frontiers | Research Topics

Bacteriophages, prophages, and their products: regulating bacterial populations

Edited by
Barbara Maciejewska, Agata Dorotkiewicz-Jach, Zuzanna Drulis-Kawa and Gamaliel López-Leal

Published in
Frontiers in Microbiology

ISSN 1664-8714
ISBN 978-2-8325-6463-9
DOI 10.3389/978-2-8325-6463-9

About Frontiers

Frontiers is more than just an open access publisher of scholarly articles: it is a pioneering approach to the world of academia, radically improving the way scholarly research is managed. The grand vision of Frontiers is a world where all people have an equal opportunity to seek, share and generate knowledge. Frontiers provides immediate and permanent online open access to all its publications, but this alone is not enough to realize our grand goals.

Frontiers journal series

The Frontiers journal series is a multi-tier and interdisciplinary set of open-access, online journals, promising a paradigm shift from the current review, selection and dissemination processes in academic publishing. All Frontiers journals are driven by researchers for researchers; therefore, they constitute a service to the scholarly community. At the same time, the *Frontiers journal series* operates on a revolutionary invention, the tiered publishing system, initially addressing specific communities of scholars, and gradually climbing up to broader public understanding, thus serving the interests of the lay society, too.

Dedication to quality

Each Frontiers article is a landmark of the highest quality, thanks to genuinely collaborative interactions between authors and review editors, who include some of the world's best academicians. Research must be certified by peers before entering a stream of knowledge that may eventually reach the public - and shape society; therefore, Frontiers only applies the most rigorous and unbiased reviews. Frontiers revolutionizes research publishing by freely delivering the most outstanding research, evaluated with no bias from both the academic and social point of view. By applying the most advanced information technologies, Frontiers is catapulting scholarly publishing into a new generation.

What are Frontiers Research Topics?

Frontiers Research Topics are very popular trademarks of the *Frontiers journals series*: they are collections of at least ten articles, all centered on a particular subject. With their unique mix of varied contributions from Original Research to Review Articles, Frontiers Research Topics unify the most influential researchers, the latest key findings and historical advances in a hot research area.

Find out more on how to host your own Frontiers Research Topic or contribute to one as an author by contacting the Frontiers editorial office: frontiersin.org/about/contact

Bacteriophages, prophages, and their products: regulating bacterial populations

Topic editors

Barbara Maciejewska — University of Wrocław, Poland
Agata Dorotkiewicz-Jach — University of Wrocław, Poland
Zuzanna Drulis-Kawa — University of Wrocław, Poland
Gamaliel López-Leal — Laboratory of Computational Biology and Integrative Viromics, Center for Research in Cellular Dynamics-UAEM, Mexico

Citation

Maciejewska, B., Dorotkiewicz-Jach, A., Drulis-Kawa, Z., López-Leal, G., eds. (2025). *Bacteriophages, prophages, and their products: regulating bacterial populations*. Lausanne: Frontiers Media SA. doi: 10.3389/978-2-8325-6463-9

Table of contents

frontiers | Frontiers in Microbiology

TYPE Editorial
PUBLISHED 03 June 2025
DOI 10.3389/fmicb.2025.1628912

OPEN ACCESS

EDITED AND REVIEWED BY
Sangryeol Ryu,
Seoul National University, Republic of Korea

*CORRESPONDENCE
Barbara Maciejewska
barbara.maciejewska@uwr.edu.pl
Gamaliel López-Leal
gamaliel.lopez@docentes.uaem.edu.mx

RECEIVED 15 May 2025
ACCEPTED 20 May 2025
PUBLISHED 03 June 2025

CITATION
Maciejewska B, Dorotkiewicz-Jach A, Drulis-Kawa Z and López-Leal G (2025) Editorial: Bacteriophages, prophages, and their products: regulating bacterial populations. *Front. Microbiol.* 16:1628912. doi: 10.3389/fmicb.2025.1628912

Editorial: Bacteriophages, prophages, and their products: regulating bacterial populations

Barbara Maciejewska[1]*, Agata Dorotkiewicz-Jach[1], Zuzanna Drulis-Kawa[1] and Gamaliel López-Leal[2]*

[1]Department of Pathogen Biology and Immunology, University of Wroclaw, Wroclaw, Poland, [2]Laboratorio de Biología Computacional y Virómica Integrativa, Centro de Investigación en Dinámica Celular, Universidad Autónoma del Estado de Morelos, Cuernavaca, Morelos, Mexico

KEYWORDS

phages, phage therapy, phage diversity, bacteriophages, prophages, phage host interactions, phage evolution, antimicrobial resistance

Editorial on the Research Topic
Bacteriophages, prophages, and their products: regulating bacterial populations

Bacteriophages, the most numerous biological entities on Earth, can be found as separate particles in the environment as well as in various forms within bacterial genomes, ranging from intact inducible prophages to incomplete phage genes. As the main bacterial predator, they are powerful regulators of microbial populations and influence bacterial evolution by selection, and gene exchange. Moreover, both bacteriophages and their derivatives offer a critical solution to the growing threat of antimicrobial resistance. This Research Topic includes articles that contribute to broadening our knowledge in three themes: phage biology, ecology and evolution, and phage therapy and biocontrol. Together, they illustrate the multifaceted roles phages and their products play in bacterial evolution, community dynamics, and the development of novel antimicrobial strategies.

Several articles in this Research Topic expand our arsenal against resistant pathogens through the characterization of new bacteriophages and highlighting their therapeutic potential against multidrug-resistant pathogens and bacterial diseases of agricultural. Khazani Asforooshani et al. introduced a newly isolated *Enterococcus faecium* phage EF-M80 that shows a broad host range (against resistant strains), biofilm-degrading ability, and resilience to high temperatures and pH. Based on this, researchers developed a hydrogel-encapsulated version, which was applied in a wound infection mouse model and led to enhanced healing by increasing the presence of neutrophils, fibroblasts, blood vessels, and collagen. The results suggest that the hydrogel-encapsulated EF-M80 phage holds promising potential for the treatment of infections caused by antibiotic-resistant *E. faecium*. Shamsuzzaman et al. isolated and characterized four lytic phages from hospital sewage water (which belong to the *Tequatrovirus* and *Kuravirus* genus) with broad host ranges and demonstrated their efficacy in reducing *Escherichia coli* ST131 infections *in vivo*. This pandemic clone poses a significant challenge to current treatments, and their findings mark a critical step toward phage-based interventions. On the other hand, Köhne et al. isolated and characterized phages active against *Streptococcus equi* subsp. *Zooepidemicus* (a major causative agent of infections in foals and adult horses), revealing strong *in vitro* lytic activity and providing a basis for future development of phage therapeutics in veterinary medicine, and expanding the catalog of phages with therapeutic potential.

In agriculture, Chantapakul et al. tested phage cocktails—mostly of the families *Autographiviridae* and *Pootjesviridae*—against *Rhizobium radiobacter*, the causative agent of crown gall disease in blueberries. The study demonstrated a significant bacterial reduction in a soil-based model, pointing to promising phage applications in plant protection. Although temperate, Miller et al. reported a phage with a narrow host range that infects *Klebsiella quasipneumoniae* and exhibits features such as biofilm disruption and phage–antibiotic synergy. While temperate phages are not commonly used in phage therapy, characterizing these phage populations remains important, as they may hold therapeutic potential through genetic engineering.

Beyond their role as lytic agents, phages encode proteins with potent antimicrobial activity. In this sense, Tian et al. report a novel phage, PA1, showing broad lytic activity against *Pantoea ananatis*. Based on the phage PA1 genome, they identified and produced an endolysin (PA1-Lys) and a hypothetical protein (PA1-LRP), enhancing the activity of the endolysin PA1-Lys. These findings reveal new insight into phage-induced lysis mechanisms and indicate PA1-LRP as a novel lysis-related protein with potential applications in phage therapy. Moreover, Zhao et al. identified the 73-amino acid Icd protein from phage P1 as a potent inhibitor of *E. coli* growth. Icd directly binds the essential division protein FtsZ, disrupting Z-ring formation. What's more, a core region (aa 12–51) retains full antibacterial activity, highlighting a novel mechanism to suppress bacterial growth and a minimal peptide with potential for antibacterial design. Both articles help to better understand the phage-host relationship and provide clues for the development of new antimicrobial proteins.

In addition to the emphasis on the use of phages and phage enzymes in combating bacteria, it is equally important to advance our understanding of phage interactions with bacterial hosts, the dynamic nature of these relationships, and the broader ecological roles and diversity of phages. Barrio-Pujante et al. focus on minimizing phage resistance in *Klebsiella pneumoniae* by inhibiting Quorum Sensing (QS) with cinnamaldehyde (CAD). Results show that CAD effectively reduces QS activity, allowing phages to infect previously resistant *K. pneumoniae* strains. This combined treatment enhances phage proliferation and significantly reduces bacterial growth, suggesting QS inhibitors could be valuable in phage therapy and phage-antibiotic combinations to combat antimicrobial resistance. DiSalvo et al. explore the dynamics of bacteriophage interactions within the *Paraburkholderia-Dictyostelium discoideum* symbiosis system. This study is noteworthy due to the versatility of this genus and the interactions of different species with various hosts. By isolating and characterizing six environmental *Paraburkholderia* phages, the research examines their impact on bacterial symbionts and host amoebae. The study reveals diverse phage effects on symbiont infection prevalence and host fitness, highlighting the complexity of tripartite interactions and laying the groundwork for future investigations into phage therapy and bacterial evolution.

To use bacteriophages as alternative strategies to antibiotics, it is essential to identify and characterize prophage populations within key pathogens such as *Acinetobacter baumannii*. In this context, Arellano-Maciel et al. analyzed the prophage diversity in *A. baumannii* isolates from various geographic regions, identifying 13 major clusters and revealing the global prevalence of *Vieuvirus*-related prophages. Studies like this provide valuable insights into the diversity and distribution of prophages across regions. The identification of distinct geographically prophage populations underscores the importance of further research into how phage–host interactions evolve in different environments. On the other hand, Zaychikova et al. reported the isolation of Vic9, the first subcluster B2 mycobacteriophage identified in Russia. Although it lysed *Mycobacterium tuberculosis* with low efficiency, its genome revealed unique features—including a recombination event and queuosine biosynthesis genes—shedding light on phage evolution and host adaptation.

Finally, in this Research Topic, Hellwig et al. introduced a novel methodology using biorthogonal non-canonical amino acid tagging (BONCAT) and click chemistry to label and isolate phage-host complexes without cultivation. This approach paves the way for studying phages in complex microbial communities, enabling high-resolution detection of active infection events *in situ*.

Author contributions

BM: Conceptualization, Project administration, Supervision, Writing – original draft, Writing – review & editing. AD-J: Data curation, Supervision, Validation, Writing – review & editing. ZD-K: Writing – review & editing, Validation, Writing – original draft. GL-L: Conceptualization, Investigation, Project administration, Supervision, Validation, Writing – original draft, Writing – review & editing.

Conflict of interest

The authors declare that the research was conducted in the absence of any commercial or financial relationships that could be construed as a potential conflict of interest.

The author(s) declared that they were an editorial board member of Frontiers, at the time of submission. This had no impact on the peer review process and the final decision.

Publisher's note

frontiers | Frontiers in Microbiology

TYPE Original Research
PUBLISHED 26 June 2024
DOI 10.3389/fmicb.2024.1416628

OPEN ACCESS

EDITED BY
Agata Dorotkiewicz-Jach,
University of Wrocław, Poland

REVIEWED BY
Swapnil Ganesh Sanmukh,
Université Clermont Auvergne, France
Tahir Hussain,
Abdul Wali Khan University Mardan, Pakistan

*CORRESPONDENCE
María Tomás
✉ MA.del.Mar.Tomas.Carmona@sergas.es

†These authors have contributed equally to this work

RECEIVED 12 April 2024
ACCEPTED 12 June 2024
PUBLISHED 26 June 2024

CITATION
Barrio-Pujante A, Bleriot I, Blasco L, Fernández-Garcia L, Pacios O, Ortiz-Cartagena C, Cuenca FF, Oteo-Iglesias J and Tomás M (2024) Regulation of anti-phage defense mechanisms by using cinnamaldehyde as a quorum sensing inhibitor.
Front. Microbiol. 15:1416628.
doi: 10.3389/fmicb.2024.1416628

Regulation of anti-phage defense mechanisms by using cinnamaldehyde as a quorum sensing inhibitor

Antonio Barrio-Pujante[1,2†], Inés Bleriot[1,2†], Lucía Blasco[1,2], Laura Fernández-Garcia[1,2], Olga Pacios[1,2], Concha Ortiz-Cartagena[1,2], Felipe Fernández Cuenca[3,4,5], Jesús Oteo-Iglesias[4,5,6] and María Tomás[1,2,5*]

[1]Grupo de Microbiología Traslacional y Multidisciplinar (MicroTM)-Servicio de Microbiología Instituto de Investigación Biomédica A Coruña (INIBIC), Hospital A Coruña (CHUAC), Universidad de A Coruña (UDC), A Coruña, Spain, [2]Study Group on Mechanisms of Action and Resistance to Antimicrobials (GEMARA) the Behalf of the Spanish Society of Infectious Diseases and Clinical Microbiology (SEIMC), Madrid, Spain, [3]Unidad Clínica de Enfermedades Infecciosas y Microbiología Clínica, Hospital Universitario Virgen Macarena, Instituto de Biomedicina de Sevilla (Hospital Universitario Virgen Macarena/CSIC/Universidad de Sevilla), Sevilla, Spain, [4]CIBER de Enfermedades Infecciosas (CIBERINFEC), Instituto de Salud Carlos III, Madrid, Spain, [5]MEPRAM, Proyecto de Medicina de Precisión Contra las Resistencias Antimicrobianas, Madrid, Spain, [6]Laboratorio de Referencia e Investigación de Resistencias a Antibióticos e Infecciones Sanitarias, Centro Nacional de Microbiología, Instituto de Salud Carlos III, Madrid, Spain

Background: Multidrug-resistant bacteria and the shortage of new antibiotics constitute a serious health problem. This problem has led to increased interest in the use of bacteriophages, which have great potential as antimicrobial agents but also carry the risk of inducing resistance. The objective of the present study was to minimize the development of phage resistance in *Klebsiella pneumoniae* strains by inhibiting quorum sensing (QS) and thus demonstrate the role of QS in regulating defense mechanisms.

Results: Cinnamaldehyde (CAD) was added to *K. pneumoniae* cultures to inhibit QS and thus demonstrate the role of the signaling system in regulating the anti-phage defense mechanism. The QS inhibitory activity of CAD in *K. pneumoniae* was confirmed by a reduction in the quantitative expression of the *lsrB* gene (AI-2 pathway) and by proteomic analysis. The infection assays showed that the phage was able to infect a previously resistant *K. pneumoniae* strain in the cultures to which CAD was added. The results were confirmed using proteomic analysis. Thus, anti-phage defense-related proteins from different systems, such as cyclic oligonucleotide-based bacterial anti-phage signaling systems (CBASS), restriction–modification (R–M) systems, clustered regularly interspaced short palindromic repeat-Cas (CRISPR-Cas) system, and bacteriophage control infection (BCI), were present in the cultures with phage but not in the cultures with phage and CAD. When the QS and anti-phage defense systems were inhibited by the combined treatment, proteins related to phage infection and proliferation, such as the tail fiber protein, the cell division protein DamX, and the outer membrane channel protein TolC, were detected.

Conclusion: Inhibition of QS reduces phage resistance in *K. pneumoniae*, resulting in the infection of a previously resistant strain by phage, with a significant increase in phage proliferation and a significant reduction in bacterial growth. QS inhibitors could be considered for therapeutic application by including them in phage cocktails or in phage-antibiotic combinations

to enhance synergistic effects and reduce the emergence of antimicrobial resistance.

KEYWORDS

cinnamaldehyde, phage resistance, *Klebsiella pneumoniae*, proteome, quorum sensing, anti-phage defense mechanisms

Introduction

Klebsiella pneumoniae is a Gram-negative enterobacteria (Wang et al., 2020), included by the World Health Organization (WHO) in the list of ESKAPE pathogens (*Enterococcus faecium*, *Staphylococcus aureus*, *K. pneumoniae*, *Acinetobacter baumannii*, *Pseudomonas aeruginosa*, and *Enterobacter*). The pathogens pose a serious threat to public health, as these multidrug-resistant (MDR) bacteria can be life-threatening in both hospitalized patients and immunocompromised individuals. Moreover, many of these pathogens can persist stably in biofilms formed on catheters, ventilators, as well as other medical devices (Mancuso et al., 2021).

In this context of clinical urgency, the use of phage therapy has recently re-emerged in the West as one of the main options for treating MDR bacteria (Nikolich and Filippov, 2020). Phage therapy has several advantages over the use of antibiotic therapy. Phages, i.e., viruses that are obligate intracellular parasites of bacteria (Salmond and Fineran, 2015), are highly specific, infecting individual bacterial species or subgroups of species, and are therefore considered narrow-spectrum antimicrobials (Gordillo Altamirano and Barr, 2019; Nikolich and Filippov, 2020). They do not act on the patient's normal microbiota, they are highly effective against MDR pathogens, and they can be used in conjunction with antibiotics to produce synergetic effects and/or restore the sensitivity of pathogens to antibiotics (Kortright et al., 2019; Gordillo Altamirano et al., 2021). Another advantage of phages is that they can replicate inside the target cell at the site of infection and they are easy to isolate. Moreover, as the most abundant biological entities on the planet, they may represent an inexpensive means of obtaining new antimicrobials (Gordillo Altamirano and Barr, 2019; Nikolich and Filippov, 2020). However, the most important problem regarding phages is the rapid acquisition of resistance in bacteria, as both phages and bacteria are involved in a constant "arms race" to develop resistance and protective mechanisms (Nikolich and Filippov, 2020; Ambroa et al., 2021). In addition, phage therapy also has certain requirements, as the phages must be strictly lytic, have no lysogeny genes such as integrases and recombinases, must have good antibacterial activity to target the pathogen, and bacterial remains and endotoxins must be eliminated (Young and Gill, 2015).

The main mechanisms of phage resistance in bacteria include the following: (i) use of outer membrane vesicles (OMVs) as a decoy for phages, which will inject their DNA into the vesicle (Azam and Tanji,

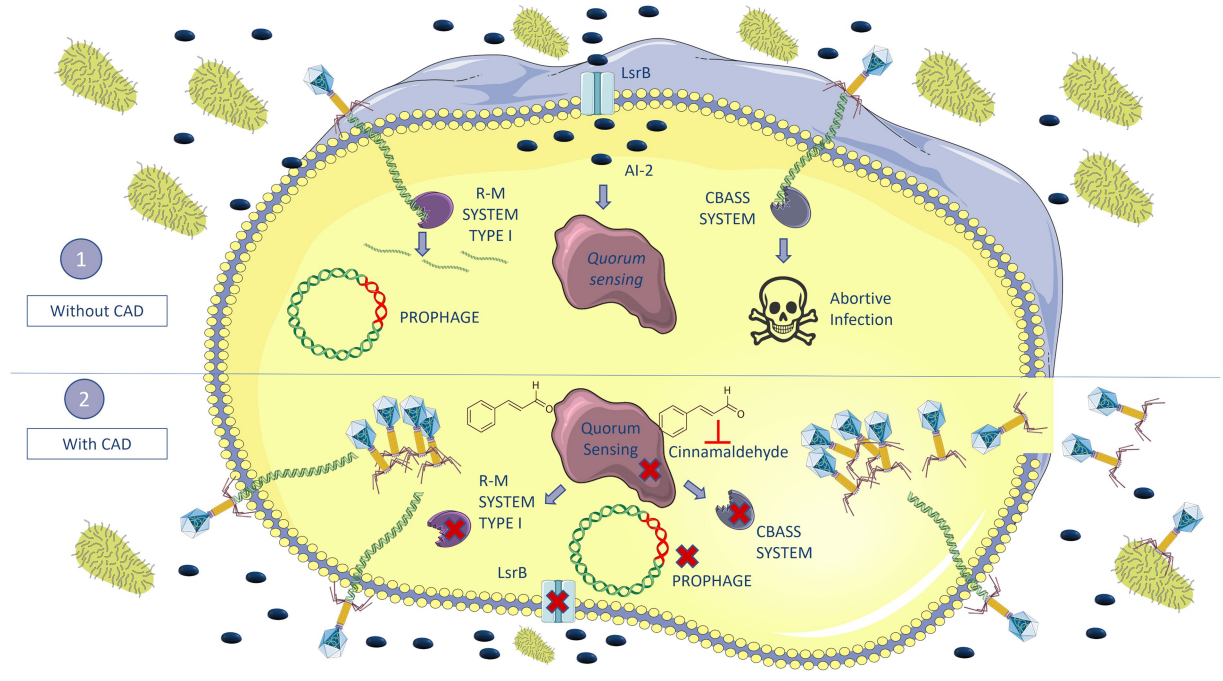

GRAPHICAL ABSTRACT

2019); (ii) blocking phage adsorption to prevent binding to the specific membrane receptor, i.e., by modifying the receptors through mutations (Labrie et al., 2010), or masking them by capsule production or by biofilm formation (Flemming et al., 2023); (iii) blocking nucleic acid injection, i.e., superinfection exclusion (Sies) system (Azam and Tanji, 2019); (iv) degradation of viral nucleic acid—if the phages manage to enter the bacteria, the bacteria may activate defense mechanisms such as exogenous DNA cutting, such as restriction–modification (R–M) (Rusinov et al., 2018), or clustered regularly interspaced short palindromic repeat (CRISPR-Cas) systems (Barrangou et al., 2007); (v) inhibition of phage DNA replication, i.e., by the bacteriophage exclusion (BREX) system (Azam and Tanji, 2019; Rousset et al., 2023); (vi) interference with phage assembly, i.e., phage-inducible chromosomal island (PICI); and (vii) abortive infection (Abi) systems, whereby bacteria being infected by phage cause their own death, thus protecting the rest of the bacterial population and preventing spread of the infection, i.e., toxin/antitoxin (TA) systems and the cyclic oligonucleotide-based antiphage signaling (CBASS) system (Azam and Tanji, 2019; Ambroa et al., 2021).

Many bacteria regulate the expression of defense mechanisms against phages by quorum sensing (QS) (Høyland-Kroghsbo et al., 2017; Rémy et al., 2018). QS is defined as a cellular communication process based on the production, secretion, and detection of extracellular signaling molecules called autoinducers (AIs), which accumulate in the local environment in a cell density-dependent manner (Xavier and Bassler, 2003). QS enables bacteria to regulate several processes such as fluorescence, virulence, biofilm formation, antibiotic resistance, bacterial competition factors, and phage resistance mechanisms such as prophages, CBASS system, and CRISPR-Cas immunity (Galloway et al., 2011; Broniewski et al., 2021; Lazar et al., 2021; Pacheco et al., 2021; Severin et al., 2023).

The QS of *K. pneumoniae* mainly relies on the action of autoinducer-2 (AI-2), a furanosyl borate diester molecule encoded by LuxS synthase, for interspecies communication. Moreover, this species can detect other AIs in the medium, such as exogenous *N*-acyl homoserine lactone (AHL), known as AI-1 (Lazar et al., 2021; Pacheco et al., 2021).

In this study, the role of QS in controlling anti-phage defense mechanisms was tested in *K. pneumoniae* by using the QS inhibitor cinnamaldehyde (CAD). CAD has previously been shown to interfere with the AI-2-based QS *Vibrio* spp. and *Burkholderia* spp. by reducing the DNA binding activity of the response regulator LuxR (Brackman et al., 2008, 2009, 2011). It also possesses antimicrobial activity and can inhibit both microbial growth and toxin production (Doyle and Stephens, 2019); it has been reported to exert antiviral activity against influenza A/PR/8 virus by inhibiting viral protein synthesis at the post-transcriptional level thereby reducing the growth of the virus (Hayashi et al., 2007). CAD can cause allergic reactions when included in perfumes and cosmetics, and the dermatological no-observed-adverse-effect level has been established as 0.5% (Shreaz et al., 2016). In addition, when inhaled in e-cigarettes, CAD has been shown to be toxic to lung cells by inhibiting cell growth and differentiation, increasing cell death and DNA strand breaks (Behar et al., 2016; Zhu et al., 2017).

Finally, CAD has been recognized by both the Flavor and Extract Manufacturers Association (FEMA) and the U.S. Food and Drug Administration (FDA) as a safe compound (Friedman, 2017).

In this study, the role of the QS in the anti-phage defense was determined by the use of CAD to sensitize a phage-resistant *K. pneumoniae* clinical isolate.

Materials and methods

Bacterial and phage strains

Two lytic phages that infect *K. pneumoniae* were used in the study: the vB_KpnM_VAC36 phage (VAC36) (Family *Myoviridae* and Genus *Marfavirus*) and the vB_KpnM_VAC66 phage (VAC66) (Family *Myoviridae* and Genus *Slopekvirus*) (Bleriot et al., 2023). The genomes of both phages are available via the GenBank BioProject with accession number PRJNA739095: VAC36 (GenBank SAMN20298872) and VAC66 (GenBank SAMN22059211).

Three clinical isolates of *K. pneumoniae* with different sensitivity to the phages were used: K3318, a phage-resistant clinical isolate (GenBank SAMEA3649518); K3573, a clinical isolate sensitive to phage VAC36 (GenBank SAMEA3649559); and ST974-OXA48, a clinical isolate sensitive to phage VAC66 (GenBank WRWT00000000). All clinical isolates of *K. pneumoniae* were obtained from the Virgen Macarena University Hospital (Seville, Spain) and the National Center for Microbiology (Carlos III Health Institute, Spain).

Propagation and collection of phages

Phages were propagated by the double-layer agar method (Da Silva et al., 2021). An overnight inoculum of each of the different strains of *K. pneumoniae* (phage host) was diluted 1/100 in Luria–Bertani (LB) broth and grown until the absorbance at 600 nm (optical density, OD_{600}) reached 0.5. Aliquots of 50 µL of phage were then added to 200 µL of the corresponding *K. pneumoniae* host and mixed with 4 mL of soft agar (0.5% NaCl, 1% tryptone, and 0.4% agar) in TA plates (0.5% NaCl, 1% tryptone, and 1.5% agar) and incubated at 37°C for 24 h. The TA plates were washed with 3 mL of SM buffer (0.1 M NaCl, 10 mM $MgSO_4$, and 20 mM Tris–HCl) and placed on a shaker at room temperature for 3 h. All of the liquid was then recovered in 15 mL tubes, to which 1% chloroform was added, and the mixture was held for 20 min. Finally, the suspension was centrifuged for 15 min at 3,400 × *g* and filtered through 0.45 nm filters. The supernatant with the phages was collected and stored at 4°C.

Cinnamaldehyde minimal inhibitory concentration assay

The CAD (3-phenylprop-2-enal; Sigma-Aldrich) minimum inhibitory concentrations (MICs) for *K. pneumoniae* clinical strains K3318, K3573, and ST974-OXA48 were established by microdilution broth assay (Wikler and Clinical, 2006; Pacios et al., 2021). Briefly, nine serial double dilutions of CAD were prepared in Muller–Hinton broth (MHB) in 96-well microtiter plates. Finally, each well was then inoculated with the corresponding strain of *K. pneumoniae* to a final concentration of 5×10^5 CFU/mL, diluted from an overnight culture. A row of MHB inoculated with *K. pneumoniae* was included as a positive control and a row including only MHB was included as a

A

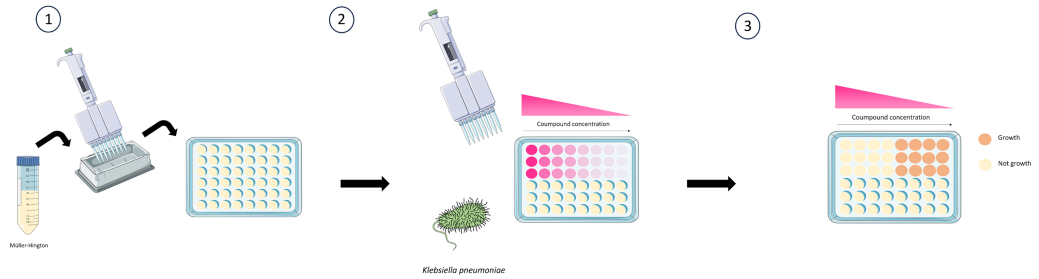

B

Name	K3318	K3573	ST974-OXA48
CAD (µg/mL)	6.125 mM	2.5 mM	3.125 mM

C

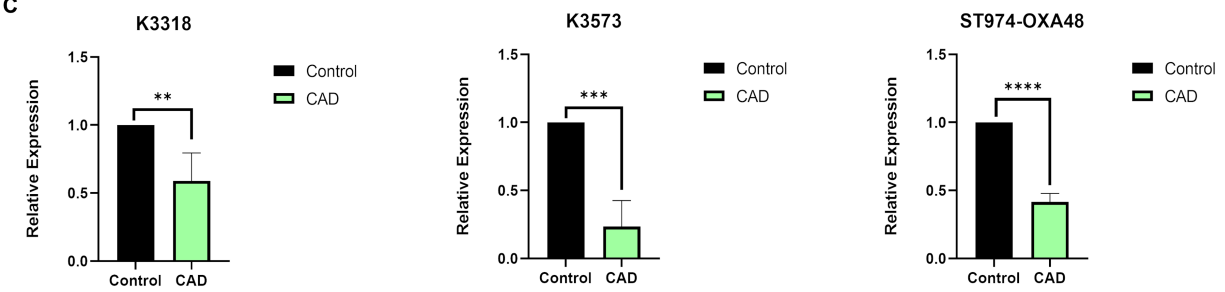

FIGURE 1
Illustration of the microdilution broth assay used to determine the MICs of Cinnamaldehyde (CAD) and to quantify *lsrB* gene expression. **(A)** Illustration of the microdilution broth assay process for different strains of *K. pneumoniae* in the presence of CAD. **(B)** MICs of CAD for different strains of *K. pneumoniae*. **(C)** Quantification of *lsrB* gene expression in the presence of 1 mM CAD relative to the control. The asterisks refer to statistical significance, the more asterisks, the more significant the difference between the groups compared. *p<0,0332; **p<0,0021; ***p<0,0002; ****p<0,0001.

negative control. The plates were incubated for 24 h at 37°C, and finally, the MICs were determined as the concentration of CAD in the first well where no bacterial growth was observed (Pacios et al., 2021). All experiments were performed in triplicate (Figure 1A).

Quantitative expression of the *lsrB* gene

Expression of the *lsrB* gene, which is responsible for transporting AI-2 into the cell (Figure 2), was quantified in the presence of a subinhibitory concentration of CAD (1 mM) in the three clinical isolates of *K. pneumoniae*. For this purpose, 200 µL of an overnight culture of the corresponding *K. pneumoniae* clinical isolate was inoculated in 20 mL flasks of LB broth containing 1 mM CAD (two biological samples of each strain). The flasks were then incubated at 37°C with shaking at 180 rpm, until an OD_{600} of 0.3 was reached. Duplicate aliquots of 1 mL were taken from each flask for subsequent RNA extraction with the High Pure RNA Isolation Kit (Roche). The extraction was conducted following the manufacturer's instructions. The RNA extracted from each sample was measured in a Nanodrop spectrophotometer (NanoDrop Technologies) and adjusted to 50 ng/µL with nuclease-free water for use in qRT-PCR (LightCycler® 480). Specific primers for the *lsrB* gene and its corresponding UPL probe and specific primers for the *rho* gene, included as a housekeeping gene (Gomes et al., 2018), with the corresponding UPL probe (Table 1), were used in the assay (conducted with the LightCycler® 480 Control Kit from Roche). Student's *t*-test (GraphPad Prism 9.0.0) was used to determine any statistically significant differences (p-value < 0.05) in gene expression.

Phage infection assays

Phage infection curves were constructed for strains K3318, ST974-OXA48, and K3573, and phages VAC36 and VAC66. Briefly, an overnight culture of the *K. pneumoniae* strain to be tested was diluted 1/100 in LB broth. Five different conditions were prepared with the bacterial culture at an initial OD_{600} of 0.3: a growth control; *K. pneumoniae* culture with 1 mM CAD; *K. pneumoniae* strain with the corresponding phage at a multiplicity of infection (MOI) 1; *K. pneumoniae* strain in combination with the phage at MOI 1 and 1 mM CAD; and a negative control with LB broth. A final volume of 200 µL was added to each corresponding well of 96-well plates.

The plates were incubated at 37°C with shaking at 559 cycles per minute (CPM) for 24 h in a BioTek Epoch 2.0 (Agilent). The contents of three wells for each condition were recovered at different time points, and the bacteria and phages were quantified by counting colony-forming units (CFUs/mL) and plaque-forming units (PFUs/mL) at 0 h (T0), 5 h (T5), and 24 h (T24). To quantify the CFUs, 100 µL of culture was removed at the appropriate time and diluted to the correct dilution for counting the cells. Finally, 100 µL of the dilution was plated on LB plates. For the quantification of PFUs, the phages were isolated as described below. At the corresponding time points, 100 µL of culture was removed, 1% chloroform was added, and the mixture was shaken for 20 min. The suspension was then centrifuged at 10,000 × *g* for 5 min and serially diluted to the correct dilution for counting. Finally, the double-layer agar method was used to obtain the PFUs (Da Silva et al., 2021); the plates were incubated for 24 h at 37°C,

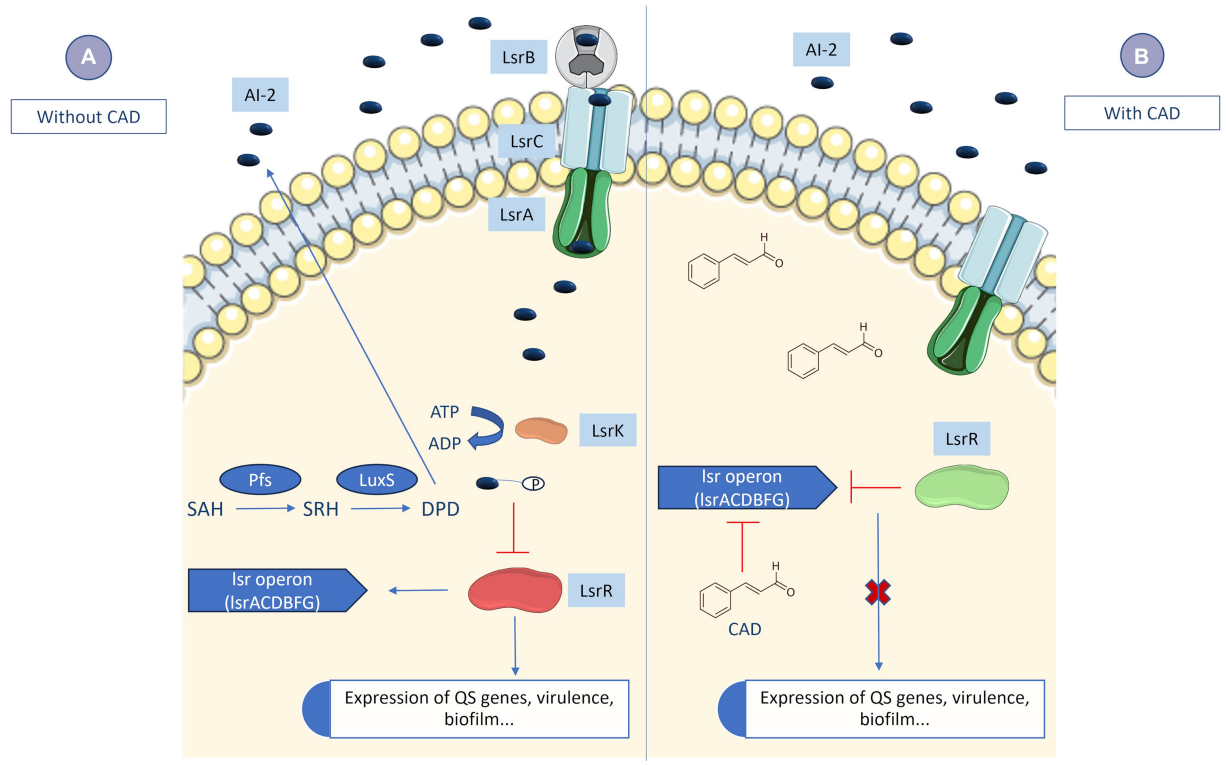

FIGURE 2
QS inhibition by the action of CAD. **(A)** Under normal conditions, the bacteria synthesize AI-2 in the extracellular environment. AI-2 from the extracellular environment is internalized via LsrB into the bacteria. Subsequently, the AI-2 will be phosphorylated by LsrK. The phosphorylated AI-2 molecule represses LsrR (repressor of the *lsrACDBFG operon*) so that much more AI-2 begins to be transported into the bacteria. Transport of AI-2 into the cell, together with the repression of LsrR, leads to the transcription of numerous genes related to bacterial virulence, biofilm, QS, etc. **(B)** When cinnamaldehyde (CAD) is inside the cell, expression of the *lsrB* gene is inhibited, preventing extracellular AI-2 from being internalized. Thus, LsrR itself continues to inhibit the *lsrACDBFG operon,* and transcription of the aforementioned genes does not occur, so the QS cascade is inhibited.

TABLE 1 Primers and probes used for *rho* and *lsrB* genes in the qRT-PCRs.

Primer name	Sequences	Probes	References
***lsrB* gene (AI-2 transport)**			
Kp_lsrB_Fow	CAGTATGAGGCGAAGGGCAA	74	This study
Kp_lsrB_Rev	TCGTAGTTGTTGATGTTCTCTTTGC	74	This study
***rho* gene (Housekeeping gene)**			
Kp_rho_Fow	CGACGGCGTACTGGAGATAC	17	This study
Kp_rho_Rev	TTGGCTGGGGGATACGTAGA	17	This study

and the CFUs/mL and PFUs/mL were counted. All experiments were performed in triplicate. Student's *t*-test was used to determine any statistically significant differences ($p < 0.05$) in the bacteria counts (GraphPad Prism 9.0.0).

Proteomic analysis

A proteomic study was conducted to determine the inhibition of anti-phage defense mechanisms and QS by using LC–MS and NanoUHPLC-Tims-QTOF analysis.

Strain K3318 (obtained from an overnight inoculum) was inoculated into 50 mL flasks containing LB broth at 1/100 dilution, and the culture was incubated until an OD_{600} of 0.3 (approximately 1×10^7 CFU/mL) was reached. The four previously described treatments were tested in duplicate. The culture strains were allowed to grow for 3 h, before 25 mL of the suspension was removed from each flask, placed in 50 mL tubes, and placed on ice for 10 min. The tubes were centrifuged for 20 min at 4°C and 4,500 rpm, and the pellet obtained after discarding the supernatant was frozen at −80°C. On the following day, the pellet was resuspended in phosphate-buffered saline (PBS) medium and sonicated with an ultrasonic processor (UP200S, Hielscher Ultrasonics) at an amplitude of 80% and a cycle of 0.5 per second for periods of 90 s with the sample on ice. The sonicated pellets were centrifuged for 20 min at 4°C at 4,500 × *g*. The supernatant was recovered and used in the proteomic analysis.

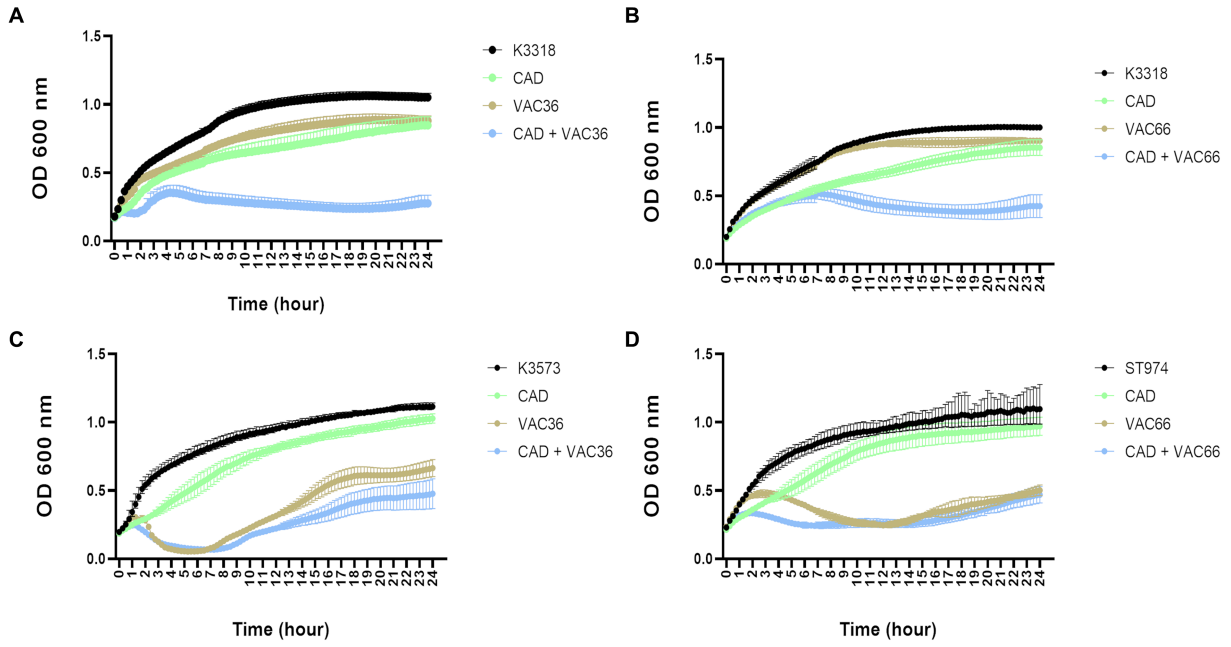

FIGURE 3
Infection curves for the three clinical isolates of *K. pneumoniae* with phage alone and phage in combination with CAD. **(A)** Strain K3318 infected with VAC36. **(B)** Strain K3318 infected with VAC66. **(C)** Strain K3573 infected with VAC36. **(D)** Strain ST974-OXA48 infected with phage VAC66.

A quantitative analysis of proteins was conducted with 200 ng of supernatant from each sample using the NanoUHPLC-Tims-QTOF in a TimsTof Pro mass spectrophotometer (Bruker), with a nanoESI source (CaptiveSpray), a QTOF-time analyzer and a nanoELUTE chromatograph (Bruker). The samples were prepared by tryptic digestion in solution with reduction-alkylation, followed by ZipTip desalting. The data were obtained in a nanoESI positive ionization mode, Scan PASEF-MSMS mode, and CID fragmentation mode, with an acquisition range of 100–1,700 m/z. The products were separated on a ReproSil C18 column (150 × 0.075 mm, 1.9 µm, and 120 Å) (Bruker) at 50°C with an injection volume of 2 µL. The mobile phases consisted of 0.1% H_2O/formic acid (A) and 0.1% acetonitrile/formic acid (B). The flow rate was 0.4 µL/min, and the gradient program was 11% B (0–5 min), 16% B (5–10 min), 35% B (10–16 min), 95% B (16–18 min), and 95% B (18–20 min). Finally, different types of software were used for data acquisition: Compass HyStar 5.1 (Bruker), TimsControl (Bruker), DataAnalysis (Bruker), and PEAKS studio (Bioinformatics Solutions).

Student's *t*-test was used to detect any statistically significant differences (p-value < 0.05) in the results (GraphPad Prism 9.0.0).

Results

CAD microdilution broth assay

The microdilution broth assay was used to determine the MICs of CAD for clinical isolates of *K. pneumoniae* (Figure 1B). The MICs were 6.125 mM for clinical strain K3318, 2.5 mM for clinical strain K3573, and 3.125 mM for clinical strain ST974-OXA48.

Quantitative expression of the *lsrB* gene

In order to confirm the role of CAD in inhibiting the *K. pneumoniae* QS, the expression of the AI-2 QS periplasmic transporter *lsrB* gene (Figure 2) was measured (Zhang et al., 2020). Expression of *lsrB* was significantly lower in the presence of CAD than in the absence of CAD (Figure 1C). This difference was observed for the three isolates of *K. pneumoniae* used in the study, thus confirming the inhibitory effect of CAD on QS in *K. pneumoniae*.

Phage infection assays

The phage infection assays were performed to test the infectivity of phages in the presence of the QS inhibitor CAD. The corresponding infection curves showed a decrease in the OD_{600} of strain K3318 when the bacteria were infected with the phages in combination with CAD (Figures 3A,B), as this strain was resistant to both phages. The control infection curve showed similar growth. In the sensitive strains, K3573 and ST974-OXA48, no differences were observed when the bacteria were infected with the phage alone or in combination with CAD (Figures 3C,D). A slight reduction in initial growth was observed in the CAD condition in all three strains. To confirm the OD_{600} results, CFUs and PFUs were counted at 0 h, 7 h, and 24 h (Figures 4A,B). The results revealed a significant decrease in the number of CFUs at 7 h and a significant increase in the PFUs for strain K3318 when infected with the combination of CAD and each of the phages. No decrease in CFUs or increase in PFUs was observed when the bacteria were infected with each phage alone. At 24 h, the number of CFUs was higher in the cultures

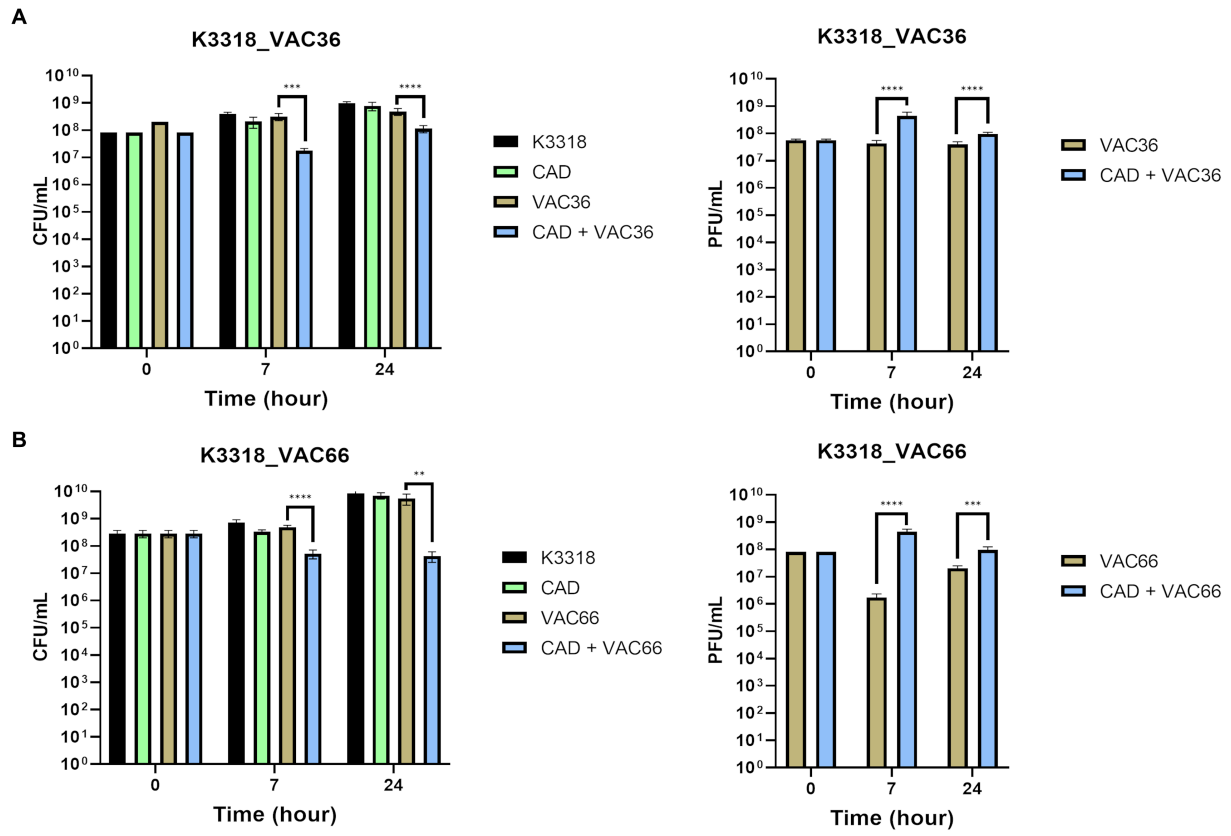

FIGURE 4
Quantification of bacteria and phages by CFU/mL and PFU/mL counts in phage infection assays. **(A)** CFU/mL and PFU/mL of strain K3318 infected with phage VAC36. **(B)** CFU/mL and PFU/mL of strain K3318 infected with phage VAC66. The asterisks refer to statistical significance, the more asterisks, the more significant the difference between the groups compared. *p<0,0332; **p<0,0021; ***p<0,0002; ****p<0,0001.

with CAD plus phage but significantly lower than in the control with phage and growth control. At 24 h, although the number of PFUs was lower, it was significantly higher than the number corresponding to each phage alone. No significant differences in CFUs between the control group and the CAD condition were observed. These results are consistent with a productive phage infection after the addition of CAD, suggesting that CAD favors phage infection by inhibiting bacterial defense mechanisms.

Host strains K3573 and ST974-OXA48 were sensitive to phage infection, but there were no significant differences between the treatment with phage alone and the treatment with CAD plus phage (Figures 3C,D). Owing to the lack of any differences, the CFUs and PFUs were not quantified. As the phage was able to infect the culture in the control condition, it seems that no efficient bacterial defense mechanisms were activated in this case, and the CAD did not have any effect.

Study of the proteins related to anti-phage defense mechanisms and QS

A proteomic analysis (NanoUHPLC-Tims-QTOF) was conducted to confirm that the anti-phage defense mechanisms are regulated by QS. The analysis identified a total of 1,222 proteins among all samples, grouped according to function and abundance across all conditions (Supplementary Table S1; Figure 5A). For example, 406 proteins were identified in the CAD plus VAC36 treatment, and 344 proteins were identified in the condition with phage alone (Figures 5B,C).

The analysis showed that the main representative proteins in all conditions were related to bacterial metabolism and protein metabolism. These proteins were less abundant in the treatments, including phage (Supplementary Table S1; Figures 5A–C). Although the relative abundance of proteins related to nucleic acid metabolism was reduced in the treatment with phage, it was slightly higher in the CAD plus VAC36 treatment (Figure 5A). Interestingly, the analysis revealed a higher relative abundance of proteins related to anti-phage defense when CAD was not added to the culture. Proteins related to functions such as cell division, the outer membrane, and cell wall production were also less abundant in the treatment with phage (Figure 5A). The effect of CAD on phage infection was highlighted, as in this condition only phage-related proteins were detected. In addition, the outer membrane proteins, which usually act as phage receptors, were also more abundant in this treatment relative to the treatment with phage alone (Figure 5A).

Proteins related to anti-phage defense mechanisms were present when the culture was only infected with phage and was absent in the treatment, including CAD (Table 2). The defense system proteins identified belong to the CBASS system, such as purine-nucleoside phosphorylase (WFM04862.1), uridine phosphorylase (WGN84707.1), ubiquitin-like protein (WP_289465582.1), and polyubiquitin (WP_223807730.1). They also belonged to the CRISPR-Cas type I-E defense system, such as CRISPR-associated

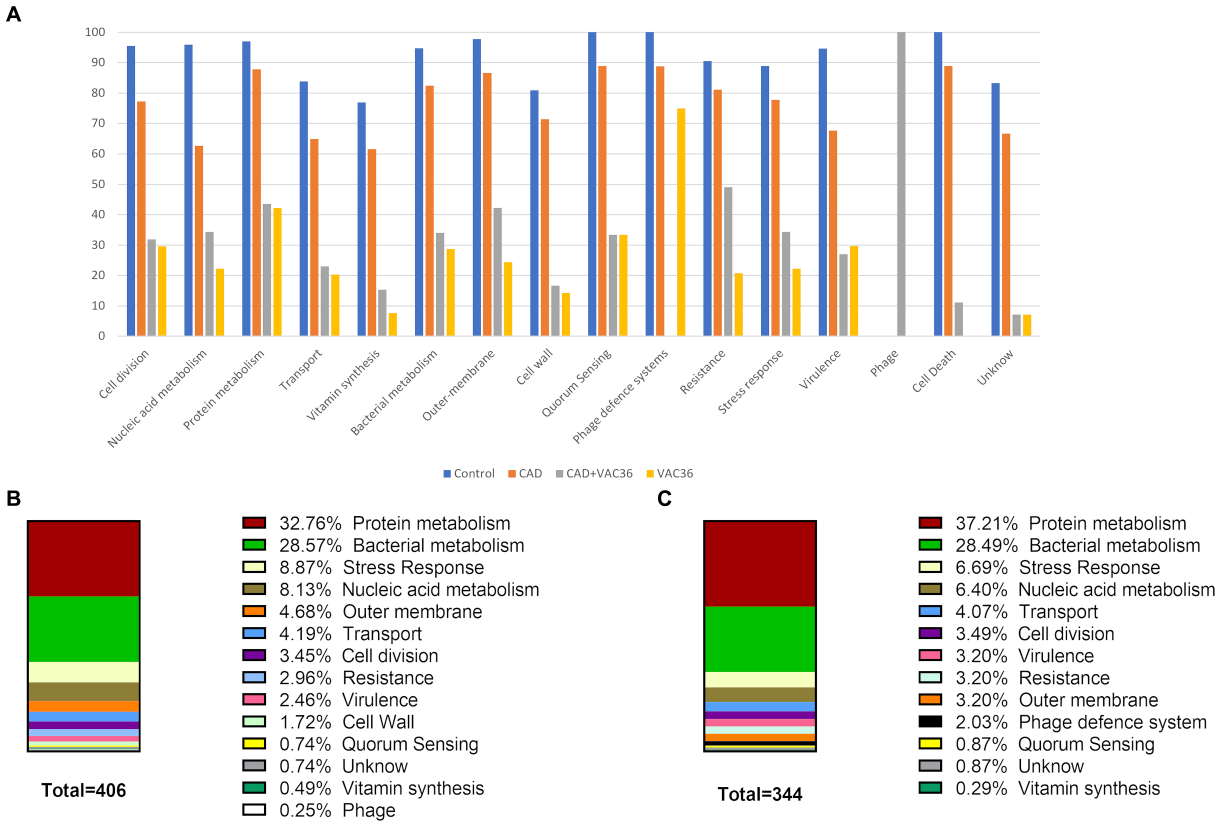

FIGURE 5
Graphical representation of proteomic analysis. **(A)** Relative abundance of each functional protein group in K3318. **(B)** Abundance of proteins belonging to each functional group in the CAD plus VAC36 treatment. **(C)** Abundance of proteins belonging to each functional group in the VAC36 treatment. Parts of the figure were drawn using diagrams available from Servier Medical Art. Servier Medical Art by Servier is licensed under a Creative Commons Attribution 3.0 Unported License (https://creativecommons.org/licenses/by/3.0/).

protein Cas7/Cse4/CasC (WAY94155.1), to the R-M system, including restriction endonuclease subunit S (WAD08528.1), and finally to a prophage-related defense system known as bacteriophage control infection (BCI) (UZL08287.1), previously described by our research group (Ambroa et al., 2020). In addition, a tail phage protein (WP_153932364.1) was only present in significant amounts when both phage and CAD were added to the culture. Other proteins, such as the cell division protein DamX (UZL52976.1), which contributes to more efficient infection of the phage, and the outer membrane channel protein TolC (WBL85855.1), a phage receptor, were more abundant in the cultures to which CAD was included than in the corresponding cultures without the compound, confirming active infection. These results confirmed the regulatory activity of the QS in the anti-phage defense mechanisms.

Interestingly, the abundance of protein confirmed the inhibitory effect of CAD on QS. Thus, quorum quenching proteins related to QS extinction, such as (4S)-4-hydroxy-5-phosphonooxypentane-2,3-dione isomerase (UZL69991.1) and alpha/beta fold hydrolase (WCN21377.1), were also more abundant in the cultures with CAD than in the control culture. LuxR (WP_265783091.1), a known QS receptor, was only present in the control culture, and the ribosome-associated translation inhibitor RaiA (UZL23362.1), another protein of interest related to bacterial persistence, was less abundant in the presence of CAD.

Discussion

Phage therapy provides a great opportunity to advance in the fight against MDR bacteria; phages can be used alone and in cocktails, and they can also be used in combination with antibiotics to restore bacterial sensitivity to these agents (Chan et al., 2016; Blasco et al., 2023). Phages have many advantages over conventional antimicrobials: they are cheap and easy to obtain, highly specific and self-replicating, and they do not act on the patient's normal microbiota (Gordillo Altamirano and Barr, 2019; Kortright et al., 2019; Nikolich and Filippov, 2020; Gordillo Altamirano et al., 2021). However, the main problem with their use is the rapid acquisition of resistance in bacteria, which possess numerous defense mechanisms against phages (Nikolich and Filippov, 2020; Ambroa et al., 2021). Therefore, inhibiting anti-phage defense mechanisms, currently achieved by combining both antibiotic and phage therapies, is an important strategy to improve phage therapy, although the current strategy only works for those bacteria with phage receptors involved in antibiotic resistance (Blasco et al., 2019, 2023; Cesta et al., 2023; Bleriot et al., 2024).

In this context, the present study aimed to determine whether anti-phage resistance mechanisms are regulated by QS in *K. pneumoniae*. Previous studies have shown that QS regulates anti-phage defense mechanisms in bacteria under conditions of high cell

TABLE 2 Proteins associated with quorum sensing (QS), anti-phage defense mechanisms, and phage proliferation, detected in the proteomic analysis.

Quorum related								
Description	Accession no.	−10LgP	Control	CAD	CAD + VAC	VAC	Mechanism	References
(4S)-4-hydroxy-5-phosphonooxypentane-2,3-dione isomerase [*Klebsiella pneumoniae*]	UZL69991.1	1.48E+07	7.07E+06	1.93E+07	0.00E+00	0.00E+00	Quorum Quenching	Marques et al. (2011)
Alpha/beta fold hydrolase [*Klebsiella pneumoniae*]	WCN21377.1	1.39E+07	8.80E+06	3.04E+07	0.00E+00	0.00E+00	Quorum Quenching	Sikdar and Elias (2020)
LuxR C-terminal-related transcriptional regulator, partial	WP_265783091.1	9.21E+06	1.18E+07	0.00E+00	0.00E+00	0.00E+00	Quorum Sensing	Pacheco et al. (2021)
Ribosome-associated translation inhibitor RaiA	UZL23362.1	2.08E+07	4.61E+07	2.22E+05	0.00E+00	0.00E+00	Persistence	Lang et al. (2021)
Anti-phage defense								
Type I-E CRISPR-associated protein Cas7/Cse4/CasC	WAY94155.1	2.02 + 06	1.66E+07	0.00E+00	0.00E+00	0.00E+00	CRISPR-Cas	Barrangou et al. (2007), Makarova et al. (2011)
Bacteriophage Control Infection (BCI)	UZL08287.1	1.87E+07	1.43E+07	3.22E+07	0.00E+00	1.93E+06	Virulence	Ambroa et al. (2020)
Purine-nucleoside phosphorylase	WFM04862.1	2.46E+06	7.40E+07	1.56E+07	0.00E+00	1.88E+07	CBASS System	Rousset et al. (2023)
Uridine phosphorylase	WGN84707.1	1.88E+07	4.51E+07	1.61E+07	0.00E+00	2.42E+06	CBASS System	Rousset et al. (2023)
Uridine phosphorylase	WBY12188.1	1.44E+07	1.57E+05	1.68E+07	0.00E+00	1.44E+06	CBASS System	Rousset et al. (2023)
Restriction endonuclease subunit S	WAD08528.1	6.03E+07	1.53E+06	1.77E+07	0.00E+00	2.32E+07	R-M System	Loenen et al. (2014)
Ubiquitin-like protein, partial	WP_289465582.1	1.32E+07	2.05E+07	4.45E+07	0.00E+00	6.72E+06	CBASS System	Jenson et al. (2023)
Polyubiquitin, partial	WP_223807730.1	2.02E+07	6.70E+06	7.49E+06	0.00E+00	6.72E+06	CBASS System	Jenson et al. (2023)
Phage related								
Tail fiber domain-containing protein	WP_153932364.1	1.73E+07	0.00E+00	0.00E+00	4.65E+07	0.00E+00	Tail phage	Olszak et al. (2017)
Cell division protein DamX	UZL52976.1	2.79E+07	1.86E+07	8.05E+06	3.90E+07	1.54E+06	Cell Division	Wenzel et al. (2024)
Outer membrane channel protein TolC	WBL85855.1	1.90E+07	2.89E+07	5.16E+07	7.23E+06	0.00E+00	Phage receptor	Hasan and Ahn (2022)

10.3389/fmicb.2024.1416628

density: the bacteria are more exposed to phages as the viruses are more abundant in densely populated environments, as they need bacteria to proliferate (Høyland-Kroghsbo et al., 2013).

In the present study, the relationship between QS and the anti-phage defense mechanism was tested by inhibiting QS with CAD. The QS autoinductor in *K. pneumoniae* is the AI-2 synthesized by an ortholog of LuxS synthase, which is also related to biofilm production (Balestrino et al., 2005). The relationship between anti-phage defense and QS has been demonstrated in *Escherichia coli* in a study in which the AI-2 induced a defensive response against phages by decreasing both the overall host metabolism and the phage receptors (Ding et al., 2021).

Inhibition of QS in clinical isolates of *K. pneumoniae* was confirmed in the present study by the *lsrB* gene, known to encode an AI-2 transporter with a previously demonstrated role in anti-phage defense (Zhang et al., 2020; Ding et al., 2021). The role of CAD in QS inhibition was demonstrated in uropathogenic *E. coli* strains, in a study in which CAD reduced QS and biofilm production (Capper-Parkin et al., 2023). The inhibitory effect of CAD on QS has also been demonstrated in other bacteria such as *Vibrio* spp. and *Burkholderia* spp. (Brackman et al., 2008, 2009, 2011; Capper-Parkin et al., 2023). The inhibitory role of CAD was established in the present study for *K. pneumoniae,* as a 60% decrease in *lsrB* expression levels was observed when CAD was present at subinhibitory concentrations (1 mM) (Figure 1C).

The role of QS in regulating anti-phage defense mechanisms was previously demonstrated by Hoque et al., who observed that QS in *V. cholerae* (via cholera AI-1- and AI-2-like AIs) regulates the production of haemagglutinin protease (HAP), which is responsible for inactivating viral particles and deregulating phage receptors, particularly the LPS O-antigen receptor, thereby preventing phage adhesion (Hoque et al., 2016). Moreover, the high cell density caused by QS in *V. cholerae* cultures has been associated with the transcription of two essential components of the CBASS defense system, the oligonucleotide cyclase and the phospholipase effector (Severin et al., 2023). Numerous studies have confirmed the activation of the CRISPR-Cas defense system at high cell densities. Thus, in *Serratia* spp., an increase in type I-E, I-F, and III CRISPR-Cas systems was shown to be caused by QS regulation (Patterson et al., 2016). In *P. aeruginosa*, QS was demonstrated to be involved in regulating CRISPR-Cas genes and activating three key aspects of the system, namely expression, activity, and adaptation (Høyland-Kroghsbo et al., 2017; Broniewski et al., 2021). In addition, it has been suggested that *P. aeruginosa* regulates cell death by using the Pseudomonas quinolone signal (PQS) to prevent the spread of phage infection (Shah et al., 2021). In *E. coli*, activation of QS was shown to reduce the number of phage λ receptors on the cell surface in order to evade infection (Høyland-Kroghsbo et al., 2013; Ding et al., 2021). Finally, the Brex defense system is also linked to QS through S-adenosyl methionine (SAM), a precursor in the synthesis of AI-2 that may be a necessary cofactor in the system (Xavier and Bassler, 2003; Andriianov et al., 2023). We are not aware of any studies specifically linking *K. pneumoniae* QS to anti-phage defense mechanisms such as those described above.

The role of QS in the expression of anti-phage defense mechanisms was tested by infecting the phage-resistant strain *K. pneumoniae* K3318 with two different phages in combination with 1 mM CAD. The infection curves obtained for two phages showed a significant reduction in the OD_{600} when resistant strain K3318 was infected with phages in combination with CAD (Figures 3A,B), as well as a reduction in the CFU/mL and an increase in the PFU/mL after 7 h and 24 h (Figures 4A,B). As isolate K3318 was initially resistant to phages VAC36 and VAC66, the results of the control infection were similar to those obtained for the growth control. In the sensitive strains (Figures 3C,D), no resistance was observed as both strains were killed by their respective phages, and no effect of phage in combination with CAD was observed as the results of infection in the presence and absence of CAD were similar. In the growth curves for the presence of CAD alone, the growth of both strains was slightly reduced. This effect was also observed for the resistant strain K3318, but the difference was not large enough to be reflected in the CFU counts. Although the antimicrobial activity of CAD has been demonstrated (Doyle and Stephens, 2019), it seems that this effect was negligible at the subinhibitory concentration used in the present study. The antiviral activity of the CAD was also established for the influenza virus but was not observed in the present study (Hayashi et al., 2007), as the CAD did not affect infection of the sensitive strains; in the case of the resistant strain K3318, the presence of CAD favored the infection, and the counts of PFUs increased, thus indicating increased phage replication and inhibition of defense mechanisms.

The results of the proteomic study confirmed those revealed by the infection curve and the relationship between QS and anti-phage defense mechanisms. Moreover, the CAD-mediated QS inhibition was validated by the lower or higher expression of some proteins related to QS in the cultures with CAD than in the control culture (Table 2). Some of these proteins are directly related to quenching of the QS signal and were found to be more abundant in the presence of CAD, e.g., (4S)-4-hydroxy-5-phosphonoxypoxypentane-2,3-dione isomerase, which is directly involved in the degradation of phospho-AI-2, as it converts the molecule (4S)-4-hydroxy-5-phosphonoxypoxypentane-2,3-dione (P-DPD) (a precursor of the AI-2) into 3-hydroxy-5-phosphonoxypoxypentane-2,4-dione (P-HPD), closing the signaling cycle and leading to termination of the expression of the *lsr operon* (Marques et al., 2011). The alpha/beta-fold hydrolase protein shows a preference for a wide variety of AHL substrates and may have lactonase activity (Sikdar and Elias, 2020). The orphan LuxR C-terminal-related transcriptional regulator, another protein related to AI receptors, was not present in cultures with CAD or phage. In *K. pneumoniae*, this protein detects (but does not produce) exogenous AHL from other bacterial species and also regulates virulence factors such as biofilm formation, expression of fimbriae, cell division, and production of QS AIs (Pacheco et al., 2021). Finally, the ribosome-associated translation inhibitor RaiA, a ribosome-associated protein related to the transition to the stationary phase, was less abundant in the cultures to which CAD was added than in the control culture, owing to persistence mechanisms (Lang et al., 2021).

The relationship between QS and phage resistance was also reflected by the abundance of some phage-related proteins present when the CAD was added along with the phage. The relative abundance of proteins related to DNA metabolism was slightly higher when the cultures were infected with CAD plus VAC36 than when they were infected with the phage alone (Figure 5A), probably due to active replication of the phage. In the phage infection, the number of proteins related to cell division, cell wall, or outer membrane was reduced. However, in cultures to which CAD was added along with the phage, the outer membrane proteins were almost two times more abundant than in cultures infected with phage alone. One of the main

anti-phage defense mechanisms is receptor masking (Bleriot et al., 2024). The proteins that act as receptors were present in the cultures to which CAD was added, as no defense mechanisms were activated; however, the same proteins were undetectable in the cultures to which only phage was added, as a result of receptor masking. These proteins include some outer membrane proteins (Hantke, 2020), in particular the outer membrane channel protein TolC (Table 2), which has been shown to act as a phage receptor in *E. coli* (phage TLS) and *Salmonella* spp. (phages ST27, ST29, and ST35) (Hasan and Ahn, 2022). The cell division protein DamX, an important component of the episome, has been reported to play a supportive role during phage replication by increasing replication efficiency (Wenzel et al., 2024). Although this protein is more abundant in the CAD condition due to phage replication, it is also present in other conditions because it is involved in cell division (Wenzel et al., 2024) (Table 2). The absence of resistance and the active infection in the presence of CAD were finally confirmed by the presence of a tail phage protein, which was not present in the cultures without CAD (Table 2), i.e., during the absence of infection as observed in the infection curves (Figures 3A,B). The presence of this protein in the synergistic interaction between CAD and phage shows that a productive infection was taking place in this treatment and new phage progeny was being produced (Olszak et al., 2017). The proteins related to anti-phage defense mechanisms were only detected when the infection was established in the absence of CAD, which suggests that CAD is involved in inhibiting the anti-phage defense mechanism. Many of these proteins belong to the CBASS defense system, an Abi system composed of an oligonucleotide cyclase that is responsible for activating the effector upon sensing the infection and a cyclic oligonucleotide-sensitive effector that kills the infected cell (Jenson et al., 2023; Rousset et al., 2023; Severin et al., 2023). The CBASS proteins were present in the cultures infected with phage alone, but not in the cultures in which QS was inhibited by the addition of CAD. The CBASS proteins identified were purine-nucleoside phosphorylase, uridine phosphorylase, ubiquitin-like protein, and polyubiquitin. The two first proteins act as effector proteins in the CBASS, as both are purine nucleoside phosphorylases (PNP), forming part of the cyclic oligonucleotide-sensitive effector (Rousset et al., 2023). Ubiquitin and polyubiquitin are involved in coding *cap2*, a gene whose catalytic activity is essential for the correct functioning of the CBASS system (Jenson et al., 2023). The restriction endonuclease subunit S protein, which is related to the R-M defense system, was also absent in cultures to which CAD was added along with phage (Mruk and Kobayashi, 2014). The R-M system provides a type of innate immunity that protects prokaryote cells from the insertion of foreign DNA, including a restriction endonuclease (REase), which recognizes and cuts short DNA sequences, and a methyltransferase (Mtase), which methylates host DNA so that it cannot be cut by REase (Birkholz et al., 2022). The restriction endonuclease subunit S belongs to the R–M type I system, which is encoded by three genes: *hsdR,* which encodes the restriction subunit (R); *hsdM*, which encodes the modification subunit (M); and *hsdS*, which encodes the recognition subunit (S for specificity) (Loenen et al., 2014). A CRISPR-associated protein Cas7/Cse4/CasC, a bacterial defense-related protein, was detected in the control cultures and belongs to the CRISPR-Cas type I–E system (Makarova et al., 2011). The absence of this protein in the phage-only condition, in which the anti-phage defense mechanisms are active, may be explained by the mode of action of the CRISPR-Cas system, which needs to carry a specific spacer for the phage, and if it does not (because there has been no previous contact between the phage and bacteria), the system would not be activated (Makarova et al., 2011). The BCI protein, a carbon storage family protein present in prophages and involved in controlling infection by other phages, was also detected. Expression of BCI has been shown to favor the activation of the QS (Ambroa et al., 2020). This protein was totally inhibited by the combination of CAD and phage and present in all other conditions, possibly because its expression is regulated by QS, and when inhibited, it cannot provide protection against phage infection.

Finally, in the cultures to which phage was added along with CAD, multiple resistance mechanisms, such as efflux pumps, were activated (Figure 5A; Supplementary Table S1). This finding can probably be attributed to the presence of CAD. In *P. aeruginosa*, exposure to subinhibitory concentrations of CAD resulted in the expression of efflux pump encoding operons (Tetard et al., 2019).

The present study demonstrated that bacterial defense mechanisms are directly linked to and controlled by QS in *K. pneumoniae*. Inhibition of QS reduces phage resistance, and inhibitory compounds could be included in phage cocktails or in phage-antibiotic combinations, potentially further enhancing the synergy and reducing the emergence of resistance. This would partly resolve the drawback of using phages by themselves.

The study findings indicate that QS inhibition appears to be a promising strategy for evading bacterial defense. However, a limited number of phages and bacterial strains were tested in the present study, and an examination of the effect of CAD on a larger number of phages and phage-resistant strains is recommendable. QS inhibition may be the missing piece of the puzzle that will enable the great potential of phages to be fulfilled, thus providing a possible solution to the ever-increasing problem of MDR bacteria and the lack of antibiotics.

Data availability statement

The original contributions presented in the study are included in the article/Supplementary material, further inquiries can be directed to the corresponding author.

Author contributions

AB-P: Investigation, Methodology, Writing – original draft. IB: Supervision, Validation, Writing – review & editing. LB: Supervision, Validation, Writing – review & editing, Investigation. LF-G: Investigation, Writing – review & editing, Visualization. OP: Writing – review & editing, Data curation, Validation. CO-C: Data curation, Validation, Writing – review & editing, Conceptualization, Visualization. FC: Visualization, Writing – review & editing, Resources. JO-I: Visualization, Writing – review & editing, Investigation, Supervision, Validation. MT: Investigation, Supervision, Validation, Visualization, Writing – review & editing, Funding acquisition, Methodology.

Funding

The author(s) declare that financial support was received for the research, authorship, and/or publication of this article. This study was funded by Instituto de Salud Carlos III (ISCIII), through projects

PI19/00878 and PI22/00323, and co-funded by the European Union and by the Study Group on Mechanisms of Action and Resistance to Antimicrobials, GEMARA (SEIMC). (SEIMC, http://www.seimc.org/). The study was also supported by CIBERINFEC (CIBER21/13/00095) and by a *personalized and precision medicine* grant from the Instituto de Salud Carlos III (MePRAM Project, PMP22/00092). MT was financially supported by the Miguel Servet Research Programme (SERGAS and ISCIII). OP, LF-G, and M. López were financially supported by grants IN606A-2020/035, IN606B-2021/013, and IN606C-2022/002, respectively (GAIN, Xunta de Galicia). IB was financially supported by the pFIS programme (ISCIII, FI20/00302).

Acknowledgments

The authors are grateful to the PIRASOA laboratory (Virgen Macarena Hospital, Seville), the reference laboratory for molecular typing of nosocomial pathogens and detection of mechanisms of resistance to antimicrobials of health interest in Andalusia, for providing the clinical isolates. The authors thank Alvaro Pascual (Virgen Macarena Hospital, Seville) and Luis Martínez-Martínez (Reina Sofia Hospital, Cordoba) for supervision of the research.

Conflict of interest

The authors declare that the research was conducted in the absence of any commercial or financial relationships that could be construed as a potential conflict of interest.

Publisher's note

Supplementary material

The Supplementary material for this article can be found online at: https://www.frontiersin.org/articles/10.3389/fmicb.2024.1416628/full#supplementary-material

References

Ambroa, A., Blasco, L., Lopez, M., Pacios, O., Bleriot, I., Fernandez-Garcia, L., et al. (2021). Genomic analysis of molecular bacterial mechanisms of resistance to phage infection. *Front. Microbiol.* 12:784949. doi: 10.3389/fmicb.2021.784949

Ambroa, A., Blasco, L., López-Causapé, C., Trastoy, R., Fernandez-García, L., Bleriot, I., et al. (2020). Temperate bacteriophages (prophages) in *Pseudomonas aeruginosa* isolates belonging to the international cystic fibrosis clone (CC274). *Front. Microbiol.* 11:556706. doi: 10.3389/fmicb.2020.556706

Andriianov, A., Trigüis, S., Drobiazko, A., Sierro, N., Ivanov, N. V., Selmer, M., et al. (2023). Phage T3 overcomes the BREX defense through SAM cleavage and inhibition of SAM synthesis by SAM lyase. *Cell Rep.* 42:112972. doi: 10.1016/j.celrep.2023.112972

Azam, A. H., and Tanji, Y. (2019). Bacteriophage-host arm race: an update on the mechanism of phage resistance in bacteria and revenge of the phage with the perspective for phage therapy. *Appl. Microbiol. Biotechnol.* 103, 2121–2131. doi: 10.1007/s00253-019-09629-x

Balestrino, D., Haagensen, J. A., Rich, C., and Forestier, C. (2005). Characterization of type 2 quorum sensing in Klebsiella pneumoniae and relationship with biofilm formation. *J. Bacteriol.* 187, 2870–2880. doi: 10.1128/JB.187.8.2870-2880.2005

Barrangou, R., Fremaux, C., Deveau, H., Richards, M., Boyaval, P., Moineau, S., et al. (2007). CRISPR provides acquired resistance against viruses in prokaryotes. *Science* 315, 1709–1712. doi: 10.1126/science.1138140

Behar, R. Z., Luo, W., Lin, S. C., Wang, Y., Valle, J., Pankow, J. F., et al. (2016). Distribution, quantification and toxicity of cinnamaldehyde in electronic cigarette refill fluids and aerosols. *Tob. Control.* 25:ii94-ii102. doi: 10.1136/tobaccocontrol-2016-053224

Birkholz, N., Jackson, S. A., Fagerlund, R. D., and Fineran, P. C. (2022). A mobile restriction-modification system provides phage defence and resolves an epigenetic conflict with an antagonistic endonuclease. *Nucleic Acids Res.* 50, 3348–3361. doi: 10.1093/nar/gkac147

Blasco, L., Ambroa, A., Lopez, M., Fernandez-Garcia, L., Bleriot, I., Trastoy, R., et al. (2019). Combined use of the Ab105-2φΔCI lytic mutant phage and different antibiotics in clinical isolates of multi-resistant. *Microorganisms* 7:556. doi: 10.3390/microorganisms7110556

Blasco, L., López-Hernández, I., Rodríguez-Fernández, M., Pérez-Florido, J., Casimiro-Soriguer, C. S., Djebara, S., et al. (2023). Case report: Analysis of phage therapy failure in a patient with a *Pseudomonas aeruginosa* prosthetic vascular graft infection. *Front. Med. (Lausanne)* 10:1199657. doi: 10.3389/fmed.2023.1199657

Bleriot, I., Blasco, L., Pacios, O., Fernández-García, L., López, M., Ortiz-Cartagena, C., et al. (2023). Proteomic study of the interactions between phages and the bacterial host. *Microbiol. Spectr.* 11:e0397422. doi: 10.1128/spectrum.03974-22

Bleriot, I., Pacios, O., Blasco, L., Fernandez-Garcia, L., Lopez, M., Ortiz-Cartagena, C., et al. (2024). Improving phage therapy by evasion of phage resistance mechanisms. *JAC Antimicrob. Resist.* 6:dlae017. doi: 10.1093/jacamr/dlae017

Brackman, G., Celen, S., Hillaert, U., Van Calenbergh, S., Cos, P., Maes, L., et al. (2011). Structure-activity relationship of cinnamaldehyde analogs as inhibitors of AI-2 based quorum sensing and their effect on virulence of *Vibrio* spp. *PLoS One* 6:e16084. doi: 10.1371/journal.pone.0016084

Brackman, G., Defoirdt, T., Miyamoto, C., Bossier, P., Van Calenbergh, S., Nelis, H., et al. (2008). Cinnamaldehyde and cinnamaldehyde derivatives reduce virulence in Vibrio spp. by decreasing the DNA-binding activity of the quorum sensing response regulator LuxR. *BMC Microbiol.* 8:149. doi: 10.1186/1471-2180-8-149

Brackman, G., Hillaert, U., Van Calenbergh, S., Nelis, H. J., and Coenye, T. (2009). Use of quorum sensing inhibitors to interfere with biofilm formation and development in Burkholderia multivorans and *Burkholderia cenocepacia*. *Res. Microbiol.* 160, 144–151. doi: 10.1016/j.resmic.2008.12.003

Broniewski, J. M., Chisnall, M. A. W., Høyland-Kroghsbo, N. M., Buckling, A., and Westra, E. R. (2021). The effect of quorum sensing inhibitors on the evolution of CRISPR-based phage immunity in *Pseudomonas aeruginosa*. *ISME J.* 15, 2465–2473. doi: 10.1038/s41396-021-00946-6

Capper-Parkin, K. L., Nichol, T., Smith, T. J., Lacey, M. M., and Forbes, S. (2023). Antimicrobial and cytotoxic synergism of biocides and quorum-sensing inhibitors against uropathogenic Escherichiacoli. *J Hosp Infect.* 134, 138–146. doi: 10.1016/j.jhin.2023.02.004

Cesta, N., Pini, M., Mulas, T., Materazzi, A., Ippolito, E., Wagemans, J., et al. (2023). Application of phage therapy in a case of a chronic hip-prosthetic joint infection due to. Open forum. *Infect. Dis.* 10:ofad051. doi: 10.1093/ofid/ofad051

Chan, B. K., Sistrom, M., Wertz, J. E., Kortright, K. E., Narayan, D., and Turner, P. E. (2016). Phage selection restores antibiotic sensitivity in MDR *Pseudomonas aeruginosa*. *Sci. Rep.* 6:26717. doi: 10.1038/srep26717

Da Silva, R. T., De Souza Grilo, M. M., Magnani, M., and De Souza Pedrosa, G. T. (2021). "Double-layer plaque assay technique for enumeration of virus surrogates" in Detection and enumeration of Bacteria, yeast, viruses, and protozoan in foods and freshwater. ed. M. Magnani (New York, NY: Springer US), 157–162.

Ding, Y., Zhang, D., Zhao, X., Tan, W., Zheng, X., Zhang, Q., et al. (2021). Autoinducer-2-mediated quorum-sensing system resists T4 phage infection in *Escherichia coli*. *J. Basic Microbiol.* 61, 1113–1123. doi: 10.1002/jobm.202100344

Doyle, A. A., and Stephens, J. C. (2019). A review of cinnamaldehyde and its derivatives as antibacterial agents. *Fitoterapia* 139:104405. doi: 10.1016/j.fitote.2019.104405

Flemming, H. C., Van Hullebusch, E. D., Neu, T. R., Nielsen, P. H., Seviour, T., Stoodley, P., et al. (2023). The biofilm matrix: multitasking in a shared space. *Nat. Rev. Microbiol.* 21, 70–86. doi: 10.1038/s41579-022-00791-0

Friedman, M. (2017). Chemistry, antimicrobial mechanisms, and antibiotic activities of Cinnamaldehyde against pathogenic Bacteria in animal feeds and human foods. *J. Agric. Food Chem.* 65, 10406–10423. doi: 10.1021/acs.jafc.7b04344

Galloway, W. R., Hodgkinson, J. T., Bowden, S. D., Welch, M., and Spring, D. R. (2011). Quorum sensing in gram-negative bacteria: small-molecule modulation of AHL and AI-2 quorum sensing pathways. *Chem. Rev.* 111, 28–67. doi: 10.1021/cr100109t

Gomes, A. I., Stuchi, L. P., Siqueira, N. M. G., Henrique, J. B., Vicentini, R., Ribeiro, M. L., et al. (2018). Selection and validation of reference genes for gene expression studies in *Klebsiella pneumoniae* using reverse transcription quantitative real-time PCR. *Sci. Rep.* 8:9001. doi: 10.1038/s41598-018-27420-2

Gordillo Altamirano, F. L., and Barr, J. J. (2019). Phage therapy in the postantibiotic era. *Clin. Microbiol. Rev.* 32:e00066-18. doi: 10.1128/CMR.00066-18

Gordillo Altamirano, F., Forsyth, J. H., Patwa, R., Kostoulias, X., Trim, M., Subedi, D., et al. (2021). Bacteriophage-resistant *Acinetobacter baumannii* are resensitized to antimicrobials. *Nat. Microbiol.* 6, 157–161. doi: 10.1038/s41564-020-00830-7

Hantke, K. (2020). Compilation of *Escherichia coli* K-12 outer membrane phage receptors - their function and some historical remarks. *FEMS Microbiol. Lett.* 367:fnaa013. doi: 10.1093/femsle/fnaa013

Hasan, M., and Ahn, J. (2022). Evolutionary dynamics between phages and Bacteria as a possible approach for designing effective phage therapies against antibiotic-resistant bacteria. *Antibiotics (Basel)* 11:915. doi: 10.3390/antibiotics11070915

Hayashi, K., Imanishi, N., Kashiwayama, Y., Kawano, A., Terasawa, K., Shimada, Y., et al. (2007). Inhibitory effect of cinnamaldehyde, derived from Cinnamomi cortex, on the growth of influenza A/PR/8 virus *in vitro* and *in vivo*. *Antivir. Res.* 74, 1–8. doi: 10.1016/j.antiviral.2007.01.003

Hoque, M. M., Naser, I. B., Bari, S. M., Zhu, J., Mekalanos, J. J., and Faruque, S. M. (2016). Quorum regulated resistance of *Vibrio cholerae* against environmental bacteriophages. *Sci. Rep.* 6:37956. doi: 10.1038/srep37956

Høyland-Kroghsbo, N. M., Maerkedahl, R. B., and Svenningsen, S. L. (2013). A quorum-sensing-induced bacteriophage defense mechanism. *MBio* 4, e00362–e00312. doi: 10.1128/mBio.00362-12

Høyland-Kroghsbo, N. M., Paczkowski, J., Mukherjee, S., Broniewski, J., Westra, E., Bondy-Denomy, J., et al. (2017). Quorum sensing controls the *Pseudomonas aeruginosa* CRISPR-Cas adaptive immune system. *Proc. Natl. Acad. Sci. USA* 114, 131–135. doi: 10.1073/pnas.1617415113

Jenson, J. M., Li, T., Du, F., Ea, C. K., and Chen, Z. J. (2023). Ubiquitin-like conjugation by bacterial cGAS enhances anti-phage defence. *Nature* 616, 326–331. doi: 10.1038/s41586-023-05862-7

Kortright, K. E., Chan, B. K., Koff, J. L., and Turner, P. E. (2019). Phage therapy: A renewed approach to combat antibiotic-resistant Bacteria. *Cell Host Microbe* 25, 219–232. doi: 10.1016/j.chom.2019.01.014

Labrie, S. J., Samson, J. E., and Moineau, S. (2010). Bacteriophage resistance mechanisms. *Nat. Rev. Microbiol.* 8, 317–327. doi: 10.1038/nrmicro2315

Lang, M., Krin, E., Korlowski, C., Sismeiro, O., Varet, H., Coppée, J. Y., et al. (2021). Sleeping ribosomes: bacterial signaling triggers RaiA mediated persistence to aminoglycosides. *iScience* 24:103128. doi: 10.1016/j.isci.2021.103128

Lazar, V., Holban, A. M., Curutiu, C., and Chifiriuc, M. C. (2021). Modulation of quorum sensing and biofilms in less investigated gram-negative ESKAPE pathogens. *Front. Microbiol.* 12:676510. doi: 10.3389/fmicb.2021.676510

Loenen, W. A., Dryden, D. T., Raleigh, E. A., and Wilson, G. G. (2014). Type I restriction enzymes and their relatives. *Nucleic Acids Res.* 42, 20–44. doi: 10.1093/nar/gkt847

Makarova, K. S., Haft, D. H., Barrangou, R., Brouns, S. J., Charpentier, E., Horvath, P., et al. (2011). Evolution and classification of the CRISPR-Cas systems. *Nat. Rev. Microbiol.* 9, 467–477. doi: 10.1038/nrmicro2577

Mancuso, G., Midiri, A., Gerace, E., and Biondo, C. (2021). Bacterial antibiotic resistance: the most critical pathogens. *Pathogens* 10:1310. doi: 10.3390/pathogens10101310

Marques, J. C., Lamosa, P., Russell, C., Ventura, R., Maycock, C., Semmelhack, M. F., et al. (2011). Processing the interspecies quorum-sensing signal autoinducer-2 (AI-2): characterization of phospho-(S)-4,5-dihydroxy-2,3-pentanedione isomerization by LsrG protein. *J. Biol. Chem.* 286, 18331–18343. doi: 10.1074/jbc.M111.230227

Mruk, I., and Kobayashi, I. (2014). To be or not to be: regulation of restriction-modification systems and other toxin-antitoxin systems. *Nucleic Acids Res.* 42, 70–86. doi: 10.1093/nar/gkt711

Nikolich, M. P., and Filippov, A. A. (2020). Bacteriophage therapy: developments and directions. *Antibiotics (Basel)* 9:135. doi: 10.3390/antibiotics9030135

Olszak, T., Latka, A., Roszniowski, B., Valvano, M. A., and Drulis-Kawa, Z. (2017). Phage life cycles behind bacterial biodiversity. *Curr. Med. Chem.* 24, 3987–4001. doi: 10.2174/0929867324666170413100136

Pacheco, T., Gomes, A. I., Siqueira, N. M. G., Assoni, L., Darrieux, M., Venter, H., et al. (2021). SdiA, a quorum-sensing regulator, suppresses fimbriae expression, biofilm formation, and quorum-sensing signaling molecules production in *Klebsiella pneumoniae*. *Front. Microbiol.* 12:597735. doi: 10.3389/fmicb.2021.597735

Pacios, O., Fernández-García, L., Bleriot, I., Blasco, L., González-Bardanca, M., López, M., et al. (2021). Enhanced antibacterial activity of repurposed Mitomycin C and imipenem in combination with the lytic phage vB_KpnM-VAC13 against clinical isolates of *Klebsiella pneumoniae*. *Antimicrob. Agents Chemother.* 65:e0090021. doi: 10.1128/AAC.00900-21

Patterson, A. G., Jackson, S. A., Taylor, C., Evans, G. B., Salmond, G. P. C., Przybilski, R., et al. (2016). Quorum sensing controls adaptive immunity through the regulation of multiple CRISPR-Cas systems. *Mol. Cell* 64, 1102–1108. doi: 10.1016/j.molcel.2016.11.012

Rémy, B., Mion, S., Plener, L., Elias, M., Chabrière, E., and Daudé, D. (2018). Interference in bacterial quorum sensing: A biopharmaceutical perspective. *Front. Pharmacol.* 9:203. doi: 10.3389/fphar.2018.00203

Rousset, F., Yirmiya, E., Nesher, S., Brandis, A., Mehlman, T., Itkin, M., et al. (2023). A conserved family of immune effectors cleaves cellular ATP upon viral infection. *Cell* 186, 3619–3631.e13. doi: 10.1016/j.cell.2023.07.020

Rusinov, I. S., Ershova, A. S., Karyagina, A. S., Spirin, S. A., and Alexeevski, A. V. (2018). Avoidance of recognition sites of restriction-modification systems is a widespread but not universal anti-restriction strategy of prokaryotic viruses. *BMC Genomics* 19:885. doi: 10.1186/s12864-018-5324-3

Salmond, G. P., and Fineran, P. C. (2015). A century of the phage: past, present and future. *Nat. Rev. Microbiol.* 13, 777–786. doi: 10.1038/nrmicro3564

Severin, G. B., Ramliden, M. S., Ford, K. C., Van Alst, A. J., Sanath-Kumar, R., Decker, K. A., et al. (2023). Activation of a *Vibrio cholerae* CBASS anti-phage system by quorum sensing and folate depletion. *MBio* 14:e0087523. doi: 10.1128/mbio.00875-23

Shah, M., Taylor, V. L., Bona, D., Tsao, Y., Stanley, S. Y., Pimentel-Elardo, S. M., et al. (2021). A phage-encoded anti-activator inhibits quorum sensing in *Pseudomonas aeruginosa*. *Mol. Cell* 81, 571–583.e6. doi: 10.1016/j.molcel.2020.12.011

Shreaz, S., Wani, W. A., Behbehani, J. M., Raja, V., Irshad, M., Karched, M., et al. (2016). Cinnamaldehyde and its derivatives, a novel class of antifungal agents. *Fitoterapia* 112, 116–131. doi: 10.1016/j.fitote.2016.05.016

Sikdar, R., and Elias, M. (2020). Quorum quenching enzymes and their effects on virulence, biofilm, and microbiomes: a review of recent advances. *Expert Rev. Anti-Infect. Ther.* 18, 1221–1233. doi: 10.1080/14787210.2020.1794815

Tetard, A., Zedet, A., Girard, C., Plésiat, P., and Llanes, C. (2019). Cinnamaldehyde induces expression of efflux pumps and multidrug resistance in *Pseudomonas aeruginosa*. *Antimicrob. Agents Chemother.* 63:e01081-19. doi: 10.1128/AAC.01081-19

Wang, G., Zhao, G., Chao, X., Xie, L., and Wang, H. (2020). The characteristic of virulence, biofilm and antibiotic resistance of *Klebsiella pneumoniae*. *Int. J. Environ. Res. Public Health* 17:17. doi: 10.3390/ijerph17176278

Wenzel, S., Hess, R., Kiefer, D., and Kuhn, A. (2024). Involvement of the cell division protein DamX in the infection process of bacteriophage T4. *Viruses* 16:487. doi: 10.3390/v16040487

Wikler, M. A.Clinical (2006). Methods for dilution antimicrobial susceptibility tests for bacteria that grow aerobically: Approved standard.

Xavier, K. B., and Bassler, B. L. (2003). LuxS quorum sensing: more than just a numbers game. *Curr. Opin. Microbiol.* 6, 191–197. doi: 10.1016/S1369-5274(03)00028-6

Young, R., and Gill, J. J. (2015). Phage therapy redux—what is to be done? *Science* 350, 1163–1164. doi: 10.1126/science.aad6791

Zhang, L., Li, S., Liu, X., Wang, Z., Jiang, M., Wang, R., et al. (2020). Sensing of autoinducer-2 by functionally distinct receptors in prokaryotes. *Nat. Commun.* 11:5371. doi: 10.1038/s41467-020-19243-5

Zhu, R., Liu, H., Liu, C., Wang, L., Ma, R., Chen, B., et al. (2017). Cinnamaldehyde in diabetes: A review of pharmacology, pharmacokinetics and safety. *Pharmacol. Res.* 122, 78–89. doi: 10.1016/j.phrs.2017.05.019

frontiers | Frontiers in Microbiology

TYPE Original Research
PUBLISHED 28 June 2024
DOI 10.3389/fmicb.2024.1416971

OPEN ACCESS

EDITED BY
Barbara Maciejewska,
University of Wrocław, Poland

REVIEWED BY
Joanna Marta Majewska,
University of Wrocław, Poland
Laura Fernandez-Garcia,
Institute of Biomedical Research of A Coruña (INIBIC), Spain
Nallelyt Segundo-Arizmendi,
Facultad de Farmacia de la Universidad Autónoma del Estado de Morelos, Mexico

*CORRESPONDENCE
Ameneh Elikaei
✉ a.elikaei@alzahra.ac.ir
Morvarid Shafiei
✉ drshafiei80@gmail.com

RECEIVED 13 April 2024
ACCEPTED 13 June 2024
PUBLISHED 28 June 2024

CITATION
Khazani Asforooshani M, Elikaei A, Abed S, Shafiei M, Barzi SM, Solgi H, Badmasti F and Sohrabi A (2024) A novel *Enterococcus faecium* phage EF-M80: unveiling the effects of hydrogel-encapsulated phage on wound infection healing.
Front. Microbiol. 15:1416971.
doi: 10.3389/fmicb.2024.1416971

A novel *Enterococcus faecium* phage EF-M80: unveiling the effects of hydrogel-encapsulated phage on wound infection healing

Mahshid Khazani Asforooshani[1,2], Ameneh Elikaei[1]*, Sahar Abed[3], Morvarid Shafiei[2]*, Seyed Mahmoud Barzi[2], Hamid Solgi[4], Farzad Badmasti[2] and Aria Sohrabi[5]

[1]Department of Microbiology, Faculty of Biological Sciences, Alzahra University, Tehran, Iran, [2]Department of Bacteriology, Pasteur Institute of Iran, Tehran, Iran, [3]Department of Microbial Biotechnology, Faculty of Basic Sciences and Advanced Technologies in Biology, University of Science and Culture, Tehran, Iran, [4]Isfahan Endocrine and Metabolism Research Center, Isfahan University of Medical Sciences, Isfahan, Iran, [5]Department of Epidemiology and Biostatistics, Research Center for Emerging and Reemerging Infectious Diseases, Pasteur Institute of Iran, Tehran, Iran

Background: *Enterococcus faecium* is one of the members of ESKAPE pathogens. Due to its resistance to antimicrobial agents, treating this bacterium has become challenging. The development of innovative approaches to combat antibiotic resistance is necessary. Phage therapy has emerged as a promising method for curing antibiotic-resistant bacteria.

Methods: In this study, *E. faecium* phages were isolated from wastewater. Phage properties were characterized through *in vitro* assays (*e.g.* morphological studies, and physicochemical properties). In addition, whole genome sequencing was performed. A hydrogel-based encapsulated phage was obtained and its structure characteristics were evaluated. Wound healing activity of the hydrogel-based phage was assessed in a wound mice model.

Results: The purified phage showed remarkable properties including broad host range, tolerance to high temperature and pH and biofilm degradation feature as a stable and reliable therapeutic agent. Whole genome sequencing revealed that the genome of the EF-M80 phage had a length of 40,434 bp and harbored 65 open reading frames (ORFs) with a GC content of 34.9% (GenBank accession number is OR767211). Hydrogel-based encapsulated phage represented an optimized structure. Phage-loaded hydrogel-treated mice showed that the counting of neutrophils, fibroblasts, blood vessels, hair follicles and percentage of collagen growth were in favor of the wound healing process in the mice model.

Conclusion: These findings collectively suggest the promising capability of this phage-based therapeutic strategy for the treatment of infections associated with the antibiotic-resistant *E. faecium*. In the near future, we hope to expect the presence of bacteriophages in the list of antibacterial compounds used in the clinical settings.

KEYWORDS

Bacteriophage, *Enterococcus faecium*, genome analysis, Hydrogel, wound infection

1 Introduction

Enterococcus faecium as a Gram-positive bacterium exhibits a remarkable tolerance to hostile conditions. It has a highly adaptable metabolism that allows it to grow in a variety of environments. *E. faecium* along with *Enterococcus faecalis* are common bacteria in the gastrointestinal tract (Pradal et al., 2023). However, *E. faecium* has acquired several capabilities that contribute to its success within hospital settings. These include an increasing resistance to antimicrobial agents that were previously considered first-line antibiotics (e.g., ampicillin, vancomycin and aminoglycosides) for the treatment of enterococcal infections, (Yim et al., 2017). In addition, *E. faecium* has acquired virulence genes that promote the formation of biofilm apparatus and improve its ability to colonize (Zhou et al., 2020). Biofilms are frequently encountered in the context of wound infections, and numerous studies have identified *Enterococcus* spp. as one of the most prevalent bacteria found in chronic wound infections. *Enterococcus* spp. has been consistently isolated from diabetic foot ulcers, venous leg ulcers, and burn wounds (Melo et al., 2019). The antibiotic susceptibility of entrapped bacteria in biofilms is significantly reduced due to metabolic and structural changes, leading to a 1000-fold reduction in antibiotic permeability. This situation exacerbates the eradication of infections associated with biofilm. High doses of antibiotics are leading to the development of antimicrobial resistance among bacteria, presenting a significant challenge to healthcare providers (Lebeaux et al., 2014; Vestby et al., 2020).

Recently, bacteriophages have become interesting alternatives for targeting superbugs and biofilm removal (Lin et al., 2017). Bacteriophages, also known as phages, are natural predators of bacteria that specifically replicate within bacteria. Notably, the potential of bacteriophages as therapeutic agents against bacterial infections, known as phage therapy, has sparked significant interest (Węgrzyn, 2022). Meanwhile, *Enterococcus* phages have attracted the attention of the biomedical research community as promising candidates for the development of therapeutics against drug-resistant enterococci (Canfield and Duerkop, 2020).

While the isolation of an lytic *Enterococcus* phage offers a promising initial step, translating this potential into a viable therapeutic requires *in vivo* evaluation in an animal model, where the complex interplay between the phage, host, and immune system can be accurately investigated (El Haddad et al., 2022). For proper release of the phage in wound site and to improve the healing process, design of a hydrogel based on sodium alginate (SA) and hyaluronic acid (HA) would be a promising route. Hydrogels are three-dimensional networks of hydrophilic polymers. They have substantial water absorption capability while retaining their structure. These compounds are being intensively investigated as wound dressings and drug depots for the sustained release of therapeutic agents (Yan et al., 2021). These properties make hydrogels interesting candidates for the delivery of bacteriophages in wound healing process, owing to their moisture retention, high adsorption capacity, biocompatibility, and ability to control the release of phages (Chang et al., 2021). In addition, the hydrophilicity of hydrogels minimizes cell adhesion and painless removal, offering advantages over conventional dressings (Shafigh Kheljan et al., 2023).

A study by Bean et al. observed a distinct zone of inhibition against *Staphylococcus aureus* using Phage K encapsulated within a hyaluronic acid methacrylate (HAMA)/agarose hydrogel system (Bean et al., 2014). Furthermore, Kaur et al. reported a significant reduction in bacterial biomass following treatment with a polyvinyl alcohol-sodium alginate (PVA-SA) hydrogel membrane encapsulated with a phage cocktail (MR10, Kpn5, and PA5). This treatment significantly reduced the amount of *S. aureus* bacteria by 6-log, *Klebsiella pneumoniae* by 6.37-log and *Pseudomonas aeruginosa* by 4.6-log after only 6 hours *in vitro* evaluation (Kaur et al., 2019). Treatment with an MR10-loaded hydrogel in a murine model of *S. aureus* burn injury led to both accelerated wound closure and a significant decrease in mortality rates. Additionally, Kumari et al. reported that the administration of phage Kpn5 encapsulated within an hydroxypropyl methylcellulose (HPMC) hydrogel significantly improved the percentage of survived animals which infected with *K. pneumoniae* compared to treatment with traditional antimicrobials like gentamicin (Kumari et al., 2011).

The aim of this study was the isolation and characterization of a lytic bacteriophage against clinical isolates of *E. faecium*. In addition, the morphological examination, determination of host range, ability to remove biofilms and other biological properties of the phage were evaluated. Finally, the therapeutic capability of the phage encapsulated in hydrogel on an *E. faecium* biofilm-induced wound infection model in mice was explored.

2 Methods and materials

2.1 Isolation of *Enterococcus faecium* strains

In this study, 50 clinical strains of *E. faecium* and the standard strain (*E. faecium* ATCC 1959) were considered. All clinical strains were isolated from patients in Imam Khomeini hospital in 2022 (Tehran, Iran) following standard protocols for bacterial culture and identification. Identification of *E. faecium* was confirmed by a combination of conventional biochemical tests and polymerase chain reaction (PCR) assay. The specific primers for *sodA* gene were previously reported as forward primer sequence (5′-GAAAAAACAATAGAAGAATTAT-3′) and the reverse primer sequence (5′-TGCTTTTTTGAATTCTTCTTTA-3′) (Alduhaidhawi et al., 2022). It should be noted that *E. faecium* strain used in all subsequent experiments was a clinical strain that originated from a lesion sample.

2.2 Antimicrobial susceptibility testing

The susceptibility of all isolates to various antibiotic classes was determined using two methods. The disk diffusion method, following the guidelines of the Clinical and Laboratory Standards Institute (Clinical and Laboratory Standards Institute [CLSI], 2023) was employed on Mueller-Hinton agar (Merck, Germany). A panel of ten antibiotics representing nine antibiotic classes was used: ampicillin-sulbactam (10/10 μg), streptomycin (300 μg), gentamicin (30 μg), chloramphenicol (30 μg), ciprofloxacin (5 μg), erythromycin (15 μg), linezolid (30 μg), rifampin (5 μg), teicoplanin (30 μg), and tetracycline (30 μg) (MAST Co., UK).

For vancomycin (Sigma-Aldrich, USA), the minimum inhibitory concentration (MIC) was determined using the broth

microdilution method in sterile 96-well microtiter plates according to CLSI guidelines. Stock solutions of antibiotics were prepared in Mueller Hinton Broth and serially two-fold diluted from 256 to 0.5 μg/mL. Bacterial suspensions without antibiotics served as positive controls, while sterile medium represented negative controls. Each well was inoculated with a standardized inoculum of 1.5×10^8 CFU/mL of the bacterial suspension. Following both disk diffusion and MIC procedures, plates were incubated at 37°C for 18–24 h. Interpretation of results for both methods followed based on established CLSI breakpoints.

2.3 Bacteriophage isolation and particle enrichment

Phage was collected and isolated from wastewater from Imam Khomeini hospital before chemical treatment. To remove bacterial cells and contaminants, the sample was centrifuged (8,000 rpm for 20 minutes) and filtered through a 0.22 μm membrane. To enrich the phage population, an equal volume of fresh Brain Heart Infusion (BHI) broth was added to the filtered effluent. This mixture was then inoculated with the fresh culture of *E. faecium* and incubated for 24 h at 37°C with shaking (150 rpm). After incubation, the new culture was centrifuged and filtered to separate the bacterial cells from the free phage particles. The double layer plaque assay (DLA), as described by Gong et al. (2016), was then used to concentrate and further purify the phage.

The enriched phage broth was serially diluted and the 0.1 ml aliquots from each dilution were co-incubated with 0.1 mL of *E. faecium* at 37°C for 10 min in a static incubator. This mixture was added to 5 ml of softened agar (0.4% agar) and then plated onto a solidified agar plate. After overnight incubation, clear zones (plaques) formed on the bacterial lawn, indicating areas where the phage lysed the bacteria. A single isolated plaque was picked and transferred to a sodium-magnesium buffer (100 mM NaCl, 8 mM MgSO4, 50 mM Tris-Cl) to be purified by two more rounds of plaque isolation.

2.4 Transmission electron microscopy

Transmission electron microscopy (TEM) was used to visualize the morphology of purified phage particles, following the method described by Lee et al. (2019). Briefly, 5 μl of the purified phage was fixed with 1% glutaraldehyde and placed on a Copper Mesh 400 grid coated with Formvar charcoal for a duration of 3–5 min. Subsequently, the sample was negatively stained with 2% PTA (phosphotungstic acid). The grid was then allowed to air-dry and subsequently analyzed using a Zeiss EM900 TEM apparatus (Carl Zeiss LEO EM 906 E, Germany) at a voltage of 50 kV.

2.5 Phage characteristics

2.5.1 Host range determination

The host specificity of the isolated bacteriophage was assessed against 50 clinical *E. faecium* isolates. Bacterial susceptibility was evaluated using the spot test method. In brief, 10 μl of the purified phage suspension (7×10^{14} PFU/ml) was placed on a freshly cultured lawn of each bacterial strain and then incubated at 37°C for 24 hours in a static incubator. The procedure was replicated three times. The formation of plaques indicated susceptibility to the phage. In addition, the activity of the bacteriophage against other clinically relevant bacterial species, including *Enterococcus faecalis*, *Escherichia coli*, *Staphylococcus aureus*, *Streptococcus pneumoniae*, *Klebsiella pneumoniae* and *Pseudomonas aeruginosa*, was investigated to further determine the host range (Daubie et al., 2022).

2.5.2 Environmental stability assay

To assess the sensitivity of phage to temperature ranges, 0.1 ml of selected phages with a titer of 7×10^{16} PFU/ml was inoculated into 0.9 ml of BHI broth. The suspensions were incubated for one hour at the following temperatures: −20°C, 4°C, 20°C, 37°C, 60°C, 70°C and 80°C in a static incubator. After incubation, the titer of the target phage was determined using the double-layer agar method (Litt and Jaroni, 2017).

The sensitivity of the phage to pH was investigated by preparing BHI broth media adjusted to the following pH values: 2, 4, 7, 10 and 14. Then 0.1 mL from the selected phage with titer of 7×10^{16} PFU/ml was added to 0.9 mL of the pH-adjusted culture medium in each medium. The suspensions were incubated at 37°C for one hour in a static incubator. The quantification of the phage titer was subsequently assessed through the utilization of the double-layer agar technique (Khawaja et al., 2016).

To investigate the stability of the phage particles in different NaCl concentrations, 0.1 mL of the phage (7×10^{16} PFU/ml) was added to 0.9 mL of BHI broth with different NaCl concentrations (5%, 10%, 15%). The suspensions were subjected to incubation at 37°C for an hour in a static incubator. The titer of the target phage was then determined using the double-layer agar method. Experiments were repeated three times for each condition.

2.5.3 Determination of optimal multiplicity of infection (MOI)

Multiplicity of infection is the ratio of infecting or adsorbing phages to bacteria during infection (Abedon, 2016). For assessing the optimal MOI, the *E. faecium* strain was first grown in BHI broth at 37°C until early logarithmic growth phase ($OD_{625nm} = 0.4$). To achieve MOIs of 10, 1 and 0.1, different phage titers were prepared (10^9 PFU/ml, 10^8 PFU/ml, 10^7 PFU/ml, respectively). Mixtures containing a bacterial growth of 1.5×10^8 CFU/ml and various MOIs of phage were incubated with shaking (150 rpm) at 37°C for 4 h. The OD_{625nm} values were measured at 30-minute intervals and the experiment was done in triplicate. The MOI that resulted in the highest reduction in bacterial density was considered the optimal MOI (Ji et al., 2020).

2.5.4 One-step growth culture and phage adsorption assay

To depict a one-step growth curve, EF-M80 phage (10^9 PFU/ml) was mixed with host bacteria (1.5×10^8 CFU/ml). This mixture was then incubated for 15 minutes at 37°C in a static incubator, followed by centrifugation at 10,000 rpm for 1 min. The supernatant was removed, and the remaining pellet containing phage-infected bacterial cells was re-suspended with 5 ml of fresh

BHI broth. This suspension was then incubated with shaking at 150 rpm at 37°C. Aliquots were collected at 10-minute intervals, and their phage titers were immediately determined using the double-layer agar method. The experiment was repeated three times. The average burst size, quantified as the ratio of the phages formed during the rise period to the initial count of infected bacterial cells, was also determined (Wang et al., 2016). The rate of phage adsorption was detected using the double layer agar method. Host strain culture was exposed to bacteriophage at the titer of 7×10^{16} PFU/ml and incubated at 37°C. At predetermined time intervals (0, 5 and 10 min), 100 µl subsamples were collected from the suspension. These aliquots were then centrifuged to pellet bacterial cells. The resulting supernatants were assayed for unabsorbed bacteriophages at each time point. The procedure repeated for three times based on the protocol (Zhou W. et al., 2018) The phage adsorption rate determined as the ratio of the difference between the initial phage titer (P0) and the titer of unabsorbed phage at a given time point (Pt), to the initial phage titer (P0) (Pan et al., 2022).

2.6 Effect of bacteriophage on biofilm degradation

The biofilm plate assay, previously described, was utilized to assess the disruption of biofilm (Yazdi et al., 2018). In this assay, an overnight culture of *E. faecium* was diluted in BHI broth and transferred into 96-well flat-bottomed polystyrene tissue culture microtiter plates. Following incubation at 37°C for 24 h, the wells were discharged and washed with phosphate-buffered saline (PBS, pH = 7). Subsequently, the wells were treated with different dilutions of the phage particles from 10^1 to 10^{10}-fold and sterile physiological saline serving as the negative control. After 24 h of exposure at 37°C, the wells underwent washing with PBS followed by staining of the attached biofilm layer using Triphenyl Tetrazolium Chloride (TTC). The absorbance (at OD_{480nm}) of each well was then measured. The lower OD showed more degradation of biofilm layers using phage intervention in a specific phage dilution. This method was applied for evaluation of the phage effect on 3-day and 5-day old of *E. faecium* biofilms and each experiment repeated for three times. Based on the data, the optimum phage dilutions were detected.

2.7 Phage genome sequencing and *de novo* assembly

DNA extraction was performed using a Viral Nucleic Acid Extraction Kit (FavorPrep^{TM}, Favorgen). Genome libraries were prepared and sequenced using the Illumina HiSeq 2000 platform (Illumina, Inc., San Diego, CA, USA). Paired-end sequence reads of 150 bp length were generated on an Illumina NextSeq (Micromon, Clayton, Australia) apparatus. The quality of the FASTQ paired-end files was checked using FastQC software (Brown et al., 2017). The trimming and filtering of the Fastq files was performed with the AfterQC (Chen et al., 2017). *De novo* assembly of short-read sequences was performed with QIAGEN CLC Genomics Workbench version 20. The quality of the assembly was assessed using the QUAST tool (Gurevich et al., 2013) and misassembles were corrected by the Mauve software (Darling et al., 2004). The *Enterococcus* phage genome sequence was annotated using the Prokka (rapid prokaryotic genome annotation) v1.14.5 (Seemann, 2014). Finally, the phage genome was submitted in the GenBank database via the BankIt submission route.

2.8 Comparative genome analysis

A dataset of related *Enterococcus* phages strain EF-M80, including 55 genomes (cut-off was coverage $\geq$ 70, and identity $\geq$ 70), was collected from GenBank and compared in the DNA and protein layers with the isolated *Enterococcus* phages. We conducted a distribution analysis of the accessory genomic elements using the ClustAGE (Ozer, 2018). The presence/absence matrix of DNA fragments is then converted into a dendrogram based on the unweighted pair-group method with arithmetic mean (UPGMA) using the Anvi'o tool (Eren et al., 2015). The dendrogram was visualized using the Interactive Tree Of Life (iTOL) platform and categorized based on the 50% threshold line (Letunic and Bork, 2021). In addition, the pan/core proteome analysis and the matrix of the present/absent genes were determined through the Roary (Rapid large-scale prokaryote pan-genome analysis) version 3.11.2 (Page et al., 2015). The inputs were annotated assemblies in GFF format generated by the Prokka version 1.14.5. The pan/core plot and dendrogram were depicted using the Python-based roary_plots.py tool.

2.9 Hydrogel preparation

Sodium alginate (SA) served as the primary natural polymer in this process. To fabricate the hydrogel, 4 g of SA was gradually dissolved in 100 ml of preheated (40°C) distilled water under continuous stirring to ensure a homogenous solution. The amount of 0.2 *g* of Carboxymethylcellulose (CMC) was dissolved by slow addition to 10 ml of distilled water with continues stirring to prevent aggregation. Hyaluronic acid (HA) was independently dissolved in deionized water at room temperature. Subsequently, all three solutions were combined, and the final mixture was autoclaved. Following sterilization and cooling, the solution was used to create hydrogel. The phage suspension was then thoroughly mixed with the hydrogel solution for 10 minutes to ensure homogenous phage distribution. To induce gelation, sterile 1% CaCl2 solution was subsequently incorporated into the mixture using a syringe. For film formation, the final solution containing phage and CaCl2 was immediately cast onto a plate and maintained at 20°C for 18-24 h. The solidified hydrogel film was then further cross-linked by adding 8 ml of 10% $CaCl_2$ solution onto its surface. After one hour, excess liquid was discarded (Shafigh Kheljan et al., 2023).

2.10 Characterization of the hydrogel

2.10.1 Determination of the swelling index

The hydrogel film was divided into 2 × 2 cm segments and allowed to dry at ambient temperature. Subsequent to determining

the weight of the dried hydrogel (W_0), it was exposed in distilled water and subsequently extracted at hourly intervals, as well as after a duration of 24 h. The excess water was eliminated by employing tissue paper, and the hydrogel was weighed (W_S). The swelling index was determined using the designated formula (Gupta and Shivakumar, 2012)

$$\text{Swelling index}(\%) = [(W_S - W_0)/W_0] \times 100$$

2.10.2 Phage release

A hydrogel piece (2 × 2 cm) loaded with phage particles was aseptically transferred into a sterile culture tube containing BHI broth medium. The medium was supplemented with 1.5×10^8 CFU/ml of *E. faecium* bacteria. The tube was then incubated at 37°C in a shaking incubator for 24 h. To determine phage release, the optical density (OD_{625nm}) of the culture supernatant was measured. A control tube containing only BHI broth and bacteria, without the hydrogel, was processed identically for background subtraction.

2.10.3 *In vitro* antibacterial activity assay

The antimicrobial activity of the hydrogels was assessed qualitatively via the disc diffusion method (Kaur et al., 2019). An overnight culture of bacteria, standardized to a 0.5 McFarland turbidity, was spread uniformly onto BHI agar plates using a sterile swab. Subsequently, disks were punched from both phage-loaded and phage-free hydrogels (negative control). These disks were then placed onto the solidified bacterial lawn and incubated at 37°C for 24 h. A clear inhibition zone surrounding each disk was evaluated after overnight incubation.

2.10.4 Scanning electron microscopy (SEM) of hydrogels

Control and phage-loaded hydrogel films were characterized using scanning electron microscopy (SEM) to determine pore size and particle distribution and overall structure. Following complete dehydration, the hydrogels were sputter-coated with a thin layer of gold to enhance conductivity before SEM analysis (Martinez-Garcia et al., 2022).

2.10.5 Fourier transform infrared spectroscopy (FTIR)

Fourier-transform infrared (FTIR) spectroscopy was employed to characterize the functional groups and bonding environment within the hydrogel samples. KBr pellet formation was utilized to prepare the samples for analysis. The infrared spectra were recorded in the range of 4,000–400 cm^{-1} using a spectrometer (Perkin–Elmer FTIR model 2000). The acquired spectra were then analyzed to identify characteristic absorption bands corresponding to the vibrational modes of functional groups present in the hydrogel (Mansur et al., 2008).

2.11 *In vivo* studies

In vivo experiments were conducted to examine the therapeutic efficacy of bacteriophage to evaluate the functionality of the designed hydrogel as a substitution for delivering the phage to the site of the wound infection. The study was authorized by the Ethics Committee of Al-Zahra University (Ir.ALZAHRA.REC.1401.015). Female BALB/c mice were obtained and given a week to acclimate to their new environment before commencing the experiments. To induce anesthesia, each mouse was injected intraperitoneal with 200 μl of ketamine/xylazine (in a 4:1 ratio). A bilateral full-thickness wound was created in the back skin of the mice using a 5 mm biopsy punch. The wound site was prepared by shaving the surrounding hair. Worth mentioning that the wound was created to a depth below the epidermis and superficial dermis, while avoiding damage to the muscles and minimizing bleeding with peak skin density. All wounds (except for the negative control group, which was treated with sterile distilled water) were infected with 50 μl of a 1.5×10^8 CFU/ml suspension of *E. faecium* bacteria, and after 24 h, they were treated with the desired bacteriophage at optimal MOI of 0.1 (which in this case corresponds to 10^7 PFU/ml) except for the positive control group. Following the experiments, each group of mice was placed in individual cages with sufficient availability to food and water. The mice were maintained in a 12-h light/dark cycle. All animals involved in this experiment received appropriate and compassionate care (Kaur et al., 2019). The wound healing process was monitored for over a period of 14 days. The mice were categorized into six groups, each consisting of five mice. All groups were as follows:

Healthy Control (HC): Unwounded, untreated mice.

Negative Control (NC): Wounded mice treated using sterile distilled water.

Positive Control (B): Wounded, *E. faecium*-infected, untreated mice.

Phage-Treated Group (Ph): Wounded, *E. faecium*-infected, phage-treated mice.

Phage Hydrogel Group (Ph-hyd): Wounded, *E. faecium*-infected, phage-loaded hydrogel-treated mice.

Hydrogel Control Group (Hyd): Wounded, *E. faecium*-infected, phage-free hydrogel-treated mice.

2.12 Histopathology studies

Following a 14-day observation period, the healed skin areas of the mice were excised and preserved in 10% formalin solution for subsequent pathological analysis. Hematoxylin and eosin (H&E) staining was performed to assess wound healing progression. The cell quantifying was done for neutrophils, fibroblasts, blood vessels, and hair follicles using the counting chamber. In addition, the percentage of collagen deposition and epidermal thickness were measured. To evaluate the wound-healing trajectory, standardized photographs were captured on days 3, 7, 10, and 14. Notably, this experiment was conducted concurrently with a separate comparative study that included healthy and uninfected wounded mice as the negative controls (Mansouri et al., 2022).

2.13 Statistical analysis

The data were tested for normal distribution using the Shapiro–Wilk test for small sample size. Groups were compared using a one-way analysis of variance (ANOVA) or multiple *t*-tests.

P-values from statistical analyses were obtained, and $P < 0.05$ was considered statistically significant. GraphPad Prism software version 10 was employed for analyzing the data.

3 Results

3.1 Bacterial strains

A total of 50 *E. faecium* strains were isolated from hospital patients and identified to the species level by biochemical tests and confirmed through PCR assay. The percentage of antibiotic resistance of the isolates was as follows: ampicillin-sulbactam (92%), streptomycin (100%), gentamicin (92%), vancomycin (100%), chloramphenicol (16%), ciprofloxacin (100%), erythromycin (100%), linezolid (6%), rifampin (100%), teicoplanin (70%), and tetracycline (72%). Antibiogram profile of bacterial isolates is available in the (Supplementary Table 1). The *E. faecium* strain serving as the host for EF-M80 phage isolation and propagation was designated EF.11 within our collection. Notably, EF.11 originated from a clinical lesion sample and displayed the highest level of sensitivity towards EF-M80, as evidenced by the formation of numerous clear plaques. Due to these observations, EF.11 was employed for subsequent experiments, including those investigating biofilm formation and *in vivo* efficacy.

3.2 Phage isolation and morphology

The results of the DLA assay demonstrated that the purified phage, which has been named *Enterococcus* phage EF-M80, is effective against *E. faecium* (Figure 1A). Plaques were observed at a dilution of 10^{14}-fold, indicating a high concentration of isolated phage in the initial stock. An estimated 7×10^{16} PFU/ml were present based on the average of 70 plaques observed at this dilution. The morphological characteristics of EF-M80 were represented through TEM, which revealed an icosahedral head and tail with approximate 35 nm in diameter and the length of 53 nm, respectively (Figure 1B). These findings, along with genomic analysis, suggest that EF-M80 belongs to the *Efquatrovirus* genus within the class of *Caudoviricetes*, as determined by the ICTV guidelines (Fauquet, 2005).

3.3 Phage characteristics

3.3.1 Host range of the phage

Host range analysis was performed using a spot test to determine the phage's lytic activity against a panel of thirty *E. faecium* clinical isolates. Sixty percent of the strains exhibited susceptibility, suggesting a broad host range within *E. faecium*. The phage demonstrated no lytic activity against other bacterial species such as *E. faecalis*, *E. coli*, *S. aureus*, *S. pneumoniae*, *K. pneumoniae* and *P. aeruginosa*.

3.3.2 Phage stability tests

The effects of environmental conditions on the stability of phage were investigated, including temperature, pH and salt concentration. The optimal temperature for phage stability was found to be 37°C, with the detectable stability between 4°C and 50°C (Figure 2A). Phage exhibited a broad pH tolerance and remained active from pH = 4 to 10 range (Figure 2B). However, stability decreased at both extremes of the pH range, reaching zero at pH = 2 and 14. The phage was demonstrated to remain stable over a range of NaCl concentrations of 5%, 10% and 15%, as illustrated in Figure 2C.

3.3.3 MOI determination of the phage

A sufficient MOI is necessary to ensure efficient bacterial lysis, ultimately impacting the therapeutic efficacy of phages. As depicted in Figure 2D, all three MOIs showed a significant impact on the host cell population contrasted with the control group. Interestingly, the most reduction in bacterial growth was observed at MOI = 0.1, yet the differences among tested MOIs were not statistically significant. This finding suggests that multiple rounds of infection may be necessary to infect all of the bacterial cells in the culture.

3.3.4 One-step growth and phage adsorption rate

The one-step growth curve analysis revealed a latent period of approximately 20 min and a total phage multiplication cycle of 60 min for this bacteriophage. In addition, the burst size was determined to be 12.6 PFU/infected cell (Figure 2E). Notably, the phage adsorption rate curve indicated that nearly 40% of the phages were adsorbed by the bacterial population within the initial ten minutes (Figure 2F). Understanding these key parameters is crucial for optimizing phage fitness, achieving a balance in early infection dynamics, and ultimately, for the successful implementation of phage therapy.

3.4 Biofilm degradation properties of the phage

Our findings demonstrate that phage treatment resulted in a decrease in absorbance within the wells compared to the control, indicating effective biofilm disruption. The phage dilution exhibiting the lowest absorbance, relative to the control, was designated as the most effective concentration for biofilm eradication. For one-day biofilms, the most effective phage dilution was 10^5-fold. This value decreased to 10^4-fold and 10^3-fold for three-day and five-day biofilms, respectively (See Supplementary Table 3). These results suggest a positive correlation between biofilm maturity and the required phage concentration for an effective eradication.

3.5 Phage genome and proteome characterization

The genome of the EF-M80 phage has a total length of 40,434 bp and harbors 65 open reading frames (ORFs) with a GC content of 34.9% (GenBank accession number is OR767211). The genomic structure is illustrated in Figure 3, which displays their gene categorization into seven main groups: DNA packaging termination, head and tail structure, bacterial lysis, DNA replication, transcriptional regulation factors, membrane proteins, and hypothetical proteins. Six proteins were selected for analysis of sequence similarity among 56 *Enterococcus* phages.

10.3389/fmicb.2024.1416971

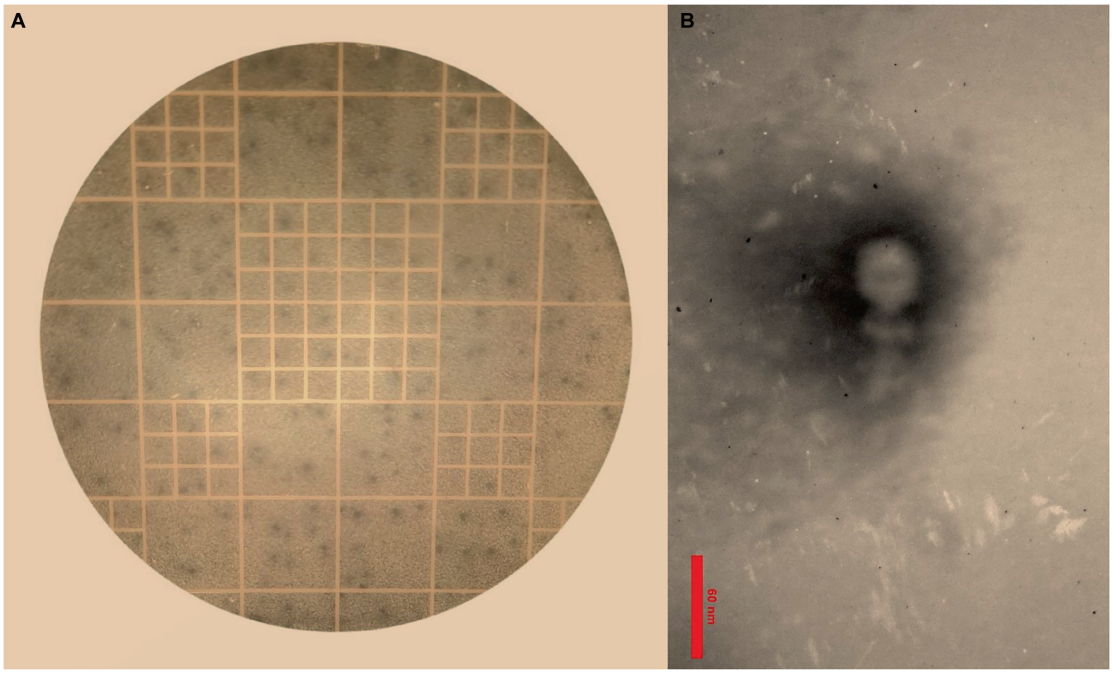

FIGURE 1
Isolation of *Enterococcus* phage strain EF-M80 from hospital sewage. **(A)** Plaque formation on double layer agar plate is showing the lytic activity of the phage against *E. faecium*. **(B)** Electron microscopy of the isolated phage negatively stained with 2% PTA at the scale bar of 60 nm. EF-M80 phage has icosahedral head and a collar structure consists of six long fibers.

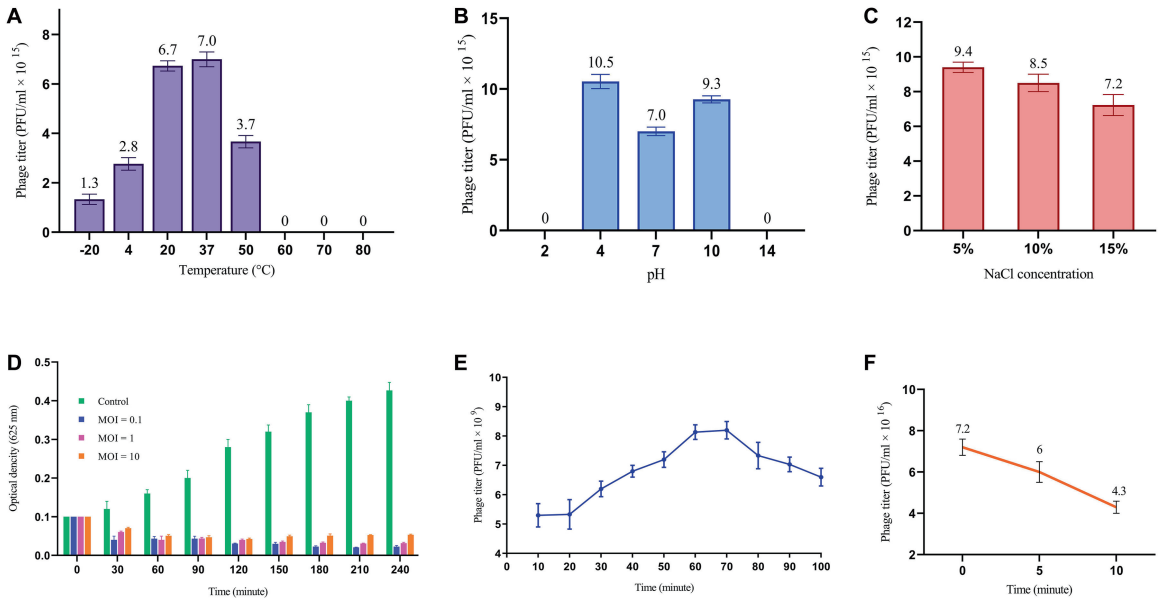

FIGURE 2
Phage replication cycle and its stability in different environmental conditions. **(A)** Phage titer changes at different temperatures. All differences in phage titers were statistically significant except group 20°C vs. 37°C. **(B)** The effects of different pH on phage titer. All differences were statistically significant except pH 2 vs. 14. **(C)** Lytic activity of the phage at high concentration of NaCl. All differences in phage titers were statistically significant except group with the concentration of 5% vs. 10%. See Supplementary Table 2. **(D)** MOI determination graph. **(E)** One-step growth cure revealing information about the life cycle of the phage. **(F)** The titer of non-adsorbed phage particles showing adsorption rate of almost 40% within 10 minutes.

The portal protein and XhlA-like hemolysin were found to have 100% coverage and identity with other *Enterococcus* phages (see Supplementary Table 4).

The phylogenetic analysis of EF-M80 with other *Enterococcus* phage genomes revealed that it was most closely related to phage vB_EfaS_AL3 with accession number MH203383, with

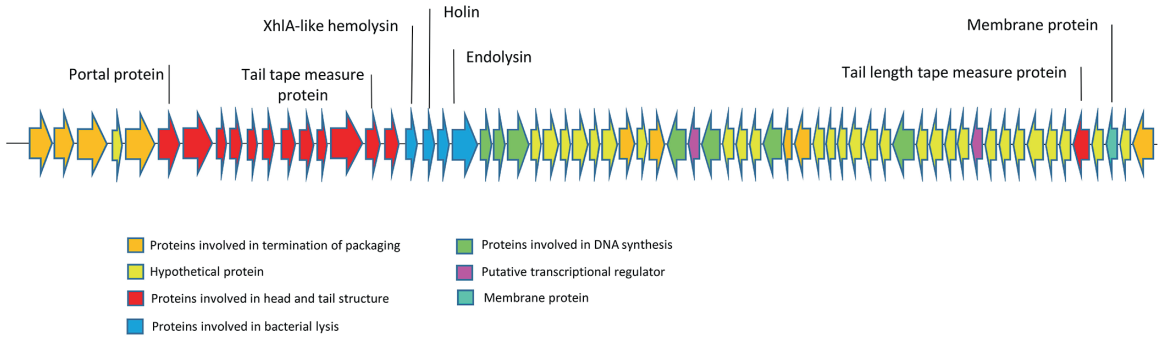

FIGURE 3
The genome structure of *Enterococcus* phage strain EF-M80. Hypothetical proteins and proteins involved in DNA replication were distributed across the genomes. The lytic cassette of EF-M80 (shown in blue) comprises enzymes (endolysins, holin) and a putative toxin (XhlA-like hemolysin) that act cooperatively to mediate phage-induced host cell lysis and release of progeny virions.

90% coverage and 97.61% identity (Figure 4). The clustering and distribution analysis of phages' accessory genomic elements showed seven clades in DNA comparison, while a pan/core plot by Roary (sequence identity cut-off = 80%) revealed 332 gene clusters in proteome comparison. Pan/core analysis showed that a total of 10 proteins belong to the core region, while 97 proteins are in the shell (8 < genome < 53), and 225 proteins belong to the cloud (genome < 8). The neighbor-joining phylogenetic dendrogram of the genomes based on the presence/absence gene matrix revealed a high level of diversity among the *Enterococcus* phages (Figure 5).

3.6 Preparation and characterization of the hydrogel carrying EF-M80 phage

3.6.1 Swelling ratio

As depicted in Figure 6A, the hydrogel's swelling behavior aligns with previous reports (Shafigh Kheljan et al., 2023). Following immersion for 24 hours, the hydrogel demonstrated a swelling index of 20%. This enhanced swelling capacity is expected to facilitate the sustained release of the phage. However, it is crucial to maintain a balance, as excessive swelling can compromise the hydrogel's structural integrity. Therefore, hydrogels exhibiting moderate swelling characteristics may be most optimal for wound healing applications (Zhou Q. et al., 2018).

3.6.2 Phage release and antibacterial activity of the hydrogel

Consistent with the results in Figure 6B, the phage-loaded hydrogel effectively inhibited bacterial growth in the broth culture medium. In contrast, the control group represented a significant increase in turbidity after 24 hours which suggests the effective release of the phage from the hydrogel. The disk diffusion assay further confirmed these results. A clear halo zone surrounding the phage-containing hydrogel disk indicated bacterial inhibition by the released phage particles. In contrast, the empty hydrogel disk, which served as a negative control, revealed no halo formation (Figure 7).

3.6.3 SEM analysis

The morphology of the hydrogel at different magnifications using scanning electron microscopy has been shown in Figure 8. The image reveals a continuous, interconnected porous structure, possibly formed by a combination of phase separation during hydrogel formation and sublimation of water removed by the freezing process. The observed pores have an average diameter of approximately 80 nm, suggesting a potential applicability for phage encapsulation.

3.6.4 FTIR spectroscopy

FTIR was used to characterize the chemical composition of the hydrogel, both empty and loaded with phage as shown in Figure 9. The spectra were consistent with previous studies on similar hydrogels (Zhang et al., 2021). The broad peak in the range of 3200–3500 cm^{-1} corresponds to the stretching vibration of O-H bonds, which are likely due to inter- and intramolecular hydrogen bonding in the polysaccharides (sodium alginate, CMC and hyaluronic acid) within the hydrogel. The peaks at approximately 1620 cm^{-1} and 1420 cm^{-1} can be attributed to the amide I vibrations (C = O stretching) of carboxyl groups and the stretching vibrations of primary amine bonds (C-N), respectively. Finally, the peak observed at about 1020 cm^{-1} is assigned to the C-O stretching vibration of primary alcohols. The intensity of the peak at 2330 cm^{-1} appears to be higher in the phage-loaded hydrogel. While this wavenumber may indicate primary or secondary amines in protein structures, it could possibly provide evidence for phage encapsulation in the hydrogel.

3.7 *In vivo* results

3.7.1 Wound healing process

Wound closure and epithelialization were monitored in all six groups of mice (Figure 10). Results demonstrated significant wound healing in the phage-loaded hydrogel group (Ph-hyd) compared to all other groups. Complete wound closure was observed in the Ph-hyd group by day 14, with healing starting as early as day 3. In addition, the phage-treated group (Ph) showed a faster healing process compared to the wounded control group (NC) and the untreated infectious group (B), achieving significant

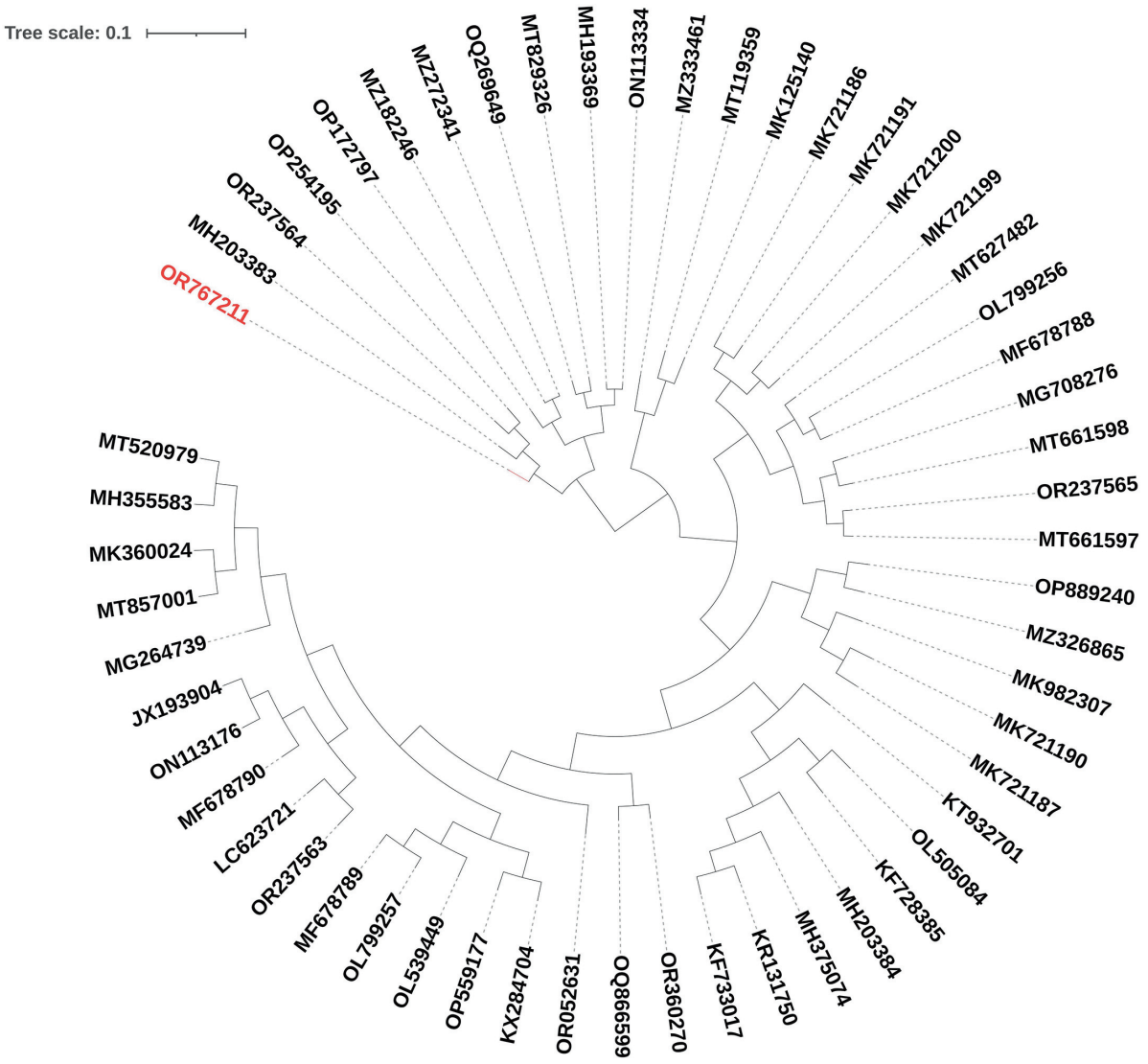

FIGURE 4
Phylogenetic positioning of EF-M80 phage within the *Enterococcus* phage landscape. A dendrogram constructed using the ClustAGE software depicts the evolutionary relationships between phage EF-M80 (colored in red) and other 55 *Enterococcus* phage genomes. The analysis revealed EF-M80's closest relatives (MH203383) within the cluster, providing insights into its potential origins and evolutionary trajectory.

wound closure by day 14. However, the healing rate was slower than in the Ph-hyd group, suggesting that although phage therapy promotes wound healing, its efficacy is optimized by a suitable delivery system such as the hydrogel. The NC group displayed delayed wound closure compared to the Ph and Ph-hyd groups, with a remaining large wound on day 10. The slowest healing rate was observed in the B group, highlighting the detrimental effects of untreated infection on wound healing.

3.7.2 Histopathological studies

Histopathologic analysis of tissue samples collected from the wounds on day 14 revealed incomplete epidermal regeneration in the positive control (B) and negative control (NC) groups. These groups displayed significantly increased epidermal thickness compared to the phage-loaded hydrogel group (Ph-hyd). In contrast, the healthy negative control (HC) and the Ph-hyd groups exhibited normal epidermal thickness, indicating efficient epidermal repair (Figure 11A). Interestingly, hair follicles and blood vessels in the hydrogel-treated groups (Ph-hyd and hyd) displayed a morphology closely resembling those observed in healthy skin. They promote the restoration of essential skin structures, potentially contributing to the accelerated healing and epithelialization observed in these groups Fibroblast density, a marker of skin regeneration and proliferation, was significantly higher in the Ph-hyd and phage-treated (Ph) groups compared to the control groups. These results support the positive impact of phage therapy in promoting tissue regeneration. In addition, the presence of neutrophils, a marker of inflammation and potential infection, was significantly lower in the Ph-hyd group compared to the positive control group. This indicates that the hydrogel delivery system was effective in reducing inflammation within the wound area. At the same time, the results indicate the highest level of inflammation for the control group (Figure 11B).

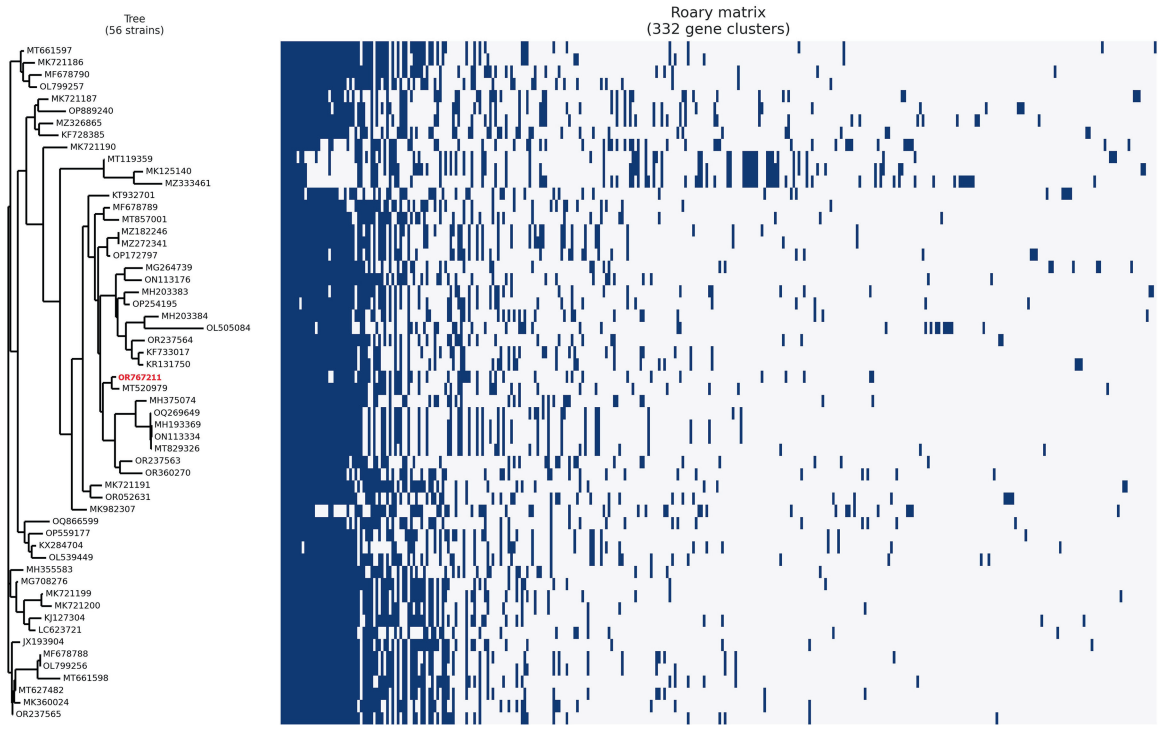

FIGURE 5
Unveiling the *Enterococcal* phage accessory genome: a pan/core proteomic analysis. This dendrogram shows the clustering patterns of 55 *Enterococcus* phage and EF-M80 phage (accession number in red color) proteomes generated using the Roary software. The analysis categorized the phage genomes into 332 gene clusters including core, accessory and unique components, revealing the common essential genes (core) and highlighting the diversity of accessory genes encoding auxiliary functions.

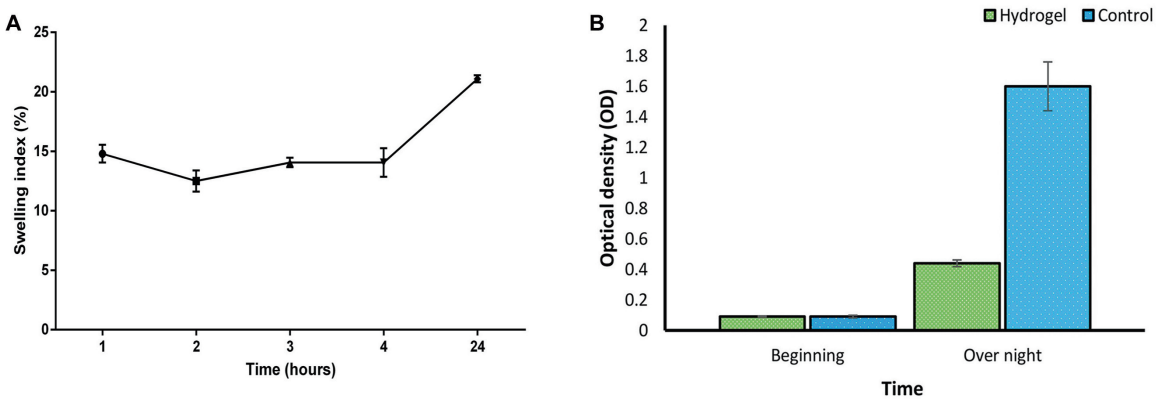

FIGURE 6
(A) Swelling index of SA/CMC/HA hydrogel showing a gradual increase in hydrogel mass with the most water uptake of 20% after 24 h. Swelling of the hydrogel triggers an expansion of the polymer network. **(B)** Suppression of bacterial growth in liquid culture by the phage-loaded hydrogel (green) compared to the control group without the hydrogel (blue). These two groups were statistically significant in overnight situation (P-value < 0.0001). See Supplementary Tables 5, 6 for more details.

4 Discussion

E. faecium is one of the main causes of hospital-acquired infections. Owing to its resistance to antibiotics treating this bacterium in hospital settings has become challenging (Peng et al., 2022). The rise in superbugs in clinical settings, accentuates the need for the development of innovative treatment approaches to effectively address the escalating threat of antimicrobial resistance. Among these novel approaches, phage therapy has emerged as an encouraging method for combating antibiotic-resistant bacteria.

To ensure the successful performance of the isolated phage as an antibacterial tool, we investigated its key properties through a series of experiments. EF-M80 exhibited strong lytic activity, a proper host spectrum, anti-biofilm activity and acceptable stability under environmental conditions. Also, analysis of the phage life

cycle through the lens of adsorption rate, one-step growth curve, and MOI determination offers valuable perceptions into critical parameters like burst size, latent period, and optimal lysis time. Burst size reflects the average number of progeny phages released per infected host cell (Kannoly et al., 2023). Its variability across different phages highlights the unique replication efficiency. Latent period signifies the duration between phage adsorption to the host and the subsequent release of new phages through cell lysis. This parameter essentially represents the time required for the intracellular replication cycle of the phage to complete (Abedon et al., 2003). The burst size and latent period observed for the EF-M80 phage were similar to the previously reported *Enterococcus* phages (Abed et al., 2024).

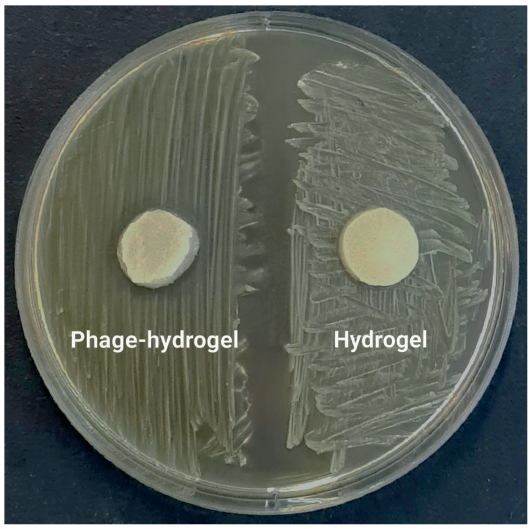

FIGURE 7
The inhibitory effect of the phage-loaded hydrogel on bacterial growth demonstrated by the inhibition zone in the disk diffusion assay.

Adsorption rate provides vital information regarding the efficiency and speed of the early stages of infection, particularly phage-host recognition and attachment (Grygorcewicz et al., 2022). The high adsorption rate of the EF-M80 phage indicates a strong binding affinity between its ligands and the corresponding receptors on the bacterial cell surface. This translates to a faster initiation of the infection cycle, potentially contributing to the effectiveness, survival, and competitive advantage of the phage over other phages or host defense mechanisms (Gallet et al., 2009).

Genome sequencing of the EF-M80 phage genome revealed that there are no genes encoding proteins associated with the lysogenic cycle like integrase, recombinase, repressors, or excisionase. These genes are key markers of temperate viruses (Necel et al., 2020). The finding supports the hypothesis that EF-M80 preferentially undergoes the lytic cycle, minimizing the risk of lysogenic transformation in phage therapy applications. This property may be advantageous in phage therapy where rapid elimination of bacteria is desired.

Before initiating phage therapy, it is essential to perform whole-genome sequencing of newly isolated bacteriophages to identify missing resistance and virulence genes to ensure safety. This approach helps optimize treatment outcomes while minimizing resource consumption (Liu et al., 2022). In this study, the potential of bacteriophage EF-M80 to act as a vector for horizontal gene transfer (HGT) of antibiotic resistance genes (ARGs) and virulence factors was investigated. While bacteriophages are known

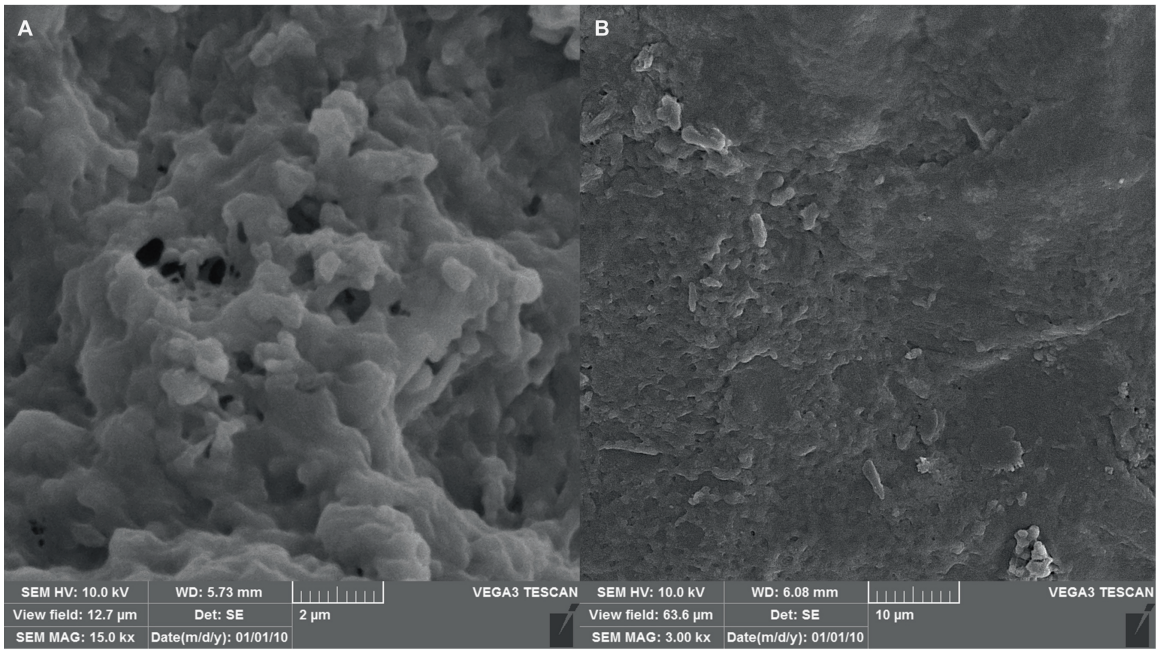

FIGURE 8
SEM micrographs of the hydrogel with scale bars of **(A)** 2 µm and **(B)** 10 µm, indicating successful formation of the hydrogel structure as well as proper shape and size.

10.3389/fmicb.2024.1416971

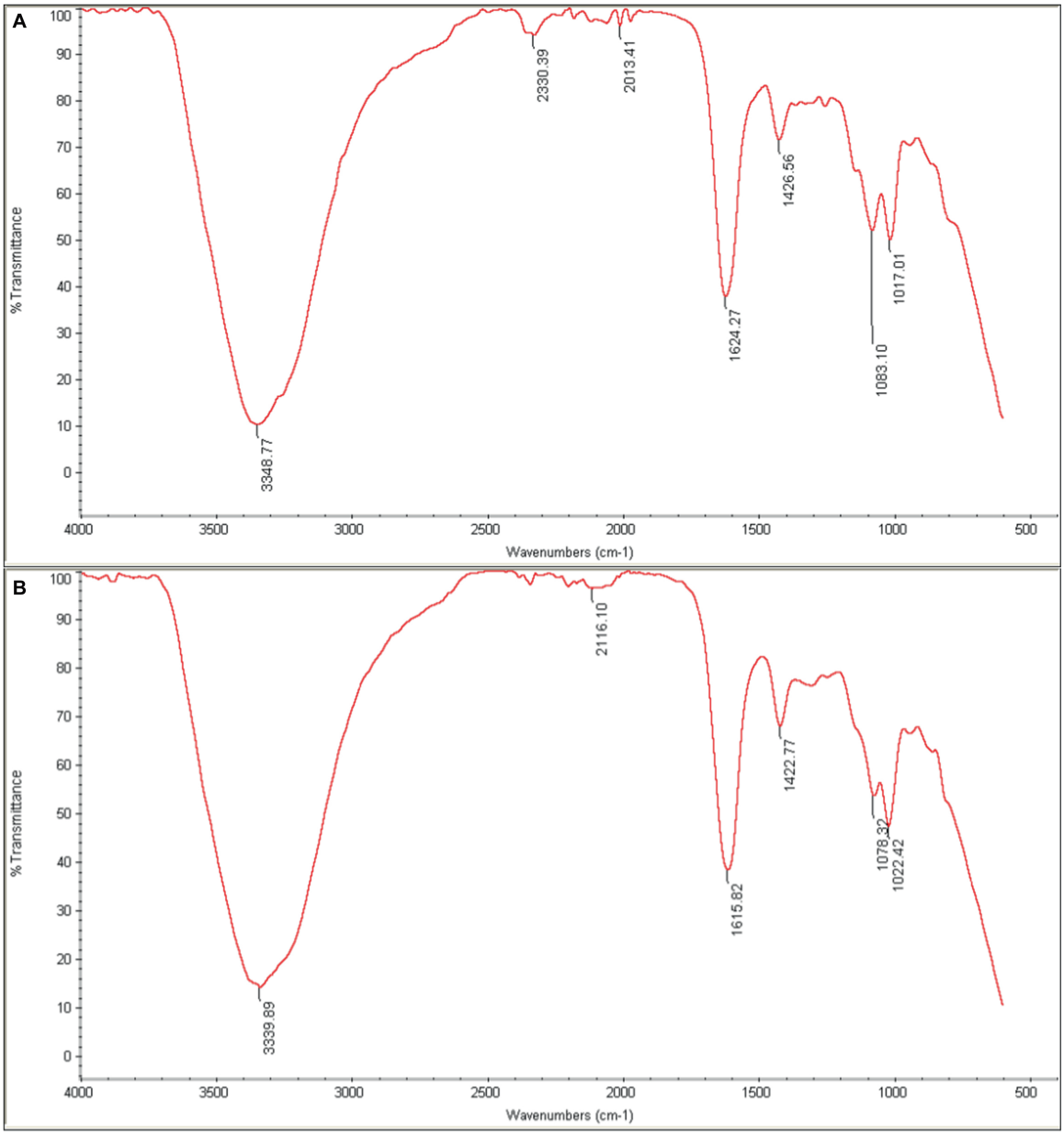

FIGURE 9
FTIR spectra of **(A)** phage-loaded hydrogel and **(B)** control hydrogel. The peaks in the range 3200–3500 cm^{-1} are related to (O–H), those in the 1620–1420 cm^{-1} range to (C=O and C–N) bonds, and at 1020 cm^{-1} to (C–O) bonds. The presence of the distinctive 2330 cm^{-1} peak in the phage-loaded hydrogel spectra indicated the possible retention of phage in the hydrogel.

facilitators of HGT (Wójcicki et al., 2021), we did not identify any ARGs or virulence factor genes within the EF-M80 genome.

EF-M80 encodes a set of lytic proteins, including endolysins, XhlA-like hemolysin, and holin (ORFs 18, 19, 20, and 21), which render its potency as an antibacterial product. In the cytoplasmic membrane, holins form micron-sized pores that allow endolysins to penetrate and degrade the peptidoglycan. Eventually, the bacterial cytoplasmic membrane is ruptured by the endopeptidase (Zaki et al., 2023). Some bacteriophages, like those we studied, have a holin-like gene in the hemolytic cassette that encodes a protein with an XhlA domain, which is characteristic of the hemolytic process. In *Enterococcus* phages, XhlA is always associated with the holin, presumably forming a membrane complex required for endolysin release across the membrane (Viglasky et al., 2023).

Additionally, the comparative genomic analysis revealed that EF-M80 shares a similar genomic structure with previously characterized phages, but with variations in non-coding regions. Notably, pan/core analysis of 56 genomes revealed that proteins involved in lysis, membrane protein, tail tape measure protein, and portal protein were the core of bacteriophages and had single or multiple amino acid polymorphisms. Interestingly, a substantial portion of the phage proteome displayed diversity in presence/absence across different phages. These findings highlight the importance of protein-level comparisons for establishing

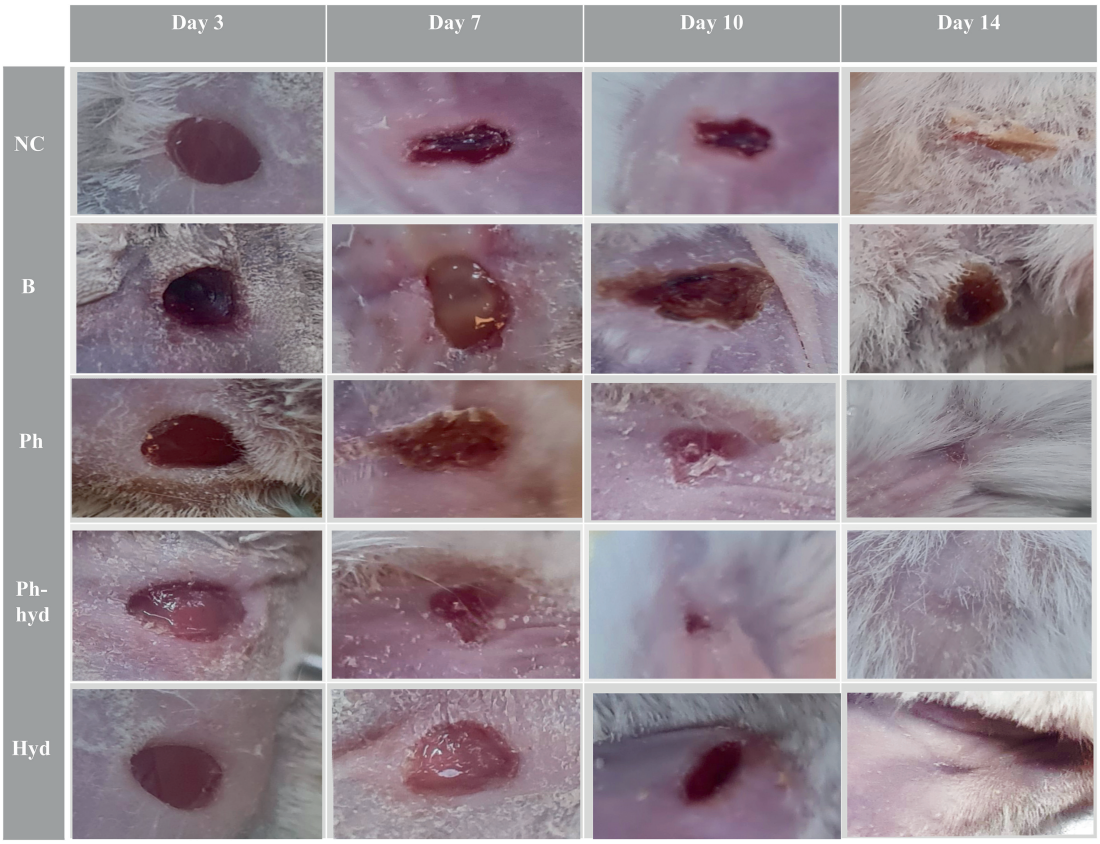

FIGURE 10
Visualizing wound healing efficacy across treatment groups. The wound healing progress is shown in five different treatment groups over a 14-day period (days 3, 7, 10, and 14 are illustrated). A progression is evident, with the phage hydrogel group (Ph-hyd) demonstrating a clear wound closure. Notably, the (Ph) group also exhibited an obvious healing effect, ranking second in wound closure efficacy. NC: Negative control. B: Positive control. Ph: Phage-treated group. Ph-hyd: Phage hydrogel group. Hyd: Hydrogel control group.

phylogenetic relationships among bacteriophages. Unlike DNA-based methods, which can be confounded by genomic mosaicism arising from frequent recombination and segment exchange, protein profiles offer a meaningful comparison for phage phylogeny (Khot et al., 2020). Intriguingly, this study showed that the tertiary structure of endolysin of the EF-M80 phage is very similar to chain A of the LytA protein from *Streptococcus pneumonia* (data have not shown). It appears that the source of the endolysin family proteins can be traced back to bacteriophages and that their integration into the bacterial chromosome occurs during the transduction process.

The growing prevalence of multidrug-resistant (MDR) *Enterococcus* spp. infections in soft tissues, wounds, and surgical sites necessitates the exploration of novel therapeutic strategies (Rajkumari et al., 2014). Biomaterials have emerged as promising tools for controlled drug delivery, and in particular hydrogels, show great potential as wound dressings. This study investigates the efficacy of a novel delivery system—encapsulated bacteriophages in a sodium alginate-based hydrogel – for treating murine wound infections caused by *E. faecium*. Hydrogels offer a near-ideal environment for wound healing. They maintain a moist environment, facilitate gas exchange, and exhibit biocompatibility, promoting optimal healing conditions (Jacob et al., 2021). The hydrogel composition and crosslinking chemistry played a significant role in preserving phage infectivity during storage. The hydrated nano-fibrous network, optimized porosity and mild crosslinking conditions provided a favorable microenvironment within the hydrogels to entrap and stabilize phage particles while retaining their antimicrobial function. Additionally, the amphoteric character of the phage allowed for easy mixing with negatively charged polysaccharides like alginate, facilitating the encapsulation process (Rana and De la Hoz Siegler, 2024). Previous reports have shown that hydrogels with similar formulations to ours can maintain phage stability for at least 2 weeks (Shafigh Kheljan et al., 2023). These findings support the idea that the hydrogel microenvironment can influence phage stability.

The current hydrogel formulation leverages a three-component design, each component contributing specific functionalities. Sodium alginate serves as a carrier for therapeutic agents, ensuring their targeted delivery to the wound site. Sodium alginate plays a crucial role in optimizing the properties of hydrogel (Lee and Mooney, 2012). Carboxymethyl cellulose (CMC) enhances the hydrogel's functionality by imparting superabsorbent properties, thermal stability, and the formation of interconnected pores within the structure, facilitating efficient phage encapsulation (Tuan Mohamood et al., 2021). Hyaluronic acid (HA), the third element of the hydrogel, is a core component of the extracellular matrix and significantly impacts wound healing processes. During inflammation, HA fragments bind to fibrinogen, initiating clotting

10.3389/fmicb.2024.1416971

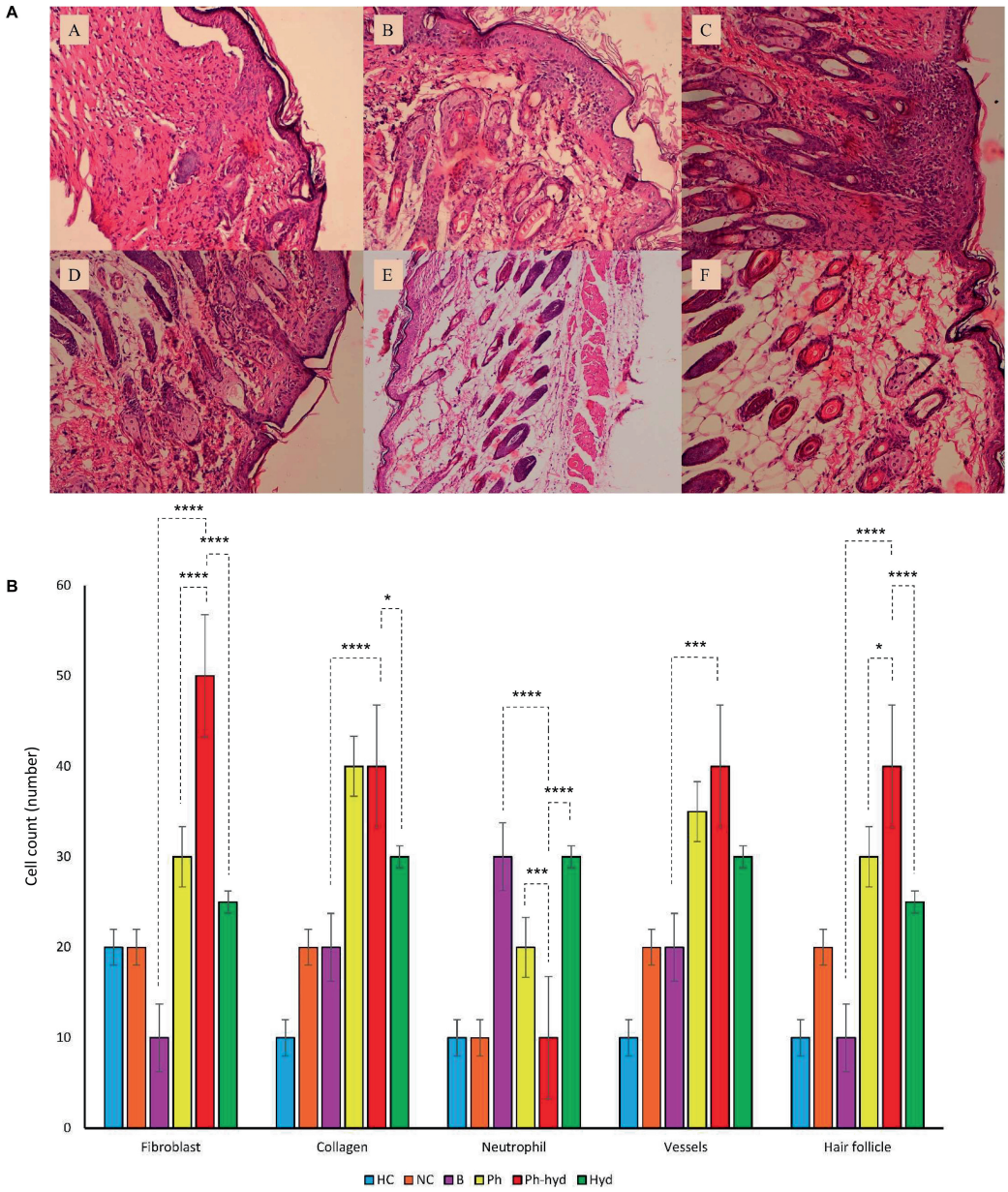

FIGURE 11

(A) Histopathological sections of skin obtained on 14th day post wound infection (A: NC, B: HC, C: B, D: Ph, E: Ph-hyd, F: Hyd). **(B)** The neutrophil, fibroblast, blood vessel, and hair follicle counts and the percentage of collagen growth as markers for the evaluation of the wound healing process in all experimental groups. One-way ANOVA test showed that the differences among some groups are statistically significant (*P* value < 0.05). The p-values of fibroblast, collagen, neutrophil, vessels, hair follicle among all vs. all groups have been shown in Supplementary Table 7. The p-values of Ph-hyd vs. B, Ph-hyd vs. Ph and Ph-hyd vs. Hyd, group were as follows: < 0.0001, < 0.0001 and < 0.0001 (for fibroblast), < 0.0001, 0.9361 and 0.0111 (for collagen), < 0.0001, 0.0003 and < 0.0001 (for neutrophil) *p-value < 0.05, ***p-value < 0.001, and ****p-value < 0.0001, 0.0002, 0.2123 and 0.1271 (for vessel) and < 0.0001, 0.0179 and < 0.0001 (for hair follicle) respectively. The underlined P-values are not significant.

and creating a scaffold for immune cell migration (Frenkel, 2014). Studies have shown that exogenous HA enhances re-epithelialization, highlighting its importance in tissue repair (Nyman et al., 2019). The observed improvements in granulation, collagen deposition, fibroblast presence, and epithelialization in the hydrogel-treated groups can be attributed to the multifaceted roles of HA in wound healing.

Beyond alginate-based hydrogels, various formulations and production methods have been explored for developing phage-delivering hydrogels. These include materials such as polyethylene glycol (PEG), polyvinyl alcohol (PVA), hydroxypropyl methylcellulose (HPMC), and agarose-hyaluronic acid methacrylate (HAMA). These alternative hydrogels hold promise for treating a range of infections, including implant-related osteomyelitis, urinary tract infections from catheters, and trauma-associated wound infections (Kim et al., 2021). Studies have demonstrated the use of PVA hydrogels for catheter blockage prevention. Milo et al. designed a surface coating PVA hydrogel loaded with phage to target biofilms formed by *Proteus mirabilis* (Milo et al., 2017). Alginate-nanohydroxyapatite hydrogels loaded

with bacteriophage have also shown efficacy. Barros et al. reported that these hydrogels reduced the ability of multidrug-resistant *E. faecalis* to adhere and form colonies in femoral tissues following bone graft implantation (Barros et al., 2020). Combination therapy using phages and antibiotics (phage-antibiotic synergy, PAS) has also been explored. Mukhopadhyay et al. employed an HPMC hydrogel containing a specific phage (vB_AbaM-IME-AB2) and the antibiotic colistin to eradicate both biofilm and planktonic forms of *Acinetobacter baumannii* (Mukhopadhyay et al., 2023).

The *in vivo* histopathological evaluation demonstrated that EF-M80 phage retained its antibacterial properties, effectively lysing *E. faecium* within the host environment. On the other hand, encapsulation of the phage within a hydrogel delivery system significantly enhanced its efficacy in promoting wound healing in wound-infected mice models. These findings collectively suggest the promising potential of this phage-based therapeutic method for the treatment of infections associated with antibiotic-resistant *E. faecium*.

5 Conclusion

Increasing antibiotic resistance of the ESKAPE bacteria causing hospital-acquired infections is alarmingly raised as a health problem all over the world. Until now, to prevent the antimicrobial resistance, the use of various methods, and strategies has been suggested. Bacteriophages seem to be efficient and attractive tools against antibiotic-resistant bacteria. In this study, EF-M80 phage revealed that it can be used against *E. faecium* in terms of promising physicochemical and genetic characteristics. The stability of the EF-M80 phage to environmental conditions and its lysis property on *E. faecium* highlighted that it could be a promising tool against this bacterium. Furthermore, the genome sequencing of *Enterococcus* phage strain EF-M80 revealed lysis cassettes that act cooperatively to mediate phage-induced host cell lysis. The phage encapsulated in the hydrogel texture represented a synergistic effect on the wound healing process. This study may provide the basis for the future use of hydrogel-encapsulated EF-M80 phage in curing biofilm related *E. faecium* infections.

Data availability statement

The Enterococcus phage strain EF-M80 was deposited in the GenBank database under accession number OR767211. In addition, all bacteriophage genomes considered in this study were retrieved from the GenBank database. The accession number(s) can be found in the article/Supplementary material.

Ethics statement

The requirement of ethical approval was waived by this project was done based on ethical guidelines as previously approved by the Al-Zahra University (Ir.ALZAHRA.REC.1401.015). for the studies on humans because samples without names and codes. The studies were conducted in accordance with the local legislation and institutional requirements. Written informed consent for participation was not required from the participants or the participants' legal guardians/next of kin in accordance with the national legislation and institutional requirements. The human samples used in this study were acquired from primarily isolated as part of your previous study for which ethical approval was obtained. The animal study was approved by this project was done based on ethical guidelines as previously approved by the Al-Zahra University (Ir.ALZAHRA.REC.1401.015).

Author contributions

MK: Data curation, Formal analysis, Software, Visualization, Writing—original draft. AE: Conceptualization, Project administration, Supervision, Validation, Writing—review and editing. SA: Data curation, Formal analysis, Writing—review and editing. MS: Project administration, Supervision, Validation, Writing—review and editing. SB: Data curation, Writing—review and editing. HS: Data curation, Formal analysis, Writing—review and editing. FB: Data curation, Formal analysis, Software, Writing—review and editing. AS: Data curation, Writing—review and editing.

Funding

The author(s) declare that no financial support was received for the research, authorship, and/or publication of this article.

Acknowledgments

The authors would like to thank the personnel in the bacteriology department of the Pasture Institute of Iran for their help. In addition, Mrs. Khazani wants to say a special thanks to Mrs. Zolykha Sherafat for obtaining sample collection.

Conflict of interest

The authors declare that the research was conducted in the absence of any commercial or financial relationships that could be construed as a potential conflict of interest.

Publisher's note

All claims expressed in this article are solely those of the authors and do not necessarily represent those of their affiliated organizations, or those of the publisher, the editors and the reviewers. Any product that may be evaluated in this article, or claim that may be made by its manufacturer, is not guaranteed or endorsed by the publisher.

Supplementary material

The Supplementary Material for this article can be found online at: https://www.frontiersin.org/articles/10.3389/fmicb.2024.1416971/full#supplementary-material

References

Abed, S., Sholeh, M., Khazani Asforooshani, M., Shafiei, M., Hashemi Shahraki, A., and Nasr, S. (2024). Insights into the novel *Enterococcus faecalis* phage: A comprehensive genome analysis. *PLoS One* 19:e0301292. doi: 10.1371/journal.pone.0301292

Abedon, S. (2016). Phage therapy dosing: The problem(s) with multiplicity of infection (MOI). *Bacteriophage* 6:e1220348. doi: 10.1080/21597081.2016.1220348

Abedon, S., Hyman, P., and Thomas, C. (2003). Experimental examination of bacteriophage latent-period evolution as a response to bacterial availability. *Appl. Environ. Microbiol.* 69, 7499–7506. doi: 10.1128/AEM.69.12.7499-7506.2003

Alduhaidhawi, A., AlHuchaimi, S., Al-Mayah, T., Al-Ouqaili, M., Alkafaas, S., Muthupandian, S., et al. (2022). Prevalence of CRISPR-cas systems and their possible association with antibiotic resistance in *Enterococcus faecalis* and *Enterococcus faecium* collected from hospital wastewater. *Infect. Drug Resist.* 15, 1143–1154. doi: 10.2147/IDR.S358248

Barros, J., Melo, L., Silva, R., Ferraz, M., Azeredo, J., Pinheiro, V., et al. (2020). Encapsulated bacteriophages in alginate-nanohydroxyapatite hydrogel as a novel delivery system to prevent orthopedic implant-associated infections. *Nanomedicine* 24:102145. doi: 10.1016/j.nano.2019.102145

Bean, J. E., Alves, D. R., Laabei, M., Esteban, P. P., Thet, N. T., Enright, M. C., et al. (2014). Triggered release of bacteriophage K from agarose/hyaluronan hydrogel matrixes by *Staphylococcus aureus* virulence factors. *Chem. Mater.* 26, 7201–7208.

Brown, J., Pirrung, M., and McCue, L. A. (2017). FQC Dashboard: Integrates FastQC results into a web-based, interactive, and extensible FASTQ quality control tool. *Bioinformatics* 33, 3137–3139. doi: 10.1093/bioinformatics/btx373

Canfield, G., and Duerkop, B. (2020). Molecular mechanisms of enterococcal-bacteriophage interactions and implications for human health. *Curr. Opin. Microbiol.* 56, 38–44. doi: 10.1016/j.mib.2020.06.003

Chang, R., Okamoto, Y., Morales, S., Kutter, E., and Chan, H. (2021). Hydrogel formulations containing non-ionic polymers for topical delivery of bacteriophages. *Int. J. Pharm.* 605:120850. doi: 10.1016/j.ijpharm.2021.120850

Chen, S., Huang, T., Zhou, Y., Han, Y., Xu, M., and Gu, J. (2017). AfterQC: Automatic filtering, trimming, error removing and quality control for fastq data. *BMC Bioinform.* 18:80. doi: 10.1186/s12859-017-1469-3

Clinical and Laboratory Standards Institute [CLSI]. (2023). *Performance standards for antimicrobial susceptibility testing; 33rd Informational Supplement*. M100-S32. Wayne, PA: CLSI.

Darling, A., Mau, B., Blattner, F., and Perna, N. (2004). Mauve: Multiple alignment of conserved genomic sequence with rearrangements. *Genome Res.* 14, 1394–1403. doi: 10.1101/gr.2289704

Daubie, V., Chalhoub, H., Blasdel, B., Dahma, H., Merabishvili, M., Glonti, T., et al. (2022). Determination of phage susceptibility as a clinical diagnostic tool: A routine perspective. *Front. Cell. Infect. Microbiol.* 12:1000721. doi: 10.3389/fcimb.2022.1000721

El Haddad, L., Angelidakis, G., Clark, J., Mendoza, J., Terwilliger, A., Chaftari, C., et al. (2022). Genomic and functional characterization of vancomycin-resistant enterococci-specific bacteriophages in the *Galleria mellonella* wax moth larvae model. *Pharmaceutics* 14:1591. doi: 10.3390/pharmaceutics14081591

Eren, A., Esen, ÖC., Quince, C., Vineis, J. H., Morrison, H. G., Sogin, M. L., et al. (2015). Anvi'o: An advanced analysis and visualization platform for 'omics data. *PeerJ* 3:e1319. doi: 10.7717/peerj.1319

Fauquet, C. (2005). *International committee on taxonomy of viruses, international union of microbiological societies. Virology Division. Virus taxonomy: Classification and nomenclature of viruses: Eighth report of the international committee on the taxonomy of viruses*. Boston, MA: Elsevier Academic Press.

Frenkel, J. (2014). The role of hyaluronan in wound healing. *Int. Wound J.* 11, 159–163. doi: 10.1111/j.1742-481X.2012.01057.x

Gallet, R., Shao, Y., and Wang, I. (2009). High adsorption rate is detrimental to bacteriophage fitness in a biofilm-like environment. *BMC Evol. Biol.* 9:241. doi: 10.1186/1471-2148-9-241

Gong, P., Cheng, M., Li, X., Jiang, H., Yu, C., Kahaer, N., et al. (2016). Characterization of *Enterococcus faecium* bacteriophage IME-EFm5 and its endolysin LysEFm5. *Virology* 492, 11–20. doi: 10.1016/j.virol.2016.02.006

Grygorcewicz, B., Rakoczy, R., Roszak, M., Konopacki, M., Kordas, M., Piegat, A., et al. (2022). Rotating magnetic field-assisted reactor enhances mechanisms of phage adsorption on bacterial cell surface. *Curr. Issues Mol. Biol.* 44, 1316–1325. doi: 10.3390/cimb44030088

Gupta, N., and Shivakumar, H. (2012). Investigation of Swelling behavior and mechanical properties of a ph-sensitive superporous hydrogel composite. *Iran. J. Pharm. Res.* 11, 481–493.

Gurevich, A., Saveliev, V., Vyahhi, N., and Tesler, G. (2013). QUAST: Quality assessment tool for genome assemblies. *Bioinformatics* 29, 1072–1075. doi: 10.1093/bioinformatics/btt086

Jacob, S., Nair, A., Shah, J., Sreeharsha, N., Gupta, S., and Shinu, P. (2021). Emerging role of hydrogels in drug delivery systems, tissue engineering and wound management. *Pharmaceutics* 13:357. doi: 10.3390/pharmaceutics13030357

Ji, J., Liu, Q., Wang, R., Luo, T., Guo, X., Xu, M., et al. (2020). Identification of a novel phage targeting methicillin-resistant *Staphylococcus aureus* In vitro and In vivo. *Microb. Pathog.* 149:104317. doi: 10.1016/j.micpath.2020.104317

Kannoly, S., Oken, G., Shadan, J., Musheyev, D., Singh, K., Singh, A., et al. (2023). Single-cell approach reveals intercellular heterogeneity in phage-producing capacities. *Microbiol. Spectr.* 11:e0266321. doi: 10.1128/spectrum.02663-21

Kaur, P., Gondil, V., and Chhibber, S. (2019). A novel wound dressing consisting of PVA-SA hybrid hydrogel membrane for topical delivery of bacteriophages and antibiotics. *Int. J. Pharm.* 572:118779. doi: 10.1016/j.ijpharm.2019.118779

Khawaja, K., Abbas, Z., and Rehman, S. (2016). Isolation and characterization of lytic phagesTSE1-3 against *Enterobacter cloacae*. *Open Life Sci.* 11, 287–292.

Khot, V., Strous, M., and Hawley, A. (2020). Computational approaches in viral ecology. *Comput. Struct. Biotechnol. J.* 18, 1605–1612. doi: 10.1016/j.csbj.2020.06.019

Kim, H., Chang, R., Morales, S., and Chan, H. (2021). Bacteriophage-delivering hydrogels: Current progress in combating antibiotic resistant bacterial infection. *Antibiotics (Basel)* 10:130. doi: 10.3390/antibiotics10020130

Kumari, S., Harjai, K., and Chhibber, S. (2011). Bacteriophage versus antimicrobial agents for the treatment of murine burn wound infection caused by *Klebsiella pneumoniae* B5055. *J. Med. Microbiol.* 60, 205–210. doi: 10.1099/jmm.0.018580-0

Lebeaux, D., Ghigo, J., and Beloin, C. (2014). Biofilm-related infections: Bridging the gap between clinical management and fundamental aspects of recalcitrance toward antibiotics. *Microbiol. Mol. Biol. Rev.* 78, 510–543. doi: 10.1128/MMBR.00013-14

Lee, D., Im, J., Na, H., Ryu, S., Yun, C., and Han, S. (2019). The novel *Enterococcus* phage vB_EfaS_HEf13 has broad lytic activity against clinical isolates of *Enterococcus faecalis*. *Front. Microbiol.* 10:2877. doi: 10.3389/fmicb.2019.02877

Lee, K., and Mooney, D. (2012). Alginate: Properties and biomedical applications. *Prog. Polym. Sci.* 37, 106–126. doi: 10.1016/j.progpolymsci.2011.06.003

Letunic, I., and Bork, P. (2021). Interactive tree of life (iTOL) v5: An online tool for phylogenetic tree display and annotation. *Nucleic Acids Res.* 49, W293–W296. doi: 10.1093/nar/gkab301

Lin, D., Koskella, B., and Lin, H. (2017). Phage therapy: An alternative to antibiotics in the age of multi-drug resistance. *World J. Gastrointest. Pharmacol. Ther.* 8, 162–173. doi: 10.4292/wjgpt.v8.i3.162

Litt, P., and Jaroni, D. (2017). Isolation and physiomorphological characterization of *Escherichia coli* O157:H7-infecting bacteriophages recovered from beef cattle operations. *Int. J. Microbiol.* 2017:7013236. doi: 10.1155/2017/7013236

Liu, M., Hernandez-Morales, A., Clark, J., Le, T., Biswas, B., Bishop-Lilly, K., et al. (2022). Comparative genomics of *Acinetobacter baumannii* and therapeutic bacteriophages from a patient undergoing phage therapy. *Nat. Commun.* 13:3776. doi: 10.1038/s41467-022-31455-5

Mansouri, M., Barzi, S., Zafari, M., Chiani, M., Chehrazi, M., Nosrati, H., et al. (2022). Electrosprayed cefazolin-loaded niosomes onto electrospun chitosan nanofibrous membrane for wound healing applications. *J. Biomed. Mater. Res. B Appl. Biomater.* 110, 1814–1826. doi: 10.1002/jbm.b.35039

Mansur, H. S., Sadahira, C. M., Souza, A. N., and Mansur, A. A. P. (2008). FTIR spectroscopy characterization of poly (vinyl alcohol) hydrogel with different hydrolysis degree and chemically crosslinked with glutaraldehyde. *Mater. Sci. Eng.* 28, 539–548.

Martinez-Garcia, F., Fischer, T., Hayn, A., Mierke, C., Burgess, J., and Harmsen, M. C. (2022). A beginner's guide to the characterization of hydrogel microarchitecture for cellular applications. *Gels* 8:535. doi: 10.3390/gels8090535

Melo, L., Ferreira, R., Costa, A., Oliveira, H., and Azeredo, J. (2019). Efficacy and safety assessment of two enterococci phages in an in vitro biofilm wound model. *Sci. Rep.* 9:6643. doi: 10.1038/s41598-019-43115-8

Milo, S., Hathaway, H., Nzakizwanayo, J., Alves, D., Esteban, P., Jones, B., et al. (2017). Prevention of encrustation and blockage of urinary catheters by *Proteus mirabilis* via pH-triggered release of bacteriophage. *J. Mater. Chem. B* 5, 5403–5411. doi: 10.1039/c7tb01302g

Mukhopadhyay, S., To, K., Liu, Y., Bai, C., and Leung, S. S. Y. (2023). A thermosensitive hydrogel formulation of phage and colistin combination for the management of multidrug-resistant *Acinetobacter baumannii* wound infections. *Biomater. Sci.* 12, 151–163. doi: 10.1039/d3bm01383a

Necel, A., Bloch, S., Nejman-Faleńczyk, B., Grabski, M., Topka, G., Dydecka, A., et al. (2020). Characterization of a bacteriophage, vB_Eco4M-7, that effectively infects many *Escherichia coli* O157 strains. *Sci. Rep.* 10:3743. doi: 10.1038/s41598-020-60568-4

Nyman, E., Henricson, J., Ghafouri, B., Anderson, C., and Kratz, G. (2019). Hyaluronic acid accelerates re-epithelialization and alters protein expression in a human wound model. *Plast. Reconstr. Surg. Glob. Open* 7:e2221. doi: 10.1097/GOX.0000000000002221

Ozer, E. (2018). ClustAGE: A tool for clustering and distribution analysis of bacterial accessory genomic elements. *BMC Bioinform.* 19:150. doi: 10.1186/s12859-018-2154-x

Page, A., Cummins, C., Hunt, M., Wong, V., Reuter, S., Holden, M., et al. (2015). Roary: Rapid large-scale prokaryote pan genome analysis. *Bioinformatics* 31, 3691–3693. doi: 10.1093/bioinformatics/btv421

Pan, L., Li, D., Sun, Z., Lin, W., Hong, B., Qin, W., et al. (2022). First characterization of a Hafnia phage reveals extraordinarily large burst size and unusual plaque polymorphism. *Front. Microbiol.* 12:754331. doi: 10.3389/fmicb.2021.754331

Peng, Z., Yan, L., Yang, S., and Yang, D. (2022). Antimicrobial-resistant evolution and global spread of *Enterococcus faecium* clonal complex (CC) 17: Progressive change from gut colonization to hospital-adapted pathogen. *China CDC Wkly.* 4, 17–21. doi: 10.46234/ccdcw2021.277

Pradal, I., Casado, A., Del Rio, B., Rodriguez-Lucas, C., Fernandez, M., Alvarez, M., et al. (2023). Enterococcus faecium bacteriophage vB_EfaH_163, a new member of the herelleviridae family, reduces the mortality associated with an *E. faecium* vanR clinical isolate in a *Galleria mellonella* animal model. *Viruses* 15:179. doi: 10.3390/v15010179

Rajkumari, N., Mathur, P., and Misra, M. (2014). Soft tissue and wound infections due to *Enterococcus* spp. Among hospitalized trauma patients in a developing country. *J. Glob. Infect. Dis.* 6, 189–193. doi: 10.4103/0974-777X.145253

Rana, M., and De la Hoz Siegler, H. (2024). Evolution of hybrid hydrogels: Next-generation biomaterials for drug delivery and tissue engineering. *Gels* 10:216. doi: 10.3390/gels10040216

Seemann, T. (2014). Prokka: Rapid prokaryotic genome annotation. *Bioinformatics* 30, 2068–2069. doi: 10.1093/bioinformatics/btu153

Shafigh Kheljan, F., Sheikhzadeh Hesari, F., Aminifazl, M., Skurnik, M., Gholadze, S., and Zarrini, G. (2023). Design of phage-cocktail-containing hydrogel for the treatment of *Pseudomonas aeruginosa*-infected wounds. *Viruses* 15:03. doi: 10.3390/v15030803

Tuan Mohamood, N., Abdul Halim, A., and Zainuddin, N. (2021). Carboxymethyl cellulose hydrogel from biomass waste of oil palm empty fruit bunch using calcium chloride as crosslinking agent. *Polymers (Basel)* 13:4056. doi: 10.3390/polym13234056

Vestby, L., Grønseth, T., Simm, R., and Nesse, L. (2020). Bacterial biofilm and its role in the pathogenesis of disease. *Antibiotics (Basel)* 9:59. doi: 10.3390/antibiotics9020059

Viglasky, J., Piknova, M., and Pristas, P. (2023). Gene and domain shuffling in lytic cassettes of *Enterococcus* spp. bacteriophages. *3 Biotech* 13:388. doi: 10.1007/s13205-023-03775-w

Wang, Z., Zheng, P., Ji, W., Fu, Q., Wang, H., Yan, Y., et al. (2016). SLPW: A virulent bacteriophage targeting methicillin-resistant *Staphylococcus aureus* in vitro and in vivo. *Front. Microbiol.* 7:934. doi: 10.3389/fmicb.2016.00934

Węgrzyn, G. (2022). Should bacteriophages be classified as parasites or predators? *Pol. J. Microbiol.* 71, 3–9. doi: 10.33073/pjm-2022-005

Wójcicki, M., Średnicka, P., Błażejak, S., Gientka, I., Kowalczyk, M., Emanowicz, P., et al. (2021). Characterization and genome study of novel lytic bacteriophages against prevailing saprophytic bacterial microflora of minimally processed plant-based food products. *Int. J. Mol. Sci.* 22:12460. doi: 10.3390/ijms222212460

Yan, W., Banerjee, P., Liu, Y., Mi, Z., Bai, C., Hu, H., et al. (2021). Development of thermosensitive hydrogel wound dressing containing *Acinetobacter baumannii* phage against wound infections. *Int. J. Pharm.* 602:120508. doi: 10.1016/j.ijpharm.2021.120508

Yazdi, M., Bouzari, M., and Ghaemi, E. (2018). Isolation and characterization of a lytic bacteriophage (vB_PmiS-TH) and its application in combination with ampicillin against planktonic and biofilm forms of *Proteus mirabilis* isolated from urinary tract infection. *J. Mol. Microbiol. Biotechnol.* 28, 37–46. doi: 10.1159/000487137

Yim, J., Smith, J., and Rybak, M. (2017). Role of combination antimicrobial therapy for vancomycin-resistant *Enterococcus faecium* infections: Review of the current evidence. *Pharmacotherapy* 37, 579–592. doi: 10.1002/phar.1922

Zaki, B., Fahmy, N., Aziz, R., Samir, R., and El-Shibiny, A. (2023). Characterization and comprehensive genome analysis of novel bacteriophage, vB_Kpn_ZCKp20p, with lytic and anti-biofilm potential against clinical multidrug-resistant *Klebsiella pneumoniae*. *Front. Cell. Infect. Microbiol.* 13:1077995. doi: 10.3389/fcimb.2023.1077995

Zhang, K., Wang, Y., Wei, Q., Li, X., Guo, Y., and Zhang, S. (2021). Design and fabrication of sodium alginate/carboxymethyl cellulose sodium blend hydrogel for artificial skin. *Gels* 7:115. doi: 10.3390/gels7030115

Zhou, W., Feng, Y., and Zong, Z. (2018). Two new lytic bacteriophages of the myoviridae family against carbapenem-resistant *Acinetobacter baumannii*. *Front. Microbiol.* 9:850. doi: 10.3389/fmicb.2018.00850

Zhou, Q., Kang, H., Bielec, M., Wu, X., Cheng, Q., Wei, W., et al. (2018). Influence of different divalent ions cross-linking sodium alginate-polyacrylamide hydrogels on antibacterial properties and wound healing. *Carbohydr. Polym.* 197, 292–304. doi: 10.1016/j.carbpol.2018.05.078

Zhou, X., Willems, R., Friedrich, A., Rossen, J., and Bathoorn, E. (2020). *Enterococcus faecium*: From microbiological insights to practical recommendations for infection control and diagnostics. *Antimicrob. Resist. Infect. Control* 9:130. doi: 10.1186/s13756-020-00770-1

frontiers | Frontiers in Microbiology

TYPE Original Research
PUBLISHED 02 August 2024
DOI 10.3389/fmicb.2024.1437536

OPEN ACCESS

EDITED BY
Gamaliel López-Leal,
Center for Research in Cellular Dynamics-UAEM, Mexico

REVIEWED BY
Swapnil Ganesh Sanmukh,
Université Clermont Auvergne, France
Rosa Isela Santamaria,
National Autonomous University of Mexico, Mexico

*CORRESPONDENCE
Siyun Wang
✉ siyun.wang@ubc.ca

RECEIVED 23 May 2024
ACCEPTED 27 June 2024
PUBLISHED 02 August 2024

CITATION
Chantapakul B, Sabaratnam S and Wang S (2024) Isolation and characterization of bacteriophages for controlling *Rhizobium radiobacter* – causing stem and crown gall of highbush blueberry.
Front. Microbiol. 15:1437536.
doi: 10.3389/fmicb.2024.1437536

Isolation and characterization of bacteriophages for controlling *Rhizobium radiobacter* – causing stem and crown gall of highbush blueberry

Bowornnan Chantapakul[1], Siva Sabaratnam[2] and Siyun Wang[1]*

[1]Food, Nutrition and Health, University of British Columbia, Vancouver, BC, Canada, [2]Abbotsford Agriculture Centre, Ministry of Agriculture and Food, Abbotsford, BC, Canada

Introduction: Stem and crown gall disease caused by the plant pathogen *Rhizobium radiobacter* has a significant impact on highbush blueberry (*Vaccinium corymbosum*) production. Current methods for controlling the bacterium are limited. Lytic phages, which can specifically target host bacteria, have been widely gained interest in agriculture.

Methods: In this study, 76 bacteriophages were recovered from sewage influent and screened for their inhibitory effect against *Rhizobium* spp. The phages were genetically characterized through whole-genome sequencing, and their lytic cycle was confirmed.

Results: Five potential candidate phages (isolates IC12, IG49, AN01, LG08, and LG11) with the ability to lyse a broad range of hosts were chosen and assessed for their morphology, environmental stability, latent period, and burst size. The morphology of these selected phages revealed a long contractile tail under transmission electron microscopy. Single-step growth curves displayed that these phages had a latent period of 80–110 min and a burst size ranging from 8 to 33 phages per infected cell. None of these phages contained any antimicrobial resistance or virulence genes in their genomes. Subsequently, a combination of two-, three- and four-phage cocktails were formulated and tested for their efficacy in a broth system. A three-phage cocktail composed of the isolates IC12, IG49 and LG08 showed promising results in controlling a large number of *R. radiobacter* strains *in vitro*. In a soil/peat-based model, the three-phage cocktail was tested against *R. radiobacter* PL17, resulting in a significant reduction ($p < 0.05$) of 2.9 and 1.3 $\log_{10}$ CFU/g after 24 and 48 h of incubation, respectively.

Discussion: These findings suggest that the three-phage cocktail (IC12, IG49 and LG08) has the potential to serve as a proactive antimicrobial solution for controlling *R. radiobacter* on blueberry.

KEYWORDS

bacteriophage, gall disease, *Rhizobium radiobacter*, blueberry, biocontrol, genomic analysis

1 Introduction

Rhizobium radiobacter, formerly known as *Agrobacterium tumefaciens*/*A. radiobacter*, has been identified as the causative agent of stem and crown gall disease in blueberries (Kuzmanović et al., 2019). The general characteristics of *R. radiobacter* are gram-negative rod-shaped bacterium and generally found in soil environments and roots of plants (Guo et al., 2017). Most

plant-pathogenic *Rhizobium* species possess a tumor-inducing plasmid (pTi) responsible for developing gall in wounded plant cells. The transfer DNA (T-DNA) segment of pTi plasmid, upon integration into plant genome, results in the imbalance of plant growth hormones such as auxin and cytokinin (Gohlke and Deeken, 2014). Once the equilibrium of plant hormones is disrupted, the abnormal growth of cells develops into galls that resemble tumors (Kunkel and Harper, 2018). Gall, typically seen as ball-shaped or knob-like structures on various parts of plants such as roots, crowns and stems or even flowers and stems, can obstruct the vascular system of plants, resulting in obstruction of conducting water and nutrients beyond the gall's location (Aloni and Ullrich, 2008). While galls typically do not cause serious effects on the adult plant, they can have significant impacts on young blueberry plants (Pulawska, 2010). Although cases related to stem gall disease in blueberries were rarely found until recently, blueberry farmers in British Columbia have reported incidents and requested a solution to minimize the impact of gall disease. In addition, the Canadian blueberry industry, being one of the World's largest suppliers, faces economical loss from stem and crown gall disease, estimated at $11.2 million per year (Carter, 1989).

The method for controlling gall disease involves the use of chemicals such as copper and acids (Sawalha et al., 2013; Mary Opisa et al., 2020). However, heavy use of these chemicals can contribute to soil pollution, the development of resistant strains, and potential harm to humans. Commercial biocontrol therapies have been available for decades to prevent *R. radiobacter* in some plants. For instance, *A. radiobacter* strain K84 has been shown to produce bacteriocin called agrocin 84 and used to control *A. tumefaciens* in cherry (Stockwell et al., 1993; Penyalver et al., 2001). While this inhibitory compound is very effective against *R. radiobacter*, the application may adversely affect beneficial microbes that are closely related to other *Rhizobium* species. To date, there is no effective method for curing stem gall disease in highbush blueberry. The best strategy for controlling gall disease is proactive prevention before the onset of the disease.

The use of bacteriophage (phage) has perceived the interest in plant disease management due to their unique trait that overcomes other biocontrol methods. Phage specifically binds to bacterial host cells through a particular receptor, leading to the lysis of specific target bacterial hosts. In other words, phage cannot attach to nonbacterial hosts and rarely any evidence of cross-binding to other genera, minimizing the risk of damage to non-target and beneficial species. Over the past decades, successful developments of phage treatments in agriculture have demonstrated their ability to outperform other biocontrol strategies. Phages have been used to control soft rot in potato (Adriaenssens et al., 2012; Czajkowski et al., 2015), bacterial wilt in tomato (Fujiwara et al., 2011), bacterial spot in citrus (Balogh et al., 2008), and bacterial blight in leek (Rombouts et al., 2016). In the context of phage biocontrol targeting gall disease-causing bacteria, phage Atu_ph02, isolated from wastewater, showed the ability to subdue *Agrobacterium* in potato discs (Attai et al., 2017). Recently, phage OLIVR 1 to 6, isolated from tomato greenhouses, demonstrated the inhibitory effect against *Agrobacterium* biovar 1 strain in a hydroponic solution (Fortuna et al., 2023). In addition, a commercially successful phage treatment, AgriPhage™, has been used in agricultural field to control *Xanthomonas campestris* or *Pseudomonas syringae* in Tomato (Ly-Chatain, 2014). However, in the case of gall disease, neither phages nor chemicals can penetrate the shell of galls once they have developed. Phages, however, manifest potential as biocontrol agents because they can enter through the roots of the plants and be applied directly to soil to inhibit target pathogens (Buttimer et al., 2017). In addition, to the best of our knowledge, the application of phage biocontrol to manage stem gall disease-causing bacterium in blueberry has not been explored. Therefore, the objectives of this study were to optimize isolation techniques and isolate phages from natural environment, characterize the selected phages for efficacy against *R. radiobacter,* and evaluate their inhibitory effect against *R. radiobacter* in a soil/peat-based system.

2 Materials and methods

2.1 Bacterial strains and growth conditions

The *Rhizobium* strains, previously isolated from blueberry farms, were used as the host strains for phage isolation in this study (Table 1). In addition, *R. radiobacter* ATCC 25235 and *R. radiobacter* ATCC 33970 from the American Type Culture Collection (ATCC) were used as a control. All strains were stored at −80°C in nutrient broth (NB; BD/Difco, East Rutherford, NJ, United States) supplemented with a final concentration of 20% glycerol. For working stocks, all *R. radiobacter* strains were grown at 28 ± 2°C in nutrient agar (NA; BD/Difco, East Rutherford, NJ, United States). For each experiment, new sets of bacterial cultures were prepared by inoculating a single colony into 10 mL of NB and incubating at 28 ± 2°C and 150 rpm for 24 h on an orbital shaker (311DS, Labnet, Edison, NJ, United States).

2.2 Phage isolation and purification

Isolation of phages was performed with modifications of previously published protocols (Mendum et al., 2001; Halmillawewa et al., 2015; Fong et al., 2017). Strains of *R. radiobacter,* as listed in Table 1, including *R. radiobacter* ATCC 25235 and *R. radiobacter* ATCC 33970, were used as hosts for the isolation of phages. Briefly, 20 g of samples from the soil collected from the vicinity of stem gall infected blueberry plants, 20 mL water samples from drainage ditches in stem gall infected blueberry farms, and 20 mL of sewage influent from waste water treatment plant in metro Vancouver region were prepared by adding 20 mL of 2X NB and a cocktail of 400 µL of sets of five overnight cultures of *Rhizobium* strains of the 28 strains at a time as hosts were placed in 50 mL centrifuge tubes. The samples were incubated in a shaker at 150 rpm and 28 ± 2°C for 24 h. Then, the supernatant was centrifuged at 4,000 *x g* for 10 min and filtrated through a 0.45 µm filter (Cytiva, Marlborough, MA, United States). A 100 µL aliquot of the filtrate was mixed with 300 µL of an overnight culture of each of the 28 *Rhizobium* strains and 4 mL of 0.7% NB agar in 90 mm Petri dish using the double agar overlay technique (Kropinski et al., 2009).

The plates were incubated at 28 ± 2°C for 24–48 h to visualize plaque activity in the bacterial colonies. Upon observing the presence of plaque activity, plaques were removed from the agar surface using a sterile inoculating loop and suspended in 200 µL of SM buffer (100 mM NaCl, 8 mM $MgSO_4.7H_2O$, 50 mM Tris-Cl pH 7.5, and dH_2O). The suspension was left at room temperature for at least 6 h.

TABLE 1 *Rhizobium* strains used in this study.

Strain	Species	Source
Bn18	*Rhizobium rhizogenes*	Blueberry
Bn37	*Rhizobium radiobacter*	Cucumber
Bn38	*Rhizobium radiobacter*	Cucumber
Bn42	*Rhizobium rhizogenes*	Blueberry
Bn46	*Rhizobium rhizogenes*	Blueberry
14736-1	*Rhizobium rhizogenes*	Blueberry
14736-2	*Rhizobium rhizogenes*	Blueberry
M11	*Rhizobium rhizogenes*	Blueberry
M13	*Rhizobium rhizogenes*	Blueberry
Edr1-6	*Rhizobium rhizogenes*	Blueberry
M22	*Rhizobium rhizogenes*	Blueberry
M26	*Rhizobium rhizogenes*	Blueberry
M29	*Rhizobium rhizogenes*	Blueberry
M30	*Rhizobium rhizogenes*	Blueberry
M33	*Rhizobium radiobacter*	Blueberry
M35	*Rhizobium rhizogenes*	Blueberry
PL3	*Rhizobium radiobacter*	Blueberry
PL8	*Rhizobium rhizogenes*	Blueberry
PL9	*Rhizobium rhizogenes*	Blueberry
PL10	*Rhizobium rhizogenes*	Blueberry
PL11	*Rhizobium rhizogenes*	Blueberry
PL12	*Rhizobium rhizogenes*	Blueberry
PL13	*Rhizobium rhizogenes*	Blueberry
PL14	*Rhizobium rhizogenes*	Blueberry
PL15	*Rhizobium rhizogenes*	Blueberry
PL16	*Rhizobium rhizogenes*	Blueberry
PL17	*Rhizobium radiobacter*	Blueberry
25235S	*Rhizobium radiobacter*	Potato
25235L	*Rhizobium radiobacter*	Potato
33970	*Rhizobium radiobacter*	Cherry gall

Double agar overlay technique was used with the suspension from the previous step for phage purification. To obtain a pure plaque, this step was repeated at least 5 times, and the purified phages were stored in SM buffer at 4°C for long-term storage.

2.3 Host range assessment

The assessment of host range of the isolated phages (76 isolates) was performed as described by Kutter (2009) with some modifications. Phage ATCC 25235b and 25236b were served as positive controls as they have been proven to target *R. radiobacter*. Briefly, 5 µL aliquots of ~10^6 PFU/mL of each of the 76 phages from the phage collection were spotted on the lawn of *Rhizobium* host in duplicate in Petri dish. The phage droplets were allowed to air dry under a biosafety cabinet and then incubated at 28 ± 2°C. After 24 h, the zones of lytic activity on the lawn of *Rhizobium* hosts were recorded using a scale of 0–4, where 0 = no activity and 4 = complete lysis. The assessment of host range and lytic activity of the phages was done in triplicate.

2.4 Lysis efficacy of *Rhizobium* phages in broth

The overnight-grown cultures of *R. radiobacter* hosts were prepared as previously mentioned in the section 2.1 "Bacterial strains and growth conditions." After centrifugation at 4000 ×*g* for 10 min, the cell pellets were washed three times with fresh NB and adjusted to a final concentration of 5×10^6 CFU/mL. Then, 50 µL aliquots of the cultures were transferred into a 96-well plate and treated with the 12 selected phages (IG09, IG14, IC12, IG49, IG57, IG58, AN01, LL05, LL09, LG08, LL11, and LL10) at the multiplicity of infection (MOI) of 100 PFU/CFU. Plates were placed into a plate reader (SpectraMax M2, Molecular Devices, Sunnyvale, CA, United States) set to 25°C and the cell density measurements (OD_{600}) were taken every 6 h for 48 h. Each experiment was independently done in duplicate.

2.5 Transmission electron microscopy

Morphology of the phage isolates was identified using negative staining transmission electron microscopy (TEM). The method was performed as previously described by Alexeeva et al. (2018) with some modifications. Briefly, a high concentration of the phage lysates (~10^{11} PFU/mL) was centrifuged at 4°C for 1 h at 21130 ×*g*. The supernatant was carefully discarded, retaining the last 100 µL of the phage suspension. Subsequently, 1.5 mL of 0.1 M sterile ammonium acetate was added to the suspension and centrifuged at 4°C for 1 h at 21130 ×*g*. This step was repeated twice. After concentration, the purified phage suspension was applied to carbon coated copper grids (Ted Pella, Redding, CA, United States) followed by glow-discharge and then stained with 0.5% uranyl acetate. The phage images were taken using a Tecnai Spirit TEM (Fei company, Hillsboro, OR, United States) at an accelerating voltage of 80 kV.

2.6 Single-step growth curves

The single-step growth curve was used to determine the latent period and burst size of the phages in their respective hosts. Briefly, 1 mL of bacterial host corresponding to the phage amplification was diluted to 10^8 CFU/mL using a calibration curve. Subsequently, the phages (IC12, IG49, AN01, LG08 or LG11) were individually added to an MOI equal to 0.01 or approximately 10^6 PFU/mL. After allowing the phage to attach to the host for 5 min, unattached phages were removed by centrifuging at 4°C for 10 min at 4000 ×*g*. The supernatant was discarded, and a 1 mL aliquot of NB was added to resuspend the pellet. Immediately, the co-culture was incubated at room temperature and enumerated at 10-min intervals for 150 min. The assay was performed in triplicate.

2.7 Temperature and pH stability assay

The stability of the five most potential phages was examined in order to determine their viability under different pH and temperature

conditions. For the pH stability test, the phages, IC12, IG49, AN01, LG08 and LG11, were diluted to ~10^6 PFU/mL in SM buffers at pH 4, 6 and 8, and incubated at 22°C. Similar to the evaluation for the stability of the phages at various pH, phages were diluted in SM buffer at ~10^6 PFU/mL and placed at 4, 22, and 37°C. To test the stability of the phage suspensions at −20°C, phages were aliquoted into 100 µL portions and placed in microcentrifuge tubes to prevent the freeze–thaw cycle. The concentrations of the phages were assessed on days 0, 1, 3, 5, 7, 10, 15, 20, 25 and 30. All experiments were done in triplicate.

2.8 DNA extraction and sequencing

Total genomic DNA from 71 phage isolates was extracted using the Norgen Biotek Phage DNA isolation kit (Norgen Biotek, ON, Canada) following the manufacturer's specifications with some modifications. Briefly, 1 mL of high concentration of phage lysates (~10^9–10^{11} PFU/mL) was treated with the DNase 1 kit (Norgen Biotek) to degrade host nucleic acid, following manufacturer's instructions, and lysis buffer was added to the phage lysates and incubated at 65°C for 30 min. Afterward, the phage lysates were washed and eluted as per manufacturer's instructions.

The DNA library was constructed using Nextera XT DNA Library Preparation Kit (Illumina, Hayward, CA, United States) according to manufacturer's instructions and high-throughput sequencing was performed using Illumina MiSeq platform (Illumina).

2.9 Genome analysis

Contigs obtained from Illumina MiSeq were quality-checked using FastQC (Andrews, 2010) and low-quality reads were trimmed with Trimmomatic (Bolger et al., 2014). High quality paired-end reads were assembled into single circular contigs via Unicycler (Wick et al., 2016). The quality and %GC content of the genome assemblies were assessed using QUAST (Mikheenko et al., 2018). Open reading frames (ORFs) were identified and annotated with Pharokka using the Phanotate gene predictor (Bouras et al., 2022). Antimicrobial resistance genes and virulence genes were screened with ABRicate using Resfinder and VFDB database (Seemann, 2016), respectively. The phage life cycle was determined with Bacphlip (Hockenberry and Wilke, 2021). The completed phage genome was searched against other phage nucleotides using BLASTn of National Center for Biotechnology Information (NCBI) database. For phylogenetic tree, complete phage nucleotide sequences were aligned using ClustalW algorithms (Larkin et al., 2007) and the phylogenetic tree was constructed by the Maximum-Likelihood method using IQ-tree with 1,000 bootstrap replicates (Nguyen et al., 2014). The phylogenetic tree was visualized using iTOL (Letunic and Bork, 2021).

2.10 Application of a phage cocktail in artificially contaminated soil

A soil/peat-based (hereafter referred to as soil-based) *R. radiobacter* system was used to evaluate the efficacy of a phage cocktail (IC12, IG49, and LG08) *in vitro*. Soil-based substrate was obtained from Sun Gro Horticulture® (MA, United States) that comprised 65–75% Canadian Sphagnum peat moss, perlite, dolomite lime, and a wetting agent. An overnight culture of *R. radiobacter* PL17 was centrifuged at 4000 *x g* for 10 min and washed three times with NB. Parallelly, 1 g of the autoclaved soil-based substrate was added to a 50 mL centrifuge tube, and 5 mL of the *R. radiobacter* was inoculated to the soil-based substrate at a final concentration of 10^6 CFU/mL. For the treatment group, an equal amount of phage cocktail (IC12, IG49, and LG08) or phage IG49 was added after the bacterial host reached an MOI of 100. Soil-based substrate added with 10 mL of 0.1% peptone water (PW) was used as a control group to check the background. In addition, the phage cocktail was added to the soil-based substrate as a phage quality control. Tubes were incubated at 22°C and 200 rpm for three days. At each 24-h interval, a 1-mL suspension was diluted in 0.1% PW and plated onto NA. Plates were incubated at 22°C- for 48–72 h and *R. radiobacter* colonies were enumerated. The experiment was done in triplicate.

2.11 Statistical analysis

All statistical tests were conducted using GraphPad Prism 9.2 (GraphPad Software, Inc., San Diego, CA, United States). For the phage stability tests, Student's *t*-test was used to compare the means of two study groups. To compare multiple biocontrol treatments at the same time point, a one-way and two-way analysis of variance (one-way/two-way ANOVA) was conducted. All statistical analysis was performed at the significance level (α) at 0.05.

3 Results

3.1 Phage isolation and host range determination

A total of 105 phages based on the lysis of *Rhizobium* as host were isolated from the sewage samples, with only 76 phages (72.38% recovery rate) were successfully recovered and confirmed to be stable after five times purification and stored at 4°C at least 30 days. Notably, no phages were isolated from either soils or drainage water samples from gall disease-infected blueberry fields. The majority of the phages were recovered with the *Rhizobium* host M11, M13, M22, M30, M35, Edr1-6, PL8, PL9, PL14, PL15, and PL17.

The host range of the 76 phage isolates was assessed against 28 strains of *Rhizobium*, including *R. radiobacter* ATCC 25235 and ATCC 33970 (Figure 1). Among these phages ($n = 76$), 18/76 (23.68%) showed the ability to lyse at least 15/28 (53.57%) *Rhizobium* strains and 10/76 (13.16%) phages exhibited the ability to lyse at least 21/28 (75%) *Rhizobium* strains. However, only two phages (LL05 and LL13) exhibited lytic ability against *R. radiobacter* isolate PL3. None of the phages were able to lyse *R. radiobacter* ATCC 33970 on the spot test. Based on the host range determination, only 12 phages were selected for further assessment.

3.2 Assessment of phages for lytic activity in broth

In order to identify the most effective single phages for designing an effective phage cocktail against *R. radiobacter*, 12 individual phages were tested against *R. radiobacter* isolate PL17 at a MOI of 100 PFU/

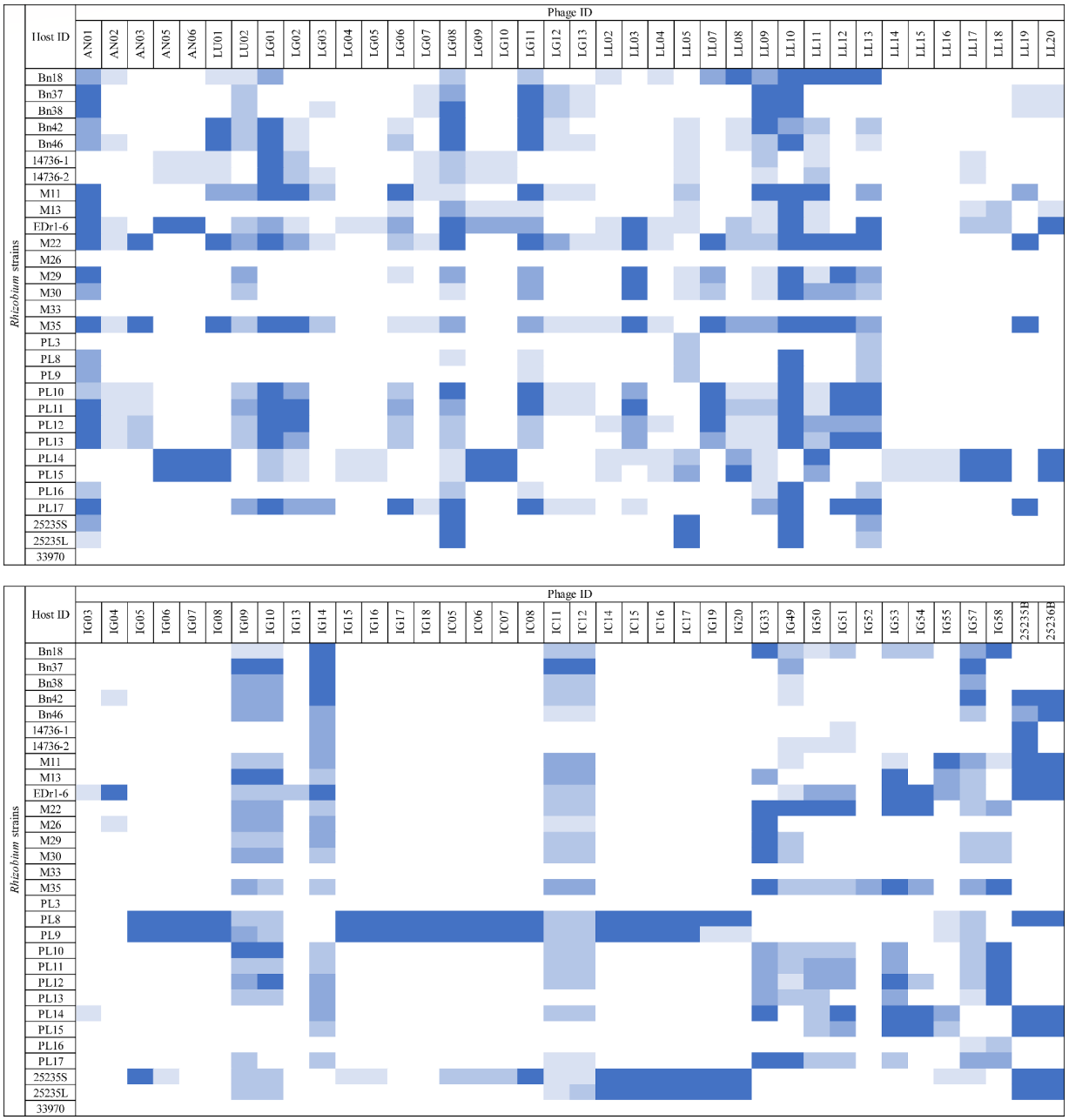

FIGURE 1
Host range assessment of phages. *Rhizobium* isolates susceptible to lytic phages were determined by the inhibition zones (□ = no lysis, ■ = low lysis, ■ = medium lysis, ■ = almost complete lysis, and ■ = complete lysis).

CFU at 25°C (Figure 2). The lytic activity of each phage was assessed based on its ability to either delay or inhibit the bacterial growth. The growth of *R. radiobacter* PL17 began to increase after 12 h. During that period, the treatment with phage LL09 did not suppress the growth of *R. radiobacter* PL17, while the other phages displayed inhibitory effects. By 18 h, treatments with single phage IG09, IG14, IC12, IG49, IG57, IG58, AN01, LG08, LG11 and LL10 showed a significant reduction ($p < 0.05$) when compared to the no-phage treatment. During the period of 24 h, the lytic ability of single phage IG09 and IG14 began to diminish, and no longer delayed the growth of *R. radiobacter* PL17. After 36 h, only the treatments with single phage IC12, IG49, IG57, LG08 and LL05 showed a significant decrease ($p < 0.05$) in the growth of *R. radiobacter* PL17. Only the treatment with phage IG49 completely inhibited the growth of *R. radiobacter* PL17 for 48 h, while the treatment with single phage IG57, LG08 and LL05 delayed the growth of the bacterium for 48 h. To qualitatively compare the inhibitory effect of each phage on the 28 *Rhizobium* isolates in a broth system, single phage-host efficacy graphs were converted to a heatmap, as shown in the Supplementary Figure S1.

To assess the synergistic effect of the phages in a broth-based system, various combinations of three- and four-phages cocktails consisting of the 5 most effective phages, based on the single phage efficacy results, were tested against *R. radiobacter* PL17 (Figure 3). All combinations of three- and four-phage cocktails were effective during

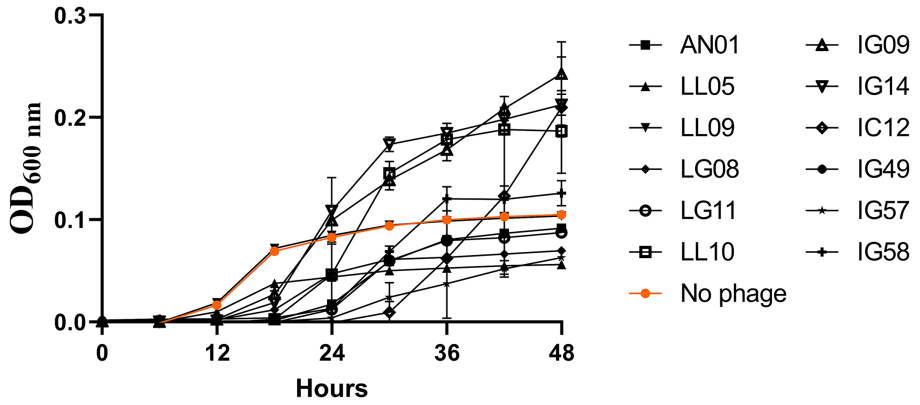

FIGURE 2
Single phage efficacy against *Rhizobium radiobacter* PL17 at MOI = 100.

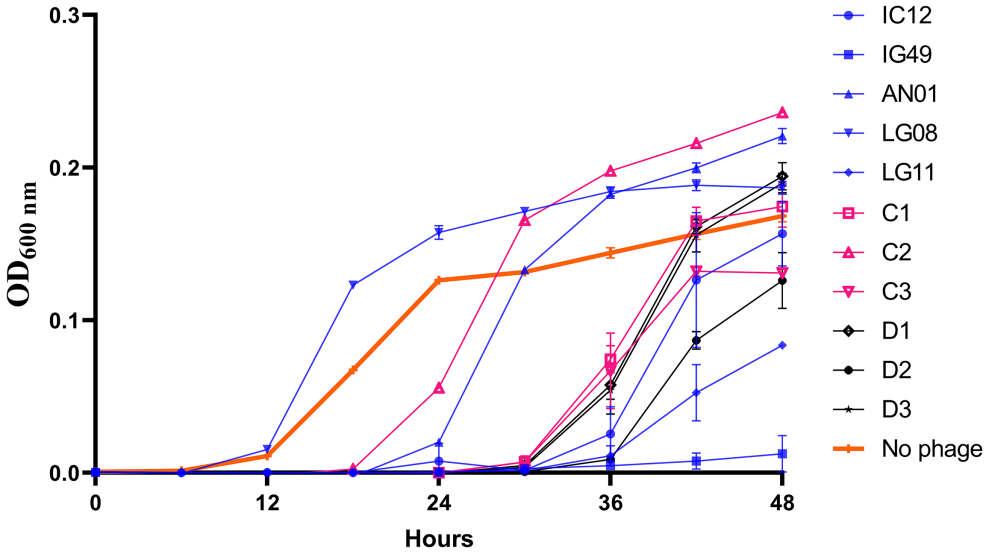

FIGURE 3
Efficacy of a combination of phage cocktail against *Rhizobium radiobacter* PL17 at MOI = 100. C1 – IG49, LG08 and IC12; C2 – IG49, LG08 and AN01; C3 – IG49, LG08 and LG11; D1 – IG49, LG08, IC12 and AN01; D2 – IG49, LG08, IC12 and LG11; D3 – IG49, LG08, AN01 and LG11. *Colored graph indicates the number of phages in each formulation. Blue is a single phage; Pink is a three-phage cocktail; Black is a four-phage cocktail.

the first 24 h, and thereafter the lytic activity began to decrease after 36 h. At 48 h; it appeared that only the treatments with three-phage cocktail (IG49, LG08, and LG11; C3) and the four-phage cocktail (IG49, LG08, IC12, and LG11; D2) were effective in delaying the growth of *R. radiobacter* PL17.

3.3 General characterization of phages

3.3.1 Latent period and burst size

The single-step growth curve was used to study the activity of phage amplification within the host cell, allowing to identify both latent period and burst size of the phages (Figure 4). These parameters are crucial for determining the most effective candidate phages to formulate different combinations of phage cocktail, aimed at assessing their efficacy against *R. radiobacter*. The latent period indicates the time taken for phages to propagate within the host cells, leading to the release of phase progenies upon cell lysis. The observed latent periods for the phages IC12, IG49, AN01, LG08 and LG11 were 110, 100, 90, 90 and 80 min, respectively. The burst size, calculated by the difference in the phage titer just after host lysis, determined the number of progenies produced per infected host cell. The burst size of IC12, IG49, AN01, LG08 and LG11 was determined as 14, 33, 9, 4 and 8 phages per infected host cell, respectively.

3.3.2 pH and temperature stability

The survivability of phage IC12, IG49, AN01, LG08 and LG11 at different temperatures is shown in Figure 5. The 30-days storage period was chosen to assess the lytic activity over storage time and for potential phage application in field trials. None of the five phages were able to survive at −20°C (Figure 5A). Phages IC12, IG49,

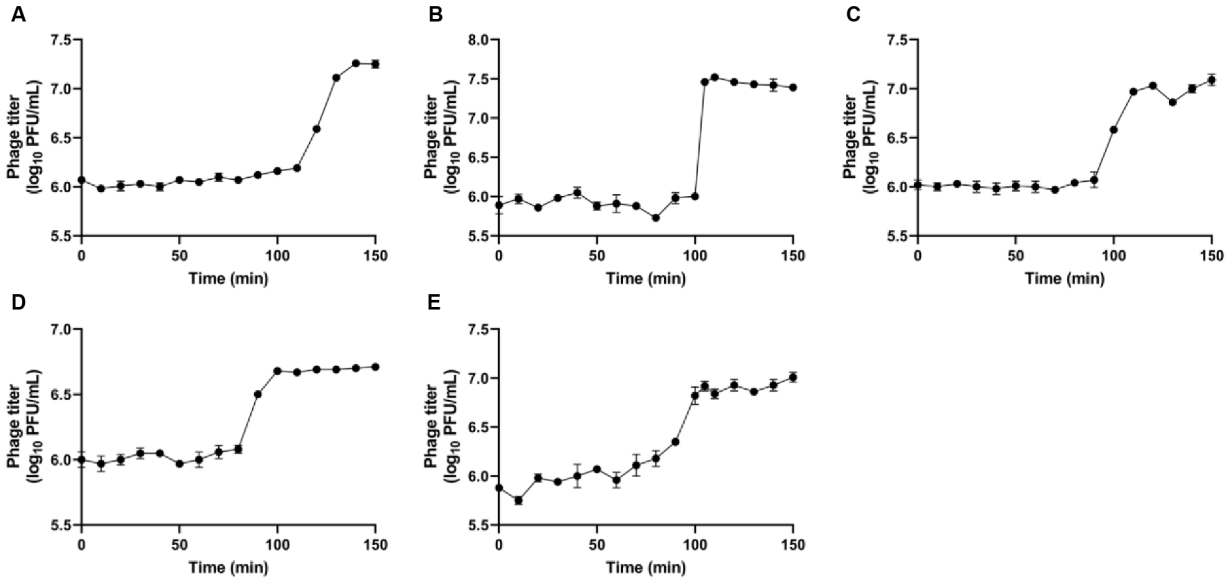

FIGURE 4
Single-step growth curves of the phages **(A)** IC12, **(B)** IG49, **(C)** AN01, **(D)** LG08, and **(E)** LG11. Data shown are the mean of three replicates ± SD.

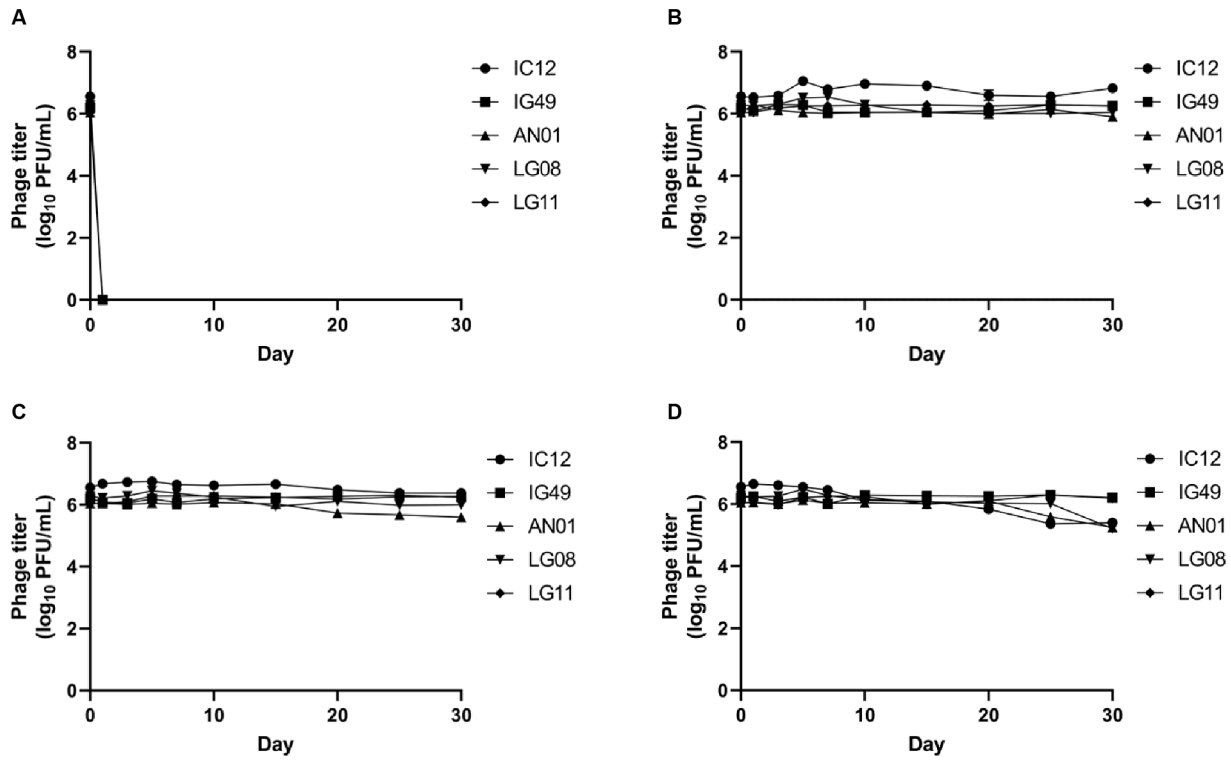

FIGURE 5
Stability of phage IG12, IC49, AN01, LG08, LG11 at **(A)** −20°C, **(B)** 4°C, **(C)** 22°C, and **(D)** 37°C over 30 days.

AN01, LG08 and LG11 were significantly ($p > 0.05$) stable at 4°C (Figure 5B) and 22°C (Figure 5C) for 30 days. However, at 37°C, the concentration of phage IC12, AN01 and LG08 was reduced by 1 $\log_{10}$ PFU/mL after 30-day of storage, while phages IG49 and LG11 remained significantly ($p > 0.05$) stable at 37°C (Figure 5D). These results suggested that these five phages remained stable at 4–37°C during 30 days of storage.

The concentrations of phages IC12, IG49, AN01, LG08 and LG11 at pH 4, 6 and 8 after 30 days of storage are presented in Figure 6. At pH 4 and 6, phages IC12, IG49, and AN01 remained stable throughout

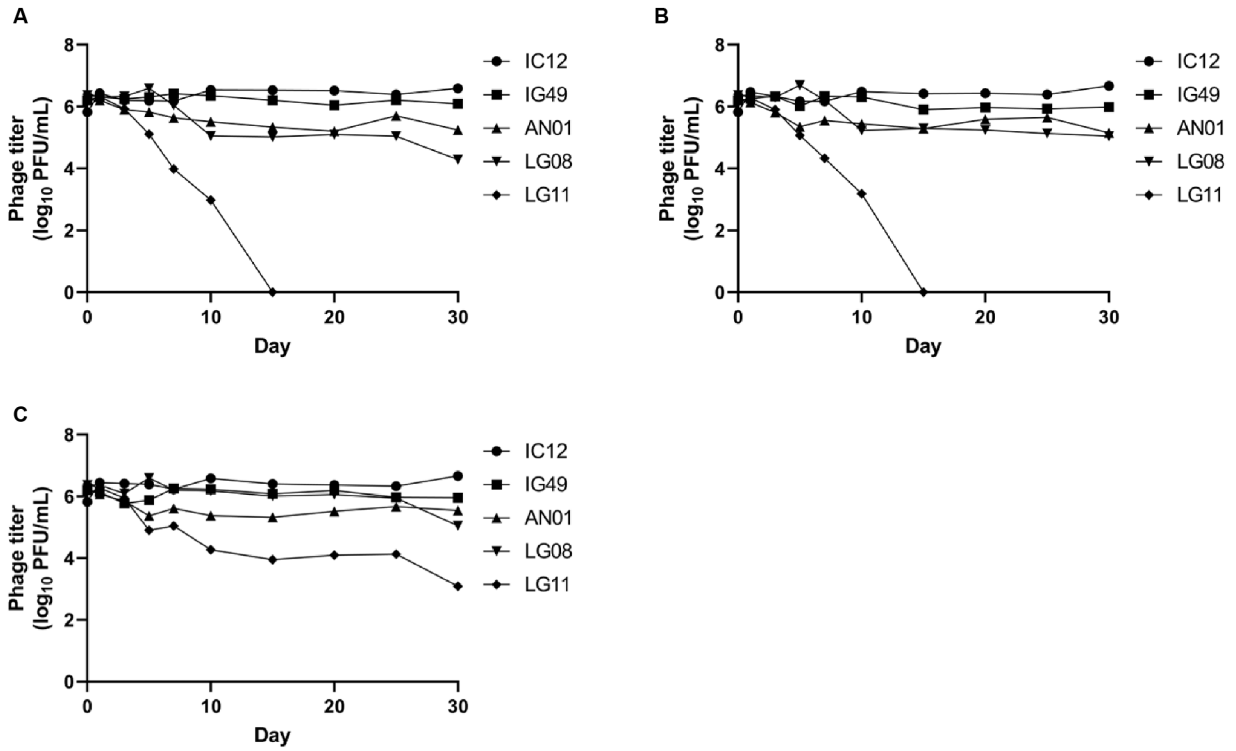

FIGURE 6
Stability of phage IG12, IC49, AN01, LG08, LG11 at **(A)** pH 4, **(B)** pH 6, and **(C)** pH 8 over 30 days.

the 30 days, while the concentration of phage LG08 slightly decreased by day 30. Phage LG11, however, declined from 10^6 PFU/mL to 10^4 PFU/mL starting on day 7 and thereafter rapidly declined to undetectable levels after 15 days. At pH 8, all phages except LG11 remained stable over 30 days. Phage LG11 significantly decreased ($p < 0.05$) from 10^6 PFU/mL to 10^4 PFU/mL after 10-day of storage, then remained stable until day 25, before decreasing to 10^3 PFU/mL by the end of storage period. These results suggest that phage LG11 is the least stable biocontrol agent in acidic conditions, while other candidate phages remained stable in acidic conditions.

3.3.3 Phage morphology under TEM

The morphology of the phage was revealed through TEM. All five phages isolated from different sewage sources possessed the same structure: an icosahedral head and a long contractile tail, characteristics that classify them under the family *Myoviridae*. The specific length of the head and tail for each phage are illustrated in Figure 7.

3.4 General features of the phage genomes

The complete genome of 71 phages used in the formulation of three phage cocktails for potential biocontrol agents for *R. radiobacter* was obtained through whole-genome sequencing. Phage IC12 (Accession no. PP417939), IG49 (Accession no. PP429226), and LG08 (Accession no. PP429227) have circular dsDNA genomes with the sizes of 150,526 bp, 151,705 bp, and 149,984 bp, and the GC contents of 47.26, 46.86 and 47.12%, respectively.

Genome annotation using Pharokka revealed that phage IC12 contains 255 putative open reading frames (ORFs) and two tRNAs, with 60 annotated and 195 uncharacterized ORFs (Supplementary Figure S2A). These annotated ORFs were classified into four functional elements: phage structural and packaging-related proteins (22 ORFs), DNA-associated proteins (33 ORFs), lysis-associated protein (1 ORFs) and auxiliary genes (5 ORFs). Additionally, no integrase module was found in this phage genome. The genome sequence of phage IC12, aligned with NCBI database, revealed 93% coverage and 94.99% identity with *Agrobacterium* phage OLIVR5 (Accession no. NC_055841.1).

The genome of IG49 consists of 269 ORFs and two tRNAs, with 69 annotated and 200 uncharacterized ORFs (Supplementary Figure S2B). The predicted elements were categorized into four functional elements: phage structural and packaging-related proteins (24 ORFs), DNA-associated proteins (38 ORFs), lysis-associated protein (1 ORFs) and auxiliary genes (6 ORFs). Phage IG49 does not contain any lysogeny-related module such as integrase. The genome of phage IG49 was aligned to *Agrobacterium* phage OLIVR5 (Accession no. NC_055841.1) with the highest of 95% coverage and 96.64% identity.

The genome of LG08 contains 256 ORFs and two tRNAs, with 63 annotated and 193 uncharacterized ORFs (Supplementary Figure S2C). These annotated ORFs were divided into four functional elements: phage structural and packaging-related proteins (24 ORFs), DNA-associated proteins (32 ORFs), lysis-associated protein (1 ORFs) and auxiliary genes (6 ORFs). Phage LG08 also does not contain any lysogeny-related module. The genome of phage LG08 was aligned to *Agrobacterium* phage OLIVR5 (Accession no. NC_055841.1) with 92% coverage and 93.46% identity.

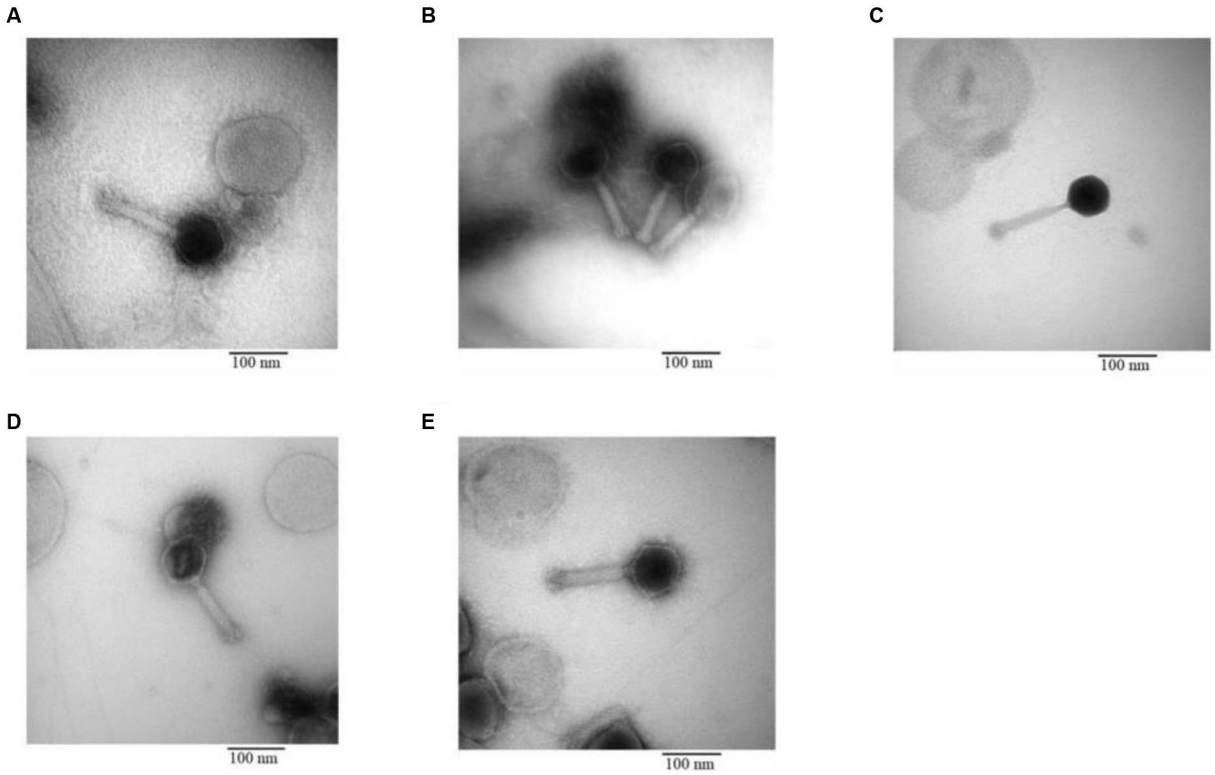

FIGURE 7
Transmission electron microscopy of phage **(A)** IC12, **(B)** IG49, **(C)** AN01, **(D)** LG08, **(E)** LG11.

3.5 Phylogenetic analysis

A Phylogenetic tree was constructed using whole-genome sequencing data from 71 isolates of phages (Figure 8). The complete genomes were searched through Blastn, revealing that most of the phages were belonged to *Autographiviridae* and *Pootjesviridae* (> 50% coverage and 75% identity). Only 17 phages were assigned to unidentified family due to low coverage and %identity. According to the tree, phage IC12, IG49 and LG08 belong to the same family, *Pootjesviridae*, but are located in different branches with a bootstrap value exceeding 70%, indicating the results are reliable. In addition, the life cycle of these phages was predicted through Bacphlip. A total of 22 phages were classified as temperate phages, showing the presence of integrase, recombinase, or transposase, while the majority of the phages was classified as virulent or lytic (probability of having a virulent lifestyle >0.8). Phages IC12, IG49, and LG08 were classified to have a lytic cycle. A search for virulence factors or antimicrobial resistance genes found that none of the phages contained any of these factors, suggesting that these phages possessed potential lytic ability and are safe for use in agricultural systems (Fernández et al., 2019).

3.6 Efficacy of a phage cocktail in reducing *Rhizobium radiobacter* in soil

The lytic ability of the phage cocktail with IC12, IG49, and LG08 to control *R. radiobacter* PL17 in a soil-based substrate was assessed, using an MOI of 100 PFU/CFU as determined by phage lysis efficacy in broth.

Treatment with the phage cocktail resulted in a significant ($p < 0.05$) reduction of 2.9 $\log_{10}$ CFU/g from 8.43 $\log_{10}$ CFU/g of *R. radiobacter* PL17 after 24 h of treatment (Figure 9). Treatment with a single phage (IG49) also resulted in a significant decrease ($p < 0.05$) in the host cells from 8.43 $\log_{10}$ CFU/g to 5.42 $\log_{10}$ CFU/g after 24 h of treatment. Furthermore, treatment with the phage cocktail showed no significant difference ($p > 0.05$) when compared to the treatment with a single phage. After 48 h of treatment, the phage cocktail demonstrated a significant reduction ($p < 0.05$) from 8.98 $\log_{10}$ CFU/g to 7.69 $\log_{10}$ CFU/g of the host cells, while treatment with a single phage showed only a 0.93 $\log_{10}$ CFU/g reduction ($p < 0.05$) in the host cells when compared to the no-phage treatment. However, treatment with the phage cocktail or single phage was not significantly different ($p > 0.05$) from the no-phage treatment after 72 h of treatment.

4 Discussion

The emergence of stem or crown gall disease in blueberry, especially in highbush varieties, has posed a significant challenge for farmers in British Columbia. Knowledge regarding effectively controlling stem or crown gall disease has been lacking. Current methods involve pruning infected branches and root treatment with *A. radiobacter* K84 (Dygall®) at planting. In addition, use of antibiotics or chemicals like copper to control bacterial diseases is restricted, and their intensive use may lead to the development of copper- and antibiotic-resistant strains through processes like horizontal gene transfer (Song et al., 2021). Moreover, these

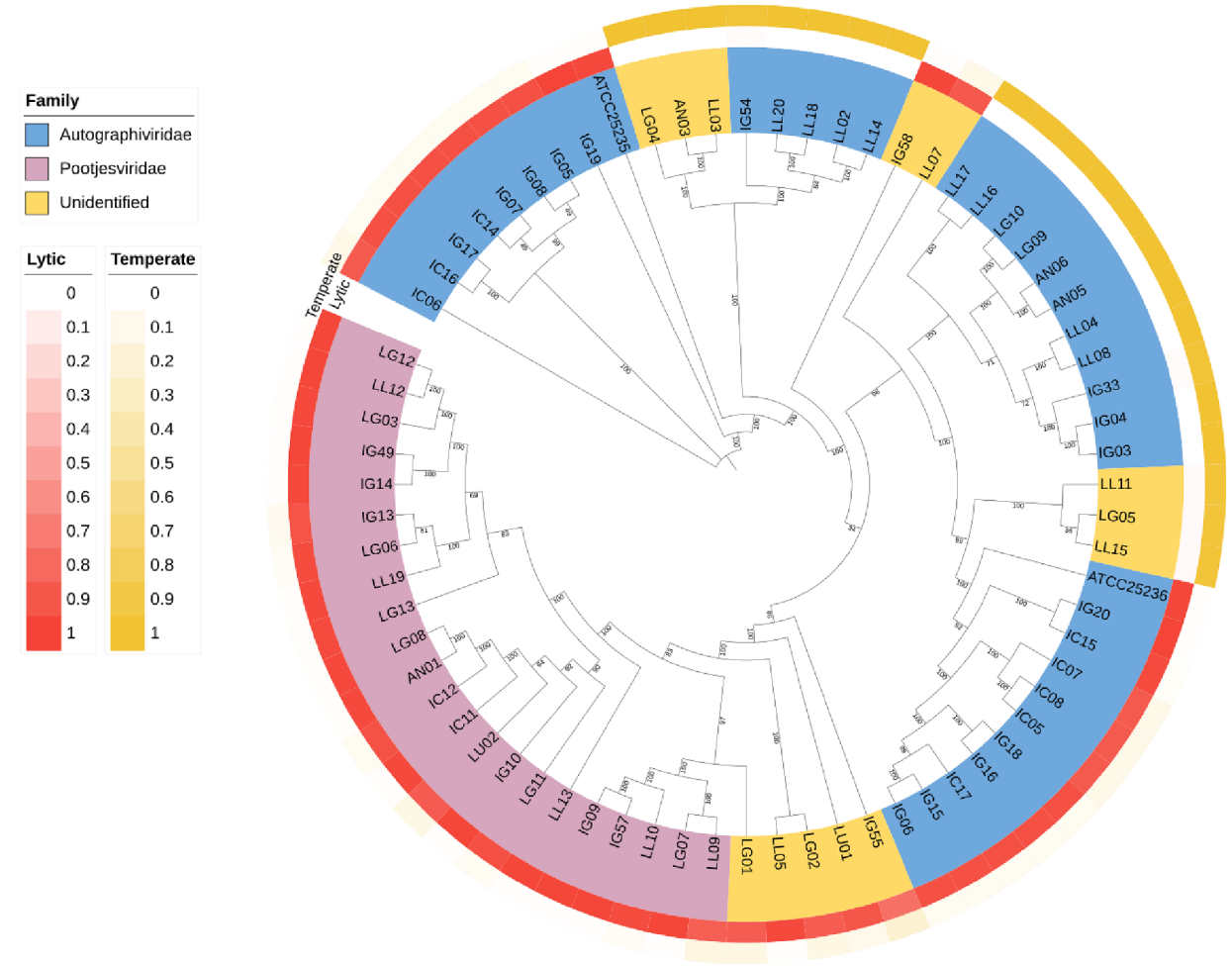

FIGURE 8
Phylogenetic tree of the whole genome sequencing of 71 isolates of phages. The genomic sequences were aligned using ClustalW alignment and the tree was constructed using Maximum-Likelihood method using IQ-TREE with 1,000 bootstrap replicates.

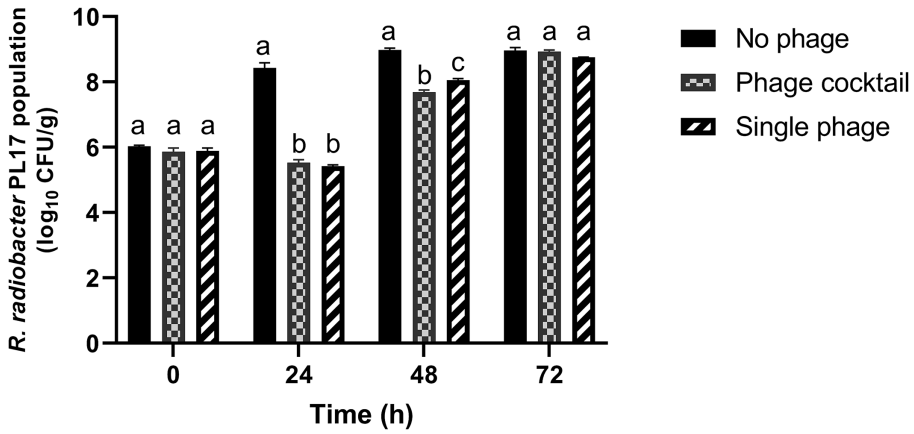

FIGURE 9
Control of *R. radiobacter* PL17 in a soil-based system with the phage cocktail IC12, IG49 and LG08 and single phage IG49. Data shown are the mean of three replicates ±SD. Lowercase letters indicate a significant difference in the bacterial population number ($p < 0.05$).

methods can harm beneficial microbes. Therefore, a phage-based control strategy with high host specificity offers a targeted solution to this issue.

Phages are ubiquitous and can be found in close proximity to their target hosts. In our study, however, *Rhizobium* phages were not found in soil samples collected from blueberry fields infected with stem gall.

This can be contributed to several factors, including a long-term storage of soil samples in the laboratory and the negative effect of ice crystals on phages when samples were frozen during storage. In addition, phages can undergo a lysogenic cycle and become temperate phages at low temperatures (Shan et al., 2014). In the fresh soil samples collected around the blueberry plants with stem gall symptoms and processed immediately after collection, no phages were recovered. It could be due to phages potentially binding to soil particles or presented in low concentrations, making them difficult to extract through centrifugation and filtration. Another possibility could be the absence of *R. radiobacter* as a host in the soil, as phages require a host to coexist and propagate; however, *R. radiobacter,* being a soil-inhabitant, is expected to be present in the infected fields. In addition, isolation of phages was unsuccessful from the water samples collected from a drainage ditch in a blueberry farm with stem gall disease. In a study conducted by Boyd et al., *Rhizobium* phages were successfully recovered from sewage (Boyd et al., 1970). Therefore, sewage appears to be a potential source of *Rhizobium* phages, as evidenced by the recovery of 76 phages in this study.

Previous studies have showed that combinations of lytic phages in a cocktail could overcome phage resistance developed by bacteria and significantly enhance the efficacy in controlling pathogens (Ye et al., 2019). In formulating an effective phage cocktail, factors such as lytic ability, high progeny production, and host specificity need to be considered (Merabishvili et al., 2018; Villalpando-Aguilar et al., 2022). In our study, we identified five candidate phages for the formulation of phage cocktail based on the host range assessment and other characteristics. Single-step growth curves were used to determine how fast a phage replicates in the host cell and the number of progenies produced at the time of lysis. Phage IG49 displayed a burst size of 33 phages per infected cell, higher than the other phages tested, while phage LG08 had a low burst size of 4 phages per infected cell. Although an effective phage-host interaction is expected to have a short latent period and a high burst size (Kalatzis et al., 2016), phage LG08 displayed lytic ability across a wide host range, making it a suitable candidate to be used in the phage cocktail treatment.

The long-term stability of the phages is essential for developing a phage-based biocontrol system that can be readily used in agriculture. The optimal temperature for growing highbush blueberries typically ranges from 20 to 25°C, depending on the cultivar (Hao et al., 2019). For blueberries, optimal soil pH falls between 4.2–5.5. A pH beyond this range can affect the growth, physiological metabolism, and yield of blueberries (Zhou et al., 2022). In our study, phages IC12, IG49, AN01, and LG08 demonstrated stability at pH 4, 6, and 8. However, phage LG11 showed a decrease to below the limit of detection (LOD) after 15 days of storage, indicating the instability of the phage over a period of time. Regarding temperature stability, the selected phages remained stable at 4, 22 and 37°C after 30 days of storage. These results suggest that the phages retained their stability within the expected temperature and pH range that is relevant to the growing conditions of highbush blueberry.

Whole-genome sequencing has been recognized as a method to study the genetic elements of phages, providing insights into their characteristics and safety for both human and environmental applications. Based on our study, none of the candidate phages presented an integrase gene, indicating a probability of being a lytic phage greater than 0.9. Lytic phages do not integrate their genetic material into genome of host bacteria, making them suitable for biocontrol applications (Huss and Raman, 2020). Furthermore, the absence of virulent genes and antimicrobial resistance genes in the genomes confirmed their safe use in agricultural. These findings are important to ensure that the phages selected in this study do not contribute to the development of antibiotic resistance. Based on the phylogenetic tree, phage IC12, IG49 and LG08 could be classified as new members of the *Pootjesviridae* family, with more than 93 percent identity to *Agrobacterium* phage OLIVR5 (accession no. NC_055841.1) (Fortuna et al., 2023). According to Fortuna et al. (2023), the morphology of phages in the *Pootjesviridae* family contain a long contractile tail. The TEM study confirmed the morphology of the three phages, IC12, IG49 and LG08, suggesting a structural analogy to the family *Myoviridae*, and the whole-genome sequencing offers a more in-depth understanding regarding taxonomic classification.

From these characteristics and whole-genome sequencing analysis, a combination of two-, three-, and four-phage cocktail was formulated against *R. radiobacter*. *R. radiobacter* strain PL17 was selected as the model strain due to the presence of *virB* gene cascade, identified by Biolog and whole-genome sequencing (unpublished data). This *virB* gene cascade accounts for delivering T-DNA to plant cells and causing gall disease (Li and Christie, 2018). Phage efficacy results indicated that the ideal phage cocktail formulation would be a 3-phage cocktail system, consisting of IG49, LG08, and IC12. Despite the effectiveness of phage LG11 and AN01 against *R. radiobacter* PL17, they were excluded from the final cocktail due to specific reasons. Specifically, phage LG11 was unstable at different pH levels, and phage AN01 had a host range similar to phage LG08. These considerations highlight the importance of carefully selecting phages to ensure the overall effectiveness and environmental stability of the phage cocktail. The decision to opt for a 3-phage cocktail, rather than a higher or lower number of phages, aims to maintain a balance between efficacy and production costs.

The efficacy of a 3-phage cocktail in the control of *R. radiobacter* PL17 was evaluated in pasteurized soil-based system to eliminate unintended variables such as soil microbes or other living organisms. The phage cocktail showed an inhibitory effect against *R. radiobacter*, resulting in approximately a 3-$\log_{10}$ CFU/g reduction of *R. radiobacter* PL17 after 24 h and a 1.5 $\log_{10}$ CFU/g reduction after 48 h. These results showed that the phages successfully interacted with the bacterial host in the soil-based system. While previous reports suggested that cocktail of phages can synergistically enhance the lytic ability against host cells (Glonti and Pirnay, 2022), our study tested a single phage IG49 against *R. radiobacter* PL17 in the soil-based system. Interestingly, the log reduction of bacterial host cells by the single phage was not significantly different when compared to the efficacy of the 3-phage cocktail. A previous study showed that a single phage (OLIVR1) had the ability to reduce *Agrobacterium* host to below the limit of detection in hydroponic solution, suggesting the potential of phage application in hydroponic greenhouse systems (Fortuna et al., 2023). However, compared to our soil-based system, the effectiveness of phage application could be reduced due to factors such as a high concentration of the bacterial host, designed to represent a highly infected blueberry field, or the composition of the growth substrates. The hydroponic nutrient solution used in the study conducted by Fortuna et al. provided more nutrients when compared to 0.1% peptone and soil solution used in this study. In addition, phage-host interaction plays an important role in phage treatment. In our system, soil characteristics may limit the mobility of bacteria due to water absorption within soil particles. Although *R. radiobacter* is motile, most of phages are non-motile, which limit the interaction between phage and host (Li et al., 2020).

5 Conclusion

The cocktail of the three-phage system comprising of IC12, IG49 and LG08 was chosen based on their efficacy, stability, and the presence or absence of essential genes. This selected phage system exhibited significant inhibitory ability against *R. radiobacter* in a soil/peat-based system, showing a great potential for preventing stem gall disease of blueberry. Further studies on the assessment of efficacy of the phage system against *R. radiobacter* in stem/crown gall *in planta* and infected blueberry fields are crucial to confirm the effectiveness of this biocontrol agent. Overall, the approach discussed is effective for conceptualizing formulation and commercialization of the bacteriophage system, offering potential benefits to the blueberry industry.

Data availability statement

The sequences of phage IC12, IG49 and LG08 have been deposited in the GenBank under accession numbers of PP417939, PP429226, and PP429227, respectively.

Author contributions

BC: Formal analysis, Investigation, Methodology, Visualization, Writing – original draft. SS: Conceptualization, Funding acquisition, Resources, Writing – review & editing. SW: Conceptualization, Funding acquisition, Project administration, Resources, Supervision, Writing – review & editing.

Funding

The author(s) declare financial support was received for the research, authorship, and/or publication of this article. This study was funded by the Canadian Agricultural Partnership, a federal, provincial, and territorial initiative by the Government of Canada, for research and development (project: URA23CP001).

Acknowledgments

We would like to sincerely thank the blueberry farmers in the Lower Mainland, British Columbia who provided access to their farms for sampling and Rob MacArthur from Metro Vancouver Wastewater Treatment Plant for providing us with sewage influence for phage isolation.

Conflict of interest

The authors declare that the research was conducted in the absence of any commercial or financial relationships that could be construed as a potential conflict of interest.

Publisher's note

All claims expressed in this article are solely those of the authors and do not necessarily represent those of their affiliated organizations, or those of the publisher, the editors and the reviewers. Any product that may be evaluated in this article, or claim that may be made by its manufacturer, is not guaranteed or endorsed by the publisher.

Supplementary material

The Supplementary material for this article can be found online at: https://www.frontiersin.org/articles/10.3389/fmicb.2024.1437536/full#supplementary-material

References

Adriaenssens, E. M., Van Vaerenbergh, J., Vandenheuvel, D., Dunon, V., Ceyssens, P.-J., De Proft, M., et al. (2012). T4-related bacteriophage LIMEstone isolates for the control of soft rot on potato caused by '*Dickeya solani*'. *PLoS One* 7:e33227. doi: 10.1371/journal.pone.0033227

Alexeeva, S., Guerra Martínez, J. A., Spus, M., and Smid, E. J. (2018). Spontaneously induced prophages are abundant in a naturally evolved bacterial starter culture and deliver competitive advantage to the host. *BMC Microbiol.* 18:120. doi: 10.1186/s12866-018-1229-1

Aloni, R., and Ullrich, C. I. (2008) in Biology of Crown Gall Tumors BT - Agrobacterium: From Biology to Biotechnology. eds. T. Tzfira and V. Citovsky (New York: Springer), 565–591.

Andrews, S. (2010). FastQC A Quality Control Tool for High Throughput Sequence Data. Available at: http://www.bioinformatics.babraham.ac.uk/projects/fastqc/ (Accessed May 1, 2024).

Attai, H., Rimbey, J., Smith, G. P., and Brown, P. J. B. (2017). Expression of a peptidoglycan hydrolase from lytic bacteriophages Atu_ph02 and Atu_ph03 triggers lysis of *Agrobacterium tumefaciens*. *Appl. Environ. Microbiol.* 83:e01498-17. doi: 10.1128/AEM.01498-17

Balogh, B., Canteros, B. I., Stall, R. E., and Jones, J. B. (2008). Control of citrus canker and citrus bacterial spot with bacteriophages. *Plant Dis.* 92, 1048–1052. doi: 10.1094/PDIS-92-7-1048

Bolger, A. M., Lohse, M., and Usadel, B. (2014). Trimmomatic: a flexible trimmer for Illumina sequence data. *Bioinformatics* 30, 2114–2120. doi: 10.1093/bioinformatics/btu170

Bouras, G., Nepal, R., Houtak, G., Psaltis, A. J., Wormald, P.-J., and Vreugde, S. (2022). Pharokka: a fast scalable bacteriophage annotation tool. *Bioinformatics* 39:btac776. doi: 10.1093/bioinformatics/btac776

Boyd, R. J., Hildebrandt, A. C., and Allen, O. N. (1970). Specificity patterns of *Agrobacterium tumefaciens* phages. *Arch. Mikrobiol.* 73, 324–330. doi: 10.1007/BF00412299

Buttimer, C., McAuliffe, O., Ross, R. P., Hill, C., O'Mahony, J., and Coffey, A. (2017). Bacteriophages and bacterial plant diseases. *Front. Microbiol.* 8:1–15. doi: 10.3389/fmicb.2017.00034

Carter, A. (1989). Decision Document: Order – Eubacteriales family – Enterobacteriaceae Agrobacterium radiobacter. Available at: https://publications.gc.ca/collections/Collection/H113-4-89-02E.pdf

Czajkowski, R., Ozymko, Z., De Jager, V., Siwinska, J., Smolarska, A., Ossowicki, A., et al. (2015). Genomic, proteomic and morphological characterization of two novel broad host lytic bacteriophages ΦPD10.3 and ΦPD23.1 infecting pectinolytic *Pectobacterium* spp. and *Dickeya* spp. *PLoS One* 10:e0119812. doi: 10.1371/journal.pone.0119812

Fernández, L., Gutiérrez, D., García, P., and Rodríguez, A. (2019). The perfect bacteriophage for therapeutic applications—a quick guide. *Antibiotics* 8:126. doi: 10.3390/antibiotics8030126

Fong, K., LaBossiere, B., Switt, A. I. M., Delaquis, P., Goodridge, L., Levesque, R. C., et al. (2017). Characterization of four novel bacteriophages isolated from British Columbia for control of non-typhoidal *Salmonella* in vitro and on sprouting alfalfa seeds. *Front. Microbiol.* 8, 1–14. doi: 10.3389/fmicb.2017.02193

Fortuna, K. J., Holtappels, D., Venneman, J., Baeyen, S., Vallino, M., Verwilt, P., et al. (2023). Back to the roots: *Agrobacterium* -specific phages show potential to disinfect nutrient solution from hydroponic greenhouses. *Appl. Environ. Microbiol.* 89:e00215-23. doi: 10.1128/aem.00215-23

Fujiwara, A., Fujisawa, M., Hamasaki, R., Kawasaki, T., Fujie, M., and Yamada, T. (2011). Biocontrol of *Ralstonia solanacearum* by treatment with lytic bacteriophages. *Appl. Environ. Microbiol.* 77, 4155–4162. doi: 10.1128/AEM.02847-10

Glonti, T., and Pirnay, J. P. (2022). In vitro techniques and measurements of phage characteristics that are important for phage therapy success. *Viruses* 14:1490. doi: 10.3390/v14071490

Gohlke, J., and Deeken, R. (2014). Plant responses to *Agrobacterium tumefaciens* and crown gall development. *Front. Plant Sci.* 5:155. doi: 10.3389/fpls.2014.00155

Guo, H., Glaeser, S. P., Alabid, I., Imani, J., Haghighi, H., Kämpfer, P., et al. (2017). The abundance of endofungal bacterium *Rhizobium radiobacter* (syn. *Agrobacterium tumefaciens*) increases in its fungal host *Piriformospora indica* during the tripartite sebacinalean symbiosis with higher plants. *Front. Microbiol.* 8:629. doi: 10.3389/fmicb.2017.00629

Halmillawewa, A. P., Restrepo-Córdoba, M., Yost, C. K., and Hynes, M. F. (2015). Genomic and phenotypic characterization of *Rhizobium gallicum* phage vB_RglS_P106B. *Microbiology (United Kingdom)* 161, 611–620. doi: 10.1099/mic.0.000022

Hao, L., Guo, L., Li, R., Cheng, Y., Huang, L., Zhou, H., et al. (2019). Responses of photosynthesis to high temperature stress associated with changes in leaf structure and biochemistry of blueberry (*Vaccinium corymbosum* L.). *Sci. Hortic.* 246, 251–264. doi: 10.1016/j.scienta.2018.11.007

Hockenberry, A. J., and Wilke, C. O. (2021). BACPHLIP: predicting bacteriophage lifestyle from conserved protein domains. *PeerJ* 9:e11396. doi: 10.7717/peerj.11396

Huss, P., and Raman, S. (2020). Engineered bacteriophages as programmable biocontrol agents. *Curr. Opin. Biotechnol.* 61, 116–121. doi: 10.1016/j.copbio.2019.11.013

Kalatzis, P. G., Bastías, R., Kokkari, C., and Katharios, P. (2016). Isolation and characterization of two lytic bacteriophages, φst2 and φgrn1; phage therapy application for biological control of *Vibrio alginolyticus* in aquaculture live feeds. *PLoS One* 11, 1–18. doi: 10.1371/journal.pone.0151101

Kropinski, A. M., Mazzocco, A., Waddell, T. E., Lingohr, E., and Johnson, R. P. (2009). "Enumeration of bacteriophages by double agar overlay plaque assay" in Bacteriophages: Methods and Protocols, Volume 1: Isolation, Characterization, and Interactions. eds. M. R. J. Clokie and A. M. Kropinski (Humana Press), 69–76. doi: 10.1007/978-1-60327-164-6_7

Kunkel, B. N., and Harper, C. P. (2018). The roles of auxin during interactions between bacterial plant pathogens and their hosts. *J. Exp. Bot.* 69, 245–254. doi: 10.1093/jxb/erx447

Kutter, E. (2009). Phage Host Range and Efficiency of Plating BT - Bacteriophages: Methods and Protocols, Volume 1: Isolation, Characterization, and Interactions. eds. M. R. J. Clokie and A. M. Kropinski (Humana Press), 141–149. doi: 10.1007/978-1-60327-164-6_14

Kuzmanović, N., Behrens, P., Idczak, E., Wagner, S., Götz, M., Spröer, C., et al. (2019). A novel group of *Rhizobium tumorigenes* -like *agrobacteria* associated with crown gall disease of rhododendron and blueberry. *Phytopathology* 109, 1840–1848. doi: 10.1094/PHYTO-05-19-0167-R

Larkin, M. A., Blackshields, G., Brown, N. P., Chenna, R., McGettigan, P. A., McWilliam, H., et al. (2007). Clustal W and Clustal X version 2.0. *Bioinformatics* 23, 2947–2948. doi: 10.1093/bioinformatics/btm404

Letunic, I., and Bork, P. (2021). Interactive tree of life (iTOL) v5: an online tool for phylogenetic tree display and annotation. *Nucleic Acids Res.* 49, W293–W296. doi: 10.1093/nar/gkab301

Li, Y. G., and Christie, P. J. (2018). "The Agrobacterium VirB/VirD4 T4SS: mechanism and architecture defined through in vivo mutagenesis and chimeric systems" in Agrobacterium Biology. ed. S. B. Gelvin, vol. *418* (Springer International Publishing), 233–260. doi: 10.1007/82_2018_94

Li, X., Gonzalez, F., Esteves, N., Scharf, B. E., and Chen, J. (2020). Formation of phage lysis patterns and implications on co-propagation of phages and motile host bacteria. *PLoS Comput. Biol.* 16:e1007236. doi: 10.1371/journal.pcbi.1007236

Ly-Chatain, M. H. (2014). The factors affecting effectiveness of treatment in phages therapy. *Front. Microbiol.* 5:51. doi: 10.3389/fmicb.2014.00051

Mary Opisa, O., Achwanya, O. S., Otaye, D. O., and Muthamia, J. M. (2020). The efficacy of sterilizing agents, copper oxychloride, vegetable oil and agrowipe (botanic neem extract) against crown gall disease of roses in Kericho, Kenya. *Afr. J. Biol. Sci.* 2:115. doi: 10.33472/AFJBS.2.4.2020.115-121

Mendum, T. A., Clark, I. M., and Hirsch, P. R. (2001). Characterization of two novel *Rhizobium leguminosarum* bacteriophages from a field release site of genetically-modified rhizobia. *Anton. Leeuw. Int. J. Gen. Mol. Microbiol.* 79, 189–197. doi: 10.1023/A:1010238412538

Merabishvili, M., Pirnay, J.-P., and De Vos, D. (2018). "Guidelines to compose an ideal bacteriophage cocktail" in Bacteriophage Therapy: From Lab to Clinical Practice. eds. J. Azeredo and S. Sillankorva (New York: Springer), 99–110.

Mikheenko, A., Prjibelski, A., Saveliev, V., Antipov, D., and Gurevich, A. (2018). Versatile genome assembly evaluation with QUAST-LG. *Bioinformatics* 34, i142–i150. doi: 10.1093/bioinformatics/bty266

Nguyen, L.-T., Schmidt, H. A., von Haeseler, A., and Minh, B. Q. (2014). IQ-TREE: a fast and effective stochastic algorithm for estimating maximum-likelihood phylogenies. *Mol. Biol. Evol.* 32, 268–274. doi: 10.1093/molbev/msu300

Penyalver, R., Oger, P., López, M. M., and Farrand, S. K. (2001). Iron-binding compounds from *Agrobacterium* spp.: biological control strain *Agrobacterium rhizogenes* K84 produces a hydroxamate siderophore. *Appl. Environ. Microbiol.* 67, 654–664. doi: 10.1128/AEM.67.2.654-664.2001

Pulawska, J. (2010). Crown gall of stone fruits and nuts, economic significance and diversity of its causal agents: tumorigenic *Agrobacterium* spp. *J. Plant Pathol.* 92, S87–S98.

Rombouts, S., Volckaert, A., Venneman, S., Declercq, B., Vandenheuvel, D., Allonsius, C. N., et al. (2016). Characterization of novel bacteriophages for biocontrol of bacterial blight in leek caused by *Pseudomonas syringae* pv. Porri. *Front. Microbiol.* 7:279. doi: 10.3389/fmicb.2016.00279

Sawalha, H., Al-Badawi, S., Hamdan, H., and Houshia, O. (2013). Chemical antibacterial agents used to disinfect cultivation tools against the crown gall disease of stone fruits. *J. Biol.* 3, 30–39.

Seemann, T. (2016). ABRicate: Mass Screening of Contigs for Antiobiotic Resistance Genes. Available at: https://github.com/tseemann/abricate (Accessed May 1, 2024).

Shan, J., Korbsrisate, S., Withatanung, P., Adler, N. L., Clokie, M. R. J., and Galyov, E. E. (2014). Temperature dependent bacteriophages of a tropical bacterial pathogen. *Front. Microbiol.* 5, 1–7. doi: 10.3389/fmicb.2014.00599

Song, Z., Zuo, L., Li, C., Tian, Y., and Wang, H. (2021). Copper ions facilitate the conjugative transfer of SXT/R391 integrative and conjugative element across bacterial genera. *Front. Microbiol.* 11:616792. doi: 10.3389/fmicb.2020.616792

Stockwell, V. O., Moore, L. W., and Loper, J. E. (1993). Fate of *Agrobacterium radiobacter* K84 in the environment. *Appl. Environ. Microbiol.* 59, 2112–2120. doi: 10.1128/aem.59.7.2112-2120.1993

Villalpando-Aguilar, J. L., Matos-Pech, G., López-Rosas, I., Castelán-Sánchez, H. G., and Alatorre-Cobos, F. (2022). Phage therapy for crops: concepts, experimental and bioinformatics approaches to direct its application. *Int. J. Mol. Sci.* 24:325. doi: 10.3390/ijms24010325

Wick, R. R., Judd, L. M., Gorrie, C. L., and Holt, K. E. (2016). Unicycler: Resolving bacterial genome assemblies from short and long sequencing reads. *Unicycler: Resolving Bacterial Genome Assemblies From Short and Long Sequencing Reads*. 13:e1005595. doi: 10.1371/journal.pcbi.1005595

Ye, M., Sun, M., Huang, D., Zhang, Z., Zhang, H., Zhang, S., et al. (2019). A review of bacteriophage therapy for pathogenic bacteria inactivation in the soil environment. *Environ. Int.* 129, 488–496. doi: 10.1016/j.envint.2019.05.062

Zhou, Y., Liu, Y., Zhang, X., Gao, X., Shao, T., Long, X., et al. (2022). Effects of soil properties and microbiome on highbush blueberry (*Vaccinium corymbosum*) growth. *Agronomy* 12:1263. doi: 10.3390/agronomy12061263

frontiers | Frontiers in Microbiology

TYPE Original Research
PUBLISHED 03 September 2024
DOI 10.3389/fmicb.2024.1434301

OPEN ACCESS

EDITED BY
Gamaliel López-Leal,
Center for Research in Cellular Dynamics-UAEM, Mexico

REVIEWED BY
Bozena Nejman-Falenczyk,
University of Gdansk, Poland
William C. Nelson,
Pacific Northwest National Laboratory (DOE), United States
Markus De Raad,
Berkeley Lab (DOE), United States

*CORRESPONDENCE
Patrick Hellwig
✉ hellwig@mpi-magdeburg.mpg.de
Dirk Benndorf
✉ benndorf@mpi-magdeburg.mpg.de

RECEIVED 17 May 2024
ACCEPTED 15 August 2024
PUBLISHED 03 September 2024

CITATION
Hellwig P, Dittrich A, Heyer R, Reichl U and Benndorf D (2024) Detection, isolation and characterization of phage-host complexes using BONCAT and click chemistry. *Front. Microbiol.* 15:1434301. doi: 10.3389/fmicb.2024.1434301

Detection, isolation and characterization of phage-host complexes using BONCAT and click chemistry

Patrick Hellwig[1,2]*, Anna Dittrich[3], Robert Heyer[4,5], Udo Reichl[1,2] and Dirk Benndorf[1,2,6]*

[1]Chair of Bioprocess Engineering, Otto-von-Guericke University Magdeburg, Magdeburg, Germany, [2]Bioprocess Engineering, Max Planck Institute for Dynamics of Complex Technical Systems Magdeburg, Magdeburg, Germany, [3]Department of Systems Biology, Institute of Biology, Otto-von-Guericke University Magdeburg, Magdeburg, Germany, [4]Multidimensional Omics Analyses Group, Leibniz-Institut für Analytische Wissenschaften – ISAS – e.V., Dortmund, Germany, [5]Multidimensional Omics Analyses Group, Faculty of Technology, Bielefeld University, Universitätsstraße, Bielefeld, Germany, [6]Department of Microbiology, Anhalt University of Applied Sciences, Köthen, Germany

Introduction: Phages are viruses that infect prokaryotes and can shape microbial communities by lysis, thus offering applications in various fields. However, challenges exist in sampling, isolation and accurate prediction of the host specificity of phages as well as in the identification of newly replicated virions in response to environmental challenges.

Methods: A new workflow using biorthogonal non-canonical amino acid tagging (BONCAT) and click chemistry (CC) allowed the combined analysis of phages and their hosts, the identification of newly replicated virions, and the specific tagging of phages with biotin for affinity chromatography.

Results: Replication of phage λ in *Escherichia coli* was selected as a model for workflow development. Specific labeling of phage λ proteins with the non-canonical amino acid 4-azido-L-homoalanine (AHA) during phage development in *E. coli* was confirmed by LC–MS/MS. Subsequent tagging of AHA with fluorescent dyes via CC allowed the visualization of phages adsorbed to the cell surface by fluorescence microscopy. Flow cytometry enabled the automated detection of these fluorescent phage-host complexes. Alternatively, AHA-labeled phages were tagged with biotin for purification by affinity chromatography. Despite biotinylation the tagged phages could be purified and were infectious after purification.

Discussion: Applying this approach to environmental samples would enable host screening without cultivation. A flexible and powerful workflow for the detection and enrichment of phages and their hosts in pure cultures has been established. The developed method lays the groundwork for future workflows that could enable the isolation of phage-host complexes from diverse complex microbial communities using fluorescence-activated cell sorting or biotin purification. The ability to expand and customize the workflow through the growing range of compounds for CC offers the potential to develop a versatile toolbox in phage research. This work provides a starting point for these further studies by providing a comprehensive standard operating procedure.

KEYWORDS

BONCAT, click chemistry, bacteriophage, biotin, proteomics, LC–MS/MS, host screening, fluorescence

Introduction

Phages are viruses that infect prokaryotes and play a major role in the composition and evolution of microbial communities (Anderson et al., 2011; Heyer et al., 2019b; Howard-Varona et al., 2017; Kristensen et al., 2010; Marsh and Wellington, 1994; Suttle, 2007). Phages are also considered a potential alternative to antibiotics for infection control (Clark and March, 2006; Fernández et al., 2021; Kutateladze and Adamia, 2010; Sieiro et al., 2020). Therefore, the identification and characterization of phages in natural, biotechnological and clinical areas, including patients, is of considerable interest.

So far, DNA sequencing and genome annotation are crucial for phage detection and characterization. However, associating an annotated phage DNA sequence with a corresponding host is challenging (Hwang et al., 2023). Furthermore, DNA sequencing does not cover RNA phages (Fernández et al., 2021; Gregory et al., 2019; Paez-Espino et al., 2016) and cannot distinguish whether a phage genome is expressed or only integrated into the genome of the host cell. Heyer et al., 2019b demonstrated that metaproteomics helps to close these knowledge gaps by analyzing the expression of phage proteins in microbial communities. Nevertheless, analyzing phages in complex microbial communities remains challenging due to their low contribution to the total biomass, the elaborate methods required for phage enrichment and the lack of approaches to co-enrich their hosts.

The enrichment and purification of low-abundant phages and the visualization of phage-host complexes are keys to overcome these limitations. In the past, developments have been made to detect phages together with their hosts by staining the phage genome and by isolating phages attached to their host (Deng et al., 2014; Džunková et al., 2019; Ohno et al., 2012). There have also been attempts to analyze phages with their host at the single cell level (Sakowski et al., 2021). These methods efficiently allow to detect phages and hosts and are used for the sequencing of phage genomes in conjunction with the host genome, making cultivation unnecessary in many cases. However, they often need prior knowledge of phage genomes for fluorescent dye selection and prone to non-specific staining (Low et al., 2020). In general, the adsorption of the phage does not inevitably result in infection (Džunková et al., 2019).

The tagging of phage proteins represents a novel innovative alternative approach that allows the specific identification of newly replicated phages independent of the genome (RNA/DNA) while recognizing important proteins involved in the host infection process. Labeling of proteins, particularly by biorthogonal non-canonical amino acid tagging (BONCAT) and click chemistry (CC), represents a versatile approach to mark phage proteins (Dieterich et al., 2006; Kolb et al., 2001). CC is very flexible as for example, fluorescent dyes of a wide range of wavelengths and affinity markers with different properties can be attached to the proteins, which makes this technology easily adaptable to the existing laboratory equipment.

The bottleneck of this technology is the necessity to cultivate phages and hosts for effective labeling, and it is crucial that the phages are adequately labeled with ncAAs. Hatzenpichler et al. (2014) demonstrated the efficacy of labeling newly synthesized proteins in microbial communities using BONCAT and CC. Pasulka et al. (2018) further extended this approach, utilizing fluorescence microscopy to quantify virulent phage replication. Additionally, a new labeling method called "THRONCAT" shows promise in addressing the issues of insufficient labeling effectiveness in the future (Ignacio et al., 2023).

In this paper we demonstrate successful isolation of phage host complexes from a laboratory culture system and thus provide a basis for possible future applications in microbial ecology. In particular, we present a workflow (Figure 1) that allows to enrich and analyze phage-host complexes. The BONCAT workflow depends on incorporating 4-azido-L-homoalanine (AHA) into newly synthesized phage proteins. Combined with copper-free CC, fluorescent dyes or biotin were attached to AHA-labeled phages without denaturation. Combining BONCAT and CC allowed the detection of phage proteins adsorbed to the host surface and the specific enrichment of labeled phages. The workflow was evaluated using *E. coli* and phage λ as a well-established model system.

Materials and methods

The workflow established is shown in Figure 1. A detailed description of the methods, including a step-by-step standard operation procedure, can be found in Supplementary material S2. Briefly, replication of phage λ was induced with mitomycin C (MMC) and the newly synthesized phage λ proteins were labeled with AHA (Figure 1, step 1 and 2). After centrifugation and filtration of the AHA-labeled phages, CC was used to attach fluorescent dyes or biotin (Figure 1, step 3a and b). Coupling of fluorescent dyes to phages enabled the detection of phages adsorbed to their host cells by fluorescence microscopy and flow cytometry (Figure 1, step 4a). In addition, biotin coupling allowed the purification and enrichment of phages via affinity chromatography (Figure 1, step 4b). This enrichment allowed the detection of the phages by liquid chromatography-mass spectrometry/mass spectrometry (LC–MS/MS). Alternatively, well established approaches for DNA/RNA sequencing could be applied at this step.

Induction and replication of AHA-labeled phages

Escherichia coli K12 (DSM 5911) with genome-integrated phage λ and *E. coli* K12 (DSM 5911) without phage integration were cultured in M9 minimal medium at 37°C and 130 rpm overnight. Overnight cultures diluted to an optical density of 600 nm (OD_{600}) ≈ 0.145 were used as inoculum to start new batches. After incubation of the bacteria for 1 h at 37°C and 130 rpm, 0.5 µg/mL MMC and/or 0.1 mM AHA were added as indicated in Figure 2 and Supplementary Table M1. Samples were taken to monitor bacterial growth, and OD_{600} was measured every hour. After 4 h or 6 h, phage λs were harvested by centrifugation of the culture (3,000 × g, 12 min, 4°C). The supernatant was collected, and samples were adjusted to pH 7 with 1 M

Abbreviations: AF, alexafluor; AHA, 4-azido-L-homoalanine; BONCAT, biorthogonal non-canonical amino acid tagging; CC, click chemistry; CID, collision induced dissociation; CY, cyanin; DBCO, dibenzylcyclooctyne; DDA, data dependent acquisition; DIA, data independent acquisition; EdU, 5-ethynyl-2′-deoxyuridine; FACS, fluorescence activated cell sorting; FASP, Filter Aided Sample Preparation; LC–MS/MS, liquid chromatography-mass spectrometry/mass spectrometry; MMC, mitomycin c; Moi, multiplicity of infection; ncAA, non-canonical amino acids; OD, optical density; PASEF, parallel Accumulation Serial Fragmentation; PBS, phosphate-buffered saline; PSM, peptide spectrum match; Rpm, rounds per minute; RT, room temperature; TIMS, trapped ion mobility spectrometry; TFA, trifluoroacetic acid.

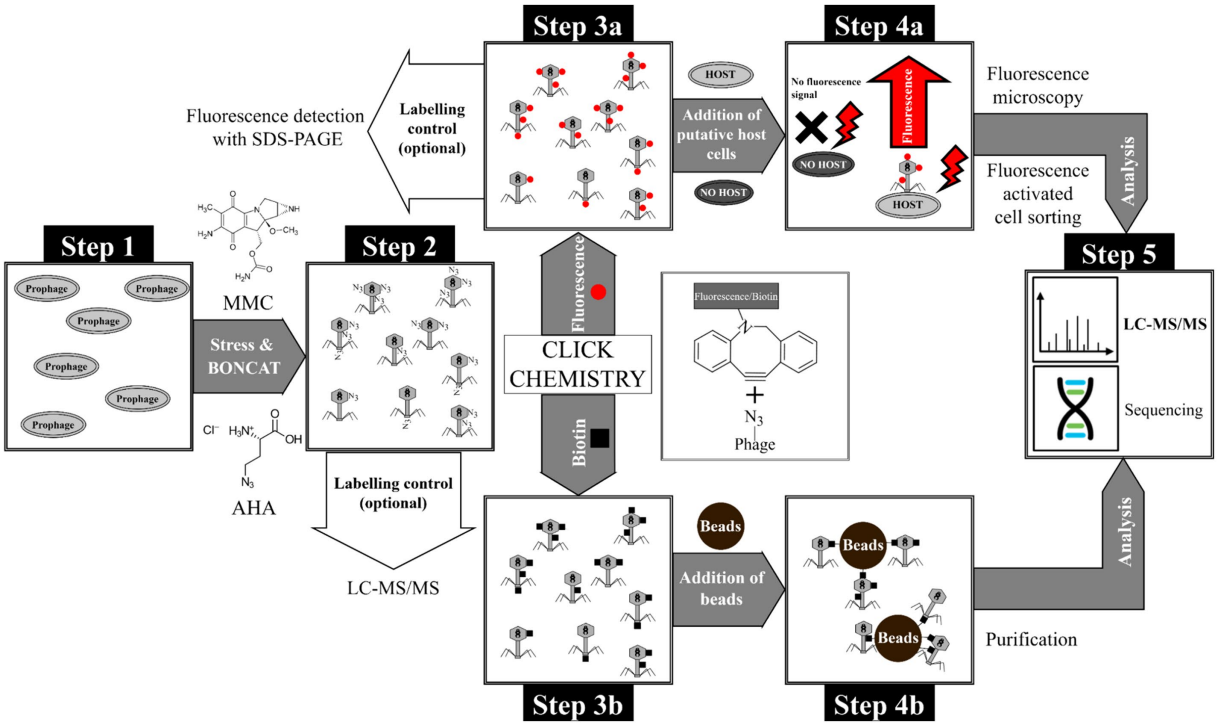

FIGURE 1
Overview of the BONCAT workflow for detection of phages and purification of phage-host complexes. Step 1: Cultivation of *E. coli* with genome-integrated phage λ, Step 2: Induction of phage replication with MMC and subsequent incorporation of the non-canonical amino acid AHA into phage proteins. The incorporation of AHA into newly synthesized proteins was subsequently verified by LC–MS/MS. Step 3: Tagging of AHA-labeled phages with (a) fluorophores or (b) biotin using CC. In-gel detection is possible using a fluorescent dye (after CC) as quality control for CC. Step 4a: Incubation of fluorescent phages with putative host cells and identification/sorting of adsorbed phages by fluorescence microscopy and flow cytometry, respectively. Step 4b: Purification of biotin-labeled phages using magnetic beads (monomeric avidin beads). Step 5: Analysis of purified phages or phage-host complexes by LC–MS/MS or sequencing (not used in this study).

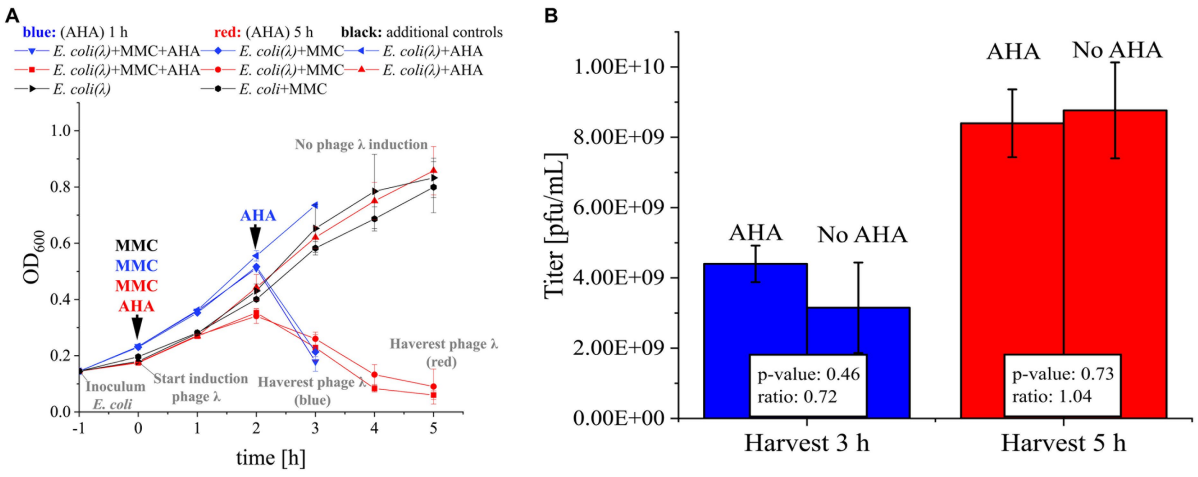

FIGURE 2
MMC induction and AHA labeling of phage λ. **(A)** *E. coli* (DSM 5911, control for toxicity of MMC) and *E. coli* with integrated phage λ (*E. coli* (λ)) were cultivated. The time course of OD_{600} for 3 h (blue) resp. 5 h (red) was recorded. MMC was added to the indicated cultures after 1 h of incubation (0 h). Corresponding cultures were marked with "+ MMC." AHA was added ("+ AHA") at the same time as MMC (AHA 5 h, red) or 1 h before the drop of the OD_{600} (AHA 1 h, blue). In each case, controls were included that were cultivated with MMC only, AHA only, or without either (as indicated)., see Supplementary Protocol S1; **(B)** Phage titer (pfu/mL) determined by plaque assay of the harvested phages from A. Mean and standard deviation of the phage λ titer for three independent experiments; differences in titer not significant ($p > 0.05$; t-test with Benjamini-Hochberg correction). Raw data: see Supplementary Table S1.

NaOH. Next, samples were clarified using a syringe with a filter cascade (5 µm, 1.2 µm, 0.8 µm, 0.45 µM, Sartorius AG). The cell pellets were not further analyzed. For details, see Supplementary Protocol S1.

Plaque-assay

The phage suspensions were sequentially diluted (10^{-6} to 10^{-7}), and 100 µL of each dilution was mixed with 4 mL of melted overlay agar and 100 µL of a fresh overnight culture of *E. coli* K12. Mixtures were poured onto a plate with underlay agar. Hardened agar plates were incubated at 37°C overnight. Based on the number of plaques on plates, the phage titer was calculated: Number of plaques × 10 × reciprocal of dilution = pfu/mL. For details, see Supplementary Protocol S2.

Protein extraction, protein quantification, and sample preparation for LC–MS/MS

Proteins from 4 mL of each phage suspension were extracted with chloroform-methanol. Then, proteins were resuspended in 1 mL 8 M urea buffer. The protein concentration was quantified using amido black assay. 25 µg of total protein was used for Filter Aided Sample Preparation (FASP) digestion with MS-approved trypsin (1:100 µg protein) (Heyer et al., 2019a). The resulting peptide solutions were dried in a vacuum centrifuge and solubilized in 75 µL loading buffer A [LC–MS water and 0.1% trifluoroacetic acid (TFA)]. For details, see Supplementary Protocol S3.

LC–MS/MS

LC–MS/MS analysis was performed using an UltiMate® 3,000 nano splitless reversed-phase nanoHPLC (Thermo Fisher Scientific, Dreieich) coupled online to a timsTOF™ pro mass spectrometer (Bruker Daltonik GmbH, Bremen). For details, see Supplementary Protocol S3.

Identification of AHA incorporation using MASCOT

MS/MS raw data files were processed with the Compass DataAnalysis software (version 5.3.0, Bruker Corporation, Bremen, Germany) and converted to Mascot Generic Files (.mgf). The files were uploaded to MASCOT Daemon (Version 2.6.0) (Perkins et al., 1999) and searched against a filtered UniProt database containing only *E. coli* K12 (taxonomy_id: 83333, 23.03.2023) and *Enterobacteria phage lambda* (taxonomy_id: 10710, 23.03.2023) entities. The following modifications were used: oxidation of methionine, carbamidomethyl, AHA, and reduced AHA (see Supplementary Table M2).

Fluorophore/biotin tagging of BONCAT phages by click chemistry

Phage suspensions were collected on a 100 kDa filter via centrifugation (5 min, 3,500 × g, RT). Afterwards, phosphate-buffered saline (PBS) was added and samples were centrifuged again (5 min, 3,500 × g, RT). 100 mM iodoacetamide in PBS was added, and samples were incubated in the dark at 37°C for 1 h. Afterwards, 0.15 µM dibenzylcyclooctyne (DBCO)-cyanin 5.5 or 0.15 µM DBCO-Alexafluor 555 or 0.15 mM DBCO-PEG_4-biotin were added. Next, samples were incubated in the dark for 30 min at 37°C, washed thrice with PBS, and resuspended in 1 mL PBS. Finally, phage suspensions were transferred to 1.5 mL LoBind® tubes and stored at 4°C in the dark. For details, see Supplementary Protocol S4.

Specific adsorption of labeled phages to host cells

Escherichia coli and *Pseudomonas fluorescens* (DSM 50090) were cultured in standard nutrient broth (Carl Roth, # 1533.1, plus 5 mM $MgSO_4$) at 37°C, 130 rpm overnight. Next, bacteria were diluted with fresh standard nutrient broth in sterile 1.5 mL tubes to 1.80×10^7 cells/mL and incubated for 20 min at 30°C and 600 rpm. Fluorescent phages were added to adjust a multicity of infection (moi) ≈ 2. As a control, only medium was added to the bacteria. 200 µL samples were taken after 0 min, 10 min, 20 min, 30 min, and 60 min. The samples were immediately centrifuged (5 min, 16,400 × g, 4°C). The supernatants of the samples were removed, and cell pellets were immediately fixed with 4% formaldehyde in PBS for 1 h at 4°C. The fixation solution was removed by centrifugation (5 min, 16,400 × g, 4°C). Cells were resuspended in PBS and stored at 4°C. For details, see Supplementary Protocol S4.

Fluorescence microscopy

Phage-host complexes were visualized with an Imager.M1 fluorescence microscope (Carl Zeiss, Jena, Germany) using a 100X objective (EC-Neoflur 100x/1.3 Oil Ph3) and phase contrast. For details, see Supplementary Protocol S4.

Flow cytometry

Flow cytometric analysis was performed using a FACS Canto II equipped with three lasers (405 nm, 488 nm, 663 nm), Firmware Version 1.47 (BD Biosciences, Franklin Lakes, NJ, United States). The data were analyzed with the software FlowJo™ (BD Biosciences,10.8.1). For details, see Supplementary Protocol S4.

Native purification of biotinylated phages via magnetic beads

Biotinylated phages were purified with BcMag™ Monomeric Avidin Magnetic Beads (Bioclone, MMI-101) kit according to the manufacturer's instructions. After binding of the phages, beads were washed with PBS. The supernatant of each washing step was collected for further analysis (fraction "Washing phase"). The biotinylated phages bound to the beads were eluted with 2 mM biotin and collected in a new tube (fraction "Elution"). Lastly, the beads were boiled at 60°C for 5 min with an SDS-buffer, and the supernatant was collected for further analysis (fraction "SDS-boiled"). All fractions were analyzed with an untreated control (fraction "Not purified") with a SDS-PAGE. The phage titer in the "Elution" was also determined with a plaque assay. For details, see Supplementary Protocol S4.

SDS-PAGE

SDS-PAGE was performed with 1 mm SDS-PAGE gels with 12% separation and 4% stacking gel (Laemmli, 1970). For details, see Supplementary Protocol S4.

Staining and scanning of SDS gels loaded with biotinylated or fluorescent proteins

After electrophoresis and fixation, gels with fluorescent proteins were scanned with Licor Odyssey ODY-2600 (LI-COR Biosciences - GmbH) or Typhoon Trio Variable Mode Imager System (GE Healthcare). Subsequently, the gels were counterstained with Coomassie staining solution overnight and scanned with a Biostep ViewPix900 scanner (Seiko Epson Corporation) (Supplementary Table M3). Gels with biotinylated proteins were fixed,

stained with Coomassie, and scanned with a Biostep ViewPix900 scanner (Seiko Epson Corporation) (Supplementary Table M3).

In-gel digestion

The method was performed as described in Heyer, Schallert and Büdel et al., 2019a. For each protein band isolated from an SDS gel, 1 µg of protein content was assumed to calculate the amount of MS-approved trypsin (1 µg trypsin:100 µg protein).

Replicates, biostatistics, and visualization

All experiments were performed in biological triplicates or as indicated. R-Statistics (version 4.1.2) with R studio (version 2021.09.1 Build 372) was used for statistical analysis. Normal distribution was confirmed by the Shapiro–Wilk test; for group-wise differences, a t-test with Benjamini-Hochberg correction was used.

Results and discussion

BONCAT labeling of phage λ in *Escherichia coli*

Efficient phage replication induced by MMC was a critical precondition for the subsequent labeling of phages with AHA. The addition of MMC to exponentially growing *E. coli* resulted in a growth arrest at 2 h and a subsequent decrease of biomass (OD_{600}), indicating cell lysis and phage replication (Figure 2A). Based on OD_{600}, the addition of AHA for labeling did not reduce phage replication. Similar phage titers confirmed this result for incubations with and without addition of AHA (Figure 2B; $p > 0.05$). Earlier harvest (3 h post infection) resulted in lower phage titers, showing that phage replication was still ongoing until final sampling at 5 h.

In summary, AHA addition did neither inhibit the MMC-induced production of phage λ in *E. coli* nor the production and infectivity of phage λ. This is consistent with recent studies investigating the impact of AHA addition on the growth of *E. coli* (Landor et al., 2023; Steward et al., 2020).

Verification of the incorporation of AHA by LC–MS/MS

The successful labeling of proteins with AHA was subsequently confirmed using LC–MS/MS. Here, the incorporation of AHA instead of methionine caused specific mass shifts of tryptic peptides. Overall, LC–MS/MS allowed the assignment of 5,046 ± 1,200 peptide spectrum matches (PSMs) related to phage λ proteins (Figure 3A). After 5 h labeling with AHA, 271 ± 50 PSMs showed incorporation of AHA instead of methionine. Since AHA is incorporated only in place of methionine, the incorporation rate of AHA should be referenced to methionine-containing PSMs (51.82% ± 1.15% of all PSMs). AHA was detected in 5.68% ± 0.23% of all PSMs and in 10.97% ± 0.50% of methionine-containing PSMs. Interestingly, shorter labeling with AHA (1 h) resulted in a similar incorporation rate of AHA (5.24% ± 2.14% of all PSMs) (Figure 3A; Supplementary Table S2), showing that AHA incorporation started soon after addition. Compared to eukaryotic cells, where AHA is only incorporated at 1 out of 400–500 methionine sites (Calve et al., 2016; Kiick et al., 2002; Ngo et al., 2009; van Bergen et al., 2022), the incorporation rate of AHA observed for phage λ was higher. The high incorporation rate of AHA in phage λ proteins has several advantages. A higher incorporation rate provides many reactive sites for subsequent coupling of fluorophores or affinity tags and it may partially compensate for the lower occurrence of methionine in some phages. To further increase the incorporation, the AHA concentration could be further increased (up to 1 mM) or AHA could be added continuously at low concentrations to reduce its impact on the physiology of host cells (Hatzenpichler et al., 2014; Landor et al., 2023; Steward et al., 2020).

Detailed analysis of PSMs allowed to identify 44 ± 1 different phage λ proteins (Figure 3B) associated with the infection cycle. The most abundant phage protein was the major capsid protein, where AHA was incorporated in all methionine positions (Figure 3C). The objective of incorporating AHA should be to provide adequate binding sites for the CC while retaining the functionality of phages. The incorporation of AHA failed only in 1 out of the top 10 identified phage λ proteins (Figure 3B). This result indicates that the high incorporation of AHA may impact the stability or the function of labeled proteins, potentially interfering with the infectivity of the phages (Landor et al., 2023). However, according to the results obtained from plaque assays, labeling with AHA at the given concentration does not significantly affect titers (Figure 2B). Heterogeneity of incorporation of AHA in proteins of phage λ might be caused either by selective incorporation of AHA or by removal of dysfunctional/misfolded proteins after protein synthesis.

During phage-induced cell lysis, the phage harvest may become contaminated with *E. coli* proteins, which could interfere with the subsequent dye or biotin labeling steps of the CC. LC–MS/MS analysis of phage harvest after purification by centrifugation showed the presence of a relatively large number (46,636 ± 11,934 PSMs) of *E. coli* background proteins containing 1.18% ± 0.10% AHA labeled PSMs for 5 h AHA labeling, and 0.38% ± 0.15% AHA labeled PSMs for 1 h AHA labeling. Therefore, shorter labeling with AHA (1 h) in a later phase of infection (2 h after the addition of MMC) should be preferred in situations where labeling of *E. coli* background proteins is detrimental (Figure 3A) despite lower overall labeling efficiency. However, interfering background proteins could also be removed by CsCl centrifugation or PEG precipitation (Boulanger, 2009; Nasukawa et al., 2017; Yamamoto et al., 1970). Nevertheless, every additional purification step might also reduce the yield of phages (Carroll-Portillo et al., 2021).

In summary, both tested AHA incubation periods allowed successful AHA-labeling of the phages. However, the parallel incubation of cells with the phage replication inducer (here MMC) and AHA is more practical, especially for cultures with unknown cell growth dynamics and phage replication kinetics. Therefore, the 5 h incubation period with simultaneous MMC and AHA addition was used in the further course of this study.

Fluorescence tagging of AHA-labeled phages

AHA-labeling was a precondition for the attachment of fluorescent dyes by CC to identify newly synthesized proteins by SDS-PAGE and fluorescence microscopy (Figure 1 Step 3a) (Dieterich et al., 2007; Hatzenpichler et al., 2014; Pasulka et al., 2018).

Previously published protocols for CC apply precipitation with ethanol to remove excess reagents. However, the denaturation of

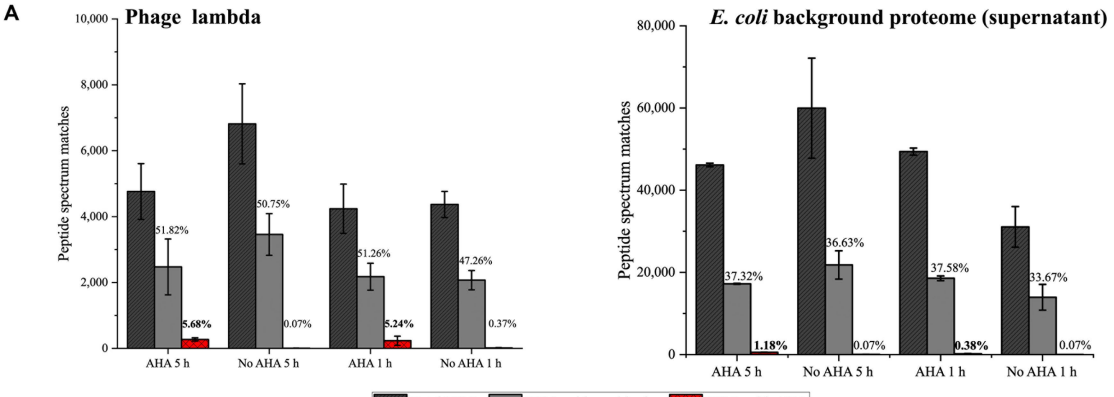

B

Accession	Protein description	Part of the virion	Amino acids	Peptide spectrum matches	Sequence coverage	Number of methionines	Number of AHA Incorporations*
P03713	Major capsid protein	yes	341	1117 ± 265 (130 ± 10 non-duplicate, 988 ± 255 duplicate)	90% ± 1%	13	11 ± 2
C6ZCY7	Tail assembly protein	yes	246	247 ± 20 (26 ± 1 non-duplicate, 221 ± 20 duplicate)	84% ± 1%	6	3 ± 1
A0A0K2FIZ6	Tail fiber protein	yes	774	125 ± 15 (25 ± 2 non-duplicate, 101 ± 13 duplicate)	29% ± 1%	9	0 ± 1
C6ZCY3	Capsid and scaffold protein	no	132	128 ± 22 (20 ± 0 non-duplicate, 108 ± 22 duplicate)	89% ± 3%	3	2 ± 0
P03712	Capsid decoration protein	yes	110	149 ± 25 (31 ± 4 non-duplicate, 118 ± 20 duplicate)	89% ± 0%	3	3 ± 0
P03749	Tip attachment protein J	yes	1132	129 ± 14 (48 ± 5 non-duplicate, 81 ± 10 duplicate)	54% ± 3%	19	1 ± 0
C6ZCX9	Portal protein B	yes	533	92 ± 17 (37 ± 1 non-duplicate, 56 ± 16 duplicate)	69% ± 2%	19	1 ± 1
C6ZCZ0	Tape measure protein	yes	853	88 ± 10 (36 ± 2 non-duplicate, 52 ± 9 duplicate)	56% ± 2%	25	0 ± 0
P03735	Tail assembly protein GT	no	279	109 ± 6 (37 ± 3 non-duplicate, 72 ± 5 duplicate)	70% ± 9%	15	5 ± 1
A0A0K2FI65	Serine/threonine protein phosphatase	no	221	84 ± 12 (22 ± 5 non-duplicate, 62 ± 8 duplicate)	73% ± 11%	5	1 ± 0
	34 ± 1 other lambda phage proteins						

* Different positions of the incorporation of AHA, detected in at least one peptide

C

Major capsid protein

Protein sequence coverage: 91%

Matched peptides shown in ***bold red***.

```
  1 MSMYTTAQLL AANEQKFKFD PLFLRLFFRE SYPFTTEKVY LSQIPGLVNM
 51 ALYVSPIVSG EVIRSRGGST SEFTPGYVKP KHEVNPQMTL RRLPDEDPQN
101 LADPAYRRRR IIMQNMRDEE LAIAQVEEMQ AVSAVLKGKY TMTGEAFDPV
151 EVDMGRSEEN NITQSGGTEW SKRDKSTYDP TDDIEAYALN ASGVVNIIVF
201 DPKGWALFRS FKAVKEKLDT RRGSNSELET AVKDLGKAVS YKGMYGDVAI
251 VVYSGQYVEN GVKKNFLPDN TMVLGNTQAR GLRTYGCIQD ADAQREGINA
301 SARYPKNWVT TGDPAREFTM IQSAPLMLLA DPDEFVSVQL A
```

FIGURE 3
Screening for AHA containing PSMs from phage λ and the *E. coli* background proteome. PSMs were identified by data-dependent acquisition LC–MS/MS using the MASCOT search engine. **(A)** A total number of phage λ and *E. coli* (not cell pellet); only PSMs of the same sample were analyzed. AHA 5 h, AHA 1 h: AHA incubation times of 1 h and 5 h; No AHA 5 h, No AHA 1 h: controls. PSMs with methionine indicate the percentage of methionine-containing PSMs of all identified PSMs. PSMs with AHA indicate the percentage of AHA-containing PSMs of all PSMs. Mean and standard deviation of three independent experiments (Supplementary Table S2). **(B)** The 10 most abundant identified phage λ proteins (by PSM count) containing AHA after MASCOT search for sample AHA 5 h (3 replicates) were analyzed—the order of the 10 phage λ proteins corresponds to replicate 1. PSM: Mean and standard deviation of three replicates. **(C)** The major capsid protein was the most abundant protein detected in all samples (90% ± 1 sequence coverage). Black underlined letters in the amino acid sequence shows the position of methionine.

phages by ethanol precipitation should be omitted for subsequent fluorescence microscopy. Therefore, the protocol for labeling the AHA-labeled phages with fluorophores was adapted so that all CC and washing steps were performed using a 100 kDa filter. The native phages were retained on the filter, while the chemicals passed through in the flow through after CC (Bichet et al., 2021; Bonilla et al., 2016; Erickson, 2009; Hietala et al., 2019). Ultracentrifugation was not considered here, as pelleting phages was considered too time-consuming and potentially reducing overall yield. The newly established filter-based protocol for tagging phages with DBCO Alexafluor (AF) 555 allowed the successful detection of fluorescence in SDS-PAGE (see Supplementary Figure S1). Two fluorescent bands with molecular weights of approximately 37 kDa and 60 kDa were detected for both labeling conditions (1 h and 5 h labeling with AHA). In contrast, no fluorescent proteins were detected in the control sample. The 37 kDa band could correspond to the highly labeled major capsid protein, and the 60 kDa band to the portal protein B. Further, these fluorophore-tagged phages are termed "AF555 phages." Alternatively, AHA-labeled phages were coupled to DBCO Cyanin (CY) 5.5 by CC (see Supplementary Figure S4). The fluorescence gels showed higher fluorescence intensity with additional bands besides the two main bands at 37 kDa and 60 kDa. In the following, these fluorophore-tagged phages are termed "CY5.5 phages".

In summary, the AHA-labeled phages had sufficient binding sites for detectable fluorescence tagging via CC. This also confirms the results of the MS measurements, where a high level of incorporation with AHA was found. In addition, sufficient phages could be recovered from the filters for phage protein detection via Coomassie stain and fluorescence detection. This should also allow fluorescence microscopy detection, which will be verified below.

Detection of phage-host complexes via fluorescence microscopy

The binding of AF555 phages to *E. coli* was confirmed by fluorescence microscopy. AF555 phages were incubated for 30 min with *E. coli* or *P. fluorescens* as negative control.

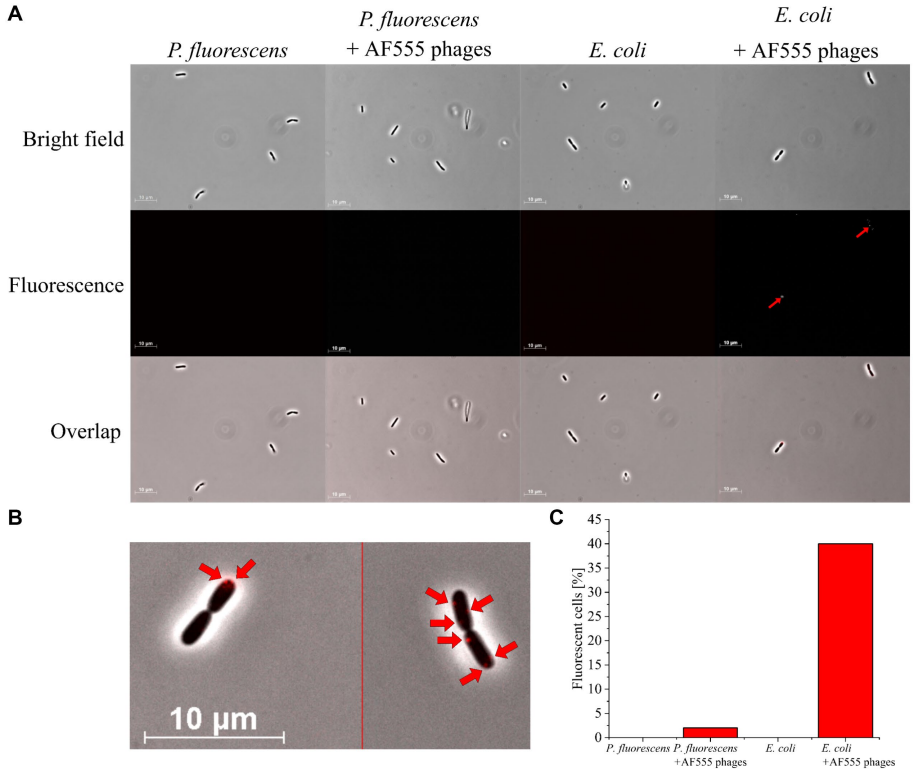

FIGURE 4
Fluorescence microscopy of *E. coli* and *P. fluorescens* (control) with AF555 phages. Cells were incubated for 30 min with and without AF555 phages. All pictures were taken with an Imager M1 fluorescence microscope (Carl Zeiss, Jena) using the software AxioVision (Version 4.8.2 SP3); brightfield and fluorescence (excitation 546/12 nm; beam splitter: FT 560; emission 575–640 nm), 1,000x, phase contrast. **(A)** Representative pictures of *P. fluorescens* and *E. coli* cells with and without AF555 phages after incubation for 30 min; only *E. coli* cells show a positive fluorescence after the addition of AF555 phages (red arrow). **(B)** *E. coli* cells with attached AF555 phages (red arrow, enlarged from overlap in **(A)**. **(C)** Percentage of fluorescent cells after scanning in greyscale mode (see Supplementary Figure S2).

Neither *P. fluorescens* nor *E. coli* showed background fluorescence at the selected wavelength (Figure 4A). *E. coli* incubated with AF555 phages emitted fluorescence (Figure 4A), whereas *P. fluorescens* incubated with AF555 phages in most cases did not emit fluorescence. Despite their small size, AF555 phages were even visible as red dots on the surface of *E. coli* cells (Figure 4B). We were even able to observe free fluorescent phages in the supernatant (Supplementary Figure S3, see Pasulka et al. (2018)).

About 40% of *E. coli* cells showed AF555 phages-specific fluorescence signals after 30 min incubation, whereas only 2% of *P. fluorescens* showed a fluorescence signal (Figure 4C). The small proportion of AF555 phages bound to *P. fluorescens* could be explained by the non-specific binding of phages to glycans of the extracellular membrane of many gram-negative bacteria (Dennehy and Abedon, 2021; Maffei et al., 2021) that are similar to carbohydrates of the *E. coli* membrane.

In summary, a workflow for AHA-labeling and CC-based addition of DBCO AF555 to phage λ proteins was established. The AF555 phages specifically bound to their host cells.

Quantification of fluorescent phage-host complexes via flow cytometry

Fluorescence microscopy was used to monitor the absorption of AF555 phages on their host cells (Figure 4). In addition, flow cytometry was applied for automated analysis to quantify phage-host interaction (Figure 1 Step 4a).

First, CY5.5 phages were incubated with *E. coli* or *P. fluorescens* for up to 60 min (Figure 5A "λ"). *E. coli* and *P. fluorescens* incubated without CY5.5 phages served as control (Figure 5A "C"). Pure bacteria (without phages) and pure CY5.5 phages were used to exclude clumped bacteria and unbound fluorescent phages from counting as positive signals for phage-host interaction analysis (see Supplementary Figure S5).

When incubated with CY5.5 phages, the percentage of fluorescent *E. coli* increased from 1.35% ± 0.04 to 24.55% ± 7.14%. A rapid increase in fluorescence of *E. coli* from 7.05% ± 0.42 to 24.55% ± 7.14% was observed between 30 min and 60 min incubation with CY5.5 phages. In contrast, the fluorescence of *P. fluorescens* did not increase significantly within the first 30 min of incubation using CY5.5 phages. After 60 min of incubation of *P. fluorescens* with CY5.5 phages, 7.50% ± 1.41% of the cells were fluorescent, indicating non-specific binding of CY5.5 phages due to the extended incubation time (Figure 5). Non-specific adsorption of CY5.5 phages to non-host cells such as *P. fluorescens* might cause false positive results. Therefore, short incubation times are suggested. Alternatively, non-specific binding could be minimized by extensive washing steps with PBS after harvest.

In our analysis of three biological replicates, we observed a slower adsorption of CY5.5 phages in one replicate, where the increase in

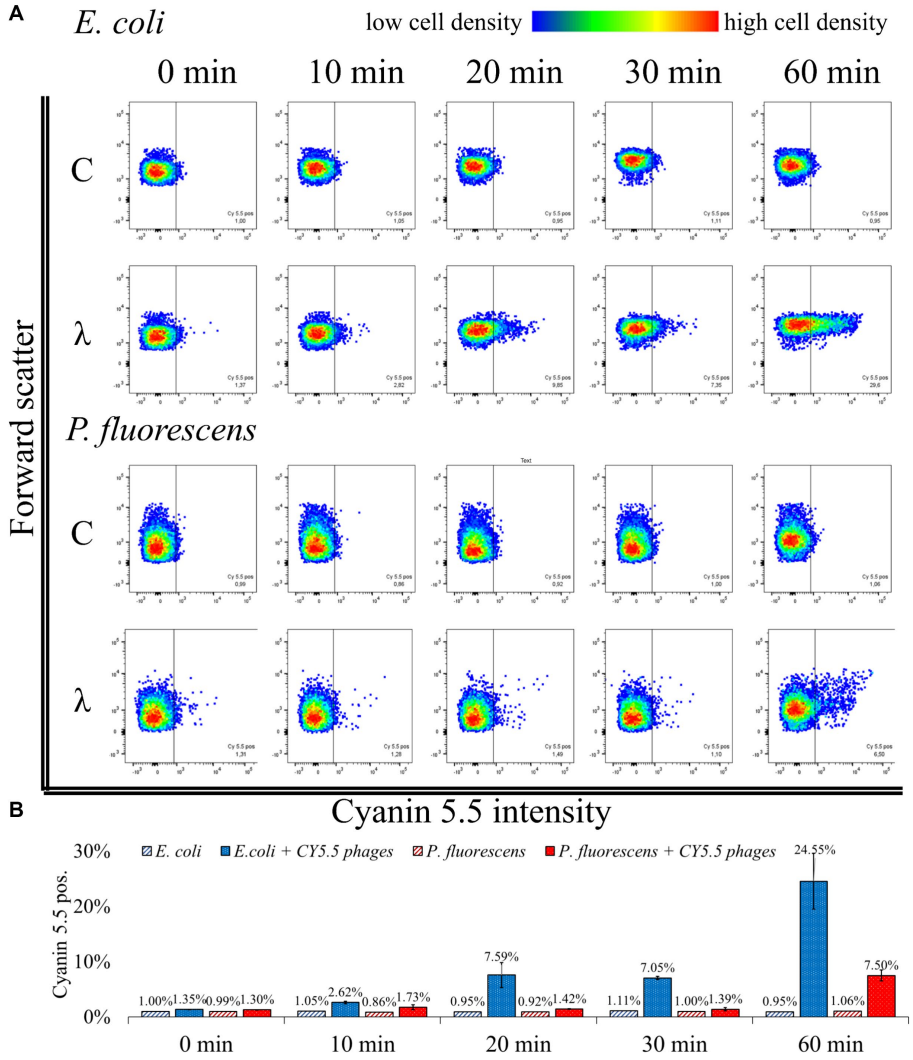

FIGURE 5
Flow cytometric analysis of phage-host complexes. **(A)** *E. coli* or *P. fluorescens* were incubated with CY5.5 phages for the indicated period (λ); control (C): without the addition of CY5.5 phages. Bacteria were harvested and treated with 4% formaldehyde for fixation. The fluorescence intensity was determined for n = 10,000 bacteria per condition. Forward scatter as an indicator of cell size was plotted against the intensity of cyanin 5.5 fluorescence. The threshold for background fluorescence of bacteria incubated without phages was set to about 1% (vertical line in the scatter plots). **(B)** Mean percentage of cyanin 5.5 positive phage-host complexes from two independent biological replicates with standard derivation. The third replicate showed different adsorption kinetics and the raw data can be found in Supplementary Table S3: FACS analysis.

fluorescence from *E. coli* after CY5.5 phage addition only increased from 1.12 to 4.13% after 60 min, while the fluorescence of *P. fluorescens* remained at 1.17% (Supplementary Table S3). A longer incubation time might have also increased the fluorescence signal in this experiment, similar to the other replicates.

In the case of a low number of fluorescent cells, it may be beneficial to increase the moi to enhance the number of phages bound to host cells. Since phage infections follow a Poisson distribution, a higher moi can statistically increase the number of phages per cell surface, leading to more fluorescent cells (Arkin et al., 1998; Ellis and Delbrück, 1939; Kourilsky, 1973; Marcelli et al., 2020). In particular, for unknown phage titers, the optimal adsorption conditions must be determined by analyzing different ratios of cells and phages.

In summary, the analysis of fluorescent phage-host complexes by flow cytometry confirms the results obtained from fluorescence microscopy (Figure 4) and offers the advantage of automated quantification. In addition, it allows the enrichment and isolation of fluorescent phage-host complexes by Fluorescence Activated Cell Sorting (FACS) in subsequent studies. Compared to genome staining (Deng et al., 2012), this approach has the advantage that the number of available fluorescent dyes for CC is steadily increasing, which facilitates the adaptation of the workflow to other detection methods (Van Kasteren and Rozen, 2023). In addition, only phages that are actively replicating are labeled, so that non-specifically stained fragments on cell surfaces are not analyzed. Consequently, the number of phage-host complexes identified by BONCAT and CC will be lower than in genome staining-based approaches, but the detection of those present is highly specific. Nevertheless, a combination with genome staining methods could be advantageous for subsequent studies, as the use of two dyes could allow more accurate sorting (Hardy et al., 1982).

Purification of biotinylated phages via magnetic beads

CC of AHA-labeled proteins allows coupling of affinity tags, such as biotin, permitting specific enrichment of tagged proteins with corresponding binding partners, such as avidin (Bayer and Wilchek, 1990). Enrichment of intact biotinylated phages from complex cultures would allow subsequent analyses of the isolated phages, including DNA/RNA sequencing, LC–MS/MS-based proteomics, or follow-up infection experiments (Figure 1 Step 3b and 4b).

AHA labeled phages were tagged with DBCO-PEG4-biotin (biotinylated phages) and purified with magnetic beads functionalized with monomeric avidin. The different fractions obtained were analyzed by SDS-PAGE (Figure 6A). The biotinylated phages eluted easily using a surplus of biotin (Figure 6 A "biotinylated phages" SDS gel lane "Elution"). In contrast, the elution of non-biotinylated phages (control) failed (Figure 6 A "non-biotinylated phages" SDS gel lane "Elution"). The low protein content in the collected washing fractions of beads (Figure 6 A, SDS gel lanes 'Washing phase') indicates that mild washing with PBS releases only low amounts of proteins from the beads with PBS. In contrast, boiling the beads with an SDS-buffer after the elution step removed many proteins from the beads, indicating non-specific binding to the bead surface, which is independent of biotinylation (Figure 6 A SDS gel lanes "SDS-boiled"). However, the non-specific binding of proteins to the monomeric avidin beads does not seem to affect the purification of phages since exclusively biotinylated phages were collected after the selective elution with biotin (Figure 6 A "biotinylated phages" SDS gel lane "Elution").

The most abundant protein from the "Elution" of the biotinylated phages had a molecular weight of about 37 kDa. It corresponded to the major band of AF555 and CY5.5 phages identified by SDS-PAGE (Figure 6A and Supplementary Figures S1, S4). LC–MS/MS confirmed that this band mostly contained the major capsid protein of phage λ (Figure 6B red). The analysis of the SDS-boiled fractions showed a low proportion of major capsid protein but a high proportion of *E. coli* PSMs. Obviously, destroying the beads with SDS mostly released

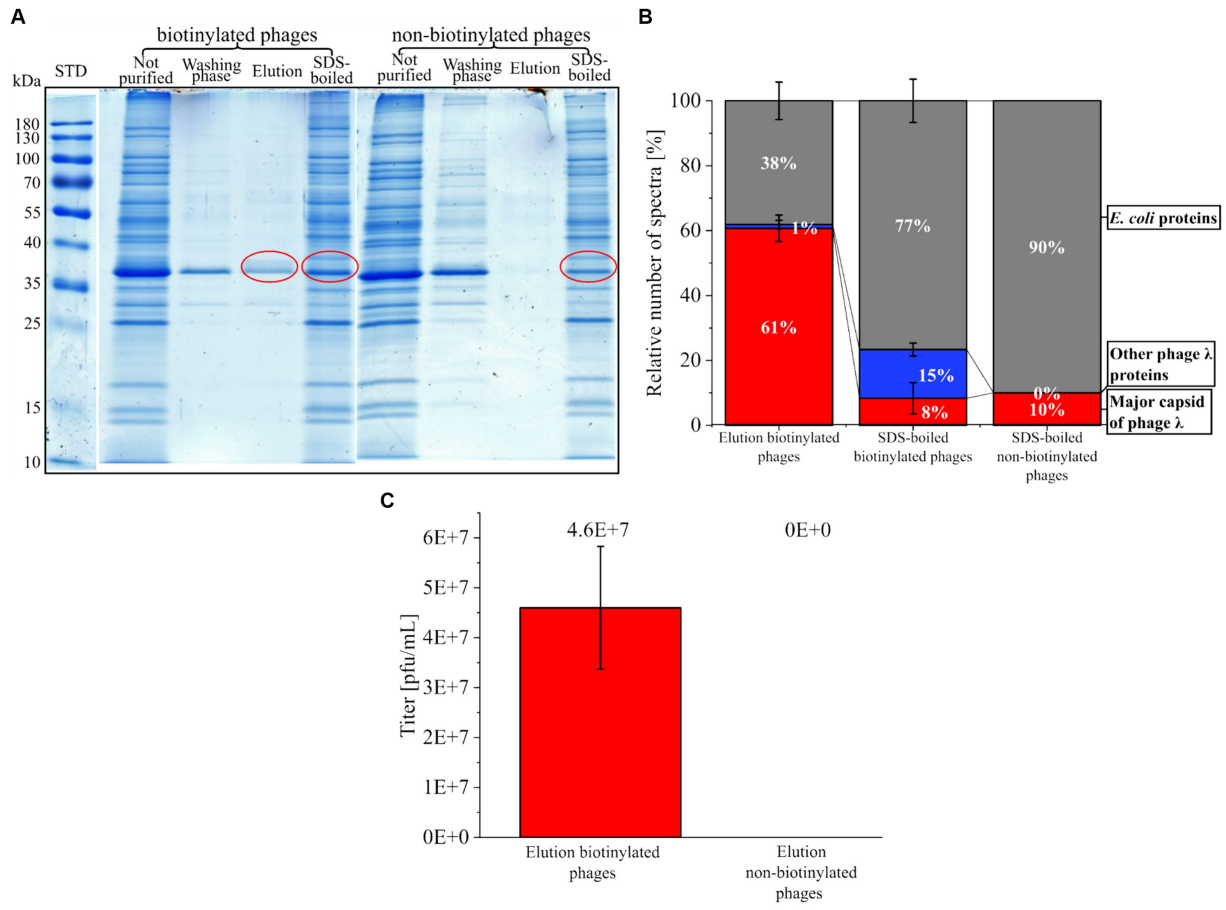

FIGURE 6
Purification of biotinylated phages with magnetic monomeric avidin beads. **(A)** SDS gel from different fractions collected during purification of phages (biotinylated or non-biotinylated) stained with Coomassie blue. The fraction "not purified" corresponds to the control (sample before the addition of beads). The "washing phase" comprises fractions of all washing steps of the beads with PBS. "Elution" includes all proteins eluted from avidin beads with a surplus of biotin. The fraction "SDS-boiled" is the collected supernatant of avidin beads after boiling (5min, 60°C) with SDS buffer. Red circles indicate protein fractions that were further analyzed by LC–MS/MS. For the original gels, see Supplementary Figure S6. STD: protein standard (Thermo Scientific, PageRuler Prestained Protein Ladder #26616) **(B)** Relative percentage of the spectra measured with LC–MS/MS after in-gel digestion of the protein fractions marked in **A**. MS data were screened for the major capsid protein from phage λ, other phage λ proteins, and *E. coli* proteins from the background of the phage λ suspension. For raw data, see Supplementary Table S4 MS in-gel. **(C)** Plaque titer from the elution fraction of biotinylated and non-biotinylated phages; three independent experiments with mean and standard derivation below the detection limit for the elution of non-biotinylated phages.

background proteins (Figure 6B), whereas a mild elution with 2 mM biotin is highly specific. Blocking the beads with amino acids or gelatin could be considered in future applications to prevent the non-specific binding of host proteins (Nicora et al., 2013; Richter et al., 2021).

Plaque assays were performed to assess the infectivity of the collected phages. Here, biotinylated phages eluted from beads showed infectivity with 4.60E+07 pfu/mL ± 1.23E+07 pfu/mL (Figure 6C), whereas the elution fraction of beads loaded with unlabeled phages showed no plaques. The missing plaques in the control experiment confirmed the specific binding of biotinylated phages, as already concluded from LC–MS/MS data.

In summary, it is possible to tag phages with biotin using CC without compromising their infectivity. Biotin tagging allows the purification of the biotinylated phages with monomeric avidin beads. The specific bead-bound phages could also be used for specific host screening in follow-up studies, where the phages bind the hosts, and the phage-host complexes are specifically released from the beads by an excess of biotin (mild condition).

Future application of the established workflow in microbial ecology and personalized medicine

The new workflow established fluorescence labeling of phage λ for subsequent monitoring by fluorescence microscopy and flow cytometry in pure culture. A specific enrichment of infectious biotin-labeled phage λ fractions is possible using monomeric avidin beads. Other phage-host systems could be tested for future applications in microbial ecology and personalized medicine. As BONCAT approaches have been applied to a wide range of species (e.g., Babin et al., 2017; Franco et al., 2018; Metcalfe et al., 2021; Pasulka et al., 2018) no major difficulties in the transfer to other phage-host systems are anticipated. Fluorescent labeling of defined phages from phage collections would enable high throughput flow cytometry screening for alternative hosts in bacterial strain collections or the personalized selection of candidates for phage therapy using a pathogenic isolate from patient as target. In the future the screening could also be widened to non-cultivable bacteria enriched from environmental samples. Flow cytometry-based cell sorting and subsequent sequencing or proteomics could support the identification and description of new hosts for phages already available in phage collections. Induction of phage replication by MMC or other environmental stressors followed by BONCAT could also be applied to complex microbial communities (e.g., Howard-Varona et al., 2017; Jiang and Paul, 1998; Rossi et al., 2022). Phages could be separated from cells by filtration or ultracentrifugation for subsequent labeling with fluorescent dyes or affinity tags. Afterwards, flow cytometry and cell sorting could be applied to identify and characterize the corresponding hosts, including non-cultivable bacteria from the same microbial community. A preliminary experiment conducted on a co-culture of *E. coli* and *Priestia megaterium* revealed that following the addition of fluorescent phages, only the host *E. coli* exhibited fluorescence due to the specific phage adsorption (see Supplementary Figure S7).

Alternatively, biotinylated phages previously immobilized on monomeric avidin magnetic beads can be enriched from corresponding hosts for subsequent sequencing and characterization by adsorption on the surface of host cells. While applying the workflow presented here to complex microbiomes is ambitious, it holds great potential for identifying and monitoring phage-host interactions in natural environments. Comprehensive experiments are required to evaluate its application in microbiome research, a topic that extends beyond the current focus on pure cultures.

Conclusion

A workflow for the analysis of phage λ infection in *E. coli* and the detection and purification of fluorescent phage-host complexes was established. First, phages were labeled with AHA using BONCAT. Second, labeled phages were tagged with either fluorescent dyes or biotin using CC. Using BONCAT followed by CC, is a novel strategy and flexible tool for studying microbial communities (Hatzenpichler et al., 2020). The method was demonstrated on pure cultures. Its potential application in microbial communities, including environmental or patient samples, requires further assessment of the workflow under complex environmental conditions. Furthermore, fluorescent phages could be applied for specific screening of phage libraries for the therapy of infectious diseases. Finally, due to the increasing repertoire of substances for CC, it can be safely assumed that the BONCAT and CC approach will evolve into a very flexible toolbox for phage research and therapy (van Kasteren and Rozen, 2023).

Data availability statement

The datasets presented in this study can be found in online repositories. The names of the repository/repositories and accession number(s) can be found at: https://www.ebi.ac.uk/pride/archive/, PXD044316.

Author contributions

PH: Conceptualization, Data curation, Formal analysis, Investigation, Methodology, Visualization, Writing – original draft, Writing – review & editing. AD: Investigation, Methodology, Resources, Writing – review & editing. RH: Writing – review & editing. UR: Conceptualization, Project administration, Resources, Supervision, Writing – review & editing. DB: Conceptualization, Project administration, Supervision, Writing – review & editing.

Funding

The author(s) declare financial support was received for the research, authorship, and/or publication of this article. This study was funded by Deutsche Forschungsgemeinschaft (DFG, German Research Foundation) – INST 272/284-1 FUGG.

Acknowledgments

We thank Andreas Kuhn (University of Hohenheim, Germany) for providing *E. coli* with integrated phage λ and the helpful feedback to the manuscript and Helga Tietgens (Max Planck Institute for Dynamics of Complex Technical Systems Magdeburg, Germany) for support in fluorescence microscopy.

Conflict of interest

The authors declare that the research was conducted in the absence of any commercial or financial relationships that could be construed as a potential conflict of interest.

Publisher's note

All claims expressed in this article are solely those of the authors and do not necessarily represent those of their affiliated organizations, or those of the publisher, the editors and the reviewers. Any product that may be evaluated in this article, or claim that may be made by its manufacturer, is not guaranteed or endorsed by the publisher.

Supplementary material

The Supplementary material for this article can be found online at: https://www.frontiersin.org/articles/10.3389/fmicb.2024.1434301/full#supplementary-material

References

Anderson, R. E., Brazelton, W. J., and Baross, J. A. (2011). Is the genetic landscape of the deep subsurface biosphere affected by viruses? *Front. Microbiol.* 2:219. doi: 10.3389/fmicb.2011.00219

Arkin, A., Ross, J., and McAdams, H. H. (1998). Stochastic kinetic analysis of developmental pathway bifurcation in phage lambda-infected *Escherichia coli* cells. *Genetics* 149, 1633–1648. doi: 10.1093/genetics/149.4.1633

Babin, B. M., Atangcho, L., van Eldijk, M. B., Sweredoski, M. J., Moradian, A., Hess, S., et al. (2017). Selective proteomic analysis of antibiotic-tolerant cellular subpopulations in *Pseudomonas aeruginosa* biofilms. *MBio* 8:17. doi: 10.1128/mbio.01593-17

Bayer, E. A., and Wilchek, M. (1990). Application of avidin-biotin technology to affinity-based separations. *J. Chromatogr.* 24, 3–11. doi: 10.1016/s0021-9673(01)93733-1

Bichet, M. C., Patwa, R., and Barr, J. J. (2021). Protocols for studying bacteriophage interactions with in vitro epithelial cell layers. *STAR Protocols* 2:100697. doi: 10.1016/j.xpro.2021.100697

Bonilla, N., Rojas, M. I., Netto Flores Cruz, G., Hung, S. H., Rohwer, F., and Barr, J. J. (2016). Phage on tap-a quick and efficient protocol for the preparation of bacteriophage laboratory stocks. *PeerJ* 4:e2261. doi: 10.7717/peerj.2261

Boulanger, P. (2009). Purification of bacteriophages and SDS-PAGE analysis of phage structural proteins from ghost particles. *Methods Mol. Biol.* 502, 227–238. doi: 10.1007/978-1-60327-565-1_13

Calve, S., Witten, A. J., Ocken, A. R., and Kinzer-Ursem, T. L. (2016). Incorporation of non-canonical amino acids into the developing murine proteome. *Sci. Rep.* 6:32377. doi: 10.1038/srep32377

Carroll-Portillo, A., Coffman, C. N., Varga, M. G., Alcock, J., Singh, S. B., and Lin, H. C. (2021). Standard bacteriophage purification procedures cause loss in numbers and activity. *Viruses* 13:328. doi: 10.3390/v13020328

Clark, J. R., and March, J. B. (2006). Bacteriophages and biotechnology: vaccines, gene therapy and antibacterials. *Trends Biotechnol.* 24, 212–218. doi: 10.1016/j.tibtech.2006.03.003

Deng, L., Gregory, A., Yilmaz, S., Poulos, B. T., Hugenholtz, P., and Sullivan, M. B. (2012). Contrasting life strategies of viruses that infect photo-and heterotrophic bacteria, as revealed by viral tagging. *MBio* 3:12. doi: 10.1128/mBio.00373-12

Deng, L., Ignacio-Espinoza, J. C., Gregory, A. C., Poulos, B. T., Weitz, J. S., Hugenholtz, P., et al. (2014). Viral tagging reveals discrete populations in Synechococcus viral genome sequence space. *Nature* 513, 242–245. doi: 10.1038/nature13459

Dennehy, J. J., and Abedon, S. T. (2021). "Adsorption: phage Acquisition of Bacteria" in Bacteriophages. ed. D. R. Harper (Cham: Springer International Publishing), 93–117.

Dieterich, D. C., Lee, J. J., Link, A. J., Graumann, J., Tirrell, D. A., and Schuman, E. M. (2007). Labeling, detection and identification of newly synthesized proteomes with bioorthogonal non-canonical amino-acid tagging. *Nat. Protoc.* 2, 532–540. doi: 10.1038/nprot.2007.52

Dieterich, D. C., Link, A. J., Graumann, J., Tirrell, D. A., and Schuman, E. M. (2006). Selective identification of newly synthesized proteins in mammalian cells using bioorthogonal noncanonical amino acid tagging (BONCAT). *Proc. Natl. Acad. Sci. U. S. A.* 103, 9482–9487. doi: 10.1073/pnas.0601637103

Džunková, M., Low, S. J., Daly, J. N., Deng, L., Rinke, C., and Hugenholtz, P. (2019). Defining the human gut host-phage network through single-cell viral tagging. *Nat. Microbiol.* 4, 2192–2203. doi: 10.1038/s41564-019-0526-2

Ellis, E. L., and Delbrück, M. (1939). The growth of bacteriophage. *J. Gen. Physiol.* 22, 365–384. doi: 10.1085/jgp.22.3.365

Erickson, H. P. (2009). Size and shape of protein molecules at the nanometer level determined by sedimentation, gel filtration, and electron microscopy. *Biol. Proc. Online* 11, 32–51. doi: 10.1007/s12575-009-9008-x

Fernández, L., Duarte, A. C., Rodríguez, A., and García, P. (2021). The relationship between the phageome and human health: are bacteriophages beneficial or harmful microbes? *Benefic. Microbes* 12, 107–120. doi: 10.3920/BM2020.0132

Franco, M., D'haeseleer, P. M., Branda, S. S., Liou, M. J., Haider, Y., Segelke, B. W., et al. (2018). Proteomic profiling of *Burkholderia thailandensis* during host infection using bio-orthogonal noncanonical amino acid tagging (BONCAT). *Front. Cell. Infect. Microbiol.* 8:370. doi: 10.3389/fcimb.2018.00370

Gregory, A. C., Zayed, A. A., Conceição-Neto, N., Temperton, B., Bolduc, B., Alberti, A., et al. (2019). Marine DNA viral macro-and microdiversity from pole to pole. *Cell* 177, 1109–1123.e14. doi: 10.1016/j.cell.2019.03.040

Hardy, R. R., Hayakawa, K., Haaijman, J., and Herzenberg, L. A. (1982). B-cell subpopulations identifiable by two-color fluorescence analysis using a dual-laser FACS. *Ann. N. Y. Acad. Sci.* 399, 112–121. doi: 10.1111/j.1749-6632.1982.tb25667.x

Hatzenpichler, R., Krukenberg, V., Spietz, R. L., and Jay, Z. J. (2020). Next-generation physiology approaches to study microbiome function at single cell level. *Nat. Rev. Microbiol.* 18, 241–256. doi: 10.1038/s41579-020-0323-1

Hatzenpichler, R., Scheller, S., Tavormina, P. L., Babin, B. M., Tirrell, D. A., and Orphan, V. J. (2014). In situ visualization of newly synthesized proteins in environmental microbes using amino acid tagging and click chemistry. *Environ. Microbiol.* 16, 2568–2590. doi: 10.1111/1462-2920.12436

Heyer, R., Schallert, K., Büdel, A., Zoun, R., Dorl, S., Behne, A., et al. (2019a). A robust and universal Metaproteomics workflow for research studies and routine diagnostics within 24 h using phenol extraction, FASP Digest, and the MetaProteomeAnalyzer'. *Front. Microbiol.* 10:1883. doi: 10.3389/fmicb.2019.01883

Heyer, R., Schallert, K., Siewert, C., Kohrs, F., Greve, J., Maus, I., et al. (2019b). Metaproteome analysis reveals that syntrophy, competition, and phage-host interaction shape microbial communities in biogas plants. *Microbiome* 7:69. doi: 10.1186/s40168-019-0673-y

Hietala, V., Horsma-Heikkinen, J., Carron, A., Skurnik, M., and Kiljunen, S. (2019). The removal of Endo-and enterotoxins from bacteriophage preparations. *Front. Microbiol.* 10:1674. doi: 10.3389/fmicb.2019.01674

Howard-Varona, C., Hargreaves, K. R., Abedon, S. T., and Sullivan, M. B. (2017). Lysogeny in nature: mechanisms, impact and ecology of temperate phages. *ISME J.* 11, 1511–1520. doi: 10.1038/ismej.2017.16

Hwang, Y., Roux, S., Coclet, C., Krause, S. J. E., and Girguis, P. R. (2023). Viruses interact with hosts that span distantly related microbial domains in dense hydrothermal mats. *Nat. Microbiol.* 8, 946–957. doi: 10.1038/s41564-023-01347-5

Ignacio, B. J., Dijkstra, J., Mora, N., Slot, E. F. J., van Weijsten, M. J., Storkebaum, E., et al. (2023). THRONCAT: metabolic labeling of newly synthesized proteins using a bioorthogonal threonine analog. *Nat. Commun.* 14:3367. doi: 10.1038/s41467-023-39063-7

Jiang, S. C., and Paul, J. H. (1998). Significance of Lysogeny in the marine environment: studies with isolates and a model of lysogenic phage production. *Microb. Ecol.* 35, 235–243. doi: 10.1007/s002489900079

Kiick, K. L., Saxon, E., Tirrell, D. A., and Bertozzi, C. R. (2002). Incorporation of azides into recombinant proteins for chemoselective modification by the Staudinger ligation. *Proc. Natl. Acad. Sci. USA* 99, 19–24. doi: 10.1073/pnas.012583299

Kolb, H. C., Finn, M. G., and Sharpless, K. B. (2001). Click chemistry: diverse chemical function from a few good reactions. *Angew. Chem. Int. Ed.* 40, 2004–2021. doi: 10.1002/1521-3773(20010601)40:11<2004::AID-ANIE2004>3.0.CO;2-5

Kourilsky, P. (1973). Lysogenization by bacteriophage lambda. I. Multiple infection and the lysogenic response. *Mol. Gen. Genet. MGG* 122, 183–195. doi: 10.1007/BF00435190

Kristensen, D. M., Mushegian, A. R., Dolja, V. V., and Koonin, E. V. (2010). New dimensions of the virus world discovered through metagenomics. *Trends Microbiol.* 18, 11–19. doi: 10.1016/j.tim.2009.11.003

Kutateladze, M., and Adamia, R. (2010). Bacteriophages as potential new therapeutics to replace or supplement antibiotics. *Trends Biotechnol.* 28, 591–595. doi: 10.1016/j.tibtech.2010.08.001

Laemmli, U. K. (1970). Cleavage of structural proteins during the assembly of the head of bacteriophage T4. *Nature* 227, 680–685. doi: 10.1038/227680a0

Landor, L. A. I., Bratbak, G., Larsen, A., Tjendra, J., and Våge, S. (2023). Differential toxicity of bioorthogonal non-canonical amino acids (BONCAT) in *Escherichia coli*. *J. Microbiol. Methods* 206:106679. doi: 10.1016/j.mimet.2023.106679

Low, H. Z., Böhnlein, C., Sprotte, S., Wagner, N., Fiedler, G., Kabisch, J., et al. (2020). Fast and easy phage-tagging and live/dead analysis for the rapid monitoring of bacteriophage infection. *Front. Microbiol.* 11:602444. doi: 10.3389/fmicb.2020.602444

Maffei, E., Shaidullina, A., Burkolter, M., Heyer, Y., Estermann, F., Druelle, V., et al. (2021). Systematic exploration of *Escherichia coli* phage-host interactions with the BASEL phage collection. *PLoS Biol.* 19:e3001424. doi: 10.1371/journal.pbio.3001424

Marcelli, B., Karsens, H., Nijland, M., Oudshoorn, R., Kuipers, O. P., and Kok, J. (2020). *Poisson distribution describing the proportion of cells in a population infected with a certain number of phages, at MOIs ranging from 0.1 to 10*. Available at: https://plos.figshare.com/articles/figure/Poisson_distribution_describing_the_proportion_of_cells_in_a_population_infected_with_a_certain_number_of_phages_at_MOIs_ranging_from_0_1_to_10_/12953081/1 (Accessed February 14, 2023).

Marsh, P., and Wellington, E. (1994). Phage-host interactions in soil. *FEMS Microbiol. Ecol.* 15, 99–107. doi: 10.1111/j.1574-6941.1994.tb00234.x

Metcalfe, K. S., Murali, R., Mullin, S. W., Connon, S. A., and Orphan, V. J. (2021). Experimentally-validated correlation analysis reveals new anaerobic methane oxidation partnerships with consortium-level heterogeneity in diazotrophy. *ISME J.* 15, 377–396. doi: 10.1038/s41396-020-00757-1

Nasukawa, T., Uchiyama, J., Taharaguchi, S., Ota, S., Ujihara, T., Matsuzaki, S., et al. (2017). Virus purification by CsCl density gradient using general centrifugation. *Arch. Virol.* 162, 3523–3528. doi: 10.1007/s00705-017-3513-z

Ngo, J. T., Champion, J. A., Mahdavi, A., Tanrikulu, I. C., Beatty, K. E., Connor, R. E., et al. (2009). Cell-selective metabolic labeling of proteins. *Nat. Chem. Biol.* 5, 715–717. doi: 10.1038/nchembio.200

Nicora, C. D., Anderson, B. J., Callister, S. J., Norbeck, A. D., Purvine, S. O., Jansson, J. K., et al. (2013). Amino acid treatment enhances protein recovery from sediment and soils for metaproteomic studies. *Proteomics* 13, 2776–2785. doi: 10.1002/pmic.201300003

Ohno, S., Okano, H., Tanji, Y., Ohashi, A., Watanabe, K., Takai, K., et al. (2012). A method for evaluating the host range of bacteriophages using phages fluorescently labeled with 5-ethynyl-2′-deoxyuridine (EdU). *Appl. Microbiol. Biotechnol.* 95, 777–788. doi: 10.1007/s00253-012-4174-1

Paez-Espino, D., Eloe-Fadrosh, E. A., Pavlopoulos, G. A., Thomas, A. D., Huntemann, M., Mikhailova, N., et al. (2016). Uncovering Earth's virome. *Nature* 536, 425–430. doi: 10.1038/nature19094

Pasulka, A. L., Thamatrakoln, K., Kopf, S. H., Guan, Y., Poulos, B., Moradian, A., et al. (2018). Interrogating marine virus-host interactions and elemental transfer with BONCAT and nanoSIMS-based methods. *Environ. Microbiol.* 20, 671–692. doi: 10.1111/1462-2920.13996

Perkins, D. N., Pappin, D. J. C., Creasy, D. M., and Cottrell, J. S. (1999). Probability-based protein identification by searching sequence databases using mass spectrometry data. *Electrophoresis* 20, 3551–3567. doi: 10.1002/(SICI)1522-2683(19991201)20:18<3551::AID-ELPS3551>3.0.CO;2-2

Richter, Ł., Księżarczyk, K., Paszkowska, K., Janczuk-Richter, M., Niedziółka-Jönsson, J., Gapiński, J., et al. (2021). Adsorption of bacteriophages on polypropylene labware affects the reproducibility of phage research. *Sci. Rep.* 11:7387. doi: 10.1038/s41598-021-86571-x

Rossi, A., Morlino, M. S., Gaspari, M., Basile, A., Kougias, P., Treu, L., et al. (2022). Analysis of the anaerobic digestion metagenome under environmental stresses stimulating prophage induction. *Microbiome* 10:125. doi: 10.1186/s40168-022-01316-w

Sakowski, E. G., Arora-Williams, K., Tian, F., Zayed, A. A., Zablocki, O., Sullivan, M. B., et al. (2021). Interaction dynamics and virus-host range for estuarine actinophages captured by epicPCR. *Nat. Microbiol.* 6, 630–642. doi: 10.1038/s41564-021-00873-4

Sieiro, C., Areal-Hermida, L., Pichardo-Gallardo, Á., Almuiña-González, R., de Miguel, T., Sánchez, S., et al. (2020). A hundred years of bacteriophages: can phages replace antibiotics in agriculture and aquaculture? *Antibiotics (Basel, Switzerland)* 9:493. doi: 10.3390/antibiotics9080493

Steward, K. F., Eilers, B., Tripet, B., Fuchs, A., Dorle, M., Rawle, R., et al. (2020). Metabolic implications of using BioOrthogonal non-canonical amino acid tagging (BONCAT) for tracking protein synthesis. *Front. Microbiol.* 11:197. doi: 10.3389/fmicb.2020.00197

Suttle, C. A. (2007). Marine viruses--major players in the global ecosystem. *Nat. Rev. Microbiol.* 5, 801–812. doi: 10.1038/nrmicro1750

van Bergen, W., Heck, A. J. R., and Baggelaar, M. P. (2022). Recent advancements in mass spectrometry-based tools to investigate newly synthesized proteins. *Curr. Opin. Chem. Biol.* 66:102074. doi: 10.1016/j.cbpa.2021.07.001

Van Kasteren, S., and Rozen, D. E. (2023). Using click chemistry to study microbial ecology and evolution. *ISME Commun.* 3:9. doi: 10.1038/s43705-022-00205-5

Yamamoto, K. R., Alberts, B. M., Benzinger, R., Lawhorne, L., and Treiber, G. (1970). Rapid bacteriophage sedimentation in the presence of polyethylene glycol and its application to large-scale virus purification. *Virology* 40, 734–744. doi: 10.1016/0042-6822(70)90218-7

frontiers | Frontiers in Microbiology

TYPE Original Research
PUBLISHED 15 October 2024
DOI 10.3389/fmicb.2024.1472729

OPEN ACCESS

EDITED BY
Gamaliel López-Leal,
Center for Research in Cellular Dynamics-UAEM, Mexico

REVIEWED BY
Laura Bonofiglio,
University of Buenos Aires, Argentina
Kotsoana Peter Montso,
Stellenbosch University, South Africa

*CORRESPONDENCE
Ruhul H. Kuddus
✉ Ruhul.kuddus@uvu.edu

RECEIVED 30 July 2024
ACCEPTED 23 September 2024
PUBLISHED 15 October 2024

CITATION
Miller IP, Laney AG, Zahn G, Sheehan BJ, Whitley KV and Kuddus RH (2024) Isolation and preliminary characterization of a novel bacteriophage vB_KquU_φKuK6 that infects the multidrug-resistant pathogen *Klebsiella quasipneumoniae*.
Front. Microbiol. 15:1472729.
doi: 10.3389/fmicb.2024.1472729

Isolation and preliminary characterization of a novel bacteriophage vB_KquU_φKuK6 that infects the multidrug-resistant pathogen *Klebsiella quasipneumoniae*

Isaac P. Miller, Alma G. Laney, Geoffrey Zahn, Brock J. Sheehan, Kiara V. Whitley and Ruhul H. Kuddus*

Department of Biology, Utah Valley University, Orem, UT, United States

Background: *Klebsiella quasipneumoniae* (previously known as *K. pneumoniae* K6) strains are among the multidrug-resistant hypervirulent bacterial pathogens. Phage therapy can help treat infections caused by such pathogens. Here we report some aspects of virology and therapeutic potentials of vB_KquU_φKuK6, a bacteriophage that infects *Klebsiella quasipneumoniae*.

Methods: *K. quasipneumoniae* (ATCC 700603) was used to screen wastewater lytic phages. The isolate vB_KquU_φKuK6 that consistently created large clear plaques was characterized using standard virological and molecular methods.

Results: vB_KquU_φKuK6 has a complex capsid with an icosahedral head (~60 nm) and a slender tail (~140 nm × 10 nm). The phage has a 51% AT-rich linear dsDNA genome (51,251 bp) containing 121 open reading frames. The genome contains genes encoding spanin, endolysin, and holin proteins necessary for lytic infection and a recombinase gene possibly involved in lysogenic infection. vB_KquU_φKuK6 is stable at −80 to +67°C, pH 4–9, and brief exposure to one volume percent of chloroform. vB_KquU_φKuK6 has a narrow host range. Its lytic infection cycle involves a latency of 20 min and a burst size of 435 plaque-forming units. The phage can cause lysogenic infection, and the resulting lysogens are resistant to lytic infection by vB_KquU_φKuK6. vB_KquU_φKuK6 reduces the host cells' ability to form biofilm but fails to eliminate that ability. vB_KquU_φKuK6 demonstrates phage-antibiotic synergy and reduces the minimum inhibitory concentration of chloramphenicol and neomycin sulfate by about 8 folds.

Conclusion: vB_KquU_φKuK6 cannot be directly used for phage therapy because it is a temperate bacteriophage. However, genetically modified strains of vB_KquU_φKuK6 alone or combined with antibiotics or other lytic *Klebsiella* phages can have therapeutic utilities in treating *K. quasipneumoniae* infections.

KEYWORDS

***Klebsiella quasipneumoniae*, MDR bacterial pathogens, phage therapy, lytic/lysogenic infection cycle, biofilm, phage-antibiotic synergy**

1 Introduction

Antibiotics are the first-line therapeutic agents in treating bacterial infections, but pathogenic antibiotic-resistant bacteria (ARB) have become a formidable challenge to this norm. Despite the superior healthcare infrastructure in the United States, the Center for Disease Control and Prevention (CDC) estimates that about 2.8 million US citizens (about 1% of the population) contract ARB infections, and about 35,000 die of such infections every year (CDC, 2019). The World Health Organization (WHO) estimates that ARB infections kill over 0.7 million patients per year globally, and the number would rise to 10 million per year by 2050 if new therapeutic interventions to combat ARB infections are not found (Mancuso et al., 2021). The severity of the crisis led the WHO to declare that a "post-antibiotic" era, where common bacterial infections can be fatal, is imminent (Reardon, 2014). Experts from the European Center for Disease Prevention and Control (ECDC) and the US Center for Disease Control and Prevention (CDC) categorized ARBs as multidrug-resistant (MDR) if the isolates are "non-susceptible to ≥1 agent in ≥3 antimicrobial categories," extensively drug-resistant (XDR) if the isolates have "non-susceptibility to at least one agent in all but two or fewer antimicrobial categories (i.e., bacterial isolates remain susceptible to only one or two categories)," and pan drug-resistant (PDR) if the isolates show "non-susceptibility to all agents in all antimicrobial categories" (Magiorakos et al., 2011).

Klebsiella pneumoniae is among the WHO-designated six highest-priority ARB pathogens besides *Enterococcus faecium, Staphylococcus aureus, Acinetobacter baumannii, Pseudomonas aeruginosa,* and *Enterobacter* sp. (WHO, 2017). In 2015, the species *K. pneumoniae* was divided into three species, *K. pneumoniae, K. quasipneumoniae,* and *K. variicola,* based on the genomic diversity of the species (Holt et al., 2015). About 2–4% of clinical infections attributed to *K. pneumoniae* are caused by *K. quasipneumoniae* (Chew et al., 2021; Long et al., 2017). *K. quasipneumoniae* strains constitute up to one-third of the hospital bacterial isolates in some Asian countries (Chew et al., 2021; Crellen et al., 2019). Disease signs due to *K. pneumoniae* or *K. quasipneumoniae* infections are similar (Chew et al., 2021), and like *K. pneumoniae*, *K. quasipneumoniae* has MDR and hypervirulent strains (Altayb et al., 2023; Arabaghian et al., 2019). Furthermore, *K. quasipneumoniae* strains readily acquire antibiotic-resistance genes and plasmids from other species of Enterobacteriaceae (Mathers et al., 2019). Altogether, *K. quasipneumoniae* is an important emerging bacterial pathogen.

The principal strategies to prevent and combat antibiotic resistance include infection control, containment, judicious use of antibiotics, finding new and more effective antibiotics, regulating clinical and industrial use of antibiotics, public education, and global surveillance (Ventola, 2015). In addition, phage therapy, the application of naturally occurring or genetically manipulated lytic bacteriophages, is suggested as an "alternative to antibiotics" in treating infections caused by MDR and XDR pathogens (Romero-Calle et al., 2019; Lin et al., 2017, reviewed by Strathdee et al., 2023). Although veterinary and clinical phage therapy was initiated by Felix d'Herelle (1873–1949), one of the discoverers of bacteriophages, in 1921 (Keen, 2012), phage therapy is not yet approved as a routine therapeutic method by the US Food and Drug Administration and European Medicines Agency, indicating some uncertainties regarding availability, quality assurance, efficacy, safety, and public trust in phage therapy. However, case-by-case compassionate applications and clinical trials of phage therapy have been approved (Yang et al., 2023).

Research in phage therapy gained momentum in 2021 when public funding for research on phage therapy was initiated in the United States, followed by Australia, the UK, and some other member nations of the European Union (National Institute of Allergy and Infectious Diseases, 2024; New South Wales Government, 2024; Fabijan et al., 2023). Worldwide, about 90 clinical trials of phage therapy including four in the United States are currently being carried out with more in the pipeline (Balthazar, 2024). The present study screened, identified, and characterized a strain of novel bacteriophage that efficiently kills a clinical isolate of *K. quasipneumoniae*. This study labels a few challenges in finding new bacteriophages for phage therapy and suggests some amends.

2 Materials and methods

2.1 Bacterial strains

Klebsiella quasipneumoniae strain K6 700603 (previously known as *Klebsiella pneumoniae* Strain K6) was obtained from the American Type Culture Collection (Manassas VA). Additional strains of *Klebsiella pneumoniae, K. oxytoca*, *Escherichia coli, Pseudomonas aeruginosa, Citrobacter freundii*, *Proteus mirabilis, Salmonella enterica,* and *Serratia marcescens* were obtained from ATCC or BEI Resource Depository (Manassas VA).

2.2 Bacterial culture, phage screening, and phage titration

Bacterial strains (including *K. quasipneumoniae*) were grown and infected by bacteriophages in trypticase soy broth (TSB) containing 0.2% maltose and 10 mM $MgSO_4$, or TSB containing 1.5% agar (TSA plates). The overlay semi-solid medium contained 0.6% agar. Bacteriophages were sampled from wastewater processing facilities in the Utah Valley area. Raw wastewater (10 mL) was transported to the laboratory on ice, centrifuged at 13,000 × g for 3 min to remove cells and particulates, and passed through 0.2-micron Acrodisc Supor™ membrane low protein-binding filters (Pall Lab, New York, NY) before use. Phages were enriched by mixing 0.5 mL of the filtrate, 0.5 mL of overnight bacterial culture of the host bacterium (*K. quasipneumoniae*), and 9 mL of TSB, incubating the mixture at 37°C overnight with moderate agitation (250 rotation/min). The culture supernatant was processed similarly to wastewater and then serially diluted with TSB for phage titration. For titration, the host bacterium (*K. quasipneumoniae*) growing in the log phase (20 mL, A600 = 0.4–0.5)

Abbreviations: ARB, Antibiotic-resistant bacteria; CDC, US Center for Disease Control and Prevention; CFU, Colony-forming units; ESBL, Extended-spectrum beta-lactamase; FIC, Fractional inhibitory concertation; MDR, Multidrug resistant; MIC, Minimum inhibitory concentration; MIM, Minimum inhibitory multiplicity of infection (MOI); MOI, Multiplicity of infection; ORF, Open reading frame; PAS, Phage-antibiotic synergy; PCR, Polymerase chain reaction; PDR, Pan-drug-resistant; PFU, Plaque-forming units; PDR, Pan drug-resistant; TPF, 1, 3, 5 triphenyl formazan; TSA, Trypticase soy agar; TSB, Trypticase soy broth; TTC, 2,3,5 triphenyl tetrazolium chloride; WHO, World Health Organization; XDR, Extensively drug-resistant; ZOI, Zone of inhibition.

was harvested by centrifugation at 5,000 × g for 5 min, and the pellet was suspended in 20 mL of cold 10 mM $MgSO_4$ solution. For plaque assays (done in duplicates), 0.1 mL of the 10-fold serially diluted phage samples were mixed in a 13 mL tube with 0.1 mL of the bacterial suspension and incubated for 20 min at 37°C. Melted overlay agar medium (3 mL) adjusted at 50°C was added to the tube, mixed on a Vortex Genie (USA Scientific, Ocala FL), and poured on top of prewarmed (to 37°C) 10-cm TSB agar plates. The plates were sealed with parafilm, inverted, and incubated at 37°C for 16–20 h. The number of plaque-forming units (PFU) was counted by placing the plates on a transilluminator using the formula N = n/(dv), where N = PFU/ml of the undiluted phage sample; n = number of plaques on the plate, d = dilution factor, and v is the volume of virus suspension (in ml) used for infection. Plates having 40–400 plaques were counted.

2.3 Plaque purification and storage of phages

Viruses were plaque-purified through four rounds of bacterial infection. In each round, a sterile cotton-tipped applicator or a sterile 200-µl pipette tip was used to touch a well-isolated plaque, and the applicator was washed with 1 ml TSB in a microfuge tube. The wash was filtered, 10-fold serially diluted, and then used for infecting bacteria as described in the previous section. In the fifth round, the phage was mass-produced by infecting 50 mL of host bacterial culture. For short-term storage, the phage-infected bacterial culture was refrigerated. A previously described method (Clark, 1962) was utilized for the long-term storage of plaque-purified phages. Briefly, the culture medium was centrifuged (at 13,000 × g), filtered using a 0.45-micron Acrodisc Supor™ membrane low protein-binding filter (Pall Lab), and then an equal volume of sterile glycerol was mixed with the filtrate, the mixture was chilled in a refrigerator and then stored at −80°C.

2.4 Phage precipitation and DNA extraction

Phage particles were precipitated for DNA extraction as described previously (Antibody Design Laboratories, 2024). Briefly, the phage-infected bacterial culture was centrifuged at 13,000 × g for 5 min, and the supernatant was filtered using a 0.45-micron filter cartridge. To 12 mL of the filtrate, 3 mL of 5× PEG-NaCl solution (20% PEG8000, 2.5 M NaCl) was added and mixed by inversion. The mixture was incubated on ice for 1 h and then centrifuged at 13,000 × g for 3 min to precipitate the phage particles. The pellet was suspended in 1 ml of 1× Tris-buffered saline (50 mM Tris–HCl pH 7.5, 0.15 M NaCl). The suspension was incubated on ice for 1 h. The suspension was centrifuged at 13,000 × g for 1 min. The clear phage solution was transferred to a new tube.

Before DNA extraction, the bacteriophage preparation (in 0.5 mL of Tris-buffered saline, pH 7.5) was treated with 20 units/mL of DNase I (NEB, Beverly MA) and 0.02 µg/mL of RNaseA (Roche, Indianapolis IN) at 37°C for 1 h, to remove any nucleic acids of the host bacterium. DNase was then inactivated by heating the sample to 75°C for 5 min, and the sample was treated with 1 mg/mL of proteinase K (ThermoFisher, Waltham MA) in a buffer containing 0.1% SDS at 55°C for 1 h. The sample was then cooled to room temperature and extracted with an equal volume of phenol-chloroform-isoamyl alcohol reagent (ThermoFisher) on a rocking platform for 1 h. The mixture was then centrifuged for 5 min at 13,000 × g and the upper aqueous layer was transferred to a new tube. DNA was ethanol-precipitated following standard protocols. DNA was further cleaned using QIAquick cartridges (Qiagen, Germantown MD). DNA concentration was measured using a NanoDrop spectrometer (ThermoFisher).

2.5 DNA sequencing, assembly, and annotation

Phage DNA was sequenced using the MinION flow cell v10.4.1, using the Rapid DNA sequencing kit (Oxford Nanopore, New York, NY). The sequencing run was programmed for 20 h using the MinKNOW software package (Oxford Nanopore). The FASTQ files were assembled into contigs using FLYE (Kolmogorov et al., 2019). The median sequencing coverage was 360x (range 19–1,750×). The assembled genome was annotated with Pharokka v1.2.0.[1] Nucleotide BLAST[2] was utilized for comparative viral genomics and to check the presence of any integrated bacterial DNA and anti-CRISPR genes in the bacteriophage genome.

2.6 One-step growth curve

The latency period and burst size of the bacteriophage were determined from the one-step growth curve as described (Oliveira et al., 2020). Briefly, bacteria growing in log phage (A600 = 0.4–0.5) were harvested by centrifugation. The cells were suspended in 10 mM $MgSO_4$, and the cell count/ml was estimated using the formula: 0.5 MacFarland Standard = 1.5×10^8 colony-forming units (CFU)/ml (McFarland, 1907). The cell volume was adjusted with TSB to 2×10^{10} CFU/ml. To accomplish a multiplicity of infection (MOI) of 0.01, 1 ml of the bacterial suspension was mixed with 0.1 mL phage suspension containing 2×0^8 PFU. The mixture was incubated at 37°C for 5 min and then centrifuged at 13,000 × g for 5 min to remove any unabsorbed phages. The cell pellet was suspended in 10 mL of TSB and incubated at 37°C with mild agitation. One ml of post-infection sample was harvested at 10-min intervals over 70 min. The sample was centrifuged at 13,000 × g for 5 min to remove bacterial cells. The supernatant was 10-fold serially diluted, and 0.1 mL of the diluted samples were used to infect bacterial cells using the agar overlay method. The plates were incubated at 37°C for 16–20 h and the phage titer was calculated as described in the previous section. The latency period was determined from two independent experiments from the time point before lysis of the host cells, and the burst size was calculated by quantifying the infection centers (i.e., dividing the average PFU/ml of three higher viral titers by the average of three lower virus titer) (Rivera et al., 2022).

2.7 Electron microscopy

Electron microscopy was done at the Brigham Young University Electron Microcopy Facility, Provo UT. Phage particles were harvested from infected host cells in broth culture as described in the

1 https://bear-apps.bham.ac.uk/applications/2022a/pharokka/1.2.0/
2 https://blast.ncbi.nlm.nih.gov/Blast.cgi

previous section, or from webbed overlay culture plates by washing with TSB containing 1.0 mM $CaCl_2$. The wash was centrifuged at 13,000 × g for 5 min to remove cellular debris. A 5 µL sample of the clean supernatant/wash was placed on copper grids. The grids were incubated at room temperature for 2 min. The fluid was then removed by touching the margin of the grids with a blotting paper and the grids were stained for 2 min with 0.5% aqueous uranyl acetate solution. The grids were examined, and the images were digitally documented using a Helios NanoLab™ 600 DualBeam scope (Hillsboro OR).

2.8 Host range and stability of phage particles

The host range of the phage was tested using the spotting method (Huang et al., 2018), by placing 10.0 µl samples of cell-free phages (10^9 PFU/ml) on a bacterial lawn created using the agar overlay method. The inoculated plates were incubated at 37°C for 20 h before visual examination for plaque formation.

The temperature and pH stability of the phage were tested as described (Oliveira et al., 2020; Khawaja et al., 2016), in the range that can be encountered during storage, transportation, formulation, and administration of therapeutic phages. For temperature sensitivity, cell-free bacteriophages (10^8 PFU/ml) were incubated at the constant temperature of 37°C, 47°C, 57°C, 67°C, or 77°C for 75 min. We also assayed cell-free bacteriophages stored at −80°C and bacteriophages in infected host cell cultures stored at 4°C. For pH sensitivity, 1 ml cell-free bacteriophage (10^9 PFU) was mixed with 9 mL of TSB previously adjusted to pH 3, 5, 7, 9, or 11 (by adding NaOH or HCl solutions) and incubated at room temperature for 75 min. The treated samples were 10-fold serially diluted using TSB and the phage titer was determined by the agar overlay method.

2.9 Lysogenic infection and lysogen immunity tests

Temperate phages, having lytic and lysogenic life cycles, are generally not desirable for phage therapy (Monteiro et al., 2019), because temperate phages may transduce bacterial genes including virulence factor genes and the integrated proviral genome may prevent lytic infections of the lysogens. Whether the *Klebsiella* phage we isolated causes lysogenic infection of the host bacterium was tested using a previously described protocol (Altamirano and Barr, 2021). Briefly, fresh TSA plates were streaked using a sterile applicator or a 200-µl pipette tip that touched the center of an isolated viral plaque. The plates were incubated overnight at 37°C. Several potential lysogen colonies from the plate were grown to pure culture through sequential agar plate streaking experiments. Lysogeny was tested by PCR using DNA extracted from pure cultures of the potential lysogens (as the test item), uninfected *K. pneumoniae* cells (as a negative control), and cell-free bacteriophages (as a positive control) as the template. The primer pairs used were 5′ CGATCGTCAGCCATGCAAAG3′, and 5′GCGAG TCATTCGATGTTGGC3′. The primers were designed based on the nucleotide sequence of the genome of the *Klebsiella* phage using Primer-BLAST software.[3] Nucleotide BLAST analyses indicated that the primer pair, part of the DNA Primase Gene of the *Klebsiella* phage, is not related to genomic DNA sequences of any known species of *Klebsiella*. The reaction mixture (20 µL) contained 1x Platinum *Taq* II Master Mix (ThermoFisher), 20 picomoles of the primer pairs, and 20 ng of DNA template. The thermocycler was programmed as the following: 94°C for 5 min (one cycle), 94°C for 30 s, 59°C for 30 s and 72°C for 40 s, (37 cycles), and 72°C for 5 min (one cycle). The amplified DNA fragments were resolved in 6% polyacrylamide gels, stained with ethidium bromide (10 µg/ml), and digitally documented. PCR-positive colonies were considered lysogens. Immunity of the lysogens to the phage was tested by infecting the potential lysogens with the bacteriophage using the spot assay method.

2.10 Minimum inhibitory multiplicity of Infection (MIM)

MIM of the phage for the host bacterial strain was tested as described (Nikolic et al., 2022). Briefly, the host bacterium grown overnight was pelleted by centrifugation (5,000 × g for 5 min). The pellet was suspended in 0.1 M $MgSO_4$ solution to 0.5 McFarland Standard (~1.5×10^8 CFU/ml). This stock was diluted 1:10 with TSB, and then 0.1 mL of the diluted bacterial preparation (~1×10^6 CFU) was seeded into a 96-well plate. The virus preparation was 10-fold serially diluted (10^9–10^1 PFU/ml), and 0.1 mL of the diluted virus preparation was added to the wells of the 96-well plate, in triplicates. Uninfected cells (0.1 mL bacterial cells mixed with 0.1 mL of TSB) served as the control. The plate was incubated at 37°C for 20 h. At that point, 20 µl of 0.1% aqueous solution of 2,3,5 triphenyl tetrazolium chloride (TTC) (Sigma-Aldrich, St. Louis MO) was added to the plate. The plate was incubated for another 3 h for any surviving bacteria in the wells to reduce TTC (a colorless chemical) to 1, 3, 5 triphenyl formazan (TPF), a red dye. The MIM is the lowest MOI of phage solution that prevented bacterial growth, indicated by a complete lack of TPF synthesis.

2.11 Inhibition of biofilm formation by the bacteriophage

K. quasipneumoniae is a biofilm-forming bacterium, and the ability to form a biofilm is a crucial virulence factor of *Klebsiella* spp. (Guerra et al., 2022). Whether the bacteriophage interferes with the bacterium's capacity to form biofilm was tested as described previously (Bernal-Bayard et al., 2023). Briefly, 1×10^6 CFU (in 0.1 mL) of bacteria growing in the log phase were seeded into a 96-well plate. Ten-fold serially diluted bacteriophage preparation (0.1 mL, 1×10^9–1×10^1 PFU/well) was also added to the wells in triplicates. Uninfected *Pseudomonas aeruginosa* (ATCC 27853), and uninfected *K. quasipneumoniae* cells served as the controls. The plate was incubated at 37°C for 24 h. Bacterial growth was measured using a BioTek Synergy I plate reader (Agilent, Santa Clara CA) at 600 nm. The liquid medium was aspirated, and the plates were washed thrice

3 https://www.ncbi.nlm.nih.gov/tools/primer-blast/

with water and then stained for 15 min using 0.2 mL of 0.5% aqueous solution of crystal violet. The crystal violet solution was then rinsed by repeatedly immersing the plate in tap water. The plate was air-dried for 10 min and 0.2 mL of 30% glacial acetic acid solution was added to the wells. After incubating for 5 min at room temperature, 0.18 mL of the fluid was transferred to a new 96-well plate. The absorbance (A585) of the solution was measured using a BioTek Synergy I plate reader.

2.12 Phage-antibiotic synergy (PAS)

PAS refers to a decrease in the inhibitory/lethal dose of an antibiotic to a bacterium in the presence of a virus that infects the bacterium (Comeau et al., 2007). Initially, antibiotic sensitivity of the bacterial strain was tested following the standard Kirby-Bauer Disk Diffusion Susceptibility test protocol (Hudzicki, 2009) in 15-cm Muller Hinton Agar plates using antibiotic-impregnated Sensi-Disks™ (BD BBL, Franklyn Lake NJ) and the zone of inhibition (ZOI) was measured. The minimum inhibitory concentration (MIC) of the two antibiotics to which the bacterium was found susceptible was then determined. Overnight-grown bacterial culture was centrifuged, and the pellet was suspended in 0.1 M $MgSO_4$ to 0.5 McFarland standard. The preparation was further diluted to 1:10 with TSB, and 0.1 mL of bacterial suspension (~1×10^6 CFU) was seeded into a 96-well plate, in triplicates. The selected antibiotics were diluted to 512 μg/ml to 1 μg/ml and 0.1 mL of the diluted antibiotic was added to the wells (i.e., the final antibiotic concentration was 256 to 0.5 μg/ml). The plate was incubated at 37°C for 20 h and bacterial viability was tested by TTC conversion assay as described in the previous section. The lowest concentration of the drug that prevented conversion of TTC to TPF was considered the MIC.

PAS was tested using the checkerboard method as described previously (Nikolic et al., 2022). Briefly, 0.05 mL of a diluted bacterial preparation (~1×10^6 CFU) was seeded into a 96-well plate. Two-fold serially diluted antibiotic solutions (0.05 mL) were added to the wells in rows to the final concentration 1–256 μg/ml. Ten-fold serially diluted bacteriophage preparations (0.1 mL, 10^9–10^1 PFU/well, corresponding MOI 1,000 to 0.000001) were added to the wells in columns. The experiments were repeated once. The plate was incubated at 37°C for 20 h. Bacterial viability was tested by reduction of TTC to TPF as described in the previous section. The fractional inhibitory concertation (FIC) was determined by the relation $FIC = (MIC_{\text{phage-antibiotic combination}}/MIC_{\text{antibiotic alone}})$.

3 Results

3.1 Structure of the virus and its genome

Lytic phages in raw wastewater were screened using *Klebsiella quasipneumoniae* strain K6 (ATCC 700603). A phage isolate that consistently generated large transparent plaques (~2 mm in diameter) was plaque-purified for further analyses. Electron microscopic imaging of the negatively stained samples of the cell-free bacteriophage isolate magnified to 350,000× showed naked complex capsids having an icosahedral spherical head (62 ± 3 nm in diameter) and a slender (137 ± 12 nm × 11 ± 1.36 nm) tail with an inconspicuous tail base plate (Figure 1). At this magnification of the negatively stained samples, the tail fibers, if present, were not visible.

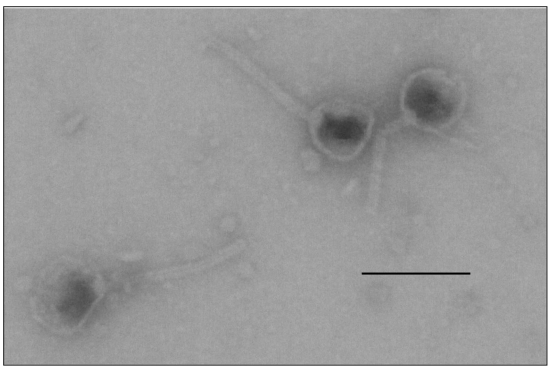

FIGURE 1
Structure of the capsids of the bacteriophage vB_KquU_φKuK6. Shown is a photograph of electron microscopic images of phage capsids with a roundish icosahedral head (about 60 nm), and a slender tail (about 140 nm × 10 nm), original magnification 349,908×. The bar is 100 nm.

The nucleotide sequence of the genome of the virus (GenBank accession number is PP874908) indicated that the isolate has an AT-rich (51% AT), linear double-stranded DNA genome 51,251 base pairs in size, containing 121 open reading frames (ORFs). A Pharokka plot of the identified genes and putative genes of the virus are shown in Figure 2. Majority of the genes including all the genes encoding the structural proteins for the head and tail of the capsid and the putative genes are in the top strand of the genome. Genes encoding nucleases, helicases, and enzymes involved in DNA replication (such as primases, and single-strand DNA binding proteins) are in the bottom strand of the genome. The genome contains a putative spanin gene, an endolysin gene, and a holin gene, which are necessary for a lytic infection cycle. The Pharokka v1.2.0. annotation software was unable to detect a genome integration/excision module needed for the lysogenic life cycle. However, the genome contains a gene encoding Erf-like ssDNA binding protein/recombinase in the location 36,705–37,382. A search of the open protein and genome databases using the BLAST software (Altschul et al., 1990) indicated that the genome of the bacteriophage isolate is most closely related to the genome of the *Klebsiella* phage vB_KpnS_SXFY507 (GenBank: ON045001.1) with a Query Cover of 95%, and Percent Identity of 98.17%, and is also related to several other *Klebsiella* phages of the Family *Drexlerviridae*. We named the isolate vB_KquU_φKuK6 (vB- bacterial virus, Kqu- abbreviated for the name of the host species, U- unknown virus genus, φKuK6- the name of the isolate) following the proposed naming convention (Adriaenssens and Brister, 2017).

3.2 Host range

Twelve additional strains of gram-negative bacteria (Table 1) were tested to evaluate the host range of vB_KquU_φKuK6. The phage failed to create plaques in the lawn of any of the strains other than *K. quasipneumoniae* within 24 h of the incubation period, indicating its narrow host range.

10.3389/fmicb.2024.1472729

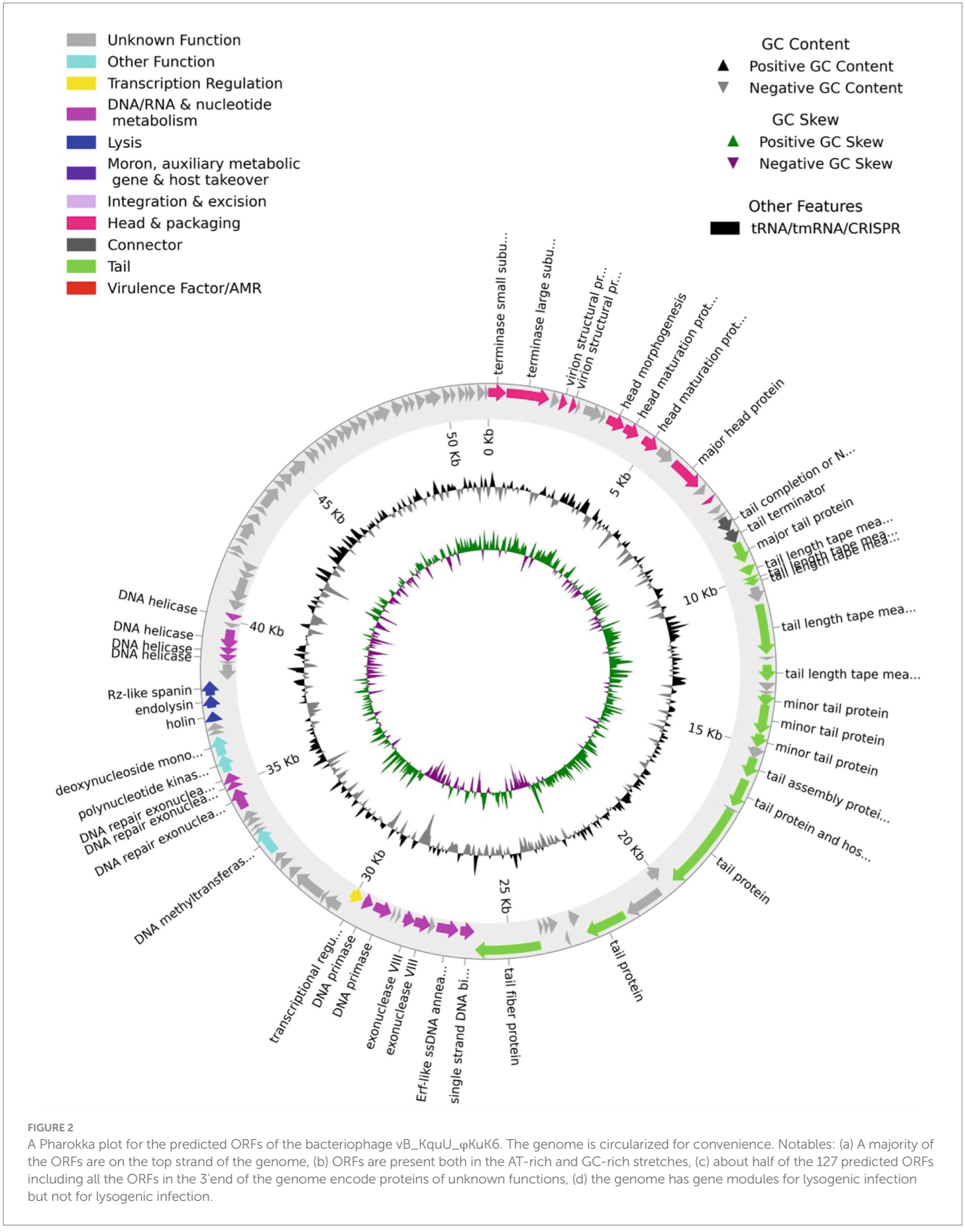

FIGURE 2
A Pharokka plot for the predicted ORFs of the bacteriophage vB_KquU_φKuK6. The genome is circularized for convenience. Notables: (a) A majority of the ORFs are on the top strand of the genome, (b) ORFs are present both in the AT-rich and GC-rich stretches, (c) about half of the 127 predicted ORFs including all the ORFs in the 3′end of the genome encode proteins of unknown functions, (d) the genome has gene modules for lysogenic infection but not for lysogenic infection.

3.3 One-step growth curve and lytic infection

The one-step growth curve of the phage (Figure 3A) indicates a latency period of about 20 min, a growth plateau of about 40 min, and a burst size of 435. Although the phage created large (diameter 2.0 ± 0.13 mm) clear (non-turbid) plaques (Figure 3B), it was unable to lyse the host bacterial lawns to a completion (Figure 3C) or clear the turbid broth culture of the infected host bacterium at any MOI

TABLE 1 Host range of the bacteriophage vB_KquU_φKuK6.

Bacterial strain	Lysis
Klebsiella quasipneumoniae Strain K6 (ATCC 700603)	+
Klebsiella pneumoniae strain 160_1080 (BEI: NR-44349)	–
Klebsiella oxytoca strain MIT 10–5,243 (BEI: HM-624)	–
Citrobacter freundii strain ATCC 13316 (ATCC 8090)	–
Escherichia coli FDA strain Seattle 1946 (ATCC 25922)	–
Escherichia coli stain EDL 931 (ATCC 35150) (BEI: NR-3)	–
Escherichia coli stain DH5α (ThermoFisher)	–
Proteus mirabilis strain WGLW6 (BEI: HM-753)	–
Pseudomonas aeruginosa strain Pa1651 (BEI: NR-51336)	–
Pseudomonas aeruginosa strain Boston 41,501 (ATCC 27853)	–
Salmonella enterica Tennessee (BEI NR-20742)	–
Serratia marcescens Bizio (ATCC 13880)	–
Shigella flexneri strain serotype 2a (BEI: NR-517)	–
Shigella sonnei strain WRAIR I Virulent (BEI: NR-519)	–

tested (Supplementary Figure 1). At high MOI, bacterial mesas grew in the overlay agar plates (Figure 3C).

3.4 Sensitivity to physical and chemical factors

The titer of the progeny phages of thermally treated vB_KquU_φKuK6 is shown in Figure 4. There was no reduction in the titer of progeny phages for parental phages treated at 37°C, 47°C, and 57°C. The titer of the progeny phages was reduced by about two orders of magnitude for parental phages treated at 67°C. vB_KquU_φKuK6 treated at 77°C for 75 min was completely inactivated (produced no progeny phage) (Figure 4A). Titer of vB_KquU_φKuK6 refrigerated in infected bacterial culture remained unchanged for at least 4 months and purified vB_KquU_φKuK6 in 50% glycerol stored at −40°C and −80°C remained biologically active for at least 10 months (Supplementary Figure 2).

The titer of progeny phages of parental vB_KquU_φKuK6 treated at different pH is shown in Figure 4B. Phages treated at pH 3 were inactivated (generated no progeny phage). There was no reduction in the titer of progeny phages for parental phages treated at pH 5 and pH 7. The progeny virus titer was reduced by about two orders of magnitude for parental phages treated at pH 9 or pH 11 (Figure 4B). Phages released by infected host bacterial cells treated with 1% (by volume) of chloroform for 1 min remain biologically active (Supplementary Figure 3).

3.5 Lysogenic infection

vB_KquU_φKuK6 reduced growth (measured by A600) of the host bacterium at all MOI (i.e., 0.00001 to 1,000) tested. However, the TTP dye reduction assay indicated that the phage failed to completely halt bacterial growth irrespective of the MOI (Figure 5A), indicating a possible lysogenic mode of infection. To confirm this finding, we isolated potential lysogens from the center of isolated plaques on overlay agar plates to pure culture to examine the genome of the cells for the presence of a potential provirus. PCR tests using vB_KquU_φKuK6 genome-specific primers and the genomic DNA of the isolated potential lysogens as templates indicated the presence of a potential provirus in the genome of the potential lysogen clone #2 (Figure 5B). Spot assay showed that the PCR-positive lysogen clone #2 was resistant to infection by vB_KquU_φKuK6 (Figure 5C), indicating immunity of the lysogens to vB_KquU_φKuK6 reinfection.

3.6 Interference to biofilm production by the host bacterium

vB_KquU_φKuK6 inhibited biofilm production of the host bacterium in a dose-dependent manner, where the higher MOI (1,000-1) reduced biofilm production by approximately 75% and lower MOI (0.1–0.001) reduced biofilm production by about 50% (Figure 6). However, none of the tested MOIs completely negated the ability of the host cells to secrete biofilms.

3.7 Phage-antibiotic synergy

Initial disk-diffusion tests indicated that the host bacterial strain is completely resistant (i.e., no ZOI) to cephalothin (30 μg), and erythromycin (15 μg) and resistant/intermediately resistant (Hudzicki, 2009) to chloramphenicol (30 μg, ZOI 11 mm), neomycin sulfate (30 μg, ZOI 8 mm), moxifloxacin (5 μg, ZOI 11 mm), and sulfamethoxazole-trimethoprim (23.75 μg/1.25 μg, ZOI 12 mm) (Supplementary Figure 4). We randomly chose chloramphenicol and neomycin sulfate for further study and determined the MIC for these two drugs to be 64 μg/mL and 256 μg/mL, respectively (Supplementary Figure 5). When phages and antibiotics were combined, bacterial growth was completely inhibited at 8 μg/mL of chloramphenicol in combination with a phage MOI of 0.01, giving a fractional inhibitory concentration (FIC) of 0.125 (Figure 7). However, higher MOIs increased the FIC (for example, the MOI of 1,000 increased the FIC to 0.25). Neomycin sulfate also completely inhibited bacterial growth at 32 μg per ml in combination with a phage MOI of 1,000, giving an FIC of 0.13 (Figure 7).

4 Discussion

K. quasipneumoniae strain K6 (previously named *K. pneumoniae* stain K6) was isolated from the urine of a hospitalized patient in 1994. The strain has been extensively characterized (Rasheed et al., 2000) and its genome has been sequenced and analyzed (Elliott et al., 2016). Pathologists use the strain as the reference strain for bacterial extended-spectrum beta-lactamase (ESBL) production. Although some strains of *K. quasipneumoniae* colonize the gastrointestinal tract of some healthy subjects (Holt et al., 2015), MDR/hypervirulent strains of *K. quasipneumoniae* have been reported from clinically infected subjects (Altayb et al., 2023; Arabaghian et al., 2019). For having MDR, XDR, PDR, and hypervirulent strains, *Klebsiella* spp. has been a model candidate for phage therapy. Several phages have been reported to have potential use in phage therapy against

K. quasipneumoniae (Bird et al., 2024; Liu et al., 2024) and *K. pneumoniae* (Fayez et al., 2023; Han et al., 2023; Kondo et al., 2023; Lourenço et al., 2023; Peng et al., 2023; Kim et al., 2022; Nazir et al., 2022; Townsend et al., 2021; Zurabov and Zhilenkov, 2021; reviewed in Herridge et al., 2020) over past few years. The present report describes one such phage vB_KquU_φKuK6, adding to this rapidly growing body of information.

vB_KquU_φKuK6 is a typical coliphage with a spherical icosahedral head (about 60 nm) and a long slender tail (about 140 nm × 10 nm). A nucleotide BLAST search indicated vB_KpnS_SXFY507, a phage that infects *K. pneumoniae* strain SFX506 (Feng et al., 2023), as the closest genetic relative of vB_KquU_φKuK6. The size of the head and tail of vB_KpnS_SXFY507 was reported to be 56 nm and 175 nm, respectively (Feng et al., 2023), which is comparable to that of vB_KquU_φKuK6. The total volume of a vB_KquU_φKuK6 particle is about 1.8×10^5 cubic nanometers (or about 0.0002 cubic micrometers). We initially screened the phage by filtering wastewater using 0.2-micron, low protein-binding filters. After plaque purification, we used 0.45-micron low protein-binding filters because we observed that the phage titer was reduced from typically about 1.5×10^{10} PFU/ml to about 1.5×10^8 PFU/ml (on average, by about two orders of magnitude) if 0.2-micron filters were used. A previous report indicated that the recovery of different phages is negatively affected by certain types of membranes and smaller pore sizes of the filtration devices (Larsen et al., 2023).

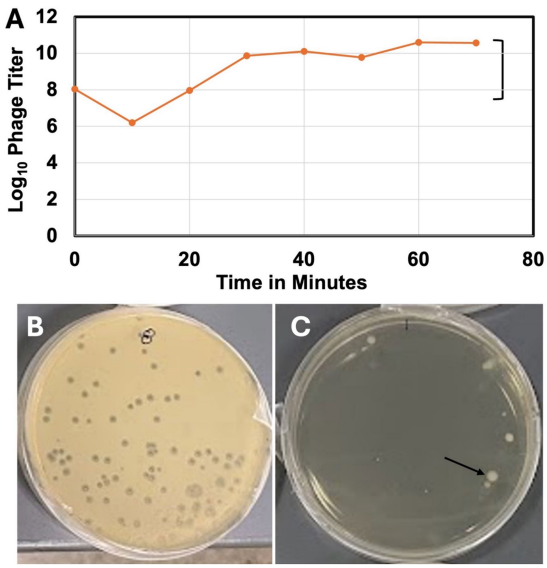

FIGURE 3
One-step growth curve and some lytic properties of vB_KquU_φKuK6. **(A)** One-step growth curve of the bacteriophage. **(B)** A photograph showing plaques (~2 mm in diameter) created on a bacterial lawn infected at the MOI of 0.001. **(C)** A photograph showing bacterial mesas (indicated by the arrow) on a lawn infected at a MOI of 1,000.

The genome of vB_KquU_φKuK6 is made of a linear dsDNA molecule 51,251 bp in size, comparable to the genome (53,122 bp) of its nearest relative vB_KpnS_SXFY507 (Feng et al., 2023). The structure of the capsids and genomes of vB_KquU_φKuK6 and vB_KpnS_SXFY507 indicate that the two phages are different taxonomic entities. The structures of the virion and the genome indicate that vB_KquU_φKuK6 (along with vB_KpnS_SXFY507 and *Escherichia* phage T1) belongs to the Family *Drexlerviridae*. Several bacteriophages of this family that infect *Klebsiella* spp. have been reported and extensive comparative genomic studies on these viruses have been conducted (Ndiaye et al., 2024; Fayez et al., 2023; Feng et al., 2023; Lourenço et al., 2023; Pertics et al., 2023; Nazir et al., 2022; Martins et al., 2022). The genome of vB_KquU_φKuK6 and many of these related viruses have several gene modules such as: (a) DNA packaging module containing genes for terminases and some other proteins involved in incorporating viral DNA into the capsid, (b) morphogenesis modules containing genes encoding the head and tail proteins of the capsid, (c) genome replication/maintenance modules containing genes involved in nucleotide metabolism, genome replication, genome modification, and recombinases, (d) lysis module containing genes encoding proteins involved in the lysis of the infected host cells such as holins, endolysins, and spanins, (e) modules containing over 50 ORFs encoding proteins of unknown function, and a gene for transcription regulation (Fayez et al., 2023; Feng et al., 2023; Pertics et al., 2023; Nazir et al., 2022; Ku et al., 2021). We found no genes for bacterial virulence, or toxin genes, in the genome of vB_KquU_φKuK6, although we cannot rule out the possibility of those genes given the abundance of ORFs coding proteins of unknown function. A previous study also reported a lack of such genes in the genome of a related virus of the Family

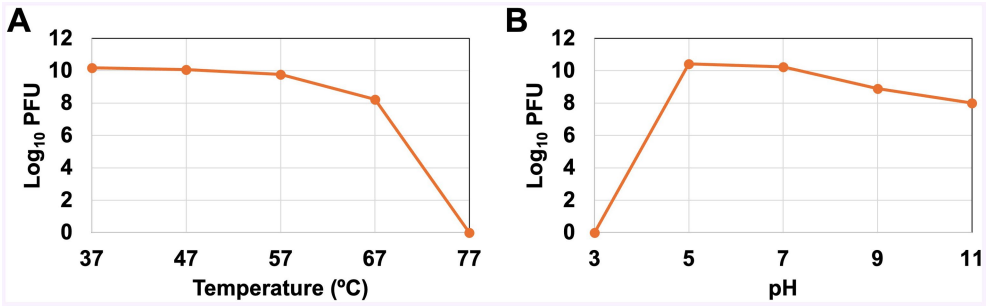

FIGURE 4
Stability of vB_KquU_φKuK6 at different temperatures and pH. **(A)** Temperature sensitivity. A graph showing $\log_{10}$ of phage titer (PFU/ml) after the phage was incubated at indicated temperatures. The phage is unaffected at 37–57°C. Phages incubated at 67°C yielded a titer two orders of magnitude lower. Phages incubated at 77°C were inactivated. **(B)** A graph showing $\log_{10}$ of phage titer (PFU/ml) after the phage was incubated at the indicated pH. Phages incubated at pH 3 were inactivated. Phages incubated at pH 5 and pH 7 yielded similar progeny titers. Phages incubated at pH 9 and pH 11 produced a titer reduced by about two orders of magnitude.

10.3389/fmicb.2024.1472729

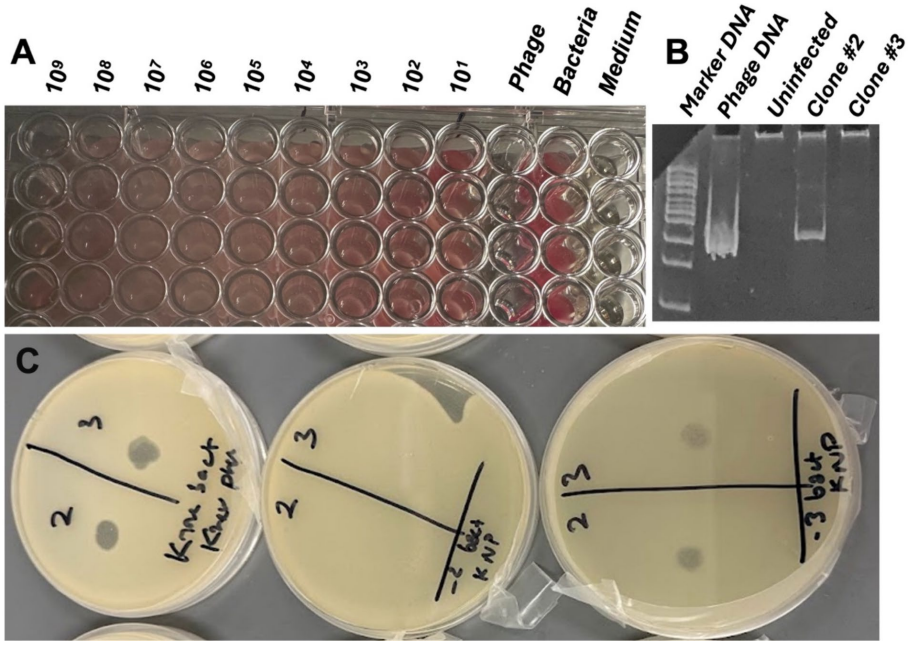

FIGURE 5
Lysogenic mode of infection by vB_KquU_φKuK6. **(A)** vB_KquU_φKuK6 failed to completely stop the growth of the host bacterium. Shown is a photograph of a part of a 96-well plate growing the host bacterium exposed to different MOIs of vB_KquU_φKuK6 for 20 h. The red dye in the wells indicates the presence of live cells. Phage- phages only, no host bacterium added (the wells were clean; the redness on the right corner of the wells is because of the reflection of the wells on the right side). Bacteria- host cells only, no phage added. Medium- medium only, no bacteria or virus added. **(B)** A PCR-test for lysogenic infection. A photograph of an agarose gel that resolved DNA fragments amplified with a vB_KquU_φKuK6 genome-specific primers. The genomic DNA of plaque-purified vB_KquU_φKuK6 and potential lysogen clone #2 generated the PCR product of the expected size, the genomic DNA of uninfected host cells and potential lysogen clone #3 did not. **(C)** Immunity of the lysogen clone #2 to superinfection. vB_KquU_φKuK6 (10^7 PFU) was spotted on overlay agar plates seeded with the uninfected host cells (left), clone #2 cells (middle), and clone #3 cells (right). Plaques developed on plates on spots 2 and 3 of the uninfected host cells and potential lysogen clone #3, but the plate growing potential lysogen Clone #2 cells resisted plaque formation.

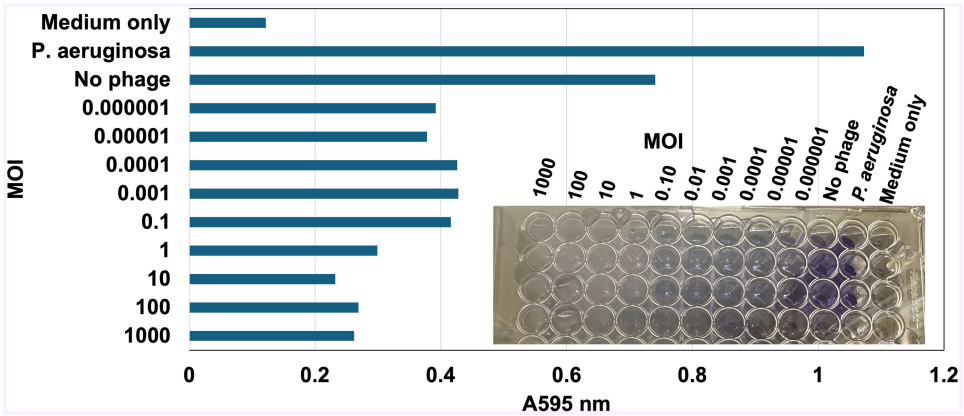

FIGURE 6
vB_KquU_φKuK6 inhibited the ability of biofilm formation of the host bacterium. Shown is a bar graph of light scattering (A595) by the biofilm formed by uninfected *K. quasipneumoniae* cells (No phage) or the same exposed to a MOI of 1,000 to 0.000001 of vB_KquU_φKuK6. Uninfected *K. quasipneumoniae*, Cells (No phage) uninfected *P. aeruginosa* cells, and uninoculated medium (TSB) served as controls. Inset: A photograph showing biofilm formation indicated by the retention of crystal violet dye in the wells of a repeatedly washed 96-well plate.

Drexlerviridae (Fayez et al., 2023). We also found no anti-CRISPR genes in the genome of vB_KquU_φKuK6 although some members of the *Drexlerviridae* family have such genes (Kondo et al., 2023; Kumar et al., 2021). Two other reported phages, EKq1, and KL0, that infect *K. quasipneumoniae*, are not closely related to vB_KquU_φKuK6. The genome of EKq1 is about 48.2 kbp in size and the phage has a putative anti-CRSPR gene (Bird et al., 2024). The genome of KL01 is about 44 kb and the virus is a member of Autophagoviridae (Liu et al., 2024).

The lysis module of the genome of vB_KquU_φKuK6 with the hollin, spanin, and endolysin genes indicates a lytic infection cycle.

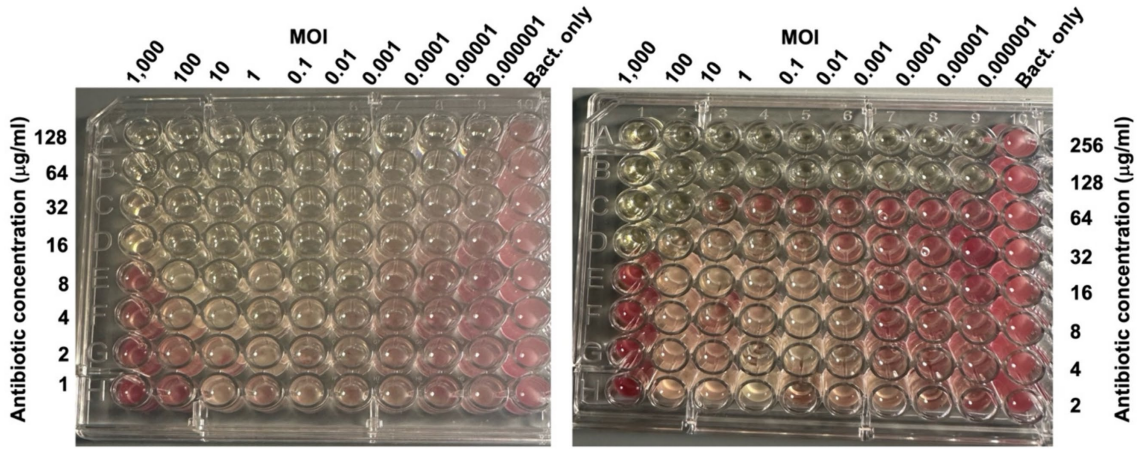

FIGURE 7
Phage-Antibiotic synergy. Photographs of 96 well plates seeded with the host bacterium (10^6 CFU) exposed to the indicated MOIs of vB_KquU_φKuK6 (in columns), and the indicated amounts of chloramphenicol (left) or neomycin sulfate in rows (right). The antibiotics or phages were not added to the control wells. The plates were incubated for 20 h and then TTC was added. The picture was taken 3 h after TTC was added. The lack of red color formation indicates complete inhibition of bacterial growth.

Hollins accumulate in the plasma membrane and create holes that depolarize the infected cell; endolysins degrade the cell wall polysaccharides; and spanins disrupt the inner and outer membranes (Abeysekera et al., 2022). The genome of many members of the *Drexlerviridae* family contains an Erf-like ssDNA annealing protein/recombinase gene (Ndiaye et al., 2024; Feng et al., 2023; Nazir et al., 2022; Kumar et al., 2021). The genes of the Erf-like ssDNA annealing protein/recombinase family encode proteins that bind ssDNA and supercoiled DNA but not dsDNA (Caldwell et al., 2022; Cheong et al., 2022). Thus, it is unclear if these proteins are involved in conserved site-specific recombination (CSSR) needed for phage genome integration and excision. Our initial analysis of the genome of vB_KquU_φKuK6 indicated an absence of an integration/excision genes module needed for lysogenic infection. However, we observed that vB_KquU_φKuK6 fails to completely lyse bacterial culture irrespective of MOI indicating the possibility of lysogenic infection mode. Our molecular and culture-based assays indicated that vB_KquU_φKuK6 is a temperate phage capable of causing lysogenic infection of *K. quasipneumoniae*. Our PCR test for lysogeny does not confirm whether the lysogens have chromosome-integrated proviruses or episomal genomes of the bacteriophage. Thus, the viral infection can be lysogenic or pseudolysogenic (Hobbs and Abedon, 2016). However, our results indicate that the resulting lysogens are immune to lytic infection by vB_KquU_φKuK6. Other phages capable of lysogenic infection of *Klebsiella* spp. have been reported (Kondo et al., 2023). Lysogeny is naturally selected because it is a part of the survival strategies of bacteriophages (Poteete and Fenton, 1983) and is potentially beneficial to the host bacterium (Howard-Varona et al., 2017). Since lytic/non-lysogenic phages are preferred for phage therapy, candidate phages should be screened by molecular and cellular methods for lysogenic infection. Our limited analysis indicates that comparative genome analysis alone may not rule out the possibility of lysogenic infection by a bacteriophage.

Our preliminary analyses indicate that vB_KquU_φKuK6 has a narrow host range. An ideal therapeutic phage should have a somewhat broader host range (it should be able to infect many pathogenic strains of the target species but not the members of the resident normal biota). However, most of the reported *Klebsiella* phages have a narrow host range because of the diversity of the capsule of the host cells and the substrate-specificity of the depolymerase gene of the phages (Beamud et al., 2023). Because of this and other reasons (including the ability of potential lysogenic infection by many phages, and the ability of the host cells to develop resistance to phage infection), a phage cocktail containing many phage species, is suggested for phage therapy (Beamud et al., 2023; Yoo et al., 2023; Abedon et al., 2021).

A temperate phage, although less desirable, can be useful for phage therapy (Monteiro et al., 2019). Therefore, we investigated if vB_KquU_φKuK6 has some useful attributes of therapeutic phages. An ideal therapeutic phage should infect host cells rapidly and the virions should be stable at a wide range of environmental conditions suitable for formulation, storage, and transport of the phage preparations. We observed that vB_KquU_φKuK6 has a short latency period of about 20 min and a bust size of over 400. The vB_KquU_φKuK6 titer plateaued in 40 min to reach 10^{11} PFU/ml within 2–48 h post-infection. vB_KquU_φKuK6 is resistant to a short exposure to 1% chloroform (an agent used in lysing intact infected bacteria to release phages) and quite stable at −80°C to about 57°C and a pH of 4–11. However, vB_KquU_φKuK6 gets inactivated at pH 3, indicating that its oral application would require manipulation of the stomach pH. Of some *Klebsiella* phages of the Family *Drexlerviridae,* VB_Kpn_ZC2 showed a latency period of 22 min, a burst size of 650 PFU, and stability at −40°C to +50°C and pH 4–9 (Fayez et al., 2023). The *Klebsiella* phage IME268 showed a latency period of 30 min, and a plateau time of 90 min, but the phage is sensitive to chloroform, temperature above 50°C, and pH <4 and >11 (Nazir et al., 2022). The *Klebsiella* phage vB_KpnS_SXFY507 showed a latency period of 20 min, a burst size of 246, stability at 50°C and pH 4–12, and the phage showed a relatively wider host range (Feng et al., 2023). The *Klebsiella* phage KM18 showed a latency period of 20 min and a burst size of 12 (Ku et al., 2021).

Overall, several *Klebsiella* phages of the Family *Drexlerviridae* have some good attributes of a therapeutic phage.

Biofilm secretion is a major virulence factor of *Klebsiella* spp. (Guerra et al., 2022) and most other pathogenic bacteria (Domenico et al., 2017). Infection by a lytic phage prevents capsule secretion by the infected bacterium, reducing the possibility of biofilm formation. vB_KquU_φKuK6 reduced biofilm secretion of its host strain by up to 75% in a MOI dose-dependent manner, but the phage failed to completely stop biofilm production at any MOIs tested. A previous report indicated that the *Klebsiella* phage KM18 (Family *Drexlerviridae*) significantly reduced (but was unable to stop) biofilm production by *Klebsiella michiganensis*, by killing host bacterial cells (Ku et al., 2021).

K. quasipneumoniae is resistant to many antibiotics (Altayb et al., 2023). vB_KquU_φKuK6 demonstrated phage-antibiotic synergy (PAS) by reducing the MIC of chloramphenicol from 64 μg/ml to 8 μg/m at a MOI of 0.01. However, at higher MOI (of 1–1,000) a higher dose of the antibiotic was needed to stop bacterial growth, indicating that some host cells may become rapidly lysogenized and the lysogens required a higher dose of antibiotics for lysis. vB_KquU_φKuK6 also reduced the MIC of neomycin sulfate from 256 ug/ml to 32 ug/ml. A previous report indicated a *Klebsiella* phage that reduced MIC of cefepime and tetracycline for two MDR strains of *K. pneumoniae* (Qurat-ul-Ain et al., 2021). PAS has been demonstrated in other pathogenic bacteria including biofilm-producing bacteria such as *Pseudomonas aeruginosa* (Holger et al., 2023; Osman et al., 2023). We anticipate simultaneous application of PAS and a phage cocktail to be clinically more effective in treating MDR/XDR bacterial infections.

5 Conclusion

We have isolated a new bacteriophage (vB_KquU_φKuK6) that infects and effectively lyses *K. quasineumoniae*, an MDR pathogen. The phage is stable at clinically relevant ranges of temperatures and pH. The phage rapidly infects the host strain and generates a high virus titer. However, vB_KquU_φKuK6 has a narrow host range, it causes lysogenic infections, and the resulting lysogens are resistant to lytic infection by vB_KquU_φKuK6. Despite these shortcomings, vB_KquU_φKuK6 has potential for therapeutic applications because the phage significantly reduces its host's ability to produce biofilm and the minimum inhibitory concentration of certain antibiotics. Further research is needed to create a genetically modified vB_KquU_φKuK6 incapable of lysogenic infection. Such an agent, preferably in combination with antibiotics and/or other therapeutic *Klebsiella* phages, can be used in treating infections caused by *K. quasineumoniae* and possibly some other strains of *K. pneumoniae*.

Data availability statement

The genomic dataset presented in this study can be found in online repository. The names of the repository/repositories and accession number(s) can be found below: https://www.ncbi.nlm.nih.gov/genbank/, PP874908.

Author contributions

IPM: Funding acquisition, Investigation, Methodology, Writing – original draft, Writing – review & editing. AGL: Data curation, Investigation, Methodology, Project administration, Software, Supervision, Writing – original draft, Writing – review & editing. GZ: Data curation, Investigation, Methodology, Software, Writing – original draft, Writing – review & editing. BJS: Investigation, Methodology, Writing – original draft, Writing – review & editing. KVW: Investigation, Methodology, Project administration, Resources, Writing – original draft, Writing – review & editing. RHK: Investigation, Methodology, Project administration, Resources, Writing – original draft, Writing – review & editing, Conceptualization, Data curation, Formal analysis, Funding acquisition, Supervision.

Funding

The author(s) declare that financial support was received for the research, authorship, and/or publication of this article. An Undergraduate Research Scholarly and Creative Activities (URSCA) grant to IPM partially supported this research. Utah Valley University supported AGL, GZ, and RHK through reassigned time and paid the publication fee for this article.

Acknowledgments

The authors are grateful to Anna Smithee, Caleb Conrad, and Brian Bona for conducting some preliminary experiments and to Michael Standing of Brigham Young University Electron Microscopy Facility, Provo Utah, for preparing the electron microscopic images of the bacteriophage.

Conflict of interest

The authors declare that the research was conducted in the absence of any commercial or financial relationships that could be construed as a potential conflict of interest.

Publisher's note

Supplementary material

The Supplementary material for this article can be found online at: https://www.frontiersin.org/articles/10.3389/fmicb.2024.1472729/full#supplementary-material

References

Abedon, S. T., Danis-Wlodarczyk, K. M., and Wozniak, D. J. (2021). Phage cocktail development for bacteriophage therapy: toward improving spectrum of activity breadth and depth. *Pharmaceuticals (Basel)* 14:1019. doi: 10.3390/ph14101019

Abeysekera, G. S., Love, M. J., Manners, S. H., Billington, C., and Dobson, R. C. (2022). Bacteriophage-encoded lethal membrane disruptors: Advances in understanding and potential applications. *Front. Microbiol.* 13:1044143. doi: 10.3389/fmicb.2022.1044143

Adriaenssens, E. M., and Brister, J. R. (2017). How to name and classify your phage: an informal guide. *Viruses* 9:70. doi: 10.3390/v9040070

Altamirano, F. L. G., and Barr, J. (2021). Screening for lysogen activity in therapeutically relevant bacteriophages. *Bio Protoc.* 11:e3997. doi: 10.21769/BioProtoc.3997

Altayb, H. N., Hosawi, S., Baothman, O., Kazmi, I., Chaieb, K., Zeid, I. M. A., et al. (2023). Molecular insights into novel environmental strains of *Klebsiella quasipneumoniae* harboring different antimicrobial-resistance genes. *Front. Public Health* 10:2022. doi: 10.3389/fpubh.2022.1068888

Altschul, S. F., Gish, W., Miller, W., Myers, E. W., and Lipman, D. J. (1990). Basic local alignment search tool. *J. Mol. Biol.* 215, 403–410. doi: 10.1016/S0022-2836(05)80360-2

Antibody Design Laboratories (2024). Small-scale preparation of bacteriophage by peg precipitation. Available at: http://www.abdesignlabs.com/technical-resources/bacteriophage-preparation/ (Accessed July 15, 2024).

Arabaghian, H., Salloum, T., Alousi, S., Panossian, B., Araj, G. F., and Tokajian, S. (2019). Molecular characterization of carbapenem resistant *Klebsiella pneumoniae* and *Klebsiella quasipneumoniae* isolated from Lebanon. Sci. Rep. (2019). doi: 10.1038/s41598-018-36554-2, 9

Balthazar, D. (2024). Phage therapy: Researchers sharpen another arrow in the quiver against antibiotic resistance. Available at: https://www.statnews.com/2024/02/20/phage-therapy-research-antibiotic-resistance/#:~:text=Clinical%20trials%20of%20phages&text=There%20are%20about%2090%20clinical,in%20the%20pipeline%2C%20Strathdee%20said (Accessed July 29, 2024).

Beamud, B., García-González, N., Gómez-Ortega, M., González-Candelas, F., Pilar Domingo-Calap, P. D., and Sanjuan, R. (2023). Genetic determinants of host tropism in *Klebsiella phages*. *Cell Rep.* 42:112048. doi: 10.1016/j.celrep.2023.112048

Bernal-Bayard, J., Thiebaud, J., Brossaud, M., Beaussart, A., Caillet, C., Waldvogel, Y., et al. (2023). Bacterial capsular polysaccharides with antibiofilm activity share common biophysical and electrokinetic properties. *Nat. Commun.* 14:2553. doi: 10.1038/s41467-023-37925-8

Bird, J. T., Burke, K. A., Urick, C. D., Braverman, J. L., Mzhavia, N., Ellison, D. W., et al. (2024). Genome sequence of the *Klebsiella quasipneumoniae* bacteriophage EKq1 with activity against *Klebsiella pneumoniae*. *Microbiol. Resour. Announc.* 13, e00954–e00923. doi: 10.1128/MRA.00954-23

Caldwell, B. J., Norris, A. S., Karbowski, C. F., Karbowski, C. F., Wiegand, A. M., Wysocki, V. H., et al. (2022). Structure of a RecT/Redβ family recombinase in complex with a duplex intermediate of DNA annealing. *Nat. Commun.* 13:7855. doi: 10.1038/s41467-022-35572-z

CDC. (2019). Antibiotic Resistance Threats in the United States, 2019. Atlanta, GA: U.S. Department of Health and Human Services, CDC. Available at: https://www.hhs.gov/sites/default/files/michael-craig-cdc-talk-thursday-am-508.pdf (Accessed July 15, 2024).

Cheong, K. H., Wen, T., Benler, S., Koh, J. M., and Koonin, E. V. (2022). Alternating lysis and lysogeny is a winning strategy in bacteriophages due to Parrondo's paradox. *Proc. Natl. Acad. Sci. USA* 119:e2115145119. doi: 10.1073/pnas.2115145119

Chew, K. L., Octavia, S., Lai, D., Lin, R. T. P., and Teo, J. W. P. (2021). *Klebsiella quasipneumoniae* from clinical specimens in Singapore. *Antimicrob. Agents Chemother.* 65, e00412–e00421. doi: 10.1128/AAC.00412-21

Clark, W. A. (1962). Comparison of Several methods for preserving bacteriophages. *Appl. Microb.* 10, 466–471. doi: 10.1128/am.10.5.466-471.1962

Comeau, A. M., Tétart, F., Trojet, S. N., Prère, M. F., and Krisch, H. M. (2007). Phage-antibiotic synergy (PAS): beta-lactam and quinolone antibiotics stimulate virulent phage growth. *PLoS One* 2:e799. doi: 10.1371/journal.pone.0000799

Crellen, T., Turner, P., Pol, S., Baker, S., Nguyen Thi Nguyen, T., Stoesser, N., et al. (2019). Transmission dynamics and control of multidrug-resistant *Klebsiella pneumoniae* in neonates in a developing country. *eLife* 8:e50468. doi: 10.7554/eLife.50468

Domenico, E. G. D., Farulla, I., Prignano, G., Gallo, M. T., Vespaziani, M., Cavallo, I., et al. (2017). Biofilm is a major virulence determinant in bacterial colonization of chronic skin ulcers independently from the multidrug resistant phenotype. *Int. J. Mol. Sci.* 18:1077. doi: 10.3390/ijms18051077

Elliott, E. G., Ganesamoorthy, D., Coin, L., Cooper, M. A., and Cao, M. D. (2016). Complete genome sequence of *Klebsiella quasipneumoniae* subsp. similipneumoniae strain ATCC 700603. *Genome Announc.* 4, e00438–e00416. doi: 10.1128/genomeA.00438-16

Fabijan, A. P., Iredell, J., Danis-Wlodarczyk, K., Kebriaei, R., and Abedon, S. T. (2023). Translating phage therapy into the clinic: Recent accomplishments but continuing challenges. *PLoS Biol.* 21:e3002119. doi: 10.1371/journal.pbio.3002119

Fayez, M. S., Hakim, T. A., Zaki, B. M., Makky, S., Abdelmoteleb, M., Essam, K., et al. (2023). Morphological, biological, and genomic characterization of *Klebsiella pneumoniae* phage vB_Kpn_ZC2. *BMC Virol. J.* 20:86. doi: 10.1186/s12985-023-02034-x

Feng, J., Li, F., Sun, L., Dong, L., Gao, L., Wang, H., et al. (2023). Characterization and genome analysis of phage vB_KpnS_SXFY507 against *Klebsiella pneumoniae* and efficacy assessment in *Galleria mellonella* larvae. *Front. Microbiol.* 14:2023. doi: 10.3389/fmicb.2023.1081715

Guerra, M. E. S., Destro, G., Vieira, B., Lima, A. S., Ferraz, L. F. C., Hakansson, A. P., et al. (2022). *Klebsiella pneumoniae* biofilms and their role in disease pathogenesis. *Front. Cell. Infect. Microbiol.* 12:877995. doi: 10.3389/fcimb.2022.877995

Han, P., Pu, M., Li, Y., Fan, H., and Tong, Y. (2023). Characterization of bacteriophage BUCT631 lytic for K1 *Klebsiella pneumoniae* and its therapeutic efficacy in *Galleria mellonella* larvae. *Virol. Sin.* 38, 801–812. doi: 10.1016/j.virs.2023.07.002

Herridge, W. P., Shibu, P., O'Shea, J., Brook, T. C., and Hoyles, L. (2020). Bacteriophages of *Klebsiella* spp., their diversity and potential therapeutic uses. *J. Med. Microbiol.* 69, 176–194. doi: 10.1099/jmm.0.001141

Hobbs, Z., and Abedon, S. T. (2016). Diversity of phage infection types and associated terminology: the problem with 'Lytic or lysogenic. *FEMS Microbiol. Lett.* 363:fnw047. doi: 10.1093/femsle/fnw047

Holger, D. J., El Ghali, A., Bhutani, N., Lev, K. L., Kyle Stamper, K., Kebriaei, R., et al. (2023). Phage-antibiotic combinations against multidrug-resistant *Pseudomonas aeruginosa* in *in vitro* static and dynamic biofilm models. *Antimicrob. Chemother.* 67:e0057823. doi: 10.1128/aac.00578-23

Holt, K. E., Wertheim, H., Zadoks, R. N., and Thomson, N. R. (2015). Genomic analysis of diversity, population structure, virulence, and antimicrobial resistance in *Klebsiella pneumoniae*, an urgent threat to public health. *Proc. Natl. Acad. Sci. USA* 112, E3574–E3581. doi: 10.1073/pnas.150104911

Howard-Varona, C., Hargreaves, K. R., Abedon, S. T., and Sullivan, M. B. (2017). Lysogeny in nature: mechanisms, impact and ecology of temperate phages. *ISME J.* 11, 1511–1520. doi: 10.1038/ismej.2017.16

Huang, C., Virk, S. M., Shi, J., and Zhou, Y. (2018). Isolation, characterization, and application of bacteriophage LPSE1 against *Salmonella enterica* in ready to eat (RTE) foods. *Front. Microbiol.* 9:1046. doi: 10.3389/fmicb.2018.01046

Hudzicki, J. (2009). Kirby-Bauer disk diffusion susceptibility test protocol. American Society for Microbiology Protocols. Available at: https://asm.org/protocols/kirby-bauer-disk-diffusion-susceptibility-test-pro (Accessed July 15, 2024).

Keen, E. C. (2012). Phage Therapy: Concept to Cure. *Front. Microbiol.* 3:238. doi: 10.3389/fmicb.2012.00238

Khawaja, K. A., Abbas, Z., and Rehman, S. (2016). Isolation and characterization of lytic phages TSE1-3 against *Enterobacter cloacae*. *Open Life Sci.* 11, 287–292. doi: 10.1515/biol-2016-0038

Kim, Y., Lee, S.-M., Nong, L. K., Kim, J., Kim, S. B., and Kim, D. (2022). Characterization of *Klebsiella pneumoniae* bacteriophages, KP1 and KP12, with deep learning-based structure prediction. *Front. Microbiol.* 13. doi: 10.3389/fmicb.2022.990910

Kolmogorov, M., Yuan, J., Lin, Y., and Pevzner, P. A. (2019). Assembly of long, error-prone reads using repeat graphs. *Nat. Biotechnol.* 37, 540–546. doi: 10.1038/s41587-019-0072-8

Kondo, K., Nakano, S., Hisatsune, J., Sugawara, Y., Kataoka, M., Kayama, S., et al. (2023). Characterization of 29 newly isolated bacteriophages as a potential therapeutic agent against IMP-6-producing *Klebsiella pneumoniae* from clinical specimens. *Microbiol. Spectr.* 11, e04761–e04722. doi: 10.1128/spectrum.04761-22

Ku, H., Kabwe, M., Chan, H. T., Stanton, C., Petrovski, S., Batinovic, S., et al. (2021). Novel Drexlerviridae bacteriophage KMI8 with specific lytic activity against *Klebsiella michiganensis* and its biofilms. *PLoS One* 16:e0257102. doi: 10.1371/journal.pone.0257102

Kumar, P., Meghvansi, M. K., and Kamboj, D. V. (2021). Isolation, phenotypic characterization and comparative genomic analysis of 2019SD1, a polyvalent enterobacteria phage. *Sci. Rep.* 11:22197. doi: 10.1038/s41598-021-01419-8

Larsen, F., Offersen, S. M., Li, V. R., Deng, L., Nielsen, D. S., and Rasmussen, T. S. (2023). Choice of ultrafilter affects recovery rate of bacteriophages. *Viruses* 15:2051. doi: 10.3390/v15102051

Lin, D. M., Koskella, B., and Lin, H. C. (2017). Phage therapy: An alternative to antibiotics in the age of multi-drug resistance. *World J. Gastrointest. Pharmacol. Ther.* 8, 162–173. doi: 10.4292/wjgpt.v8.i3.162

Liu, Y., Wang, J., Zhao, R., Xiaoping Liu, X., Dong, Y., Shi, W., et al. (2024). Bacterial isolation and genome analysis of a novel *Klebsiella quasipneumoniae* phage in southwest China's karst area. *Virol. J.* 21:56. doi: 10.1186/s12985-024-02321-1

Long, S. W., Linson, S. E., Saavedra, M. O., Cantu, C., Davis, J. J., Brettin, T., et al. (2017). Whole-genome sequencing of human clinical *Klebsiella pneumoniae* isolates reveals misidentification and misunderstandings of *Klebsiella pneumoniae*, *Klebsiella*

*v*ariicola, and *Klebsiella quasipneumoniae*. *mSpehere* 2, e00290–e00217. doi: 10.1128/mSphereDirect.00290-17

Lourenço, M., Osbelt, L., Passet, V., Gravey, F., Megrian, D., Strowig, T., et al. (2023). Phages against noncapsulated *Klebsiella pneumoniae*: broader host range, slower resistance. *Microbiol. Spectr.* 11, e04812–e04822. doi: 10.1128/spectrum.04812-22

Magiorakos, A.-P., Srinivasan, A., Carey, R. B., Carmeli, Y., Falagas, M. E., Giske, C. G., et al. (2011). Multidrug-resistant, extensively drug-resistant and pandrug-resistant bacteria: an international expert proposal for interim standard definitions for acquired resistance. *Clin. Micobiol. Infect.* 18, 268–281. doi: 10.1111/j.1469-0691.2011.03570.x

Mancuso, G., Midiri, A., Gearce, E., and Biondo, C. (2021). Bacterial antibiotic resistance: the most critical pathogens. *Pathogens* 10:1310. doi: 10.3390/pathogens10101310

Martins, W. M. B. S., Cino, J., Lenzi, M. H., Sands, K., Portal, E., Hassan, B., et al. (2022). Diversity of lytic bacteriophages against XDR *Klebsiella pneumoniae* sequence type 16 recovered from sewage samples in different parts of the world. *Sci. Total Environ.* 839:156074. doi: 10.1016/j.scitotenv.2022.156074

Mathers, A. J., Crook, D., Vaughan, A., Barry, K. E., Vegesana, K., Stoesser, N., et al. (2019). *Klebsiella quasipneumoniae* provides a window into carbapenemase gene transfer, plasmid rearrangements, and patient interactions with the hospital environment. *Antimicrob. Agents Chemother.* 63:e02513-18. doi: 10.1128/aac.02513-18

McFarland, J. (1907). Nephelometer: an instrument for media used for estimating the number of bacteria in suspensions used for calculating the opsonic index and for vaccines. *JAMA J. Am. Med. Assoc.* 14, 1176–1178. doi: 10.1001/jama.1907.25320140022001f

Monteiro, R., Pires, D. P., Costa, A. R., and Azeredo, J. (2019). Phage therapy: going temperate? *Trends Microbiol.* 27, 368–378. doi: 10.1016/j.tim.2018.10.008

National Institute of Allergy and Infectious Diseases (2024). NIH awards grants to support bacteriophage therapy research. Available at: https://www.nih.gov/news-events/news-releases/nih-awards-grants-support-bacteriophage-therapy-research (Accessed July 15, 2024).

Nazir, A., Qi, C., Shi, N., and Gao, X. (2022). Characterization and genomic analysis of a novel drexlervirial bacteriophage IME268 with lytic activity against *Klebsiella pneumoniae*. *Infect. Drug Resist.* 15, 1533–1546. doi: 10.2147/IDR.S347110

Ndiaye, I., Debarbieux, L., Diagne, M. M., and Sow, O. (2024). Complete genome sequences of two *Klebsiella pneumoniae* phages from Dakar, Senegal. *Microbiol. Resour. Announc.* 13, e00047–e00024. doi: 10.1128/mra.00047-24

New South Wales Government. Major funding boost for phage therapy manufacturing in NSW. (2024). Available at: https://www.health.nsw.gov.au/news/Pages/20230707_01.aspx (Accessed July 30, 2024).

Nikolic, I., Vukovic, D., Gavric, D., Cvetanovic, J., Sabo, V. A., Gostimirovic, S., et al. (2022). An optimized checkerboard method for phage-antibiotic synergy detection. *Viruses* 14, 14:1542. doi: 10.3390/v14071542

Oliveira, V. C., Bim, F. L., Monteiro, R. M., Macedo, A. P., Santos, E. S., Silva-Lovato, C. H., et al. (2020). Identification and characterization of new bacteriophages to control multidrug-resistant *Pseudomonas aeruginosa* biofilm on endotracheal tubes. *Front. Microbiol.* 11:580779. doi: 10.3389/fmicb.2020.580779

Osman, A.-H., Kotey, F. C. N., Odoom, A., Darkwah, S., Yeboah, R. K., Dayie, N. T. K. D., et al. (2023). The potential of bacteriophage-antibiotic combination therapy in treating infections with multidrug-resistant bacteria. *Antibiotics* 12:1329. doi: 10.3390/antibiotics12081329

Peng, Q., Ma, Z., Han, Q., Xiang, F., Wang, L., Zhang, Y., et al. (2023). Characterization of bacteriophage vB_KleM_KB2 possessing high control ability to pathogenic *Klebsiella pneumoniae*. *Sci. Rep.* 13:9815. doi: 10.1038/s41598-023-37065-5

Pertics, B. Z., Kovacs, T., and Schneider, G. (2023). Characterization of a lytic bacteriophage and demonstration of its combined lytic effect with a K2 depolymerase on the hypervirulent *Klebsiella pneumoniae* strain 52145. *Microorganisms* 11:669. doi: 10.3390/microorganisms11030669

Poteete, A. R., and Fenton, A. C. (1983). DNA-binding properties of the Erf protein of bacteriophage P22. *J. Mol. Biol.* 162, 257–275. doi: 10.1016/0022-2836(83)90006-2

Qurat-ul-Ain, H., Ijaz, M., Siddique, A. B., Muzammil, S., Shafique, M., Rasool, M. H., et al. (2021). Efficacy of phage-antibiotic combinations against multidrug-resistant *Klebsiella pneumoniae* clinical isolates. *Jundishapur J. Microbiol.* 14:e111926. doi: 10.5812/jjm.111926

Rasheed, J. K., Anderson, G. J., Yigit, H., Queenan, A. M., Doménech-Sánchez, A., Swenson, J. M., et al. (2000). Characterization of the extended-spectrum β-lactamase reference strain, *Klebsiella pneumoniae* K6 (ATCC 700603), which produces the novel enzyme SHV-18. *Antimicrob. Agents Chemother.* 44, 2382–2388. doi: 10.1128/AAC.44.9.2382-2388.2000

Reardon, S. (2014). WHO warns against 'post-antibiotic' era. *Nature*. doi: 10.1038/nature.2014.15135

Rivera, D., Moreno-Switt, A., Denes, T. G., Hudson, L. K., Peters, T. L., Samir, R., et al. (2022). Novel *Salmonella* phage, vB_Sen_STGO-35-1, characterization and evaluation in chicken meat. *Microorganisms* 10:606. doi: 10.3390/microorganisms10030606

Romero-Calle, D., Benevides, R. G., Góes-Neto, A., and Billington, C. (2019). Bacteriophages as alternatives to antibiotics in clinical care. *Antibiotics (Basel)* 8:138. doi: 10.3390/antibiotics8030138

Strathdee, S. A., Hatfull, G. F., Mutalik, V. K., and Schooley, R. T. (2023). Phage therapy: From biological mechanisms to future directions. *Cell* 186, 17–31. doi: 10.1016/j.cell.2022.11.017

Townsend, E., Kelly, L., Gannon, L., Muscatt, G., Dunstan, R., and Michnieswki, S. (2021). Isolation and characterization of *Klebsiella* phages for phage therapy. *Phage (New Rochelle)* 2, 26–42. doi: 10.1089/phage.2020.0046

Ventola, C. L. (2015). The antibiotic resistance crisis, part 2: management strategies and new agents. *PT* 40, 344–352.

WHO. (World Health Organization). (2017). Global priority list of antibiotic-resistant bacteria to guide research, discovery, and development of new antibiotics. Available at: http://www.who.int/medicines/publications/WHO-PPL-Short_Summary_25Feb-ET_NM_WHO.pdf?ua=1 (Accessed 30 July 2024).

Yang, Q., Le, S., Zhu, T., and Wu, N. (2023). Regulations of phage therapy across the world. *Front. Microbiol.* 14:1250848. doi: 10.3389/fmicb.2023.1250848

Yoo, S., Lee, K.-M., Kim, N., Nguyen, T., Abadie, R., and Yong, D. (2023). Designing phage cocktails to combat the emergence of bacteriophage-resistant mutants in multidrug-resistant *Klebsiella pneumoniae*. *Microbiol. Spectr.* 12:e0125823. doi: 10.1128/spectrum.01258-23

Zurabov, F., and Zhilenkov, E. (2021). Characterization of four virulent *Klebsiella pneumoniae* bacteriophages, and evaluation of their potential use in complex phage preparation. Virol. J. 18:9. doi: 10.1186/s12985-020-01485-w

frontiers | Frontiers in Microbiology

TYPE Original Research
PUBLISHED 23 October 2024
DOI 10.3389/fmicb.2024.1463192

OPEN ACCESS

EDITED BY
Barbara Maciejewska,
University of Wrocław, Poland

REVIEWED BY
Magdalena Plotka,
University of Gdansk, Poland
Bozena Nejman-Falenczyk,
University of Gdansk, Poland

*CORRESPONDENCE
Jianfei Lu
✉ 1095232712@qq.com
Yanli Wang
✉ ylwang88@aliyun.com
Bin Li
✉ libin0571@zju.edu.cn

RECEIVED 11 July 2024
ACCEPTED 09 October 2024
PUBLISHED 23 October 2024

CITATION
Tian Y, Xu X, Ijaz M, Shen Y, Shahid MS, Ahmed T, Ali HM, Yan C, Gu C, Lu J, Wang Y, Ondrasek G and Li B (2024) Role of hypothetical protein PA1-LRP in antibacterial activity of endolysin from a new *Pantoea* phage PA1.
Front. Microbiol. 15:1463192.
doi: 10.3389/fmicb.2024.1463192

Role of hypothetical protein PA1-LRP in antibacterial activity of endolysin from a new *Pantoea* phage PA1

Ye Tian[1], Xinyan Xu[1], Munazza Ijaz[1], Ying Shen[2], Muhammad Shafiq Shahid[3], Temoor Ahmed[1,4,5], Hayssam M. Ali[6], Chengqi Yan[7], Chunyan Gu[8], Jianfei Lu[2]*, Yanli Wang[9]*, Gabrijel Ondrasek[10] and Bin Li[1]*

[1]State Key Laboratory of Rice Biology and Breeding, Ministry of Agriculture Key Laboratory of Molecular Biology of Crop Pathogens and Insects, Zhejiang Key Laboratory of Biology and Ecological Regulation of Crop Pathogens and Insects, Institute of Biotechnology, Zhejiang University, Hangzhou, China, [2]Station for the Plant Protection & Quarantine and Control of Agrochemicals of Zhejiang Province, Hangzhou, China, [3]Department of Plant Sciences, College of Agricultural and Marine Sciences, Sultan Qaboos University, Al-Khoud, Muscat, Oman, [4]Xianghu Laboratory, Hangzhou, China, [5]Department of Life Sciences, Western Caspian University, Baku, Azerbaijan, [6]Department of Botany and Microbiology, College of Science, King Saud University, Riyadh, Saudi Arabia, [7]Crop Institute, Ningbo Academy of Agricultural Sciences, Ningbo, China, [8]Institute of Plant Protection and Agricultural Product Quality and Safety, Anhui Academy of Agricultural Sciences, Hefei, China, [9]State Key Laboratory for Managing Biotic and Chemical Threats to the Quality and Safety of Agro-Products, Institute of Plant Protection and Microbiology, Academy of Agricultural Sciences, Zhejiang, Hangzhou, China, [10]Faculty of Agriculture, University of Zagreb, Svetošimunska Cesta, Zagreb, Croatia

Introduction: *Pantoea ananatis* has emerged as a significant plant pathogen affecting various crops worldwide, causing substantial economic losses. Bacteriophages and their endolysins offer promising alternatives for controlling bacterial infections, addressing the growing concerns of antibiotic resistance.

Methods: This study isolated and characterized the *Pantoea* phage PA1 and investigated the role of PA1-LRP in directly damaging bacteria and assisting endolysin PA1-Lys in cell lysis, comparing its effect to exogenous transmembrane domains following the identification and analysis of the PA1-Lys and the PA1-LRP based on whole genome analysis of phage PA1. Additionally, this study also explored how hydrophobic region of PA1-LRP (HPP) contributes to bacterial killing when combined with PA1-Lys and examined the stability and lytic spectrum of PA1-Lys under various conditions.

Results and discussion: Phage PA1 belonging to the *Chaseviridae* family exhibited a broad host range against *P. ananatis* strains, with a latent period of 40 minutes and a burst size of 17.17 phages per infected cell. PA1-Lys remained stable at pH 6-10 and temperatures of 20-50°C and showed lytic activity against various Gram-negative bacteria, while PA1-Lys alone could not directly lyse bacteria, its lytic activity was enhanced in the presence of EDTA. Surprisingly, PA1-LRP inhibited bacterial growth when expressed alone. After 24 h of incubation, the OD_{600} value of pET28a-LRP decreased by 0.164 compared to pET28a. Furthermore, the lytic effect of co-expressed PA1-LRP and PA1-Lys was significantly stronger than each separately. After 24 h of incubation, compared to pET28a-LRP, the OD_{600} value of pET28a-Lys-LRP decreased by 0.444, while the OD_{420} value increased by 3.121. Live/dead cell staining, and flow cytometry experiments showed that the fusion expression of PA1-LRP and PA1-Lys resulted in 41.29% cell death, with bacterial morphology changing from rod-shaped to filamentous. Notably, PA1-LRP provided stronger support for endolysin-mediated cell lysis than exogenous transmembrane domains. Additionally, our results demonstrated that the HPP

fused with PA1-Lys, led to 40.60% cell death, with bacteria changing from rod-shaped to spherical and exhibiting vacuolation. Taken together, this study provides insights into the lysis mechanisms of *Pantoea* phages and identifies a novel lysis-related protein, PA1-LRP, which could have potential applications in phage therapy and bacterial disease control.

KEYWORDS

phage, endolysin, lysis, novel lysed protein, fusion expression

1 Introduction

In recent years, *Pantoea ananatis* has emerged as a significant rice pathogen across numerous countries, causing a spectrum of detrimental effects including grain discoloration, reduced seed germination rates, tissue decay, and leaf sheath necrosis, ultimately resulting in substantial yield losses (Xue et al., 2021; Zhang et al., 2022). Additionally, *P. ananatis* can lead to reduced production of wheat, corn, mulberry, strawberry, and water bamboo, and even cause plant death (Krawczyk et al., 2020; Wu et al., 2021; Xiao et al., 2022; Yuan et al., 2023). As natural enemies of bacteria, phages can specifically identify and effectively kill target bacteria, and they can co-evolve with host bacteria, thus exhibiting excellent biological safety (Piel et al., 2022; Rehman et al., 2019). In agriculture, phages are considered the most promising biopesticides (Ahmed and Li, 2023; Jamal et al., 2019). Phages have strong environmental adaptability, making them widely distributed in various environments, even extreme ones (Chevallereau et al., 2022; Hatfull et al., 2022). However, their high host specificity and bacterial resistance limit the application of phages (Luong et al., 2020).

Endolysins, encoded by phages and synthesized by host bacteria, are classified based on their functions as lytic transglycosidases, lysozyme, amidases, glycosidases and endopeptidases (Wong et al., 2022). Compared to phages, endolysins with lower host specificity and higher lethality have recently been explored as antibacterial agents (Ho et al., 2022; Lai et al., 2020). In addition to their individual antibacterial effectiveness, endolysins can also synergistically act with antibiotics, showing broad application prospects in the prevention and treatment of multidrug-resistant pathogen infections (Ghose and Euler, 2020; Hong et al., 2022). In the future, endolysins have broad application prospects in many industries such as food, feed, detergents, and pharmaceuticals (Cho et al., 2021; Pallesen et al., 2023; Shannon et al., 2020). Endolysin can directly hydrolyze the peptidoglycan cell wall of Gram-positive bacteria, causing cell lysis. However, the outer membrane of Gram-negative bacteria, which contains lipopolysaccharides, acts as a barrier preventing most endolysin from directly entering the cell. Outer membrane permeation agents such as chloroform and ethylenediaminetetraacetic acid (EDTA) have been reported to alter cell membrane permeability, thereby helping endolysins enter Gram-negative bacteria and inhibit their growth (Yuan et al., 2021).

The holin-endolysin pathway is the most common phage lysis mechanism for phages of Gram-negative bacteria (Basit et al., 2021). Holins are small hydrophobic proteins with at least one transmembrane domain (TMD), forming holes in the inner membrane to help endolysins hydrolyze peptidoglycan, ultimately leading to cell death (Brüser and Mehner-Breitfeld, 2022). Additionally, some phages produce endolysins that can traverse the plasma membrane without the assistance of holins. In the phages of Gram-negative bacteria, some endolysins contain a signal-anchor-release (SAR) domain at their N-terminal, allowing them to autonomously split cells (Cahill and Young, 2019). Besides endolysin and holin operation, membrane fusion proteins are required for bacterial lysis (Gontijo et al., 2021). The direct fusion of endolysins and antimicrobial peptides not only enhances antibacterial activity, but also expands the antibacterial spectrum (Gouveia et al., 2022). Furthermore, endolysins modified with cationic/hydrophobic amino acids significantly enhance bacterial cell membrane permeability and effectively kill bacteria (Wang et al., 2017).

In this study, we isolated and characterized the *Pantoea* phage PA1. We identify and analyze the endolysin (PA1-Lys) and the hypothetical protein PA1-LRP based on whole genome analysis of phage PA1. Additionally, we investigated the role of PA1-LRP in directly damaging bacteria and assisting PA1-Lys in cell lysis, comparing its effect to exogenous TMD. We also explored how hydrophobic region of PA1-LRP (HPP) contributes to bacterial killing when combined with PA1-Lys. Furthermore, we examined the stability and lytic spectrum of PA1-Lys under various conditions. Overall, our study provides a theoretical basis for understanding the lysis mechanisms of *Pantoea* phages and potentially develop new strategies for bacterial control.

2 Materials and methods

2.1 Bacterial strains, plasmid, and reagents

In this study, strains of *P. ananatis* (ZJU1 - ZJU14), *Escherichia coli* (DH5α, BL21 (DE3), S17, and XL1-Blue), *Xanthomonas oryzae* pv. *oryzae* (Xoo) (Y4, PXO99^{A}, and C2), *Xanthomonas oryzae* pv. *oryzicola* (Xoc) (BLS256 and RS105), *Acidovorax avenae* subsp. *avenae* (Ao) (RS1 and RS2), *Pantoea dispersa* strain 19,001, *Bacillus* sp. strain RP12, and *Paenibacillus polymyxa* strain RP31 stored in our laboratory were utilized. *E. coli* strains were cultured in Luria-Bertani (LB) broth at 37°C, while other strains were cultured in nutrient broth (NB) at 30°C. The *E. coli* BL21 strains containing plasmids pET28a, pET28a-Lys, pET28a-LRP, pET28a-Lys-LPP, pET28a-Lys-LRP, pET28a-Lys-LVP, pET28a-Lys-ATMD, and pET28a-Lys-HPP were abbreviated as 28a, 28a-Lys, 28a-LRP, 28a-Lys-LPP, 28a-Lys-LRP, 28a-Lys-LVP, 28a-Lys-ATMD, and 28a-Lys-HPP, respectively. 28a and 28a-Lys were used as negative controls to study the lytic activity of the lytic related proteins (Table 1).

Moreover, the concentrations of antibiotics we used in this study were as follows: kanamycin at 50 μg/mL, tetracycline at 12.5 μg/mL, or chloramphenicol at 34 μg/mL. SM buffer (pH 7.5) consists of 8 mM magnesium sulfate, 0.1 mM sodium chloride, 1% gelatin and 50 mM Tris–HCl, which was used for preservation and dilution of phages. Furthermore, Isopropyl-β-D-thiogalactopyranoside (IPTG) was used as a protein inducer at a final concentration of 0.5 mmol/L. In addition to this, the Live/Dead Bacterial Staining Kit was purchased from Thermo Fisher Scientific (Waltham, MA, USA). Lysozyme used as a positive control is a commercial lysozyme extracted from egg whites, which was purchased from Beyotime Biotechnology (Haimen, China).

TABLE 1 Plasmids used in this study.

Plasmids	Description	Sources
pET28a	Km^R; cloning vector	Laboratory collection
pBT	Chl^R; encode λcI; bait plasmid	Laboratory collection
pTRG	Tet^R; encode α-NTD; target plasmid	Laboratory collection
pET28a-Lys	Km^R; pET28a containing gene Lys	This study
pET28a-LRP	Km^R; pET28a containing gene LRP	This study
pET28a-Lys-LPP	Km^R; pET28a containing gene Lys and LPP	This study
pET28a-Lys-LRP	Km^R; pET28a containing gene Lys and LRP	This study
pET28a-Lys-LVP	Km^R; pET28a containing gene Lys and LVP	This study
pET28a-Lys-ATMD	Km^R; pET28a containing gene Lys and ATMD	This study
pET28a-Lys-HPP	Km^R; pET28a containing gene Lys and HPP	This study
pBT-Lys	Chl^R; pBT containing gene Lys	This study
pTRG-LRP	Tet^R; pTRG containing gene LRP	This study

Km^R/Chl^R/Tet^R: kanamycin–/ chloramphenicol–/ tetracycline-resistant.

Besides, the BCA protein quantitative kit, Phosphate Buffer Solution (PBS), EDTA, Tris–HCl buffer and IPTG were also purchased from Beyotime Biotechnology (Haimen, China).

2.2 Isolation, purification, and morphology of phage PA1

To isolate phages, we utilized a traditional isolation method devised by Liu et al. (2021). Rice leaves were ground using a sterilized mortar, and the resulting homogenate was centrifuged at 11,000 × g for 10 min to obtain the supernatant. The supernatant was then filtered through a 0.22 μm filter (Millipore, Ireland) to remove bacteria completely. Various *P. ananatis* strains (ZJU1-ZJU14) were selected to identify the presence of phages in the supernatant. The supernatant filtrate was spotted onto double-layer plates containing 1 mL of each *P. ananatis* suspension and 7 mL of molten NB semi-solid broth (0.8% agar). After air drying, the plates were incubated overnight at 30°C. The presence of transparent plaques on the double-layer plates indicated the presence of lytic phages. These plaques were picked with sterile tips and placed in SM buffer, and the mixed SM buffer was left overnight at 4°C. After that, 7 mL of molten NB semi-solid broth, 1 mL of *P. ananatis* ZJU1, and 100 μL of the diluted phage SM buffer were mixed and poured onto NB plates. A single plaque was then selected and the process was repeated five times until a uniform single transparent plaque appeared. At this point, the purified phage was named PA1. For higher titers of phage samples, the purified phage was concentrated according to previous studies (Sasaki et al., 2021). Finally, for morphological and structural observation, the PA1 phage suspension was placed on carbon-coated copper grids (Ted Pella Inc., USA) and observed under a transmission electron microscope (TEM) (JEM-1230, JEOL, Akishima, Japan).

2.3 Phage host range and optimal multiplicity of infection (MOI)

The spot assay method, as described by Huang et al. (2022), was used to investigate the host range of phage PA1. In this method, a 5 μL suspension of phage PA1 was applied onto double-layer agar plates containing lawns of various bacterial strains, followed by incubation at 30°C. The presence of clear, transparent spots signified bacterial susceptibility to phage PA1. To determine the optimal multiplicity of infection (MOI), we adapted and modified the protocol outlined in Cao et al. (2022). Given the high lytic efficiency of phage PA1 against *P. ananatis* ZJU1, this particular strain was selected for further investigation. During the exponential growth phase of *P. ananatis* ZJU1, different ratios of phage PA1 to *P. ananatis* ZJU1 (ranging from 1:1000 to 1,000:1) were mixed in NB and incubated at 30°C for 4 h. Post-incubation, the mixtures were centrifuged at 12,000 × g for 10 min and subsequently filtered to isolate the supernatant. The phage titer was then quantified using the double-layer plate method, with the MOI yielding the highest phage titer identified as optimal. This experiment was conducted in triplicate, with each replication performed independently.

2.4 Phage adsorption rate and one-step growth curve

The phage adsorption rate was examined following the methodology devised by Xuan et al. (2022). Briefly, *P. ananatis* ZJU1 at a concentration of 1×10^6 CFU/mL was infected with phage PA1 at the predetermined optimal MOI of 0.01. Supernatant samples were collected at multiple time points: 0, 1, 2, 3, 4, 5, 6, 7, 8, 9, 10, 15, 20, 25, and 30 min. The quantity of unabsorbed phage particles was determined using the double-layer plate assay. The adsorption rate was calculated using the formula: adsorption rate (%) = [(initial phage titer – unabsorbed phage titer)/initial phage titer] × 100%. The one-step growth assay was conducted in accordance with the protocol established by Gašić et al. (2022). Specifically, once *P. ananatis* ZJU1 reached its exponential phase, phage PA1 was introduced at an MOI of 0.01. The mixture was incubated at 30°C for 20 min, followed by centrifugation at 12,000 × g for 2 min at 4°C to remove unabsorbed phages, after which the supernatant was discarded. The resultant pellet was resuspended in NB broth and incubated at 30°C. Samples were taken at 20-min intervals up to 240 min. The supernatant samples

TABLE 2 PCR primers used in this study.

Primer Name	Nucleotide Sequence (5′–3′)	Characterization
28a-Lys-F	GGAATTCCATATGATGATCAGTAAAAACGCAATTG (N)	Gene of PA1-Lys from phage PA1
28a-Lys-R	CGGGATCCTAAGAATCTCAAGCAATCTTTATAACG (B)	
28a-LRP-F	CGGGATCCATGGTAAGGCGCAGACG (B)	Gene of PA1-LRP from phage PA1
28a-LRP-R	CCGCTCGAGCTTTTGCTGTTCTACTTTCTGGA (X)	
28a-LPP-F	CGGGATCCATGGTTCAAATCTACGTCAGGC (B)	Gene of PA1-LPP from phage PA1
28a-LPP-R	CCGCTCGAGACTAGAACGGAACCAGCCG (X)	
28a-LVP-F	CGGGATCCATGAACTGGCAAGACATTGG (B)	Gene of PA1-LVP from phage PA1
28a-LVP-R	CCGCTCGAGTAACGGTAGACCTAACTCAGC (X)	
ATMD-F	CGGGATCCAGCCTCGGCAACTGGC (B)	Gene of ATMD
ATMD-R	CCGCTCGAGTGACCACCCCTCTCGCC (X)	
HPP-F	CGGGATCCAGGACTATTTTGATCAGCTG (B)	Gene of HPP
HPP-R	CCGCTCGAGAGCAGGCGCTAAGTCATAG (X)	
PBT-Lys-F	CGGAATTCATGATCAGTAAAAACGCAATTG (E)	Gene of PA1-Lys from phage PA1
PBT-Lys-R	CGGGATCCTTATAAGAATCTCAAGCAATCTTTATAACG (B)	
PTRG-LRP-F	ATAAGAATGCGGCCGCATGGTAAGGCGCAGACG (No)	Gene of PA1-LRP from phage PA1
PTRG-LRP-R	CGGAATTCTTACTTTTGCTGTTCTACTTTCTGGA (E)	

Lys, PA1-Lys; LRP, PA1-LRP; LPP, PA1-LPP; LVP, PA1-LVP; ATMD, transmembrane domain of endolysin in phage AP1; HPP, hydrophobic region of PA1-LRP. The parentheses contain the abbreviation for restriction endonuclease and the cleavage site is marked with an underline (N, NdeI; B, BamHI; X, XhoI; E, EcoRI; No, NotI).

were then filtered and subjected to gradient dilution. The phage titer was subsequently assessed via the double-layer plate method. All experiments were performed in triplicate to ensure reproducibility.

2.5 Phage stability

To elucidate the factors influencing the stability of phage PA1, the double-layer plate method was used to ascertain the phage titer following various treatments. Drawing upon previous studies, both temperature and pH stability assays were performed. The pH stability experiment involved incubating phage PA1 in SM buffer across a pH gradient ranging from 3 to 12 at 25°C for 60 min. For the thermal resistance assay, phage PA1 was exposed to a series of temperatures (4, 25, 40, 50, 60, 70, and 80°C) at a neutral pH of 7 for a duration of 1 h. The activity of the treatment exhibiting the highest phage titer was designated as 100%. Each experiment was conducted in triplicate, with all replicates executed independently to ensure robustness and reproducibility of the results.

2.6 Genome sequencing and phylogenetic analysis of phage PA1

Genomic DNA of phage PA1 was extracted utilizing the λ phage genome kit (Sangon Biotech, Shanghai, China). Whole genome sequencing was subsequently performed at Biozeron (Shanghai, China) employing the Illumina HiSeq paired-end platform, with quality control of the raw reads conducted using Trimmomatic. Following trimming, the paired-end reads were assembled via AbySS.[1] Open reading frames (ORFs) were predicted using both the RAST server,[2] GeneMarkS[3] and Pharokka.[4] Protein functions were annotated within the non-redundant protein database through BLASTp.[5] The detection of tRNA was executed using tRNAscan-SE v2.0.[6] A circular representation of the phage PA1 genome was generated using Proksee[7] as outlined by Vu et al. (2021). Phylogenetic trees, based on the phage PA1 genome and TERL (termination enzyme large subunit), were constructed using MEGA6 software.

2.7 Recombinant plasmid construction

We have named the proteins encoded by ORF11, ORF12, ORF13, and ORF16 as PA1-LPP, PA1-Lys, PA1-LRP, and PA1-LVP, respectively. In order to construct recombinant plasmids, the genes encoding PA1-Lys, PA1-LPP, PA1-LRP, and PA1-LVP were amplified using phage PA1 as a template, and the gene encoding ATMD was amplified using Ao phage AP1 as a template. Cloning of various gene fragments into different plasmids were done using specific restriction enzymes and T4 ligases. The conjugated product was transfected into *E. coli* DH5α by the heat shock method to obtain a recombinant plasmid. Gene sequences used in this study are listed Supplementary Table S2 and the primers used in this study are listed in Table 2.

1 http://www.bcgsc.ca/platform/bioinfo/software/abyss

2 http://rast.nmpdr.org/rast.cgi

3 http://topaz.gatech.edu/GeneMark/genemarks.cgi

4 https://github.com/gbouras13/Pharokka

5 http://blast.ncbi.nlm.nih.gov/

6 http://lowelab.ucsc.edu/tRNAscanSE/

7 https://proksee.ca/projects/

2.8 Bioinformatics and physicochemical properties analysis

ExPASY prot param tool[8] was used to predict the basic physicochemical properties of PA1-Lys, including isoelectric point, stability index, aliphatic index, and hydrophobicity. Analysis of protein conserved functional domains was obtained through the Conserved Domain Database in NCBI.[9] Application of TMHMM-2.0[10] and SignalP-5.0 Server[11] to analyze the TMD and signal peptide. SWISS-MODEL[12] and phyre2 analysis[13] were used to predict the structure of protein.

2.9 Expression and purification of PA1-Lys

The recombinant *E. coli* 28a-Lys was cultured overnight in LB broth containing 50 μg/mL kanamycin at 37°C and 200 rpm. Following this, 200 μL of the overnight culture was inoculated into 200 mL of LB broth and incubated at 37°C. Upon reaching an OD_{600} of 0.6, protein expression was induced by adding 200 μL of 0.5 M IPTG, followed by incubation at 20°C for 20 h. The bacterial cells were harvested by centrifugation, washed three times with 0.1 M PBS, and resuspended in 0.1 M PBS. The cells were then lysed using an ultrasonic homogenizer (400 W, 5 s on, 10 s off) for a total of 10 min. The resulting lysate was centrifuged at 11,000 × g for 30 min at 4°C to separate the supernatant and sediment. Protein purification was performed using the ProteinIso™ Ni-NTA Resin (Genscript, China). After elution with imidazole, the purified protein was analyzed by SDS-PAGE and Western blotting. The PA1-Lys protein was concentrated using a 3 kDa protein ultrafiltration tube (Pell, USA), and the concentrated PA1-Lys was stored in 50 mM Tris–HCl buffer (pH 8.0). Protein concentration was determined using the BCA protein quantitation kit.

2.10 Lytic capacity of PA1-Lys

2.10.1 Turbidity reduction assay

The turbidity reduction assay was conducted with slight modifications to the previously described method by Zhang et al. (2021). Overnight cultures of *P. ananatis* strain ZJU1 were centrifuged, and the resulting bacterial pellet was resuspended in 0.1 M PBS and then treated with 0.5% (*v*/*v*) chloroform for 5 min. The treated bacteria were centrifuged at 6,000 × g for 4 min, and the resulting pellet was washed three times with 0.1 M PBS. The bacterial pellet was subsequently resuspended in 50 mM Tris–HCl buffer (pH 8.0) containing 0.1% Triton X-100. The 20 μL PA1-Lys (0.2 mg/mL) was added to 200 μL of chloroform-treated bacterial suspension, and the value of OD_{450} was measured every 5 min by a microplate photometer (Thermo Fisher Scientific Inc., Waltham, MA, USA). Lysozyme (0.2 mg/mL) was utilized as a positive control, while 0.1 M PBS buffer served as a negative control. Each experiment was repeated independently three times to ensure reproducibility.

2.10.2 Synergistic lysis of viable Bacteria by PA1-Lys and EDTA

Overnight cultures of *P. ananatis* strain ZJU1 were centrifuged, and the resulting bacterial pellet was resuspended in 50 mM Tris–HCl buffer (pH 8.0) to achieve a suspension with an OD_{600} of 0.8 (equivalent to 2×10^8 CFU/mL). To this bacterial suspension, a mixture comprising 100 μL of recombinant PA1-Lys protein (0.2 mg/mL) and 100 μL of EDTA solution (0.01 mol/L) was added to 800 μL of the bacterial suspension. As a control, 100 μL of 50 mM Tris–HCl buffer (pH 8.0) was combined with 100 μL of PA1-Lys and 800 μL of the bacterial suspension. Following incubation at 25°C for both 30 and 60 min, bacterial counts were determined using plate counting methods. Each experiment was independently repeated three times to ensure the validity and reproducibility of the results.

2.10.3 Lysis spectrum of PA1-Lys

Pantoea ananatis, *P. dispersa*, *E. coli*, Xoo, Xoc, Ao, *P. polymyxa* and *Bacillus* were used as indicator bacteria to determine the lytic spectrum of PA1-Lys. Gram-negative bacteria require pre-treatment with chloroform, while Gram-negative bacteria do not require treatment. The lytic effect of PA1-Lys was measured using a turbidity analysis method.

$$\text{Lytic activity}(\%) = \begin{bmatrix} (OD_{450}\ \text{value of bacteria before PA1} - \text{Lys treatment}) \\ -OD_{450}\ \text{value of bacteria after PA1} - \text{Lys treatment} \\ /OD_{450}\ \text{value of bacteria before PA1} - \text{Lys treatment} \end{bmatrix} \times 100\%.$$

2.11 Biochemical characterization of PA1-Lys

The method described by Jiang et al. (2021) was used to determine the optimal conditions for PA1-Lys activity. To assess the thermal stability of PA1-Lys, the protein was subjected to various temperatures (ranging from 20°C to 70°C) for durations of 30 and 60 min, respectively. The lytic activity was then evaluated at 25°C using a turbidity reduction assay. The effect of pH on the lytic activity was also investigated. Specifically, overnight cultures of *P. ananatis* strain ZJU1 were centrifuged at 6,000 × g for 4 min, and the resulting bacterial pellet was resuspended in 0.1 M PBS. A mixture of 20 μL PA1-Lys and 200 μL chloroform was added to the bacterial suspension. The pH of the suspension was adjusted to a range from 2 to 11 using sodium hydroxide or hydrochloric acid. The OD_{450} value was monitored after 30 and 60 min of incubation at 25°C. Additionally, the influence of various metal ions on lytic activity was assessed. Metal ions such as $FeCl_3$, $ZnCl_2$, $CuCl_2$, $MnCl_2$, NaCl, KCl, FeCl2, $MgCl_2$, and $CaCl_2$ were added to the chloroform-treated bacterial suspension at a final concentration

8 https://web.expasy.org/protparam/; accessed on: 30 December 2021

9 https://www.ncbi.nlm.nih.gov/Structure/cdd/wrpsb.cgi; accessed on: 30 December 2021.

10 https://services.healthtech.dtu.dk/services/TMHMM-2.0; accessed on: 30 December 2021.

11 https://services.healthtech.dtu.dk/services/SignalP-5.0; accessed on: 30 December 2021.

12 https://swissmodel.expasy.org; accessed on: 30 December 2021.

13 http://www.sbg.bio.ic.ac.uk/phyre2/phyre2_output/41b500971e497a23/summary.html

of 10 mmol/L each. Subsequently, 20 μL PA1-Lys was added to 200 μL of the treated bacterial resuspension. The OD_{450} value was then monitored every 5 min at 25°C. Each experiment was independently repeated three times to ensure the robustness and reproducibility of the results.

2.12 Bacterial growth assays

According to previous research (Wu et al., 2021), when the OD_{600} of BL21 strains containing the recombinant plasmid reached 0.4, IPTG (0.5 M, 5 μL) was added to 5 mL of bacterial culture. The induced bacteria were then cultured at 20°C and 180 rpm. At intervals of 6-, 12-, 18-, and 24-h post-induction, the absorbance at 600 nm of the BL21 strains was measured using a microplate reader (Thermo Fisher Scientific Inc., Waltham, MA, USA). This experiment was conducted three times independently to ensure reliability and consistency of the results.

2.13 Determination of β-galactosidase activity

To evaluate the effect of recombinant proteins on the permeability of the cell membrane, we measured β-Galactosidase activity as described previously with minor modifications (Ning H. et al., 2021). Bacterial suspensions induced by IPTG were centrifuged (12,000 × *g*, 5 min), and the supernatant was collected. The 100 μL 20 mM O-nitrophenyl-β-D-galactopyranoside (ONPG) was added to 500 μL extracellular supernatant. After placing it at 45°C for 30 min, an equal volume of Na_2CO_3 (0.5 mM) was added to terminate the reaction. The activity of galactosidase was evaluated by measuring the OD_{420} of the samples with a microplate reader.

2.14 Live/dead cell and flow cytometry assay

Following the methodology outlined by Wu et al. (2021), 5 μL of 0.5 M IPTG was added to a 5 mL bacterial suspension for induction at 20°C over a 24-h period. Subsequently, bacterial sediment was harvested by centrifugation at 6000 × g for 3 min and washed three times with 0.1 M PBS. To assess bacterial viability, the BacLight bacterial viability kit (Thermo-Fisher Scientific, Waltham, MA, USA), containing SYTO 9 and propidium iodide (PI) dyes, was utilized. Bacterial samples were stained with a mixture of SYTO 9 and PI in the dark for 30 min, followed by centrifugation (6,000 × g, 3 min) to remove the staining solution. Stained bacteria were examined using an Olympus inverted confocal microscope (Leica-SP8, Heidelberg, Germany). For flow cytometry analysis, the preparation of bacterial samples mirrored the live/dead experiments. PI dye was specifically used to identify dead bacteria. Bacterial samples were incubated with PI in the dark for 30 min, followed by washing with 0.1 M PBS to remove excess dye, as per the protocol described by Daei et al. (2022). Stained bacteria were then analyzed using the FACSVerse cytometer (BD Biosciences, San Jose, CA, USA). This approach allowed for precise quantification of bacterial viability and death under the experimental conditions.

2.15 TEM observation

The changes in the bacterial microstructure induced by IPTG were studied by TEM (JEM-1230, JEOL, Akishima, Japan). Bacterial pellets were fixed overnight with 2.5% (*v*/*v*) glutaraldehyde, coated with agar and washed 3 times with 0.1 M PBS. Subsequently, bacterial blocks were treated with 1% (*w*/*v*) osmic acid for 1 h. After washing three times with PBS, the bacterial samples were dehydrated in different concentrations of alcohol (30–80%, *v*/*v*). Afterwards, the samples were dehydrated in different acetone solutions (90–100%, *v*/*v*). After embedding, infiltration, and sectioning, the bacterial samples were observed.

2.16 Bacterial two-hybrid assay

The bacterial two-hybrid assay method was adapted from the protocol described by Liu et al. (2017). Initially, the PBT-Lys vector and PTRG-LRP vector were co-transformed into *E. coli* XL1-Blue, and subsequent screening was conducted to verify the correct dual hybrid vectors. *E. coli* XL1-Blue strains containing PBT-LGF2 and PTRG-Gal11^{P} served as positive controls, while strains containing PBT and PTRG acted as negative controls. Subsequently, 3 μL of bacterial suspension from each transformation was inoculated onto non-selective medium plates supplemented with corresponding antibiotics, as well as onto M9 + His-Dropout double selective media plates containing antibiotics, 3 mM 3-AT (3-amino-1, 2, 4-triazole), and 12.5 μg/mL streptomycin. All plates were then incubated at 25°C for 24 h. This experimental setup allowed for the selective growth and assessment of interactions between the proteins encoded by the co-transformed vectors under specific conditions.

3 Results

3.1 Biological characteristics of phage PA1

Our study characterized the isolated phage, which formed small, clear, circular plaques on *P. ananatis* ZJU1 (Figure 1A). Upon further purification, the isolated phage exhibited distinct features including bright patches, well-defined edges, and a uniform size (2 mm), leading to its designation as phage PA1. TEM analysis revealed that phage PA1 possesses a head diameter of 80 ± 6.2 nm and a contractile, flexible tail approximately 120 ± 5.4 nm in length (Figure 1B). According to the latest ICTV classification criteria, phage PA1 belongs to the *Chaseviridae* family. Sequencing of phage PA1's genome unveiled a circular double-stranded DNA (dsDNA) with a length of 69,452 bp and an average G + C content of 46.1%. Using RAST servers, GeneMarkS and Pharokka, a total of 105 putative open reading frames (ORFs) were identified, with 46 located on the minus strand and the remainder on the plus strand. Among these, 41 ORFs were

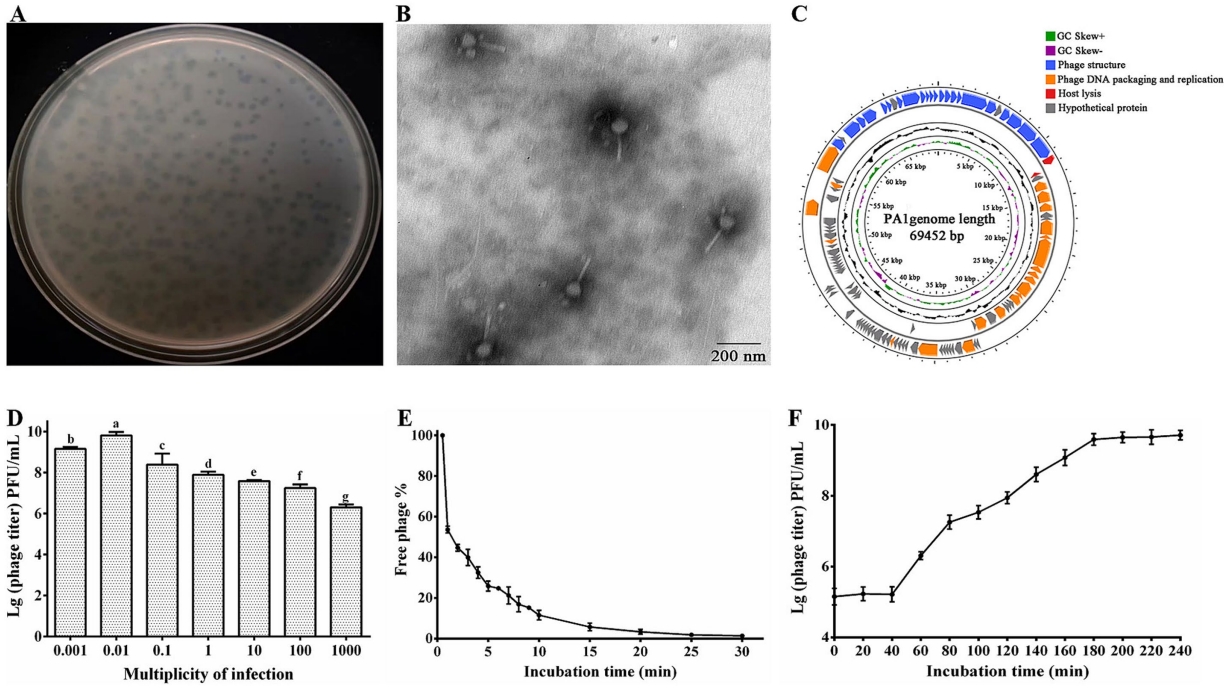

FIGURE 1
Morphological identification and biological features of phage PA1. **(A)** Plaque morphology of phage PA1. **(B)** TEM image of phage PA1 particles. Scale bar = 200 nm, Magnification = 12,000x. **(C)** Genome map of PA1. The open reading frames (ORFs) are indicated by specific colors according to their functional categories. The direction of each arrow represents the direction of transcription. Genes in four functional modules are represented in blue (phage structure), orange (phage DNA packaging and replication), red (host lysis), and gray (hypothetical protein). GC skew is shown as inner circles holograms in purple and green. GC content is indicated by black circular hologram. **(D)** Optimal multiplicity of infection (MOI) of phage PA1. **(E)** Adsorption assay of phage PA1. **(F)** One-step growth curve of phage PA1. Different letters on the Bar chart represents significant differences between samples. Error bars indicates the mean of three replicates ($n = 3 \pm$ standard deviation).

functionally annotated while 64 were categorized as hypothetical proteins. No transfer RNA (tRNA) sequences were detected within the phage genome using tRNAscan-SE.

Bioinformatics analysis revealed that the genome of phage PA1 is organized into four functional modules: phage structure, DNA packaging and replication, host lysis, and hypothetical proteins (Figure 1C). The genomic architecture of phage PA1 demonstrates a modular organization where genes with related functions are clustered together. The complete genome sequence of phage PA1 has been deposited in the NCBI database under accession number PP537389. This comprehensive genomic characterization provides insights into the genetic composition and functional potential of phage PA1 within its ecological niche.

Through bioinformatics prediction, we found that 22 genes related to phage structural function, including baseplate protein, tail fiber protein, head-tail connector protein, capsid protein, and tail sheath protein. Terminase large subunit encoded by ORF85 is responsible for phage genome packaging and phage protease encoded by ORF88 which plays a role in phage morphogenesis and is also present in DNA packaging module (Evseev et al., 2021; Golz and Kemper, 1999; Thomas et al., 2012). Replication-related genes encoding DNA polymerase, DNA helicase, DNA ligase, and other related proteins, bacterial lysis genes, and phage-encoded enzymes attacking peptidoglycans were studied in many previous studies (Vu et al., 2021; Yang et al., 2021; Young, 1992). PA1-Lys encoded by ORF12 is associated with host lysis. However, since most of the proteins encoded by the ORFs are predicted to be hypothetical proteins, further investigation of the roles of the encoded gene products is needed. In this study, it was discovered that the ORF13 encoded hypothetical protein (PA1-LRP) directly lyse bacteria. Hence, the PA1-LRP was classified into lysis module.

The research findings indicated that the optimal MOI for phage PA1 was determined to be 0.01 (Figure 1D). Adsorption experiments revealed that phage PA1 achieved an adsorption rate of 97% within 20 min (Figure 1E). To further elucidate the proliferation dynamics, including incubation time and burst size, a one-step growth curve was conducted. The curve illustrated that phage PA1 had a latent period of 40 min and a burst size of 17.17 phages per infected bacterial cell (Figure 1F). These results provided valuable insights into the infectivity and replication characteristics of phage PA1 under experimental conditions.

3.2 Biological characteristics of phage PA1

Our study demonstrated that phage PA1 exhibited peak activity at 4°C and 25°C following treatment at various temperatures for 1 h. Phage activity declined sharply by 98.8% at 70°C and was completely deactivated at 80°C (Figure 2A), indicating high-temperature adaptability within a specific range. Additionally, phage PA1 exhibited optimal survival at pH 7, with a noticeable decrease in survival rates observed at pH 10 and pH 3 (Figure 2B). These results suggest that phage PA1 displays sensitivity to extreme acidic and alkaline conditions, highlighting its preference for neutral pH environments.

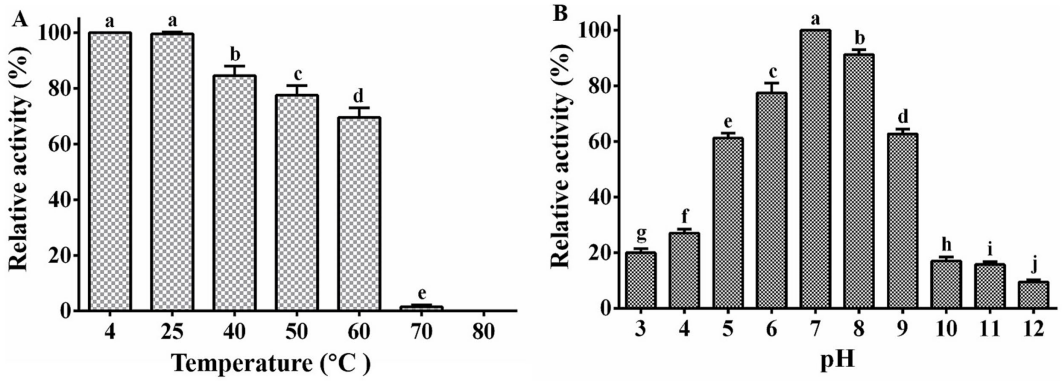

FIGURE 2
Stability of phage PA1. **(A)** Temperature stability of phage PA1. **(B)** pH stability of phage PA1. Different letters on the Bar chart represents significant differences between samples. Error bars indicates the mean of three replicates ($n = 3 \pm$ standard deviation).

TABLE 3 Host range of phage PA1.

Strain	Infection	Strain	Infection
P. ananatis ZJU1	+++	*P. ananatis* ZJU13	+++
P. ananatis ZJU2	++	*P. ananatis* ZJU14	++
P. ananatis ZJU3	++	*P. dispersa* 19,001	–
P. ananatis ZJU4	++	Xoo PXO99^{A}	–
P. ananatis ZJU5	++	Xoo C2	–
P. ananatis ZJU6	++	Xoc BLS256	–
P. ananatis ZJU7	+	Xoc RS105	–
P. ananatis ZJU8	+	Ao RS1	–
P. ananatis ZJU9	++	Ao RS2	–
P. ananatis ZJU10	+++	*Bacillus* sp. RP12	–
P. ananatis ZJU11	++	*P. polymyxa* RP31	–
P. ananatis ZJU12	++		

"+++" means dense patches appearing on the plate, but the background clearness; "++" means dense patches appearing on the plate, but the background is blurry; "+" means only a few patches on the plate; "–" no patche on the plate. All strains were isolated from rice leaves.

3.3 Host range of phage PA1

The host range test showed that phage PA1 has a broad host range, as it had lytic ability against all tested strains of *P. ananatis* (Table 3), but phage PA1 displayed different infection rates when tested against different strains of *P. ananatis*. Specifically, phage PA1 showed strong lytic ability against ZJU1, ZJU10 and ZJU13 strains, but its lytic ability was limited when tested against ZJU7 and ZJU8 strains. Notably, phage PA1 did not have lytic ability on other bacterial genera.

3.4 Phylogenetic analysis

Based on the phylogenetic analysis of the entire genome sequence and the amino acid sequence of the conserved protein (terminal large subunit), we found that phage PA1 clustered into a distinct branch. Phage PA1 is closely related to *Escherichia* phage based on the terminase large subunit (Figure 3A). However, according to the entire genome sequence, phage PA1 exhibits a phylogenetic relationship similar to that of *Pantoea* phages (Figure 3B). The whole genome sequencing of phage PA1 showed relatively low similarity to other phages in the NCBI database. We therefore believed that phage PA1 to be a new *Pantoea* phage.

3.5 Bioinformatics and physicochemical properties of PA1-Lys

PA1-Lys contains 217 amino acids with a molecular weight of 23.7 kDa (Supplementary Table S1). PA1-Lys possess a lysozyme-like domain at amino acid site 18–195, belonging to the Lyz-like superfamily (Figure 4A). Bioinformatics analysis showed that the isoelectric point of PA1-Lys is 9.21 and the aliphatic index of PA1-Lys is 71.66. As a stable hydrophilic protein, PA1-Lys has 22 negatively charged residues and 29 positively charged residues. Moreover, PA1-Lys lacks a TMD domain structure or signal peptide. According to Phyre2 analysis, PA1-Lys consists of 1 beta-sheets and 8

10.3389/fmicb.2024.1463192

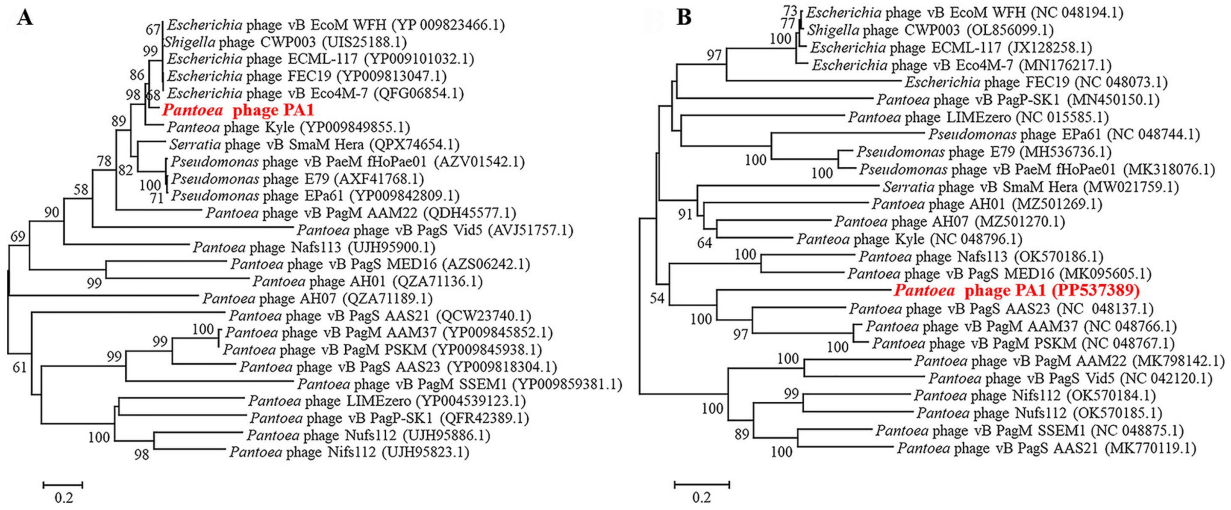

FIGURE 3
Neighbor-joining phylogenetic analysis of phage PA1. **(A)** Phylogenetic tree based on the amino acid sequences of terminal large subunit. **(B)** Phylogenetic tree based on Genome sequence.

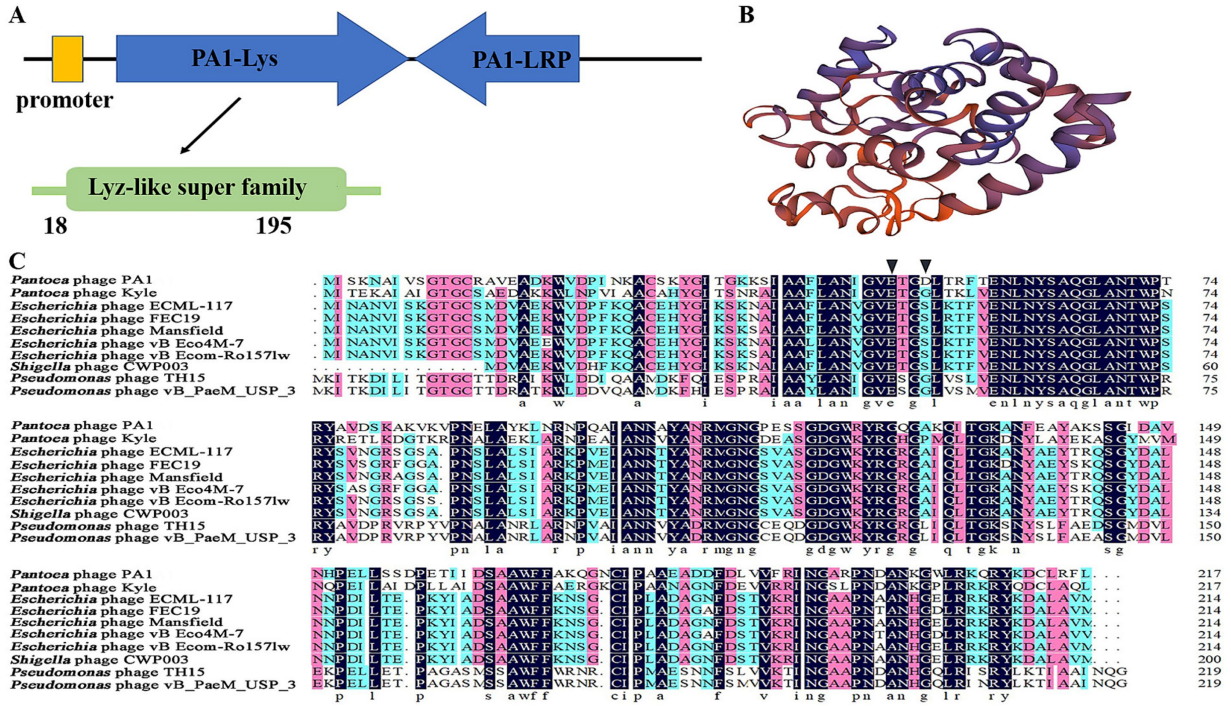

FIGURE 4
Bioinformatics and physicochemical properties of PA1-Lys. **(A)** Schematic diagram of the position of PA1-Lys in the phage PA1 genome. **(B)** 3D structure prediction of PA1-Lys. **(C)** Sequence alignment of PA1-Lys with that endolysin of *Pantoea* phage kyle (YP_009849889.1), *Escherichia* phage ECML-117 (YP_009101063.1), *Escherichia* phage FEC19 (YP_009813017.1), *Escherichia* phage Mansfield (QEG09877.1), *Escherichia* phage vB_Eco4M-7 (QFG06885.1), *Escherichia* phage vB_EcoM-Ro157lw (AVZ45696.1), *Shigella* phage CWP003 (UIS25194.1), *Pseudomonas* phage TH15 (QQO38587.1), and *Pseudomonas* phage vB_PaeM_USP_3 (QLI49345.1). The black arrow represents the predicted conserved motifs responsible for catalysis binding.

alpha-helices. So we believed that PA1-Lys has a spiral structure (Figure 4B). Besides, Phyre2 analysis showed PA1-Lys has the most similar protein structure to *Salmonella Typhimurium* bacteriophage spnls endolysin. The 208 residues (96% of PA1-Lys) have been modeled with 99.5% confidence by the single highest scoring template. NCBI blastp results showed that nine proteins have the most similar genetic relationship with PA1-Lys. Both of them are endolysins from *Pantoea* phage kyle (YP_009849889.1), *Escherichia* phage ECML-117 (YP_009101063.1), *Escherichia* phage FEC19 (YP_009813017.1), *Escherichia* phage Mansfield (QEG09877.1), *Escherichia* phage vB_Eco4M-7 (QFG06885.1), *Escherichia* phage vB_EcoM-Ro157lw (AVZ45696.1), *Shigella* phage CWP003 (UIS25194.1), *Pseudomonas*

phage TH15 (QQO38587.1) and *Pseudomonas* phage vB_PaeM_USP_3 (QLI49345.1) (Chen et al., 2021; D'Souza et al., 2019; Liao et al., 2019; Necel et al., 2020). Align the amino acid sequence of PA1-Lys with the amino acid sequences of the nine similar protein and results showed that the amino acid sequence of PA1-Lys is different from that of the 9 proteins.

Due to NCBI's conservative domain prediction, no conserved motifs responsible for catalysis or substrate binding were identified. Generally speaking, the catalytic motifs of phage endolysins typically include amino acid residues in the active site, such as glycine (G), glutamic acid (E), serine (S), and aspartic acid (D), which directly participate in the enzyme's catalytic reaction (Schmelcher et al., 2012; Vázquez et al., 2018). We speculated that the catalytic binding of PA1-Lys are E50 and D53, while the catalytic binding of other phages endolysin are E50 and G53 or E53 and S53. The differences in catalytic motifs among endolysins suggested that PA1-Lys may affect the structure and stability of bacterial cell walls through different mechanisms, which can lead to variations in their lytic efficacy and specificity against bacteria (Figure 4C).

3.6 Lytic activity of PA1-Lys

Our research found that the PA1-Lys mainly exists in the lysate supernatant. As shown in Figure 5A, the size of PA1-Lys is about 28 kDa, which is consistent with the results obtained from the bioinformatics analysis. Previous studies have shown that the cell wall of Gram-negative bacteria has an outer membrane with a lipopolysaccharide layer, which prevents endolysin from entering the peptidoglycan layer, thus preventing endolysin from lysing bacteria (Kim et al., 2020). Outer membrane permeabilizers (chloroform and EDTA) can facilitate endolysin enter the bacteria (Shen et al., 2023). Previous study have reported that phage endolysin has a certain specificity (Skorynina et al., 2020). After adding chloroform, there was no significant change in the OD_{450} of the bacteria. However, after adding PA1-Lys for 5 min, the OD_{450} value of bacteria treated with chloroform decreased by 61.59%, and lysozyme (positive control) reduced the OD_{450} value of bacteria treated with chloroform by 52.40%. However, the OD_{450} value of bacteria pretreated with chloroform did not change after adding 0.1 M PBS (Figure 5B). Besides, EDTA also enhanced the inhibitory effect of PA1-Lys on the *P. ananatis* strain ZJU1. EDTA alone decreased bacterial count by 41.92%, while the combination of EDTA and PA1-Lys reduced bacterial count by 63.65% (Figure 5C). PA1-Lys can effectively destroy a variety of Gram-negative bacteria pretreated with chloroform, such as *P. ananatis*, *P. dispersa*, *E. coli*, Xoo, and Xoc, but it was unable to lyse Ao. Notably, PA1-Lys can not lyse Gram-positive bacteria (*Bacillus* and *P. polymyxa*) that do not require chloroform pretreatment (Figure 5D).

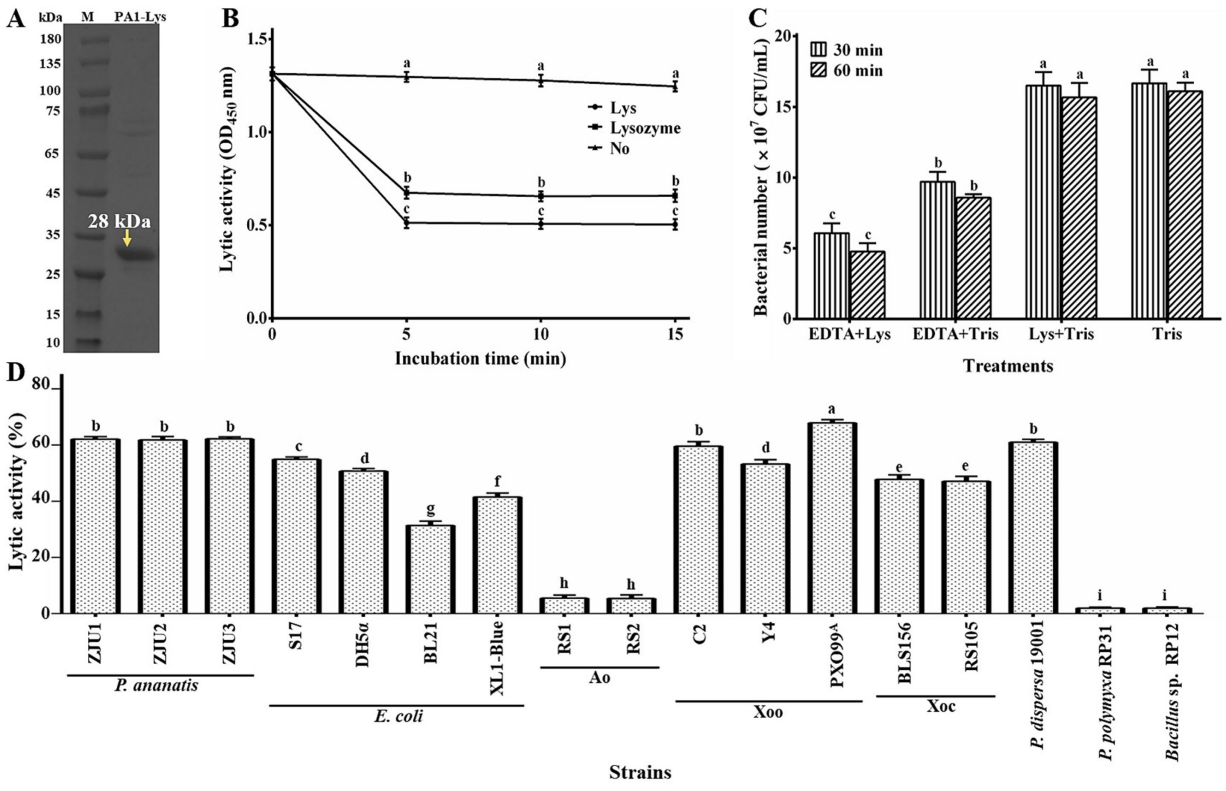

FIGURE 5
Lytic activity of PA1-Lys. **(A)** *In vitro* expression of PA1-Lys **(B)** Lytic effect of PA1-Lys on chloroform-pretreated *P. ananatis* strains ZJU1. **(C)** Lytic effect of PA1-Lys combined with EDTA. **(D)** Lytic spectrum of PA1-Lys. The error bars shows the mean of three replicates ($n = 3 \pm$ standard deviation). Different letters indicates significant differences in lytic activity among the different treatment groups at the same time point ($p < 0.05$).

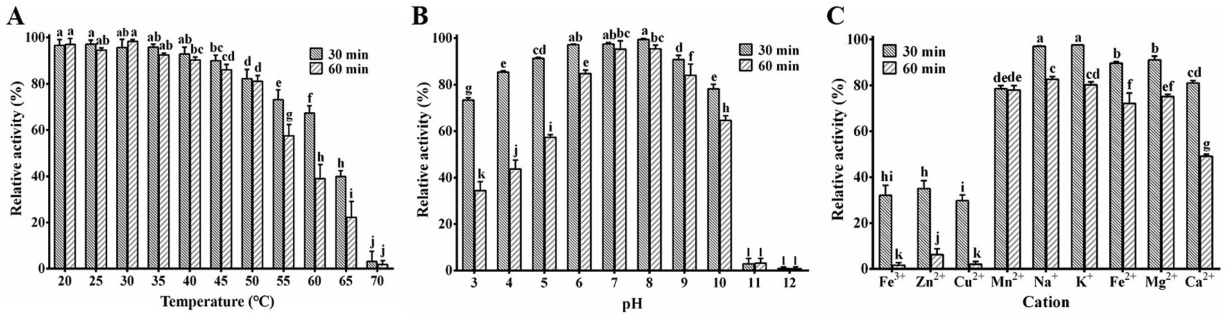

FIGURE 6
Stability of PA1-Lys. **(A)** Thermal stability of PA1-Lys. **(B)** pH stability of PA1-Lys. **(C)** Cation stability of PA1-Lys. The error bars stands for the mean of three replicates ($n = 3 \pm$ standard deviation). Different letters represents significant differences in the stability of PA1-Lys caused by different treatments at the same time point ($p < 0.05$).

3.7 Stability of PA1-Lys

The study on the thermal stability of PA1-Lys revealed robust lytic activity (>80%) across temperatures ranging from 20°C to 50°C (Figure 6A). However, the activity of PA1-Lys decreased notably with higher temperatures, showing a 96.83% decrease after incubation at 70°C for 30 min. Temperature exposure between 55°C and 65°C also significantly impacted PA1-Lys activity over time. Regarding pH stability (Figure 6B), PA1-Lys exhibited strong lytic activity across the pH range of 5 to 10. Optimal lytic activity was observed at pH 8, where PA1-Lys displayed 99.47% activity after 30 min and 95.4% after 60 min. The duration of treatment notably affected PA1-Lys activity, particularly at pH levels 3 to 6, where longer treatment times (60 min) resulted in decreased lytic activity compared to shorter treatments (30 min).

Furthermore, the study investigated the impact of cations on PA1-Lys activity (Figure 6C). Treatment with Fe^{3+}, Zn^{2+}, and Cu^{2+} for 30 min or 60 min significantly reduced PA1-Lys lytic activity by more than 75%. In contrast, Na^{+} and K^{+} did not affect PA1-Lys activity. However, prolonged exposure to these metal ions diminished PA1-Lys lytic activity. Interestingly, Ca^{2+} treatment initially showed no significant impact on PA1-Lys activity after 30 min but led to a significant decrease after 60 min. These findings underscore the sensitivity of PA1-Lys to temperature, pH, and specific cations, highlighting its potential application in environments where these factors can be controlled to optimize its efficacy as a biocontrol-agent.

3.8 Bacterial lysis function of PA1-Lys and PA1-LRP

Through bioinformatics analysis, we found that PA1-Lys does not possess a TMD or signal peptides, indicating that it might require the assistance of other proteins to facilitate its transmembrane transport, leading to cell lysis. Previous studies have reported that holin can assist endolysins in cell lysis (Bai et al., 2020; Chandran et al., 2022). However, we could not identify genes encoding holin through bioinformatics analysis. As we all know, lytic related proteins, such as holins, are located near the endolysins (Wang et al., 2022). PA1-Lys is expressed by the ORF12 gene of the phage PA1. Therefore, we chosed the proteins PA1-LPP and PA1-LRP expressed by ORF11 and ORF13 genes for the next research. In addition, studies have shown that some lytic related proteins contain TMD (Aslam et al., 2021). TMHMM analysis showed that among the 20 proteins near PA1-Lys, only the PA1-LVP contains three TMDs. Besides, the analysis of TMHMM showed PA1-LRP contains a hydrophobic region within the 40–60 amino acid range, while the PA1-LPP has no hydrophobic region. Then PA1-LRP, PA1-LPP, and PA1-LVP were fused and co-expressed with PA1-Lys to investigate whether the three fusion proteins could lyse bacteria. After 24 h of IPTG induction, we observed the OD_{600} value of 28a-Lys-LRP was 68.88% lower compared to 28a-Lys, declaring that the PA1-LRP can help PA1-Lys perform cell lysis functions. Therefore, ORF13 expressed protein PA1-LRP drew my attention.

According to Phyre2 analysis, we found that PA1-LRP has 2 alpha-helices and no beta-sheets. In addition, 3D structure prediction of PA1-LRP was showed in Supplementary Figure S3. Through comparison, PA1-LRP does not resemble any known protein structures in the Protein Data Bank (PDB). Through NCBI blastp, the similar proteins of PA1-LRP are all hypothetical protein. *Pantoea* phage Kyle hypothetical protein HWC52 gp058 has the highest similarity with PA1-LRP, with a query coverage of 97%. Besides, bioinformatics analysis results indicated that the size of the PA1-LRP is 8.5 kDa.

Bacterial growth assay makes it clear that after application of IPTG for 6, 12, 18, and 24 h, there was no significant difference in the OD_{600} values of 28a-Lys compared to 28a, while the OD_{600} values of 28a-LRP reduced by 13.40, 13.91, 14.18, and 19.67% (Figure 7A). The β-galactosidase assay measured the effect of PA1-Lys and PA1-LRP on cell membrane permeability. When the cell membrane is damaged, the β-galactosidase inside the cell membrane flow out, which can break down ONPG and produce yellow O-nitrophenol. Therefore, the more yellow the color of the bacterial supernatant, the greater the cell membrane permeability. After induction of IPTG for 24 h, the color of 28a was transparent, suggesting that the bacterial cell membrane was intact. However, the supernatants of 28a-Lys and 28a-LRP turned yellow, and the color of 28a-LRP was stronger than that of 28a-Lys, indicating that the cell membranes of 28a-Lys and 28a-LRP were unstable, with 28a-LRP having higher cell permeability (Figure 7B).

Further analysis of the mortality rates after 24 h of induction using flow cytometry revealed mortality rates of 3.25% for 28a-Lys

and 24.65% for 28a-LRP, while the mortality rates of 28a was only 1.03% (Figure 7C). Utilizing a live/dead bacterial staining kit, live bacteria were stained green while dead bacteria appeared red. Fluorescence microscopy observations showed that all bacteria were short rod-shaped, with a higher proportion of dead bacteria observed in 28a-LRP compared to 28a (Figure 7D). To investigate the effects of PA1-Lys and PA1-LRP on the morphology of *E. coli* in greater detail, ultrastructural analysis using TEM was performed. TEM observations indicated that both 28a and 28a-Lys exhibited intact cell structures with high-density intracellular substances (Figure 7E). In contrast, 28a-LRP showed a relatively lower density of intracellular materials compared to 28a-Lys and 28a. These findings strongly suggest that PA1-LRP contributes to cellular damage, resulting in altered cell morphology and increased mortality rates among bacterial populations.

3.9 Effects of co-expression of PA1-Lys and PA1-LRP on cells

Previous studies have shown that adding an exogenous TMD to endolysins can help them lyse cells (Wu et al., 2021). Therefore, we added an exogenous TMD at the C-terminus of PA1-Lys as a positive control (28a-Lys-ATMD). After 6, 12, 18, and 24 h of IPTG induction, the OD_{600} value of 28a-Lys-ATMD decreased by 38.21, 53.88, 59.68, and 60.89%, compared to the negative control of 28a while the OD_{600} value of 28a-Lys-LRP decreased by 43.92, 65.84, 72.46 and 75.40% (Figure 8A). After 6 h of induction, the supernatant of 28a-Lys-LRP turned dark yellow and showed a stronger color compare to 28a-Lys-ATMD (Figure 8B). Flow cytometry measurement results suggested that the mortality rates of 28a-Lys-LRP and 28a-Lys-ATMD were 43.18 and 39.94%, respectively (Figure 8C). Compared with the positive control, the co-expression of PA1-Lys and PA1-LRP possessed strong antibacterial properties.

To further elucidate the synergistic mechanism of PA1-Lys and PA1-LRP in bacterial lysis, we observed the morphological and structural changes of cells using fluorescence and TEM. The morphology of all bacteria in the 28a-Lys-LRP sample was filamentous, while the morphology of 28a and 28a-Lys were short rod-shaped. Moreover, some bacteria in the 28a-Lys-ATMD sample became spherical (Figure 8D). The field of view of the 28a-Lys-LRP samples contained relatively fewer bacteria and a higher proportion of dead bacteria, consistent with the bacterial growth experiments and flow cytometry results.

Compared with 28a and 28a-Lys, the cells of 28a-Lys-LRP and 28a-Lys-ATMD were enlarged, with lower intracellular material density, lighter cell color, and even some cells formed vacuoles due to complete loss of contents (Figure 8E). These results indicated that co-expression of PA1-Lys and PA1-LRP can effectively inhibit bacterial growth, ultimately

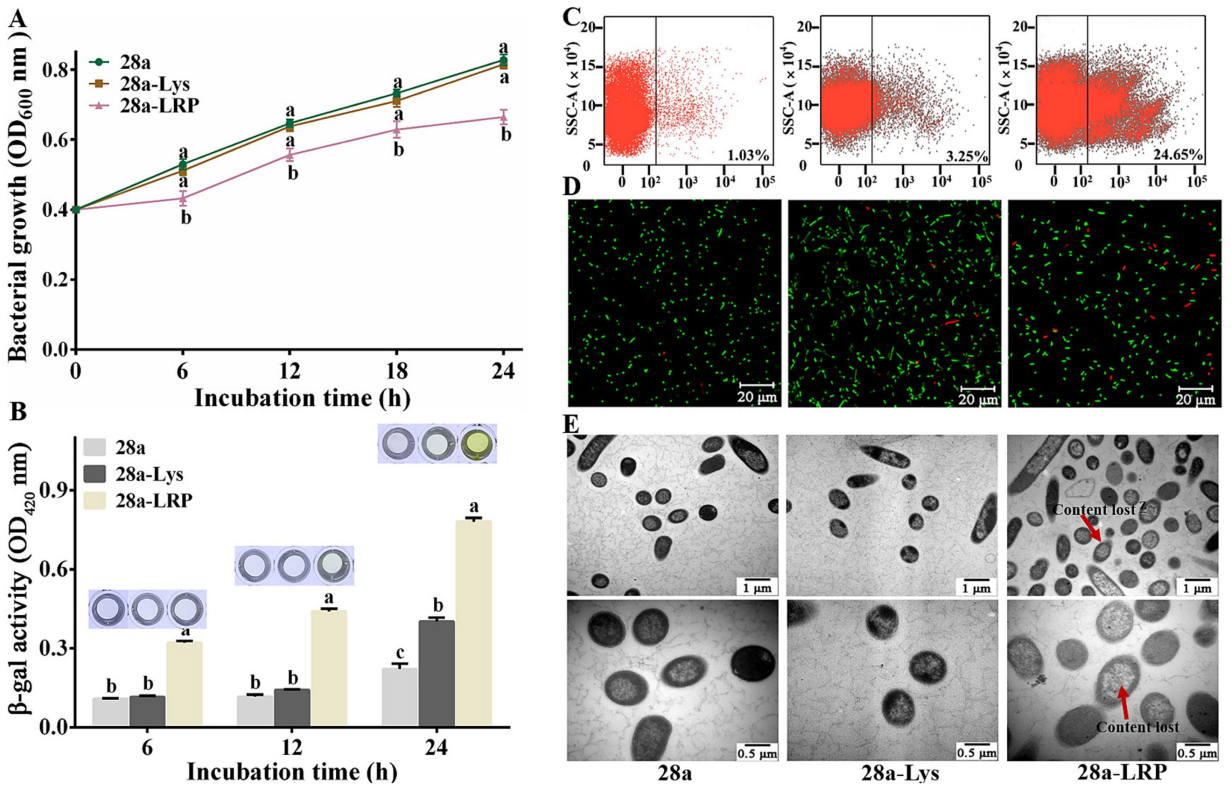

FIGURE 7
Effects of PA1-Lys and PA1-LRP on cell. **(A)** Bacterial growth curve. The statistically significant results are based on the OD_{600} values of 28a, 28a-Lys and 28a-LRP induced at the same induction time. **(B)** Determination of β-galactosidase in bacterial supernatant. The statistically significant results are based on the OD_{420} values of 28a, 28a-Lys and 28a-LRP induced at the same induction time. **(C)** Flow cytometry analysis. **(D)** Live/dead cell staining analysis. **(E)** TEM images of bacterial ultrastructure. The red arrow represents the lost of cell contents. Magnification was 20,000 x and 40,000 x, respectively. The error bars stands for the mean of three replicates (n = 3 ± standard deviation). Different letters represents significant differences caused by different treatments at the same time point ($p < 0.05$).

leading to bacterial death. Moreover, PA1-LRP has a stronger auxiliary effect than exogenous TMD in helping PA1-Lys perform cell lysis functions. Due to the synergistic destructive effect of PA1-LRP and PA1-Lys on *E. coli*, we conducted the bacterial two-hybrid experiment to explore whether they directly interact *in vivo*. Positive colonies grew well on the selected culture medium. However, the colonies of *E. coli* XL1-Blue co-expressing PA1-LRP and PA1-Lys was unable to grow on the selected medium, consistent with the negative colonies. The bacterial two-hybrid experiment showed that there was no direct interaction between PA1-Lys and PA1-LRP (Supplementary Figure S2).

3.10 Effects of co-expression of PA1-Lys and HPP on cells

Previous research has shown that fusion expression of endolysin and hydrophobic peptides can damage cells (Sitthisak et al., 2023). We engineered a fusion of HPP at the C-terminus of PA1-Lys to investigate its impact on PA1-Lys function. Following induction periods of 6, 12, 18, and 24 h, the OD_{600} values of 28a-Lys-HPP decreased by 39.77, 61.55, 67.84, and 70.16%, respectively, compared to 28a-Lys (Figure 9A). Notably, after just 6 h of induction, the supernatant of 28a-Lys-HPP exhibited a yellow color (Figure 9B), suggesting cellular disruption and metabolic changes. Flow cytometry analysis revealed a 38.44% higher mortality rate in 28a-Lys-HPP compared to 28a-Lys (Figure 9C). Fluorescence microscopy observations further supported these findings, revealing predominantly long rod-shaped bacteria in 28a-Lys-HPP samples, accompanied by a lower total bacterial count and increased presence of dead bacteria relative to 28a-Lys (Figure 9D). TEM imaging of 28a-Lys-HPP samples depicted significant cellular content leakage, vacuole formation, and substantial cell debris, similar to observations in 28a-Lys-LRP samples (Figure 9E). These results collectively demonstrate that HPP enhances PA1-Lys's ability to disrupt cell membranes, leading to effective bacterial cell destruction.

4 Discussion

In recent years, *P. ananatis* has been recognized as a new type of pathogenic bacteria affecting various plants, and is widely distributed in nature (Xiao et al., 2022; Xu et al., 2021). As natural enemies of bacteria, phages can not only specifically recognize and effectively kill target bacteria, but also co-evolve with the host, demonstrating excellent biosafety (Oyejobi et al., 2023). Therefore, phages are very important for the treatment of pathogenic bacteria. However, despite their potential use, research on *P. ananatis* phage is limited.

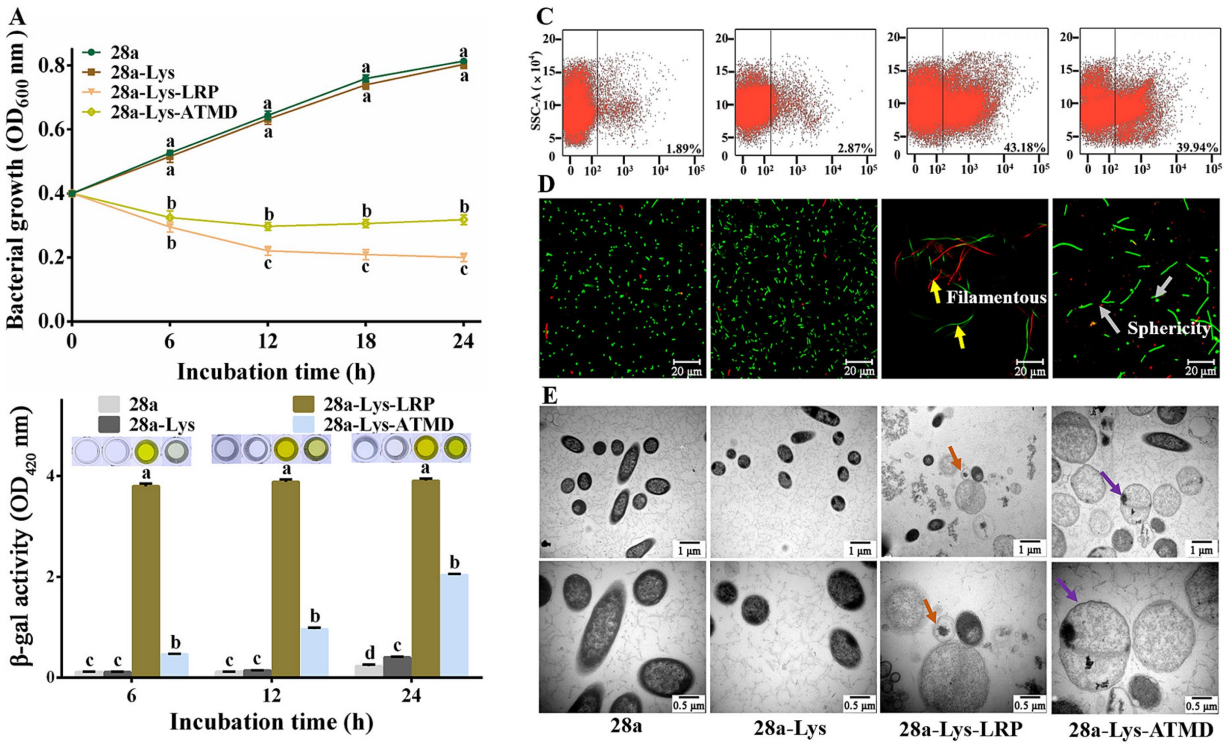

FIGURE 8
Effects of co-expression of PA1-Lys and PA1-LRP on cell. **(A)** Bacterial growth curve. The statistically significant results are based on the OD_{600} values of 28a, 28a-Lys, 28a-Lys-LRP and 28a-Lys-ATMD induced at the same induction time. **(B)** Determination of β-galactosidase in bacterial supernatant. The statistically significant results are based on the OD_{420} values of 28a, 28a-Lys, 28a-Lys-LRP and 28a-Lys-ATMD induced at the same induction time. **(C)** Flow cytometry analysis. **(D)** Live/dead cell staining analysis. The yellow arrows point to the bacteria becoming filamentous, while the gray arrows points to the bacteria becoming spherical. **(E)** TEM images of bacterial ultrastructure. The orange arrow represents the transformation of bacteria into vacuoles, and the purple arrow represents bacterial enlargement. The magnification was 20,000x and 40,000x, respectively. The error bars stands for the mean of three replicates ($n = 3 \pm$ standard deviation). Different Minuscule mean significant differences caused by different treatments at the same time point ($p < 0.05$).

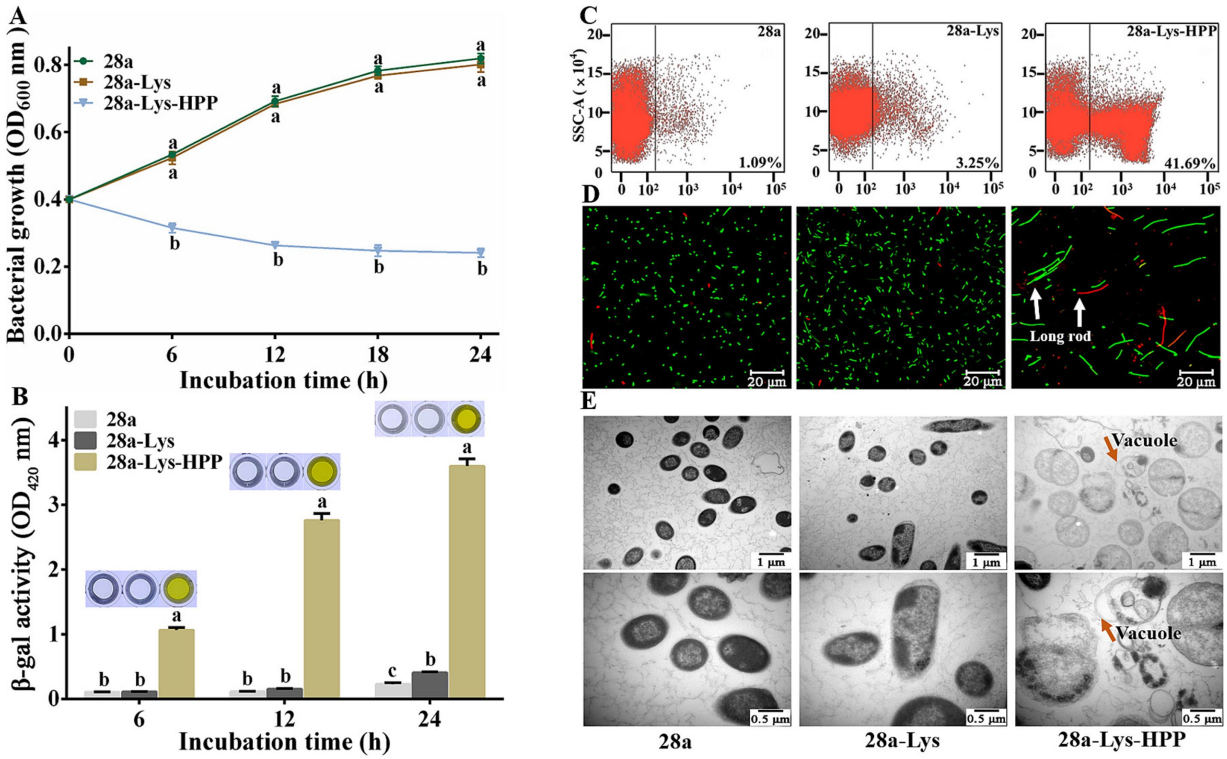

FIGURE 9
Effects of Co-Expression of PA1-Lys and HPP on cell. **(A)** Bacterial growth curve. The statistically significant results are based on the OD_{600} values of 28a, 28a-Lys and 28a-Lys-HPP induced at the same induction time. **(B)** Determination of β-galactosidase in bacterial supernatant. The statistically significant results are based on the OD_{420} values of 28a, 28a-Lys and 28a-Lys-HPP induced at the same induction time. **(C)** Flow cytometry analysis. **(D)** Live/dead cell staining analysis. The white arrow points to long rod-shaped bacteria **(E)** TEM images of bacterial ultrastructure. The orange arrow represents the transformation of bacteria into vacuoles. The magnification was 20,000x and 40,000x, respectively. The error bars stand for the mean of three replicates ($n = 3 \pm$ standard deviation). Different letters represent significant differences caused by different treatments at the same time point ($p < 0.05$).

In this study, we isolated a phage with specific lysis capabilities against *P. ananatis* from rice leaves and named it PA1. The whole genome sequencing of phage PA1 showed relatively low similarity to other phages in the NCBI database. Although different annotation tools were used to annotate the PA1 phage proteins, there are still many hypothetical proteins among the 105 putative open reading frames, which may be related to the limited number of reported *Pantoea* phages.

However, the evolutionary tree indicated a close genetic relationship between phage PA1 and *Pantoea* phages. TEM observation confirmed that phage PA1 has an icosahedron head and a contractile tail, classifying it under the *Chaseviridae* family. Previous studies have shown that phages with larger burst sizes tend to have more effective lysis effects (Manohar et al., 2018). The results of the one-step growth experiment showed that phage PA1 has a latent period of 40 min and a burst size of 17.17, indicating its potential as a biocontrol agent against diseases caused by *P. ananatis*. As a biocontrol agent, phages should remain stable under various environmental conditions, including pH and temperature (Liu et al., 2021). Phage stability testing showed that phage PA1 was stable within a pH range of 6 to 8 and a temperature range of 4 to 60°C, signifying its suitability for biological control.

However, phage therapy faces several obstacles, including the limitations in phage infection spectrum and the development of bacterial resistance to phages (Hatfull et al., 2022). Phage endolysins are peptidoglycan hydrolases encoded by phages and synthesized by host bacteria (Li et al., 2021; Zhang et al., 2022). Due to their broad lytic spectrum, phage endolysins have emerged as potential novel antibacterial agents (Wan et al., 2021). In our study, we analyzed the sequencing data of phage PA1 and identified the phage endolysin PA1-Lys. PA1-Lys can break down various chloroform-treated bacteria, including *P. ananatis*, *P. dispera,* Xoo, Xoc and *E. coli*. Also, PA1-Lys remaines stable under different pH levels (6 to 10) and temperatures (20 to 50°C).

In this study, the PA1-Lys cannot directly lyse cells. Bioinformatics analysis showed that PA1-Lys possesses a Lyz-like superfamily domain. Notably, unlike Gram-positive bacteria, Gram-negative bacteria have an outer membrane containing lipopolysaccharide, which makes it impossible for the endolysins lacking transmembrane and SAR domains to directly hydrolyze the bacterial cell wall through the outer membrane. Therefore, the endolysins of Gram-negative bacteria cannot directly penetrate the bacteria (Rahman et al., 2021). Studies have shown that the addition of EDTA and chloroform can disrupt the outer membrane of Gram-negative bacteria, thereby helping endolysins to destroy bacteria (Legotsky et al., 2014; Nie et al., 2022; Wang et al., 2024). Consequently, this study confirmed that PA1-Lys exhibits enhanced lytic activity in the presence of EDTA and chloroform.

Phage holins can form pores in the bacterial cytoplasmic membrane at specific times, (Xu et al., 2021) facilitating the endolysin to damage cell wall peptidoglycan and leading to rapid dissolution of the host cells (Zhou et al., 2021). Previous studies have shown that the transport function of holins may be determined by their TMD (Wu et al., 2021). In this study, an exogenous TMD with PA1-Lys was fused and the fusion protein indeed caused cell lysis. Since PA1-Lys alone was unable to directly lyse bacteria, we speculated whether the presence of a holin to assist in its lysis effect. However, no holin gene was observed through RAST analysis. Previous studies have shown that some lytic related proteins, such as holins, located near the endolysins and contain at least one TMD (Guo et al., 2022; Lu et al., 2020). TMHMM analysis showed that among the 20 proteins near PA1-Lys, only the PA1-LVP contains three TMDs. PA1-Lys is expressed by the ORF12 gene of the phage PA1. Therefore, we also chosed the proteins PA1-LPP and PA1-LRP expressed by ORF11 and ORF13 genes for the next research. We fused PA1-Lys with PA1-LPP, PA1-LRP, and PA1-LVP for expression, and the results showed that only PA1-LRP fused with PA1-Lys can inhibit bacterial growth. Additionally, we found PA1-LRP was found to inhibit bacterial growth and cause cell death. Moreover, the lytic effect of co-expressing PA1-LRP with PA1-Lys was significantly stronger than expressing PA1-LRP or PA1-Lys alone. After 24 h, the OD_{600} value of 28a-Lys-LRP was 0.444 lower than that of 28a-LRP. In addition to inhibiting bacterial growth, the co-expression of PA1-LRP with PA1-Lys altered the bacterial shape from short rod to filamentous, suggesting a potential inhibitory effect on bacterial cell division. Thus we consider PA1-LRP to be a novel lysis-related protein. Bioinformatics analysis indicated that PA1-LRP contains a hydrophobic region. Previous studies have shown that hydrophobic regions assist endolysins in degrading bacterial cells (Ning H. Q. et al., 2021; Xu et al., 2021). *E. coli* phages endolysin Lysep3 modified with hydrophobic amino acids can undergo external lysis of *E. coli* (Yan et al., 2019). Hydrophobic fusion of intracellular endolysin (lysAB-vT2 fusion) can dissolve the cell wall of Gram-negative bacteria (Sitthisak et al., 2023). The co-expression of the HPP with PA1-Lys also led to cell death. Therefore, PA1-LRP, using HPP, can assist PA1-Lys in disrupting bacterial cells.

5 Conclusion

In summary, this study successfully isolated and characterized *Pantoea* phage PA1 belonging to the *Chaseviridae* family. Phage PA1 exhibited promising characteristics as a biocontrol agent, including a large burst size of 17.17 phages per infected cell and stability over a range of pH and temperature conditions. Genomic analysis identified the endolysin PA1-Lys, which showed broad lytic activity against various chloroform-treated Gram-negative bacteria. Importantly, this research uncovered a novel lysis-related protein, PA1-LRP, which enhanced the bactericidal activity of PA1-Lys. Co-expression of PA1-Lys with PA1-LRP resulted in significant bacterial growth inhibition, cell shape alterations, and increased cell death compared to either protein alone. The HPP was found to be crucial in assisting PA1-Lys to disrupt bacterial cells. These findings contribute to our understanding of phage lysis mechanisms and offer new strategies for combating bacterial infections. The synergistic effect of PA1-Lys and PA1-LRP presents a promising approach for developing more effective antimicrobial agents. Further research into the precise mechanisms of PA1-LRP lytic activity and its potential applications could lead to novel therapeutic interventions against antibiotic-resistant pathogens.

Data availability statement

The original contributions presented in the study are included in the article/Supplementary material, further inquiries can be directed to the corresponding authors.

Author contributions

YT: Writing – original draft, Methodology, Investigation, Formal analysis, Data curation, Conceptualization. XX: Writing – review & editing, Validation, Formal analysis. MI: Writing – review & editing, Validation, Formal analysis. YS: Writing – review & editing, Validation, Formal analysis. MS: Writing – review & editing, Investigation, Formal analysis, Data curation. TA: Writing – original draft, Investigation, Formal analysis, Data curation. HA: Writing – review & editing, Investigation, Formal analysis, Data curation. CY: Writing – review & editing, Validation, Investigation. CG: Writing – review & editing, Project administration, Formal analysis. JL: Writing – review & editing, Project administration, Formal analysis. YW: Writing – review & editing, Supervision, Project administration, Methodology, Funding acquisition, Formal analysis, Conceptualization. GO: Writing – review & editing, Supervision, Project administration, Methodology, Funding acquisition, Formal analysis, Conceptualization. BL: Project administration, Methodology, Funding acquisition, Formal analysis, Conceptualization, Writing – review & editing.

Funding

The author(s) declare that financial support was received for the research, authorship, and/or publication of this article. The work is partially supported by the "Pioneer" and "Leading Goose" R&D Program of Zhejiang (2022C02047 and 2023C02018), National Natural Science Foundation of China (32072472, 32372614), Zhejiang Provincial Natural Science Foundation of China (LZ24C140004), Hangzhou Science and Technology Development Plan Project (20231203A05), State Key Laboratory for Managing Biotic and Chemical Threats to the Quality and Safety of Agro-products (2021DG700024-KF202415). This study has been partly conducted under the WAST2GROW project (NPOO.C3.2.R3-I1.04.0143) founded by the Ministry of Science and Education, R. of Croatia. This work was funded by the Researchers Supporting Project number (RSP2024R123), King Saud University, Riyadh, Saudi Arabia.

Acknowledgments

The authors would like to extend their sincere appreciation to the Researchers Supporting Project number (RSP2024R123), King Saud University, Riyadh, Saudi Arabia.

Conflict of interest

The authors declare that the research was conducted in the absence of any commercial or financial relationships that could be construed as a potential conflict of interest.

Publisher's note

All claims expressed in this article are solely those of the authors and do not necessarily represent those of their affiliated organizations, or those of the publisher, the editors and the reviewers. Any product that may be evaluated in this article, or claim that may be made by its manufacturer, is not guaranteed or endorsed by the publisher.

Supplementary material

The Supplementary material for this article can be found online at: https://www.frontiersin.org/articles/10.3389/fmicb.2024.1463192/full#supplementary-material

References

Ahmed, T., and Li, B. (2023). Phage-plant interactions: a way forward toward sustainable agriculture. *Viruses* 15:329. doi: 10.3390/v15020329

Aslam, B., Arshad, M. I., Aslam, M. A., Muzammil, S., Siddique, A. B., Yasmeen, N., et al. (2021). Bacteriophage proteome: insights and potentials of an alternate to antibiotics. *Infect. Dis. Ther.* 10, 1171–1193. doi: 10.1007/s40121-021-00446-2

Bai, J., Lee, S., and Ryu, S. (2020). Identification and in vitro Characterization of a Novel Phage Endolysin that Targets Gram-Negative Bacteria. *Microorganisms.* 8:447. doi: 10.3390/microorganisms8030447

Basit, A., Qadir, S., Qureshi, S., and Rehman, S. U. (2021). Cloning and expression analysis of fused holin-endolysin from RL bacteriophage; exhibits broad activity against multi drug resistant pathogens. *Enzym. Microb. Technol.* 149:109846. doi: 10.1016/j.enzmictec.2021.109846

Brüser, T., and Mehner-Breitfeld, D. (2022). Occurrence and potential mechanism of holin-mediated non-lytic protein translocation in bacteria. *Microb Cell* 9, 159–173. doi: 10.15698/mic2022.10.785

Cahill, J., and Young, R. (2019). Phage lysis: multiple genes for multiple barriers. *Adv. Virus Res.* 103, 33–70. doi: 10.1016/bs.aivir.2018.09.003

Cao, S., Yang, W., Zhu, X., Liu, C., Lu, J., Si, Z., et al. (2022). Isolation and identification of the broad-spectrum high-efficiency phage vB_SalP_LDW16 and its therapeutic application in chickens. *BMC Vet. Res.* 18:386. doi: 10.1186/s12917-022-03490-3

Chandran, C., Tham, H. Y., Abdul Rahim, R., Lim, S. H. E., Yusoff, K., and Song, A. (2022). Lactococcus lactis secreting phage lysins as a potential antimicrobial against multi-drug resistant Staphylococcus aureus. *PeerJ.* 10:e12648. doi: 10.7717/peerj.12648

Chen, F., Cheng, X., Li, J., Yuan, X., Huang, X., Lian, M., et al. (2021). Novel lytic phages protect cells and mice against *Pseudomonas aeruginosa* infection. *J. Virol.* 95, e01832–e01820. doi: 10.1128/JVI.01832-20

Chevallereau, A., Pons, B. J., van Houte, S., and Westra, E. R. (2022). Interactions between bacterial and phage communities in natural environments. *Nat. Rev. Microbiol.* 20, 49–62. doi: 10.1038/s41579-021-00602-y

Cho, J. H., Kwon, J. G., O'Sullivan, D. J., Ryu, S., and Lee, J. H. (2021). Development of an endolysin enzyme and its cell wall-binding domain protein and their applications for biocontrol and rapid detection of *Clostridium perfringens* in food. *Food Chem.* 345:128562. doi: 10.1016/j.foodchem.2020.128562

Daei, S., Ziamajidi, N., Abbasalipourkabir, R., Aminzadeh, Z., and Vahabirad, M. (2022). Silver Nanoparticles Exert Apoptotic Activity in Bladder Cancer 5637 Cells Through Alteration of Bax/Bcl-2 Genes Expression. *Chonnam Med J.* 58, 102–109. doi: 10.4068/cmj.2022.58.3.102

D'Souza, G. M., Klotz, K., Moreland, R., Liu, M., and Ramsey, J. (2019). Complete genome sequence of *Escherichia coli* Myophage Mansfield. *Microbiol Resour Announc* 8, e01038–e01019. doi: 10.1128/MRA.01038-19

Evseev, P., Lukianova, A., Sykilinda, N., Gorshkova, A., Bondar, A., Shneider, M., et al. (2021). *Pseudomonas* phage MD8: genetic mosaicism and challenges of taxonomic classification of lambdoid bacteriophages. *Int. J. Mol. Sci.* 22:10350. doi: 10.3390/ijms221910350

Gašić, K., Obradović, M., Kuzmanović, N., Zlatković, N., Ivanović, M., Ristić, D., et al. (2022). Isolation, characterization and draft genome analysis of bacteriophages infecting *Acidovorax citrulli*. *Front. Microbiol.* 12:803789. doi: 10.3389/fmicb.2021.803789

Ghose, C., and Euler, C. W. (2020). Gram-negative bacterial Lysins. *Antibiotics* 9:74. doi: 10.3390/antibiotics9020074

Golz, S., and Kemper, B. (1999). Association of Holliday-structure resolving endonuclease VII with gp20 from the packaging machine of phage T4. *J. Mol. Biol.* 285, 1131–1144. doi: 10.1006/jmbi.1998.2399

Gontijo, M. T. P., Jorge, G. P., and Brocchi, M. (2021). Current status of Endolysin-based treatments against gram-negative Bacteria. *Antibiotics* 10:1143. doi: 10.3390/antibiotics10101143

Gouveia, A., Pinto, D., Veiga, H., Antunes, W., Pinho, M. G., and Sao-Jose, C. (2022). Synthetic antimicrobial peptides as enhancers of the bacteriolytic action of *staphylococcal* phage endolysins. *Sci. Rep.* 12:1245. doi: 10.1038/s41598-022-05361-1

Guo, T., Cui, Y., Zhang, L., Xu, X., Xu, Z., and Kong, J. (2022). Holin-assisted bacterial recombinant protein export. *Biotechnol. Bioeng.* 119, 2908–2918. doi: 10.1002/bit.28179

Hatfull, G. F., Dedrick, R. M., and Schooley, R. T. (2022). Phage therapy for antibiotic-resistant bacterial infections. *Annu. Rev. Med.* 73, 197–211. doi: 10.1146/annurev-med-080219-122208

Ho, M. K. Y., Zhang, P., Chen, X., Xia, J., and Leung, S. S. Y. (2022). Bacteriophage endolysins against gram-positive bacteria, an overview on the clinical development and recent advances on the delivery and formulation strategies. *Crit. Rev. Microbiol.* 48, 303–326. doi: 10.1080/1040841X.2021.1962803

Hong, H. W., Kim, Y. D., Jang, J., Kim, M. S., Song, M., and Myung, H. (2022). Combination effect of engineered Endolysin EC340 with antibiotics. *Front. Microbiol.* 13:821936. doi: 10.3389/fmicb.2022.821936

Huang, S., Tian, Y., Wang, Y., García, P., Liu, B., Lu, R., et al. (2022). The broad host range phage vB_CpeS_BG3P is able to inhibit *Clostridium perfringens* growth. *Viruses* 14:676. doi: 10.3390/v14040676

Jamal, M., Bukhari, S., Andleeb, S., Ali, M., Raza, S., Nawaz, M. A., et al. (2019). Bacteriophages: an overview of the control strategies against multiple bacterial infections in different fields. *J. Basic Microbiol.* 59, 123–133. doi: 10.1002/jobm.201800412

Jiang, Y., Xu, D., Wang, L., Qu, M., Li, F., Tan, Z., et al. (2021). Characterization of a broad-spectrum endolysin LysSP1 encoded by a *Salmonella* bacteriophage. *Appl. Microbiol. Biotechnol.* 105, 5461–5470. doi: 10.1007/s00253-021-11366-z

Kim, S., Lee, D. W., Jin, J. S., and Kim, J. (2020). Antimicrobial activity of LysSS, a novel phage endolysin, against *Acinetobacter baumannii* and *Pseudomonas aeruginosa*. *J Glob Antimicrob Resist* 22, 32–39. doi: 10.1016/j.jgar.2020.01.005

Krawczyk, K., Wielkopolan, B., and Obrepalska-Steplowska, A. (2020). *Pantoea ananatis*, a new bacterial pathogen affecting wheat plants (*Triticum L.*) in Poland. *Pathogens* 9:1079. doi: 10.3390/pathogens9121079

Lai, W. C. B., Chen, X., Ho, M. K. Y., Xia, J., and Leung, S. S. Y. (2020). Bacteriophage-derived endolysins to target gram-negative bacteria. *Int. J. Pharm.* 589:119833. doi: 10.1016/j.ijpharm.2020.119833

Legotsky, S. A., Vlasova, K. Y., Priyma, A. D., Shneider, M. M., Pugachev, V. G., Totmenina, O. D., et al. (2014). Peptidoglycan degrading activity of the broad-range *Salmonella* bacteriophage S-394 recombinant endolysin. *Biochimie* 107, 293–299. doi: 10.1016/j.biochi.2014.09.017

Liao, Y.-T., Sun, X., Quintela, I. A., Bridges, D. F., Liu, F., Zhang, Y., et al. (2019). Discovery of Shiga toxin-producing *Escherichia coli* (STEC)-specific bacteriophages from non-fecal composts using genomic characterization. *Front. Microbiol.* 10:627. doi: 10.3389/fmicb.2019.00627

Liu, P., Huang, D., Hu, X., Tang, Y., Ma, X., Yan, R., et al. (2017). Targeting inhibition of SmpB by peptide aptamer attenuates the virulence to protect zebrafish against *Aeromonas veronii* infection. *Front. Microbiol.* 8:1766. doi: 10.3389/fmicb.2017.01766

Liu, Y., Liu, M., Hu, R., Bai, J., He, X., and Jin, Y. (2021). Isolation of the novel phage PHB09 and its potential use against the plant pathogen *Pseudomonas syringae* pv. *Actinidiae*. *Viruses* 13:2275. doi: 10.3390/v13112275

Li, X., Zhang, C., Wei, F., Yu, F., and Zhao, Z. (2021). Bactericidal activity of a holin-endolysin system derived from *Vibrio alginolyticus* phage HH109. *Microb. Pathog.* 159:105135. doi: 10.1016/j.micpath.2021.105135

Lu, N., Sun, Y., Wang, Q., Qiu, Y., Chen, Z., Wen, Y., et al. (2020). Cloning and characterization of endolysin and holin from *Streptomyces avermitilis* bacteriophage phiSASD1 as potential novel antibiotic candidates. *Int. J. Biol. Macromol.* 147, 980–989. doi: 10.1016/j.ijbiomac.2019.10.065

Luong, T., Salabarria, A. C., and Roach, D. R. (2020). Phage therapy in the resistance era: where do we stand and where are we going? *Clin. Ther.* 42, 1659–1680. doi: 10.1016/j.clinthera.2020.07.014

Manohar, P., Tamhankar, A. J., Lundborg, C. S., and Ramesh, N. (2018). Isolation, characterization and in vivo efficacy of *Escherichia* phage myPSH1131. *PLoS One* 13:e0206278. doi: 10.1371/journal.pone.0206278

Necel, A., Bloch, S., Nejman-Faleńczyk, B., Grabski, M., Topka, G., Dydecka, A., et al. (2020). Characterization of a bacteriophage, vB_Eco4M-7, that effectively infects many *Escherichia coli* O157 strains. *Sci. Rep.* 10:3743. doi: 10.1038/s41598-020-60568-4

Nie, T., Meng, F., Lu, F., Bie, X., Zhao, H., Sun, J., et al. (2022). An endolysin Salmcide-p1 from bacteriophage fmb-p1 against gram-negative bacteria. *J. Appl. Microbiol.* 133, 1597–1609. doi: 10.1111/jam.15661

Ning, H., Cong, Y., Lin, H., and Wang, J. (2021). Development of cationic peptide chimeric lysins based on phage lysin Lysqdvp001 and their antibacterial effects against *Vibrio parahaemolyticus*: a preliminary study. *Int. J. Food Microbiol.* 358:109396. doi: 10.1016/j.ijfoodmicro.2021.109396

Ning, H. Q., Lin, H., and Wang, J. X. (2021). Synergistic effects of endolysin Lysqdvp001 and ε-poly-lysine in controlling Vibrio parahaemolyticus and its biofilms. *Int. J. Food Microbiol.* 343:109112. doi: 10.1016/j.ijfoodmicro.2021.109112

Oyejobi, G. K., Zhang, X., Xiong, D., Ogolla, F., Xue, H., and Wei, H. (2023). Phage-bacterial evolutionary interactions: experimental models and complications. *Crit. Rev. Microbiol.* 49, 283–296. doi: 10.1080/1040841X.2022.2052793

Pallesen, E. M. H., Gluud, M., Vadivel, C. K., Buus, T. B., de Rooij, B., Zeng, Z., et al. (2023). Endolysin inhibits skin colonization by patient-derived *staphylococcus aureus* and malignant T-cell activation in cutaneous T-cell lymphoma. *J. Invest. Dermatol.* 143, 1757–1768.e3. doi: 10.1016/j.jid.2023.01.039

Piel, D., Bruto, M., Labreuche, Y., Blanquart, F., Goudenège, D., Barcia-Cruz, R., et al. (2022). Phage-host coevolution in natural populations. *Nat. Microbiol.* 7, 1075–1086. doi: 10.1038/s41564-022-01157-1

Rahman, M. U., Wang, W., Sun, Q., Shah, J. A., Li, C., Sun, Y., et al. (2021). Endolysin, a promising solution against antimicrobial resistance. *Antibiotics* 10:1277. doi: 10.3390/antibiotics10111277

Rehman, S., Ali, Z., Khan, M., Bostan, N., and Naseem, S. (2019). The dawn of phage therapy. *Rev. Med. Virol.* 29:e2041. doi: 10.1002/rmv.2041

Sasaki, R., Miyashita, S., Ando, S., Ito, K., Fukuhara, T., and Takahashi, H. (2021). Isolation and characterization of a novel jumbo phage from leaf litter compost and its suppressive effect on Rice seedling rot diseases. *Viruses* 13:591. doi: 10.3390/v13040591

Schmelcher, M., Donovan, D. M., and Loessner, M. J. (2012). Bacteriophage endolysins as novel antimicrobials. *Future Microbiol.* 7, 1147–1171. doi: 10.2217/fmb.12.97

Shannon, R., Radford, D. R., and Balamurugan, S. (2020). Impacts of food matrix on bacteriophage and endolysin antimicrobial efficacy and performance. *Crit. Rev. Food Sci. Nutr.* 60, 1631–1640. doi: 10.1080/10408398.2019.1584874

Shen, K., Shu, M., Zhong, C., Zhao, Y., Bao, S., Pan, H., et al. (2023). Characterization of a broad-spectrum endolysin rLysJNwz and its utility against *Salmonella* in foods. *Appl. Microbiol. Biotechnol.* 107, 3229–3241. doi: 10.1007/s00253-023-12500-9

Sitthisak, S., Manrueang, S., Khongfak, S., Leungtongkam, U., Thummeepak, R., Thanwisai, A., et al. (2023). Antibacterial activity of vB_AbaM_PhT2 phage hydrophobic amino acid fusion endolysin, combined with colistin against *Acinetobacter baumannii*. *Sci. Rep.* 13:7470. doi: 10.1038/s41598-023-33822-8

Skorynina, A. V., Piligrimova, E. G., Kazantseva, O. A., Kulyabin, V. A., Baicher, S. D., Ryabova, N. A., et al. (2020). *Bacillus*-infecting bacteriophage Izhevsk harbors thermostable endolysin with broad range specificity. *PLoS One* 15:e0242657. doi: 10.1371/journal.pone.0242657

Thomas, J. A., Weintraub, S. T., Wu, W., Winkler, D. C., Cheng, N., Steven, A. C., et al. (2012). Extensive proteolysis of head and inner body proteins by a morphogenetic protease in the Giant *pseudomonas aeruginosa*phage φKZ. *Mol. Microbiol.* 84, 324–339. doi: 10.1111/j.1365-2958.2012.08025.x

Vázquez, R., García, E., and García, P. (2018). Phage Lysins for fighting bacterial respiratory infections: a new generation of antimicrobials. *Front. Immunol.* 9:2252. doi: 10.3389/fimmu.2018.02252

Vu, H. T. K., Stasiewicz, M. J., Benjakul, S., and Vongkamjan, K. (2021). Genomic analysis of prophages recovered from *Listeria monocytogenes* Lysogens found in seafood and seafood-related environment. *Microorganisms* 9:1354. doi: 10.3390/microorganisms9071354

Wang, S., Gu, J., Lv, M., Guo, Z., Yan, G., Yu, L., et al. (2017). The antibacterial activity of *E. coli* bacteriophage lysin lysep3 is enhanced by fusing the *Bacillus amyloliquefaciens* bacteriophage endolysin binding domain D8 to the C-terminal region. *J. Microbiol.* 55, 403–408. doi: 10.1007/s12275-017-6431-6

Wang, X., Han, L., Rong, J., Ren, H., Liu, W., and Zhang, C. (2022). Endolysins of bacteriophage vB_Sal-S-S10 can naturally lyse *Salmonella enteritidis*. *BMC Vet. Res.* 18:410. doi: 10.1186/s12917-022-03514-y

Wang, Y., Wu, J., Li, J., Yu, C., Gao, J., Song, F., et al. (2024). Isolation and characterization of duck sewage source *Salmonella* phage P6 and antibacterial activity for recombinant endolysin LysP6. *Poult. Sci.* 103:104227. doi: 10.1016/j.psj.2024.104227

Wan, X., Geng, P., Sun, J., Yuan, Z., and Hu, X. (2021). Characterization of two newly isolated bacteriophages PW2 and PW4 and derived endolysins with lysis activity against *Bacillus cereus* group strains. *Virus Res.* 302:198489. doi: 10.1016/j.virusres.2021.198489

Wong, K. Y., Megat Mazhar Khair, M. H., Song, A. A.-L., Masarudin, M. J., Chong, C. M., in, L. L. A., et al. (2022). Endolysins against *streptococci* as an antibiotic alternative. *Front. Microbiol.* 13:935145. doi: 10.3389/fmicb.2022.935145

Wu, Z., Zhang, Y., Xu, X., Ahmed, T., Yang, Y., Loh, B., et al. (2021). The Holin-Endolysin lysis system of the OP2-like phage X2 infecting *Xanthomonas oryzae* pv. *Oryzae*. *Viruses* 13:1949. doi: 10.3390/v13101949

Xiao, Z., Deng, J., Zhou, X., Zhu, L., He, X., Zheng, J., et al. (2022). Shoot rot of *Zizania latifolia* and the first record of its pathogen *Pantoea ananatis* in China. *J Zhejiang Univ Sci B* 23, 328–338. doi: 10.1631/jzus.B2100682

Xuan, G., Lin, H., Kong, J., and Wang, J. (2022). Phage resistance evolution induces the sensitivity of specific antibiotics in *Pseudomonas aeruginosa* PAO1. *Microbiol Spectr* 10:e0135622. doi: 10.1128/spectrum.01356-22

Xu, D., Zhao, S., Dou, J., Xu, X., Zhi, Y., and Wen, L. (2021). Engineered endolysin-based "artilysins" for controlling the gram-negative pathogen *Helicobacter pylori*. *AMB Express* 11:63. doi: 10.1186/s13568-021-01222-8

Xue, Y., Hu, M., Chen, S., Hu, A., Li, S., Han, H., et al. (2021). *Enterobacter asburiae* and *Pantoea ananatis* causing Rice bacterial blight in China. *Plant Dis.* 105, 2078–2088. doi: 10.1094/PDIS-10-20-2292-RE

Yang, M., Xia, Q., Du, S., Zhang, Z., Qin, F., and Zhao, Y. (2021). Genomic characterization and distribution pattern of a novel marine OM43 phage. *Front. Microbiol.* 12:651326. doi: 10.3389/fmicb.2021.651326

Yan, G., Yang, R., Fan, K., Dong, H., Gao, C., Wang, S., et al. (2019). External lysis of *Escherichia coli* by a bacteriophage endolysin modified with hydrophobic amino acids. *AMB Express* 9:106. doi: 10.1186/s13568-019-0838-x

Young, R. (1992). Bacteriophage lysis: mechanism and regulation. *Microbiol. Rev.* 56, 430–481. doi: 10.1128/mr.56.3.430-481.1992

Yuan, T., Huang, Y., Luo, L., Wang, J., Li, J., Chen, J., et al. (2023). Complete genome sequence of *Pantoea ananatis* strain LCFJ-001 isolated from bacterial wilt mulberry. *Plant Dis.* 107, 2500–2505. doi: 10.1094/PDIS-10-22-2473-A

Yuan, Y., Li, X., Wang, L., Li, G., Cong, C., Li, R., et al. (2021). The endolysin of the *Acinetobacter baumannii* phage vB_AbaP_D2 shows broad antibacterial activity. *Microb. Biotechnol.* 14, 403–418. doi: 10.1111/1751-7915.13594

Zhang, G., Ye, Z., Mao, B., Lou, T., and Shen, L. (2022). First report of *Pantoea ananatis* causing crown necrobiosis on strawberry in China. *Plant Dis.* doi: 10.1094/PDIS-10-22-2333-PDN

Zhang, Y., Huang, H. H., Duc, H. M., Masuda, Y., Honjoh, K. I., and Miyamoto, T. (2021). Endolysin LysSTG2: characterization and application to control *Salmonella Typhimurium* biofilm alone and in combination with slightly acidic hypochlorous water. *Food Microbiol.* 98:103791. doi: 10.1016/j.fm.2021.103791

Zhou, B., Wu, Y., and Su, Z. (2021). Computational simulation of Holin S105 in membrane bilayer and its dimerization through a Helix-turn-Helix motif. *J. Membr. Biol.* 254, 397–407. doi: 10.1007/s00232-021-00187-w

frontiers | Frontiers in Microbiology

TYPE Original Research
PUBLISHED 28 October 2024
DOI 10.3389/fmicb.2024.1448958

OPEN ACCESS

EDITED BY
Gamaliel López-Leal,
Center for Research in Cellular Dynamics-UAEM, Mexico

REVIEWED BY
Swapnil Ganesh Sanmukh,
Université Clermont Auvergne, France
Mei Liu,
Texas A and M University, United States

*CORRESPONDENCE
Martin Köhne
✉ martin.koehne@tiho-hannover.de

RECEIVED 14 June 2024
ACCEPTED 10 October 2024
PUBLISHED 28 October 2024

CITATION
Köhne M, Hüsch R, Tönissen A, Schmidt M, Müsken M, Böttcher D, Hirnet J, Plötz M, Kittler S and Sieme H (2024) Isolation and characterization of bacteriophages specific to *Streptococcus equi* subspecies *zooepidemicus* and evaluation of efficacy *ex vivo*.
Front. Microbiol. 15:1448958.
doi: 10.3389/fmicb.2024.1448958

Isolation and characterization of bacteriophages specific to *Streptococcus equi* subspecies *zooepidemicus* and evaluation of efficacy *ex vivo*

Martin Köhne[1]*, Ronja Hüsch[1], Anna Tönissen[1], Matthias Schmidt[2], Mathias Müsken[3], Denny Böttcher[4], Juliane Hirnet[5], Madeleine Plötz[5], Sophie Kittler[5] and Harald Sieme[1]

[1]Unit for Reproductive Medicine – Clinic for Horses, University of Veterinary Medicine, Foundation, Hannover, Germany, [2]Department of Technical Biogeochemistry, Helmholtz Centre for Environmental Research –UFZ, Leipzig, Germany, [3]Central Facility for Microscopy, Helmholtz Centre for Infection Research – HZI, Braunschweig, Germany, [4]Institute for Veterinary Pathology, Faculty of Veterinary Medicine, Leipzig University, Leipzig, Germany, [5]Institute of Food Quality and Food Safety, University of Veterinary Medicine, Foundation, Hannover, Germany

Streptococcus (S.) equi subspecies (subsp.) *zooepidemicus* is an important facultative pathogen in horses and can cause severe infections in other species including humans. Facing the post-antibiotic era, novel antimicrobials are needed for fighting bacterial infections. Bacteriophages (phages) are the natural predators of bacteria and discussed as a promising antimicrobial treatment option. The objective of this study was to isolate and characterize *S. equi* subsp. *zooepidemicus*-specific phages for the first time and to evaluate their efficacy *in vitro* and *ex vivo*. In total, 13 phages with lytic activity were isolated and host ranges were determined. Two phages with broad host ranges and high efficiency of plating (vB_SeqZP_LmqsRe26-2 (lytic activity: 30/37 bacterial isolates) and vB_SeqZP_LmqsRe26-3 (lytic activity: 29/37 bacterial isolates)) and one phage with relatively low efficiency of plating (vB_SeqZP_LmqsRe26-1) were selected for further characterization, including electron microscopy and whole genome sequencing. In *in vitro* planktonic killing assays at two tested multiplicities of infection (MOI 1 and MOI 10), significant bacterial growth reduction was observed when the phages vB_SeqZP_LmqsRe26-2 and vB_SeqZP_LmqsRe26-3 were added. These phages were subsequently co-incubated with clinical *S. equi* subsp. *zooepidemicus* isolates in an equine endometrial explant model but did not achieve bacterial growth reduction at MOI 1 and MOI 10. However, helium ion microscopy revealed presence of particles adherent to the bacteria on the explant after incubation (25 h), suggesting possible phage-bacteria interactions. In conclusion, phages against *S. equi* subsp. *zooepidemicus* were successfully isolated and characterized. Promising results were observed in *in vitro* but no significant reduction was detected in *ex vivo* experiments, requiring additional investigations. However, after further adaptations (e.g., optimization of MOIs and phage administration or use of phage-antibiotic combination), phages could be a potential antimicrobial tool for future therapeutic use in *S. equi* subsp. *zooepidemicus* infections, although the available results do not currently support the therapeutic usage.

KEYWORDS

bacteriophage, uterus, *Streptococcus equi* subspecies *zooepidemicus*, *ex vivo* model, non-antibiotic treatment

1 Introduction

Streptococcus (S.) equi subspecies (subsp.) *zooepidemicus* is a major causative agent of infections in foals and adult horses (Timoney, 2004), leading to severe respiratory diseases (Oikawa et al., 1994) and infection of inner organs, such as liver, lung, brain, kidney as well as joints (Timoney, 2004). In foals, *S. equi* subsp. *zooepidemicus* infection is a frequent cause for neonatal bacterial sepsis (Sanchez et al., 2008). In equine reproductive medicine, *S. equi* subsp. *zooepidemicus* is the bacterial species most often detected in bacterial endometritis cases (Köhne et al., 2024b; Rathbone et al., 2023; Ricketts, 2011). However, *S. equi* subsp. *zooepidemicus* is also detected in cases of necrotizing myositis (Kittang et al., 2017), meningitis (Eyre et al., 2010) and arthritis (Friederichs et al., 2010) in humans after direct horse-human contact (Pelkonen et al., 2013) or consumption of contaminated food (Bordes-Benítez et al., 2006). Furthermore, it plays a role as opportunistic pathogen in a large variety of domestic animals including cats (Blum et al., 2010), dogs (Priestnall and Erles, 2011), mice (Literák and Mráz, 1991), pigs (Feng and Hu, 1977) and small ruminants (Steward et al., 2017).

In equine medicine, the condition of bacterial endometritis has been rated as one of the major clinical problems (Traub-Dargatz et al., 1991) and is a leading cause for reproductive failure (Hurtgen, 2006; Riddle et al., 2007; LeBlanc and Causey, 2009). Traditionally, the treatment of bacterial endometritis involves antibiotic drugs, which are administered either locally or systemically (Canisso et al., 2020; Köhne et al., 2020). In addition alternative therapeutic approaches with antibacterial properties, e.g., ozone (Köhne et al., 2023; Ávila et al., 2022) and hydrogen peroxide (Ferris et al., 2016), have been investigated *in vitro* and *in vivo* with varying degrees of success. Searching for novel antimicrobial treatment options against bacterial infections is urgently needed, considering the increasing numbers of multidrug-resistant (MDR) bacteria worldwide (Murray et al., 2022) and the presence of penicillin-resistant *S. equi* subsp. *zooepidemicus* in cases of equine bacterial endometritis (Pisello et al., 2019; Davis et al., 2013).

A promising antimicrobial approach for treating bacterial infections is the use of bacteriophages (phages) that has received increasing attention in medical research as well as in the general public (Kortright et al., 2019). Phages are viruses that exclusively infect bacterial cells, having very specific bactericidal activity against their host bacteria and leaving the physiological microbiome unaffected (Kasman and Porter, 2022; Kutateladze and Adamia, 2010). Recently, regulatory hurdles for using phages in veterinary antibacterial therapy have been reduced in the European Union (European Commission, 2019; European Medicines Agency, 2023) and phage products could be approved for veterinary medicine in the near future (Peh et al., 2023). Studies from human (Van Nieuwenhuyse et al., 2022) as well as veterinary medicine (Smith and Huggins, 1983) reported the successful use of phages in antibacterial therapy. However, promising results of *in vitro* experiments for large animal gynecology (Bicalho et al., 2010), using phages specific to *Escherichia coli* isolates associated with bovine metritis, have not been transferred into a clinical study (Machado et al., 2012). In equine medicine, studies on phages specific against equine pathogens, e.g., *Salmonella enterica* subsp. *enterica* serovar Abortusequi (Wang et al., 2020) and equine keratitis-associated *Pseudomonas aeruginosa* (Furusawa et al., 2016), have been carried out in mouse models only and have not been published for species-specific models nor *in vivo* experiments to date.

In contrast to non-target-species animal models, *ex vivo* models are suitable for studying phage efficacy while reducing animal experimentation. These models provide an environment that mimics the situation in the target organ of the target species (Thompson et al., 2020b) without using live animals. For the equine uterus, several *ex vivo* models, including isolated-perfused uteri (Köhne et al., 2022; Köhne et al., 2024a), organoid (Thompson et al., 2020a) and explant cultures (Nash et al., 2008; Monteiro de Barros et al., 2021) have been introduced and validated. In this study, an explant culture model has been selected since it provides access to the endometrial surface – contrasting endometrial organoids – and allows for the replication of experiments using one uterus, which cannot be achieved in the isolated-perfused uterus model.

To our knowledge, no phages specific to *S. equi* subsp. *zooepidemicus* have been introduced in collections for research and therapeutic purposes despite the zoonotic potential of their host and the demands for reduction of antibiotic drugs in veterinary medicine.

Hence, the objectives of the present study were to (i) isolate and characterize *S. equi* subsp. *zooepidemicus*-specific phages for the first time and (ii) to determine their bactericidal capacities *in vitro* and in an explant model, including visualization of possible phage-bacteria interactions on the endometrium.

2 Materials and methods

2.1 Bacterial isolates

Streptococcus equi subsp. *zooepidemicus* isolates ($n = 37$) from horse-derived samples (Supplementary Table S1) were provided by the Institute of Microbiology, University of Veterinary Medicine Hannover, Foundation, Germany and Labor Dr. Böse, GmbH, Harsum, Germany. The isolates were stored in cryotubes (Carl Roth GmbH + Co. KG, Karlsruhe, Germany) at −80°C. Before starting the experiments, isolates were plated out on Columbia agar supplemented with sheep blood (Oxoid Deutschland GmbH, Wesel, Germany) and incubated aerobically at 37°C overnight.

The study has been approved by the institutional review board (Doctoral Commission, Stiftung Tierärztliche Hochschule Hannover, 2023, 3.5) and the animal welfare officer (TVO-2023-V-18) as ethical.

2.2 Phage isolation and propagation

The soft-agar overlay technique was used to isolate *Streptococcus* phages from environmental samples as described previously (Shakeri et al., 2021; Steffan et al., 2021). Phages were isolated from different

horse associated samples (manure, uterine lavage fluid, drain water of horse husbandries; $n = 12$). Two grams of each sample were dispersed in sodium chloride-magnesium sulfate (SM) buffer (100 mM NaCl, 8 mM $MgSO_4$, 50 mM Tris–HCl (pH 7.5)) in falcon tubes (50 mL). Next, the dispersed samples were centrifuged (5,000 × *g*, 20 min, 4°C) and the supernatant was subsequently filtrated through a 0.2 µm polyethylene sulfone membrane (PES) syringe filter (Carl Roth GmbH + Co. KG, Karlsruhe, Germany). Subsequently, the presence of phages in the filtrate was tested using the soft agar-overlay method. In brief, overnight cultures of *S. equi* subsp. *zooepidemicus* isolates ($n = 6$) were prepared on Columbia agar supplemented with sheep blood [Oxoid Deutschland GmbH, Wesel, Germany; incubation (37°C, 18 h)]. For each isolate, a McFarland standard 3.0 was prepared and 100 µL of the bacterial suspension was transferred to a liquefied LB agar overlay suspension (0.7% agar agar) at 48°C. Next, 100 µL of filtered dispersed samples ($n = 12$) was added and the overlay was poured onto LB agar plates (1.5% agar agar) in duplicates. After incubation at room temperature for 10 min, double-agar-overlays were incubated aerobically for 24 h at 37°C. Presence of lytic phages was assumed if lytic areas, so called plaques, were present. The phages were then isolated and purified by a successive 3-fold picking and plating procedure of single plaques. Afterwards, the phages were propagated to obtain concentrations of 10^8–10^9 PFU/ml and stored at 4°C until further use. The phage titers were determined by plating 100 µL of a 10-fold serial dilution series of the phage suspension on the respective host bacterial isolate using the soft agar overlay technique as described above.

2.3 Host range and efficiency of plating

The host range of the isolated phages ($n = 13$) was determined in accordance with the plaque assay method of Korf et al. (2020), with some modifications, while susceptibility of the bacteria was indicated by efficiency of plating (EOP), as calculated and presented by Steffan et al. (2021). In short, LB-agar plates were overlaid with 5 mL LB soft agar, containing 100 µL of the respective phage suspension (10^6 – 10^9 PFU/ml) and 100 µL of the *Streptococcus equi* subsp. *zooepidemicus* isolate (10^8 CFU/mL; $n = 37$). After aerobic incubation at 37°C for 18 h, the sensitivity of the tested bacteria to the phages was determined by counting the number of plaques in the bacterial lawns. All combinations were tested in triplicate. The relative efficiency of plating was graded according to the presence of a zone of inhibition or number of plaques visible on the agar plates: no sensitivity (no plaque formation), moderately low sensitivity (presence of an opaque plaque), low sensitivity ($EOP < 0.1$), moderate sensitivity ($0.1 \leq EOP \leq 1$), high sensitivity ($1 < EOP \leq 10$), ultimate sensitivity ($10 < EOP$). EOP of 1 represented similar plaque formation as observed in the original host bacterial isolate.

2.4 Extraction of phage DNA, whole-genome sequencing, and bioinformatics analysis

For further characterization, phages ($n = 3$) were selected according to their host range and EOP (broad host range: $n = 2$; low EOP: $n = 1$). Three hundred ml of phage suspensions (10^8 – 10^{10} PFU/ml) were prepared as described above. Subsequent to filtration, the suspensions were centrifuged (24,000 × *g*, 2 h, Avanti J-26S XP, Beckmann Coulter Inc., Brea, United States) and the resulting pellets were resuspended with a small amount of SM-buffer and purified by CsCl-gradient (165,100 × *g*, 4°C, 2 h, Optima XPN-100, Beckmann Coulter Inc., Brea, United States). Thereafter, cesium chloride was removed from the phages via dialysis with SM-buffer. The resulting phage suspensions were used for both, electron micrographs and DNA isolation. Phage DNA was extracted from the purified virions treated with Norgen's RNase-Free DNase I Kit (Norgen Biotek Corp., Canada) and Phage DNA Isolation Kit (Norgen Biotek Corp., Canada) was used for DNA extraction and according to the manufacturer's instructions. The concentration of phage DNA molecules was determined using ds DNA HS Assay Kit (Life Technologies Corporation, Oregon, United States) before submission to whole genome sequencing using a Nextseq sequencing system (Microsynth AG, Balgach, Switzerland). For Phage LmqsRe26-2 long read sequencing was performed using a MinIon according to the manufactures instructions. Assembly and annotation was performed using the Galaxy platform (The Galaxy Community, 2022). Contigs were assembled using the SPAdes software (St. Petersburg genome assembler; version: 3.15.5) or Flye (Version 2.9.4). Phage termini were determined using PhageTerm (Garneau et al., 2017) and confirmed by PCR as described by Boeckman et al., 2024. Homology with previously published bacteriophages was detected by BLASTN (Basic Local Alignment Search Tool, http://www.ncbi.nlm.nih.gov Version 2.15.0; Lin et al., 2016). Annotation of CDS was conducted with Prokka (Prokaryotic genome annotation; Galaxy Version 1.14.6) and Pharokka (rapid standardized annotation tool for bacteriophage genomes and metagenomes; Galaxy Version 1.3.2). Alignment und phylogenetic tree were generated using ClustalOmega (Madeira et al., 2024).

2.5 Negative staining of phages

Phages are adsorbed for 15–30 s onto a carbon film and washed twice on TE buffer droplets (10 mM TRIS, 1 mM EDTA, pH 6.9) according to Dreiseikelmann et al. (2017). After washing, samples were negatively stained with 2% aqueous uranyl acetate by heat drying on a 60 W bulb after blotting excessive liquid with a filter paper. Samples were examined in a Zeiss TEM 910 transmission electron microscope (Zeiss, Oberkochen, Germany) at an acceleration voltage of 80 kV and at calibrated magnifications with a line replica. Images were recorded digitally with a slow-scan closed circuit device (CCD)-camera (ProScan, 1,024 × 1,024, Proscan Elektronische Systeme GmbH, Scheuring, Germany) with ITEM-Software (Olympus Soft Imaging Solutions GmbH, Münster, Germany). The head diameter and tail length were determined using the same software and calculating the average size from a minimum of 10 measurements.

2.6 Efficacy testing of phages' bacteria reduction capability in liquid culture (planktonic killing assay)

The growth of two *S. equi* subsp. *zooepidemicus* isolates (isolates 9 and 10) with and without exposure to the respective bacteriophages

(vB_SeqZP_LmqsRe26-1, vB_SeqZP_LmqsRe26-2 and vB_SeqZP_LmqsRe26-3) at different multiplicities of infection (MOI input of 1 and 10) (Danis-Wlodarczyk et al., 2021) was examined in liquid cultures using a Tecan Spark Microplate Reader (Tecan Group AG, Männedorf, Switzerland), similar to the protocol described by Steffan et al. (2021) with some modifications. Briefly, bacterial overnight cultures were adjusted to a McFarland standard of 5 in 10 mM $MgSO_4$ and used to inoculate 25 mL CBHI that was then incubated for 3 h while shaking (130 rpm). Next, wells of 48-well microplates were filled with 200 µL of the culture that was adjusted to 0.5 McFarland standard and diluted in CBHI (1:100). The phage suspensions, adjusted to 1×10^6 (MOI 1) and 1×10^7 (MOI 10), PFU/ml in CBHI were added to the respective well. The plates were aerobically incubated with double orbital shaking at 37°C for 24 h. Optical density measurements (OD_{600}) were taken hourly during incubation. Bacterial cultures inoculated with CBHI instead of phages served as positive controls. Two replicates per well were used and the experiment was performed in triplicate. The area under the curve (AUC) of OD_{600} measurements and virulence indices were calculated as described by Peh et al. (2023).

2.7 Efficacy testing of phages' bacteria reduction capability in an equine endometrial explant model

Endometrial explants culture was performed according to Monteiro de Barros et al. (2021). Equine uteri and ovaries were collected at a slaughterhouse directly after slaughter of diestrous mares ($n = 5$; 3 Warmblood and 2 American Quarter Horse mares; mean age: 15.2 years (range: 5–20 years)) and transported on ice to the laboratory. The interval between exsanguination and arrival in the laboratory was between 4 to 5 h (mean: 263 min). On arrival, cycle stage was determined as described (Köhne et al., 2022). Before the next processing steps, the serosal surface of the uteri was rinsed with ethanol (70%) and uterine horns and body were opened using a sterile scalpel. Next, endometrial samples for microbial culture and cytology were collected for exclusion of endometritis. Additionally, an endometrial tissue sample comparable to a biopsy was obtained and submitted to histopathological examination. The swab was smeared directly on Columbia agar supplemented with sheep blood in three fractions and incubated (24 h, 37°C) before microbial growth was assessed. When presence of microbial growth was noted, the results of the experiment were excluded from further analysis as it was done when cytological examination using standard procedures (Dascanio, 2003) revealed presence of polymorphonuclear granulocytes.

Endometrial explants were collected using skin biopsy punches (8 mm diameter, Eickemeyer KG, Tuttlingen, Germany), sterile forceps and scissors. Directly afterwards, explants were transferred into Hanks Balanced Salt Solution (20 mL; Gibco™ HBSS, without calcium, magnesium and phenol red, Fisher Scientific GmbH, Schwerte, Germany), supplemented with amikacin sulfate (500 µg per ml medium; Briklin® Amikacin, 500 mg, Bristol-Myers Squibb, München, Germany) for 5 min. After two washing steps in unsupplemented HBSS, every explant was weighed on a sterile petri dish and the biopsies were then placed individually in wells of a 6-well plate (BioLite 6 Well Multidish, Fisher Scientific GmbH, Schwerte, Germany). An additional swab for assessment of bacterial contamination was taken and handled as described above.

The culturing of explants was performed in duplicates for every experimental group. For every uterus, a negative (culture medium without phages or bacteria) and a positive control (culture medium with bacterial suspension) were included. Briefly, culture medium (negative control: 4000 µL supplemented William's medium (William's Liquid E Medium, Gibco™ without phenol red, Life Technologies GmbH, Darmstadt, Germany); positive control and treatment groups: 3960 µL) was added to the wells. For samples incubated with bacteria (positive control and treatment groups), 40 µL of bacterial suspension (*S. equi* subsp. *zooepidemicus* isolate 10 adjusted to 1×10^7 CFU) were added. After 1 h of incubation, specific phages were added to treatment group at two different MOIs (MOI 1: 1×10^7 PFU; MOI 10: 1×10^8 PFU). In controls, 40 µL of 0.9% saline solution were added and in one positive control per bacterial isolate, bacterial concentration was determined as described below.

For evaluation of explant viability, lactate dehydrogenase activity was determined in samples (2 mL) obtained after 6 and 24 h of incubation and storage at −20°C until analysis (Fuji DRI-CHEM NX500i, sysmex, Norderstedt, Germany). Moreover, histopathological examination was performed in one duplicate per group after 24 h of incubation. Endometrial biopsies were processed and analyzed as described elsewhere (Köhne et al., 2022). Examination of histological slides was performed by a trained examiner blinded to the treatment and results are reported descriptively.

For qualitative analysis of bacterial growth in negative controls, direct plating as described above and an enrichment culture in BHI liquid broth were performed. In cases of positive bacterial growth after incubation (37°C, 24 h), results of the experiment were excluded from further analysis. For quantitative analysis of bacterial growth, explants were transferred to a sterile saline (0.9%, 1,000 µL) and vortexed (3 ×; 10 s). Next, the explant was discarded and the suspension was used to determine the concentration of bacteria via a decimal dilution series. Concentrations were then calculated from the number of colony forming units (CFU) using the following formula:

$$\frac{total\ no.\ of\ CFU\ (all\ plates)}{no.\ of\ plates\ (lowest\ dilution) * 1 + no.\ of\ plates\ (2nd\ lowest\ dilution) * 0.1} = concentration\ [CFU / ml]$$

For determining phage concentrations, 500 µL of the explant medium were filtrated, dilution series prepared and plaque assays were performed. Phage concentrations were determined in full analogy to the previously introduced method for bacterial concentrations replacing CFU by plaque forming units (PFU) in the formula above.

2.8 Helium ion micro-imaging of phage-bacteria interaction on the explant

At the end of one of the explant experiments, explants (treatment group and negative control) were submitted to helium ion microscopy (HIM). In preparation of the micro-imaging, the samples were fixed in glutaraldehyde (3%, dissolved in sodium-cacodylate buffer, pH 7.4) overnight at 4°C. The samples were then washed in cacodylate buffer (10 min) thrice to rinse off the fixative. Subsequently the samples were post-fixed in osmium tetroxide solution (2%) at room temperature for 2 h and thereafter rinsed

thrice in distilled water (10 min). After dehydration of the samples in a graded ethanol:water series up to 75% ethanol, the samples were mailed to the Helmholtz Center for Environmental Research – UFZ, Leipzig, Germany. After completion of the ethanol series (100%), the ethanol in the samples was replaced in preparation of gentle air-drying. For that, the samples were subjected to a 1:1 mixture of ethanol and hexamethyldisilazane (HMDS, Sigma-Aldrich, Merck KGaA, Darmstadt, Germany) for 10 min and thereafter to pure HMDS for 20 min. Then the samples were placed in a dry petri dish in a fume hood to dry for 24 h. In preparation of HIM, the dried samples were mounted onto standard stubs for electron microscopy using a conductive silver epoxy glue (quick-drying conductive silver Acheson 1,415, Plano GmbH, Wetzlar, Germany). HIM imaging was done with a Zeiss Orion NanoFab (Zeiss, Peabody, MA, United States) scanning HIM using an ion-landing-energy of 25 keV, a 10-µm aperture and an Everhard-Thornley-type secondary electron detector. To achieve both high lateral resolution (≤2 nm) and a reasonable contrast, the beam current was set between 0.08 pA (high magnification) and 0.25 pA. Charge compensation during imaging was achieved with an electron flood-gun operated in line-flooding mode. In order to avoid beam damage and to allow for efficient charge compensation the dwell time of the beam on a pixel was kept between 0.5 and 1.0 µs.

2.9 Statistical analysis

Statistical analysis of the experimental data was performed using GraphPad Prism 9.2.0 (GraphPad Software, San Diego, United States). To meet the input requirements of the software, the bacterial concentration data (section 2.7) was calculated to $\log_{10}$ CFU/ml. For parametric data (Shapiro–Wilk test), an unpaired *t*-test was used. Data from efficacy testing of phages in liquid culture and on explants was analyzed with a Dunn's multiple comparison test for significant differences. For analysis of effects of incubation on LDH activity, values were grouped (50 U/L, 50–100 U/L, > 100 U/L) and comparisons were made using chi-square test. For all tests, *p*-values below 0.05 were considered significant.

3 Results

3.1 Phage isolation and characterization

In total, 12 samples from horses and horse husbandries were examined for the presence of phages using the soft-agar overlay technique with clinical isolates of *S. equi* subsp. *zooepidemicus* ($n = 6$). After min. 3-fold serial purification and propagation of plaques, purified phages ($n = 13$) were obtained. Most phages were isolated from smegma of a healthy stallion ($n = 6$) and residues of the breeding barn ($n = 4$), while in other samples (drain (stallion stable and breeding barn), manure) only few phages were found (Table 1).

The host ranges of all purified phages were analyzed as shown in Figure 1. Phage vB_SeqZP_LmqsRe26-3 (LmqsRe26-3) showed the broadest host range, forming plaques with 30 of 37 bacterial isolates (81.1%) and phage vB_SeqZP_LmqsRe26-2 (LmqsRe26-2) with 29 of 37 isolates (78.4%). The lowest host range was shown by phages vB_SeqZ_LmqsRe235-1 and vB_SeqZ_LmqsRe26-6. All purified phages showed turbid plaque formation in at least 26 tested bacterial isolates. The two bacteriophages showing the broadest host range (LmqsRe26-3 and LmqsRe26-2) and one phage with a relatively low EOP and narrow host range (vB_SeqZP_LmqsRe26-1 (LmqsRe26-1)) were selected for further characterization.

The plaque morphology formed by the selected phages on their respective hosts on overlays with 0.7% agar were clear, their size ranging from 2 (LmqsRe26-2; Figure 2B) to 5 mm (LmqsRe26-3; Figure 2C) diameter, showing a slight halo (LmqsRe26-1; Figure 2A).

Negatively stained electron micrographs of these phages revealed presence of an icosahedral head (diameter: 47.4 ± 3.1 nm (LmqsRe26-1), 45.6 ± 1.4 nm (LmqsRe26-2) and 45.9 ± 2.3 nm (LmqsRe26-3)) and short tails [23.3 ± 1.6 nm (LmqsRe26-1), 25.8 ± 1.7 nm (LmqsRe26-2) and 27.3 ± 2.8 nm (LmqsRe26-3)], as observed in podoviruses (Figures 2D–F).

For further analysis, the selected phages were subjected to whole genome sequencing. All quality parameters of the prepared DNA and DNA sequencing libraries met the necessary criteria. Contigs were assembled showing genome lengths of 16,154 bp (vB_SeqZP_LmqsRe26-1), 13,280 bp (vB_SeqZP_LmqsRe26-2) and 16,165 bp

TABLE 1 Overview of isolated phages with name, origin, bacterial isolate number, host bacterium and isolation passage.

Phage name	Origin	Isolate no. (bacterial)	*Host bacterium*	Isolation passage
vB_SeqZ_LmqsRe241-1	Residues breeding barn	5	*S. equi* subsp. *zooepidemicus*	4
vB_SeqZ_LmqsRe238-1	Drain (stallion stable)	5	*S. equi* subsp. *zooepidemicus*	4
vB_SeqZP_LmqsRe26-1	Smegma (stallion)	9	*S. equi* subsp. *zooepidemicus*	4
vB_SeqZP_LmqsRe26-3	Smegma (stallion)	10	*S. equi* subsp. *zooepidemicus*	4
vB_SeqZP_LmqsRe26-2	Smegma (stallion)	10	*S. equi* subsp. *zooepidemicus*	4
vB_SeqZ_LmqsRe241-4	Residues breeding barn	13	*S. equi* subsp. *zooepidemicus*	4
vB_SeqZ_LmqsRe26-4	Smegma (stallion)	13	*S. equi* subsp. *zooepidemicus*	4
vB_SeqZ_LmqsRe235-1	Horse manure	4	*S. equi* subsp. *zooepidemicus*	8
vB_SeqZ_LmqsRe26-6	Smegma (stallion)	4	*S. equi* subsp. *zooepidemicus*	4
vB_SeqZ_LmqsRe241-2	Residues breeding barn	5	*S. equi* subsp. *zooepidemicus*	4
vB_SeqZ_LmqsRe26-5	Smegma (stallion)	11	*S. equi* subsp. *zooepidemicus*	4
vB_SeqZ_LmqsRe237-1	Drain (wash box)	11	*S. equi* subsp. *zooepidemicus*	4
vB_SeqZ_LmqsRe241-3	Residues breeding barn	13	*S. equi* subsp. *zooepidemicus*	4

10.3389/fmicb.2024.1448958

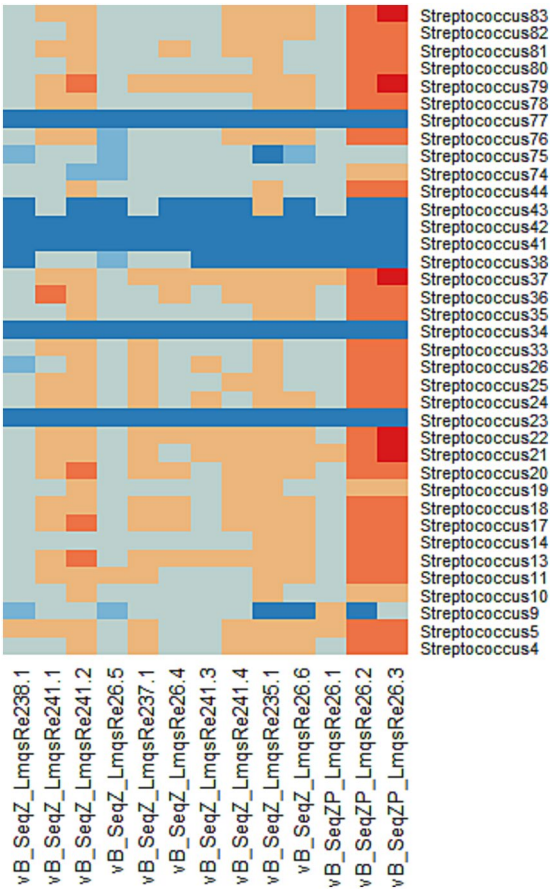

FIGURE 1
Heat map of phage host range (*Streptococcus equi* subspecies *zooepidemicus*). Phages are displayed on the x-axis and bacterial isolates on the y-axis. Dark blue: no sensitivity (no plaque formation), light blue: moderately low sensitivity (presence of an opaque plaque), grey: low sensitivity (EOP < 0.1), light orange: moderate sensitivity (0.1 ≤ EOP ≤ 1), dark orange: high sensitivity (1 < EOP ≤10), red: ultimate sensitivity (10 < EOP).

(vB_SeqZP_LmqsRe26-3), representing circularly permuted chromosomes. According to blastn analysis, the phage genomes of vB_SeqZP_LmqsRe26-1 and vB_SeqZP_LmqsRe26-3 had a 96.62and 96.17% identity, respectively, with the *Streptococcus*-phage C1 (*Fischettivirus*, family *Rountreeviridae*; Nelson et al., 2003; Clark and Clark, 1927). The most likely incomplete assembly of vB_SeqZP_LmqsRe26-2 showed a 95.85% similarity to the same phage (Figure 3). Genome annotation did not reveal the presence of genes associated with virulence or resistance or lysogenic lifecycle in any of the phages. The complete genome sequences were deposited into the GenBank database with the accession numbers PQ425460 (vB_SeqZP_LmqsRe26-1) and PQ425461 (vB_SeqZP_LmqsRe26-3).

3.2 Bacterial reduction by phages in liquid culture

A planktonic killing assay was conducted for determining the ability of phages to inhibit bacterial growth of the strains *S. equi* subsp. *zooepidemicus* 9 (LmqsRe26-1) and 10 (LmqsRe26-2 and LmqsRe26-3) in liquid culture. For this purpose, the host bacteria strains – alone or in combination with phages at different multiplicities of infection (MOIs) – were incubated for 24 h. In order to perform online cell-number measurements, the optical density (OD_{600}) was measured in parallel using a Tecan Spark Multiplate reader. Significant bacterial reduction compared to phage-free growth controls was observed at MOI 1 of LmqsRe26-2 and LmqsRe26-3, but not for LmqsRe26-1 (Figures 4A–C). At MOI 10 any significant effect was found for none of the selected phages. The virulence indices, calculated from the AUC of phage treatments and growth controls, were highest for LmqsRe26-1 at MOI 10 (52.2) and lowest for LmqsRe26-2 at MOI 10 (12.8), but, interestingly, were higher for LmqsRe26-2 and LmqsRe26-3 at MOI 1 (49.7 and 46.9) as compared to MOI 10 (12.8 and 19.3; Table 2).

3.3 Viability of explants

Explant cultures of endometrial tissue samples were incubated to provide an *ex vivo* model for investigation of phage-bacteria interactions. In total, six explant experiments were conducted for 24 h each. Preliminary results of one trial were excluded from further analysis due to bacterial contamination of the uterus. Functionality and vitality of the explant was assessed by histopathological examination of the explant and LDH activity. Histopathological analysis was performed before the experiment and after incubation. Analysis of specimens taken at arrival in the laboratory (before incubation) revealed occasional presence of periglandular fibrosis, disseminated glandular nests and glandular atrophy, indicating mild to moderate degeneration of the slaughtered mares' endometrium (Figure 5A). No signs of endometritis were detected. After incubation for 24 h, parts (up to 90%) of the luminal epithelium were either completely lost or epithelial cells appeared cuboidal and had lost their cilia (Figure 5B). Changes were more pronounced for explants co-incubated with bacteria, where the epithelial cells were absent in the majority of explants (Figure 5C), while in the control explants without co-incubation of bacteria, signs of epithelial degeneration were less pronounced. Epithelial destruction was unaffected by presence of phages (Figure 5D). Loss of typical endometrial tissue architecture – including the uterine glands – was observed in some explants, while others showed a nearly intact tissue structure, regardless of being incubated with or without bacteria (Figures 5B–D). No significant impact of time or treatment on LDH activity was detected after 6 and 24 h of incubation ($p > 0.05$; Supplementary Table S2).

3.4 Bacterial reduction efficacy of phages in an explant model

The efficacy of two phages (LmqsRe26-2 and LmqsRe26-3) for reduction of their host isolate *S. equi* subsp. *zooepidemicus* 10 was evaluated in the explant model as single phage assays. After 24 h of co-incubation, no significant effect of LmqsRe26-2 was observed with any of the tested MOIs (control: $1.71 \times 10^7 \pm 1.67 \times 10^7$ CFU/mL vs. MOI 1: $9.89 \times 10^6 \pm 9.21 \times 10^6$ CFU/ ml vs. MOI 10: $1.30 \times 10^7 \pm 1.1 \times 10^7$ CFU/mL; Figure 6A). Using LmqsRe26-3, bacterial growth was not significantly reduced either, however, a slight difference was measured in comparison to the untreated control

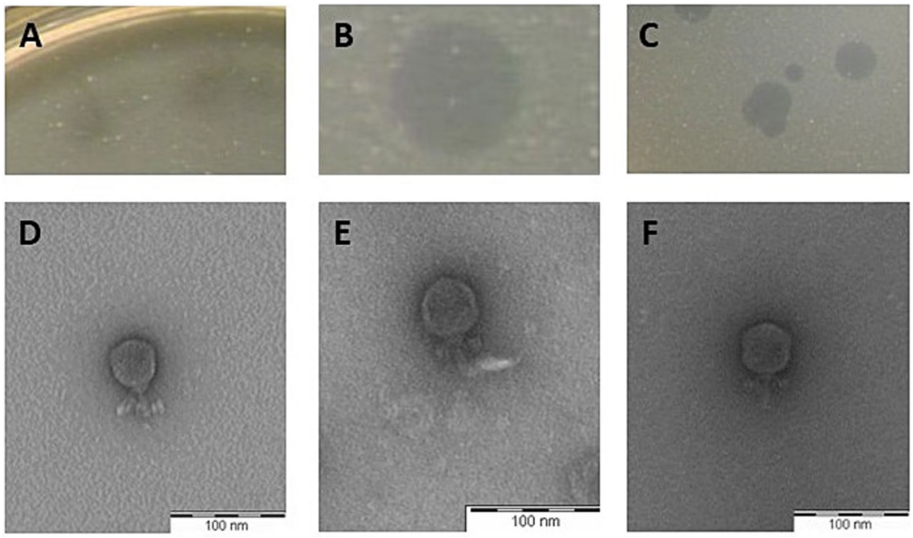

FIGURE 2
Plaque morphology of three *Streptococcus equi* subspecies *zooepidemicus*-specific phages (A–C) and transmission electron micrograph of negatively stained phages vB_SeqZP_LmqsRe26-1 (D), vB_SeqZP_LmqsRe26-2 (E) and vB_SeqZP_LmqsRe26-3 (F). Scale bar = 100 nm.

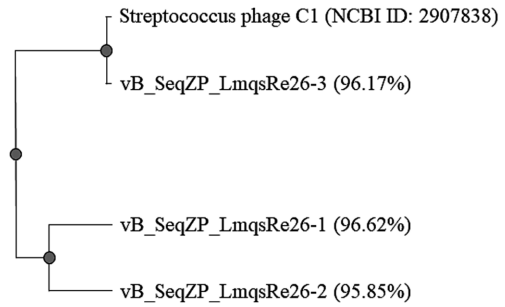

FIGURE 3
Phylogenetic analysis of newly isolated phages vB_SeqZP_LmqsRe26-1, vB_SeqZP_LmqsRe26-2, and vB_SeqZP_LmqsRe26-3 and DNA sequence identity (%) compared to the genome of *Streptococcus*-phage C1 (NCBI Nucleotide accession number: NC_004814.1) generated with Clustal Omega.

(control: $1.71 \times 10^7 \pm 1.67 \times 10^7$ CFU/mL vs. MOI 1: $1.37 \times 10^7 \pm 1.01 \times 10^7$ CFU/mL vs. MOI 10: $1.51 \times 10^7 \pm 1.15 \times 10^7$ CFU/mL; Figure 6B). The phage concentration in the medium after 24 h of incubation was $4.93 \times 10^5 \pm 7.76 \times 10^5$ PFU/ml (MOI 1) and $6.17 \times 10^5 \pm 8.28 \times 10^5$ PFU/ml (MOI 10) for LmqsRe26-2 (Figure 6C) and $6.61 \times 10^5 \pm 1.09 \times 10^6$ PFU/ml (MOI 1) and $5.83 \times 10^5 \pm 5.66 \times 10^5$ PFU/ml (MOI 10) for LmqsRe26-3 (Figure 6D), respectively.

3.5 Helium ion microscopy image analysis

After 24 h of incubation, explants without bacterial inoculate showed polygonal luminal epithelial cells with microvilli, glandular ducts and endometrial crypts (Figure 5E) in the HIM. The same technique revealed that co-incubation with phages and bacteria resulted in a complete loss of tissue architecture (Figure 5F) and presence of coccoid bacteria on the explant surface, especially within the endometrial crypts (Figure 5H). Occasional adherence of small particles to bacterial cells may suggest that phages adhered to the bacterial surface (Figure 5G; Supplementary Figures S1–S4).

4 Discussion

The isolation and characterization of phages specific to the "emerging pathogen" (Kuchipudi et al., 2021) and potentially pathogenic *S. equi* subsp. *zooepidemicus* (Kim et al., 2022) closes a gap in veterinary phage research as characterized phages specific for this important veterinary and zoonotic pathogen have not been described previously to the best of our knowledge. However, Tiwari and Timoney (2009) tested *S. equi* subsp. *zooepidemicus* isolates with the *S. equi* subsp. *equi* phage SeP9, finding no sensitivity to this phage. In 2018, Harhala et al. (2018) reported that only 3% of all published phage genomes in the NCBI (National Center of Biotechnology Information) nucleotide database were associated with phages specific to streptococci species, which has decreased to 1.3% according to NCBI blast at time of publishing. However, streptococcal infections are causing severe diseases in domestic animals (Fulde and Valentin-Weigand, 2013) and particularly *S. equi* subsp. *zooepidemicus* is a major cause for equine infertility as it has been associated with endometritis, early pregnancy loss, and placentitis in mares (LeBlanc and Causey, 2009; Rose et al., 2018; Macpherson, 2005) as well as infections in humans (Kittang et al., 2017; Eyre et al., 2010; Friederichs et al., 2010; Pelkonen et al., 2013). Thus, and due to the need to develop new non-antibiotic treatment approaches, the present study was performed.

Isolation and purification of phages from horse- and horse husbandry-associated samples resulted in the detection of 16 phages specific to *S. equi* subsp. *zooepidemicus* isolates originating from horses. All isolated phages showed EOPs of 0.1 to 1 on at least one clinical bacterial isolate. For the phages LmqsRe26-2, LmqsRe26-3, vB_SeqZ_LmqsRe241.1, and vB_SeqZ_LmqsRe241.2 even higher

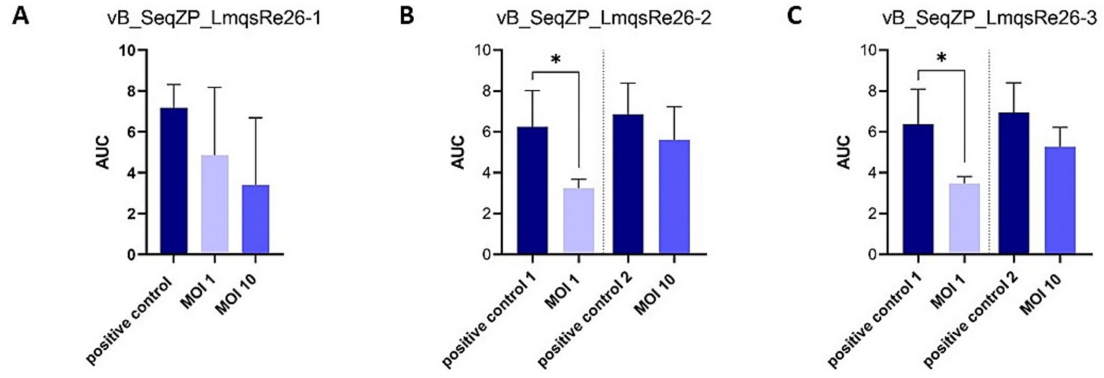

FIGURE 4
Area under the curve (optical density measurements at 600 nm; OD_{600}) after incubation of *Streptococcus equi* subspecies *zooepidemicus* isolates ($n = 2$; A–C) incubated with different phages (A) vB_SeqZP_LmqsRe26-1, (B) vB_SeqZP_LmqsRe26-2, (C) vB_SeqZP_LmqsRe26-3 for 24 h. * indicates a significant difference as determined by an unpaired t-test and Dunn's posthoc test.

TABLE 2 Virulence indices as determined by a planktonic killing assay for phages specific to *Streptococcus equi* subspecies *zooepidemicus* in different multiplicities of infection (MOIs).

Phage	Multiplicity of infection	Virulence index
vB_SeqZP_LmqsRe26-1	1	32.3
	10	52.2
vB_SeqZP_LmqsRe26-2	1	49.7
	10	12.8
vB_SeqZP_LmqsRe26-3	1	46.9
	10	19.3

EOPs (between 1 and 10) were observed when plated on some isolates. Moreover, LmqsRe26-2 and LmqsRe26-3 showed the broadest host ranges, lysing around 80% of the examined *Streptococcus* isolates. As no *S. equi* subsp. *zooepidemicus* phage characterization has been published up to now, their host ranges can only be compared with other streptococci phages. In cattle-associated *S. agalactiae* phages, the broadest lytic activity observed was 65.1% (Bai et al., 2013). In isolates of the *Streptococcus bovis/equi* complex (SBSEC), host ranges stretched from 15.4 to 35.3% in isolates originating from bovine species and 64.3 to 71.4% in caprine isolates (Park et al., 2023). Therefore, the host range presented in this study can be considered broad and therefore promising for further therapeutic use. Although the bacterial isolates used in this study did not underwent sequence typing, but the bacterial isolates differed according to their origin and growth characteristics and phage susceptibility. Therefore, the host range determination results have to be interpreted cautiously, but genetic variance in *S. equi* subsp. *zooepidemicus*-isolates from clinical samples has been reported to be large in other studies (Preziuso et al., 2019; Retamar et al., 2024).

Electron microscopy of the three selected phages revealed the presence of an icosahedral head size of 46.9–49.7 nm in diameter and short tails (23.3–27.3 nm), characteristic for podoviruses (Ackermann and Prangishvili, 2012). Genomic analysis revealed that the newly isolated phage (LmqsRe26-1) belongs to the genus *Fischettivirus*, family *Rountreeviridae* (Walker et al., 2022). The genome of LmqsRe26-1 was highly identical (96.62% identity) with the first described streptococcal phage (C_1), which was isolated in 1927 from a sewage plant sample (Clark and Clark, 1927) and demonstrated lytic activity against any group C streptococci (Lancefield, 1932). It has also been noted that the C_1 phage had lytic activity against streptococci that were not sensitive to the phage itself – a phenomenon described as "nascent lysis" in 1934 (Evans, 1934) and which has been attributed to the presence of phage-encoded endolysins later (Abdelrahman et al., 2021). While susceptibility and plaque formation was shown for the bacterial strain in planktonic killing assays, low EOP in other isolates and narrow host range could explain our results. Small host range including low EOP results might imply that even small adaptions by the bacterial strain could circumvent phage infection, e.g., in planktonic killing assays. However, further studies would be necessary to verify this hypothesis. Interestingly, the phage LmqsRe26-3, showing lower (96.17%) identity with C_1, was even more efficient in performing lysis on a broad range of host isolates as compared to the phage LmqsRe26-1. Thus, a better adaptation to *S. equi* subsp. *zooepidemicus* of LmqsRe26-3 compared to LmqsRe26-1 can be assumed. Despite the high similarity and repeated sequencing and analysis of LmqsRe26-2 no complete genome could be assembled, in contrast to the other phages. There are several possible reasons for this finding including high microdiversity of phage LmqsRe26-1, or highly repetitive regions or regions in the genome and regions with extremely high or low coverage that prevent alignment of related phage contigs (Shen and Millard, 2021; Boeckman et al., 2024).

In the planktonic killing assay, LmqsRe26-2 and LmqsRe26-3 significantly reduced bacterial growth, while LmqsRe26-1 did not. The significant growth reduction was only observed after incubation for

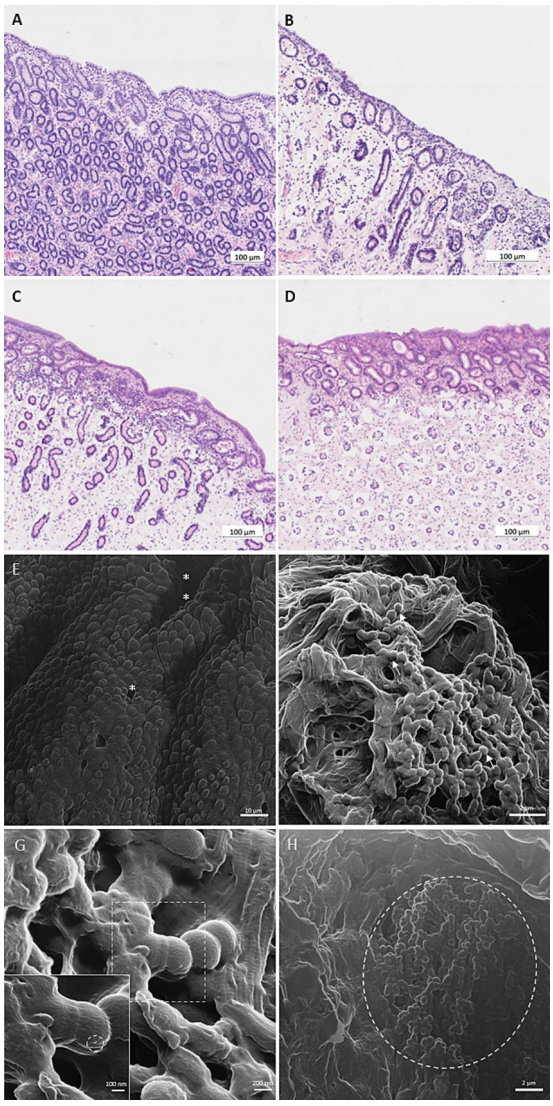

FIGURE 5
Light microscopy (A–D) and helium ion microscopy (HIM; E-H) visualization of equine endometrial explants after incubation for 24 h at 37°C. (A) HE stained endometrium (American Quarter Horse, 4 years old) after slaughter. (B) HE stained endometrium (Trakehner, 18 years old) after incubation for 24 h at 37°C in explant culture medium (negative control). (C) HE stained endometrium (Hanoverian, 18 years old) after co-incubation for 24 h at 37°C in explant culture medium with *Streptococcus (S.) equi* subspecies (subsp.) *zooepidemicus* (positive control). (D) HE stained endometrium (Trakehner, 18 years old) after co-incubation for 24 h at 37°C in explant culture medium with *S. equi* subsp. *zooepidemicus* and the specific phage vB_SeqZP_LmqsRe26-2 (multiplicity of infection (MOI): 10; treatment). Scale bars = 100 µm. (E) Negative control (HIM): incubation without bacteria or phages – note endometrial crypts (**), glandular ducts (*) and intact luminal epithelium. Scale bar = 10 µm. (F) Treatment group (HIM): incubation with *S. equi* subsp. *zooepidemicus* and the specific phage vB_SeqZP_LmqsRe26-2 at MOI 10 – note the presence of coccoid bacteria (arrows) and the complete loss of tissue architecture. Scale bar = 2 µm. (G) Treatment group (HIM): incubation with *S. equi* subsp. *zooepidemicus* and the specific phage vB_SeqZP_LmqsRe26-2 at MOI 10 – note the presence of coccoid bacteria and the adherent structure (magnification: dashed circle). Scale bar = 200 nm / 100 nm (magnification). (H) Treatment group: incubation with *S. equi* subsp. *zooepidemicus* and the specific phage vB_SeqZP_LmqsRe26-3 at MOI 10 – note the accumulation of coccoid bacteria (dashed circle) within an endometrial crypt. Scale bar = 2 µm.

24 h at MOI 1 but not at MOI 10. Loc Carrillo et al. (2005) have also reported that phages are more efficient at lower MOIs for *Campylobacter jejuni* phages. Nang et al. (2023) hypothesized that a higher phage concentration leads to higher selection pressure on phage resistance and therefore induces beneficial mutations in some bacterial cells. Possible resistance mechanisms include the loss of phage receptors on the cell surface or physical barriers, covering the phage receptor molecules (Hyman and Abedon, 2010). As bacterial isolates were neither sequenced before and after phage contact nor testing for resistances was performed after growth reduction experiments, we cannot answer this question. However, a variety of bacterial anti-phage resistance mechanisms have been reported in other streptococci species, including mutations in the methionine aminopeptidase gene (Labrie et al., 2019), activation of CRISPR-Cas systems, and the production of membrane vesicles enabling the scavenge of phage particles from the environment (Beerens et al., 2021).

To examine the *in vitro* efficient LmqsRe26-2 and LmqsRe26-3 in an environment resembling the clinical conditions in the mare, they were tested in an explant model of the equine endometrium.

Although the explants remained functional for the duration of the experiment as shown by histopathology and LDH analysis, co-incubation with *S. equi* subsp. *zooepidemicus* 10 and LmqsRe26-2 and LmqsRe26-3 resulted in alterations of the endometrium, including loss of tissue architecture and the epithelium. Since histopathological analysis of explants incubated with solely bacteria or a combination of bacteria and phages did not differ with regards to the degree of epithelial loss, we did not include explants incubated either with bacteria or phages into HIM analysis. The destructive effect of the bacteria on the endometrium is likely due to exotoxins, e.g., hemolysin, which are produced and secreted by *S. equi* subsp. *zooepidemicus* (Wittenbrink et al., 1997). This effect could have been potentiated by the fact that *S. equi* subsp. *zooepidemicus* better binds to damaged endometrial cells (Ferreira-Dias et al., 1994a).

Some of our results as well as findings in previous studies point toward a lack of phage-bacteria interaction as a reason for a lacking phage efficacy in this model: First, the altered endometrium could have contributed to a lacking efficacy of LmqsRe26-2 and LmqsRe26-3 if the binding of bacteria to the endometrium impairs the phage-bacteria interaction. However, further experiments are needed to prove this hypothesis. Second, Balcão et al. (2022) observed that the application of a phage cocktail against *E. coli* inhibited bacterial growth in an explant model of the canine endometrium for 8 h, however, after 8 h, bacterial growth normalized. The authors discussed that bacterial host cells could have been embedded in the endometrial crypts and glands, thus impairing the binding of phages to bacterial cells. In the present study, this hypothesis is supported by the fact that bacterial colonies were clustered in uterine glands as visualized by helium ion microscopy (Figure 5H). A third explanation for missing phage-bacteria interaction in this model may be related to chosen MOIs in the experiment, which might have been too low for enabling phage-bacteria interaction in the relatively large volume of the well since the phage concentration was 4×10^5 (MOI 1) or 4×10^6 (MOI 10) per well, respectively. Moreover, it was not possible to standardize the explant size in a way that only the mucosal surface was covered with a thin fluid film, where phages and bacteria could have been deposited to minimize diffusion within the culture medium. Interestingly, the phage concentration was decreased by two log levels as compared to the bacterial concentration at the end

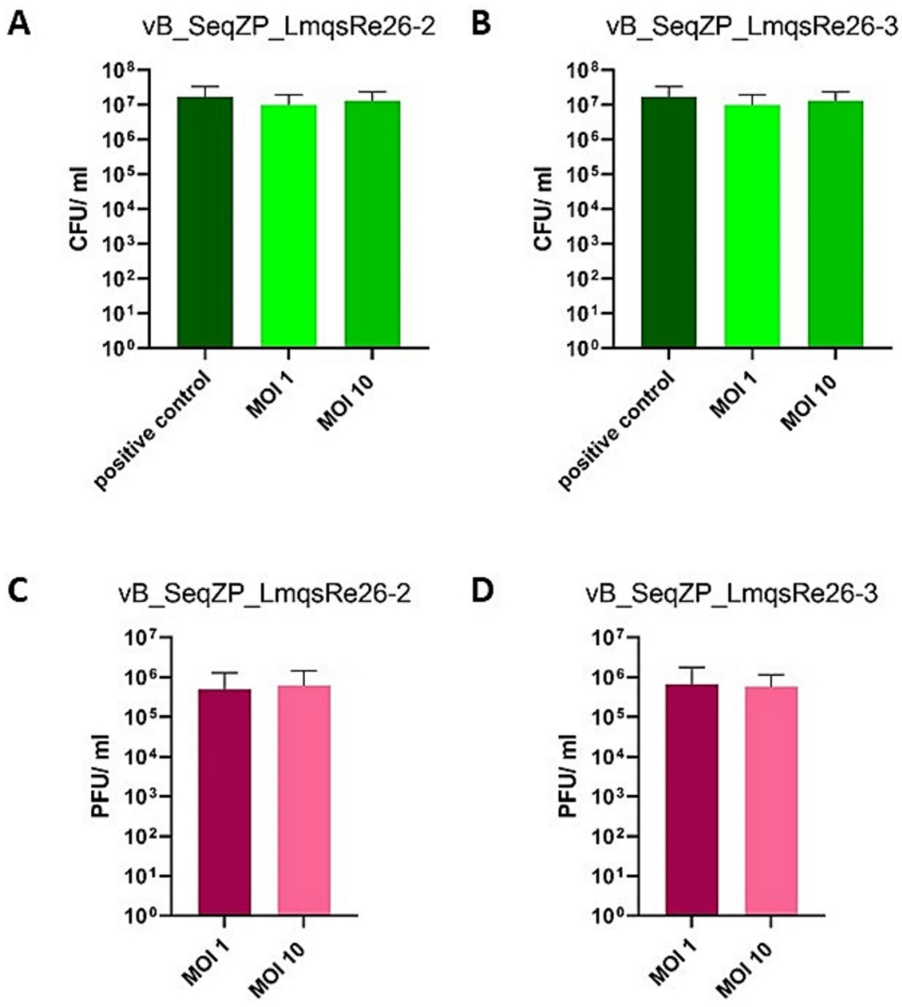

FIGURE 6
Concentration of colony forming units (CFU/ ml) of *Streptococcus equi* subspecies *zooepidemicus* (A,B) after incubation (24 h) on an equine endometrial explant in culture after infection with the specific phages vB_SeqZP_LmqsRe26-2 (A) and vB_SeqZP_LmqsRe26-3 (B) at two different multiplicities of infection (MOI 1 and MOI 10). Positive controls of bacteria were cultured without phages. Concentration (plaque forming units (PFU)/ ml) of specific phages [vB_SeqZP_LmqsRe26-2 (C) and vB_SeqZP_LmqsRe26-3 (D)] after co-incubation (24 h) with *Streptococcus equi* subspecies *zooepidemicus* on an equine endometrial explant at two different multiplicities of infection (MOI 1 and MOI 10).

of the experiment, which supports the hypothesis that no phage replication occurred or phage degradation exceeded replication. Despite the missing efficacy of phages in this experiment, a volume adapted phage concentration within the model shows potential for future experiments.

HIM was performed to visualize the explant surface and possible interactions of phages and bacteria. Images of the negative control showed polygonal epithelial cells with microvilli as described for unaltered endometrium visualized by electron microscopy (Ferreira-Dias et al., 1994b). However, loss of the regular epithelial architecture was observed after co-incubation with phages and bacteria as mentioned above. In this sample, phage-like particles were detected on bacterial cells (e.g., as displayed in Figure 5G) whose structure fits the head size of phage LmqsRe26-2 as calculated by TEM analysis. This particle was closely attached to the bacterial cell membrane as described for a podovirus infection in a previous study (Casjens and Molineux, 2012). The shape of the structure is not clearly icosahedral, however, is likely due to the long HIM sample preparation routine, compared to negative stain TEM imaging. For example, HIM images of T4 phages, which also possess icosahedral heads, have shown variable shapes during infections of bacterial cells (Leppänen et al., 2017). Moreover, the presence of extracellular matrix around the bacteria could mask the phage structure. With the same probability, the visualized structure may be a bacterial vesicle during the process of endo- or exocytosis. However, extracellular vesicles have not yet been described for *S. equi* subsp. *zooepidemicus*, while being observed in *S. pneumoniae* (Mehanny et al., 2020). Further experiments are needed to clearly visualize the phage infection of bacteria in the *ex vivo* model.

In conclusion, this paper describes the isolation and characterization of phages against *S. equi* subsp. *zooepidemicus* for the first time. A relatively broad host range and high efficacy against potential host bacteria *in vitro* emphasizes their therapeutic potential. However, while reduction has been observed in planktonic killing assays, no phage-induced bacterial growth reduction was observed in an endometrial explant model, demonstrating the need for further studies on potential phage administration (e.g., optimization of MOIs

and combined administration with antibiotics) and kinetics since the available results do not currently support the therapeutic use of the phages.

Data availability statement

The original contributions presented in the study are included in the article/Supplementary material. The complete genomes of the isolated phages can be found under the accession number PQ425460 and PQ425461 in the NCBI database (https://www.ncbi.nlm.nih.gov/).

Ethics statement

The animal study was approved by Animal Welfare Officer University of Veterinary Medicine Hannover. The study was conducted in accordance with the local legislation and institutional requirements.

Author contributions

MK: Writing – original draft, Investigation, Formal analysis, Data curation, Conceptualization. RH: Writing – review & editing, Investigation, Data curation. AT: Writing – review & editing, Investigation. MS: Writing – review & editing, Investigation. MM: Writing – review & editing, Investigation. DB: Writing – review & editing, Investigation. JH: Writing – review & editing, Investigation. MP: Writing – review & editing, Resources, Conceptualization. SK: Writing – review & editing, Resources, Project administration, Conceptualization. HS: Writing – review & editing, Resources, Project administration, Conceptualization.

Funding

The author(s) declare that no financial support was received for the research, authorship, and/or publication of this article.

Acknowledgments

The authors are thankful to the Institute of Microbiology, University of Veterinary Medicine Hannover, Foundation and Labor Böse GmbH for provision of bacterial isolates. Moreover, the authors thank the laboratory personal of the Institute of Food Quality and Food Safety, University of Veterinary Medicine Hannover, Foundation and Ina Brentrop from the EM facility for invaluable support. The authors are thankful for the use of the helium ion microscope at the Center for Chemical Microscopy (ProVIS) at UFZ Leipzig, which is supported by European Regional Development Funds (EFRE-Europe funds Saxony) and the Helmholtz Association. We acknowledge financial support by the Open Access Publication Fund of the University of Veterinary Medicine Hannover, Foundation.

Conflict of interest

The authors declare that the research was conducted in the absence of any commercial or financial relationships that could be construed as a potential conflict of interest.

Publisher's note

Supplementary material

The Supplementary material for this article can be found online at: https://www.frontiersin.org/articles/10.3389/fmicb.2024.1448958/full#supplementary-material

SUPPLEMENTARY TABLE S1
Information on bacterial isolates (isolate number, bacterial species, origin of bacterial sample).

SUPPLEMENTARY TABLE S2
Number of explants per group (negative control, positive control, treatment group) with results of lactate dehydrogenase (LDH) activity-analysis in explant culture medium (< 50 U/l; 50-100 U/l; > 100 U/l) after 6 and 24 h of incubation. No significant differences among treatment groups were determined by chi-square testing.

SUPPLEMENTARY FIGURES S1–S4
Additional helium ion microscopic images of an equine endometrial explant after incubation with *S. equi* subsp. *zooepidemicus* and the specific phage vB_SeqZP_LmqsRe26-2 at MOI 10 with particles suspected of being phages.

References

Abdelrahman, F., Easwaran, M., Daramola, O. I., Ragab, S., Lynch, S., Oduselu, T. J., et al. (2021). Phage-encoded Endolysins. *Antibiotics* 10:124. doi: 10.3390/antibiotics10020124

Ackermann, H.-W., and Prangishvili, D. (2012). Prokaryote viruses studied by electron microscopy. *Arch. Virol.* 157, 1843–1849. doi: 10.1007/s00705-012-1383-y

Ávila, A. C. A., Diniz, N. C., Serpa, R. T., de Castro Chaves, M. M. B., de Oliveira Viu, M. A., and de Oliveira, R. A. (2022). Effectiveness of ozone therapy in the treatment of endometritis in mares. *J. Equine Vet.* 112:103900. doi: 10.1016/j.jevs.2022.103900

Bai, Q., Zhang, W., Yang, Y., Tang, F., Nguyen, X., Liu, G., et al. (2013). Characterization and genome sequencing of a novel bacteriophage infecting *Streptococcus agalactiae* with high similarity to a phage from *Streptococcus pyogenes*. *Arch. Virol.* 158, 1733–1741. doi: 10.1007/s00705-013-1667-x

Balcão, V. M., Belline, B. G., Silva, E. C., Almeida, P. F., Baldo, D. Â., Amorim, L. R., et al. (2022). Isolation and molecular characterization of two novel lytic bacteriophages for the biocontrol of *Escherichia coli* in uterine infections: in vitro and ex vivo preliminary studies in veterinary medicine. *Pharmaceutics* 14:2344. doi: 10.3390/pharmaceutics14112344

Beerens, D., Franch-Arroyo, S., Sullivan, T. J., Goosmann, C., Brinkmann, V., and Charpentier, E. (2021). Survival strategies of *Streptococcus pyogenes* in response to phage infection. *Viruses* 13:612. doi: 10.3390/v13040612

Bicalho, R., Santos, T., Gilbert, R., Caixeta, L., Teixeira, L., Bicalho, M., et al. (2010). Susceptibility of *Escherichia coli* isolated from uteri of postpartum dairy cows to antibiotic and environmental bacteriophages. Part I: isolation and lytic activity estimation of bacteriophages. *J. Dairy Sci.* 93, 93–104. doi: 10.3168/jds.2009-2298

Blum, S., Elad, D., Zukin, N., Lysnyansky, I., Weisblith, L., Perl, S., et al. (2010). Outbreak of *Streptococcus equi* subsp. *zooepidemicus* infections in cats. *Vet. Microbiol.* 144, 236–239. doi: 10.1016/j.vetmic.2009.12.040

Boeckman, J., Liu, M., Ramsey, J., and Gill, J. (2024). Phage DNA extraction, genome assembly, and genome closure. *Methods Mol. Biol.* 2738, 125–144. doi: 10.1007/978-1-0716-3549-0_8

Bordes-Benítez, A., Sánchez-Oñoro, M., Suárez-Bordón, P., García-Rojas, A., Saéz-Nieto, J., González-García, A., et al. (2006). Outbreak of *Streptococcus equi* subsp. *zooepidemicus* infections on the island of gran *Canaria* associated with the consumption of inadequately pasteurized cheese. *Eur. J. Clin. Microbiol. Infect. Dis.* 25, 242–246. doi: 10.1007/s10096-006-0119-x

Canisso, I. F., Segabinazzi, L. G., and Fedorka, C. E. (2020). Persistent breeding-induced endometritis in mares—a multifaceted challenge: from clinical aspects to immunopathogenesis and pathobiology. *Int. J. Mol. Sci.* 21:1432. doi: 10.3390/ijms21041432

Casjens, S. R., and Molineux, I. J. (2012). Short noncontractile tail machines: adsorption and DNA delivery by Podoviruses. *Adv. Exp. Med. Biol.* 726, 143–179. doi: 10.1007/978-1-4614-0980-9_7

Clark, P. F., and Clark, A. S. (1927). A bacteriophage active against a virulent hemolytic Streptococcus. *Proc. Soc. Exp. Biol. Med.* 24, 635–639. doi: 10.3181/00379727-24-3498

Danis-Wlodarczyk, K., Dąbrowska, K., and Abedon, S. T. (2021). Phage therapy: the pharmacology of antibacterial viruses. *Curr. Issues Mol. Biol.* 40, 81–164. doi: 10.21775/cimb.040.081

Dascanio, J. J. (2003). "Endometrial cytology" in Current therapy in equine medicine: 5th. ed. G. S. Frazer (Philadelphia, PA: WB Saunders Co.), 226–228.

Davis, H. A., Stanton, M. B., Thungrat, K., and Boothe, D. M. (2013). Uterine bacterial isolates from mares and their resistance to antimicrobials: 8,296 cases (2003–2008). *J. Am. Vet. Med. Assoc.* 242, 977–983. doi: 10.2460/javma.242.7.977

Dreiseikelmann, B., Bunk, B., Sproer, C., Rohde, M., Nimtz, M., and Wittmann, J. (2017). Characterization and genome comparisons of three Achromobacter phages of the family Siphoviridae. *Arch. Virol.* 162, 2191–2201. doi: 10.1007/s00705-017-3347-8

European Commission. (2019). *Regulation (EU) 2019/6 of the European Parliament and of the Council of 11 December 2018 on veterinary medicinal products and repealing Directive 2001/82/EC.*

European Medicines Agency. (2023). *Guideline on quality, safety and efficacy of veterinary medicinal products specifically designed for phage therapy*. Available at: https://www.ema.europa.eu/en/quality-safety-and-efficacy-bacteriophages-veterinary-medicines-scientific-guideline (Accessed June 13, 2024).

Evans, A. C. (1934). Streptococcus bacteriophage: a study of four serological types. *Public Health Rep.* 49, 1386–1401.

Eyre, D., Kenkre, S., Bowler, I. C. J. W., and McBride, S. J. (2010). *Streptococcus equi* subspecies zooepidemicus meningitis—a case report and review of the literature. *Eur. J. Clin. Microbiol. Infect. Dis.* 29, 1459–1463. doi: 10.1007/s10096-010-1037-5

Feng, Z., and Hu, J. (1977). Outbreak of swine streptococcosis in Sichan province and identification of pathogen. *Anim. Husbandry Vet. Med. Lett.* 2, 7–12.

Ferreira-Dias, G., Nequin, L. G., and King, S. S. (1994a). Influence of estrous cycle stage on adhesion of *Streptococcus zooepidemicus* to equine endometrium. *Am. J. Vet. Res.* 55, 1028–1031. doi: 10.2460/ajvr.1994.55.07.1028

Ferreira-Dias, G., Nequin, L. G., and King, S. S. (1994b). Morphologic characteristics of equine endometrium classified as Kenney categories I, II, and III, using light and scanning electron microscopy. *Am. J. Vet. Res.* 55, 1060–1065. doi: 10.2460/ajvr.1994.55.08.1060

Ferris, R. A., McCue, P. M., Borlee, G. I., Loncar, K. D., Hennet, M. L., and Borlee, B. R. (2016). In vitro efficacy of nonantibiotic treatments on biofilm disruption of gram-negative pathogens and an in vivo model of infectious endometritis utilizing isolates from the equine uterus. *J. Cin. Microbiol.* 54, 631–639. doi: 10.1128/JCM.02861-15

Friederichs, J., Hungerer, S., Werle, R., Militz, M., and Bühren, V. (2010). Human bacterial arthritis caused by *Streptococcus zooepidemicus*: report of a case. *Int. J. Infect. Dis.* 14, e233–e235. doi: 10.1016/j.ijid.2009.08.009

Fulde, M., and Valentin-Weigand, P. (2013). Epidemiology and pathogenicity of zoonotic streptococci. *Curr. Top. Microbiol. Immunol.* 368, 368, 49–81. doi: 10.1007/82_2012_277

Furusawa, T., Iwano, H., Hiyashimizu, Y., Matsubara, K., Higuchi, H., Nagahata, H., et al. (2016). Phage therapy is effective in a mouse model of bacterial equine keratitis. *Appl. Environ. Microbiol.* 82, 5332–5339. doi: 10.1128/AEM.01166-16

Garneau, J. R., Depardieu, F., Fortier, L.-C., Bikard, D., and Monot, M. (2017). PhageTerm: a tool for fast and accurate determination of phage termini and packaging mechanism using next-generation sequencing data. *Sci. Rep.* 7:8292. doi: 10.1038/s41598-017-07910-5

Harhala, M., Barylski, J., Humińska-Lisowska, K., Lecion, D., Wojciechowicz, J., Lahutta, K., et al. (2018). Two novel temperate bacteriophages infecting *Streptococcus pyogenes*: their genomes, morphology and stability. *PLoS One* 13:e0205995. doi: 10.1371/journal.pone.0205995

Hurtgen, J. P. (2006). Pathogenesis and treatment of endometritis in the mare: a review. *Theriogenology* 66, 560–566. doi: 10.1016/j.theriogenology.2006.04.006

Hyman, P., and Abedon, S. T. (2010). Bacteriophage host range and bacterial resistance. *Adv. Appl. Microbiol.* 70, 217–248. doi: 10.1016/S0065-2164(10)70007-1

Kasman, L. M., and Porter, L. D. (2022). Bacteriophages. Treasure Island, FL: StatPearls Publishing.

Kim, M., Heo, S. T., Oh, H., Kim, M., Jo, J., Kim, Y. R., et al. (2022). Human zoonotic infectious disease caused by *Streptococcus equi* subsp. *zooepidemicus*. *Zoonoses Public Health* 69, 136–142. doi: 10.1111/zph.12895

Kittang, B. R., Pettersen, V. K., Oppegaard, O., Skutlaberg, D. H., Dale, H., Wiker, H. G., et al. (2017). Zoonotic necrotizing myositis caused by *Streptococcus equi* subsp. *zooepidemicus* in a farmer. *BMC Infect. Dis.* 17, 147–148. doi: 10.1186/s12879-017-2262-7

Köhne, M., Diel, E., Packeiser, E.-M., Böttcher, D., Tönissen, A., Unruh, C., et al. (2024a). Analysis of gene and protein expression in the endometrium for validation of an ex vivo model of the equine uterus using PCR, digital and visual histopathology. *Theriogenology* 221, 38–46. doi: 10.1016/j.theriogenology.2024.03.015

Köhne, M., Hegger, A., Tönissen, A., Heusinger, A., Hader, C., Görgens, A., et al. (2024b). Frequency of potentially pathogenic bacterial and fungal isolates among 28,887 endometrial samples from mares, with an emphasis on multi-drug resistant bacteria in Germany (2018-2022). *J. Equine Vet.* 133:105008. doi: 10.1016/j.jevs.2024.105008

Köhne, M., Hofbauer, L., Böttcher, D., Tönissen, A., Hegger, A., Görgens, A., et al. (2023). Comparison of systemic trimethoprim-sulfadimethoxine treatment and intrauterine ozone application as possible therapies for bacterial endometritis in equine practice. *Front. Vet. Sci.* 10:1102149. doi: 10.3389/fvets.2023.1102149

Köhne, M., Kuhlmann, M., Tönißen, A., Martinsson, G., and Sieme, H. (2020). Diagnostic and treatment practices of equine endometritis—a questionnaire. *Front. Vet. Sci.* 7:547. doi: 10.3389/fvets.2020.00547

Köhne, M., Unruh, C., Böttcher, D., Tönissen, A., Ulrich, R., and Sieme, H. (2022). Evaluation of an ex vivo model of the blood-perfused equine uterus. *Theriogenology* 184, 82–91. doi: 10.1016/j.theriogenology.2022.02.026

Korf, I. H., Kittler, S., Bierbrodt, A., Mengden, R., Rohde, C., Rohde, M., et al. (2020). In vitro evaluation of a phage cocktail controlling infections with *Escherichia coli*. *Viruses* 12:1470. doi: 10.3390/v12121470

Kortright, K. E., Chan, B. K., Koff, J. L., and Turner, P. E. (2019). Phage therapy: a renewed approach to combat antibiotic-resistant bacteria. *Cell Host Microbe* 25, 219–232. doi: 10.1016/j.chom.2019.01.014

Kuchipudi, S. V., Surendran Nair, M., Yon, M., Gontu, A., Nissly, R. H., Barry, R., et al. (2021). A novel real-time pcr assay for the rapid detection of virulent *Streptococcus equi* subspecies *zooepidemicus*—an emerging pathogen of swine. *Front. Vet. Sci.* 8:604675. doi: 10.3389/fvets.2021.604675

Kutateladze, M., and Adamia, R. (2010). Bacteriophages as potential new therapeutics to replace or supplement antibiotics. *Trends Biotechnol.* 28, 591–595. doi: 10.1016/j.tibtech.2010.08.001

Labrie, S. J., Mosterd, C., Loignon, S., Dupuis, M. E., Desjardins, P., Rousseau, G. M., et al. (2019). A mutation in the methionine aminopeptidase gene provides phage resistance in *Streptococcus thermophilus*. *Sci. Rep.* 9:13816. doi: 10.1038/s41598-019-49975-4

Lancefield, R. C. (1932). Note on the susceptibility of certain strains of hemolytic streptococcus to a streptococcus bacteriophage. *Proc. Soc. Exp. Biol. Med.* 30, 169–171. doi: 10.3181/00379727-30-6409

LeBlanc, M., and Causey, R. (2009). Clinical and subclinical endometritis in the mare: both threats to fertility. *Reprod. Domest. Anim.* 44, 10–22. doi: 10.1111/j.1439-0531.2009.01485.x

Leppänen, M., Sundberg, L. R., Laanto, E., de Freitas Almeida, G. M., Papponen, P., and Maasilta, I. J. (2017). Imaging bacterial colonies and phage–bacterium interaction at sub-nanometer resolution using helium-ion microscopy. *Adv. Biosyst.* 1:1700070. doi: 10.1002/adbi.201700070

Lin, Y., Yuan, J., Kolmogorov, M., Shen, M. W., Chaisson, M., and Pevzner, P. A. (2016). Assembly of long error-prone reads using de Bruijn graphs. *Proc. Natl. Acad. Sci.* 113, E8396–E8405. doi: 10.1073/pnas.1604560113

Literák, I., and Mráz, O. (1991). *Streptococcus equi* subsp. *zooepidemicus* as the cause of mass mortality among laboratory mice. *Acta Vet. Brno* 60, 51–60. doi: 10.2754/avb199160010051

Loc Carrillo, C., Atterbury, R. J., El-Shibiny, A., Connerton, P. L., Dillon, E., Scott, A., et al. (2005). Bacteriophage therapy to reduce *Campylobacter jejuni* colonization of broiler chickens. *Appl. Environ. Microbiol.* 71, 6554–6563. doi: 10.1128/AEM.71.11.6554-6563.2005

Machado, V., Bicalho, M., Pereira, R., Caixeta, L., Bittar, J., Oikonomou, G., et al. (2012). The effect of intrauterine administration of mannose or bacteriophage on uterine health and fertility of dairy cows with special focus on Escherichia coli and *Arcanobacterium pyogenes*. *J. Dairy Sci.* 95, 3100–3109. doi: 10.3168/jds.2011-5063

Macpherson, M. L. (2005). Treatment strategies for mares with placentitis. *Theriogenology* 64, 528–534. doi: 10.1016/j.theriogenology.2005.05.009

Madeira, F., Madhusoodanan, N., Lee, J., Eusebi, A., Niewielska, A., Tivey, A. R. N., et al. (2024). The EMBL-EBI job dispatcher sequence analysis tools framework in 2024. *Nucleic Acids Res.* 52, W521–W525. doi: 10.1093/nar/gkae241

Mehanny, M., Koch, M., Lehr, C.-M., and Fuhrmann, G. (2020). Streptococcal extracellular membrane vesicles are rapidly internalized by immune cells and alter their cytokine release. *Front. Immunol.* 11:499398. doi: 10.3389/fimmu.2020.00080

Monteiro de Barros, M. R., Davies-Morel, M. C., Mur, L. A., Creevey, C. J., Alison, R. H., and Nash, D. M. (2021). Characterization of an ex vivo equine endometrial tissue culture model using next-generation RNA-sequencing technology. *Animals* 11:1995. doi: 10.3390/ani11071995

Murray, C. J., Ikuta, K. S., Sharara, F., Swetschinski, L., Aguilar, G. R., Gray, A., et al. (2022). Global burden of bacterial antimicrobial resistance in 2019: a systematic analysis. *Lancet* 399, 629–655. doi: 10.1016/S0140-6736(21)02724-0

Nang, S. C., Lin, Y.-W., Fabijan, A. P., Chang, R. Y., Rao, G. G., Iredell, J., et al. (2023). Pharmacokinetics/pharmacodynamics of phage therapy: a major hurdle to clinical translation. *Clin. Microbiol. Infect.* 29, 702–709. doi: 10.1016/j.cmi.2023.01.021

Nash, D., Lane, E., Herath, S., and Martin Sheldon, I. (2008). Endometrial explant culture for characterizing equine endometritis. *Am. J. Reprod. Immunol.* 59, 105–117. doi: 10.1111/j.1600-0897.2007.00548.x

Nelson, D., Schuch, R., Zhu, S., Tscherne, D. M., and Fischetti, V. A. (2003). Genomic sequence of C1, the first streptococcal phage. *J. Bacteriol.* 185, 3325–3332. doi: 10.1128/JB.185.11.3325-3332.2003

Oikawa, M., Kamada, M., Yoshikawa, Y., and Yoshikawa, T. (1994). Pathology of equine pneumonia associated with transport and isolation of *Streptococcus equi* subsp. *zooepidemicus*. *J. Comp. Pathol.* 111, 205–212. doi: 10.1016/s0021-9975(05)80052-0

Park, S. Y., Kwon, H., Kim, S. G., Park, S. C., Kim, J. H., and Seo, S. (2023). Characterization of two lytic bacteriophages, infecting *Streptococcus bovis/equinus* complex (SBSEC) from Korean ruminant. *Sci. Rep.* 13:9110. doi: 10.1038/s41598-023-36306-x

Peh, E., Szott, V., Reichelt, B., Friese, A., Rösler, U., Plötz, M., et al. (2023). Bacteriophage cocktail application for Campylobacter mitigation-from in vitro to in vivo. *BMC Microbiol.* 23:209. doi: 10.1186/s12866-023-02963-1

Pelkonen, S., Lindahl, S. B., Suomala, P., Karhukorpi, J., Vuorinen, S., Koivula, I., et al. (2013). Transmission of *Streptococcus equi* subspecies zooepidemicus infection from horses to humans. *Emerg. Infect. Dis.* 19, 1041–1048. doi: 10.3201/eid1907.121365

Pisello, L., Rampacci, E., Stefanetti, V., Beccati, F., Hyatt, D. R., Coletti, M., et al. (2019). Temporal efficacy of antimicrobials against aerobic bacteria isolated from equine endometritis: an Italian retrospective analysis (2010–2017). *Vet. Rec.* 185:598. doi: 10.1136/vr.105413

Preziuso, S., Moriconi, M., and Cuteri, V. (2019). Genetic diversity of *Streptococcus equi* subsp. *zooepidemicus* isolated from horses. *Comp. Immunol. Microbiol. Infect. Dis.* 65, 7–13. doi: 10.1016/j.cimid.2019.03.012

Priestnall, S., and Erles, K. (2011). *Streptococcus zooepidemicus*: an emerging canine pathogen. *Vet. J.* 188, 142–148. doi: 10.1016/j.tvjl.2010.04.028

Rathbone, P., Arango-Sabogal, J. C., De Mestre, A. M., and Scott, C. J. (2023). Antimicrobial resistance of endometrial bacterial isolates collected from UK thoroughbred mares between 2014 and 2020. *Vet. Rec.* 192:e2591. doi: 10.1002/vetr.2591

Retamar, G. C., Bustos, C. P., Guillemi, E. C., Becú, T., Ivanissevich, A., Mesplet, M., et al. (2024). Streptococcus equi subsp. zooepidemicus: High molecular diversity of Argentinian strains isolated from mares with endometritis. *Res. Vet. Sci.* 173:105242. doi: 10.1016/j.rvsc.2024.105242

Ricketts, S. (2011). "Uterine and clitoral cultures" in Equine Reproduction. eds. A. O. McKinnon, E. L. Squires, W. E. Vaala and D. D. Varner (Ames: Wiley-Blackwell), 1963–1978.

Riddle, W., LeBlanc, M., and Stromberg, A. (2007). Relationships between uterine culture, cytology and pregnancy rates in a thoroughbred practice. *Theriogenology* 68, 395–402. doi: 10.1016/j.theriogenology.2007.05.050

Rose, B., Firth, M., Morris, B., Roach, J., Wathes, D., Verheyen, K., et al. (2018). Descriptive study of current therapeutic practices, clinical reproductive findings and incidence of pregnancy loss in intensively managed thoroughbred mares. *Anim. Reprod. Sci.* 188, 74–84. doi: 10.1016/j.anireprosci.2017.11.011

Sanchez, L. C., Giguère, S., and Lester, G. D. (2008). Factors associated with survival of neonatal foals with bacteremia and racing performance of surviving thoroughbreds: 423 cases (1982–2007). *J. Am. Vet. Med. Assoc.* 233, 1446–1452. doi: 10.2460/javma.233.9.1446

Shakeri, G., Hammerl, J. A., Jamshidi, A., Ghazvini, K., Rohde, M., Szabo, I., et al. (2021). The lytic Siphophage vB_StyS-LmqsSP1 reduces the number of *Salmonella enterica Serovar* typhimurium isolates on chicken skin. *Appl. Environ. Microbiol.* 87:e0142421. doi: 10.1128/AEM.01424-21

Shen, A., and Millard, A. (2021). Phage annotation: where to start and where to end. *Phage* 2, 183–193. doi: 10.1089/phage.2021.0014

Smith, H. W., and Huggins, M. (1983). Effectiveness of phages in treating experimental *Escherichia coli* diarrhoea in calves, piglets and lambs. *Microbiology* 129, 2659–2675. doi: 10.1099/00221287-129-8-2659

Steffan, S. M., Shakeri, G., Hammerl, J. A., Kehrenberg, C., Peh, E., Rohde, M., et al. (2021). Isolation and characterization of group III *Campylobacter jejuni*–specific bacteriophages from Germany and their suitability for use in food production. *Front. Microbiol.* 12:761223. doi: 10.3389/fmicb.2021.761223

Steward, K. F., Robinson, C., Holden, M. T., Harris, S. R., Ros, A. F., Pérez, G. C., et al. (2017). Diversity of *Streptococcus equi* subsp. *zooepidemicus* strains isolated from the Spanish sheep and goat population and the identification, function and prevalence of a novel arbutin utilisation system. *Vet. Microbiol.* 207, 231–238. doi: 10.1016/j.vetmic.2017.06.020

The Galaxy Community (2022). The galaxy platform for accessible, reproducible and collaborative biomedical analyses: 2022 update. *Nucleic Acids Res.* 50, W345–W351. doi: 10.1093/nar/gkac247

Thompson, R. E., Johnson, A. K., Dini, P., Turco, M. Y., Prado, T. M., Premanandan, C., et al. (2020a). Hormone-responsive organoids from domestic mare and endangered Przewalski's horse endometrium. *Reproduction* 160, 819–831. doi: 10.1530/REP-20-0266

Thompson, R. E., Premanandan, C., Pukazhenthi, B. S., and Whitlock, B. K. (2020b). A review of in vivo and in vitro studies of the mare endometrium. *Anim. Reprod. Sci.* 222:106605. doi: 10.1016/j.anireprosci.2020.106605

Timoney, J. (2004). The pathogenic equine streptococci. *Vet. Res.* 35, 397–409. doi: 10.1051/vetres:2004025

Tiwari, R., and Timoney, J. F. (2009). *Streptococcus equi* bacteriophage SeP9 binds to group C carbohydrate but is not infective for the closely related *S. zooepidemicus*. *Vet. Microbiol.* 135, 304–307. doi: 10.1016/j.vetmic.2008.09.064

Traub-Dargatz, J., Salman, M., and Voss, J. (1991). Medical problems of adult horses, as ranked by equine practitioners. *J. Am. Vet. Med. Assoc.* 198, 1745–1747. doi: 10.2460/javma.1991.198.010.1745

Van Nieuwenhuyse, B., Van der Linden, D., Chatzis, O., Lood, C., Wagemans, J., Lavigne, R., et al. (2022). Bacteriophage-antibiotic combination therapy against extensively drug-resistant *Pseudomonas aeruginosa* infection to allow liver transplantation in a toddler. *Nat. Commun.* 13:5725. doi: 10.1038/s41467-022-33294-w

Walker, P. J., Siddell, S. G., Lefkowitz, E. J., Mushegian, A. R., Adriaenssens, E. M., Alfenas-Zerbini, P., et al. (2022). Recent changes to virus taxonomy ratified by the international committee on taxonomy of viruses (2022). *Arch. Virol.* 167, 2429–2440. doi: 10.1007/s00705-022-05516-5

Wang, X., Ji, Y., Su, J., Xue, Y., Xi, H., Wang, Z., et al. (2020). Therapeutic efficacy of phage PIZ SAE-01E2 against abortion caused by *Salmonella enterica* serovar abortusequi in mice. *Appl. Environ. Microbiol.* 86, e01366–e01320. doi: 10.1128/AEM.01366-20

Wittenbrink, M., Hölzle, L., and Baumeister, A. (1997). Mechanisms of bacterial pathogenesis in equine endometritis. *Pferdeheilkunde* 13, 450–452. doi: 10.21836/PEM19970505

frontiers | Frontiers in Microbiology

TYPE Original Research
PUBLISHED 12 December 2024
DOI 10.3389/fmicb.2024.1455710

OPEN ACCESS

EDITED BY
Gamaliel López-Leal,
Center for Research in Cellular Dynamics-UAEM, Mexico

REVIEWED BY
Md Mozammel Hoque,
University of Technology Sydney, Australia
Domenico Franco,
University of Messina, Italy

*CORRESPONDENCE
Jungmin Kim
✉ minkim@knu.ac.kr

RECEIVED 27 June 2024
ACCEPTED 30 October 2024
PUBLISHED 12 December 2024

CITATION
Shamsuzzaman M, Kim S and Kim J (2024) Bacteriophage as a novel therapeutic approach for killing multidrug-resistant *Escherichia coli* ST131 clone.
Front. Microbiol. 15:1455710.
doi: 10.3389/fmicb.2024.1455710

Bacteriophage as a novel therapeutic approach for killing multidrug-resistant *Escherichia coli* ST131 clone

Md Shamsuzzaman[1,2], Shukho Kim[1,2] and Jungmin Kim[1,2]*

[1]Department of Biomedical Science, The Graduate School, Kyungpook National University, Daegu, Republic of Korea, [2]Department of Microbiology, School of Medicine, Kyungpook National University, Daegu, Republic of Korea

The emergence of the multidrug-resistant (MDR) *Escherichia coli* ST131 clone has significantly impacted public health. With traditional antibiotics becoming less effective against MDR bacteria, there is an urgent need for alternative treatment options. This study aimed to isolate and characterize four lytic phages (EC.W2-1, EC.W2-6, EC.W13-3, and EC.W14-3) from hospital sewage water and determine their effectiveness against the ST131 clone. These phages demonstrated a broad host range, effectively lysing 94.4% of highly pathogenic *E. coli* ST131 isolates. Morphological observations and phylogenetic analysis indicate that EC.W2-1, and EC.W13-3 belong to the *Tequatrovirus* genus in the *Straboviridae* family, while EC.W2-6 and EC.W14-3 are part of the *Kuravirus* genus in the *Podoviridae* family. Phages remained stable at pH 2–10 for 4 h and below 80°C for 1 h. These four phages showed *in vitro* bacterial lytic activity at various MOIs (0.1–0.001). The one-step growth curve of phages exhibited a short latent period of approximately 10–20 min and a moderate burst size of 50–80 (pfu/cell). Phages' genome size ranged from 46,325–113,909 bp, with G + C content of 35.1 –38.3%. No virulence or drug resistance genes were found, which enhanced their safety profile. *In vivo*, EC.W2-6 and EC.W13.3, along with their cocktail, fully protected against the ESBL-producing *E. coli* ST131 infection model *in vivo*. Combining these phages and a 3-day repeated single phage, EC.W13-3 significantly enhanced the survival rate of *E. coli* ST131 infected mice at low MOI (0.01–0.001). The *in vivo* effectiveness of the isolated phages and the EC.W2-6 and EC.W14-3 cocktail in highly reducing bacterial load CFU/g in multiple organs strongly supports their potential efficacy. Based on *in vivo*, *in vitro*, and genomic analyses, phages have been proposed as novel and suitable candidates for killing the pandemic ST131 clone.

KEYWORDS

***Escherichia coli*, clone ST131, antibiotic resistance, bacteriophages, therapeutic efficiency, phage cocktail**

1 Introduction

Escherichia coli sequence type 131 (ST131) is a clonal group of concern, known for causing antimicrobial-resistant infections predominantly in community settings (Rogers et al., 2011). The ST131 pandemic was initially detected in 2008 using multilocus sequence typing (MLST) to identify CTX-M-15 extended-spectrum *β*-lactamase-producing *E. coli* strains across various continents. *E. coli* ST131 is mostly known as a major cause of urinary tract infections (UTIs). Besides causing UTIs, this extraintestinal pathogenic bacterium can also lead to serious infections, including bloodstream infections, sepsis, and intra-abdominal infections (Whelan

et al., 2023). These infections affect individuals of all ages and range from cystitis to life-threatening sepsis. Treatment requires a tailored approach considering antimicrobial resistance and infection site. Although phenotypic detection of ST131 is not possible, DNA-based methods like MLST and PCR are used for identification (Rogers et al., 2011; Nicolas-Chanoine et al., 2014).

The clone ST131, which is a major cause of fluoroquinolone-resistant *E. coli* infections, has a high prevalence ranging from 60 to 90% (Peirano et al., 2020). Fluoroquinolone resistance in ST131 is caused by amino acid substitutions in the QRDR genes (*gyrA, parC*, and *parE*), which reduce the effectiveness of fluoroquinolone in inhibiting bacterial DNA replication and transcription (Shariati et al., 2022). Recently, the plasmid-mediated colistin resistance gene *mcr*-1 was detected in ST131. The presence of *mcr*-1 in ST131 raises concerns about the spread of colistin resistance (Majewski et al., 2021). The ST131 clone of *E. coli* harbors different β-lactamase genes (Miyoshi-Akiyama et al., 2016). β-lactamases are enzymes produced by bacteria that can deactivate β-lactam antibiotics such as penicillins and cephalosporins. The most common types of β-lactamase genes in the ST131 clone are CTX-M family β-lactamases, with TEM, SHV, and CMY β-lactamases being less frequent. Approximately 40–80% of extraintestinal pathogenic *E. coli* strains with extended-spectrum β-lactamases (ESBLs) belong to the ST131 clone (Hibstu et al., 2022).

The geographical distribution of ST131 is not fully known; however, it is commonly found in antimicrobial-resistant *E. coli* infections in Europe, North America, Canada, Japan, and South Korea (Bevan et al., 2017). In a national survey in Japan, the ST131 clones were found in 38.1% of ESBL-producing *E. coli* isolates between 2013 and 2014. Notably, in this region, there is higher genetic diversity within the ST131 clone and a greater variety of accompanying CTX-M ESBL genes than in other areas (Miyoshi-Akiyama et al., 2016). Similarly, in South Korea, from 2016 to 2017, 27% of ESBL-producing *E. coli* isolates were ST131, with only 57% carrying an ESBL gene (Baek et al., 2021). *E. coli* ST131, an antimicrobial-resistant clone, has been found in humans, companion animals, non-companion animals, and food sources. The extensive presence of ST131 in various populations raises concerns regarding its potential transmission and its impact on public health (Banerjee and Johnson, 2014).

As mentioned previously, the ST131 clone of *E. coli* possesses various antimicrobial resistance mechanisms. However, limited information is available regarding the specific antimicrobial therapies used to treat the infections caused by this clone. This situation underscores the pressing need for innovative therapeutic approaches and development of new antimicrobial agents to effectively combat these infections (Kim et al., 2018; Rehman et al., 2019). The limited availability of new antibiotics has renewed interest in phage therapy as a potential solution, increasing the search for novel phages (Reardon, 2014). Phages are viruses that infect and kill bacteria, offering a potential alternative to antibiotics in the face of growing antimicrobial resistance. Clinical approaches to phage therapy have been reported in several countries, including the United States, Georgia, Poland, and Russia (Hibstu et al., 2022). Phages exhibit selective tropism, targeting specific bacteria via surface receptors while minimizing harm to the host microbiome. Generally safe for mammals, potential risks include immune responses and endotoxin release. Lytic phages directly kill bacteria and can be engineered for targeted drug delivery (Emencheta et al., 2024). Scientific evidence supporting the benefits of phage therapy in humans and animals has steadily increased in the recent decades (Hon et al., 2022). Additionally, they have been used as indicators of water safety (de Almeida Kumlien et al., 2021). As the availability of phages is limited, there is an urgent need to isolate safe, highly lytic, and well-characterized phages for phage therapy.

Current research focuses on isolating, characterizing, and evaluating the efficacy of novel *E. coli* phages in combating ST131 *E. coli* infections *in vitro* and *in vivo*. The goal of this study was to explore phages as an alternative strategy to combat the growing issue of MDR *E. coli* clone ST131. However, phage therapy is still in its early stages and faces challenges, such as regulatory barriers and manufacturing limitations. Nonetheless, advancements in phage therapy have provided hope for addressing antibiotic resistance and improving the treatment options for serious bacterial infections.

2 Materials and methods

2.1 Animals used in *in vivo* experiments

In vivo experiments were conducted on BALB/c mice strain from Yeangnam Bio (166 Palgong-ro, Dong-gu Daegu) with six-week-old female mice receiving sterile food and water. The procedures followed guidelines set by the National Ethics Committee and approved by the Kyungpook National University Animal Care and Use Committee (KNU: 2023–0478).

2.2 Bacterial strains and growth conditions

E. coli isolates were obtained from Kyungpook National University Hospital Culture Collection for Pathogens (KNUH-NCCP). The isolates were initially cultured on 5% sheep blood agar at 37°C for 24 h. Then, the samples were transferred to Brain Heart Infusion broth (BHI) and incubated at 37°C for 24 h. Finally, the isolates were preserved at −70°C with a 50% glycerol stock for future experiments.

2.3 Phage isolation, purification, and preparation

E. coli hosts were cultured on blood agar plates. Sewage water samples were collected from Kyungpook National University Hospital in Daegu, South Korea. Sewage water was treated by centrifugation at 12,000 × g for 10 min to remove the debris. The resulting supernatant was filtered using 0.22 µm pore-sized membrane filters. The filtrate was used to infect *E. coli* cultures in the early exponential phase. After overnight incubation at 30°C with shaking, infected cultures were stored at 4°C for 48 h. The supernatants were centrifuged again and filtered through a 0.22 µm pore-size membrane. Phage titers were determined using the double layer method. The purified phages were stored at −70°C in glycerol-supplemented medium (Kim et al., 2022).

2.4 Antimicrobial susceptibility test and MLST analysis

Antibiotic susceptibility of the 18 *E. coli* isolates was tested against 21 antibiotics from 10 families. These families include cephalosporins, monobactams, aminopenicillin, fluoroquinolones, aminoglycosides, penicillin, sulfonamide-trimethoprim, tetracycline, carbapenem, and

extended-spectrum beta-lactamases. To determine the minimum inhibitory concentration (MIC), antibiotic disks and culture materials were purchased from Becton Dickinson and Company. *E. coli* ATCC25922 was used as the control. Each isolate was tested in triplicate, according to the Clinical and Laboratory Standards Institute guidelines (CLSI, 2020; Shamsuzzaman et al., 2023). According to these guidelines, isolates were classified as resistant, intermediate, or susceptible. The MLST analysis described in our study was previously conducted by the Department of Microbiology at Kyungpook National University (Shamsuzzaman et al., 2024).

2.5 Determination of lytic activity of phages against clinical isolates of *Escherichia coli* ST131

Eighteen *E. coli* clinical isolates (ST131) were tested for susceptibility to phage lytic activity by spot tests following the method outlined by Kim et al. (2018). To prepare the bacterial lawn, 10 mL of 0.75% soft agar with 100 µL of bacterial culture in the stationary phase was poured onto a BHA agar plate. Once the overlay solidified, a 15 µL aliquot of the phage, with a concentration of approximately 10^{11-13} PFU/ml, was directly spotted on the bacterial lawn. The plates were dried and incubated overnight at 37°C. Bacterial susceptibility was determined using the clear lytic zones on the plates.

2.6 Measurement of adsorption rate and burst size of four novel *Escherichia coli* phages

Phage adsorption rate and burst size were determined following the method outlined by Rahman et al. (2011) *E. coli* cells (ATCC25922) were cultured in BHI media until they reached exponential phase. The cells were then infected with the phage at a low multiplicity of infection (MOI) of 0.0001 and incubated at room temperature. Samples were collected and centrifuged at intervals of 0, 1, 3, 5, 10, 15, and 20 min. The supernatants were used for plaque assays to determine the titers of the unabsorbed phages. The burst size of the phage was determined using a single growth-curve experiment. *E. coli* cells were harvested by centrifugation and resuspended in 1 mL of fresh BHI medium at a concentration of 5×10^9 CFU/mL. The phage was added at an MOI of 0.0001 and allowed to adsorb for 30 min at 4°C. After centrifugation at 12,000 × g for 5 min, the pellet was resuspended in 10 mL of fresh BHI medium. The mixture was then incubated at 37°C, and samples were collected at 5-min intervals for up to 45 min. The samples were promptly diluted and analyzed for phage plaque counts. Each experiment was independently repeated thrice.

2.7 Thermal and pH stability

The thermal and pH stability of the phage were evaluated following the method described by Tang et al. (2023). To assess thermal stability, the phage suspension (~10^8 PFU/mL) was incubation at temperatures ranging from 4 to 80°C for 1 h. The phage suspension (~10^8 PFU/mL) was incubated in BHI broth with pH levels ranging from 2 to 10 at 37°C for 4 h to determine pH stability. Phage titers were determined utilizing the double-layer agar method.

2.8 *In vitro* bactericidal activity at various MOIs and phage cocktail analysis

This method determines the bactericidal activity of phages and phage cocktails against *E. coli* ATCC 25922 and *E. coli* ST131. Bacterial cultures (10^8 CFU/mL) were treated with individual phages and combination phages (1:1) at various MOIs (10, 1, 0.1, 0.01, 0.001) in BHI broth at 37°C with gentle shaking. Optical density at 600 nm was measured using a UV–Vis spectrophotometer (Molecular Devices, LLC, San Jose, CA, United States) in a 96-well plate at 1 h intervals for 12 h and again at 24 h. Bacterial culture without phages served as the positive control, while BHI broth served as the negative control. All assays were performed in triplicate (Tang et al., 2023).

2.9 Bacteriophage sequencing and genome assembly

Phage DNAs were extracted using the phenol-chloroform method described by Jakočiūnė and Moodley (2018). To conduct next-generation sequencing (NGS), phage genomic DNA was sequenced using an Illumina Miseq platform in San Diego, CA, USA. The sequencing reads were assembled through the Celemics pipeline based in South Korea.[1] To analyze genome sequence similarity, BLASTn[2] was used for alignment. The RAST online website[3] was utilized to predict open reading frames (ORFs), and the predictions were cross-checked and corrected through the NCBI database. Gene function maps were created using a custom program developed in the lab and refined using Geneious Prime 2023.2.[4] The tRNAscan-SE v.2.0 tool[5] was employed to predict tRNA. ResFinder[6] and VirulenceFinder[7] were utilized to identify drug resistance genes and virulence genes, respectively. A phylogenetic tree based on the phage proteome rectangular tree circular tree were generated using VIPTree.[8] For the construction of a complete genome phylogenetic tree based on the whole genome sequence of the isolated phages, the genome-BLAST distance phylogenetic approach provided by VICTOR[9] was used. Phylogenetic trees of large terminase and minor capsid proteins were constructed using the neighbor-joining (NJ) method, and the Bootstrap method was employed to assess the reliability of the phylogenetic trees. Additionally, the complete genome sequences of the isolated phages were aligned with other phages using the BLASTn tool available in the NCBI database. The Mauve algorithm (v2.3.1) was used to visualize the complete genome sequence similarity between the isolated phages and their closest neighbor, *E. coli* phages.[10]

1 https://btseq.celemics.com/
2 https://blast.ncbi.nlm.nih.gov/Blast.cgi
3 https://rast.nmpdr.org/rast.cgi
4 https://www.geneious.com/
5 http://lowelab.ucsc.edu/cgi-bin/tRNAscan-SE2.cgi
6 https://cge.cbs.dtu.dk/services/ResFinder/
7 https://cge.cbs.dtu.dk/services/VirulenceFinder/
8 https://www.genome.jp/viptree/
9 https://ggdc.dsmz.de/submit_victor_job.php
10 https://darlinglab.org/mauve/mauve.html

2.10 *In vivo* bactericidal efficacy of phages in a murine model of *Escherichia coli* ST131

Overnight bacterial cultures were grown in BHI broth at 37°C with shaking reached an OD of approximately 2. To ensure they were in the logarithmic phase, 100 µL of the culture was reinoculated into 10 mL fresh BHI and incubated at 37°C. Once in the logarithmic phase, cultures were washed twice in 1X PBS. Viable bacteria were quantified by plating serial dilutions on bacteriological agar to calculate CFU. Following this, mice were administered an intraperitoneal injection (IP) of a 50% lethal dose (LD50) of 10^9 CFU/mL. One-hour post-infection, mice were administered intraperitoneal injections of purified phages at varying plaque-forming units (PFU) in 100 µL of PBS. The infected mice were divided into treatment groups for analysis, with each group containing 5 mice. The control group consisted of infected mice that did not receive any treatment. The phage-treated group included mice infected with *E. coli*-specific phages. The positive control group was treated with PBS, whereas the negative control group was treated with both phages and PBS. Daily survival rates were recorded for each group to evaluate the effectiveness of phage therapy in preventing mortality (Pu et al., 2022).

To determine the colony-forming units (CFU) and plaque-forming units (PFU), mice were euthanized 16–18 h post-infection. Following euthanisation, necropsies were performed under sterile conditions. Each treatment group contained 4 mice. The lungs, kidneys, liver, and spleen were weighed and homogenized in 1X PBS using sterile blades. Subsequently, organ homogenates were serially diluted and plated on LB ampicillin (100 µg/mL) plates, followed by overnight incubation at 37°C. Phage counts were quantified using a soft agar overlay assay (Green et al., 2017).

2.11 Statistical analysis

Statistical analyses were performed using GraphPad Prism (version X). Survival analysis was conducted using the Kaplan–Meier method, with differences between groups assessed through the log-rank (Mantel-Cox) test. To compare bacterial loads across different organs, one-way ANOVA was used followed by Tukey's post-hoc test for multiple comparisons. For phage analysis, data from adsorption and burst size assays were analyzed using unpaired t-tests. Results were considered statistically significant at p-values <0.05 and are presented as mean ± standard error of the mean (SEM).

3 Results

3.1 Host range and EOP of phages

Based on the spot test results, phages EC.W2-1, EC.W2-6, EC.W13-3, and EC.W14-3 exhibited high lytic activity against pathogenic ST131 isolates, lysing 94.44% (17/18) of the isolates (Table 1). These phages also showed lytic activity against 14 different ST types, including 60 multi-drug-resistant *E. coli* isolates, with lytic activity percentages ranging from 50.0 to 56.6% (Shamsuzzaman et al., 2024). However, the efficiency of plating (EOP) values of phages against *E. coli* KBN 10PO7288 (ST131) compared to the reference *E. coli* ATCC25922 were approximately 2.56×10^9, 4.56×10^6, 261.53, and 372.09, respectively (Supplementary Table S1).

3.2 Antibiotic resistance profile of clinically isolated *Escherichia coli* isolates

As shown in Figure 1, AST results revealed that all 18 *E. coli* ST131 isolates exhibited a multidrug-resistant profile, indicating an alarming 100% prevalence of MDR (18/18) (Supplementary Table S2). The antibiotic resistance and susceptibility patterns of 18 ST131 isolates were investigated, and results revealed significant resistance to cephalosporins, specifically cefazolin (100%, 14/14), ceftazidime (94.1%, 16/17), cefoxitin (57.1%, 8/14), ceftriaxone (100%, 2/2), cefotaxime (93.3%, 14/15), and cefepime (88.8%, 16/18). The monobactam family also exhibited notable resistance, with aztreonam showing 94.1% resistance (16/17). Aminopenicillins also showed resistant to amoxicillin (72.2%, 13/18) and ampicillin (100%, 12/12), demonstrating high resistance rates. Carbapenem-resistant strains were observed with imipenem (44.4%, 8/18) and meropenem (38.8%, 7/18). The isolates also showed high fluoroquinolone resistance, with 81.2% (13/16) to ciprofloxacin and 100% (6/6) to levofloxacin. The aminoglycoside family showed resistance to amikacin (11.1%, 2/18) and gentamicin (33.3%, 6/18). In addition, the penicillin family resisted piperacillin (40%, 2/5) and the sulfonamide-trimethoprim family resisted trimethoprim (50%, 4/8). ESBL were detected in 78.5% of the isolates (11/14).

3.3 Biological and morphological characterization of phages

In this study, we investigated the lytic activity, growth curve, thermal stability, and pH stability of the phages EC.W2-1, EC.W2-6, EC.W13-3, and EC.W14-3. According to the phage adsorption assay, 90% of phages could adsorb onto *E. coli* ATCC25922 within 10 min (Figures 2a–d). The results of the one-step growth curve analysis showed that the phage displayed a latent period of approximately 10–20 min, followed by rapid release of virus particles. The final titer reached a range –$10^{7.5}$ to 10^8 PFU/mL after a burst period of 30–40 min, with a burst size of approximately 50–80 PFUs/cell (Figures 2e–h). Regarding thermal stability, there were no significant changes in the titers of the four phages after incubation at temperatures ranging from 4 to 60°C for 60 min. However, phage titers showed a substantial decrease at 70°C, and were completely inactivated at 80°C. Furthermore, these phages were stable over a pH range of 2–10 within 4 h, with the optimal pH for stability being between 6 and 8 (Figures 3a–h). Four phages were isolated from the hospital sewage water. After incubation at 37°C for 18 h on a double-layer agar plate, clear plaques with diameters of approximately 1–2 mm. Transmission electron microscopy (TEM) images revealed that EC.W2-1, EC.W13-3, and EC.W14-3 had an icosahedral head measuring 100 ± 2 to 115 ± 5 nm in diameter, along with a contracted tail measuring approximately 100 ± 4 to 113 ± 2 nm in length. In contrast, the EC.W2-6 phage had a head size of 60 ± 3 nm and tail size of 8 ± 2 nm (Shamsuzzaman et al., 2024).

TABLE 1 Bacteriolytic activities of isolated bacteriophages to kill *Escherichia coli* ST131 clone.

E. coli isolates ST131	ΦEC. W2-1 (PP445228)	ΦEC. W2-6 (PP445229)	ΦEC. W13-3 (PP496997)	ΦEC. W14.3 (PP496998)
KBN10P03440	+	+	+	+
KBN10P03979	+	+	+	+
KBN10PO7282	+	+	+	+
KBN10PO7288	+	+	+	+
KBN10P01569	–	–	+	+
KBN10P03452	+	+	+	+
KBN10P03005	+	+	+	+
KBN10P00128	+	+	+	+
KBN10P00238	+	+	+	+
KBN10P02048	+	+	–	–
KBN10P00547	+	+	+	+
KBN10P05638	+	+	+	+
KBN10P06781	+	+	+	+
KBN10P06658	+	+	+	+
KBN10P02511	+	+	+	+
KBN10P05702	+	+	+	+
KBN10P05883	+	+	+	+
KBN10P01583	+	+	+	+

(+) indicates clear lysis, and (–) indicates no lysis observed.

3.4 Phylogenetic analysis of phages

The phylogenetic relationship of the novel phages was determined through a comparative analysis of their whole genome sequences with the closest known species of *Straboviridae* and *Podoviridae E. coli* phages. The analysis revealed that EC.W2-1 and EC.W13-3 exhibited the highest DNA sequence similarities to the *Tequatrovirus* genus in the *Straboviridae* family, and phages Escherichia phage vB_EcoM_G4498 (complete genome) and Escherichia phage vB_EcoM_NBG2 (complete genome). For these isolates, the query coverage and percentage identity were recorded as 99/96.45% and 92/95.40%, respectively. On the other hand, EC.W2-6 and EC.W14-3 displayed the highest DNA sequence similarities to the *Kuravirus* genus in the *Podoviridae* family, and Escherichia phage vB_EcoP_SU10 (complete genome) and Escherichia phage 172-1(complete genome), with a query coverage and percentage identity of 94/96.21% and 89/89.62%, respectively (Table 2). Based on the analysis of their sequences and phylogenetic relationships, the phages were identified as new members of the *Straboviridae* and *Podoviridae* families.

3.5 Genomic feature of four novel *Escherichia coli* phage

Whole-genome sequence analysis indicated that EC.W2-1, EC.W2-6, EC.W13-3, and EC.W14-3 had circular double-stranded DNA structures, with genome sizes of 46,325, 67,000, 113,909, and 69,164 bp, respectively. Additionally, the G + C contents were found to be 35.5, 38.3, 35.3, and 35.1%, respectively (Table 2). Genome analysis revealed the absence of virulence or drug resistance genes, which enhanced their safety profiles. The CGView server and Geneious Prime generated visual representations of circular genomes, showcasing various aspects such as sequence characteristics, base composition plots, analysis outcomes, and sequences. These visual images provide a comprehensive and intuitive visualization of the genomes, allowing for a better understanding of their structural and compositional features (Supplementary Figures S1a–d). Phylogenetic analysis carried out using the VIPtree showed that EC.W2-1 and EC.W13-3 phages were most closely related to Escherichia phage vB_EcoM_G4498 (NC_054918) Escherichia phage ECO4 (NC_054911), Escherichia phage vB_EcoM_G9062 (NC_054920), Escherichia phage MN03 (NC_070990), and Escherichia phage vB_EcoP-(NC_070989). On the other hand, EC.W2-6, and EC.W14-3 close related to Escherichia phage ECO4 (NC_054911) Escherichia phage 172–1 (NC_028903). All phages belong to the novel genera *Tequatrovirus* and *Kuravirus* within the families *Straboviridae* and *Podoviridae* (Supplementary Figure S2). In addition, alignment with their closest neighbor using the MAUVE alignment tool suggested that these isolates are closely related and share recent common ancestors. However, small localized regions were identified, indicating functional differences between these phages. These findings suggest unique characteristics and capabilities of genetic makeup (Figure 4). Phylogenetic analysis conducted through genome comparisons using the TYGS server also supported EC.W2-1, EC.W2-6, EC.W13-3, and EC.W14-3, which are novel members of the genera *Tequatrovirus and Kuravirus* (Supplementary Figure S3). Analysis of the genome sequences of EC.W2-1, EC.W2-6, EC.W13-3, and EC.W14-3 revealed that these phages contained 71, 125, 189, and

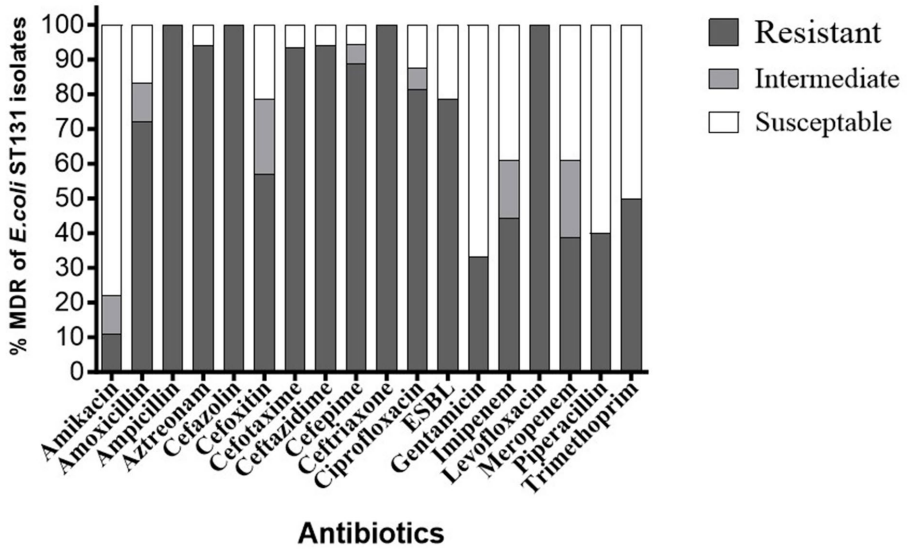

FIGURE 1
Antibiotic resistance ratios of different *E. coli* ST131 isolates. % Resistance indicates the proportion of isolates of *E. coli* ST131 that resist each antibiotic.

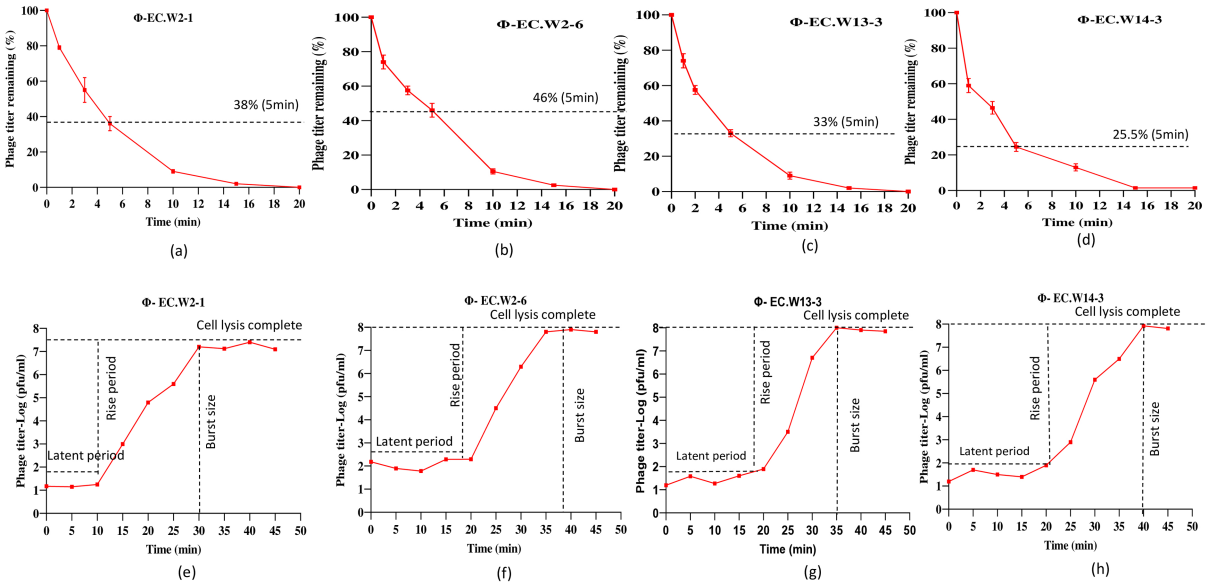

FIGURE 2
Adsorption rate and burst size of four phages to the *E. coli* ATCC25922. (a–d) Adsorption assay measuring the percentage of remaining free phages over 20 min at MOI of 0.0001 and (e–h) one-step growth curve showing the latent period and burst size of four novel *E. coli* bacteriophages in BHI medium at MOI of 0.0001. Values represent means ± standard deviations from the duplication of each treatment.

113 predicted open reading frames (ORFs), respectively. All these ORFs were located on the positive strand of the genome. There are no potential tRNA-coding genes in the genomes of these phages. Among all the ORFs identified in these phages, the predicted proteins have known potential functions related to various processes such as endolysin, holin, tail fiber protein, DNA replication/transcription/packaging, and cell lysis. On the other hand, the remaining ORFs have been classified as hypothetical proteins.

3.6 *In vitro* bactericidal activity of phages

In vitro bactericidal activity of phages against *E. coli* ATCC25922 at various MOIs (Supplementary Figure S4). Within 24 h, the OD_{600} value of the positive control increased continuously from 0.05 to 1.25, whereas that of the negative control remained unchanged. Phage treatment significantly inhibited *E. coli* ATCC25922 growth at all MOIs within the first 8 h. However, the OD_{600} values gradually increased after 8 h of phage treatment. After 24 h, there was a

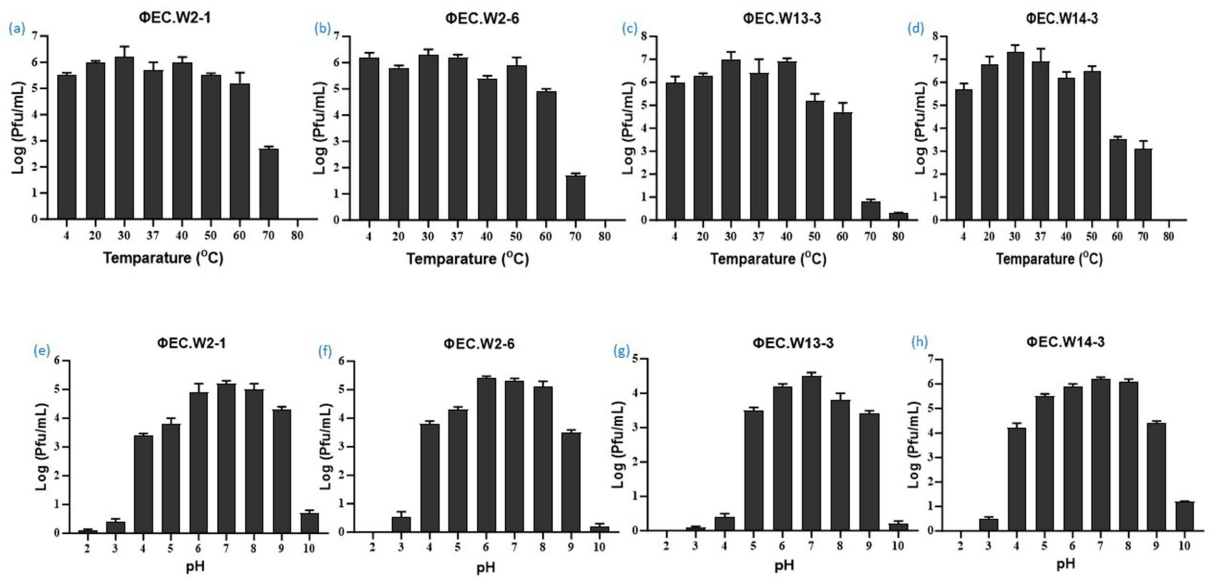

FIGURE 3
Stability of four novel *E. coli* bacteriophages. (a–d) Effect of temperature on phage stability, with phages treated at 4, 20, 30, 37, 40, 50, 60, 70, and 80°C for 1 h, and surviving phage titers calculated. (e–f) pH stability of phages, with concentrations (~10^8 PFU/mL) incubated at pH 2 to 10 at 37°C for 4 h. Values represent means ± standard deviations from triplicate treatments.

significant difference in the OD_{600} values compared to the positive control and a considerable difference in the MOI values. The OD_{600} values continued to rise gradually until 24 h. Although the bacterial counts for all MOIs exceeded 10^8 CFU/mL at 24 h, there was a significant difference between MOI 10 and 0.001 compared to the positive control. Interestingly, MOI 10 exhibited better lytic activity in the first 12 h than other MOI values. However, after 24 h, an MOI of 0.001 resulted in higher lytic activity. These findings demonstrated that these phages could significantly inhibit bacterial growth at all MOIs, with the highest bactericidal activity observed at an MOI of 0.001 after 24 h.

3.7 Comparative evaluation of *in vitro* lytic activity of individual phage's and phage cocktails

This study compared individual phages and cocktails to determine their ability to inhibit bacterial growth in two *E. coli* strains (ATCC25922-ST73 and KBN7288-ST131). Analysis of bacterial growth curves over 24 h revealed that both individual phages and phage cocktails significantly inhibited *E. coli* ATCC25922 growth throughout the study. Specifically, from 0 to 12 h, the individual phages and cocktail significantly suppressed the bacterial growth. However, during the 6–10-h timeframe, the cocktail composed of EC.W2-1 and EC.W2-6 showed slightly lower inhibition than individual phages. Notably, after 24 h, the phage cocktail consisting of EC.W2-6 and EC.W13-3 showed a high level of bacterial growth inhibition (Figure 5a). Similarly, when evaluating the lytic activity of individual phages and the phage cocktail against *E. coli* KBN 7288 (ST131), no significant changes in growth inhibition were observed within the first 4 h. However, after 4 h, the phages displayed varying levels of lytic activity. Consistent with these findings, the phage cocktail consisting of EC.W2-6 and ECW13-3 exhibited high inhibition of *E. coli* KBN 7288 growth after 24 h (Figure 5b). This study also analyzed the lytic activity against *E. coli* KBN 7288 by using various MOI of phage cocktails and compared with their single phage, where the cocktail (EC.W2-6 and ECW13-3) at MOI 10 and MOI 1 provided better lytic activity against *E. coli* KBN 7288. However, there were no significant differences among the other MOIs of the phage cocktail (Supplementary Figure S5).

3.8 Evaluation of the efficacy of phages to treat *Escherichia coli* ST 131 *in vivo*

The aim of this study was to assess the effectiveness of a phage-and-phage combination against *E. coli* ST131. Mice treated with phage EC.W13-3 at MOIs of 10 and 1 exhibited approximately 80% survival rates within 7 days. In contrast, the untreated positive control group experienced 100% mortality within 3 days, whereas the negative control group showed complete survival (Figure 6a). The study also monitored changes in the body weight of mice, revealing weight gains in mice treated with EC.W13-3 at MOIs of 10 and 0.01, indicating positive therapeutic effects. Conversely, mice exposed to a lower MOI of 0.001 or the control group displayed gradual weight loss, suggesting disease progression or ineffective treatment (Figure 6b). Additionally, a 3-day repeated treatment of EC.W13-3 at MOI 0.1 and MOI 0.001 significantly increased the survival rate by approximately 40% (Figure 6c). When investigating the effects of single phages EC.W2-6 and EC.W13-3 and their combination at MOI 01, the combination demonstrated a 100% survival rate in mice, whereas the survival rates for single phages were 60 and 80% (Figure 6d). This study evaluated the impact of individual phage treatments, including EC.W2-1, EC.W2-6, EC.W13-3, and EC.W14-3, on

TABLE 2 Genomic information of four *E. coli* bacteriophages.

Phage isolates	ΦEC.W2-1	ΦEC.W2-6	ΦEC.W13-3	ΦEC.W14-3
Accession number	PP445228	PP445229	PP496997	PP496998
Class	*Caudoviricetes*	*Caudoviricetes*	*Caudoviricetes*	*Caudoviricetes*
Family	*Straboviridae*	*Podoviridae*	*Straboviridae*	*Podoviridae*
Genus	*Tequatrovirus*	*Kuravirus*	*Tequatrovirus*	*Kuravirus*
G + C	35.5	38.3	35.3	35.1
Genome size (BP)	46,325	67,000	113,909	69,164
Hypothetical protein	31	72	26	20
Phage finder	33	13	71	12
Integration/excision	–	1	–	–
Replication/recombination	3	1	9	1
Stability/transfer/defense	–	–	2	–
Alien hunter	3	2	1	–
Endolysin	–	1	–	–
Holin	–	–	1	–
Tail fiber/spike protein	5	5	5	5
Lysis protein	2	2	3	–
Putative peptidase	–	1	–	1
Internal protein	–	1	–	–
Endonuclease	1	–	–	–
Glutaredoxin	2	–	13	–
Packaging machinery	–	2	–	3
Head protein	1	2	–	–
Thymidylate synthesis	1	1	–	1
Capsid protein	7	–	1	2
Baseplate protein	7	–	6	1
Genomic similarity	NC_054933.1	NC_028903.1	NC_042129.1	NC_027395.1
Query cover/Per. Ident (%)	99/96.4%	88/93.6%	92/95.4%	93/96.21

bacterial burden in various organs of a mouse model. Treatment with each phage substantially reduced the bacterial load across multiple organs, and phage counts (PFU/g) were calculated from the plaques on *E. coli* 10P0 KBN7288. Specifically, treatment with EC.W2-1 resulted in a significant reduction in bacterial load in the kidneys (2.5 log10 cfu/g), lungs (2.5 log10 cfu/g), liver (1.9 log10 cfu/g), and spleen (1.7 log10 cfu/g) (Figure 7a). Similarly, EC.W2-6 exhibited efficacy, demonstrating significant reductions in bacterial burden in the kidneys (3.2 log10 cfu/g), lungs (1.8 log10 cfu/g), liver (2.20 log10 cfu/g), and spleen (1.75 log10 cfu/g) (Figure 7b). Furthermore, treatment with EC.W13-3 resulted in notable reductions in log10 cfu/g, approximately 3 in the kidneys, 2.5 in the lungs, 2.55 in the liver, and 1.5 in the spleen (Figure 7c). In addition, EC.W14-3 significantly reduced log10 cfu/g by 2.7 in the lungs, 2.5 in the kidneys, 1.9 in the liver, and approximately 2.4 in the spleen (Figure 7d). Moreover, combining EC.W2-6 and EC.W13-3 in a cocktail showed enhanced effectiveness compared with individual phage treatments. This combination led to a remarkable reduction in bacterial burden in the kidneys (3.3 log10 cfu/g), lungs (3 log10 cfu/g), liver (2.5 log10 cfu/g), and spleen (2.5 log10 cfu/g) (Figure 7e).

4 Discussion

In this study, four *E. coli* phages (EC.W2-1, EC.W2-6, EC.W13-3, and EC.W14-3) were isolated in the hospital sewage water. Morphological features and sequence analysis revealed that phages have strong similarities to the *Straboviridae* and *Podoviridae* families, positioning them as promising candidates for phage-based therapies against *E. coli* infections because of their ability to effectively target and eliminate *E. coli* bacteria and combat antibiotic resistance (Koonjan et al., 2021; Wolfram-Schauerte et al., 2022). Our isolated phages displayed a broad host range, effectively targeting 94.44% (17/18) of *E. coli* ST131 isolates. Additionally, they exhibited lytic activity against 14 different ST types, including 60 MDR *E. coli* isolates, with lytic percentages ranging from 50.0 to 56.6% (Shamsuzzaman et al., 2024). The

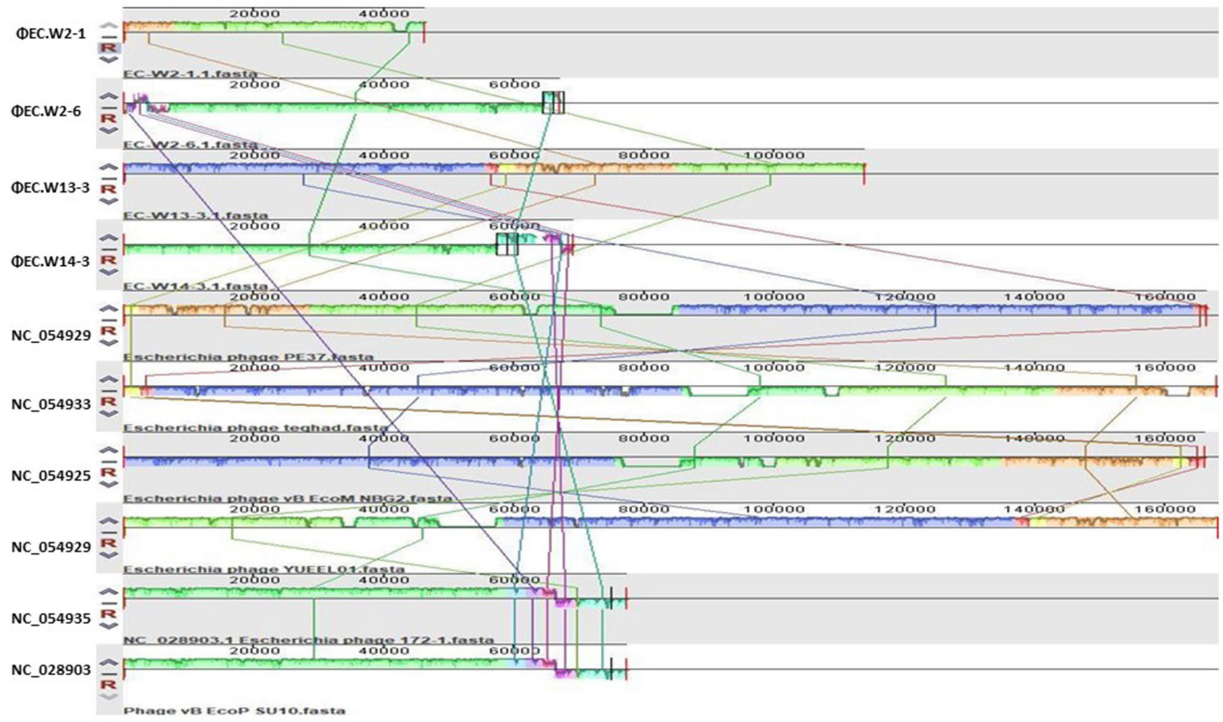

FIGURE 4
This study employed the progressive Mauve algorithm (v2.3.1) to perform multiple alignments of the genomes of 4 novel *E. coli* bacteriophages and the six closest genomes of *E. coli* bacteriophages. The objective was to investigate the rearrangement patterns and synteny in these genomes. The genomes were laid out horizontally, with homologous segments represented by colored blocks. The regions outside the blocks lacked homology and were represented by white areas, which were unique to each genome and not aligned.

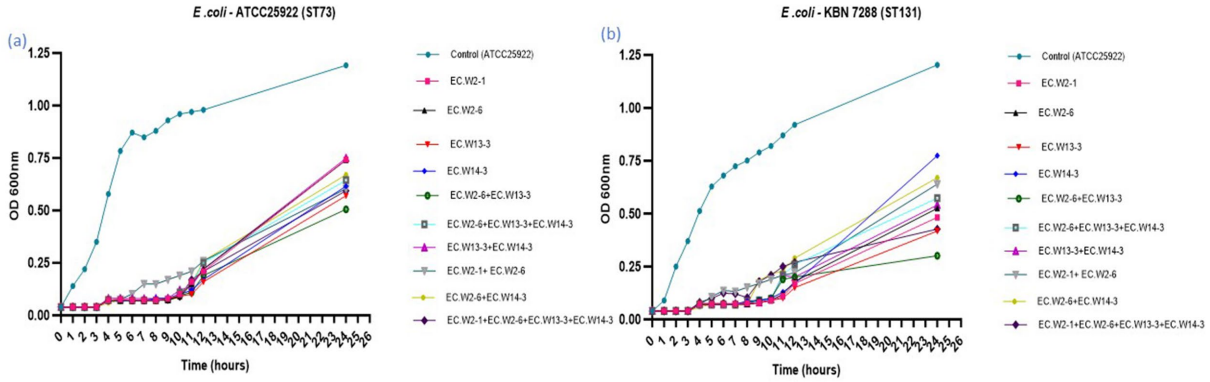

FIGURE 5
Lytic activity of four *E. coli* phages and their cocktail at MOI 0.001 against *E. coli* KBN 7288 (ST131) and *E. coli* ATCC 25922 (ST73).

phages remained stable over a wide pH range (2–10) and at temperatures ranging from 4 to 60°C, indicating their ability to survive under various environmental conditions. The extremely low optimal incubation period and moderate burst size highlighted the high proliferation efficiency and lytic activity of these phages. In an *in vivo* experiment, phage treatment significantly reduced the bacterial load, making them potential candidates for phage therapy against *E. coli* ST131 and other ST types of *E. coli* (Dufour et al., 2016; Green et al., 2017).

Whole-genome analysis revealed that none of the four phages contained virulence, antibiotic resistance, or bacterial toxin-related genes, suggesting a minimal risk of promoting antibiotic resistance and making them suitable for treating bacterial infections (Chaudhary et al., 2022). Depolymerases are enzymes that are encoded by phages infecting encapsulated bacteria, typically within open reading frames linked to structural proteins, often found in tail fibers, base plates, and neck regions (Guo et al., 2023). The analysis of isolated phage genomes revealed the presence of several

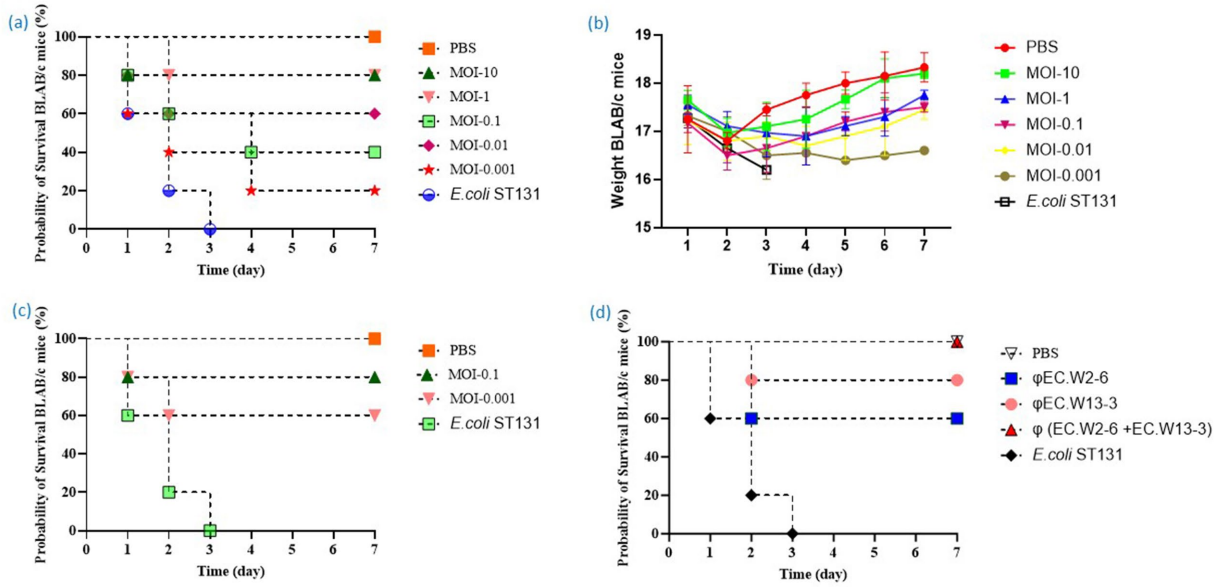

FIGURE 6
This study analyzes the toxicity of *E. coli* ST131 (KBN 7288) in BALB/c mice, identifies the optimal MOI for effective survival in phage therapy, and evaluates the efficacy of single phage and phage cocktails. (a) Survival curve of mice treated with phage EC.W13-3 at various MOIs or PBS. (b) Weight changes in mice one-week post *E. coli* administration. The weights of mice in the free phage group, mice treated with phage EC.W13-3 at various MOIs, and negative control groups were monitored for 2 week. (c) Evaluation of the efficacy of repeated phage therapy against *E. coli* ST131. The survival curve of mice given phage EC.W13-3 for 3 days at MOI-0.1 and MOI-0.001. (d) The study evaluates the efficacy of single phage and phage cocktail therapy against *E. coli* ST131 at MOI-0.1 in a mice model. The bacterial dose of 10^9 CFU was injected at 0 h, and after 1 h, the mice were infected with 10^9 PFU of phage.

tail fiber proteins with a high degree of similarity, ranging from 94 to 100%, to those found in other *E. coli* phages (Supplementary Table S3). By recognizing specific ligands on bacterial surfaces, these depolymerases specifically target capsular polysaccharides (CPSs) and lipopolysaccharides (LPSs), resulting in the breakdown of their repeating units of polysaccharides (Cai et al., 2023). Instead of directly killing bacteria, phage depolymerase strips away the protective polysaccharide layers, rendering the bacteria vulnerable to the immune system and antibacterial agents (Topka-Bielecka et al., 2021). Based on this information, we can assume that these phages could produce these enzymes, resulting in the high killing ability of *E. coli* ST131 isolates. Phage EC.W2-6 is an interesting bacteriophage that contains an endolysin with a remarkable 98.77 and 96.93% similarity to the endolysins found in Escherichia phages (YP_001671762, YP_00920818). Endolysins are enzymes that target bacterial cell wall peptidoglycans and cause cell lysis (Murray et al., 2021). Their specificity, unique mode of action, and lack of resistance mechanisms make them promising alternatives to antibiotics, particularly for combating multidrug-resistant infections (Nelson et al., 2012). Analysis of phage genomes revealed several proteins potentially crucial for combating MDR *E. coli*, especially ST131. These include holins, membrane proteins forming pores to release phage progeny (Fernandes and São-José, 2016); putative peptidases, involved in protein breakdown (Matsumi et al., 2005); replication, recombination, and repair proteins, maintaining phage genome integrity (Poteete, 2004); and packaging machinery proteins for DNA packaging and phage assembly (Isidro et al., 2004). Baseplate proteins facilitate host recognition and infection (Leiman et al., 2003). While the roles of several hypothetical proteins remain unclear, a full understanding of these proteins is essential for optimizing phage therapy (Shang et al., 2023).

To use phages to treat human bacterial infections, translation from *in vitro* activity to *in vivo* efficacy is not guaranteed, despite a high success rate (Dufour et al., 2016). Our investigation into the potential of the four isolated phages revealed that they could infect targeted ST131 isolates and reduce the bacterial load in the survival of mice models. Using animal pneumonia, septicemia, and urinary tract infection models, isolated phages LM33_P1 and HP3 showed *in vivo* efficacy in reducing bacterial load in several organs (Dufour et al., 2016; Green et al., 2017). This study found that a combination of phages (phage cocktail) and repeated phage therapy was much more effective than a single-dose phage therapy. Repeated phage therapy using the EC.W13-3 phage at an MOI of 0.1 and MOI 0.001 significantly increased the survival rate. The survival rate increased from 40 to 80% at MOI 0.1 and from 20 to 60% at MOI 0.001. Additionally, using the phage cocktails EC.W2-6 and EC.W13-3 resulted in 100% survival, whereas single-phage therapy achieved 60 and 80% survival rates at MOI-01, respectively. A previous study showed that the application of phage cocktails and repeated phage treatments can remarkably reduce the bacterial load of nosocomial pathogens in hospital wastewater (Weissfuss et al., 2023). According to this study, phage treatment effectively reduced bacterial counts in different organs. Specifically, phages EC.W2-1 and EC.W2-6 were found to have lower bacterial counts in the kidneys, lungs, liver, and spleen. Additionally, phages EC.W13-3 and EC.W14-3 also showed

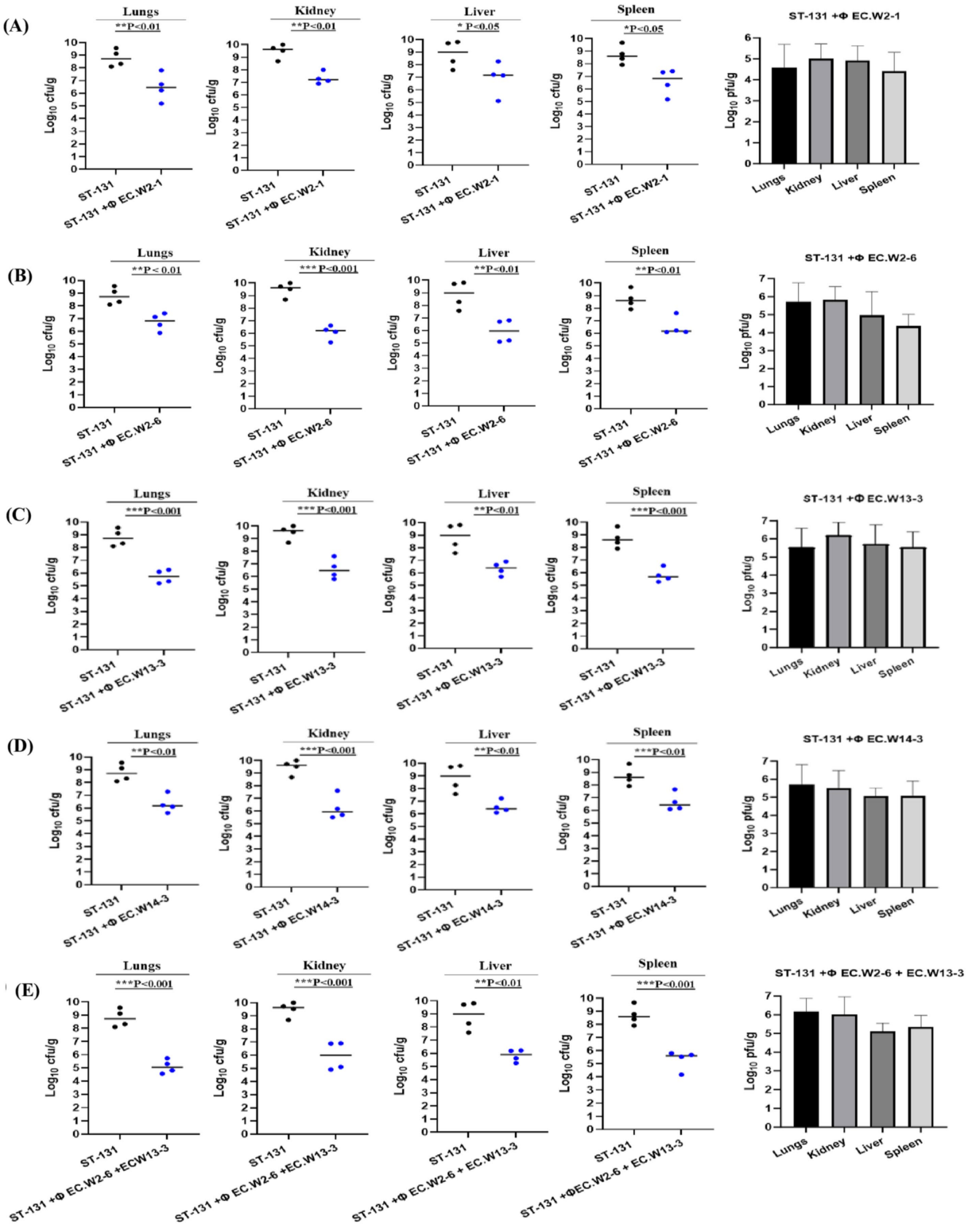

FIGURE 7
Phage therapy in a mouse model of ST131 MDR bacteraemia. BALB/c, 6-week-old female mice, were infected with an intraperitoneal (IP) injection of 10^9 CFU of *E. coli* KBN7288. One hour post-infection, mice received an IP with 10^9 PFU of four purified *E. coli* phages individually **(A)** EC.W2-1, **(B)** EC.W2-6, **(C)** EC.W13-3, **(D)** EC.W14-3, and as a cocktail **(E)** EC.W2-6 + EC.W13-3. Disease severity was evaluated, and organ samples were collected and plated to determine bacterial CFU and phage PFU. The efficacy of each treatment was assessed based on the CFU of *E. coli* KBN7288 in various organs. Black dots represent individual mice given bacteria alone, and blue dots represent the phage-treated, infected mice. Black bars represent the mean values for each group. The *p*-values were generated using a *T*-test, with one, two, or three stars denoting the significance level. One star (*) indicates $p < 0.05$, two stars (**) indicate $p < 0.01$, and three stars (***) indicate $p < 0.001$. Error bars denote standard deviation ($n = 4$).

significant reductions in the bacterial load. This study also found that combining EC.W2-6 and EC.W13-3 in a cocktail enhanced the effectiveness of treatment, resulting in reduced bacterial levels across all organs. Although these results are promising, it is essential to note that animal experiments have limitations and caution should be exercised when translating these findings to the clinical setting (Henry et al., 2013). Bacterial resistance to phage infection is a significant challenge (Örmälä and Jalasvuori, 2013), compounded by the impact of the human immune system (Łusiak-Szelachowska et al., 2014), including the production of anti-phage antibodies (Bearden et al., 2005). Previous research has shown that the vital antibody response to φX-174 serves as a crucial indicator of immune responsiveness in humans (Bearden et al., 2005), with significant implications for individuals with conditions such as HIV (Bernstein et al., 1985), genetic immunodeficiencies (Shearer et al., 2001) and those undergoing immunosuppressive treatments (Hayashi et al., 2018). In a clinical study involving immunocompromised 60% patients receiving phage therapy for bacterial infections, the local administration of phage resulted in low antibody neutralization in serum, suggesting potential efficacy in high-risk patient populations (Green et al., 2017).

This study demonstrates a significant advancement in phage therapy against MDR *E. coli* ST131. Four novel phages, isolated from hospital sewage, exhibited high individual lytic efficacy (>90%), surpassing the effectiveness of previously reported phages such as ΦLM33_P1 (70% efficacy against ST131 and ST69), ΦHP3, ΦEC1, and ΦCF2 (Dufour et al., 2016; Green et al., 2017). The increased efficacy of our phages is likely due to their greater potency and taxonomic diversity. Unlike earlier phages from the *Autographiviridae* and *Myoviridae* families, our phages belong to the *Straboviridae and Podoviridae* families, indicating distinct mechanisms of action and host interactions (Koonjan et al., 2021; Wolfram-Schauerte et al., 2022). Most importantly, our phage cocktail showed superior *in vitro* and *in vivo* performance, highlighting the promise of combination phage therapy as a more effective treatment for *E. coli* ST131 in clinical settings (Weissfuss et al., 2023).

5 Conclusion

Finally, this research highlights the serious global health threat of multidrug-resistant bacterial strains, specifically the *E. coli* ST131 clone. This study isolated four lytic phages (EC.W2-1, EC.W2-6, EC.W13-3, EC.W14-3) from hospital sewage water. These phages showed a broad host range and effectively lysed 94.4% of highly pathogenic *E. coli* ST131 isolates. They exhibited stability under different pH and temperature conditions and demonstrated strong lytic activity *in vitro*. Genomic analysis indicated the lack of virulence or drug-resistance genes. *In vivo* experiments confirmed that the phages effectively protected against MDR *E. coli* ST131 colon. In the injectional mice model, single phage and phage cocktail administrations improved survival rates and significantly reduced bacterial load in various organs. Based on this comprehensive evaluation, we propose phage EC.W2-1. EC.W2-6, EC.W13-3 and EC.W14-3 are potential solutions for targeting the ST131 pandemic. They provide hope amidst the growing threat of multidrug-resistant bacterial infections.

Data availability statement

The complete genome sequences of phages EC.W2-1, EC.W2-6, EC.W13-3, and EC.W14-3 have been deposited in GenBank with the NCBI accession numbers PP445228, PP445229, PP496997 and PP496998, respectively.

Ethics statement

The animal studies were approved by the Kyungpook National University Animal Care and Use Committee. The studies were conducted in accordance with the local legislation and institutional requirements. Written informed consent was obtained from the owners for the participation of their animals in this study.

Author contributions

MS: Conceptualization, Formal analysis, Methodology, Software, Visualization, Writing – original draft, Writing – review & editing. SK: Formal analysis, Investigation, Methodology, Resources, Validation, Visualization, Writing – review & editing. JK: Conceptualization, Funding acquisition, Project administration, Resources, Supervision, Validation, Visualization, Writing – review & editing.

Funding

The author(s) declare that financial support was received for the research, authorship, and/or publication of this article. This research was supported by a grant from the Korea Disease Control and Prevention Agency (Grant No. 2022-ER2202-00).

Conflict of interest

The authors declare that the research was conducted in the absence of any commercial or financial relationships that could be construed as a potential conflict of interest.

Publisher's note

Supplementary material

The Supplementary material for this article can be found online at: https://www.frontiersin.org/articles/10.3389/fmicb.2024.1455710/full#supplementary-material

References

Baek, Y. J., Kim, Y. A., Kim, D., Shin, J. H., Uh, Y., Shin, K. S., et al. (2021). Risk factors for extended-Spectrum-β-lactamase-producing *Escherichia coli* in community-onset bloodstream infection: impact on long-term care hospitals in Korea. *Ann. Lab. Med.* 41, 455–462. doi: 10.3343/ALM.2021.41.5.455

Banerjee, R., and Johnson, J. R. (2014). A new clone sweeps clean: the enigmatic emergence of *Escherichia coli* sequence type 131. *Antimicrob. Agents Chemother.* 58, 4997–5004. doi: 10.1128/AAC.02824-14

Bearden, C. M., Agarwal, A., Book, B. K., Vieira, C. A., Sidner, R. A., Ochs, H. D., et al. (2005). Rituximab inhibits the in vivo primary and secondary antibody response to a Neoantigen, bacteriophage phiX174. *Am. J. Transplant.* 5, 50–57. doi: 10.1111/j.1600-6143.2003.00646.x

Bernstein, L. J., Ochs, H. D., Wedgwood, R. J., and Rubinstein, A. (1985). Defective humoral immunity in pediatric acquired immune deficiency syndrome. *J. Pediatr.* 107, 352–357. doi: 10.1016/S0022-3476(85)80505-9

Bevan, E. R., Jones, A. M., and Hawkey, P. M. (2017). Global epidemiology of CTX-M β-lactamases: temporal and geographical shifts in genotype. *J. Antimicrob. Chemother.* 72, 2145–2155. doi: 10.1093/JAC/DKX146

Cai, R., Ren, Z., Zhao, R., Lu, Y., Wang, X., Guo, Z., et al. (2023). Structural biology and functional features of phage-derived depolymerase Depo32 on *Klebsiella pneumoniae* with K2 serotype capsular polysaccharides. *Microbiol. Spectr.* 11:e0530422. doi: 10.1128/SPECTRUM.05304-22

Chaudhary, N., Singh, D., Maurya, R. K., Mohan, B., Mavuduru, R. S., and Taneja, N. (2022). Whole genome sequencing and in vitro activity data of Escherichia phage NTEC3 against multidrug-resistant Uropathogenic and extensively drug-resistant Uropathogenic *E. coli* isolates. *Data Brief* 43:108479. doi: 10.1016/J.DIB.2022.108479

CLSI. (2020). Performance standards for antimicrobial susceptibility testing: 20th informational supplement. Available at: cir.nii.ac.jp (Accessed November 5, 2024).

de Almeida Kumlien, A. C. M., Borrego, C. M., and Balcázar, J. L. (2021). Antimicrobial resistance and bacteriophages: an overlooked intersection in water disinfection. *Trends Microbiol.* 29, 517–527. doi: 10.1016/j.tim.2020.12.011

Dufour, N., Clermont, O., La Combe, B., Messika, J., Dion, S., Khanna, V., et al. (2016). Bacteriophage LM33_P1, a fast-acting weapon against the pandemic ST131-O25b: H4 *Escherichia coli* clonal complex. *J. Antimicrob. Chemother.* 71, 3072–3080. doi: 10.1093/JAC/DKW253

Emencheta, S. C., Onugwu, A. L., Kalu, C. F., Ezinkwo, P. N., Eze, O. C., Vila, M. M. D. C., et al. (2024). Bacteriophages as nanocarriers for targeted drug delivery and enhanced therapeutic effects. *Mater. Adv.* 5, 986–1016. doi: 10.1039/D3MA00817G

Fernandes, S., and São-José, C. (2016). More than a hole: the holin lethal function may be required to fully sensitize bacteria to the lytic action of canonical endolysins. *Mol. Microbiol.* 102, 92–106. doi: 10.1111/MMI.13448

Green, S. I., Kaelber, J. T., Li, M., Trautner, B. W., Ramig, R. F., and Maresso, A. W. (2017). Bacteriophages from ExPEC reservoirs kill pandemic multidrug-resistant strains of clonal group ST131 in animal models of bacteremia. *Sci. Rep.* 7:46151. doi: 10.1038/srep46151

Guo, Z., Liu, M., and Zhang, D. (2023). Potential of phage depolymerase for the treatment of bacterial biofilms. *Virulence* 14:2273567. doi: 10.1080/21505594.2023.2273567

Hayashi, N., Akamatsu, H., Iwatsuki, K., Shimada-Omori, R., Kaminaka, C., Kurokawa, I., et al. (2018). Japanese dermatological association guidelines: guidelines for the treatment of acne vulgaris 2017. *J. Dermatol.* 45, 898–935. doi: 10.1111/1346-8138.14355

Henry, M., Lavigne, R., and Debarbieux, L. (2013). Predicting in vivo efficacy of therapeutic bacteriophages used to treat pulmonary infections. *Antimicrob. Agents Chemother.* 57, 5961–5968. doi: 10.1128/AAC.01596-13

Hibstu, Z., Belew, H., Akelew, Y., and Mengist, H. M. (2022). Phage therapy: a different approach to fight bacterial infections. *Biologics* 16, 173–186. doi: 10.2147/BTT.S381237

Hon, K., Liu, S., Camens, S., Bouras, G. S., Psaltis, A. J., Wormald, P. J., et al. (2022). APTC-EC-2A: a lytic phage targeting multidrug Resistant *E. coli* planktonic cells and biofilms. *Microorganisms* 10:102. doi: 10.3390/microorganisms10010102

Isidro, A., Henriques, A. O., and Tavares, P. (2004). The portal protein plays essential roles at different steps of the SPP1 DNA packaging process. *Virology* 322, 253–263. doi: 10.1016/J.VIROL.2004.02.012

Jakočiūnė, D., and Moodley, A. (2018). A rapid bacteriophage DNA extraction method.*Methods and protocols* 1:27. doi: 10.3390/mps1030027

Kim, S., Kim, S. H., Rahman, M., and Kim, J. (2018). Characterization of a *Salmonella Enteritidis* bacteriophage showing broad lytic activity against gram-negative enteric bacteria. *J. Microbiol.* 56, 917–925. doi: 10.1007/s12275-018-8310-1

Kim, S., Song, H., Jin, J. S., Lee, W. J., and Kim, J. (2022). Genomic and phenotypic characterization of Cutibacterium acnes bacteriophages isolated from acne patients. *Antibiotics* 11:1041. doi: 10.3390/antibiotics11081041

Koonjan, S., Cooper, C. J., and Nilsson, A. S. (2021). Complete genome sequence of vb_ecop_su7, a podoviridae coliphage with the rare c3 morphotype. *Microorganisms* 9:1576. doi: 10.3390/microorganisms9081576

Leiman, P. G., Shneider, M. M., Kostyuchenko, V. A., Chipman, P. R., Mesyanzhinov, V. V., and Rossmann, M. G. (2003). Structure and location of gene product 8 in the bacteriophage T4 baseplate. *J. Mol. Biol.* 328, 821–833. doi: 10.1016/S0022-2836(03)00366-8

Łusiak-Szelachowska, M., Zaczek, M., Weber-Dabrowska, B., Międzybrodzki, R., Kłak, M., Fortuna, W., et al. (2014). Phage neutralization by sera of patients receiving phage therapy. *Viral Immunol.* 27, 295–304. doi: 10.1089/VIM.2013.0128

Majewski, P., Gutowska, A., Smith, D. G. E., Hauschild, T., Majewska, P., Hryszko, T., et al. (2021). Plasmid mediated mcr-1.1 Colistin-resistance in clinical Extraintestinal *Escherichia coli* strains isolated in Poland. *Front. Microbiol.* 12:547020. doi: 10.3389/fmicb.2021.547020

Matsumi, R., Atomi, H., and Imanaka, T. (2005). Biochemical properties of a putative signal peptide peptidase from the hyperthermophilic archaeon Thermococcus kodakaraensis KOD1. *J. Bacteriol.* 187, 7072–7080. doi: 10.1128/JB.187.20.7072-7080.2005

Miyoshi-Akiyama, T., Sherchan, J. B., Doi, Y., Nagamatsu, M., Sherchand, J. B., Tandukar, S., et al. (2016). Comparative genome analysis of extended-Spectrum-β-lactamase-producing *Escherichia coli* sequence type 131 strains from Nepal and Japan. *mSphere* 1:e00289-16. doi: 10.1128/mSphere.00289-16

Murray, E., Draper, L. A., Ross, R. P., and Hill, C. (2021). The advantages and challenges of using Endolysins in a clinical setting. *Viruses* 13:680. doi: 10.3390/V13040680

Nelson, D. C., Schmelcher, M., Rodriguez-Rubio, L., Klumpp, J., Pritchard, D. G., Dong, S., et al. (2012). Endolysins as antimicrobials. *Adv. Virus Res.* 83, 299–365. doi: 10.1016/B978-0-12-394438-2.00007-4

Nicolas-Chanoine, M. H., Bertrand, X., and Madec, J. Y. (2014). *Escherichia coli* st131, an intriguing clonal group. *Clin. Microbiol. Rev.* 27, 543–574. doi: 10.1128/CMR.00125-13

Örmälä, A.-M., and Jalasvuori, M. (2013). Phage therapy. *Bacteriophage* 43, 122–125. doi: 10.4161/BACT.24219

Peirano, G., Lynch, T., Matsumara, Y., Nobrega, D., Finn, T. J., DeVinney, R., et al. (2020). Trends in population dynamics of *Escherichia coli* sequence type 131, Calgary, Alberta, Canada, 2006–2016- volume 26, number 12—December 2020- emerging infectious diseases journal - CDC. *Emerg. Infect. Dis.* 26, 2907–2915. doi: 10.3201/eid2612.201221

Poteete, A. R. (2004). Modulation of DNA repair and recombination by the bacteriophage λ Orf function in *Escherichia coli* K-12. *J. Bacteriol.* 186, 2699–2707. doi: 10.1128/JB.186.9.2699-2707.2004

Pu, M., Li, Y., Han, P., Lin, W., Geng, R., Qu, F., et al. (2022). Genomic characterization of a new phage BUCT541 against *Klebsiella pneumoniae* K1-ST23 and efficacy assessment in mouse and galleria mellonella larvae. *Front. Microbiol.* 13:950737. doi: 10.3389/fmicb.2022.950737

Rahman, M., Kim, S., Kim, S. M., Seol, S. Y., and Kim, J. (2011). Characterization of induced *Staphylococcus aureus* bacteriophage SAP-26 and its anti-biofilm activity with rifampicin. *Biofouling* 27, 1087–1093. doi: 10.1080/08927014.2011.631169

Reardon, S. (2014). Phage therapy gets revitalized. *Nature* 510, 15–16. doi: 10.1038/510015A

Rehman, S., Ali, Z., Khan, M., Bostan, N., and Naseem, S. (2019). The dawn of phage therapy. *Rev. Med. Virol.* 29:e2041. doi: 10.1002/RMV.2041

Rogers, B. A., Sidjabat, H. E., and Paterson, D. L. (2011). *Escherichia coli* O25b-ST131: a pandemic, multiresistant, community-associated strain. *J. Antimicrob. Chemother.* 66, 1–14. doi: 10.1093/JAC/DKQ415

Shamsuzzaman, M., Dahal, R. H., Kim, S., and Kim, J. (2023). Genome insight and probiotic potential of three novel species of the genus Corynebacterium. *Front. Microbiol.* 14:1225282. doi: 10.3389/fmicb.2023.1225282

Shamsuzzaman, M., Kim, S., Choi, Y.-J., Kim, B., Dahal, R. H., Shin, M., et al. (2024). Therapeutic phage candidates for targeting prevalent sequence types of Carbapenem-resistant *Escherichia coli*. *Foodborne Pathog. Dis.* doi: 10.1089/FPD.2024.0023

Shang, J., Peng, C., Tang, X., and Sun, Y. (2023). PhaVIP: phage VIrion protein classification based on chaos game representation and vision transformer. *Bioinformatics* 39, i30–i39. doi: 10.1093/BIOINFORMATICS/BTAD229

Shariati, A., Arshadi, M., Khosrojerdi, M. A., Abedinzadeh, M., Ganjalishahi, M., Maleki, A., et al. (2022). The resistance mechanisms of bacteria against ciprofloxacin and new approaches for enhancing the efficacy of this antibiotic. *Front. Public Health* 10:1025633. doi: 10.3389/fpubh.2022.1025633

Shearer, W. T., Lugg, D. J., Rosenblatt, H. M., Nickolls, P. M., Sharp, R. M., Reuben, J. M., et al. (2001). Antibody responses to bacteriophage φX-174 in human subjects exposed to the Antarctic winter-over model of spaceflight. *J. Allergy Clin. Immunol.* 107, 160–164. doi: 10.1067/MAI.2001.112269

Tang, Z., Tang, N., Wang, X., Ren, H., Zhang, C., Zou, L., et al. (2023). Characterization of a lytic *Escherichia coli* phage CE1 and its potential use in therapy against avian pathogenic *Escherichia coli* infections. *Front. Microbiol.* 14:1091442. doi: 10.3389/fmicb.2023.1091442

Topka-Bielecka, G., Dydecka, A., Necel, A., Bloch, S., Nejman-Faleńczyk, B., Węgrzyn, G., et al. (2021). Bacteriophage-derived Depolymerases against bacterial biofilm. *Antibiotics* 10:175. doi: 10.3390/ANTIBIOTICS10020175

Weissfuss, C., Wienhold, S. M., Bürkle, M., Gaborieau, B., Bushe, J., Behrendt, U., et al. (2023). Repetitive exposure to bacteriophage cocktails against *Pseudomonas aeruginosa* or *Escherichia coli* provokes marginal humoral immunity in Naïve mice. *Viruses* 15:387. doi: 10.3390/v15020387

Whelan, S., Lucey, B., and Finn, K. (2023). Uropathogenic *Escherichia coli* (UPEC)-associated urinary tract infections: the molecular basis for challenges to effective treatment. *Microorganisms* 11:2169. doi: 10.3390/MICROORGANISMS11092169

Wolfram-Schauerte, M., Pozhydaieva, N., Viering, M., Glatter, T., and Höfer, K. (2022). Integrated omics reveal time-resolved insights into T4 phage infection of *E. coli* on proteome and transcriptome levels. *Viruses* 14:2502. doi: 10.3390/v14112502

frontiers | Frontiers in Microbiology

TYPE Original Research
PUBLISHED 14 January 2025
DOI 10.3389/fmicb.2024.1513081

OPEN ACCESS

EDITED BY
Gamaliel López-Leal,
Center for Research in Cellular Dynamics-UAEM, Mexico

REVIEWED BY
Laura Bonofiglio,
University of Buenos Aires, Argentina
Rosa Isela Santamaria,
National Autonomous University of Mexico, Mexico

*CORRESPONDENCE
Marina Zaychikova
✉ spirosoma@gmail.com

RECEIVED 17 October 2024
ACCEPTED 12 December 2024
PUBLISHED 14 January 2025

CITATION
Zaychikova M, Malakhova M, Bespiatykh D, Kornienko M, Klimina K, Strokach A, Gorodnichev R, German A, Fursov M, Bagrov D, Vnukova A, Gracheva A, Kazyulina A, Shleeva M and Shitikov E (2025) Vic9 mycobacteriophage: the first subcluster B2 phage isolated in Russia.
Front. Microbiol. 15:1513081.
doi: 10.3389/fmicb.2024.1513081

Vic9 mycobacteriophage: the first subcluster B2 phage isolated in Russia

Marina Zaychikova[1]*, Maja Malakhova[1], Dmitry Bespiatykh[1], Maria Kornienko[1], Ksenia Klimina[1], Aleksandra Strokach[1], Roman Gorodnichev[1], Arina German[2], Mikhail Fursov[3], Dmitry Bagrov[1,4], Anna Vnukova[4], Alexandra Gracheva[5], Anastasia Kazyulina[5], Margarita Shleeva[2] and Egor Shitikov[1]

[1]Lopukhin Federal Research and Clinical Center of Physical-Chemical Medicine of Federal Medical Biological Agency Medicine, Moscow, Russia, [2]Federal Research Centre 'Fundamentals of Biotechnology' of the Russian Academy of Sciences, Moscow, Russia, [3]State Research Center for Applied Microbiology and Biotechnology, Obolensk, Russia, [4]Faculty of Biology, Lomonosov Moscow State University, Moscow, Russia, [5]Federal State Budgetary Institution "National Medical Research Center of Phtisiopulmonology and Infectious Diseases" of the Ministry of Health of the Russian Federation, Moscow, Russia

Mycobacteriophages are viruses that specifically infect bacteria of the Mycobacterium genus. A substantial collection of mycobacteriophages has been isolated and characterized, offering valuable insights into their diversity and evolution. This collection also holds significant potential for therapeutic applications, particularly as an alternative to antibiotics in combating drug-resistant bacterial strains. In this study, we report the isolation and characterization of a new mycobacteriophage, Vic9, using *Mycobacterium smegmatis* mc (2)155 as the host strain. Vic9 has been classified within the B2 subcluster of the B cluster. Morphological analysis revealed that Vic9 has a structure typical of siphophages from this subcluster and forms characteristic plaques. The phage adsorbs onto host strain cells within 30 min, and according to one-step growth experiments, its latent period lasts about 90 min, followed by a growth period of 150 min, with an average yield of approximately 68 phage particles per infected cell. In host range experiments, Vic9 efficiently lysed the host strain and also exhibited the ability to lyse *M. tuberculosis* H37Rv, albeit with a low efficiency of plating (EOP $\approx 2 \times 10^{-5}$), a typical feature of B2 phages. No lysis was observed in other tested mycobacterial species. The genome of Vic9 comprises 67,543 bp of double-stranded DNA and encodes 89 open reading frames. Our analysis revealed unique features in Vic9, despite its close relationship to other B2 subcluster phages, highlighting its distinct characteristics even among closely related phages. Particularly noteworthy was the discovery of a distinct 435 bp sequence within the gene cluster responsible for queuosine biosynthesis, as well as a recombination event within the structural cassette region (Vic_0033-Vic_0035) among members of the B1, B2, and B3 subclusters. These genetic features are of interest for further research, as they may reveal new mechanisms of phage-bacteria interactions and their potential for developing novel phage therapy methods.

KEYWORDS

mycobacteriophages, *Mycobacterium tuberculosis*, host range, B cluster, one-step growth curve

1 Introduction

The genus Mycobacterium contains more than 200 species, among which are pathogens responsible for various infectious diseases, including tuberculosis and leprosy (Armstrong et al., 2023). In the case of tuberculosis disease caused by *Mycobacterium tuberculosis* complex (MTBC) bacteria, one of the most pressing issues is the growing resistance of MTBC strains to antibiotics. This leads to increased costs, prolonged treatment durations, and poorer outcomes for patients. The likelihood of successful treatment of diseases caused by multidrug-resistant and extensively drug-resistant strains does not exceed 60 and 30%, respectively (WHO, 2020). Consequently, tuberculosis is increasingly associated with a poor prognosis, edging closer to being classified as a conditionally incurable disease (Seung et al., 2015). Despite extensive research into novel drugs, resistance within MTBC members rapidly develops, even to the most recent drugs, such as linezolid, bedaquiline, and clofazimine (Seung et al., 2015, Kadura et al., 2020). A similar situation is observed with non-tuberculous mycobacteria (NTM), which also exhibit significant resistance to standard antibiotic therapy and, more importantly, possess innate resistance to a range of drugs, significantly complicating treatment (Saxena et al., 2021). Another challenge in infections caused by NTM is diagnostics, as standardized testing protocols are lacking in some cases, requiring specialized laboratory methods (Bartlett et al., 2024). This highlights the urgent need for novel therapeutic strategies that can be used both in conjunction with antibiotics and as stand-alone alternatives. One such approach could be phage therapy.

Bacteriophages, or simply phages, are viruses that infect bacteria and cause their lysis. The main advantages of phages include their high specificity, which allows them, unlike antibiotics, to target specific bacterial pathogens without affecting the normal microflora of the human body. Phages also have the ability to self-replicate at the site of infection, can be used in combination with other antimicrobial agents, and remain effective against drug-resistant bacterial strains (Kortright et al., 2019). Additionally, certain phages can target bacteria residing within macrophages or biofilms, which are often difficult to eradicate with conventional antibiotics (Meneses et al., 2023; Yang et al., 2024). Despite these advantages, significant barriers hinder the widespread clinical application of phages. One of the main challenges is their high specificity: unlike broad-spectrum antibiotics, phage therapy requires precise identification of the pathogen and the selection of a corresponding phage. Another critical issue is the interaction of phages with the immune system, as phages can both elicit undesirable immune responses and be neutralized by pre-existing or therapy-induced antibodies, potentially reducing their therapeutic efficacy (Kortright et al., 2019; Champagne-Jorgensen et al., 2023).

Currently, thanks to programs like Phage Hunters Integrating Research and Education (PHIRE) and Science Education Alliance Phage Hunters Advancing Genomics and Evolutionary Science (SEA-PHAGES), mycobacteriophages — phages that infect Mycobacterium genus bacteria — are among the most studied groups of phages (Heller et al., 2024). To date, about 10,000 mycobacteriophages have been identified, of which over 2,000 have been sequenced. Mycobacteriophages are classified into clusters and subclusters, with phages not included in any cluster being called singletons. According to the actinobacteriophage database PhagesDB,[1] seven singletons and 34 clusters of mycobacteriophages have been described. Mycobacteriophages within clusters can be broadly divided into lytic and temperate phages, as phages within a cluster tend to be of the same type. However, a significant portion of known mycobacteriophages is temperate, characterized by their integration into the host genome, which limits their use in treating patients with mycobacterial infections (Hatfull, 2023).

In recent years, significant progress has been made in using mycobacteriophages as therapeutic agents. Mycobacteriophages have already been used to treat opportunistic infections caused by NTM, such as *Mycobacterium abscessus*, *Mycobacterium chelonae*, *Mycobacterium avium*, and *Mycobacterium bovis* BCG (Dedrick et al., 2019, 2021, 2023; Little et al., 2022). While human trials using mycobacteriophages to treat tuberculosis have not yet been conducted, the ongoing research shows great promise for their future use. Notably, the liposomal form of lytic mycobacteriophage D29 has shown activity against *M. tuberculosis* in both *in vitro* models of human tuberculosis granulomas and animal studies. Additionally, D29 has demonstrated efficacy as a prophylactic agent in preventing tuberculosis infection in mouse models (Avdeev et al., 2023).

These instances of successful applications of mycobacteriophages highlight the significance of their research. Further progress in this field requires creating extensive and diverse collections of mycobacteriophages, characterized by their host range, to cover a wide variety of species and strains of mycobacteria. Phages in these collections must be thoroughly characterized using microbiological methods to better understand their interactions with bacteria.

In this study, a new mycobacteriophage, Vic9, belonging to subcluster B2 of cluster B, was isolated and characterized. For this phage, as well as for other members of subcluster B2, life cycle parameters were described for the first time, and host specificity was studied across numerous Mycobacterium species. Whole-genome sequencing of Vic9 demonstrated a high level of similarity with other phages from subcluster B2; however, the phage contained several unique features that emphasize its specific genomic organization.

2 Materials and methods

2.1 Bacterial strains and culture condition

In this study we used laboratory strains of *Mycobacterium smegmatis* mc(2)155 and *Mycobacterium tuberculosis* H37Rv acquired from the A.N. Bakh Institute of Biochemistry at the Russian Academy of Science collection, as well as clinical isolates of *Mycobacterium abscessus*, *Mycobacterium fortuitum*, *Mycobacterium avium*, and *Mycobacterium kansasii* from the collection of the Federal State Budgetary Institution "NMITs FPI" of the Ministry of Health of the Russian Federation.

The mycobacteria strains were cultivated in Middlebrook 7H9 broth (Himedia, India) with 0.05% Tween-80 (Sigma-Aldrich, USA) and on solid Middlebrook 7H11 agar (Himedia, India), both containing 10% Middlebrook OADC Supplement (HiMedia, India), in a humid atmosphere with 5% CO_2 at 37°C. For *M. smegmatis* mc(2)155,

1 https://phagesdb.org; as of October 2024.

Tween-80 was not used. In experiments related to phage isolation and cultivation, Middlebrook 7H9 soft agar (0.7%) was used, and $CaCl_2$ was added to all media at a final concentration of 2 mM for *M. smegmatis* mc(2)155 and 1 mM for other mycobacteria. All manipulations with bacterial strains were performed under biosafety level 2 and 3 conditions.

2.2 Isolation of mycobacteriophage

The *M. smegmatis* mc(2)155 strain was used as a host for phage isolation. The isolation of Vic9 phage was carried out as previously described (Gong et al., 2021). Briefly, a soil sample (10 g) was co-incubated with 1 mL of *M. smegmatis* mc(2)155 suspension grown to mid-log phase and 20 µL of ampicillin (50 mg/mL) in 10 mL MP buffer (50 mM Tris–HCl; 150 mM NaCl; 10 mM $MgCl_2$; 2 mM $CaCl_2$; pH 7.5) overnight with agitation. After incubation, the sample was centrifuged at 5,000 g for 10 min at 4°C. The supernatant was first filtered through a 0.45 µm PES membrane (Millipore, USA), and then through a 0.22 µm PES membrane (Millipore, USA). The filtrate (10 mL) was added to 10 mL of double-concentrated TSB (Himedia, India), and inoculated with 2 mL of *M. smegmatis* mc(2)155 suspension grown to mid-log phase and incubated for 48 h with agitation. The double-layer agar plate method was used to detect and isolate the phage (Kropinski et al., 2009). The resulting lysate was serially diluted in Middlebrook 7H9 broth, then 100 µL aliquots were mixed with soft agar inoculated with *M. smegmatis* mc(2)155 grown to mid-log phase and poured onto a prewarmed Middlebrook 7H11 agar plate. Three rounds of single plaque purification and re-infection of exponentially growing host strains yielded pure phage suspensions. Subsequently, phage lysates were stored at 4°C.

2.3 Phage titer

The phage titer was evaluated by standard spot test methodology (Sarkis and Hatfull, 1998). Serial tenfold dilutions of the phage were spotted in 5 µL drops on double-layer agar containing 100 µL of *M. smegmatis* mc(2)155 suspension grown to mid-log phase.

2.4 Electron microscopy of phage

The phage lysate was filtered through a 0.22 µm PES membrane (Millipore, USA) and concentrated by ultracentrifugation at 75,000 g for 1 h at 4°C. The phage particles were resuspended in SM buffer (50 mM Tris–HCl pH 7.5, 100 mM NaCl, 8 mM $MgSO_4$, 0.01% gelatin). A suspension of phages (10^{12} plaque-forming units (PFU)/mL) was deposited onto carbon-coated grids (Ted Pella, USA) treated using a glow discharge device K100X (Quorum Technologies Ltd., Lewes, UK). Following one-minute deposition, the suspension was blotted, and the grids were stained with 1% uranyl acetate and subsecuently dried. The images were acquired using a transmission electron microscope (TEM) JEM-1400 (JEOL, Japan) operating at 120 kV.

2.5 Optimal multiplicity of infection

Mid-log phase *M. smegmatis* mc(2)155 cells were inoculated in Middlebrook 7H9 broth to a concentration of 1×10^7 CFU/mL. The phage was mixed with bacteria at multiplicities of infection (MOIs) of 0.001, 0.01, 0.1, 1, and 10. After incubation with shaking for 48 h, the phage titer was determined using the spot test method (Sarkis and Hatfull, 1998). The experiment was performed in three biological replicates.

2.6 Adsorption curve

The phage adsorption capacity was determined as previously described (Hendrix and Duda, 1992). Briefly, *M. smegmatis* mc(2)155 in mid-log phase and Vic9 phage were mixed at a multiplicity of infection (MOI) of 0.01 in Middlebrook 7H9 broth to a total volume of 5 mL. The mixture was incubated with agitation, and 100 µL aliquots were collected every 10 min over a 1-h period. Each aliquot was immediately centrifuged at 13,800 g for 2 min. The titer of non-adsorbed phage in the supernatant was evaluated using the double-layer agar plate method (Kropinski et al., 2009) as described previously. The experiment was carried out in three biological replicates.

2.7 One-step growth curve

The one-step growth curve of Vic9 phage was carried out as previously described (Gan et al., 2014), with modifications. *M. smegmatis* mc(2)155 in mid-log phase and Vic9 phage were mixed at a MOI of 0.01 in a total volume of 0.9 mL and incubated at 37°C for 30 min to allow phage adsorption. To inactivate unbound phages, 0.1 mL of 100 mM ferrous ammonium sulfate (Sigma-Aldrich, USA) was added to the mixture, following the optimal concentration previously demonstrated to be most effective for phage inactivation (McNerney et al., 1998). After incubation at room temperature for 5 min, the mixture was centrifuged at 13,800 g for 2 min. The pellet was resuspended in 1 mL of Middlebrook 7H9 broth, and the resulting suspension was used to determine the number of infected cells and to construct a one-step growth curve.

The number of infected cells was determined using the double-layer agar plate method (Kropinski et al., 2009) with modifications. Briefly, an aliquot of the suspension, diluted from 10^{-1} to 10^{-7}, was added to soft agar, which additionally contained *M. smegmatis* mc(2)155 in mid-log phase for better visualization. The number of plaques formed was equal to the number of infected cells.

To construct the one-step growth curve, the resulting suspension (100 µL) was additionally diluted 100-fold in Middlebrook 7H9 broth and incubated with agitation. Aliquots were collected every 30 min for 5 h and centrifuged at 13,800 g for 2 min. The titer of free phage in the supernatant was assessed using the double-layer agar plate method (Kropinski et al., 2009). The experiment was carried out in three biological replicates.

The burst size was determined as the number of phages released from each infected cell, calculated by the ratio of the final number of released phage particles to the initial number of infected bacterial cells.

2.8 Host range determination

Phage activity against mycobacterial strains was determined by spot testing on double-layer agar (Sarkis and Hatfull, 1998).

For this, 1 mL of the test bacterial culture suspension was washed twice with fresh Middlebrook 7H9 broth to remove Tween-80. The pellet was resuspended in 100 µL of Middlebrook 7H9 broth and added to 5 mL of soft agar and poured onto Middlebrook 7H11 agar. Tenfold serial dilutions of the phage in MP buffer (initial titer of 10^9 PFU/mL) were spotted in 5 µL drops on the surface of the agar. The plates were incubated for 48 h for fast-growing mycobacteria and 3 weeks for slow-growing ones. The efficiency of plating (EOP) was calculated as the ratio of the phage titer on the test strain to that on the host strain *M. smegmatis* mc(2)155.

2.9 DNA extraction and whole-genome sequencing

Phage genomic DNA was extracted from the lysate using the standard phenol-chloroform extraction protocol (Green et al., 2012). The extracted DNA (100 ng) was used for library preparation using the KAPA HyperPlus Kit (Roche, Switzerland) according to the manufacturer's protocol. The library underwent a final cleanup using KAPA HyperPure Beads (Roche, Switzerland), after which the library size distribution and quality were assessed using a high sensitivity DNA chip (Agilent Technologies). The libraries were then quantified using the Quant-iT DNA Assay Kit, High Sensitivity (Thermo Fisher Scientific). The DNA libraries underwent sequencing using the HiSeq 2,500 platform (Illumina, USA), in accordance with the manufacturer's recommendations. For this purpose, following reagent kits were employed: HiSeq Rapid PE Cluster Kit v2, HiSeq Rapid SBS Kit v2 (200 cycles), and HiSeq Rapid PE FlowCell v2. Additionally, a 2% PhiX spike-in control was included in the process.

2.10 Bioinformatics analysis

2.10.1 Genome assembly

Taxonomic confirmation of the sequenced reads was accomplished with Kraken2 v2.1.2 (Wood et al., 2019) and Bracken v2.8 (Lu et al., 2017). The quality assessment of short paired-end reads was performed using falco v1.2.1 (de Sena Brandine and Smith, 2019) and MultiQC v1.17 (Ewels et al., 2016). Adapters removal and reads filtering was performed using fastp v0.23.4 (Chen et al., 2018). The genome of the Vic9 phage was assembled using Unicycler v0.5.0 and SPAdes v3.15.5. Completeness quality of the assembled phage genome was assessed with CheckV v1.0.1 (Nayfach et al., 2021). Prokka v1.14.6 (Seemann, 2014) and Pharokka v1.7.3 (Bouras et al., 2023) were utilized to annotate the genome's assembly. Subsequently, the annotation was manually curated using GeneMarkS v4.32 (Besemer et al., 2001) to identify open reading frames. ARAGORN v1.2.41 (Laslett and Canback, 2004) was employed to search for tRNA-coding genes. Further gene annotations were carried out using BLASTp v2.13.0 and HHPred (Söding et al., 2005). BWA MEM v0.7.17-r1188 (Li and Durbin, 2009) was employed for mapping reads to the assembly, subsequently SAMtools v1.17 (Danecek et al., 2021) and mosdepth v0.3.5 (Pedersen and Quinlan, 2018) were used to compile mapping statistics. The genome of the Vic 9 phage has been deposited in GenBank under accession number PP526940.2.

2.10.2 Phylogenetic analysis

Mycobacteriophages genomes from PhagesDB (Russell and Hatfull, 2017) and ICTV (Lefkowitz et al., 2018) databases were retrieved using ncbi-acc-download v0.2.8 tool.[2] Retrieved nucleotide sequences of phage genomes were aligned using Kalign 3 v3.4.0 (Lassmann, 2019) with the following parameters: "--type dna --gpo 11 --gpe 0.85 --tgpe 0.45." The resulting alignment was subsequently trimmed using trimAl v1.4.rev15 (Capella-Gutiérrez et al., 2009) with the "-gappyout" option. SeqKit2 v2.8.2 (Shen et al., 2024) was used to remove duplicated sequences from the alignment. The maximum likelihood (ML) phylogeny was inferred from 375 sequences and 54,439 distinct patterns using IQ-TREE 2 v2.3.4 (Minh et al., 2020). Support values were determined from 10,000 ultrafast bootstrap replicates UFBoot (Hoang et al., 2018) with the "-bnni" parameter and from 10,000 replicates for Shimodaira-Hasegawa (SH) approximate likelihood ratio test with the "-altr" parameter. The best-fit model was identified by ModelFinder (Kalyaanamoorthy et al., 2017) implemented in IQ-TREE with the "-m MFP" parameter, and the model selected based on the Bayesian information criterion (BIC) was GTR + F + I + R10. The resulting phylogeny was visualized using the following R v4.3.0 (R Core Team. R: A Language and Environment for Statistical Computing. 2023) packages: tidytree v0.4.5 (Yu, 2022), phylotools v1.9-16,[3] ape v5.7–1 (Paradis and Schliep, 2019), ggnewscale v0.5.0.9000,[4] ggplot2 v3.5.1 (Wickham, 2016), ggtree v3.8.2 (Xu et al., 2022), ggtreeExtra v1.10.0 (Xu et al., 2021), ggstar v1.0.4,[5] cowplot v1.1.1,[6] ggplotify v0.1.2,[7] gtools v3.9.4,[8] colorspace v2.1–0,[9] and gginnards v0.2.0.[10]

Mycobacteriophages of the B cluster were clustered using vConTACT2 v0.11.3 and visualized by Cytoscape v3.10.2 using an edge-weighted spring-embedded model.

2.10.3 Comparative genomics

The genomic organization of the Vic9 genome was visualized using ggplot2 v3.5.1, scales v1.3.0,[11] gggenes v0.5.1,[12] gggenomes v1.0.0,[13] ggrepel v0.9.5,[14] ggwrap v0.0.0.9001,[15] ggpp v0.5.8–1,[16] cowplot v1.1.1, ggtext 0.1.2.[17] The nucleotide sequence of Vic9 was compared with other mycobacteriophages of subcluster B2 from the NCBI database using BLAST.[18] Clinker v0.0.25[19] was used to visualize

2 https://github.com/kblin/ncbi-acc-download
3 https://CRAN.R-project.org/package=phylotools
4 https://CRAN.R-project.org/package=ggnewscale
5 https://CRAN.R-project.org/package=ggstar
6 https://CRAN.R-project.org/package=cowplot
7 https://CRAN.R-project.org/package=ggplotify
8 https://CRAN.R-project.org/package=gtools
9 https://CRAN.R-project.org/package=colorspace
10 https://CRAN.R-project.org/package=gginnards
11 https://CRAN.R-project.org/package=scales
12 https://github.com/wilkox/gggenes
13 https://github.com/thackl/gggenomes
14 https://CRAN.R-project.org/package=ggrepel
15 https://github.com/wilkox/ggwrap
16 https://CRAN.R-project.org/package=ggpp
17 https://CRAN.R-project.org/package=ggtext
18 https://blast.ncbi.nlm.nih.gov/Blast.cgi
19 https://github.com/gamcil/clinker

genomic differences and to construct a comparative map of the recombinant region.

3 Results

3.1 Isolation and phenotypic characterization of the phage

Vic9 was isolated from soil samples collected at a livestock yard in the Moscow region, where small ruminants (goats) were kept. The phage plaques on the host strain *M. smegmatis* mc(2)155 were 1–3 mm in diameter, with clear edges, a round shape, and a turbid center (Figure 1A). Electron microscopy revealed that Vic9 exhibits typical siphophage morphology, characterized by an icosahedral head, 68 ± 2 nm in diameter, and a long non-contractile tail, 265 ± 10 nm in length (Figure 1B).

The optimal MOI assay of the Vic9 indicated that the highest titer, 6.9×10^9 PFU/mL, was achieved at a MOI of 0.01. The adsorption time of the phage to *M. smegmatis* mc(2)155 was approximately 30 min (Figure 2A). One-step growth curve analysis showed that Vic9 has a latent period of 90 min, followed by a rise period lasting 150 min (Figure 2B), with an estimated burst size of approximately 68 PFU per infected cell.

3.2 Host range of the Vic9 phage

To determine the host range, serial dilutions of the Vic9 phage were tested on various *Mycobacterium* species (Figure 3). The phage displayed a narrow host range, effectively lysing only the host strain and *M. tuberculosis* H37Rv. However, in contrast to *M. smegmatis* mc(2)155, the phage produced small, irregularly shaped, translucent plaques with indistinct borders on *M. tuberculosis* H37Rv. No lysis was observed on *M. kansasii*, *M. avium*, *M. fortuitum*, or *M. abscessus*, regardless of the phage titer.

3.3 General genome analysis of the phage

The complete genome of the Vic9 phage consists of linear double-stranded DNA, 67,543 bp in length, with a G + C content of 69%. A total of 89 open reading frames (ORFs) were identified, covering 63,351 bp (94% of the genome).

BLASTn analysis revealed that Vic9 shares a high degree of similarity with other phages of subcluster B2, showing over 95% query coverage and 98.9% identity. To verify its taxonomic position, a phylogenetic analysis of the phage, along with phages of cluster B ($n = 375$) from the actinobacteriophage database PhagesDB (Russell and Hatfull, 2017), was conducted. Phylogenetic analysis confirmed its affiliation with subcluster B2, with Vic9 forming a distinct group with the phages Godines (KR997932.1), Ares (JN699004.1), Qyrzula (DQ398048.1), and Laurie (KX443696.1) (Figure 4).

3.4 Functional annotation of Vic9 phage

The genomic organization of phage Vic9 is typical of subcluster B2. Functional analysis categorized its proteins into four main groups: (1) Structure and assembly (16 ORFs); (2) Host cell lysis (2 ORFs); (3) Nucleic acid metabolism and other functions (15 ORFs); and (4) Hypothetical proteins (56 ORFs) (Figure 5). The structural genes are located in the left region of the genome and are oriented on the positive strand. This module comprises several key genes, including those encoding the terminase (Vic_00007), RuvC-like resolvase (Vic_00009), portal protein (Vic_00012), MuF-like protein (Vic_00014), major head protein (Vic_00015), major capsid protein (Vic_00016), major tail protein (Vic_00021), head-tail adaptor

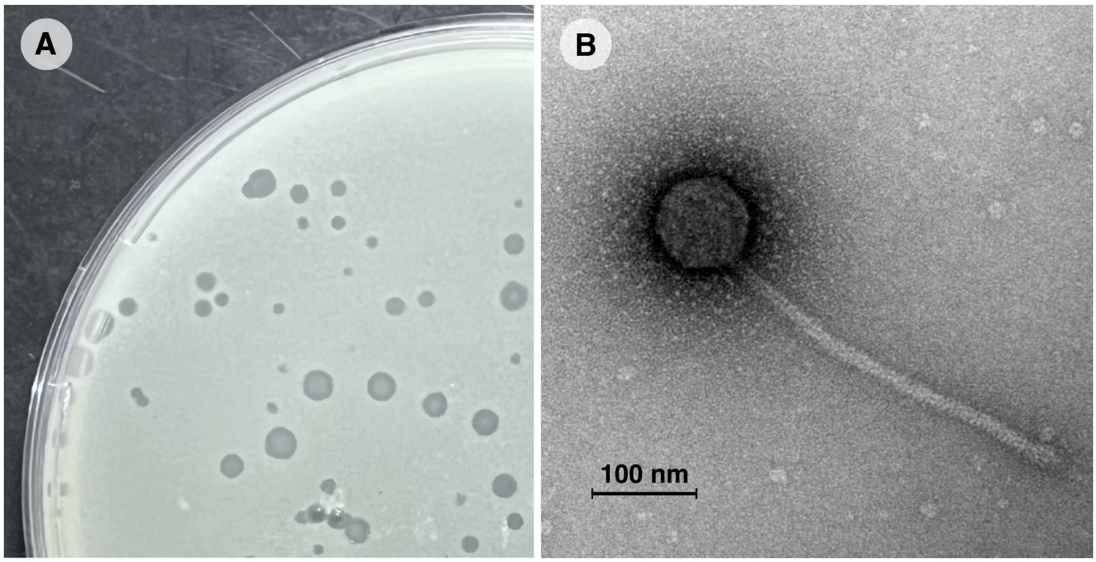

FIGURE 1
Morphological characterization of mycobacteriophage Vic9. **(A)** Plaques of phage Vic9 formed on a lawn of *M. smegmatis* mc(2)155 after 48 h of incubation. **(B)** Electron micrograph of phage Vic9, stained with 1% uranyl acetate.

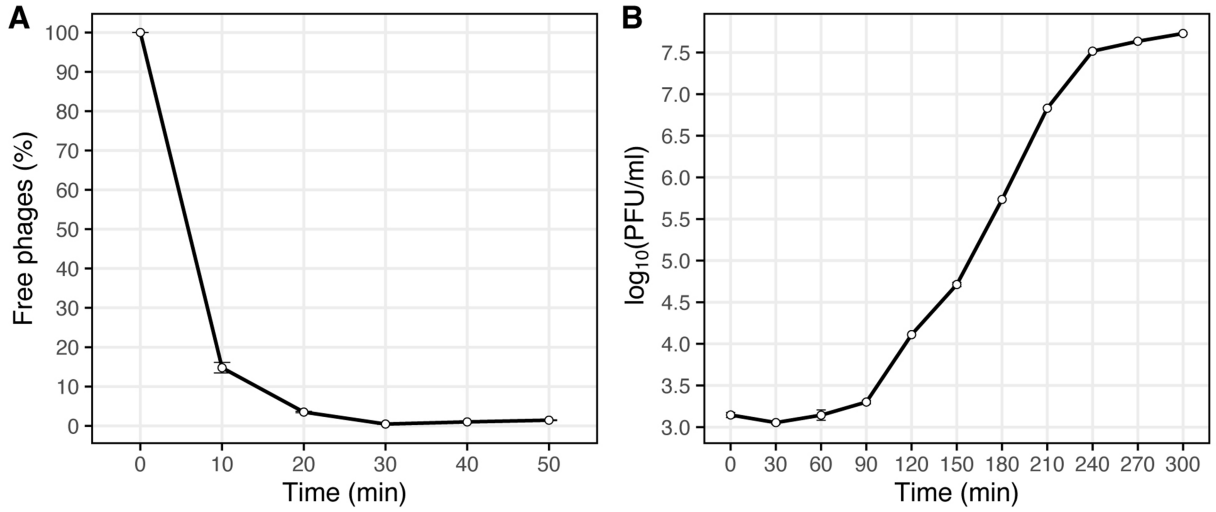

FIGURE 2
Characterization of phage Vic9 life cycle. **(A)** Adsorption curve, and **(B)** one-step growth curve.

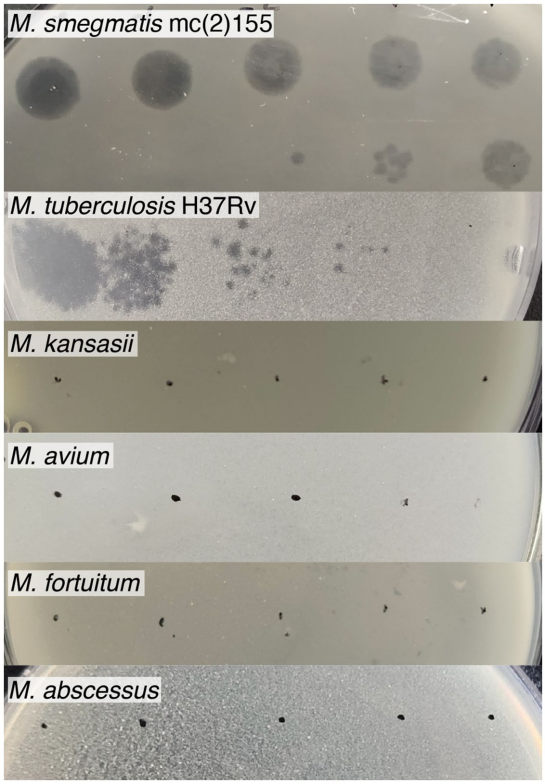

FIGURE 3
Host range of mycobacteriophage Vic9. Tenfold serial dilutions of Vic9 were spotted onto lawns of various mycobacterial species.

(Vic_00024), tail assembly chaperone (Vic_00027), tape measure protein (Vic_00029), minor tail proteins (Vic_00030-Vic_00033), head protein (Vic_00034), and virion structural protein (Vic_00042). The tape measure protein, Vic_00029, plays a crucial role in determining tail length and is composed of 1,880 amino acid residues, consistent with the observed morphology of the phage (Belcaid et al., 2011). The cell lysis module, responsible for completing the lytic cycle and releasing phage particles from the host, contains only lysin A (Vic_00058) and holin (Vic_00059).

Preceding the structural module located in the left region of the genome, a group of genes involved in nucleic acid metabolism and other functions were identified, including genes for queuosine biosynthesis from GTP. These genes include queuine tRNA-ribosyltransferase (Vic_00002), Pre-Q0 pathway QueC-like protein (Vic_00003), QueD-like 6-pyruvoyl-tetrahydropterin synthase (Vic_00004), QueE-like queuosine biosynthesis protein (Vic_00005), and GTP cyclohydrolase I (Vic_00006). Additional genes related to nucleic acid metabolism are mainly located in the right region of the genome and include DNA-binding proteins (Vic_00043, Vic_00044), DNA helicase (Vic_00050), DNA polymerase/primase (Vic_00054), DNA polymerase I (Vic_00057), Rnase E (Vic_00065), HNH endonucleases (Vic_00070, Vic_00082), and a putative elongation factor (Vic_00088).

A distinct feature of B2 subcluster members, including Vic9, is the absence of integrase, RNA polymerase, lysin B, the small terminase subunit, and tRNA-coding genes (Hatfull, 2010).

3.5 Comparative genomics of Vic9

Comparison of the nucleotide sequence of Vic9 with other mycobacteriophages of subcluster B2 from the NCBI database revealed several distinct features (Supplementary Figure S1). Vic9 contains a unique 435 bp sequence located between the genes Vic_00005 (QueE-like queuosine biosynthesis protein) and Vic_00006 (GTP cyclohydrolase I). This sequence lacks open reading frames when annotated with GeneMarkS v4.32. However, analysis using Pharokka 1.7.2 revealed that this region encodes a protein of unknown function. Notably, no homologs of this sequence or the

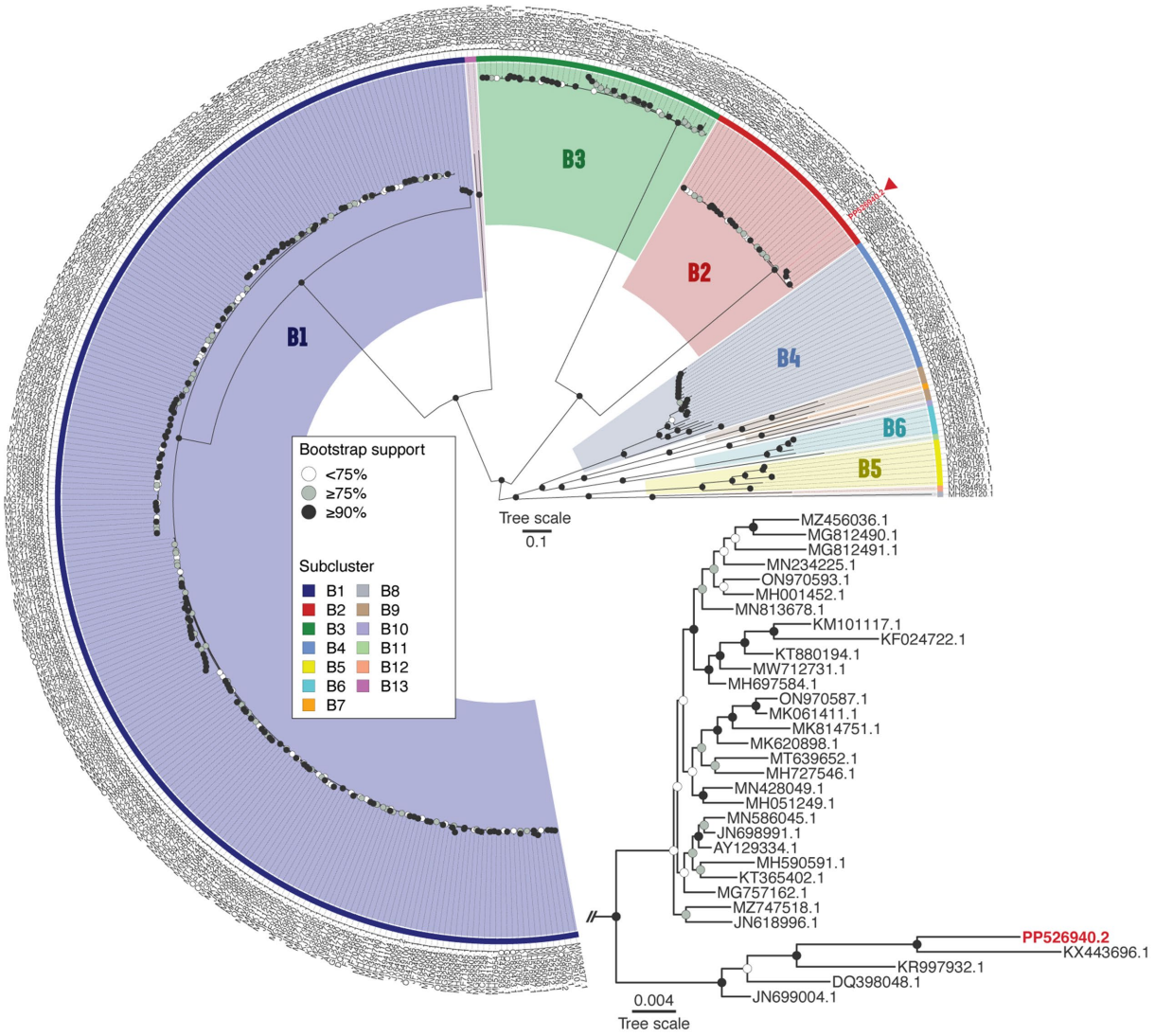

FIGURE 4
Phage Vic9 is classified within a distinct phylogenetic clade of the B2 subcluster. The midpoint-rooted maximum-likelihood phylogeny was inferred from 375 sequences and 54,439 distinct patterns obtained through whole-genome alignments of nucleotide sequences from cluster B mycobacteriophages. Bootstrap support values are indicated as white dots for values <75%, grey dots for values ≥75%, and black dots for values ≥90% on the interior nodes. Colors represent the various subclusters of cluster B, with the red triangle marking the Vic9 phage. The subtree for subcluster B2 is shown in the lower right corner.

putative protein it encodes were identified in the NCBI database. Additionally, Vic9 possesses the gene Vic_00055, encoding a protein of unknown function, homologous to FDI79_gp56 (96.15%) from phage Godines (KR997932.1) and J3996_gp55 (98.08%) from phage Laurie (KX443696.1), but absent in other cluster members. Additionally, Vic9 is missing the region between Vic_00087 and Vic_00088, which encodes a hypothetical protein in other mycobacteriophages. Notably, this deletion is also present in the phages Laurie (KX443696.1), Arbiter (JN618996.1), Phantasmagoria (ON970587.1), Holeinone (MG812490.1), and Qyrzula (DQ398048.1).

Further genomic analysis revealed that the structural cassette region Vic_0033-Vic_0035, comprising a minor tail protein, a head protein, and a protein of unknown function, shares homology with the corresponding regions in phages Godines (KR997932.1), Ares (JN699004.1), Qyrzula (DQ398048.1), and Laurie (KX443696.1). This homology places Vic9 on a distinct branch within subcluster B2. Additionally, Vic_0033-Vic_0035 showed significant homology with phages from subcluster B3, as indicated by the analysis of 28 out of 44 genomes from PhagesDB, which displayed over 75% similarity. Notably, no homology with other subcluster B2 members was observed (Figure 6).

4 Discussion

A novel lytic mycobacteriophage, Vic9, was isolated and thoroughly characterized using *M. smegmatis* mc(2)155 as the host.

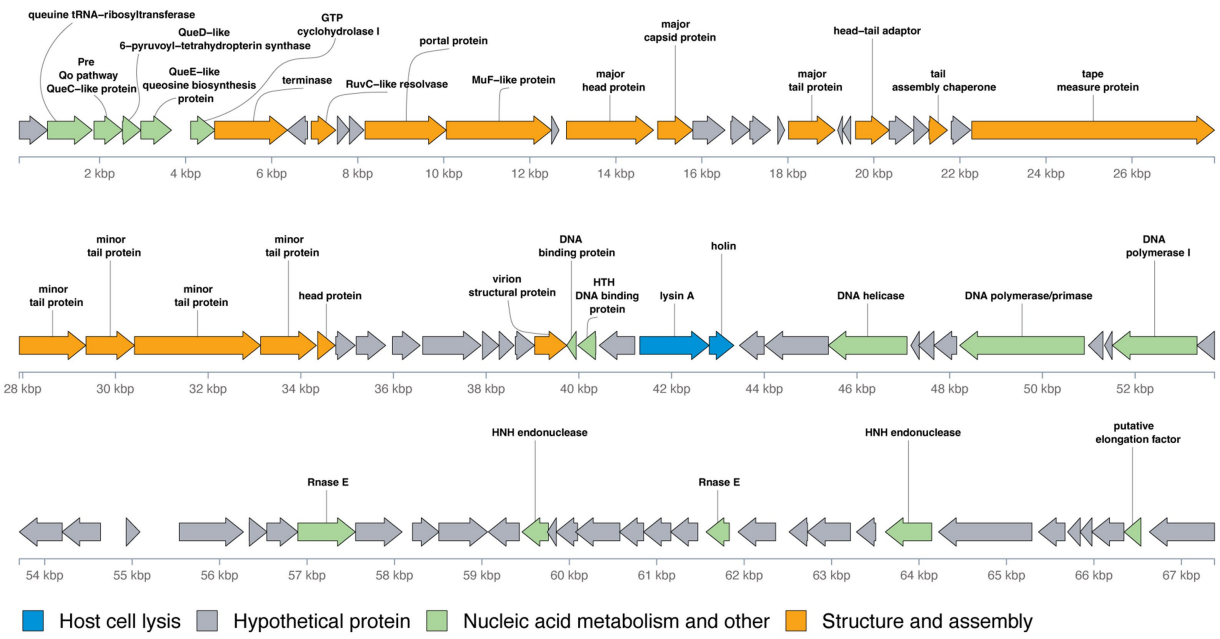

FIGURE 5
Genomic organization of mycobacteriophage Vic9. Open reading frames (ORFs) are represented as arrows, with translation frames indicated. Functional annotations of the ORFs are color-coded as follows: blue for host cell lysis, grey for hypothetical proteins, green for nucleic acid metabolism and other functions, and orange for structure and assembly.

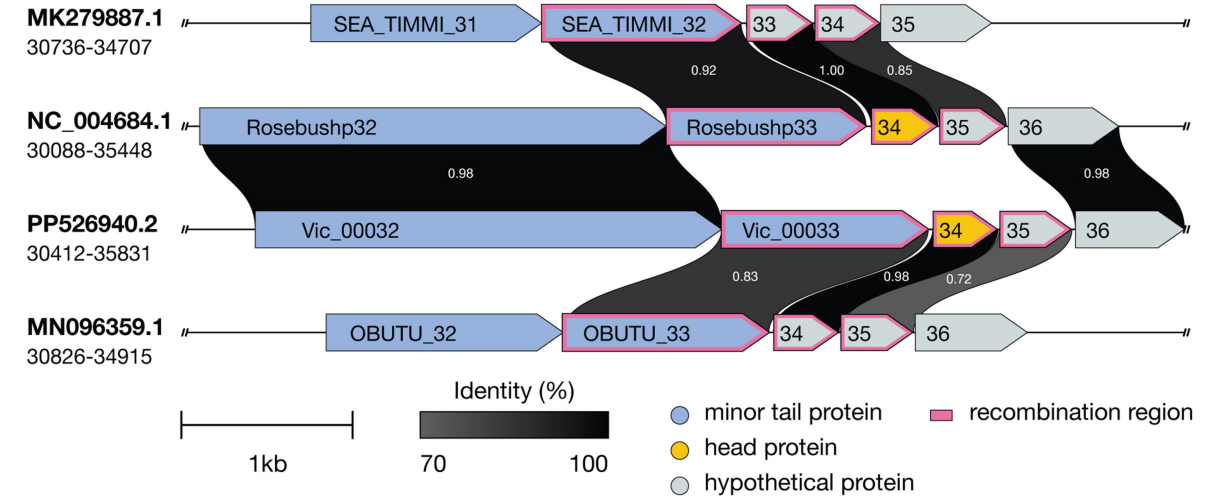

FIGURE 6
Comparative genomic organization of mycobacteriophages Timmi, Rosebush, Vic9, and Obutu reveals evidence of recombination events. Recombination events are indicated by a pink border. ORFs are represented by arrows, with grayscale shading indicating amino acid sequence identity (darker shades correspond to higher identity levels). Accession numbers and genome coordinates are noted on the left.

Vic9 belongs to subcluster B2 within the larger B cluster, which, according to the PhagesDB, is the second most represented cluster after cluster A, and the most prevalent among phages with a lytic life cycle. The B cluster comprises 13 subclusters, with subcluster B2 being the third largest, following subclusters B1 and B3 (as of October 2024). Despite the relatively large number of studied phages in subcluster B2, none have had their life cycle characteristics described, which are essential for understanding phage physiology and evaluating their therapeutic potential.

Morphologically, Vic9 is a typical representative of cluster B and, like most mycobacteriophages, belongs to the Siphoviridae family. On its host strain, Vic9 forms small plaques with a turbid center, which is a characteristic feature of B2 subcluster members, according to PhagesDB. In terms of host specificity, Vic9 efficiently lyses its host strain, *M. smegmatis* mc(2)155, and at higher titers, it also demonstrates lysis of *M. tuberculosis* H37Rv, albeit with a low efficiency of plating (EOP of 2×10^{-5}). This observation aligns with previous studies noting the relatively low efficacy of B2 subcluster

phages against *M. tuberculosis* (Jacobs-Sera et al., 2012), especially when compared to phages from clusters A2, A3, G1, K1, K2, K3, K4 and some singletons,which are considered the most promising for phage therapy (Guerrero-Bustamante et al., 2021; Yang et al., 2024).

Further investigation of Vic9's life cycle parameters, compared to phage PDRPxv (from subcluster B1), the only characterized phage of the B cluster; (Sinha et al., 2020), revealed that Vic9 has a shorter adsorption time (30 vs. 45 min) and a shorter latent period (90 vs. 135 min). However, in terms of growth, Vic9 lags significantly behind one of the most studied mycobacteriophages, D29 (Bavda and Jain, 2020), which may partly explain its low efficiency in lysing mycobacteria other than *M. smegmatis*.

At the genomic level, Vic9 shares similar organization with other B2 subcluster members, as detailed elsewhere (Hatfull, 2012). According to ICTV, Vic9 is classified under the Rosebushvirus genus, named after the first phage isolated in this group (Pedulla et al., 2003). Overall, B2 subcluster mycobacteriophages show a high degree of genetic conservation and rarely exchange genetic material with other subclusters (Supplementary Figure S1). However, in Vic9 genome, as well as in phages Ares (JN699004.1), Laurie (KX443696.1), Qyrzula (DQ398048.1), and Godines (KR997932.1), we identified three genes that show homology to B3 subcluster phages (Figure 6), suggesting possible recombination between subclusters. Interestingly, the same genes in another group of phages forming a separate group on the phylogenetic tree align with corresponding regions in B1 subcluster phages (similarity >90%), which was previously reported for the Rosebush phage (Hatfull, 2010).

Another intriguing feature unique to Vic9 is the presence of a gene encoding a protein of hypothetical function located at the left end of the genome, within a region of six genes preceding the terminase, previously described as specific to subcluster B2 mycobacteriophages (Hatfull, 2012). This gene lies between Vic_00005 and Vic_00006, which correspond to the QueE and QueF proteins involved in the biosynthesis of queuosine from GTP. This system likely plays a role in modifying the host's tRNA, although it is unknown whether it affects translation specificity or efficiency.

5 Conclusion

The isolation and characterization of Vic9, a novel mycobacteriophage from Russia, represent a significant advancement in our understanding of subcluster B2. Until now, phages from subcluster B2 have predominantly been isolated in the United States, with the exception of phage Godines (KR997932.1) from Brazil, making the isolation of Vic9 particularly interesting for evolutionary studies. Despite high conservation within the subcluster, unique genetic features were identified, such as a distinctive sequence between genes Vic_00005 and Vic_00006, as well as homology of genes Vic_0033-Vic_0035 with corresponding genes from subcluster B3. Another key aspect of our research was the investigation of Vic9 life cycle parameters, which to our knowledge has been shown for the first time for phages of the B2 subcluster. Additionally, we found that Vic9 has a narrow host range, effectively lysing only its host strain, which significantly limits its therapeutic potential. Nonetheless, the characterization of Vic9 broadens our understanding of B2 phages and highlights their relevance for evolutionary and genetic studies, while also contributing to the growing body of knowledge needed to inform future research on the potential of mycobacteriophages in biomedical applications.

Data availability statement

The data presented in the study are deposited in the GenBank repository, accession number PP526940.2.

Author contributions

MZ: Conceptualization, Formal analysis, Supervision, Writing – original draft, Resources, Writing – review & editing. MM: Investigation, Visualization, Writing – review & editing, Methodology. DBe: Data curation, Formal analysis, Software, Writing – review & editing. MK: Investigation, Methodology, Validation, Writing – review & editing. KK: Data curation, Methodology, Supervision, Writing – review & editing. AS: Formal analysis, Investigation, Software, Writing – review & editing. RG: Methodology, Validation, Visualization, Writing – review & editing. AGe: Investigation, Resources, Visualization, Writing – review & editing. MF: Investigation, Methodology, Resources, Writing – review & editing. DBa: Investigation, Methodology, Visualization, Writing – review & editing. AV: Investigation, Validation, Visualization, Writing – review & editing. AGr: Investigation, Resources, Visualization, Writing – review & editing. AK: Investigation, Resources, Visualization, Writing – review & editing. MS: Investigation, Resources, Visualization, Writing – review & editing. ES: Conceptualization, Funding acquisition, Project administration, Supervision, Writing – review & editing.

Funding

The author(s) declare that financial support was received for the research, authorship, and/or publication of this article. This work was supported by Russian Science Foundation (project ID 24-15-00514, https://rscf.ru/project/24-15-00514/).

Acknowledgments

This work was conducted using the core facilities of the Lopukhin FRCC PCM "Genomics, Proteomics, Metabolomics" (http://rcpcm.org/?p=2806). The TEM measurements were carried out at the User Facilities Center "Electron microscopy in life sciences," Lomonosov Moscow State University.

Conflict of interest

The authors declare that the research was conducted in the absence of any commercial or financial relationships that could be construed as a potential conflict of interest.

Generative AI statement

The authors declare that no Gen AI was used in the creation of this manuscript.

Publisher's note

Supplementary material

The Supplementary material for this article can be found online at: https://www.frontiersin.org/articles/10.3389/fmicb.2024.1513081/full#supplementary-material

References

Armstrong, D. T., Eisemann, E., and Parrish, N. (2023). A brief update on mycobacterial taxonomy, 2020 to 2022. *J. Clin. Microbiol.* 61:e0033122. doi: 10.1128/jcm.00331-22

Avdeev, V. V., Kuzin, V. V., Vladimirsky, M. A., and Vasilieva, I. A. (2023). Experimental studies of the liposomal form of lytic Mycobacteriophage D29 for the treatment of tuberculosis infection. *Microorganisms*. 11:1214. doi: 10.3390/microorganisms11051214

Bartlett, H. P., Dawson, C. C., Glickman, C. M., Osborn, D. W., Evans, C. R., Garcia, B. J., et al. (2024). Targeting intracellular nontuberculous mycobacteria and *M. tuberculosis* with a bactericidal enzymatic cocktail. *Microbiol. Spectr.* 12:e0353423. doi: 10.1128/spectrum.03534-23

Bavda, V. R., and Jain, V. (2020). Deciphering the role of Holin in Mycobacteriophage D29 physiology. *Front. Microbiol.* 11:883. doi: 10.3389/fmicb.2020.00883

Belcaid, M., Bergeron, A., and Poisson, G. (2011). The evolution of the tape measure protein: units, duplications and losses. *BMC Bioinformatics* 12:S10. doi: 10.1186/1471-2105-12-S9-S10

Besemer, J., Lomsadze, A., and Borodovsky, M. (2001). GeneMarkS: a self-training method for prediction of gene starts in microbial genomes. Implications for finding sequence motifs in regulatory regions. *Nucleic Acids Res.* 29, 2607–2618. doi: 10.1093/nar/29.12.2607

Bouras, G., Nepal, R., Houtak, G., Psaltis, A. J., Wormald, P.-J., and Vreugde, S. (2023). Pharokka: a fast scalable bacteriophage annotation tool. *Bioinforma. Oxf. Engl.* 39:btac776. doi: 10.1093/bioinformatics/btac776

Capella-Gutiérrez, S., Silla-Martínez, J. M., and Gabaldón, T. (2009). trimAl: a tool for automated alignment trimming in large-scale phylogenetic analyses. *Bioinforma. Oxf. Engl.* 25, 1972–1973. doi: 10.1093/bioinformatics/btp348

Champagne-Jorgensen, K., Luong, T., Darby, T., and Roach, D. R. (2023). Immunogenicity of bacteriophages. *Trends Microbiol.* 31, 1058–1071. doi: 10.1016/j.tim.2023.04.008

Chen, S., Zhou, Y., Chen, Y., and Gu, J. (2018). Fastp: an ultra-fast all-in-one FASTQ preprocessor. *Bioinforma. Oxf. Engl.* 34, i884–i890. doi: 10.1093/bioinformatics/bty560

Danecek, P., Bonfield, J. K., Liddle, J., Marshall, J., Ohan, V., Pollard, M. O., et al. (2021). Twelve years of SAMtools and BCFtools. *GigaScience* 10:giab008. doi: 10.1093/gigascience/giab008

de Sena Brandine, G., and Smith, A. D. (2019). Falco: high-speed FastQC emulation for quality control of sequencing data. *F1000Research* 8:1874. doi: 10.12688/f1000research.21142.2

Dedrick, R. M., Guerrero-Bustamante, C. A., Garlena, R. A., Russell, D. A., Ford, K., Harris, K., et al. (2019). Engineered bacteriophages for treatment of a patient with a disseminated drug-resistant *Mycobacterium abscessus*. *Nat. Med.* 25, 730–733. doi: 10.1038/s41591-019-0437-z

Dedrick, R. M., Smith, B. E., Cristinziano, M., Freeman, K. G., Jacobs-Sera, D., Belessis, Y., et al. (2023). Phage therapy of Mycobacterium infections: compassionate use of phages in 20 patients with drug-resistant mycobacterial disease. *Clin. Infect. Dis.* 76, 103–112. doi: 10.1093/cid/ciac453

Dedrick, R. M., Smith, B. E., Garlena, R. A., Russell, D. A., Aull, H. G., Mahalingam, V., et al. (2021). *Mycobacterium abscessus* strain Morphotype determines phage susceptibility, the repertoire of therapeutically useful phages, and phage resistance. *MBio* 12, e03431–e03420. doi: 10.1128/mBio.03431-20

Ewels, P., Magnusson, M., Lundin, S., and Käller, M. (2016). MultiQC: summarize analysis results for multiple tools and samples in a single report. *Bioinforma. Oxf. Engl.* 32, 3047–3048. doi: 10.1093/bioinformatics/btw354

Gan, Y., Wu, T., Liu, P., and Guo, S. (2014). Characterization and classification of Bo4 as a cluster G mycobacteriophage that can infect and lyse *M. tuberculosis*. *Arch. Microbiol.* 196, 209–218. doi: 10.1007/s00203-014-0954-6

Gong, Z., Lv, X., Li, C., Gu, Y., Fan, X., Sun, Q., et al. (2021). Genomic and proteomic portrait of a novel mycobacteriophage SWU2 isolated from China. *Infect. Genet. Evol. J. Mol. Epidemiol. Evol. Genet. Infect. Dis.* 87:104665. doi: 10.1016/j.meegid.2020.104665

Green, M. R., Sambrook, J., and Sambrook, J. (2012). Molecular cloning: A laboratory manual. *4th* Edn. Cold Spring Harbor, NY: Cold Spring Harbor Laboratory Press.

Guerrero-Bustamante, C. A., Dedrick, R. M., Garlena, R. A., Russell, D. A., and Hatfull, G. F. (2021). Toward a phage cocktail for tuberculosis: susceptibility and Tuberculocidal action of Mycobacteriophages against diverse *Mycobacterium tuberculosis* strains. *MBio* 12, e00973–e00921. doi: 10.1128/mBio.00973-21

Hatfull, G. F. (2010). Mycobacteriophages: genes and genomes. *Ann. Rev. Microbiol.* 64, 331–356. doi: 10.1146/annurev.micro.112408.134233

Hatfull, G. F. (2012). The secret lives of mycobacteriophages. *Adv. Virus Res.* 82, 179–288. doi: 10.1016/B978-0-12-394621-8.00015-7

Hatfull, G. F. (2023). Phage Therapy for Nontuberculous Mycobacteria: Challenges and Opportunities. *Pulm. Ther.* 9, 91–107. doi: 10.1007/s41030-022-00210-y

Heller, D. M., Sivanathan, V., Asai, D. J., and Hatfull, G. F. (2024). SEA-PHAGES and SEA-GENES: advancing virology and science education. *Annu. Rev. Virol.* 11, 1–20. doi: 10.1146/annurev-virology-113023-110757

Hendrix, R. W., and Duda, R. L. (1992). Bacteriophage lambda PaPa: not the mother of all lambda phages. *Science* 258, 1145–1148. doi: 10.1126/science.1439823

Hoang, D. T., Chernomor, O., von Haeseler, A., Minh, B. Q., and Vinh, L. S. (2018). UFBoot2: Improving the Ultrafast Bootstrap Approximation. *Mol. Biol. Evol.* 35, 518–522. doi: 10.1093/molbev/msx281

Jacobs-Sera, D., Marinelli, L. J., Bowman, C., Broussard, G. W., Guerrero Bustamante, C., Boyle, M. M., et al. (2012). On the nature of mycobacteriophage diversity and host preference. *Virology* 434, 187–201. doi: 10.1016/j.virol.2012.09.026

Kadura, S., King, N., Nakhoul, M., Zhu, H., Theron, G., Köser, C. U., et al. (2020). Systematic review of mutations associated with resistance to the new and repurposed *Mycobacterium tuberculosis* drugs bedaquiline, clofazimine, linezolid, delamanid and pretomanid. *J. Antimicrob. Chemother.* 75, 2031–2043. doi: 10.1093/jac/dkaa136

Kalyaanamoorthy, S., Minh, B. Q., Wong, T. K. F., von Haeseler, A., and Jermiin, L. S. (2017). ModelFinder: fast model selection for accurate phylogenetic estimates. *Nat. Methods* 14, 587–589. doi: 10.1038/nmeth.4285

Kortright, K. E., Chan, B. K., Koff, J. L., and Turner, P. E. (2019). Phage therapy: a renewed approach to combat antibiotic-resistant Bacteria. *Cell Host Microbe* 25, 219–232. doi: 10.1016/j.chom.2019.01.014

Kropinski, A. M., Mazzocco, A., Waddell, T. E., Lingohr, E., and Johnson, R. P. (2009). Enumeration of bacteriophages by double agar overlay plaque assay. *Methods Mol. Biol.* 501, 69–76. doi: 10.1007/978-1-60327-164-6_7

Laslett, D., and Canback, B. (2004). ARAGORN, a program to detect tRNA genes and tmRNA genes in nucleotide sequences. *Nucleic Acids Res.* 32, 11–16. doi: 10.1093/nar/gkh152

Lassmann, T. (2019). Kalign 3: multiple sequence alignment of large data sets. *Bioinforma. Oxf. Engl.* 36, 1928–1929. doi: 10.1093/bioinformatics/btz795

Lefkowitz, E. J., Dempsey, D. M., Hendrickson, R. C., Orton, R. J., Siddell, S. G., and Smith, D. B. (2018). Virus taxonomy: the database of the international committee on taxonomy of viruses (ICTV). *Nucleic Acids Res.* 46, D708–D717. doi: 10.1093/nar/gkx932

Li, H., and Durbin, R. (2009). Fast and accurate short read alignment with burrows-wheeler transform. *Bioinforma. Oxf. Engl.* 25, 1754–1760. doi: 10.1093/bioinformatics/btp324

Little, J. S., Dedrick, R. M., Freeman, K. G., Cristinziano, M., Smith, B. E., Benson, C. A., et al. (2022). Bacteriophage treatment of disseminated cutaneous *Mycobacterium chelonae* infection. *Nat. Commun.* 13:2313. doi: 10.1038/s41467-022-29689-4

Lu, J., Breitwieser, F. P., Thielen, P., and Salzberg, S. L. (2017). Bracken: estimating species abundance in metagenomics data. *PeerJ Comput. Sci.* 3:e104. doi: 10.7717/peerj-cs.104

McNerney, R., Wilson, S. M., Sidhu, A. M., Harley, V. S., Al Suwaidi, Z., Nye, P. M., et al. (1998). Inactivation of mycobacteriophage D29 using ferrous ammonium sulphate

as a tool for the detection of viable Mycobacterium smegmatis and *M. tuberculosis*. *Res. Microbiol.* 149, 487–495. doi: 10.1016/s0923-2508(98)80003-x

Meneses, L., Brandão, A. C., Coenye, T., Braga, A. C., Pires, D. P., and Azeredo, J. (2023). A systematic review of the use of bacteriophages for in vitro biofilm control. *Eur. J. Clin. Microbiol. Infect. Dis.* 42, 919–928. doi: 10.1007/s10096-023-04638-1

Minh, B. Q., Schmidt, H. A., Chernomor, O., Schrempf, D., Woodhams, M. D., Von Haeseler, A., et al. (2020). IQ-TREE 2: new models and efficient methods for phylogenetic inference in the genomic era. *Mol. Biol. Evol.* 37, 1530–1534. doi: 10.1093/molbev/msaa015

Nayfach, S., Camargo, A. P., Schulz, F., Eloe-Fadrosh, E., Roux, S., and Kyrpides, N. C. (2021). CheckV assesses the quality and completeness of metagenome-assembled viral genomes. *Nat. Biotechnol.* 39, 578–585. doi: 10.1038/s41587-020-00774-7

Paradis, E., and Schliep, K. (2019). ape 5.0: an environment for modern phylogenetics and evolutionary analyses in R. *Bioinformatics*. 35, 526–528. doi: 10.1093/bioinformatics/bty633

Pedersen, B. S., and Quinlan, A. R. (2018). Mosdepth: quick coverage calculation for genomes and exomes. *Bioinforma. Oxf. Engl.* 34, 867–868. doi: 10.1093/bioinformatics/btx699

Pedulla, M. L., Ford, M. E., Houtz, J. M., Karthikeyan, T., Wadsworth, C., Lewis, J. A., et al. (2003). Origins of highly mosaic mycobacteriophage genomes. *Cell* 113, 171–182. doi: 10.1016/s0092-8674(03)00233-2

Russell, D. A., and Hatfull, G. F. (2017). PhagesDB: the actinobacteriophage database. *Bioinforma. Oxf. Engl.* 33, 784–786. doi: 10.1093/bioinformatics/btw711

Sarkis, G. J., and Hatfull, G. F. (1998). Mycobacteriophages. *Methods Mol. Biol.* 101, 145–173. doi: 10.1385/0-89603-471-2:145

Saxena, S., Spaink, H. P., and Forn-Cuní, G. (2021). Drug resistance in nontuberculous mycobacteria: mechanisms and models. *Biology* 10:96. doi: 10.3390/biology10020096

Seemann, T. (2014). Prokka: rapid prokaryotic genome annotation. *Bioinforma. Oxf. Engl.* 30, 2068–2069. doi: 10.1093/bioinformatics/btu153

Seung, K. J., Keshavjee, S., and Rich, M. L. (2015). Multidrug-resistant tuberculosis and extensively drug-resistant tuberculosis. *Cold Spring Harb. Perspect. Med.* 5:a017863. doi: 10.1101/cshperspect.a017863

Shen, W., Sipos, B., and Zhao, L. (2024). SeqKit2: a Swiss army knife for sequence and alignment processing. *iMeta* 3:e191. doi: 10.1002/imt2.191

Sinha, A., Eniyan, K., Manohar, P., Ramesh, N., and Bajpai, U. (2020). Characterization and genome analysis of B1 sub-cluster mycobacteriophage PDRPxv. *Virus Res.* 279:197884. doi: 10.1016/j.virusres.2020.197884

Söding, J., Biegert, A., and Lupas, A. N. (2005). The HHpred interactive server for protein homology detection and structure prediction. *Nucleic Acids Res.* 33, W244–W248. doi: 10.1093/nar/gki408

WHO. (2020). *Global tuberculosis report 2020*. Geneva.

Wickham, H. (2016). ggplot2. Cham: Springer International Publishing.

Wood, D. E., Lu, J., and Langmead, B. (2019). Improved metagenomic analysis with kraken 2. *Genome Biol.* 20:257. doi: 10.1186/s13059-019-1891-0

Xu, S., Dai, Z., Guo, P., Fu, X., Liu, S., Zhou, L., et al. (2021). ggtreeExtra: compact visualization of richly annotated phylogenetic data. *Mol. Biol. Evol.* 38, 4039–4042. doi: 10.1093/molbev/msab166

Xu, S., Li, L., Luo, X., Chen, M., Tang, W., Zhan, L., et al. (2022). Ggtree: a serialized data object for visualization of a phylogenetic tree and annotation data. *iMeta* 1:e56. doi: 10.1002/imt2.56

Yang, F., Labani-Motlagh, A., Bohorquez, J. A., Moreira, J. D., Ansari, D., Patel, S., et al. (2024). Bacteriophage therapy for the treatment of *Mycobacterium tuberculosis* infections in humanized mice. *Commun. Biol.* 7:294. doi: 10.1038/s42003-024-06006-x

Yu, G. (2022). Data integration, manipulation and visualization of phylogenetic trees. *1st* Edn. Boca Raton: Chapman and Hall/CRC.

frontiers | Frontiers in Microbiology

TYPE Original Research
PUBLISHED 28 January 2025
DOI 10.3389/fmicb.2025.1522711

OPEN ACCESS

EDITED BY
Hany Anany,
Agriculture and Agri-Food Canada (AAFC), Canada

REVIEWED BY
Izhar Ul-Haq Khan,
Agriculture and Agri-Food Canada (AAFC), Canada
Ryan Cook,
Quadram Institute, United Kingdom

*CORRESPONDENCE
Gamaliel López-Leal
✉ gamaliel.lopez@docentes.uaem.edu.mx

RECEIVED 04 November 2024
ACCEPTED 09 January 2025
PUBLISHED 28 January 2025

CITATION
Arellano-Maciel D, Hurtado-Ramírez JM, Camelo-Valera LC, Castillo-Ramírez S, Reyes A and López-Leal G (2025) Geographic variation in abundance and diversity of *Acinetobacter baumannii Vieuvirus* bacteriophages.
Front. Microbiol. 16:1522711.
doi: 10.3389/fmicb.2025.1522711

Geographic variation in abundance and diversity of *Acinetobacter baumannii Vieuvirus* bacteriophages

Dafne Arellano-Maciel[1], Juan Manuel Hurtado-Ramírez[2], Laura Carolina Camelo-Valera[3], Santiago Castillo-Ramírez[4], Alejandro Reyes[5] and Gamaliel López-Leal[1]*

[1]Laboratorio de Biología Computacional y Virómica Integrativa, Centro de Investigación en Dinámica Celular, Universidad Autónoma del Estado de Morelos, Cuernavaca, Mexico, [2]Instituto de Biotecnología, Universidad Nacional Autónoma de México, Cuernavaca, Mexico, [3]McGill Centre for Microbiome Research, Department of Microbiology and Immunology, McGill University, Montreal, QC, Canada, [4]Programa de Genómica Evolutiva, Centro de Ciencias Genómicas, Universidad Nacional Autónoma de México, Cuernavaca, Mexico, [5]Grupo de Biología Computacional y Ecología Microbiana, Departamento de Ciencias Biológicas, Universidad de los Andes, Bogotá, Colombia

Introduction: Prophages play a crucial role in the genomic diversity of *Acinetobacter baumannii*, contributing to its pathogenicity and adaptation.

Methods: In this study, we induced and sequenced seven prophages from five isolates of *A. baumannii*. These were analyzed with 967 prophages identified from various isolates worldwide, plus 21 genomes of other phages infecting *A. baumannii* previously reported in NCBI. To have an overview of the populations of the prophages infecting *A. baumannii*.

Results: Our analysis revealed 13 major prophage clusters within the analyzed *A. baumannii* isolates. Notably, prophages belonging to the *Vieuvirus* genus were the most prevalent. Specifically, *Vieuvirus*-related phages were frequently identified in isolates from Thailand, Mexico, China, and South Korea, which show the geographic prevalence of *A. baumannii* prophages.

Discussion: This study highlights the importance of considering geographic factors to fully understand prophage diversity and their significant role in the evolutionary dynamics of *A. baumannii*.

KEYWORDS

prophages, bacteriophages, *Acinetobacter baumannii*, *Vieuvirus*, phages

Introduction

Viruses are the most abundant biological entities on Earth (Breitbart and Rohwer, 2005). Bacteriophages, or phages, specifically infect prokaryotic microorganisms. These phages replicate either through the lytic cycle, which is typical of virulent phages, or integrate into the host genome as prophages, or replicate as plasmids in the host cytoplasm (Piligrimova et al., 2021). The integrated phage genome (prophage) replicates together with the host chromosome and is transferred vertically from the initial infected cell to its progeny through cell division (Maurice et al., 2013). Integration into the bacterial chromosome can modify the host phenotype and introduce new genes and functions into the bacterial metabolic repertoir (Ramisetty and Sudhakari, 2019). Prophages encode genes responsible for antibiotic resistance and/or virulence factors (Costa et al., 2018; Kondo et al., 2021; López-Leal et al., 2020; Piña-González et al., 2024), confer adaptive benefits to their bacterial hosts (Li et al., 2017; Selva et al.,

2009), and facilitate the dissemination of these traits to other microorganisms (Wendling et al., 2021). The growing threat of antimicrobial resistance has emerged as a critical public health issue, with an estimated 700,000 deaths annually attributed to drug-resistant bacterial infections (Myers, 2016; O'Neill, 2014). *Acinetobacter baumannii* is a major cause of nosocomial multidrug-resistant (MDR) infections (Motbainor et al., 2020). It has been identified as a critical target in the World Health Organization's Priority List for Research and Development of New Antibiotics. Despite the significant knowledge available on the genomics and phylogenomics of *A. baumannii*, studies on phage and prophage populations that infect this species remain scarce. Recently, virulent phages have garnered attention as potential alternative therapies for *A. baumannii* infections and other MDR bacterial infections (Schooley et al., 2017; Wang et al., 2024), particularly for combating hospital-acquired pathogens. However, prophage populations, especially those that could be inducible or potentially active, have received far less attention. Knowing the inducible-prophage populations in target pathogens could help us to understand phage-host dynamics and whether prophages could interfere with phage therapy, as studies have reported recombination events between prophages and virulent phages when infecting their hosts (Piña-González et al., 2024; De Paepe et al., 2014; Dragos et al., 2021), as well as block cell surface receptors to prevent infection by other phages (Chung et al., 2014; Mcallister and Barrett, 1977). Advances in sequencing technologies and bioinformatics tools have increased considerably in recent years, allowing in-depth exploration of the vastness of prophage diversity (Andrade-Martínez et al., 2022). These tools are limited to only identifying the integrity and quality of prophages. A major limitation in identifying prophages is the certainty to determine whether these prophages are potentially inducible. Therefore, identifying active prophages remains a bioinformatic challenge, resulting in recourse to traditional microbiology.

In 2021, we reported a mitomycin-C-inducible phage of the genus *Vieuvirus* (accession number MT361972) isolated from an MDR *A. baumannii* strain Ab11510 (López-Leal et al., 2021), which belongs to the Sequence Type (ST) 758 lineage (Graña-Miraglia et al., 2017). At that time, very few phages of this genus had been reported in public databases, and only phages Bphi-B1251 (Jeon et al., 2012) and YMC11/11/R3177 (Jeon et al., 2015) were reported as reference Vieuviruses by the International Committee on Taxonomy of Viruses (ICTV). Additionally, exploration of prophage populations in different genomes of *A. baumannii* showed that Bphi-B1251 phages are the most prevalent type of phages in *A. baumannii* (Loh et al., 2020), suggesting that phages of the *Vieuvirus* genus may have high infectivity and a broad host range of active phage particles or that they are the most ancestral and segregate and co-evolve with the population (Loh et al., 2020). A recent study of prophage populations in 1,613 *Acinetobacter baumannii* genomes revealed that most prophage species exhibit a limited host range and are geographically restricted. However, some species are cosmopolitan and highly abundant. Despite these findings, knowledge about prophage populations in a broader genomic context, including lytic phages and inducible prophages in *A. baumannii*, remains limited (Tenorio-Carnalla et al., 2024). To expand the catalogue of inducible phages infecting *A. baumannii*, we isolated seven temperate phages from different MDR strains of *A. baumannii* and analyzed their phylogenetic relationships with 928 prophages collected from other global isolates of *A. baumannii*. This study provides a comprehensive characterization of *A. baumannii* prophage diversity.

Materials and methods

Bacteriophage isolation and genome assembly

Bacteriophages, phi9102 (PP898111), phi4197 (PQ432283), phi5013-M1 (PQ432284), phi5013-M2 (PQ432285), phi5038-11536 (PQ432286), phi11547 (PQ432287), phi5038-11551 (PQ432288), all mitomycin-C-inducible prophages were obtained from the clinical MDR *A. baumannii* strains collected from the Instituto Nacional de Cancerología (Mexico's National Institute of Oncology), a tertiary hospital located in Mexico City. Namely, GCA_004299615.1 (phi5013-M1 and phi5013-M2), GCA_003522845.1 (phi9102), GCA_004321575.1 (phi4197), GCA_004794205.1 (phi5038-11536, phi5038-11551), and GCA_001922695.1 (phi11547). In brief, the strains were treated with mitomycin C at a final concentration of 1 μg/ml in LB broth at 37°C for an overnight incubation period. Subsequently, the supernatants were collected via centrifugation (12,000 × *g* for 10 min) and utilized for host-range assays. We used the previously reported strains to propagate the phages (López-Leal et al., 2021). Specifically, 10 μl of each supernatant fraction was applied to overlay plates containing 3 ml of soft agar, followed by the addition of 300 μl of bacterial cells (López-Leal et al., 2021; Kropinski et al., 2009). After incubating overnight at 37°C, the plates were scrutinized for lysis within the spotted region. Confirmation of plaque formation in susceptible strains was achieved using a previously described method (López-Leal et al., 2021; Hyman, 2019; Santamaria et al., 2014). To summarize, 100 μl of a bacteriophage solution (or a dilution from the stock) was added with 200 μl of previously cultured, susceptible *A. baumannii* cells. The mixture was incubated for 15 min at room temperature, after which it was mixed with soft agar and spread onto LB solid medium to create a bacterial lawn. The plates were incubated at 37°C, and the formation of lytic plaques was observed. Individual plaques were picked and subjected to three consecutive rounds of replating to ensure the purity of the bacteriophage stocks. Different plaque morphologies were also considered for bacteriophage isolation. To ensure reproducibility, all experiments were conducted in triplicate. The bacteriophages were then cultivated in 6-ml cultures of *A. baumannii* strains (GCA_001922705, GCA_001922745, and GCA_001922695) in LB medium (with an OD 620 nm of 0.1), supplemented with 100 μl of each bacteriophage (average of 105 PFUs/ml). DNA isolation procedures followed established protocols (López-Leal et al., 2021; Santamaria et al., 2014), and restriction enzyme digestion analysis was performed using *Hind*III, *Eco*RI, *Eco*RV, *Bam*HI, and *Nde*I. Those phages that generated a unique restriction patterns were selected for sequencing. Phage genomic DNA sequencing was performed using a Miseq Illumina platform with a 300-bp paired-end configuration with a TruSeq DNA library. Raw reads were trimmed using TRIM_ GALORE[1] with a quality threshold of ≥30. The genome assembly was performed using the A5

1 https://www.bioinformatics.babraham.ac.uk/projects/trim_galore/

pipeline (Coil et al., 2015) with a set of ~25,000 (average of 7,215,608 reads per phage genome) randomly selected paired-end reads. Then, CheckV (v1.0.3; Nayfach et al., 2021) was used to validate the quality of each assembly. The completeness was confirmed by Bandage (v0.8.1; Wick et al., 2015), using the .gfa file.

Acinetobacter baumannii genomes used

To put our induced prophages into a genomic context with other *A. baumannii* prophages, we used a previously characterized and reported database of 1,465 *A. baumannii* isolates (Hernandez-Gonzalez et al., 2022). The genomes in this database were determined as high-quality genomes according to CheckM (v1.0.2; Parks et al., 2015). BioSample information for all *A. baumannii* genomes was obtained using efetch from E-utilities (v16.2; Sayers, 2009). Metadata was collected for the following sections: source isolate and isolation site.

Prophage identification

Prophage predictions were carried out using VirSorter2 (v2.2.4; Guo et al., 2021), and CheckV was used to determine the completeness and quality of phages and prophages sequence. Only phage sequences assigned as High-quality or Complete by checkv-quality or medium-quality were considered for downstream analysis. We followed the publicly available protocol for the validation of the first-instance prophage prediction.[2] Briefly, the final quality of prophages analyzed by CheckV were validated in a second screening using VirSorter2 (Guo et al., 2021). All (pro)phage genomes were annotated using pharokka (v1.6.1; Bouras et al., 2023).

Clustering at the genus levels and phylogenetic reconstruction

In the first instance, all prophages and phages (all the *Acinetobacter* phages reported in the NCBI) with at least 80% nucleotide similarity in at least 80% of the genome length were binned by cd-hit (v4.8.1; Fu et al., 2012). Following the parameter proposed by the ICTV (International Committee on Taxonomy of Viruses), this first clustering allowed us to select those phages and prophages that belonged to the same genus (Simmonds et al., 2023; Turner et al., 2021). In this sense, groups (phage genera) with more than five members were selected for further analysis. Then, to construct homologous groups (HG) from the selected bacteriophage genomes, we ran roary (v3.13.0; Page et al., 2015), setting the BLAST search parameters to a length coverage of ≥70% and an amino acid sequence identity of ≥40%. Next, a second clustering was made based on the optimal number of clusters determined by the hierarchical clustering of viruses based on intergenomic distances calculated from their shared protein content (pan-matrix from roary). The optimal number of clusters was determined by the average-silhouette method in R. Subsequently, hierarchical trees were constructed for each cluster with 100 bootstrap replicates. The ape (v5.6.1) and ggtree (v 3.0.4) libraries in R were used to obtain the branch length distribution. Finally, phage species and phage genera were validated using VICTOR (Meier-Kolthoff and Goker, 2017).

Phage diversity and abundance

The relationship between phage abundance and geographical location was evaluated. First, we calculated the uncertainty coefficient between bacteriophage genera and species against geographic locality. Second, the correlation between the abundance of phage species and phage genus in the different countries was computed with Pearson tests. The phage species and phage genus were taken as the result of the VICTOR analysis (Meier-Kolthoff and Goker, 2017).

Results

New inducible phages of the *Vieuvirus* genus

In previous studies, we reported that several ST-758 *A. baumannii* isolates have a high abundance and diversity of prophages (López-Leal et al., 2020). Furthermore, some of these phages belonging to the genus *Vieuvirus* were found to be active, since they could cause infections and generate progeny in other strains of the same lineage (López-Leal et al., 2020; López-Leal et al., 2021). In this study, in order to expand our understanding regarding the induced prophage sequences and the prophage population that infects *A. baumannii*, we induced seven prophages from previously reported isolates (see Methods). The phages genomes of phi9102, phi4197, phi5013-M1, phi5013-M2, phi5038-11536, phi5038-11551, and phi11547 were assembled as single contigs of 52,239 base pairs (bp), 39,359, 42,180, 49,159, 48,056, 38,492 and 25,802 bp, respectively. The assembled genomes were assigned as complete and high-quality genomes according to CheckV. No tRNA or ARGs were identified. All induced prophages were similar to the reported Ab11510-phi phage (López-Leal et al., 2021; Supplementary material 1). Interestingly, strains Ab5013 and Ab5038 harbored two genomically similar phages of the genus *Vieuvirus* (Supplementary material 2).

Thirteen most abundant putative phage genera in species of *Acinetobacter baumannii*

To obtain a better overview of the seven isolated phages in the context of the *A. baumannii* prophage populations, we used a database with 1,501 high-quality *A. baumannii* genomes, according to CheckM (Parks et al., 2015; Supplementary material 3). In an initial analysis, 4,865 prophages were collected. However, only 967 (19.87%) of the prophage predictions were assigned as high-quality by CheckV (Supplementary material 4). To place the seven induced prophages into a genomic and phylogenomic context relative to the prophage population in *A. baumannii*, only high-quality predictions were used, as this approach was considered to provide more reliable results given that prophages are prone to degradation processes (Bobay et al., 2014).

2 dx.doi.org/10.17504/protocols.io.bwm5pc86

These 928 final prophages represented an average of 1.67 prophages per genome. Additionally, we add 21 putative *Vieuvirus* genomes (Supplementary material 5), previously reported (Rastegar et al., 2024), in order to put the induced and isolated prophages (in this study) in context with other previously reported phages of the genus *Vieuvirus* and with prophage populations from *A. baumannii* isolates. Finally, we built an *A. baumannii* phage and prophage genome database with 995 genomes. Of these, we found that 30.02% of phages and prophages were singletons (see Methods), and 69.98% were grouped into 119 clusters using cd-hit. Of these, only phages that clustered with ≥5 others were selected to construct a gene content correlation matrix. This threshold was chosen to focus on the most prevalent phages, which could be grouped into potential genera, providing a clearer understanding of gene content similarity within more broadly distributed phage populations (Figure 1). Furthermore, we observed that the clustering shown in the heat map did not correlate with the groups found in the first level of clustering by cd-hit (see clusters in the top rows of Figure 1). This result suggested that mosaicism of bacteriophage genomes presents challenges to describing phage-relatedness (Gauthier and Hatfull, 2023). In other words, the clustering of gene content (homologous proteins) retrieved by the heat map did not reflect the genome-level clustering obtained by cd-hit. On the other hand, the heat map based on the gene content correlation matrix showed a considerable variation in gene content among the phages, resulting in 13 clusters (50.57% of the phage database). However, we observed some degree of relationship in gene content between phages from clusters 1, 2, 3, 6, and 9–11 (Figure 1, red rectangle). Next, we used the pangenome of the phages to perform a principal component analysis (PCA) based on the pan-matrix. Although only 45.5% of the total variation was captured by the first two components (out of 482 dimensions, Supplementary material 6), the first 10 dimensions accounted for 85.6% of the variance in our data. This suggests that the remaining variation is likely due to the presence of unique genes in each phage, which are not homologous to those in others. Two phage populations were delimited on the first principal (horizontal) axis. Namely, the phages from clusters 4, 5, 7, 8, 12, and 13 were placed within the PC1 component values >0, and the rest were located within the PC1 values <0 (Supplementary material 6). This indicates that the phages of clusters 4, 5, 7, 8, 12, and 13 do not share homologous genes with the rest of the phages or share very few homologous genes. On the contrary, phages from clusters 1, 2, 3, 6, and 9–11 (Figure 1, red rectangle) shared some or several homologous groups (see methods). To further elucidate this, we used a gene content distance matrix to construct a hierarchical clustering tree

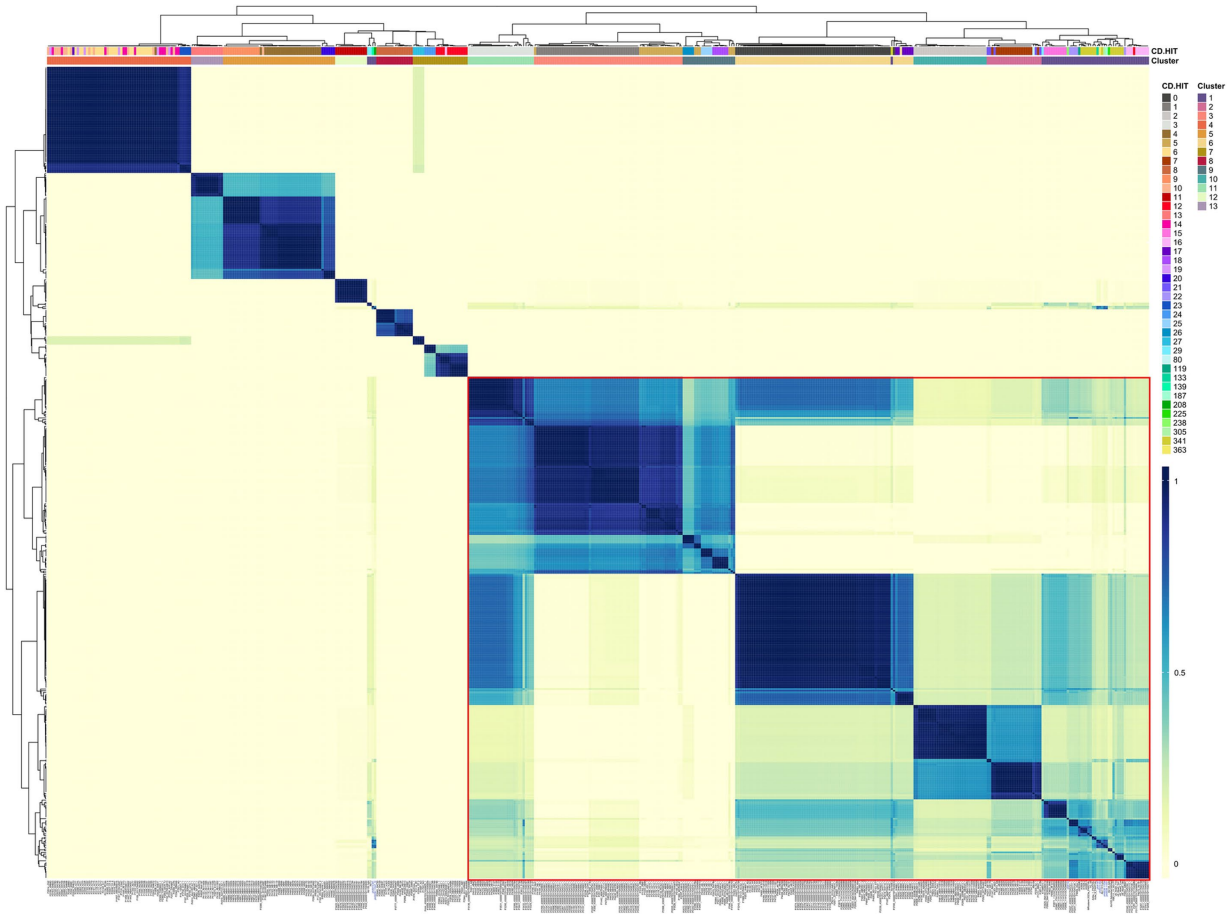

FIGURE 1
Gene content variation among the phages. A heat map of the gene content correlation matrix was used to analyze the gene content differences among the phages. Clusters according to cd-hit and the average-silhouette (using the correlation matrix) method are indicated in the color bars on the top. The red rectangle detonates those phage groups with the most shared genes.

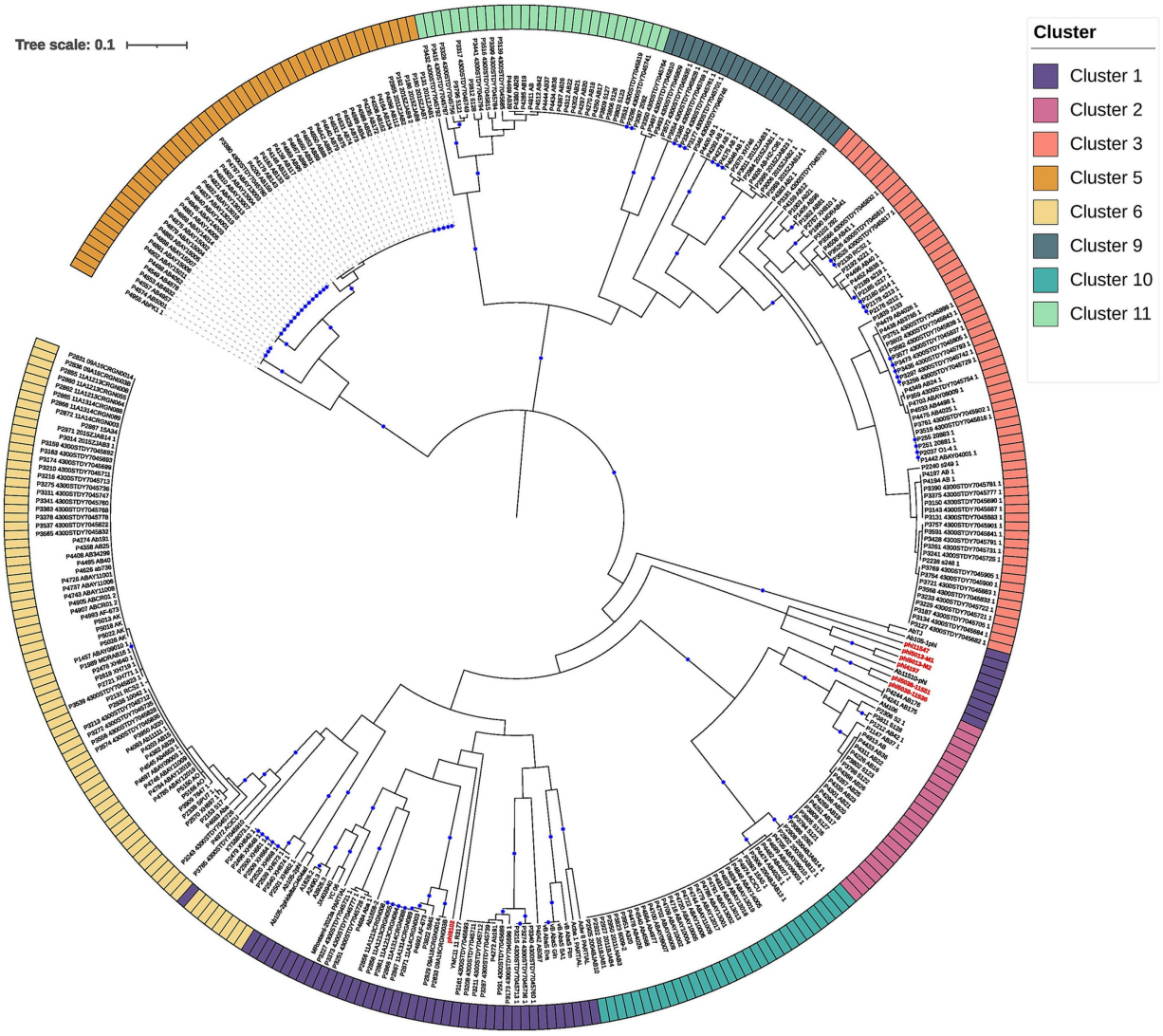

FIGURE 2
The hierarchical tree was constructed with the PC (protein clusters) from clusters 1, 2, 3, 5, 6, 9, 10, and 11 (rooted using cluster 5; see results) based on intergenomic distances. The external circle provides the clusters, which are designated by the optimal number of clusters, using the average silhouette method (see Figure 1 and Methods section). The bootstrap values higher or equal to 80 are depicted with blue circles at the internal nodes.

based on gene content (Figure 2) that only included phages from clusters 1, 2, 3, 6, and 9–11 and rooted the phylogeny using phages from Cluster 5 a closely related genus.

The first thing we noticed is that most of the clades defining the clusters (Figure 2) were well supported (>80 bootstrap values; blue circles). However, clustering boundaries between clusters 1 and 6 had weak support (bootstrap of 45). Interestingly, all members of cluster 6 correspond to prophage predictions, while phages located in cluster 1 correspond to prophage predictions and isolated phages previously reported in the NCBI (assigned as *Vieuvirus*). On this basis, we have tentatively separated these predominantly temperate *A. baumannii* phages into two clusters (Clusters 1 and 6). However, we note that this assignment was poorly supported by the phylogenetic analysis (Figure 2). Interestingly, shorter branches were observed in the Cluster 6 clade (Figure 2). Therefore, we analyzed the distribution of branch lengths for both clusters. Both distributions showed that short branches predominated in both clusters (Supplementary material 7). However, Cluster 6 (Supplementary material 7B) seems to have a higher concentration of extremely short lengths compared to Cluster 1 (Supplementary material 7A), suggesting that the prophages (Cluster 6) have a higher proportion of homolog groups or proteins very similar in sequence so they are even more closely related or have experienced less genetic divergence compared to those in Cluster 1. This indicates that the induced prophages have less HG in common; therefore, they may experience more divergence in their protein repertoire.

Finally, each cluster was validated using the VICTOR tool. Most of the clusters were validated by VICTOR at the genus level, except for phages AbTJ (Xu et al., 2020) and Ab105-1phi, which have been previously reported to share some genetic repertoire with phages of the *Vieuvirus* genus (López-Leal et al., 2021). However, according to the NCBI, these phages are unclassified *Caudoviricetes*. Another exception was for prophages P1576, P1697, P1703, P2118, and P2344

from Cluster 7 (Supplementary material 8), which showed a small degree of similarity with phage AM106 (MH115576), with a coverage of 9–15% and identity of ~90%. In other words, our approach, using the correlation of gene content variation, succeeded in grouping these phages appropriately at the genus level.

Geographic co-occurrence of bacteriophages reveals countries delimit species

With a total of 482 bacteriophages analyzed (phages and prophages from the 13 clusters), we were able to identify and validate 97 phage species and 15 phage genera (Supplementary material 8). We then determined the sequence type and isolation location of the hosts of the 467 prophages (only prophages from the 13 clusters). This collection of *A. baumannii* isolates comprised 53 different STs (according to Pasteur's MLST scheme) from 22 countries. Of these, 23.56% of the isolates primarily corresponded to 1806 STs, and 41.69% were from China (Supplementary material 9). Then, in order to identify how widely the bacteriophage genera and species were geographically spread, we first determined the uncertainty coefficient between bacteriophage genera and species. First, we determined the uncertainty coefficient between the genus-species relationships against geographic locality (country) and host ST to determine the relationship strength between these two categorical variables. We found that the mutual information was 1.27 and 0.67, for the species-country and genus-country relationships, respectively (Table 1). These values indicate that the variables share certain information, suggesting a dependence or relationship between them. Specifically, the relationship between species and country is stronger than the relationship between genus and country. Moreover, the residual uncertainty in species was 66.58% after knowing the country, whereas for genus, it was 35.11%. In addition, the residual uncertainty for the country after knowing the genus and species was 24.46 and 31.98%, respectively (Table 1). In other words, residual uncertainty is higher when species or genus is conditioned on country than vice versa, indicating that country has a considerable effect in reducing uncertainty about species or genus. Of these, phage species provide more information about the country and vice versa, compared to genus. With this information, we wanted to see the correlation between the co-occurrence of genera and phage species and the isolation country. A strong positive correlation was observed between the frequency of different species due to their co-occurrence in the same location. Of 73 phage species only located in China (28 species), Thailand (23 species), Mexico (10 species), South Korea (7 species), and Spain (5 species; Figure 3A). Of these, 26.38% of the species corresponded to the *Vieuvirus* genus (G2-Cluster 1; Figure 3B), followed by 11.11% of species for an unclassified genus (G4-Cluster 3), which are similar to the previously reported phage fLi-Aba03 (Rastegar et al., 2024). The rest of the species (with an average of 5.20% of species per genus) belonged to different genera. Interestingly, co-occurrence of phage species is mainly related to the *Vieuvirus* (Figure 3B).

Although these species belong to different genera, however, it is important to note that phages of genus G2 (Cluster 1; Figure 1) were found more frequently in Thailand, Mexico, Canada, and Iran, while phages of genus G7 (Cluster 6; Figure 1) were found mainly in China, Thailand, Canada, and South Korea (Supplementary material 8). Based on our results (Supplementary material 10), these two groups of phages could be two types of *Vieuvirus* located mainly in North America and South Asia (Cluster 2) and East Asia (Cluster 6). Additionally, the G15 genus, composed of a small number of phages (Cluster 13), was found mainly in isolates from Mexico (Supplementary material 11).

Discussion

In recent years, the use of bacteriophages as an alternative strategy to antibiotics has gained significant attention. One of the main concerns regarding phage therapy is the evolution of the host genome induced by prophages (Rohde et al., 2018). Recent studies have indicated that pathogenic species accumulate prophage sequences more frequently (Lopez-Leal et al., 2022). Therefore, identifying inducible-prophage populations or potentially active prophages in pathogens such as *A. baumannii* is crucial for studying virus-host relationships.

Here, we analyzed seven inducible prophages from *A. baumannii* combined with 4,671 prophages retrieved from 1,465 *A. baumannii* genomes. Only 19.86% of these predictions were of high quality. We chose to use only high-quality predictions because prophages, once integrated into the chromosome, can become trapped within the host genome due to genomic rearrangements and gradual decay. This domestication of prophages leads to the accumulation of mutations and the loss of genetic material (degradation), which prevents their excision during cell lysis and limits the production of phage particles, as well as lysogenization of non-lysogenic strains (Bobay et al., 2014;

TABLE 1 Relationship between phage abundance and geographic location assessed by the uncertainty coefficient.

X	Y	Mutual Information	U(X|Y)	U(X|Y)_min	U(X|Y)_max	U(Y|X)	U(Y|X)_min	U(Y|X)_max
species	country	1.272894	0.6658364	0.6275773	0.7040955	0.3458607	0.3198087	0.3719127
genus	country	0.6711771	0.3511364	0.3221173	0.3810555	0.2732039	0.2446645	0.3017434
species	host (ST)	1.963887	0.6562884	0.6258662	0.6867107	0.5335639	0.5073782	0.5597496
genus	host (ST)	2.991586	0.4067885	0.3824496	0.4311273	0.4953847	0.4632711	0.5274983

Mutual information and conditional entropy values between bacteriophage genera and species are shown in relation to geographic locality (country) and host sequence type (ST). Mutual information reflects the amount of information shared between the variables. Columns "U(X|Y)" and "U(Y|X)" indicate the uncertainty coefficient, which represents the fraction of uncertainty of X that is reduced by knowing Y, and vice versa, together with their confidence intervals (minimum "min" and maximum "max").

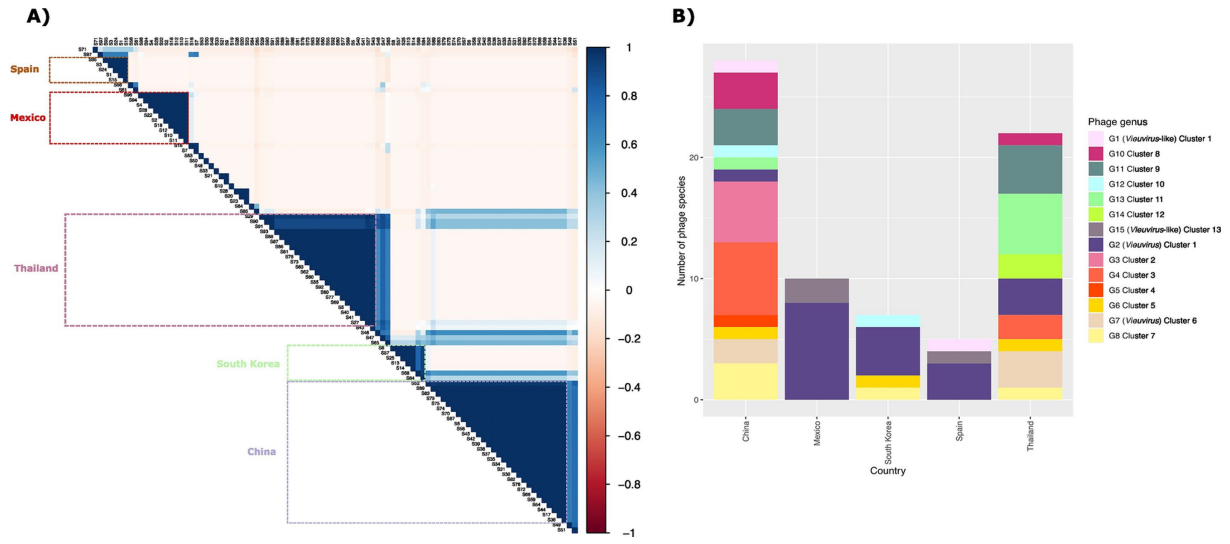

FIGURE 3
(A) Correlation matrix representing Pearson correlation between the relative abundance of species. The color intensity is relative to the correlation coefficients; negative correlations are shown in red, and positive correlations in blue. On the right, the legend shows the corresponding colors and the correlation coefficients. The boxes represent the high correlation species present in each county. **(B)** Bar plot showing the abundance of the 73 phage species by country. The colored panel indicates the genus to which the phage species belongs.

Canchaya et al., 2003). These inactive phages are often referred to as cryptic prophages. Although cryptic prophages can also play a role in phage-host dynamics, here, we aimed to explore prophage populations with active potential. On average, we found 1.6 prophages per genome, indicating a substantial prophage presence within this species. It has been reported that species from the genera *Acinetobacter*, *Enterobacter*, and *Pseudomonas* tend to accumulate more prophages (Lopez-Leal et al., 2022).

Additionally, 30.02% of these prophages were found to be singletons, reflecting that more than a quarter of the prophage population in *A. baumannii* are single prophages. Recent studies suggest that this proportion may be even higher. However, Tenorio-Carnalla et al. applied an operational species definition based on ANI values of >95% identity and >90% coverage. Our results revealed that *A. baumannii* prophages exhibit high variability in gene content, likely due to the exchange of genetic material with other phages and their bacterial hosts. This genetic exchange results in genome regions that differ significantly even among closely related phages, potentially causing ANI values to fall below the 95% identity threshold for species definition, despite the phages being functionally similar or closely related in other genomic regions (Tenorio-Carnalla et al., 2024). These observations could be critical to consider if phages that infect these species (especially *A. baumannii*) are to be viewed as an alternative strategy to antibiotic use. In this study, we used the correlation of shared homologous gene content among the phages, which allowed us to group them at the genus level. Notably, these genera were confirmed and validated using the VICTOR tool.

From a phylogenomic perspective, we found that the prophages of *A. baumannii* belong to 13 more prevalent genera, most of which are grouped as unclassified *Caudoviricetes*. However, the *Vieuvirus* genus was among the most abundant in our dataset. These results are consistent with previous studies suggesting a high prevalence of *Vieuvirus*-like prophages in *A. baumannii* (Loh et al., 2020). In this sense, one of the most relevant findings of our study is the identification of two putative *Vieuvirus* populations (Cluster 1 and Cluster 2). Interestingly, we observed shorter branches within the Cluster 6 clade than in Cluster 1. This pattern suggests that the prophages in Cluster 6 share a higher proportion of homologous groups or proteins with similar sequences, implying closer evolutionary relationships or less genetic divergence. In contrast, the prophages in Cluster 1, with longer branch lengths, appear to have undergone more divergence that could potentially result in a broader range of genetic content.

Additionally, G2 (Cluster 1) was primarily found in isolates from North America and South Asia, whereas the G7 (Cluster 6) *Vieuvirus* was mainly found in East Asia and Europe. These observations were validated by assessing the uncertainty coefficient, indicating that the identification of phage species is influenced by geographic location. In addition, some international clones (IC) of *A. baumannii* are known to be limited to specific geographic regions, and this localization is apparently timeless (Müller et al., 2023). For instance, IC9 is in the USA, whereas IC5 is in Latin America. Although it has been reported that similar lytic *A. baumannii* phages have been isolated in different geographic areas (López-Leal et al., 2021), prophage populations are geographically delimited (Tenorio-Carnalla et al., 2024).

Interestingly, of the 73 phage species that we found with a strong positive correlation between frequency and geographic co-occurrence, the species belonging to the genus *Vieuvirus* were the most prevalent (26.38%). Our results suggest that the geographic region and the circulating strains within that region could influence resistance or sensitivity to certain types of phages. Although phage and prophage detection tools may be biased by training data and genome availability, the regionality of prophage populations in *A. baumannii* has recently been reported (Tenorio-Carnalla et al., 2024). However, this has not been explored in other clinically relevant pathogens. This observation

adds another factor to consideration in using phage therapy to combat MDR pathogens since prophages prevent superinfection.

Finally, our study provides valuable insights into the diversity and geographic distribution of prophages in *A. baumannii*. Identifying two geographically distinct populations of *Vieuvirus* highlights the need for further investigation into how phage-host interactions evolve in different regions. Moreover, our results underscore the importance of considering geographic factors and inducible prophage populations when developing phage therapy strategies, particularly in the context of MDR pathogens such as *A. baumannii*. Understanding the genetic diversity and distribution of prophages will be essential for advancing the use of bacteriophages as therapeutic agents in clinical settings.

Data availability statement

The datasets presented in this study can be found in online repositories. The names of the repository/repositories and accession number(s) can be found in the article/Supplementary material.

Author contributions

DA-M: Data curation, Formal analysis, Investigation, Methodology, Software, Visualization, Writing – review & editing. JH-R: Data curation, Software, Writing – review & editing. LC-V: Formal analysis, Software, Visualization, Writing – review & editing. SC-R: Supervision, Writing – review & editing. AR: Supervision, Writing – review & editing. GL-L: Conceptualization, Data curation, Formal analysis, Funding acquisition, Investigation, Methodology, Project administration, Resources, Software, Supervision, Validation, Visualization, Writing – original draft, Writing – review & editing.

Funding

The author(s) declare that financial support was received for the research, authorship, and/or publication of this article. This project was partially funded by CONAHCyT Ciencia Básica 2024 (grant no. CBF2023-2024-3171), given to GLL.

Acknowledgments

GLL thanks Victor González, for his helpful comments and Rosa Isela Santamaria for her recommendations on the phage isolation protocol.

Conflict of interest

The authors declare that the research was conducted in the absence of any commercial or financial relationships that could be construed as a potential conflict of interest.

Generative AI statement

The author(s) declare that no Gen AI was used in the creation of this manuscript.

Publisher's note

Supplementary material

The Supplementary material for this article can be found online at: https://www.frontiersin.org/articles/10.3389/fmicb.2025.1522711/full#supplementary-material

SUPPLEMENTARY DATA 1
Blast results of isolated phage against the NCBI virus database.

SUPPLEMENTARY DATA 2
Agarose gel electrophoresis of restriction digestion products. Representative 1% agarose gel electrophoresis of restriction digestion products using *BamH*I/*Nde*I and *EcoR*I enzymes. Each gel lane corresponds to DNA from phage isolated from the same host (*A. baumannii* 5013 and/or *A. baumannii* 5038). The red arrows indicate the discriminatory bands each enzyme produces (or a mixture of enzymes), which indicates different phages.

SUPPLEMENTARY DATA 3
List of bacterial genomes used.

SUPPLEMENTARY DATA 4
CheckV report on the quality of viral sequences.

SUPPLEMENTARY DATA 5
List of phage genomes used from NCBI.

SUPPLEMENTARY DATA 6
Principal component analysis (PCA) was performed on a pan-matrix. Each phage genome is represented by a circle positioned in the pan-matrix space based on its values along the first two principal components. The colors of the circles indicate the phage clusters at the genus level. The percentages shown in the axis labels represent the total variation in the pan-matrix that is captured by each principal component. As shown in Figure 1 (see results), the circles indicate two distinct groups of phages: those that share several homologous groups (red oval) and those with few homologous groups (blue oval).

SUPPLEMENTARY DATA 7
Distributions of Cluster 1 **(A)** and Cluster 6 (right) branch lengths. The histograms show the observed branch length distributions for two clades (Cluster 1 and Cluster 6) from the tree in Figure 2.

SUPPLEMENTARY DATA 8
List of phages grouped in clusters at genus and species level.

SUPPLEMENTARY DATA 9
Table frequency of phages and prophages from the different genera (clusters) by host.

SUPPLEMENTARY DATA 10
Frequency of phages belonging to the genus *Vieuvirus* (Clusters 1 and 6) present in *A. baumannii* isolates from each geographic region.

SUPPLEMENTARY DATA 11
The hierarchical tree was constructed with the PC (protein clusters) of phages from cluster 13 based on intergenomic distances. The bootstrap values higher or equal to 80 are depicted with blue circles at the internal nodes. The color labels are found on the outer edge of the tree.

References

Andrade-Martínez, J. S., Valera, L. C. C., Cárdenas, L. A. C., Forero-Junco, L., López-Leal, G., Moreno-Gallego, J. L., et al. (2022). Computational tools for the analysis of uncultivated phage genomes. *Microbiol. Mol. Biol. R.* 86:e0000421. doi: 10.1128/mmbr.00004-21

Bobay, L. M., Touchon, M., and Rocha, E. P. C. (2014). Pervasive domestication of defective prophages by bacteria. *Proc. Natl. Acad. Sci. USA* 111, 12127–12132. doi: 10.1073/pnas.1405336111

Bouras, G., Nepal, R., Houtak, G., Psaltis, A. J., Wormald, P. J., and Vreugde, S. (2023). Pharokka: a fast scalable bacteriophage annotation tool. *Bioinformatics* 39:btac776. doi: 10.1093/bioinformatics/btac776

Breitbart, M., and Rohwer, F. (2005). Here a virus, there a virus, everywhere the same virus? *Trends Microbiol.* 13, 278–284. doi: 10.1016/j.tim.2005.04.003

Canchaya, C., Proux, C., Fournous, G., Bruttin, A., and Brussow, H. (2003). Prophage genomics. *Microbiol. Mol. Biol. Rev.* 67, 238–276. doi: 10.1128/MMBR.67.2.238-276.2003

Chung, I. Y., Jang, H. J., Bae, H. W., and Cho, Y. H. (2014). A phage protein that inhibits the bacterial ATPase required for type IV pilus assembly. *Proc. Natl. Acad. Sci. USA* 111, 11503–11508. doi: 10.1073/pnas.1403537111

Coil, D., Jospin, G., and Darling, A. E. (2015). A5-miseq: an updated pipeline to assemble microbial genomes from Illumina MiSeq data. *Bioinformatics* 31, 587–589. doi: 10.1093/bioinformatics/btu661

Costa, A. R., Monteiro, R., and Azeredo, J. (2018). Genomic analysis of prophages reveals remarkable diversity and suggests profound impact on bacterial virulence and fitness. *Sci. Rep.* 8:8. doi: 10.1038/s41598-018-33800-5

De Paepe, M., Hutinet, G., Son, O., Amarir-Bouhram, J., Schbath, S., and Petit, M. A. (2014). Temperate phages acquire DNA from defective prophages by relaxed homologous recombination: the role of Rad52-like recombinases. *PLoS Genet.* 10:e1004181. doi: 10.1371/journal.pgen.1004181

Dragos, A., Priyadarshini, B., Hasan, Z., Strube, M. L., Kempen, P. J., Maróti, G., et al. (2021). Pervasive prophage recombination occurs during evolution of spore-forming. *ISME J.* 15, 1344–1358. doi: 10.1038/s41396-020-00854-1

Fu, L., Niu, B., Zhu, Z., Wu, S., and Li, W. (2012). CD-HIT: accelerated for clustering the next-generation sequencing data. *Bioinformatics* 28, 3150–3152. doi: 10.1093/bioinformatics/bts565

Gauthier, C. H., and Hatfull, G. F. (2023). PhamClust: a phage genome clustering tool using proteomic equivalence. *mSystems* 8:e0044323. doi: 10.1128/msystems.00443-23

Graña-Miraglia, L., Lozano, L. F., Velázquez, C., Volkow-Fernández, P., Pérez-Oseguera, A., Cevallos, M. A., et al. (2017). Rapid gene turnover as a significant source of genetic variation in a recently seeded population of a healthcare-associated pathogen. *Front. Microbiol.* 8:1817. doi: 10.3389/fmicb.2017.01817

Guo, J., Bolduc, B., Zayed, A. A., Varsani, A., Dominguez-Huerta, G., Delmont TOet al. (2021). VirSorter2: a multi-classifier, expert-guided approach to detect diverse DNA and RNA viruses. *Microbiome* 9:37. doi: 10.1186/s40168-020-00990-y

Hernandez-Gonzalez, I. L., Mateo-Estrada, V., and Castillo-Ramirez, S. (2022). The promiscuous and highly mobile resistome of *Acinetobacter baumannii*. *Microb. Genom.* 8:762. doi: 10.1099/mgen.0.000762

Hyman, P. (2019). Phages for phage therapy: isolation, characterization, and host range breadth. *Pharmaceuticals* 12:35. doi: 10.3390/ph12010035

Jeon, J., D'Souza, R., Pinto, N., Ryu, C. M., Park, J. H., Yong, D., et al. (2015). Complete genome sequence of the siphoviral bacteriophage Betavarphi-R3177, which lyses an OXA-66-producing carbapenem-resistant *Acinetobacter baumannii* isolate. *Arch. Virol.* 160, 3157–3160. doi: 10.1007/s00705-015-2604-y

Jeon, J., Kim, J. W., Yong, D., Lee, K., and Chong, Y. (2012). Complete genome sequence of the Podoviral bacteriophage YMC/09/02/B1251 ABA BP, which causes the lysis of an OXA-23-producing Carbapenem-resistant isolate from a septic patient. *J. Virol.* 86, 12437–12438. doi: 10.1128/JVI.02132-12

Kondo, K., Kawano, M., and Sugai, M. (2021). Distribution of antimicrobial resistance and virulence genes within the prophage-associated regions in nosocomial pathogens. *mSphere* 6:e0045221. doi: 10.1128/mSphere.00452-21

Kropinski, A. M., Mazzocco, A., Waddell, T. E., Lingohr, E., and Johnson, R. P. (2009). Enumeration of bacteriophages by double agar overlay plaque assay. *Methods Mol. Biol.* 501, 69–76. doi: 10.1007/978-1-60327-164-6_7

Li, X. Y., Lachnit, T., Fraune, S., Bosch, T. C. G., Traulsen, A., and Sieber, M. (2017). Temperate phages as self-replicating weapons in bacterial competition. *J. R. Soc. Interface* 14:20170563. doi: 10.1098/rsif.2017.0563

Loh, B., Chen, J. Y., Manohar, P., Yu, Y. S., Hua, X. T., and Leptihn, S. (2020). A biological inventory of prophages in genomes reveal distinct distributions in classes, length, and genomic positions. *Front. Microbiol.* 11:579802. doi: 10.3389/fmicb.2020.579802

Lopez-Leal, G., Camelo-Valera, L. C., Hurtado-Ramirez, J. M., Verleyen, J., Castillo-Ramirez, S., and Reyes-Munoz, A. (2022). Mining of Thousands of prokaryotic genomes reveals high abundance of prophages with a strictly narrow host range. *mSystems* 7:e0032622. doi: 10.1128/msystems.00326-22

López-Leal, G., Reyes-Muñoz, A., Santamaria, R. I., Cevallos, M. A., Pérez-Monter, C., and Castillo-Ramírez, S. (2021). A novel vieuvirus from multidrug-resistant. *Arch. Virol.* 166, 1401–1408. doi: 10.1007/s00705-021-05010-4

López-Leal, G., Santamaria, R. I., Cevallos, M. A., Gonzalez, V., and Castillo-Ramírez, S. (2020). Prophages encode antibiotic resistance genes in. *Microb. Drug Resist.* 26, 1275–1277. doi: 10.1089/mdr.2019.0362

Maurice, C. F., Bouvier, C., de Wit, R., and Bouvier, T. (2013). Linking the lytic and lysogenic bacteriophage cycles to environmental conditions, host physiology and their variability in coastal lagoons. *Environ. Microbiol.* 15, 2463–2475. doi: 10.1111/1462-2920.12120

Mcallister, W. T., and Barrett, C. L. (1977). Superinfection exclusion by bacteriophage-T7. *J. Virol.* 24, 709–711. doi: 10.1128/jvi.24.2.709-711.1977

Meier-Kolthoff, J. P., and Goker, M. (2017). VICTOR: genome-based phylogeny and classification of prokaryotic viruses. *Bioinformatics* 33, 3396–3404. doi: 10.1093/bioinformatics/btx440

Motbainor, H., Bereded, F., and Mulu, W. (2020). Multi-drug resistance of blood stream, urinary tract and surgical site nosocomial infections of and among patients hospitalized at Felegehiwot referral hospital, Northwest Ethiopia: a cross-sectional study. *BMC Infect. Dis.* 20:92. doi: 10.1186/s12879-020-4811-8

Müller, C., Reuter, S., Wille, J., Xanthopoulou, K., Stefanik, D., Grundmann, H., et al. (2023). A global view on carbapenem-resistant *Acinetobacter baumannii*. *MBio* 14:6. doi: 10.1128/mbio.02260-23

Myers, J. (2016). This is how many people antibiotic resistance could kill every year by 2050 if nothing is done. World Economic Forum.

Nayfach, S., Camargo, A. P., Schulz, F., Eloe-Fadrosh, E., Roux, S., and Kyrpides, N. C. (2021). CheckV assesses the quality and completeness of metagenome-assembled viral genomes. *Nat. Biotechnol.* 39, 578–585. doi: 10.1038/s41587-020-00774-7

O'Neill, J. (2014). Review on antimicrobial resistance antimicrobial resistance: tackling a crisis for the health and wealth of nations. London: Review on Antimicrobial Resistance.

Page, A. J., Cummins, C. A., Hunt, M., Wong, V. K., Reuter, S., Holden, M. T., et al. (2015). Roary: rapid large-scale prokaryote pan genome analysis. *Bioinformatics* 31, 3691–3693. doi: 10.1093/bioinformatics/btv421

Parks, D. H., Imelfort, M., Skennerton, C. T., Hugenholtz, P., and Tyson, G. W. (2015). CheckM: assessing the quality of microbial genomes recovered from isolates, single cells, and metagenomes. *Genome Res.* 25, 1043–1055. doi: 10.1101/gr.186072.114

Piligrimova, E. G., Kazantseva, O. A., Kazantsev, A. N., Nikulin, N. A., Skorynina, A., Koposova, O. N., et al. (2021). Putative plasmid prophages of may hold the key to undiscovered phage diversity. *Sci. Rep.* 11:7611. doi: 10.1038/s41598-021-87111-3

Piña-González, A. M., Castelán-Sánchez, H. G., Hurtado-Ramírez, J. M., and López-Leal, G. (2024). Prophage diversity reveals pervasive recombination between prophages from different species. *Microbiol. Spectr.* 12:e0279523. doi: 10.1128/spectrum.02795-23

Ramisetty, B. C. M., and Sudhakari, P. A. (2019). Bacterial 'Grounded' prophages: hotspots for genetic renovation and innovation. *Front. Genet.* 10:10. doi: 10.3389/fgene.2019.00065

Rastegar, S., Skurnik, M., Niaz, H., Tadjrobehkar, O., Samareh, A., Hosseini-Nave, H., et al. (2024). Isolation, characterization, and potential application of *Acinetobacter baumannii* phages against extensively drug-resistant strains. *Virus Genes* 60, 725–736. doi: 10.1007/s11262-024-02103-5

Rohde, C., Resch, G., Pirnay, J. P., Blasdel, B. G., Debarbieux, L., Gelman, D., et al. (2018). Expert opinion on three phage therapy related topics: bacterial phage resistance, phage training and prophages in bacterial production strains. *Viruses* 10:178. doi: 10.3390/v10040178

Santamaria, R. I., Bustos, P., Sepúlveda-Robles, O., Lozano, L., Rodríguez, C., Fernández, J. L., et al. (2014). Narrow-host-range bacteriophages that infect *Rhizobium etli* associate with distinct genomic types. *Appl. Environ. Microbiol.* 80, 446–454. doi: 10.1128/AEM.02256-13

Sayers, E. (2009). The E-utilities in-depth: parameters, syntax and more. Available at: https://www.ncbi.nlm.nih.gov/books/NBK25499/2018 (Accessed April 25, 2022).

Schooley, R. T., Biswas, B., Gill, J. J., Hernandez-Morales, A., Lancaster, J., Lessor, L., et al. (2017). Development and use of personalized bacteriophage-based therapeutic cocktails to treat a patient with a disseminated resistant infection. *Antimicrob. Agents Chemother.* 61, e00954–e00917. doi: 10.1128/AAC.00954-17

Selva, L., Viana, D., Regev-Yochay, G., Trzcinski, K., Corpa, J. M., Lasa, I., et al. (2009). Killing niche competitors by remote-control bacteriophage induction. *Proc. Natl. Acad. Sci. USA* 106, 1234–1238. doi: 10.1073/pnas.0809600106

Simmonds, P., Adriaenssens, E. M., Zerbini, F. M., Abrescia, N. G. A., Aiewsakun, P., Alfenas-Zerbini, P., et al. (2023). Four principles to establish a universal virus taxonomy. *PLoS Biol.* 21:e3001922. doi: 10.1371/journal.pbio.3001922

Tenorio-Carnalla, K., Aguilar-Vera, A., Hernandez-Alvarez, A. J., Lopez-Leal, G., Mateo-Estrada, V., Santamaria, R. I., et al. (2024). Host population structure and species resolution reveal prophage transmission dynamics. *MBio* 15:e0237724. doi: 10.1128/mbio.02377-24

Turner, D., Kropinski, A. M., and Adriaenssens, E. M. (2021). A roadmap for genome-based phage taxonomy. *Viruses* 13:506. doi: 10.3390/v13030506

Wang, Z. T., Yang, X., Wang, H., Wang, S. X., Fang, R., Li, X. T., et al. (2024). Characterization and efficacy against carbapenem-resistant of a novel phage from sewage. *Front. Cell. Infect.* 14:1382145. doi: 10.3389/fcimb.2024.1382145

Wendling, C. C., Refardt, D., and Hall, A. R. (2021). Fitness benefits to bacteria of carrying prophages and prophage-encoded antibiotic-resistance genes peak in different environments. *Evolution* 75, 515–528. doi: 10.1111/evo.14153

Wick, R. R., Schultz, M. B., Zobel, J., and Holt, K. E. (2015). Bandage: interactive visualization of de novo genome assemblies. *Bioinformatics* 31, 3350–3352. doi: 10.1093/bioinformatics/btv383

Xu, J., Li, X., Kang, G., Bai, L., Wang, P., and Huang, H. (2020). Isolation and characterization of AbTJ, an *Acinetobacter baumannii* phage, and functional identification of its receptor-binding modules. *Viruses* 12:205. doi: 10.3390/v12020205

frontiers | Frontiers in Microbiology

TYPE Original Research
PUBLISHED 26 February 2025
DOI 10.3389/fmicb.2025.1533694

OPEN ACCESS

EDITED BY
Barbara Maciejewska,
University of Wrocław, Poland

REVIEWED BY
Thomas Brüser,
Leibniz University Hannover, Germany
Ramanujam Srinivasan,
National Institute of Science Education and Research (NISER), India

*CORRESPONDENCE
Yaodong Chen
✉ ydchen@nwu.edu.cn
Shiwei Wang
✉ wangsw@nwu.edu.cn

RECEIVED 24 November 2024
ACCEPTED 14 February 2025
PUBLISHED 26 February 2025

CITATION
Zhao K, Du S, Tian L, Wang S, Shi R, Sun H, Zhou Y, Huang C, Sun Y, Wang S and Chen Y (2025) Bacteriophage P1 protein Icd inhibits bacterial division by targeting FtsZ. *Front. Microbiol.* 16:1533694. doi: 10.3389/fmicb.2025.1533694

Bacteriophage P1 protein Icd inhibits bacterial division by targeting FtsZ

Kairui Zhao[1], Shuheng Du[1], Linlin Tian[1], Shenping Wang[1], Runqin Shi[1], Haiyu Sun[1], Yao Zhou[1], Chenhao Huang[1], Yanmei Sun[1,2], Shiwei Wang[1,2]* and Yaodong Chen[1,2]*

[1]Key Laboratory of Resources Biology and Biotechnology in Western China, Ministry of Education, College of Life Sciences, Northwest University, Xi'an, China, [2]Provincial Key Laboratory of Biotechnology of Shaanxi Province, Northwest University, Xi'an, China

The study of bacteriophage (phage) gene products and their effects on the host helps to better understand the phage-host relationship and provides clues for the development of new antimicrobial proteins. In this study, we focused on a small protein named Icd with 73 amino acids from phage P1. It inhibits the growth of *Escherichia coli* and rapidly blocks the formation of Z-ring. The results of bacterial two-hybrid and pull-down experiments showed that Icd directly targets FtsZ, a key protein in bacterial division. Furthermore, we identified the core region of Icd as amino acids 12–51; this 40-amino acid protein had similar antibacterial activity to the full-length Icd, inhibiting bacterial growth and division.

KEYWORDS

bacteriophage P1, ICD, bacterial cell division, FtsZ, phage-host

Introduction

The continued increase in pathogenic microorganisms and their drug-resistant strains pose a serious threat to human health (Munita and Arias, 2016). Drug-resistant bacteria are found in various human habitats, and the growing urgency has led to research into new antibiotics, including new antimicrobial proteins (AMP), as effective solutions.

FtsZ is an attractive target for developing novel antibiotics (Ur Rahman et al., 2020; Kusuma et al., 2019), which is conserved in most bacteria and archaea, and plays a crucial role in most pathogenic microorganisms. FtsZ is essential for bacterial division (Haeusser and Margolin, 2016; McQuillen and Xiao, 2020). It was the first identified bacterial tubulin homolog (Nogales et al., 1998; Oliva et al., 2004) with the ability to hydrolyze GTP and self-polymerize into mostly single highly dynamic protofilaments (Chen and Erickson, 2005; Chen and Erickson, 2009). FtsZ serves as a scaffold for the Z ring that assembles at the bacterial division site, recruiting dozens of proteins to form the mature divisome to complete division (McQuillen and Xiao, 2020; Bi and Lutkenhaus, 1991). Z-ring *in vivo* are very dynamic, driven by the hydrolysis of GTP by FtsZ (Stricker et al., 2002), which is consistent with the highly dynamic characteristics of FtsZ filaments (Chen and Erickson, 2005; Chen and Erickson, 2009). Recent studies have revealed that they exhibit a treadmilling pattern, adding subunits to one end of the FtsZ filaments and releasing them from another end (Bisson-Filho et al., 2017; Yang et al., 2017; McCausland et al., 2021). The dynamic Z ring not only recruits proteins to form the bacterial divisome but also directs peptidoglycan synthesis for the new cell wall (McQuillen and Xiao, 2020; Yang et al., 2021). Additionally, the contraction of the Z-ring may generate the force needed to pull the membrane inward and combine with the synthesis of the new cell wall to complete division (Osawa et al., 2008; Osawa and Erickson, 2011; Erickson and Osawa, 2017).

The gene products of phages have been extensively studied, and some have been shown to inhibit the growth and division of host bacteria by targeting proteins with important physiological function, especially bacterial cell division. Kil, a small polypeptide from phage *λ*, interferes with the formation of Z-ring in *Escherichia coli*, preventing bacterial division and causing continuous elongation (Conter et al., 1996; Haeusser et al., 2014; Hernandez-Rocamora et al., 2015). Similarly, the key bacterial division protein FtsZ has been confirmed as the target of Gp0.4 (Kiro et al., 2013; Simpkin Adam and Rigden, 2016), a gene product of phage T7, and the small polypeptide Hdi from phage T5 (Mahata et al., 2023). Simpkin Adam and Rigden (2016) predicted the structure of Gp0.4 and FtsZ, constructing a "U" model that serves as a representative for Gp0.4 analysis. Bioinformatics analysis revealed that the two *α*-helices of Gp0.4 could bind to the helices 1, 5, and 7 of the FtsZ protein. Phage peptides do not only target FtsZ proteins. De Smet et al. (2021) reported that Lgy, an early gene of *Pseudomonas aeruginosa* phage LUZ24 inhibits the DNA gyrase, thereby preventing colony formation and causing severe filamentous growth (Wagemans et al., 2015). Xu et al. (2024) discovered that protein Gp11 of *Staphylococcus aureus* phage ΦNM1 blocks cell division by inhibiting peptidoglycan biosynthesis. In addition, it has been reported that some bacteriophage proteins, such as the protein p56 of *Bacillus subtilis* phage phi29 and the UGI proteins of *B. subtilis* phages PBS-1 and PBS-2, utilize negatively charged amino acids to mimic the charge distribution of DNA and bind to uracil-DNA glycosylase to inhibit its activity (Serrano-Heras et al., 2007; Mol et al., 1995; Pearl and Savva, 1995; Savva and Pearl, 1995). Interestingly, this type of uracil-DNA glycosylase inhibitor is also present in bacteria, and the *S. aureus* protein SAUGI is the first discovered in other than bacteriophages (Wang et al., 2014).

P1 phage is a temperate phage with a double-stranded DNA genome of approximately 49.8 kb, comprising at least 119 genes (Gonzales et al., 2022). Early studies revealed that Icd (Interference with Cell Division) of phage P1 can disrupt host division (Riedel et al., 1993). This small protein consists of 73 amino acids with a molecular weight of 7.3 kDa, but its target has not yet been determined.

In this study, we found that Icd caused abnormal localization of FtsZ *in vivo* and determined, through bacterial two-hybrid and pull-down assays, that Icd inhibited bacterial division by directly binding to FtsZ. We also discovered that amino acids 12–51 of Icd was the core region which can effectively inhibit bacterial division.

Materials and methods

Bacterial strains, plasmids, and growth conditions

The strains were grown on LB or LB agar and cultured at 37°C under oxic conditions. Liquid cultures were incubated at 37°C in an oxic environment at 220 rpm. Plasmids were constructed using standard molecular biology techniques. Templates, primers, and enzymes were added to the PCR system to amplify the DNA fragments. The DNA was digested and ligated according to the reagent instructions, and the correct recombinant plasmid was screened through colony verification and confirmed by sequencing. The strains and plasmids used in this study are listed in Supplementary Table S1, and the primers are listed in Supplementary Table S2. The dual expression plasmid pBAD22a- *ftsZ-icd* was constructed, in which *ftsZ* and *icd* genes had their own ribosome binding site (rbs).

In vivo toxicity analysis

The monoclonal *E. coli* containing the pBAD22a plasmid was inoculated into 5 mL of LB liquid medium with the appropriate antibiotics. The spectrophotometer was calibrated, and once the bacterial culture reached an OD_{600} of approximately 0.4, arabinose was added to a final concentration of 0.2% to induce gene expression for 3 h. The sample with 10 μL of the bacterial solution was then taken, spotted onto LB agar, and covered with a coverslip for observation under a microscope. Cell lengths were measured for each mutant, and the results were reported as the mean ± SD. Additionally, we spotted 5 μL of dilutions from a dilution series onto LB agar plates. The plates were dried, inverted, and incubated overnight at 37°C. The number of viable bacteria was counted the next day.

For the growth curve analysis, once the bacterial culture reached an OD_{600} of approximately 0.4, 100 μL of culture was transferred into 20 mL of fresh LB medium. L-arabinose was added to a final concentration of 0.2%, and the culture was incubated in a constant temperature shaker at 37°C and 220 rpm. OD_{600} was measured at hourly intervals, and the data was used to generate a growth curve.

Microscopy and image acquisition

Fluorescence image visualization of the Z ring used a mutant strain FtsZ-G55-mNeonGreen-Q56, which replaced genomic *ftsZ* with *ftsZ-mNeonGreen* under its normal genomic control (Moore et al., 2017). After the plasmid pBAD22a carrying the *icd* gene was transferred into the strain, the bacteria were cultured in LB medium with 100 μg/mL carbenicillin until the OD_{600} reached ~0.4, followed by the addition of 0.2% arabinose for induction at 37°C for 3 h. A droplet with 10 μL of bacterial cells was placed onto an agarose spacer, and the cells were visualized using a Leica DMI3000B fluorescence microscope. A common light source was used to observe bacterial morphology, while a mercury lamp was employed for fluorescence observation, with an excitation wavelength of 488 nm for mNeonGreen. The lengths of individual cells were measured, and the results are presented as mean ± SD.

DAPI staining of bacterial nucleoids was performed using a stock solution of 20 mg/mL and a working concentration of 5 μg/mL. At room temperature (25°C), 1 mL of the working solution was applied to the bacterial cells for 8 min under dark conditions. The cells were then washed four times with PBS buffer (137 mM NaCl, 2.7 mM KCl, 10 mM Na_2HPO_4, 1.8 mM KH_2PO_4, pH 6.5). The cells were visualized using a Leica DMI3000B fluorescence microscope with an excitation wavelength of 360 nm for DAPI.

Gene expression and protein purification

The pET28a-*His-ftsZ* plasmid was transformed into *E. coli* BL21, plated on kanamycin-containing agar plates (50 μg/mL), and incubated overnight at 37°C in a constant temperature incubator. Monoclonal clones were selected and inoculated into 100 mL of TY

medium (2.4% yeast extract, 1.2% tryptone, 0.94% wt/vol K_2HPO_4, and 0.02% wt/vol KH_2PO_4) under oxic conditions, and cultured for 24 h at 37°C with shaking at 220 rpm. The cultures were centrifuged at 3000 g for 20 min at ambient temperature, with the supernatant discarded. The precipitate was resuspended in the buffer containing 50 mM Tris, 300 mM NaCl at pH 7.5, with 1% PMSF, 1% lysozyme, and 1% Triton X-100 added, and incubated on ice for 30 min. The cell disruption was performed at 1000 Bar until the lysate was clear and transparent. The lysate was centrifuged at 18,000 g for 20 min at 4°C, and the supernatants and pellets were collected and analyzed for protein production by SDS-PAGE.

The pME6032-*GST-icd* recombinant plasmid was transformed into PAO1 by electrotransformation, grown to an OD_{600} of approximately 0.6. Gene expression was induced with 0.8 mM IPTG at 16°C and 220 rpm for 24 h. Following cell lysis, the supernatant was analyzed by Western blot to examine protein production.

Bacterial two-hybrid screen

Bacterial two hybrid screening has been modified based on previous reports (Karimova et al., 1998). The plasmids pUT18-*icd* and pKNT25-*ftsZ* were simultaneously electrotransformed into *E. coli* BTH101. The bacteria were cultured on solid medium containing 40 μg/mL X-gal (5-bromo-4-chloro-3-indolyl-*β*-D-galactoside) as a chromogenic substrate and 50 μg/mL kanamycin and 100 μg/mL carbenicillin as antibiotics. IPTG (isopropyl-β-D-thiogalactoside) was typically added to the medium at a concentration of 0.5 mM to induce the expression of the full hybrid protein and the β-galactosidase reporter gene. To exclude false-positive clones, putative positive clones were selected and reseeded on LB agar plates containing 50 μg/mL kanamycin, 100 μg/mL carbenicillin, 0.5 mM IPTG, and X-gal, with true positive clones expected to yield blue colonies on these plates once again.

Bacterial cells with β-galactosidase activity to be detected were added with 0.5 mM IPTG and appropriate antibiotics in 3–5 mL LB and stirred 6 h at 220 rpm at 37°C. 50 μL bacterial suspension was added to 370 μL of Z buffer (100 mM Na_2HPO_4, 10 mM NaH_2PO_4, 10 mM KCl, 1 mM $MgSO_4$, 5.4 μL/mL β-galactosidase, pH 7.0), followed by the addition of 20 μL chloroform and 10 μL of 0.1% SDS solution. After incubation on ice for 30 min, 4 mg/mL ONPG (o-Nitrophenyl β-D-galactopyranoside) was added, and the mixture was well mixed before being placed at 30°C for the reaction. After 30 min, a yellow color was observed. The reaction was terminated by adding 250 μL of 1 M Na_2CO_3 solution, and the time of color change was accurately recorded. Absorbance at 420 nm and 550 nm was measured. Miller Units were calculated using the formula: Miller Units = 1,000 x (OD_{420}–1.75 x OD_{550})/t(min) x V(mL) x OD_{600}.

In vitro pull-down analysis

After lysing the *P. aeruginosa* PAO1 strain overexpressing *GST-icd* or the *E. coli* BL21 strain overexpression *His-ftsZ*, the samples were centrifuged at 18000 g for 20 min, and the supernatants were collected separately. After mixing the supernatants containing 1 mL of GST-Icd and 50 μL of His-FtsZ, the mixture was added to the cleaned 50 μL GST resin and incubated for 2 h then washed 5 times with PBS buffer. The mixture of GST protein and His-FtsZ protein, as well as a supernatant containing only GST-Icd or His-FtsZ were used as controls. After the protein bound to the resin, the resin was centrifuged at 3000 g for 2 min, and the supernatant was discarded. The samples were washed three times with 1 mL PBS buffer, and the final centrifugation step ensured maximum removal of the supernatant.

The samples were checked by western blotting. Proteins first were separated using SDS-PAGE gel electrophoresis and transferred from the gel to polyvinylidene fluoride (PVDF) membranes at 220 mA for 90 min and then blocked with 5% skim milk in TBST for 1 h at room temperature on a shaker. The membranes were incubated with primary antibodies overnight at 4°C, washed three times with TBST for 10 min each, and then incubated with secondary antibodies, an HRP-conjugated Goat Anti-Rabbit, for 1 h at room temperature. The membranes were washed three times with TBST for 10 min. The results of Western Blots were detected using the ECL Plus kit (Sangon Biotech). Luminol and hydrogen peroxide in the kit were mixed at a ratio of 1:1 and applied to the PVDF membrane. The membrane was then placed in the dark chamber of the chemiluminescent imaging system and exposed for 10 s to obtain the images. The ECL developing solution reacted with the HRP - labeled antibody to produce a fluorescent signal with a maximum emission wavelength of 425 nm. The primary antibodies used were Anti-GST tag and Anti-His tag antibodies, while the secondary antibody was HRP-conjugated Goat Anti-Rabbit. All antibodies were sourced from Shanghai Sangon Inc.

Result

Expression of *icd* inhibits *E. coli* division

Overexpression of *icd* has a serious impact on the growth of *E. coli*. When we introduced the pET plasmid fused with the *icd* fragment into *E. coli* strain BL21 or C41, the bacteria had difficulty forming clones and growing in liquid culture, possibly due to leakage production of the protein. After the pET28a-*GST-icd* plasmid was transformed into *E. coli* strain BL21 or C41, it took almost 48 h to form visible colonies on the plate, furthermore, when the bacteria in a single colony were transferred to liquid LB medium, the bacteria hardly grew. To study the effect of Icd on *E. coli* division, we selected the pBAD22a plasmid with stricter arabinose-inducible expression control, constructed the recombinant plasmid pBAD22a-*icd,* and transformed it into *E. coli* DH5α. Overexpression of *icd* induced by 0.2% L-arabinose resulted in severe filamentation formation of *E. coli*. The average length of bacteria was 15 ± 1.1 μm after 3 h of overexpression and 53 ± 4.9 μm after 6 h of overexpression (Figures 1A,B).

To further investigate this, we examined the sensitivity of two mutant strains, PS106 *(ftsZ84)* and PS2342 *(ftsA*)*, to Icd. PS106 *(ftsZ84)*, a *ftsZG105S* mutant, is a temperature-sensitive mutation that causes *E. coli* cells to divide severely defectively and grow into filaments at the restrictive temperature (42°C), whereas they grow normally at 37°C. This mutation FtsZG105S protein is impaired in GTP binding and GTPase, as well as in its polymerization (RayChaudhuri and Park, 1992; RayChaudhuri and Park, 1994). Another *E. coli* mutant, PS2342 *(ftsA*)*, is a mutant of *ftsA*. Compared to wild-type FtsA, the FtsA* (*ftsAR286W*, a *zipA*-bypass *ftsA* mutant allele) interacts more strongly with FtsZ than FtsA, accelerating the turnover of FtsA* in the ring (Geissler et al., 2007).

10.3389/fmicb.2025.1533694

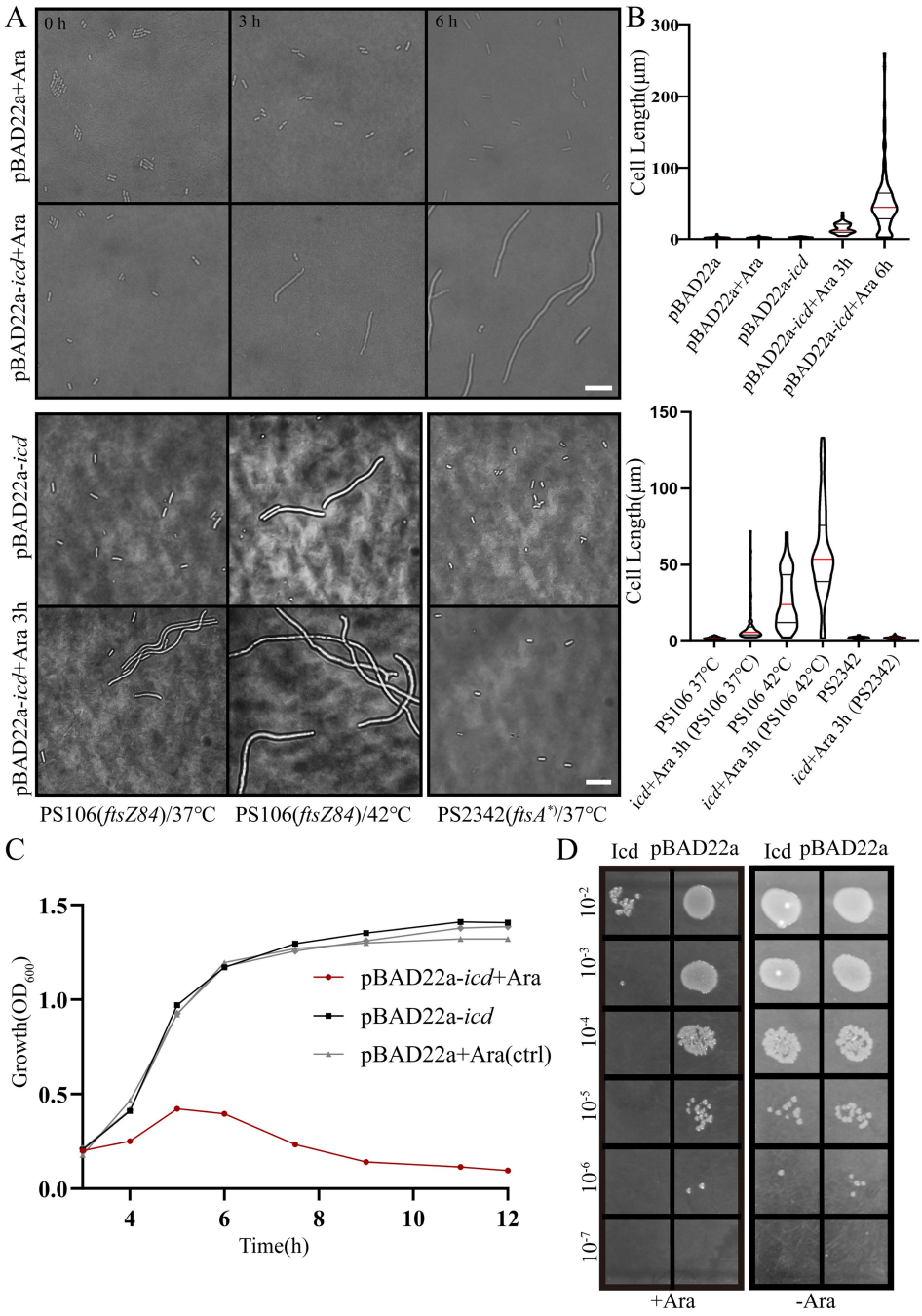

FIGURE 1
Induction of Icd interferes with *E. coli* cell growth and division. **(A)** Microscope images of *E. coli* DH5α, *E. coli* PS106 *(ftsZ84)* and PS2342 *(ftsA*)* after overexpression of *icd* for 3 and 6 h. Scale bar: 10 μm. **(B)** The violin plot shows the bacterial length after adding 0.2% L-arabinose 3 and 6 h, with the red line indicating the median and the black line representing the quartiles. **(C)** The growth curve of *E. coli* shows that overexpression of *icd* inhibits bacterial growth. **(D)** Serial spot dilutions assay shows that the number of viable bacteria decreased significantly after 6 h of overexpression of *icd*.

As shown in Figures 1A,B, Icd still inhibited cell division in PS106 *(ftsZ84)*, whereas PS2342 *(FtsA*)* was resistant to Icd. PS106 grew normally at 37°C with an average length of 2.04 ± 0.04 μm. After 3 h of *icd* gene expression, the average length of PS106 increased to 10.1 ± 1.24 μm. At 42°C, PS106 had already exhibited division defects (27.4 ± 1.7 μm), and *icd* expression exacerbated these defects, resulting in an average length of 59.2 ± 3.4 μm. Surprisingly, the expression of *icd* did not affect the growth of strain PS2342 (*ftsA**). It is possible that FtsA* enhanced the polymerization of FtsZ, thereby reducing the inhibitory effect of Icd.

Growth curve analysis showed that *E. coli* overexpressing *icd* reached its maximum OD_{600} value after 5 h and was followed by a decrease in OD_{600} value, signaling possible bacterial death or degradation (Figure 1C). Viable counts indicated that Icd caused severe

damage to *E. coli*, resulting in a 1,000-fold reduction in viable cell numbers (Figure 1D). The inhibition of bacterial growth by Icd protein was species-specific. When the pME6032-*icd* recombinant plasmid was introduced into *P. aeruginosa* and the *icd* was induced for expression, it had no significant effect on growth (Supplementary Figure S1).

Icd affects the localization of *E. coli* FtsZ

Due to the overexpression of *icd* leading to bacterial elongation, which may indicate inhibition of bacterial division, we then investigated the effect of *icd* expression on the formation of Z-ring, the bacterial divisome. Here, we used the *E. coli* mutant strain, FtsZ-G55-mNeonGreen-Q56 strain (Moore et al., 2017), in which the fluorescent protein mNeonGreen was inserted between positions 55 and 56 of FtsZ to replace the original FtsZ, to observe the Z-ring localization.

FtsZ-mNeonGreen was always located in the middle of the cell, indicating that the Z-ring was assembled. After the pBAD22a-*icd* plasmid was transferred, the cell appeared filamentous and FtsZ-mNeonGreen diffused throughout the cell, denoting that Z-ring was not assembled correctly. It has been reported that protein Gp0.4 directly inhibited FtsZ assembly in *E. coli* (Kiro et al., 2013), therefore, we used *E. coli* with a plasmid overexpressing *gp0.4* as a control. We could observe the same phenomenon with overexpression of *gp0.4* or *icd* (Figure 2A). We preliminarily speculate that Icd may directly or indirectly act on FtsZ or Z-ring binding proteins in *E. coli*.

To determine whether Icd affects bacterial DNA replication, DAPI staining was used to visualize the bacterial DNA. The results showed that although cell division was inhibited, DNA replication remained intact and unaffected (Figure 2A).

We also constructed the recombinant plasmid pBAD22a-*icd-mCherry* and introduced it into *E. coli* FtsZ-G55-mNeonGreen-Q56. After induction with a low concentration of arabinose (0.02%) for 0.5 h, both Icd-mCherry and FtsZ-mNeonGreen were unable to be located correctly and instead dispersed throughout the entire bacteria (data not shown).

Overexpression of *ftsZ* simultaneously could reduce the inhibitory effect of Icd (Figures 2B–D). After 3 h of simultaneous overexpression of *icd* and *ftsZ* using plasmid pBAD-*ftsZ-icd* and 0.2% arabinose, the length of the bacteria became longer, but was significantly shorter than that of the strain overexpressing only *icd* using plasmid pBAD22a-*icd* (Figure 2B). The average cell length was 7.8 ± 0.39 μm, which was shorter than the 15 ± 1.1 μm of a strain overexpressing *icd* alone (Figure 2C). The results of the *E. coli* growth curve further confirmed that simultaneous overexpression of *ftsZ* significantly weakened the inhibitory effect of *icd* (Figure 2D). When *icd* was overexpressed, the OD_{600} value slowly increased in the first 5 h and then began to decrease. When *ftsZ* and *icd* were overexpressed simultaneously, the OD_{600} value continued to increase and reached a maximum value at around 8 h.

Bacterial two-hybrid and pull-down experiments identified the interaction between Icd and FtsZ

The bacterial two-hybrid system is an effective method for studying the protein–protein interactions *in vivo* (Karimova et al., 1998). We recombinantly fused Icd to the T18 fragments of the adenylate cyclase, FtsZ to the T25 fragments, and transformed them into *E. coli* BTH101. We used pKNT25 and pUT18C empty plasmids as negative controls and pKNT25-*zip* and pUT18C-*zip* plasmids as positive controls. Thus, the Zip proteins could polymerize to form a dimer, resulting in *β*-galactosidase activity in the bacteria. Additionally, co-transformations of pKNT25-*ftsZ* with the pUT18C empty plasmid and pUT18C-*icd* with the pKNT25 empty plasmid into *E. coli* BTH101 served as two other negative controls (data not shown).

After the recombinant plasmid was transformed into *E. coli* BTH101 and cultured on solid medium containing IPTG and X-gal (5-bromo-4-chloro-3-indolyl-β-D-thiogalactopyranoside) for 26 h, most of the bacteria cells containing pKNT25-*ftsZ* and pUT18C-*icd* turned blue, while the negative control group remained white (Supplementary Figure S2). Figure 3A shows a single clone randomly selected from the initial culture medium, in which the cells containing pKNT25-*ftsZ* and pUT18C-*icd* and the positive control containing pKNT25-*zip* and pUT18C-*zip* were blue, while the negative control strain was white. The activity of β-galactosidase was measured by UV–VIS spectrophotometer to quantify the results of the bacterial two-hybrid measurement, further confirming that Icd and FtsZ interacted in the cells (Figure 3B).

A pull-down assay was also conducted to confirm the interaction between Icd and FtsZ. Since Icd inhibited *E. coli* growth, the production level of Icd protein expressed in *E. coli* was low, therefore, we used *P. aeruginosa* PAO1 and the recombinant plasmid pME6032-*GST-icd* to overexpress Icd protein. The cell lysates containing Icd protein were purified and enriched by GST resin, and mixed with His-FtsZ sample. We used a mixture of GST protein and His-FtsZ as a control. After elution and immunoblotting with anti-GST and anti-His antibodies, it was found that GST-Icd could pull down His-FtsZ, while the GST tag alone could not (Figure 3C). This suggested that Icd interacts directly with FtsZ.

The antibacterial core region of Icd was around 12–51

Amino acid sequence alignment revealed that Icd proteins exist not only in the P1 phage, but also in some other Enterobacteriaceae phages, although there are some sequence differences (Supplementary Figure S3). Based on the alignment, we constructed recombinant plasmids containing various lengths of *icd* gene deletions and determined the antibacterial core sequence region of Icd by observing bacterial growth. Icd sequences of different lengths are listed in Figure 4A. Icd sequences of different lengths were inserted into the pBAD22a plasmid and transformed into *E. coli* DH5α.

Firstly, we observed the effect of mutated Icd on bacterial length under a microscope (Figure 4B). We found that when the N-terminal truncation of Icd proteins exceeds 11 amino acids or the C-terminal exceeds 24 amino acids, the overexpressed *icd* mutant gene loses its antibacterial effect. Among the Icd mutants we constructed, Icd12-51 appeared to be the shortest protein with the same ability to inhibit bacterial division as full-length Icd. After overexpressing *icd12-51* for 6 h, the average length of *E. coli* reached 48 ± 5.5 μm, and the longest bacteria we observed reached 220 μm. However, the average length of bacteria overexpressing *icd12-50* decreased to 7 ± 0.34 μm, indicating a significant reduction in inhibitory ability (Figures 4B,C).

10.3389/fmicb.2025.1533694

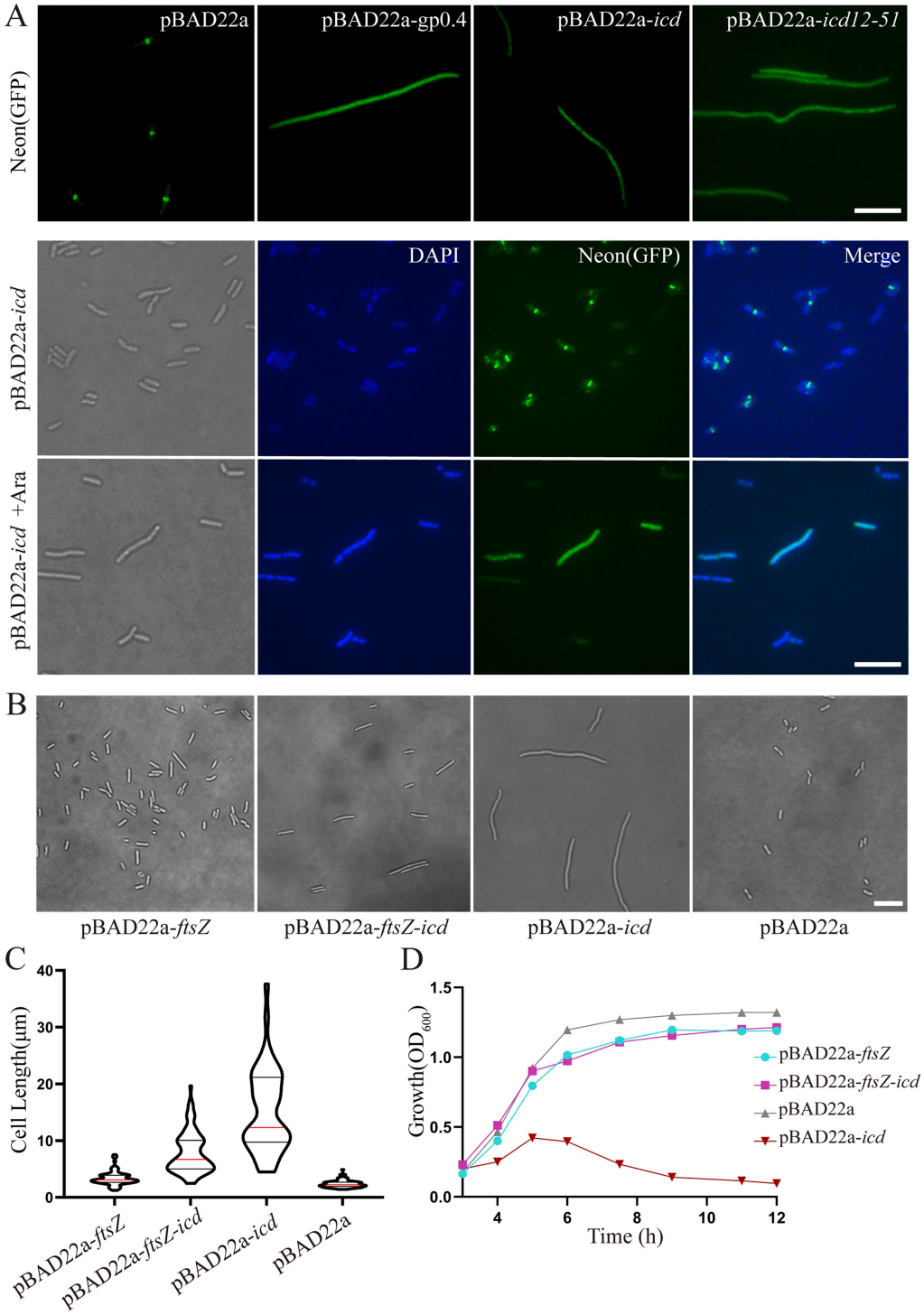

FIGURE 2
(A) Fluorescence microscopy images showed that *icd* overexpression blocked Z-ring formation. The *E. coli* mutant strain, FtsZ-G55-mNeonGreen-Q56 strain, was used to observe the Z-ring localization. When *icd* was overexpressed, FtsZ-mNeonGreen diffused in the cell, which is similar to the overexpression of FtsZ inhibitory protein GP0.4. Scale bar: 10 μm. DAPI staining was used to visualize the bacterial nucleoid. Under the influence of Icd, it was observed that bacterial division was inhibited, but the nucleolus structure remained intact and unaffected. **(B)** Comparison of microscopic images of *E. coli* DH5α overexpressing *ftsZ*, *icd* or co-overexpressing of *icd* and *ftsZ* for 3 h. Scale bar: 10 μm. **(C)** The violin plots of the bacterial length, where the red line indicates the median and the black line represents the quartile. **(D)** The growth curve results further show that the simultaneous overproduction of FtsZ reduced the inhibitory effect of Icd on bacteria.

10.3389/fmicb.2025.1533694

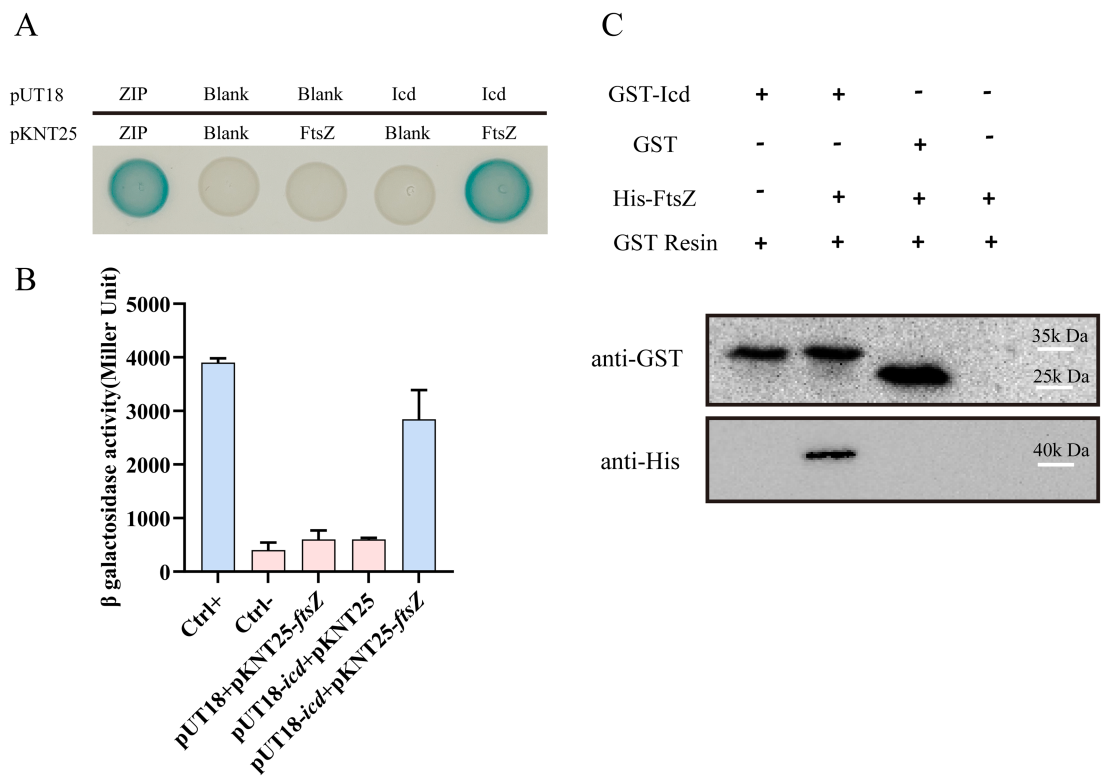

FIGURE 3
The interaction between FtsZ and Icd was confirmed by bacterial two-hybrid and pull-down assay. **(A)** Bacterial two-hybrid assay results showed the FtsZ-Icd interaction. When pKNT25-*ftsZ* and pUT18C-*icd* plasmids were transferred into the *E. coli* BTH101 strain, bacterial colonies appeared blue. All three negative controls (Ctrl-) were white spots. **(B)** The bar graph shows the statistical plot of *β*-galactosidase activity, which clearly shows the interaction between FtsZ and Icd. **(C)** Pull-down assay further validated the interaction between FtsZ and Icd. A solution containing GST-Icd was mixed with a His-FtsZ sample, separated with GST resin, and shown as an immunoblot against GST and His-tag in the cell extract. GST-Icd alone and a mixture of GST tag and FtsZ were used as controls. The results showed GST-Icd could interact with the His-FtsZ protein.

Next, we measured the bacterial growth curves to test their antibacterial activity. Overexpression of *icd* genes has a strong inhibitory effect on bacterial growth, which we used as a positive control, and the growth of bacteria containing an empty pBad22 plasmids as a negative control. The OD_{600} values of *E. coli* overexpressing *icd* genes increased slowly in the first 5 h, which may be due to an increase in bacterial numbers or the formation of filamentous bacteria. Afterwards, the OD_{600} value began to decrease and dropped to baseline after 9 h, indicating bacterial death (Figures 5A–C). Figure 5A examined the effect of overexpression of N-terminally truncated Icd mutant proteins on *E. coli* growth. The results showed that removing 7 or 11 amino acids from the N-terminus of the Icd mutant proteins still had partial inhibitory effects, while removing 16 amino acids from the N-terminus resulted in the disappearance of antibacterial activity. Figure 5B examines the effect of C-terminal truncation on the antibacterial activity of Icd proteins. Truncating the 21 amino acids at the C-terminus (Icd1-52) did not affect the antibacterial activity of the Icd protein. Figure 5C shows the antibacterial effect of Icd proteins with both N-terminal and C-terminal truncations to search for the shortest core region. The results showed that Icd12-52 had almost the same antibacterial activity as full-length Icd, with OD_{600} increasing slowly in the first 6 h then decreasing. Overexpression of *icd12-51* also had strong antibacterial activity, but no decrease in OD_{600} was observed, indicating that the antibacterial activity was partially weakened. At the same time, the antibacterial effect of overexpression of *icd12-50* was significantly weakened (Figure 5C). Interestingly, the antibacterial activity of overexpression of *icd12-52* or *icd12-51* was stronger than that of overexpression of *icd8-73*, *icd12-73* or *icd8-57*, suggesting that the extra amino acids may weaken the antibacterial activity.

Not only does an increase in the number of bacteria cause an increase in OD_{600} value, but a significant increase in bacterial length will also increase OD_{600} value. To obtain more accurate results, we used the serial spot dilution assay to measure the number of viable bacteria and assess the antibacterial activity of Icd mutant proteins. Here, we measured the viable counts after 6 h of overexpression of *icd* and its mutant genes (Figure 5D). In the absence of arabinose, the number of *E. coli* colonies was nearly identical, around 4×10^8 CFU/mL. When *icd* was overexpressed, the number of *E. coli* colonies decreases to 2×10^5 CFU/mL. Meanwhile, the number of colonies overexpressing *icd12-52* or *icd12-51* was 2×10^5 CFU/mL and 4×10^5 CFU/mL, respectively. On the other hand, the colony count of overexpressed *icd12-50* was only 4×10^6 CFU/mL, which was significantly weakened. In addition, the measurable viable counts after overexpression of *icd8-73, icd8-57 or icd12-73* were 2×10^6, 2×10^6 and 6×10^6 CFU/mL, respectively, further demonstrating that their antibacterial activity was lower than that of *icd12-51*. The colony counts after overexpression of *icd12-52* and *icd12-51* were in the same order of magnitude, which concluded that Icd12-51 can be considered

10.3389/fmicb.2025.1533694

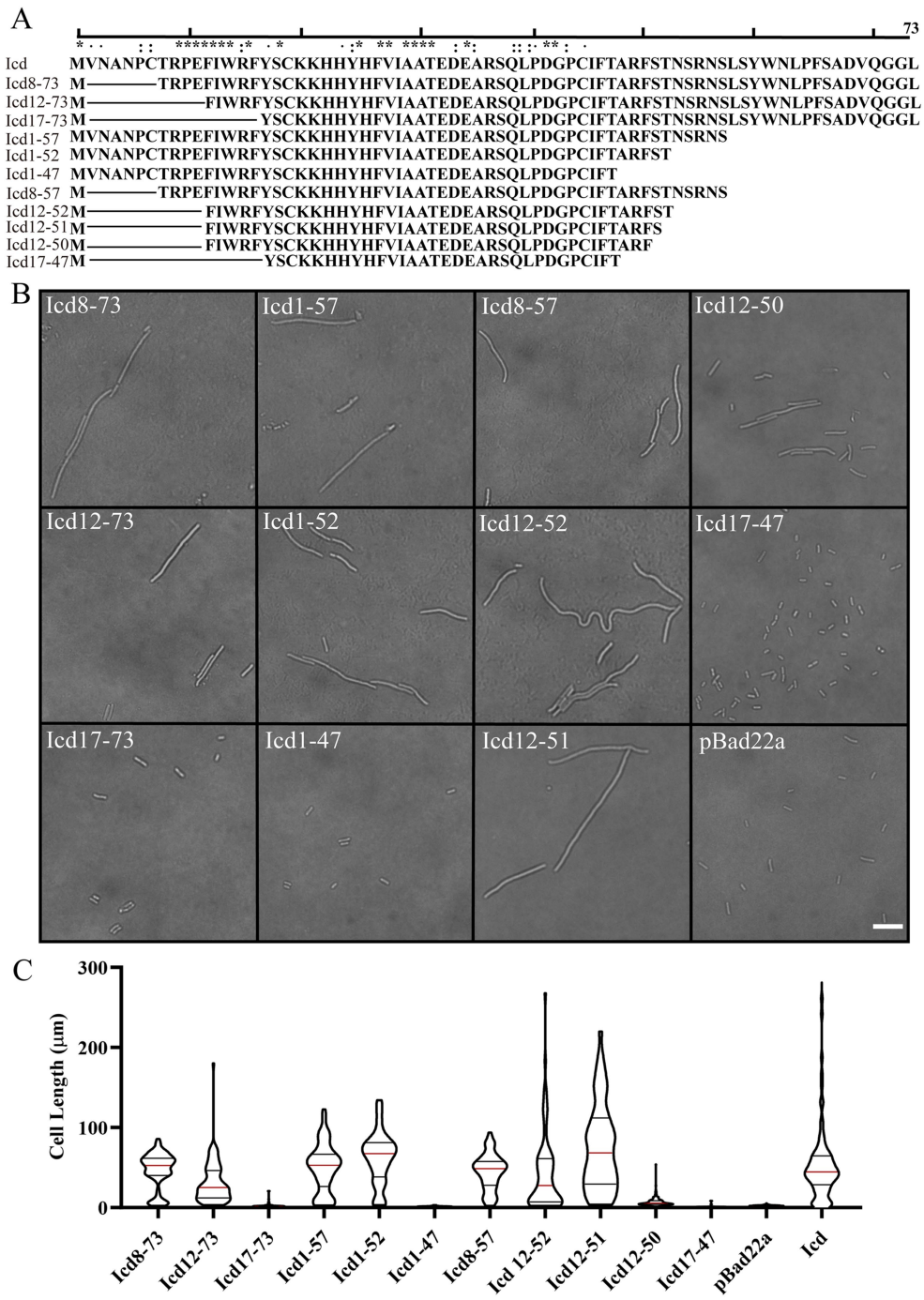

FIGURE 4
Effects of overexpression of *icd* mutant genes of different lengths on bacterial cell length. **(A)** The list of constructed Icd mutant proteins of different lengths. **(B)** Microscopic image of the effect of overexpression of *icd* mutant genes of different lengths on bacterial growth. The scale bar is 10 μm. **(C)** The violin plots summarize the statistical values of bacterial lengths after overexpression of *icd* of different lengths, with the red line indicating the median and the black lines indicating the quartiles.

as the shortest core region with antibacterial effects similar to those of the full-length Icd.

Bacterial two-hybrid experiments confirmed the interaction between Icd12-51 and FtsZ (Figures 5E,F; Supplementary Figure S2). Most of the bacteria cells containing pKNT25-*ftsZ* and pUT18C-*icd12-51* turned blue, but the color was lighter than that of bacteria containing pKNT25-*ftsZ* and pUT18C-*icd*. Moreover, the *β*-galactosidase activity was only 40% of that of the bacterial cells containing pKNT25-ftsZ and pUT18C-icd (Figures 5E,F). It can be inferred that Icd12-51 forms an effective but slightly weaker interaction with FtsZ. Meanwhile, the cells containing pKNT25-*ftsZ* and pUT18C-*icd12-50* turned a lighter blue, and the β-galactosidase activity was approximately 12% of that of the cells containing pKNT25-*ftsZ* and pUT18C-*icd* (Figures 5E,F). This

10.3389/fmicb.2025.1533694

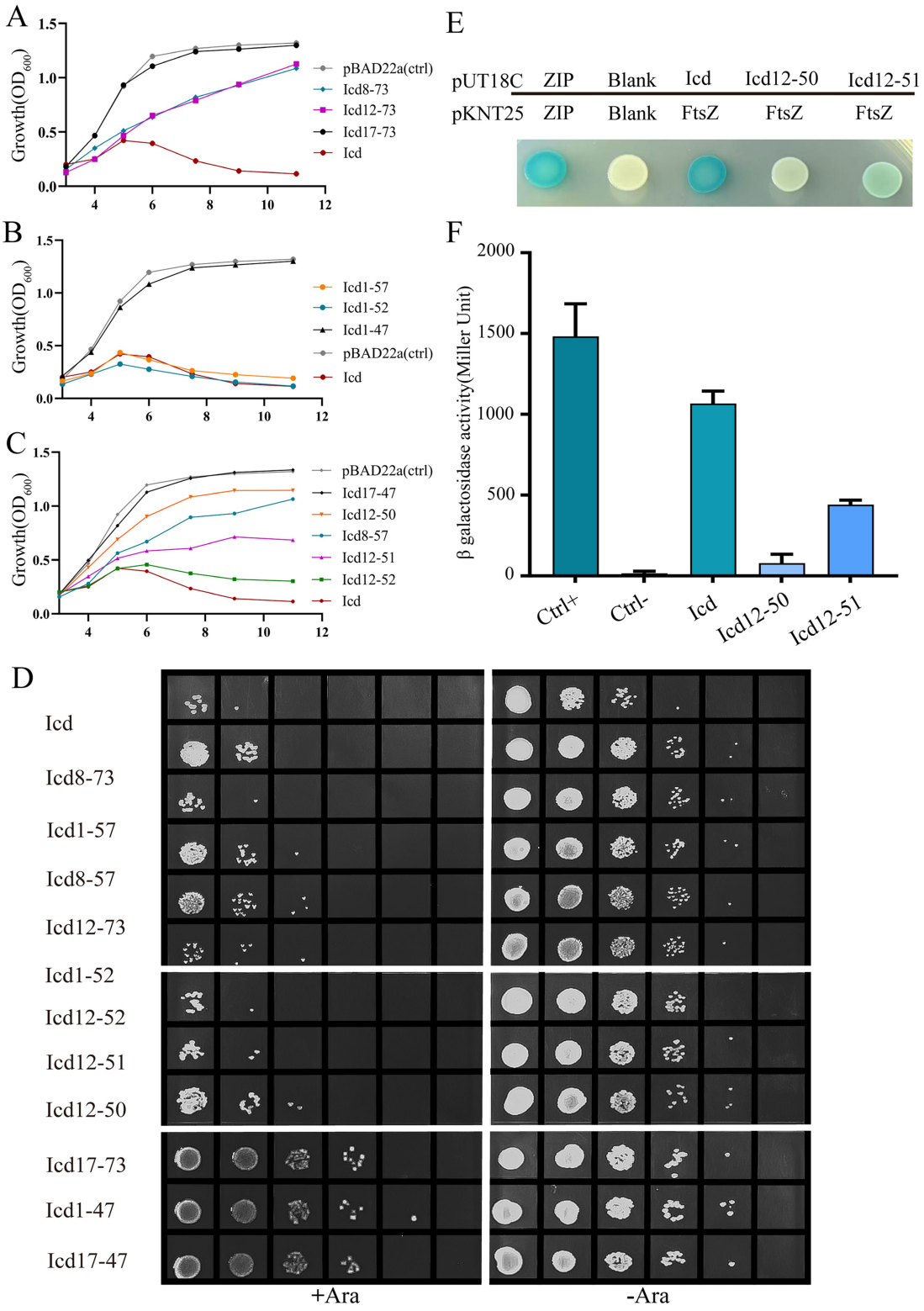

FIGURE 5
The bacterial growth curve further confirmed that the antibacterial core region of the Icd protein was 12–51. **(A–C)** Bacterial growth curve illustrating the effects of Icd of different lengths on bacterial growth. **(D)** The number of viable cells was examined by serial dilution method after overexpression of *icd* mutant genes of different lengths for 6 h. **(E,F)** Bacterial two-hybrid assay results showed the FtsZ-Icd, FtsZ-Icd12-51 and FtsZ-Icd12-50 interaction. The statistical plot of β-galactosidase activity shows and Icd12-50, and the interaction of FtsZ-Icd12-51 is weaker than that of FtsZ-Icd, while the interaction between icd12-50 and FtsZ is even weaker.

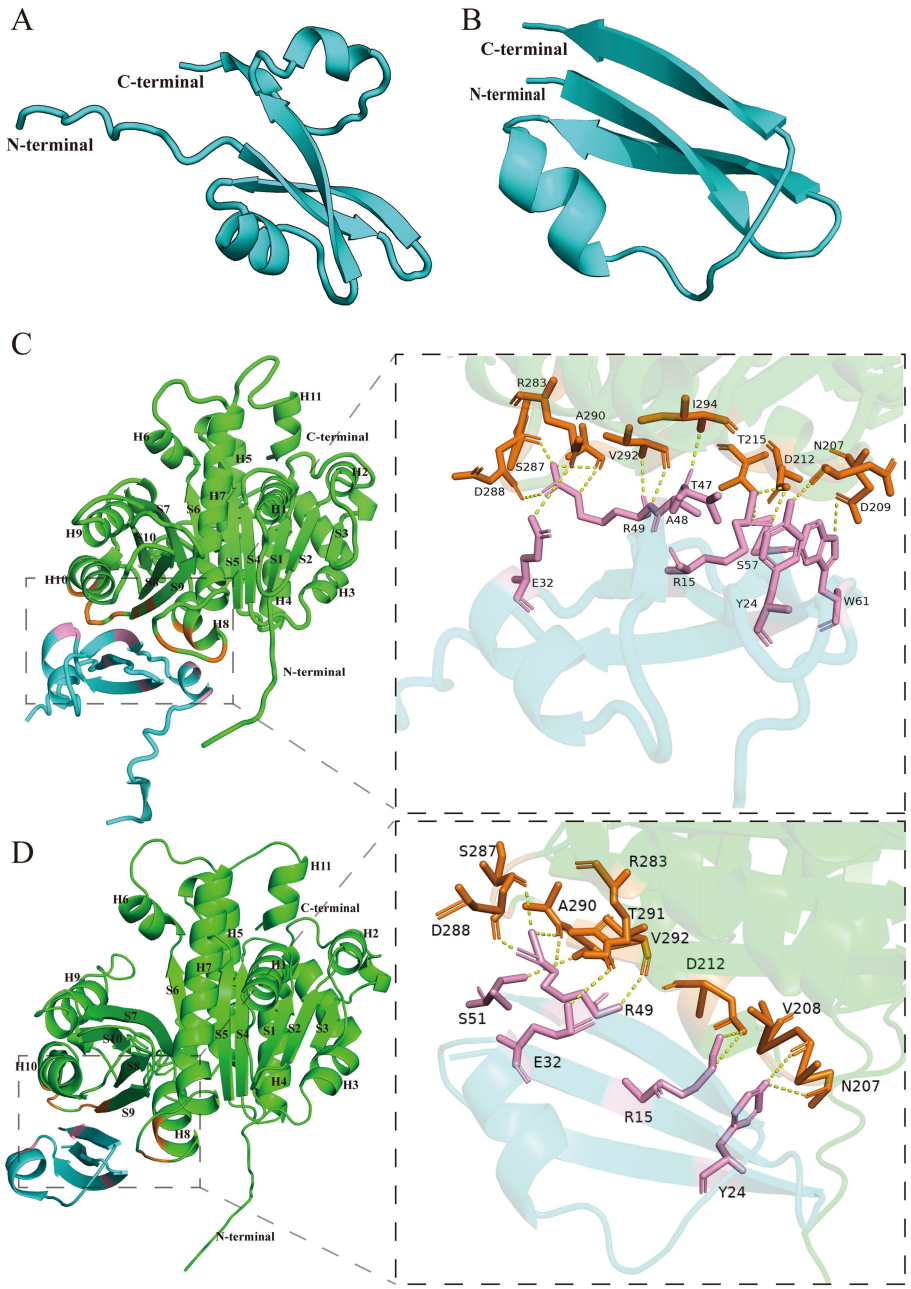

FIGURE 6
Structure prediction of Icd and the interactions between Icd and FtsZ. **(A)** Icd. **(B)** Icd12-52. **(C)** The interaction between Icd and FtsZ. The interaction interface is magnified inside the box. **(D)** The interaction between Icd12-51 and FtsZ. The interaction interface is magnified inside the box.

showed that Icd12-50 was still able to form a weaker interaction with FtsZ.

Discussion

The co-evolution between phages and hosts has enabled phages to develop a variety of special ways to inhibit the growth of host bacteria, including numerous small proteins, which can help phages effectively utilize host cell resources. Bacterial division is one of the important processes of bacterial growth and an important target for inhibition. Inhibiting host division may prevent host daughter cells from escaping and maximize the utilization of host resources (De Smet et al., 2021); it may also delay bacterial lysis, allowing bacteria to grow larger and helping phages produce more offsprings (Dhanoa et al., 2022).

In this study, we determined that the small protein Icd of P1 phage can directly target the key bacterial division protein FtsZ, thereby inhibiting the growth and division of the host *E. coli*. We also concluded that Icd12-51 was the core region, and it has nearly the same antibacterial effect as the full length of Icd. This 40-aa small peptide strongly inhibits bacterial division, and its production can lead to severe bacterial filamentation.

As we were unable to obtain high-quality protein for biochemical and structural studies, we used AlphaFold (Jumper et al., 2021) and AlphaFold3 (Abramson et al., 2024), which have advantages in the analysis of protein structure and protein–protein interaction, to predict the structure of Icd and its binding to FtsZ. The structure of Icd is bow-tie-shaped, including two small α-helix and four *β*-sheets (Figure 6A). After deleting a small α-helix and a β-sheet, its main structure Icd12-51 contains only a small α-helix and three β-sheets (Figure 6B). FtsZ from *E. coli* is a globular protein consisting of 383 amino acids, with two subdomains, N terminus (amino acids 12–195) and C terminus (amino acids 196–316) connected by the H7 helix (Oliva et al., 2004; Chen and Erickson, 2011). To predict the binding sites of Icd and FtsZ, the amino acid sequences of FtsZ and Icd or Icd12-51 were input into AlphaFold 3 to analyze the possible binding sites. We found that different Icd sequence inputs resulted in slightly different binding modes. The results showed that Icd bound to the T7-H8 region and the H10-S9 region of FtsZ, and 13 hydrogen bonds could be formed between Icd and FtsZ (Figure 6C). At the interaction interface, residues N207, D209, D212 and T215 of FtsZ interact with multiple amino acids including W61, Y24, S57 and R15 of Icd, and residues R283, S287, D288, A290, V292, and I294 of FtsZ form 5 hydrogen bonds with E32, R49, A48 and T47 of Icd. In contrast to Icd, Icd12-51 truncated one α-helix and one β-sheet, and three β-sheets and a small α-helix were retained. The predicted binding sites of Icd12-51 to FtsZ are somewhat different from those of Icd-FtsZ, but are still located in these two regions of FtsZ (Figure 6D). The predicted binding sites of Icd12-51 to FtsZ indicated that N207, V208 and D212 of FtsZ could form hydrogen bonds with Y24, R15 of Icd and R283, S287, D288, A290, T291, V292 of FtsZ interacts with E32, R49 of S51 of Icd. These predictions are consistent with our bacterial two-hybrid results. Icd12-51 is sufficient to interact with FtsZ, but its interaction is slightly weaker than that of Icd with FtsZ. The N207, D209 and D212 of FtsZ are located on the T7 loop and H8 helix, the most important amino acid sites related to FtsZ polymerization and GTPase activity. Occupancy of these sites will strongly inhibit the polymerization ability of FtsZ, which can explain why Icd has a strong antibacterial effect.

Studies searching for antibacterial proteins in phages have also reported several different types of small proteins in different phages that can specifically target FtsZ and inhibit bacterial division, such as Kil in phage *λ* (Haeusser et al., 2014; Hernandez-Rocamora et al., 2015), GP0.4 in phage T7 (Kiro et al., 2013; Simpkin Adam and Rigden, 2016) and Hdi in phage T5 (Mahata et al., 2023). All of them would lead to abnormal FtsZ localization in cells, preventing the Z-ring formation and causing cell filamentation. However, their mechanism of inhibiting FtsZ differed from that of Icd proteins.

Even though these proteins have little sequence similarity, the three small proteins Kil, GP0.4 and Hdi appear to have similar structures (Mahata et al., 2023). They all contain mainly two α-helices, forming a U-shaped or V-shaped helix-turn-helix structure. Previous studies suggested that they may have similar FtsZ binding sites and inhibitory regions. This helix-turn-helix structure was different from the bow-tie-like structure of Icd. Simpkin Adam and Rigden (2016) analyzed the interaction between GP0.4 and FtsZ and predicted that the GP0.4 protein inserts into the cleft between helices 1, 5 and 7 of FtsZ. Among them, the conserved FtsZ residues G21, N24, G47, and G107 interact with GP0.4 through hydrogen bonds, thereby inhibiting the polymerization of FtsZ. Although these proteins and Icd share the function of inhibiting FtsZ activity, it was evident that Icd has different structures and binding sites with FtsZ.

Kiro et al. (2013), in their study of GP0.4 protein, found a random mutant FtsZ, a glycine-valine repeat sequence inserted at position 18 of FtsZ, resistant to the inhibition of GP0.4. This result supports this model. However, Haeusser et al. (2014) isolated the mutants $FtsZ_{V208A}$ and $FtsZ_{L169R}$, which could resist the inhibition of bacterial division by Mahata et al. (2023) found that both $FtsZ_{F268V}$ and $FtsZ_{G191S}$ were resistant to the inhibition of Hdi and GP0.4 in *E. coli*. These mutation sites are far from the binding site and do not seem to support this model. It is possible that these mutated FtsZ proteins affect the polymerization or bundling of FtsZ or affect the interaction with other association proteins, thereby reducing the inhibitory effect of these phage peptides on bacterial growth. Therefore, further research is still needed.

Interestingly, our results show that overexpression of *icd* does not inhibit bacterial division of *ftsA** mutants, a *zipA*-bypass *ftsA* mutant allele. Considering protein FtsA* can enhance the polymerization of FtsZ (Geissler et al., 2007), it could resist the inhibitory effect of Icd. Correspondingly, Haeusser et al. (2014) found that another phage protein Kil could not inhibit the *ftsA** strain after the knockout of ZipA, although it still inhibited the *ftsA** strain. They believed that the inhibitory effect of Kil on FtsZ required the presence of ZipA. This is different from our experimental results. Subsequent biochemical studies found that the inhibitory effect of Kil on the polymerization of FtsZ does not require ZipA (Hernandez-Rocamora et al., 2015). Further studies are still needed to clarify these mechanisms.

In addition, searching for more antimicrobial proteins in phages has potential value for understanding phage-host interactions and screening new antimicrobial proteins to address the problem of multiple antibiotic resistance in pathogens.

Data availability statement

The original contributions presented in the study are included in the article/Supplementary material, further inquiries can be directed to the corresponding authors.

Author contributions

KZ: Conceptualization, Formal analysis, Investigation, Writing – original draft, Writing – review & editing. SD: Data curation, Formal analysis, Investigation, Writing – review & editing. LT: Formal analysis, Investigation, Writing – review & editing. SheW: Data curation, Investigation, Writing – review & editing. RS: Investigation, Writing – review & editing. HS: Investigation, Writing – review & editing. YZ: Investigation, Writing – review & editing. CH: Investigation, Writing – review & editing. YS: Formal analysis, Supervision, Writing – review & editing. ShiW: Formal analysis, Funding acquisition, Supervision, Writing – review & editing. YC: Conceptualization, Data curation, Formal analysis, Funding acquisition, Investigation, Project administration, Supervision, Writing – original draft, Writing – review & editing.

Funding

The author(s) declare that financial support was received for the research, authorship, and/or publication of this article. This research

was supported by the grants from the Science & Technology Fundamental Resources Investigation Program (Grant No. 2022FY101100) to YS, the National Natural Science Foundation of China (Grant No. 31970050) to YC and the National Natural Science Foundation of China (32170114) to YS.

Acknowledgments

We thank Dr. Du Shishen from Wuhan University for providing strains of *E. coli* PS106 *(ftsZ84)* and PS2342 *(ftsA*)* as gifts. We thank Ms. Cyndi Chen from North Carolina State University for her editing.

Conflict of interest

The authors declare that the research was conducted in the absence of any commercial or financial relationships that could be construed as a potential conflict of interest.

Generative AI statement

The authors declare that no Gen AI was used in the creation of this manuscript.

Publisher's note

Supplementary material

The Supplementary material for this article can be found online at: https://www.frontiersin.org/articles/10.3389/fmicb.2025.1533694/full#supplementary-material

References

Abramson, J., Adler, J., Dunger, J., Evans, R., Green, T., Pritzel, A., et al. (2024). Accurate structure prediction of biomolecular interactions with AlphaFold 3. *Nature* 630, 493–500. doi: 10.1038/s41586-024-07487-w

Bi, E., and Lutkenhaus, J. (1991). FtsZ ring structure associated with division in *Escherichia coli*. *Nature* 354, 161–164. doi: 10.1038/354161a0

Bisson-Filho, A. W., Hsu, Y. P., Squyres, G. R., Kuru, E., Wu, F., Jukes, C., et al. (2017). Treadmilling by FtsZ filaments drives peptidoglycan synthesis and bacterial cell division. *Science* 355, 739–743. doi: 10.1126/science.aak9973

Chen, Y., and Erickson, H. P. (2005). Rapid in vitro assembly dynamics and subunit turnover of FtsZ demonstrated by fluorescence resonance energy transfer. *J. Biol. Chem.* 280, 22549–22554. doi: 10.1074/jbc.M500895200

Chen, Y., and Erickson, H. P. (2009). FtsZ filament dynamics at steady state: subunit exchange with and without nucleotide hydrolysis. *Biochemistry* 48, 6664–6673. doi: 10.1021/bi8022653

Chen, Y., and Erickson, H. P. (2011). Conformational changes of FtsZ reported by tryptophan mutants. *Biochemistry* 50, 4675–4684. doi: 10.1021/bi200106d

Conter, A., Bouché, J. P., and Dassain, M. (1996). Identification of a new inhibitor of essential division gene ftsZ as the kil gene of defective prophage Rac. *J. Bacteriol.* 178, 5100–5104. doi: 10.1128/jb.178.17.5100-5104.1996

De Smet, J., Wagemans, J., Boon, M., Ceyssens, P. J., Voet, M., Noben, J. P., et al. (2021). The bacteriophage LUZ24 "Igy" peptide inhibits the DNA gyrase. *Cell Rep.* 36:109567. doi: 10.1016/j.celrep.2021.109567

Dhanoa, G. K., Kushnir, I., Qimron, U., Roper, D. I., and Sagona, A. P. (2022). Investigating the effect of bacteriophages on bacterial FtsZ localisation. *Front Cell Infect Mi.* 12:863712. doi: 10.3389/fcimb.2022.863712

Erickson, H. P., and Osawa, M. (2017). FtsZ constriction force-curved Protofilaments bending membranes. *Subcell. Biochem.* 84, 139–160. doi: 10.1007/978-3-319-53047-5_5

Geissler, B., Shiomi, D., and Margolin, W. (2007). The ftsA* gain-of-function allele of Escherichia coli and its effects on the stability and dynamics of the Z ring. *Microbiology* 153, 814–825. doi: 10.1099/mic.0.2006/001834-0

Gonzales, M. F., Piya, D. K., Koehler, B., Zhang, K. L., Yu, Z. H., Zeng, L. Y., et al. (2022). New insights into the structure and assembly of bacteriophage P1. *Viruses-Basel.* 14:678. doi: 10.3390/v14040678

Haeusser, D. P., Hoashi, M., Weaver, A., Brown, N., Pan, J., Sawitzke, J. A., et al. (2014). The Kil peptide of bacteriophage lambda blocks *Escherichia coli* cytokinesis via ZipA-dependent inhibition of FtsZ assembly. *PLoS Genet.* 10:e1004217. doi: 10.1371/journal.pgen.1004217

Haeusser, D. P., and Margolin, W. (2016). Splitsville: structural and functional insights into the dynamic bacterial Z ring. *Nat. Rev. Microbiol.* 14, 305–319. doi: 10.1038/nrmicro.2016.26

Hernandez-Rocamora, V. M., Alfonso, C., Margolin, W., Zorrilla, S., and Rivas, G. (2015). Evidence that bacteriophage lambda Kil peptide inhibits bacterial cell division by disrupting FtsZ Protofilaments and sequestering protein subunits. *J. Biol. Chem.* 290, 20325–20335. doi: 10.1074/jbc.M115.653329

Jumper, J., Evans, R., Pritzel, A., Green, T., Figurnov, M., Ronneberger, O., et al. (2021). Highly accurate protein structure prediction with AlphaFold. *Nature* 596, 583–589. doi: 10.1038/s41586-021-03819-2

Karimova, G., Pidoux, J., Ullmann, A., and Ladant, D. (1998). A bacterial two-hybrid system based on a reconstituted signal transduction pathway. *Proc. Natl. Acad. Sci. USA* 95, 5752–5756. doi: 10.1073/pnas.95.10.5752

Kiro, R., Molshanski-Mor, S., Yosef, I., Milam, S. L., Erickson, H. P., and Qimron, U. (2013). Gene product 0.4 increases bacteriophage T7 competitiveness by inhibiting host cell division. *Proc. Natl. Acad. Sci. USA* 110, 19549–19554. doi: 10.1073/pnas.1314096110

Kusuma, K. D., Payne, M., Ung, A. T., Bottomley, A. L., and Harry, E. J. (2019). FtsZ as an antibacterial target: status and guidelines for progressing this avenue. *Acs Infect Dis.* 5, 1279–1294. doi: 10.1021/acsinfecdis.9b00055

Mahata, T., Molshanski-Mor, S., Goren, M. G., Kohen-Manor, M., Yosef, I., Avram, O., et al. (2023). Inhibition of host cell division by T5 protein 008 (Hdi). *Microbiol Spectr.* 11:e0169723. doi: 10.1128/spectrum.01697-23

McCausland, J. W., Yang, X., Squyres, G. R., Lyu, Z., Bruce, K. E., Lamanna, M. M., et al. (2021). Treadmilling FtsZ polymers drive the directional movement of sPG-synthesis enzymes via a Brownian ratchet mechanism. *Nat. Commun.* 12:609. doi: 10.1038/s41467-020-20873-y

McQuillen, R., and Xiao, J. (2020). Insights into the structure, function, and dynamics of the bacterial Cytokinetic FtsZ-ring. *Annu. Rev. Biophys.* 49, 309–341. doi: 10.1146/annurev-biophys-121219-081703

Mol, C. D., Arvai, A. S., Sanderson, R. J., Slupphaug, G., Kavli, B., Krokan, H. E., et al. (1995). Crystal structure of human uracil-DNA glycosylase in complex with a protein inhibitor: protein mimicry of DNA. *Cell* 82, 701–708. doi: 10.1016/0092-8674(95)90467-0

Moore, D. A., Whatley, Z. N., Joshi, C. P., Osawa, M., and Erickson, H. P. (2017). Probing for binding regions of the FtsZ protein surface through site-directed insertions: discovery of fully functional FtsZ-fluorescent proteins. *J. Bacteriol.* 199, e00553–e00516. doi: 10.1128/JB.00553-16

Munita, J. M., and Arias, C. A. (2016). Mechanisms of antibiotic resistance. *Microbiol Spectr.* 4:1128. doi: 10.1128/microbiolspec.VMBF-0016-2015

Nogales, E., Downing, K. H., Amos, L. A., and Lowe, J. (1998). Tubulin and FtsZ form a distinct family of GTPases. *Nature Struct Biol.* 5, 451–458. doi: 10.1038/nsb0698-451

Oliva, M. A., Cordell, S. C., and Lowe, J. (2004). Structural insights into FtsZ protofilament formation. *Nat. Struct. Mol. Biol.* 11, 1243–1250. doi: 10.1038/nsmb855

Osawa, M., Anderson, D. E., and Erickson, H. P. (2008). Reconstitution of contractile FtsZ rings in liposomes. *Science* 320, 792–794. doi: 10.1126/science.1154520

Osawa, M., and Erickson, H. P. (2011). Inside-out Z rings - constriction with and without GTP hydrolysis. *Molec Microbiol.* 81, 571–579. doi: 10.1111/j.1365-2958.2011.07716.x

Pearl, L. H., and Savva, R. (1995). DNA repair in three dimensions. *Trends Biochem. Sci.* 20, 421–426. doi: 10.1016/S0968-0004(00)89092-1

RayChaudhuri, D., and Park, J. T. (1992). *Escherichia coli* cell-division gene ftsZ encodes a novel GTP-binding protein. *Nature* 359, 251–254. doi: 10.1038/359251a0

RayChaudhuri, D., and Park, J. T. (1994). A point mutation converts *Escherichia coli* FtsZ septation GTPase to an ATPase. *J. Biol. Chem.* 269, 22941–22944. doi: 10.1016/S0021-9258(17)31600-9

Riedel, H., Heinrich, J., and Schuster, H. (1993). Cloning, expression, and characterization of the icd gene in the immI operon of bacteriophage P1. *J. Bacteriol.* 175, 2833–2838. doi: 10.1128/jb.175.10.2833-2838.1993

Savva, R., and Pearl, L. H. (1995). Nucleotide mimicry in the crystal structure of the uracil-DNA glycosylase-uracil glycosylase inhibitor protein complex. *Nat. Struct. Biol.* 2, 752–757. doi: 10.1038/nsb0995-752

Serrano-Heras, G., Ruiz-Masó, J. A., del Solar, G., Espinosa, M., Bravo, A., and Salas, M. (2007). Protein p56 from the *Bacillus subtilis* phage phi29 inhibits DNA-binding ability of uracil-DNA glycosylase. *Nucleic Acids Res.* 35, 5393–5401. doi: 10.1093/nar/gkm584

Simpkin Adam, J., and Rigden, D. J. (2016). GP0.4 from bacteriophage T7: in silico characterisation of its structure and interaction with *E. coli* FtsZ. *BMC. Res. Notes* 9:343. doi: 10.1186/s13104-016-2149-5

Stricker, J., Maddox, P., Salmon, E. D., and Erickson, H. P. (2002). Rapid assembly dynamics of the *Escherichia coli* FtsZ-ring demonstrated by fluorescence recovery after photobleaching. *Proc. Natl. Acad. Sci. USA* 99, 3171–3175. doi: 10.1073/pnas.052595099

Ur Rahman, M., Wang, P., Wang, N., and Chen, Y. (2020). A key bacterial cytoskeletal cell division protein FtsZ as a novel therapeutic antibacterial drug target. *Bosn. J. Basic Med. Sci.* 20, 310–318. doi: 10.17305/bjbms.2020.4597

Wagemans, J., Delattre, A. S., Uytterhoeven, B., De Smet, J., Cenens, W., Aertsen, A., et al. (2015). Antibacterial phage ORFans of phage LUZ24 reveal a novel MvaT inhibiting protein. *Front. Microbiol.* 6:1242. doi: 10.3389/fmicb.2015.01242

Wang, H. C., Hsu, K. C., Yang, J. M., Wu, M. L., Ko, T. P., Lin, S. R., et al. (2014). *Staphylococcus aureus* protein SAUGI acts as a uracil-DNA glycosylase inhibitor. *Nucleic Acids Res.* 42, 1354–1364. doi: 10.1093/nar/gkt964

Xu, Q., Tang, L., Liu, W. L., Xu, N., Hu, Y. B., Zhang, Y., et al. (2024). Phage protein Gp11 blocks cell division by inhibiting peptidoglycan biosynthesis. *MBio* 15, e00679–e00624. doi: 10.1128/mbio.00679-24

Yang, X., Lyu, Z., Miguel, A., McQuillen, R., Huang, K. C., and Xiao, J. (2017). GTPase activity-coupled treadmilling of the bacterial tubulin FtsZ organizes septal cell wall synthesis. *Science* 355, 744–747. doi: 10.1126/science.aak9995

Yang, X., McQuillen, R., Lyu, Z., Phillips-Mason, P., De La Cruz, A., McCausland, J. W., et al. (2021). A two-track model for the spatiotemporal coordination of bacterial septal cell wall synthesis revealed by single-molecule imaging of FtsW. *Nat. Microbiol.* 6, 584–593. doi: 10.1038/s41564-020-00853-0

frontiers | Frontiers in Microbiology

TYPE Original Research
PUBLISHED 02 May 2025
DOI 10.3389/fmicb.2025.1537073

OPEN ACCESS

EDITED BY
Agata Dorotkiewicz-Jach,
University of Wrocław, Poland

REVIEWED BY
Fernando Uriel Rojas Rojas,
Universidad Nacional Autónoma de México, Mexico
Cassondra Vernier,
University of Wisconsin–Stout, United States

*CORRESPONDENCE
Susanne DiSalvo
✉ sdisalv@siue.edu

RECEIVED 29 November 2024
ACCEPTED 14 April 2025
PUBLISHED 02 May 2025

CITATION
DiSalvo S, Maness N, Braun A, Tran M and Hofferkamp A (2025) Tracking tripartite interaction dynamics: isolation, integration, and influence of bacteriophages in the *Paraburkholderia-Dictyostelium discoideum* symbiosis system.
Front. Microbiol. 16:1537073.
doi: 10.3389/fmicb.2025.1537073

Tracking tripartite interaction dynamics: isolation, integration, and influence of bacteriophages in the *Paraburkholderia-Dictyostelium discoideum* symbiosis system

Susanne DiSalvo*, Negar Maness, Andrew Braun, My Tran and Andrew Hofferkamp

Department of Biological Sciences, Southern Illinois University Edwardsville, Edwardsville, IL, United States

Introduction: Bacteriophages influence interactions between bacterial symbionts and their hosts by exerting parasitic pressure on symbiont populations and facilitating bacterial evolution through selection, gene exchange, and prophage integration. Host organisms also modulate phage-bacteria interactions, with host-specific contexts potentially limiting or promoting phage access to bacterial symbionts or driving alternative phenotypic or evolutionary outcomes.

Methods: To better elucidate tripartite phage-bacteria-host interactions in real-time, we expanded the *Dictyostelium discoideum-Paraburkholderia* symbiosis system to include *Paraburkholderia*-specific phages. We isolated six environmental *Paraburkholderia* phages from soil samples using a multi-host enrichment approach. We also identified a functional prophage from monocultures of one of the *Paraburkholderia* symbiont strains implemented in the enrichment approach. These phages were evaluated across all three amoeba-associated *Paraburkholderia* symbiont species. Finally, we treated *Paraburkholderia* infected amoeba lines with select phage isolates and assessed their effects on symbiont prevalence and host fitness.

Results: The isolated phages exhibited diverse plaquing characteristics and virion morphologies, collectively targeting *Paraburkholderia* strains belonging to each of the amoeba-symbiotic species. Following amoeba treatment experiments, we observed that phage application in some cases reduced symbiont infection prevalence and alleviated host fitness impacts, while in others, no significant effects were noted. Notably, phages were able to persist within the symbiont-infected amoeba populations over multiple culture transfers, indicating potential long-term interactions.

Discussion: These findings highlight the variability of phage-symbiont interactions within a host environment and underscore the complex nature of phage treatment outcomes. The observed variability lays the foundation for future studies exploring the long-term dynamics of tripartite systems, suggesting potential mechanisms that may shape differential phage treatment outcomes and presenting valuable avenues for future investigation.

KEYWORDS

bacteriophage, symbiosis, *Dictyostelium discoideum*, amoeba, *Paraburkholderia*

Introduction

While phages exhibit relative biological simplicity, their significance within microbial ecosystems is profound, both in terms of their abundance and functional importance (Clokie et al., 2011; Suttle, 2005). Not only do they play a pivotal role in shaping microbial assemblages, but they also serve as significant drivers of bacterial evolution (Hendrix, 2014; Koskella and Brockhurst, 2014). Efforts to comprehend phage diversity and function within ecosystems has expanded from aquatic (Suttle, 2007) to soil ecosystems (Gómez and Buckling, 2011; Srinivasiah et al., 2008), and finally, to host-associated (biotic) microbiomes (Avellaneda-Franco et al., 2023; Chatterjee and Duerkop, 2018; Duerkop et al., 2018; Koskella and Taylor, 2018; Marbouty et al., 2021; Wilde et al., 2024; Zuppi et al., 2022). The inherent complexity of some of these systems challenges our ability to directly interrogate the contribution of phages to the systems composition and function. However, evidence emphasizes that phages are powerful players that, even at the individual level, can direct large-scale changes in microbial communities. This recognition underpins the core concept of phage therapy, where phages are harnessed as treatments for bacterial infections. In a straight-forward scenario, phage administration selectively reduces the population of the bacterial pathogen, and any phage-resistant mutants can be targeted by co-evolved phages or the host immune system. Further, resistance trade-offs may be beneficial to treatment, such as reduced virulence or enhanced antibiotic susceptibility (Chan et al., 2016; Majkowska-Skrobek et al., 2021; Zhang et al., 2022). However, direct (i.e., phage-mediated genetic modifications) and indirect (i.e., expansion of opportunistic pathogens) detrimental trade-offs are also possible (Addy et al., 2012; Oechslin, 2018; Zhang et al., 2022). Although the selection of highly lytic phages helps mitigate this, context-dependent characteristics are also likely to be relevant to treatment outcomes, underscoring the need to understand the diversity of phage-bacteria interactions in eukaryotic host systems (Drulis-Kawa et al., 2012; Oromí-Bosch et al., 2023).

Phages are also relevant to the natural establishment and maintenance of beneficial relationships between eukaryotes and bacterial symbionts. For example, specific phage genotypes correspond to diverse traits associated with insect symbionts (Bordenstein and Bordenstein, 2016; LePage et al., 2017; Oliver et al., 2009; Pichon et al., 2012; Shropshire et al., 2018; Weldon et al., 2013), while phage enrichment in algae-associated bacterial communities may enhance host phenotypic plasticity by enabling rapid selective shifts in bacterial assemblages (Stiffler et al., 2024). Furthermore, in marine sponges, phages play a role in modulating the immune system, facilitating the uptake and stability of beneficial microbial partners (Horn et al., 2016; Jahn et al., 2019). Similar evidence of phage-associated immunomodulation has been demonstrated in many other systems (Dąbrowska et al., 2006; Duerkop et al., 2018; Łusiak-Szelachowska et al., 2020; Sweere et al., 2019) including germ-free models (Gogokhia et al., 2019), suggesting phages can influence eukaryotes via pathways not directly linked to bacterial intermediaries (Barr, 2019). Characteristics of eukaryote ecosystems may, in turn, structure phage-bacteria interactions. For example, anatomical, chemical, or cell-based features may restrict phage access to susceptible bacterial symbionts (Xu et al., 2016), retain phages for localized persistence (Almeida et al., 2019; Barr et al., 2013), or enhance phage clearance from host tissues (Marchi et al., 2023).

To broaden our toolkit for illuminating phage-bacteria-host dynamics, we sought to identify and integrate bacteriophages into the *Paraburkholderia-Dictyostelium discoideum* symbiosis system. The eukaryotic host in this system, *D. discoideum,* is a soil dwelling social amoeba that shares many traits with higher eukaryotes, making it a useful model organism for the study of cellular mechanisms (Annesley and Fisher, 2009; Bozzaro, 2013; Kessin, 2001; Martín-González et al., 2021) and host-pathogen interactions (Barisch et al., 2015; Bozzaro and Eichinger, 2011; Dunn et al., 2018; Steinert and Heuner, 2005; Thewes et al., 2019). During its single-cellular stage, vegetative *D. discoideum* amoeba phagocytose bacteria and multiply via binary fission. In amoeba-dense, food-scarce conditions, amoeba aggregate into a multicellular slug and migrate to a suitable location for fruiting body formation. Fruiting bodies consist of a long stalk of dead cells which support a globular sorus containing hardy spore cells which can be subsequently dispersed to new environments for germination. Throughout the social cycle, *D. discoideum* employs both cell-autonomous and innate immune-like defense mechanisms against potential pathogens (Chen et al., 2007; López-Jiménez et al., 2019; Zhang et al., 2016).

Despite these defenses, natural *D. discoideum* isolates are frequently found in association with bacterial symbionts (most notably *Chlamydiae* and *Paraburkholderia* species) which can establish intracellular infections in amoeba cells and persist through host development and dispersal cycles (Brock et al., 2011; DiSalvo et al., 2015; Haselkorn et al., 2021; Haselkorn et al., 2018). More broadly, members of the *Burkholderia*, *Paraburkholderia*, and *Caballeronia* genera encompass diverse species that engage in symbioses with a wide range of hosts, including plants, fungi, insects, and protists, where they can play roles ranging from mutualism to pathogenicity (Estrada-de Los Santos et al., 2018; Kaltenpoth and Flórez, 2020). Given their facultative nature and the tractability of their host amoeba, *Paraburkholderia* symbionts of *D. discoideum* are particularly amenable for study as they can be fluorescently labeled and co-cultured with amoeba to initiate and track infection processes and outcomes (Shu et al., 2018). Furthermore, symbionts isolated from natural isolates of *D. discoideum* belong to three species- *Paraburkholderia agricolaris, Paraburkholderia hayleyella,* and *Paraburkholderia bonniea* (listed in descending order of screening prevalence and strain diversity), representing an intriguing range of genotypic variation (Brock et al., 2018; DuBose et al., 2022; Haselkorn et al., 2018). These features enable symbiont phenotype comparisons which have emphasized connections between genotype and environmental context with infection patterns (i.e., symbiont abundance and intracellular penetrance) and symbiotic outcomes (i.e., mutualistic to pathogenic; Haselkorn et al., 2018; Khojandi et al., 2019; Miller et al., 2020).

Given the available assortment of *Paraburkholderia* symbiont strains, we reasoned that symbiont-specific phages could be isolated from the environment and employed to interrogate the interplay between phage and symbiont pairings within the context of the amoeba host ecosystem. Furthermore, the abundance and diversity represented by the *Paraburkholderia* genera broadly, which includes a striking array of environmental and symbiont species and genome characteristics, potentially promises a correlating richness in phages ripe for environmental extraction (Compant et al., 2008; Mullins and Mahenthiralingam, 2021). Indeed, a history of phage infection is evidenced by putative prophage sequences and potential phage defense mechanisms present in the majority of *Paraburkholderia* genomes assessed, and prophage induction has been successfully accomplished for at least one of these species (*Paraburkholderia terrae* strain BS437; Pratama et al., 2018; Pratama and van Elsas, 2017). Yet, reports

describing the successful isolation of *Paraburkholderia* phages from environmental sources are limited, emphasizing a gap in connecting ecological and evolutionary signatures of *Paraburkholderia*-phage associations with their contemporary dynamics and consequences.

Here, we describe six environmental phage isolates specific to *Paraburkholderia* symbionts of *D. discoideum* (named Bonzo, Paranha, Balex, Scuba, Bagra, and Scugar), which were collectively isolated following a series of environmental screening attempts. Collectively, these phages were isolated from samples originating from Texas and South Carolina using a muti-bacterial host enrichment approach. As a consequence of the enrichment process (in which sample filtrates were inoculated with *Paraburkholderia* cultures to enable target phage amplification), we also identified a functional prophage (Prozo70) from one of our symbiont strains. Individual phage isolates exhibit distinct host-ranges and plaquing patterns on the tested *Paraburkholderia* strains, providing a spectrum of lysis phenotypes. Collectively, the environmental phage isolates are characteristic of members belonging to the Siphoviridae, Podoviridae, and Myoviridae families. From this starting collection, we selected a subset of isolates to investigate within the context of the *D. discoideum*-*Paraburkholderia* symbiosis system. We found that phage persistence and the consequence of phage treatment for host amoeba and their bacterial symbionts varies by culture context and across distinct phage isolate and symbiont strain pairings. These results demonstrate the potential promise contained within this simple system to track and elucidate outcome trajectories of tripartite interactions.

Materials and methods

Bacterial and amoeba culture conditions

Bacterial strains (Supplementary Table 1) were cultured on YG medium (0.5% Yeast Extract, 0.4% Glucose, 0.1% NaCl, with 1.5% agar for solid media) or, when grown with amoeba, on SM/5 agar medium [2 g glucose, 2 g Peptone, 0.2 g yeast extract, 0.49 g $MgSO_4$, 1.9 g KH_2P0_4, 1.3 g K_2HPO_4-$3H_20$, 17 g agar (Formedium) per liter]. For plaquing assays, soft agar overlays were prepared by pouring 5 mL of melted YG top agar (0.6% agar) with 200 µL bacterial overnight cultures, over YG agar plates. Unless otherwise indicated, bacterial cultures were incubated at 24°C for all assays and liquid cultures were agitated at 150 rpm. To prepare bacterial suspensions for amoeba culturing, bacterial colonies were resuspended in KK2 buffer (2.25 g KH_2PO_4 and 0.67 g K_2HPO_4 per liter) and set to a final concentration of 1.5 OD_{600} nm.

To establish *Paraburkholderia* infections in amoeba cultures, 10^5 *Dictyostelium discoideum* spores (strains QS18 or V12) were plated on SM/5 agar plates with 200 µL of a bacterial mixture containing 95% *Klebsiella pneumoniae* and 5% *Paraburkholderia* suspension by volume. To maintain uninfected or previously infected amoeba cultures, spores were plated with pure *K. pneumoniae* suspensions. Cultures were incubated face-up under low lights at 24°C with 50–70% humidity for 5–8 d to allow fruiting body development.

Phage filtrate preparation from soil and culture samples

Surface soil (50–100 g, <8 inches deep) was collected from wooded sites in the U.S., including Edwardsville, IL; Atlanta, GA; St. Louis, MO; Houston, TX; and Bluffton, SC. Samples were suspended in YG broth (1 mL/ gram of soil) for 1 h at 100 rpm, centrifuged at 10 K rpm for 5 min, and filtered through a 0.22 µm filter. Five ml aliquots were removed and stored at 4°C as "pre-enriched" filtrates. The remaining filtrate was amended with 10x YG broth, inoculated with 100 µL of overnight liquid cultures from each of the indicated enrichment strains and incubated at 24°C for 24–48 h at 100 rpm. Samples enriched filtrates were prepared and stored as described above.

Phage isolation

Sample filtrates were spotted on bacterial soft agar overlay plates and incubated for 24–48 h. Lawn clearance indicative of bacteriophage lysis was recorded and qualitatively assessed (0 = no lysis; 5 = transparent lysis zone). Lysis producing filtrates of interest were serially diluted in phage buffer (20 mM Tris–HCl pH 7.4, 100 mM NaCl, 10 mM $MgSO_4$) and plated on susceptible strains using the double agar layer method by either spotting 10 µL of filtrate dilutions on bacterial lawns or mixing 100 µL of filtrate with 200 µL of bacterial overnight culture and 5 mL YG top agar before pouring over YG agar plates. After 24–48 h of incubation, individual plaques were extracted using pipette tips, suspended in phage buffer, and re-plated on host lawns. This purification was repeated three times to obtain pure phage isolates.

Phage amplification and enumeration

Phage stock serial dilutions were plated via the double agar layer method and incubated at 24°C for 24–48 h. Plates showing confluent lysis were incubated at room temperature for 1 h at 100 rpm with 3 mL of phage buffer added to suspend phage particles. The phage buffer from each plate was pooled into a Falcon tube, centrifuged at 10 K rpm for 5 min, and filtered through a 0.22 µm filter. Phage stocks were stored at 4°C and periodically sampled, serially diluted, and spotted on host lawns to quantify PFU titers.

Host range characterization and efficiency of plating

Purified phage lysates were spot tested on bacterial soft agar overlays and plaque presence and morphology was assessed following incubation at 24°C for 24–48 h. To determine efficiency of plating (EOP), identical phage dilutions were spotted on bacterial lawns of each tested strain, and phage titers for each were quantified following incubation and plaque formation. The efficiency of plating was calculated by dividing the phage titer produced on the test strain by the phage titer produced on the reference strain and expressed as a percentage. Reference strains were selected based on their practical suitability as hosts for each tested phage (i.e., strains that effectively amplify the phage isolate).

Phylogeny construction

ATP synthase beta chain (atpD) gene sequences corresponding to individual *Paraburkholderia* strains (for each of the *D. discoideum* symbiont strains), or to a species-representative strain (for some of the

Paraburkholderia strains that do not form a symbiosis with *D. discoideum* when strain-specific sequences were unavailable) were imported into Mega11 from NCBI (see Supplementary Table 1 for GenBank accession numbers), aligned with MUSCLE, and used to construct a neighbor end-joining tree with 1,000 bootstrap replicates.

Transmission electron microscopy

Processing and imaging of purified phage samples by transmission electron microscopy was performed by Wandy Beatty at the Washington University Molecular Microbiology Imaging Facility. Samples were fixed with 1% glutaraldehyde (Ted Pella Inc., Redding CA) and allowed to absorb onto freshly glow discharged formvar/carbon-coated copper grids for 10 min. Grids were then washed in dH_2O and stained with 1% aqueous uranyl acetate (Ted Pella Inc.) for 1 min. Excess liquid was gently wicked off and grids were allowed to air dry. Samples were viewed on a JEOL 1200EX transmission electron microscope (JEOL United States, Peabody, MA) equipped with an AMT 8-megapixel digital camera (Advanced Microscopy Techniques, Woburn, MA).

Phage stability and treatment assays

Phage stability on SM/5 plates was assessed by spreading 100 µL phage filtrate (10^8 PFU/ml for a total of 10^7 PFU's) on the agar surface in duplicate. Samples were harvested for quantification after 24 h and 7 days. For quantifying phages on uninfected and *Paraburkholderia*-infected amoeba cultures, 100 µL phage filtrate (10^8 PFU/ml), 100 µL spore suspension (10^6 spores/ml, for a total of 10^5 spores) from uninfected or infected amoeba lines, and 200 µL *K. pneumoniae* suspension (as previously described) were plated on SM/5 in duplicate (from identical sample pools, providing paired samples for two time-point assessments). One plate was harvested after 24 h, and the other was incubated for 1 week to allow fruiting body formation. 10^5 spores were transferred from these developed plates to new SM/5 plates with *K. pneumoniae*, and incubated for an additional 24 h. Following incubation, sample filtrates were prepared by adding 4 mL of phage buffer with 0.1% Igepal to the agar surface to resuspend total plate contents. A 2 mL aliquot was collected, centrifuged at 10 K rpm for 2 min, filtered (0.2 µm), serially diluted, and spotted on host lawns (corresponding to infection condition strain) for PFU enumeration.

To assess phage treatment outcomes, spore suspensions were mixed with phage filtrates (or with 100 µL phage buffer for untreated controls) and plated (in duplicate) as described above. Following 1 week incubation, total plate contents from one plate were harvested for phage enumeration and the other plate was used to harvest spores for infection prevalence quantification and (for assessment of outcomes following several social cycle passages) to initiate new amoeba cultures (as described).

Infection prevalence was quantified from suspended spores using a BD-C6 Flow Cytometer. After gating spores, the percent of *Paraburkholderia* RFP-positive spores were determined from PE-A intensity histograms, with uninfected samples used to establish fluorescent and non-fluorescent spore boundaries. An Olympus Fluoview FV1000 confocal microscope was used to acquire representative images of spores (stained with 1% calcofluor and covered with a 2% agarose overlay on a glass-bottom dish) from the treatment conditions and imaged using the Plan Ap Oil 1.4NA 60x objective. The DAPI and Cy3 channels were used to image Calcofluor and RFP, respectively, with several Z-sections (step size of 0.5 µm) acquired at a 1,024 × 1,024 resolution taken for each sample and images were processed in FIJI (imagej.net/Fiji). Total PFU's were quantified from plate suspensions as described previously, with pre-filtered suspension aliquots being reserved for spore quantification (via hemocytometer counts).

Statistics

All statistical analyses were performed using R version 4.2.3. When the assumption of normality was met, comparisons between infection outcomes (e.g., total PFUs, spore counts, or RFP values), with infection and/or treatment condition as independent variables, were assessed using ANOVA. If normality was violated, the Kruskal-Wallis test was applied instead. Post-hoc comparisons among strains were conducted using Tukey's test for significant ANOVA results or Dunn's test for significant Kruskal-Wallis results. For pairwise comparisons in phage treatment transfer experiments (e.g., PFU and spore counts between two transfers within treatment conditions), the Wilcoxon rank-sum test was used.

Results

Phage isolation and phenotypic characterization

To isolate bacteriophages specific to *Paraburkholderia* symbionts of *Dictyostelium discoideum*, we periodically collected and screened environmental samples throughout the United States. To improve detection of low-abundance phages, we implemented a multi-host enrichment method by inoculating sample filtrates with bacterial cultures and incubating for 24–48 h before preparing filtrates. Aliquots from sample filtrates collected before (pre-E) and after (post-E) enrichment with mixed *Paraburkholderia* cultures were spot tested on bacterial lawns and monitored for lysis plaques. While pre-enriched filtrates rarely produced clearance zones, post-enriched filtrates produced from Houston Arboretum (Texas) and Sun City (South Carolina) soil yielded plaques on several *Paraburkholderia* strains (Figure 1). Occasionally, faint lysis zones were observed from enriched filtrates from soil, lake, and sewage collected from other sites, but we were unable to purify symbiont-specific phages of interest from these samples.

To determine whether lysis plaques could be a product of prophages harbored by strains used for phage enrichment (rather than phages from the environmental sample), we tested filtrates from mixed and mono-cultures corresponding to the bacterial strains used during the phage enrichment process (i.e., filtrates produced from bacterial cultures without added environmental sources). From these, lysis zones were observed on two strains of *P. agricolaris* and subsequent testing of pure culture filtrates suggested that a prophage from another *P. agricolaris* strain, Pa70, was the likely source of this lysis pattern (Figure 1c). This conclusion was supported by bioinformatic identification of an intact prophage sequence in Pa70

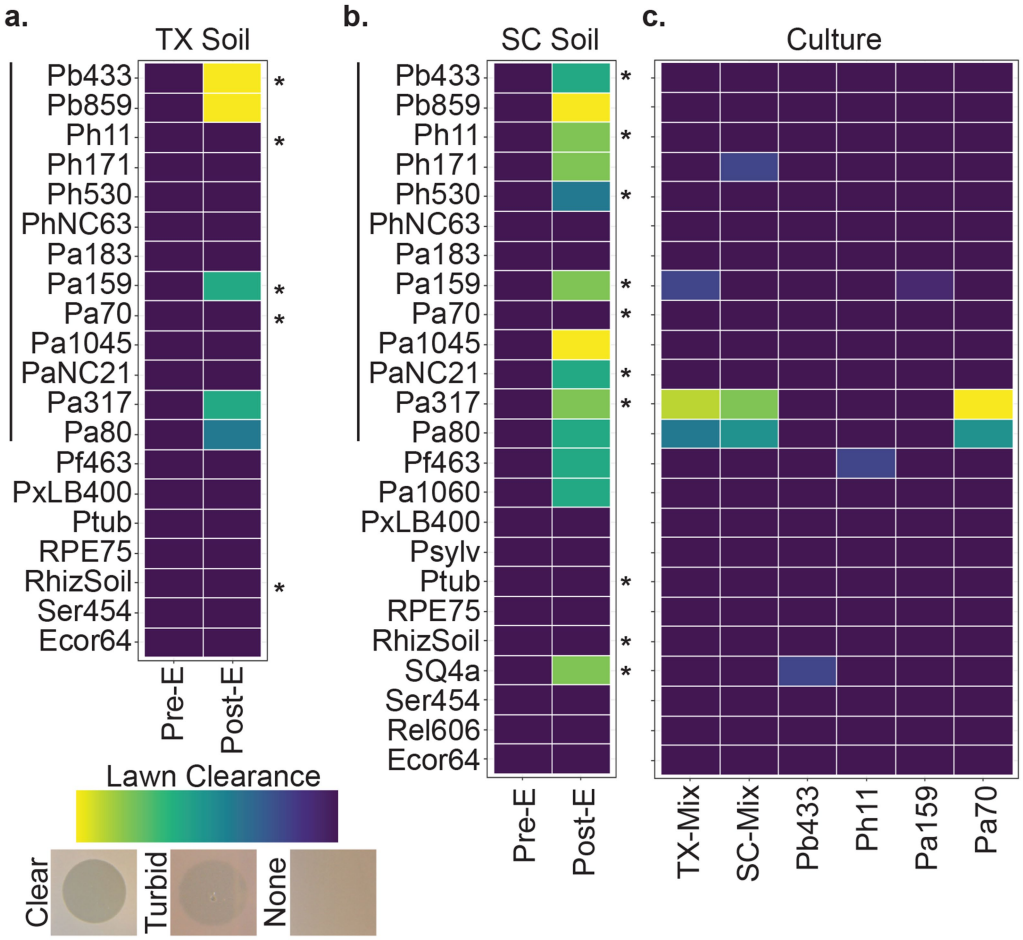

FIGURE 1
Phage screening. Tile plots representing lawn clearance from pre- and post-enriched filtrates generated from **(a)** Texas (TX) and **(b)** South Carolina (SC) soil samples, and of **(c)** culture filtrates from mixed- and mono-cultures representative of the enrichment conditions. The Y axis represents bacterial strains tested against the filtrate types indicated on the X axis. Left-hand vertical lines correspond to symbiont strains of *D. discoideum*, right-hand asterisks indicate each strain used in the multi-host enrichment condition. Observation of lysis zones were qualitatively scaled from no change (dark purple) to a full clearance (light yellow) in lawn thickness. See Supplementary Table 1 for a full list of bacterial strains.

using the PHASTER web server[1] and consistent isolation of a Pa317-targeting, replication-competent, phage from Pa70 filtrates.

Seven *Paraburkholderia* symbiont targeting phage isolates (including the Pa70 prophage) were ultimately purified from these screening efforts (Figure 2). Most phages exhibited species-specific host ranges, except for Paranha, which infected strains of *P. bonniea* and *P. hayleyella* (Figures 2, 3). Bonzo only targeted *P. bonniea*, producing notably large, clear, plaques on host lawns. The other four environmental phages (Balex, Scuba, Bagra, and Scugar) and the Pa70 prophage (Prozo) targeted a subset of *P. agricolaris* strains, and, with the exception of clearer plaques produced by Scuba and Scugar on some hosts, plaques were predominantly turbid (Figures 2, 3). To assess the efficiency of plating across susceptible host bacteria, phage titers on bacterial test strains were compared to corresponding titers on a bacterial reference strain (chosen for each phage isolate based on phage amplification and plaque formation efficacy for each phage isolate). For Bonzo, amplification was least efficient on Pb859, while for Paranha, amplification was similarly efficient on all three *P. bonniea* hosts, which produced EOP values approximately five-fold higher than *P. hayleyella* host strains (Figure 3B). For *P. agricolaris* targeting phages, phage productivity was highest on Pa1045 for Balex and Scuba, and on Pa317 for Bagra and Scugar (Figure 3B).

Transmission electron micrographs of high titer phage filtrates (>10^8 PFU/ml) suggest that the environmental phages represent members of the Myoviridae, Siphoviridae, and Podoviridae (Figure 4). Contractile tails, characteristic of Myoviridae, (138.3 nm long on average) are readily visible on Balex, while long, flexible tails, characteristic of Siphoviridae, are visible on Bagra, Bonzo, and Scuba virions (148, 164, and 178 nm long on average, respectively). Paranha and Scugar virions were harder to identify, with Podoviridae resembling particles consisting of semi-rounded capsids with small tail-like protrusions being the only phage-like particles observed from multiple high-titer filtrate preparations. Average head capsid diameters ranged from 54 nm for Bagra to 63 nm Scugar, with all others between 56.3 and 57.3 nm.

1 https://phaster.ca/

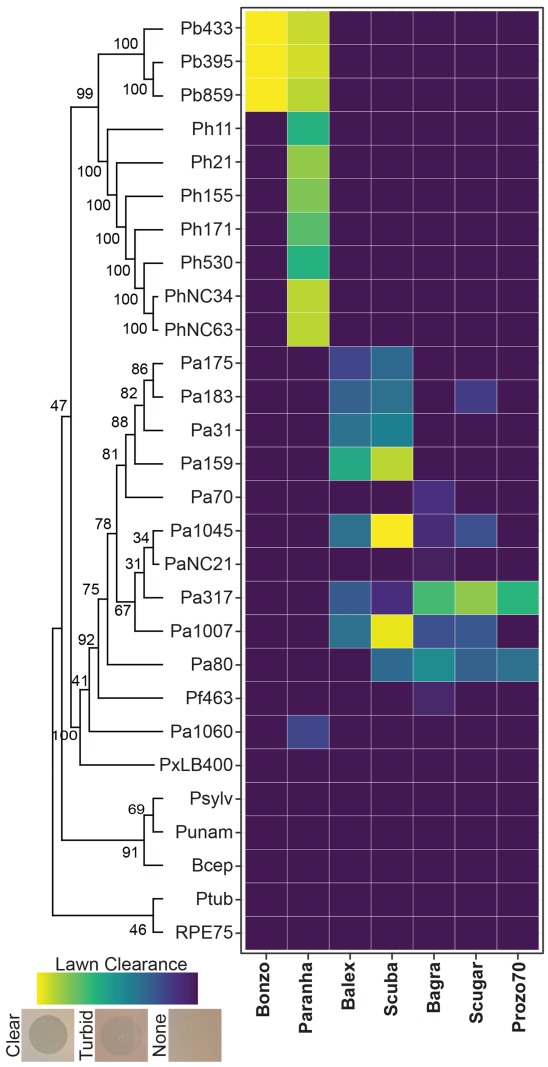

FIGURE 2
Host range and plaque clearance patterns. Tile plot representing lawn clearance values for the final phage isolates (x axis) when spot-tested on bacterial lawns (y axis). Test strains are arranged vertically according to phylogenetic relatedness based on aligned atpD gene sequences (Supplementary Table 1).

Phage stability in amoeba-associated culture conditions

Next, we wanted to explore the impact of phage integration (i.e., phage "treatment") in amoeba populations hosting phage susceptible *Paraburkholderia* symbionts (i.e., "infected" amoeba). However, before testing phage treatment outcomes for *Paraburkholderia* infected amoeba, we assessed our ability to detect and recover phages from plating contexts relevant to *D. discoideum* culturing conditions. To do this, we spread 10^7 total Bonzo PFU's on SM/5 plates alone, or with 10^5 *D. discoideum* spores harvested from uninfected or Pb433 infected amoeba lines (and plated with *K. pneumoniae* as a food source). Plates were prepared in duplicate, and total PFU's were quantified from filtrates prepared from plate contents harvested from two different time points per condition. Specifically, samples were collected 24 h after plating for all conditions, and 7 days after plating for SM/5-only samples, and, for uninfected and Pb433-infected amoeba culture conditions, after transferring spores developed from the duplicated samples (after 7 day incubations) to fresh SM/5 plates (with *K. pneumoniae*) and incubating for an additional 24 h (Figure 5).

Twenty-four hours after plating, total PFU's recovered from all conditions were lower than the initial input of total PFU's (10^7), with SM/5-only, uninfected-amoeba, and Pb433-infected amoeba, plates yielding an average 10^5, 1.65×10^5, and 6.93×10^6 total PFU's, respectively. Phage intercalation into the plating media likely limits the efficiency of recovery, accounting for some degree of phage loss following incubation. However, total PFU's varied significantly across the conditions ($df = 2$, $F = 5.55$, $p = 0.017$); with Pb433-infected amoeba cultures yielding more PFU's than either SM/5-only ($p = 0.035$) or uninfected-amoeba ($p = 0.028$) conditions (which did not significantly differ from one another, $p = 0.99$), suggesting that the presence of Pb433 bacterial symbionts carried with host spores improves/enables phage stability and/or amplification. To determine whether Bonzo could also persist throughout the amoeba social cycle and be carried to new environments during spore dispersal, we quantified total PFU's from fresh cultures seeded with spores developed from the duplicated amoeba culture plates. Interestingly, we found that phages could only be recovered from the Pb433-infected amoeba lines, which yielded phage titers comparable to their pre-transfer counterparts. These results suggest that amoeba-associated phage co-dispersal is possible but requires facilitation by phage-susceptible symbionts.

Phage, symbiont, and host outcomes in phage treated amoeba cultures

To assess the impact of phages on host-symbiont dynamics, we established *Paraburkholderia* infected amoeba host lines and inoculated (i.e., treated) these lines with select phage isolates. Each amoeba host line was infected with one of the following four rfp-labeled *Paraburkholderia* symbiont strains: Pb433, Ph171, Pa1045, or Pa159. These host lines were subsequently treated with one of the following four phage isolates: Bonzo, Paranha, Balex, or Scuba, according to the susceptibility of the symbiont infection strain to the phage isolate as indicated by plaque formation on bacterial lawns (Figure 3). Treatment consisted of plating 10^5 amoeba spores with 10^7 phage PFU's on SM/5 agar medium (supplemented with food bacteria) and incubating for 7 days to allow the completion of the amoeba social cycle and fruiting body formation. We set the phage dosage to reflect a treatment MOI of ~10, assuming that infected sori contents typically contain 10-fold *Paraburkholderia* cells than spore cells (estimating total bacterial symbiont cells plated to be ~10^6). Although these numbers are likely to vary across infection conditions, preliminary treatment trails (Supplementary Figure 1) suggested that final outcomes do not vary noticeably according to starting phage dose in the tested condition ($df = 3$, $F = 0.853$, $p = 0.5$). After establishing treatment pairings and allowing the formation of fruiting bodies, we harvested plate contents to quantify total amoeba spores, *Paraburkholderia* symbiont infection prevalence in spore populations, and total phage PFU's (Figure 6). We also visualized infection patterns in sori contents for representative samples using confocal microscopy (Figure 6A), which aligned with infection prevalence as quantified by flow cytometry (Figure 6B).

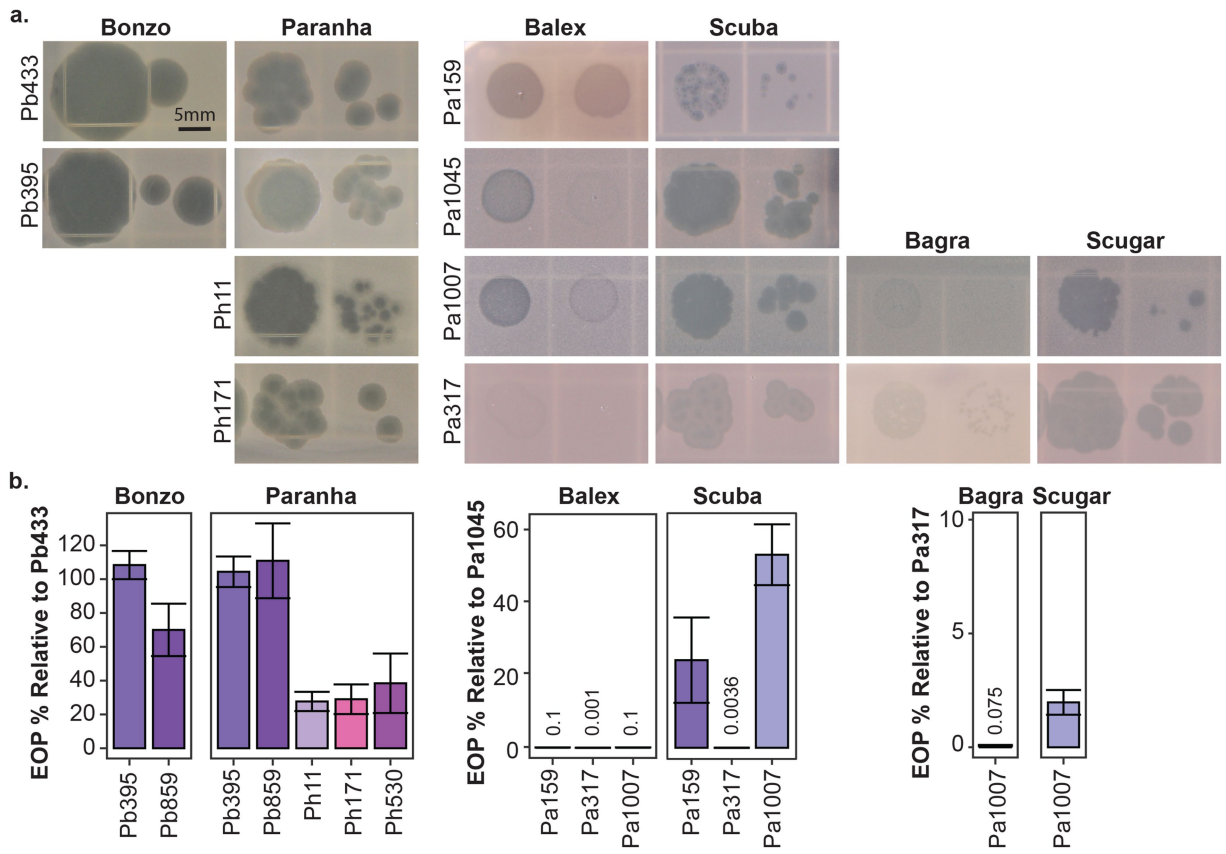

FIGURE 3
Plaque morphology and plating efficiency. Representative plaques **(a)** and efficiency of plating (EOP %) **(b)** for the environmental phage isolates on select bacterial host strains. Efficiency of plaquing is represented as the percentage of PFU/ml generated from test strains relative to PFU/ml generated from corresponding reference strains for each phage isolate (Pb433 for Bonzo and Paranha, Pa145 for Balex and Scuba, and Pa317 for Bagra and Scugar). Scale bar is representative for all images in **a**.

In line with previous reports, spore productivity is significantly impacted by *Paraburkolderia* infection status (df = 4, $F = 5.175$, $p < 0.001$), with Pa1045 and Ph171 (but not Pb433 or Pa159) resulting in a significant reduction in total spores compared to uninfected amoeba ($p < 0.05$; Figure 6B). While Paranha treatment did not significantly alleviate the fitness cost of Ph171 infections (df = 1, $X^2 = 0.43478$, $p = 0.509$), phage treatment with either Balex or Scuba ($p < 0.001$) significantly improved total spore productivity for Pa1045 infected amoeba hosts (df = 2, $F = 26.88$, $p < 0.0001$). *Paraburkholderia* symbionts also establish different rates of intracellular infections in spore populations (df = 10, $X^2 = 90.057$, $p < 0.0001$). As Pa1045 results in very low rates of intracellularly infected spores, capturing the potential significance of phage-mediated reductions in this parameter is limited. In contrast, Ph171 establishes high rates of intracellular infections, but Paranha treatment had no effect on this infection outcome. However, phage treatment with either Paranha or Bonzo phage isolates for Pb433, and with either Scuba or Balex for Pa159, significantly reduced the infection prevalence of these bacterial symbionts in host amoeba ($p < 0.001$). Finally, in regard to phage abundance in treated cultures, total pfu's significantly varied across the collective treatments (df = p6, $X^2 = 19.35$, $p < 0.005$), but within the same infection context, was only significantly different between Balex and Scuba in Pa1045 symbiont infected amoeba ($p < 0.01$).

Next, we assessed symbiont infection dynamics over multiple amoeba social cycles following phage treatment for a subset of Pb433 and Pa159 infected amoeba host lines. To do this, we replated spores developed from phage treated amoeba lines on new media plates with a fresh supply of food bacteria. Following an additional round of incubation and fruiting body formation, we harvested developed sori, quantified intracellular symbiont infection prevalence, and transferred spores to new plates. After completion of this third social cycle (following phage addition) we again quantified symbiont infection prevalence, as well as total amoeba spores and phage PFU's in developed amoeba host lines (Figure 7). Given that spore productivity is not significantly impacted by these symbionts, the lack of significant changes in this parameter following serial transfers was expected (df = 11, $F = 1.8$, $p = 0.1$). However, this also highlights that detrimental host fitness outcomes were not induced by phage treatment under these conditions. Furthermore, total Bonzo and Paranha PFU's, and phage associated reductions in Pb433 symbiont infection prevalence in amoeba host lines, remained stable between the first and last social cycle [$t(5) = 0.6$, $p = 0.56$, and $t(2) = 2.6$, $p = 0.121$]. However, in the Pb433 infected amoeba host lines that were treated with Paranha, the infection prevalence of Pb433 in host spore populations appeared to be trending upwards with each transfer, corresponding with a slight downward trend in total Paranha PFU's. For amoeba host lines infected with Pa159, symbiont infection prevalence rates for each phage

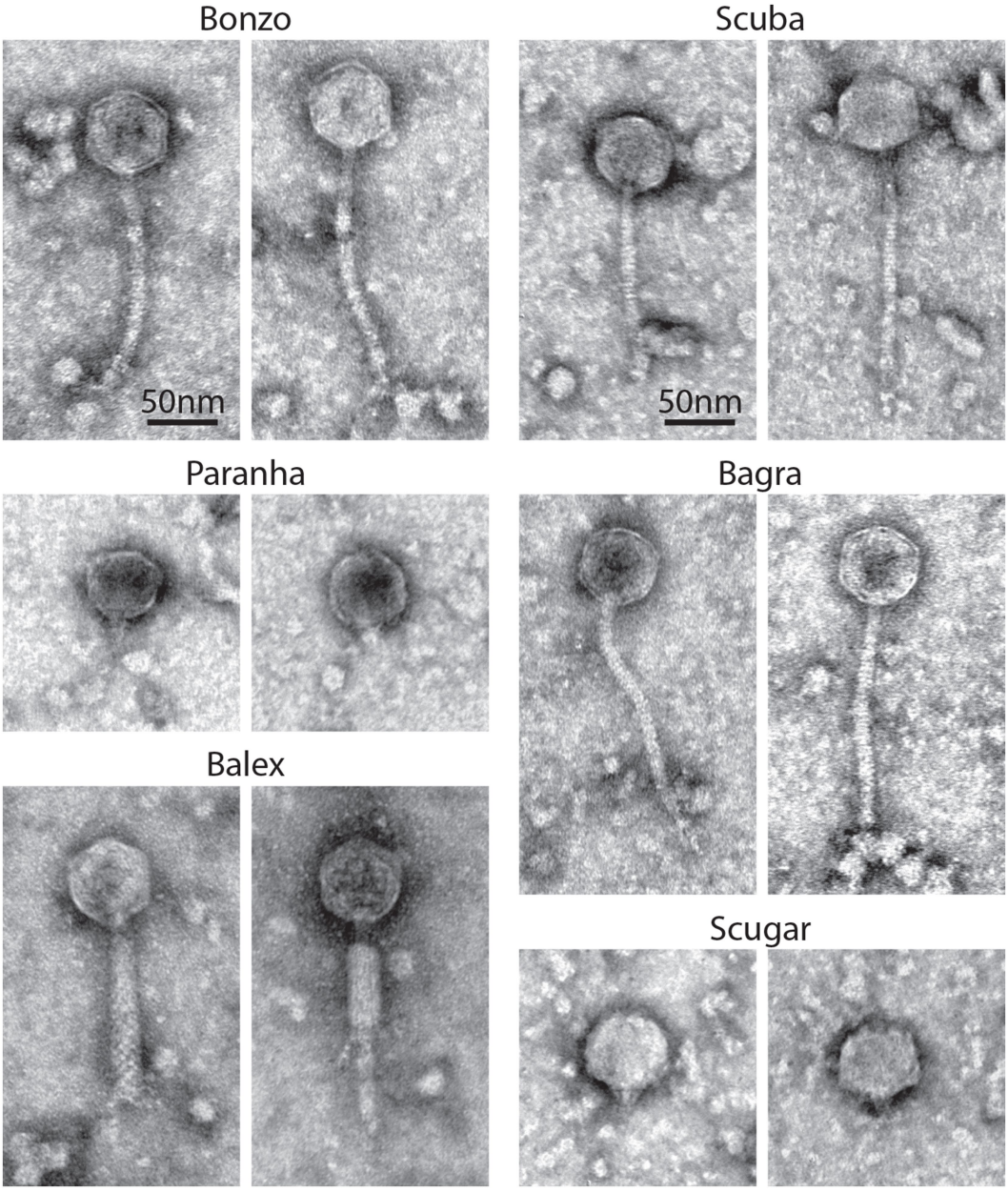

FIGURE 4
Phage virion morphology. Representative negatively stained transmission electron micrographs from high-titer filtrates of purified environmental phage isolates. Scale bars are representative for all images.

treatment condition also remained relatively stable over the tested time-period (df = 5, $X^2 = 9.1205$, *p*-value = 0.1044). However, Balex phage PFU's could not be recovered from two out of three final amoeba host lines, and these exhibited higher Pa159 symbiont infection prevalence rates, suggesting phage abundance is inversely correlated with bacterial infection levels and that phage instability or loss may enable bacterial infections to rebound following phage treatment.

Discussion

While our results demonstrate that *Paraburkholderia*-specific phages can be successfully isolated from soil, the effort we exerted toward this aim (i.e., reiterative screening attempts of water, soil, and sewage sampled collected from several states) was disproportional to our initial expectations. Presumably, the diversity and plasticity of *Paraburkholderia* species and their potential to occupy multiple overlapping habitats, should favor phage persistence, exchange, and diversification. Furthermore, at least some subset of prophage elements commonly associated with *Paraburkholderia* genomes should retain lytic potential, resulting in occasional environmental release (Pratama et al., 2018). While one study successfully induced a *Paraburkholderia* prophage, their attempts to isolate environmental phages failed to bear fruit, as has our search for additional sources describing the isolation of environmental *Paraburkholderia* phages (Pratama and van Elsas, 2017). However, accurately identifying

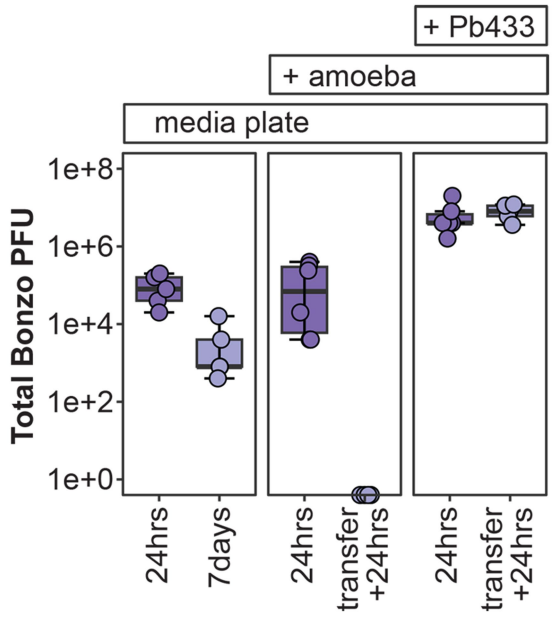

FIGURE 5
Bonzo stability in amoeba culture conditions. Total Bonzo PFU's recovered following the indicated incubation periods on agar medium alone (media plate, left), or with *D. discoideum* amoeba that were either uninfected (+ amoeba, middle), or infected with Pb433 (+ Pb433, right). For amoeba co-culture conditions, transfer + 24 h represents re-culturing from *D. discoideum* spores developed from the initial plating conditions.

relevant literature may be complicated by revolutions in phylogenomics and nomenclature, and the lag period toward consensus and broad application of new classifications. Specifically, the reclassification of the plant-beneficial-environmental clade of *Burkholderia* into a separate *Paraburkholderia* genus was proposed in 2014, and several new subdivision genera have since been proposed (Sawana et al., 2014; Dobritsa and Samadpour, 2016; Estrada-de Los Santos et al., 2018; Beukes et al., 2017). With this in mind, a prior study isolated an environmental phage active against a *Burkholderia* cinch-bug symbiont originally classified as a *Burkholderia* sp., but which is retrospectively likely to belong to the *Paraburkholderia* genera (Xu et al., 2016). Ultimately, it is unclear whether scarcity of *Paraburkholderia* phages in the literature is due to a limited number of attempted screens or limited success rates. Phage isolation is dependent on host species prevalence and characteristics, environmental context, and screening strategy (Hyman, 2019; Mattila et al., 2015; Nafarrate et al., 2020). In our own experience, local samples (~30-mile radius around Edwardsville, Illinois) have yet to yield phage isolates of interest, despite conducting over a dozen screens representing a range of seasons, sample-types, and sites. In contrast, our successful screens originated from soil collected from wooded locations in warmer climates (Texas and South Carolina), which were sent via mail for processing upon receipt, and kept aerated and moist prior to processing. Working from these successes, we hope to hone-in on sampling and screening conditions that prove most promising. However, if *Paraburkholderia* phage isolation is indeed more difficult than would be expected given the potential presence and distribution of putative bacterial hosts, this might point to an intriguing biological phenomenon inherent to *Paraburkholderia* bacteria (and/or their phages).

As a byproduct of our multi-host enrichment approach, we identified a functional prophage from the *P. agricolaris* Pa70 bacterial symbiont that could generate lysis plaques and amplify on the related Pa317 symbiont strain. This observation is intriguing and suggests several avenues for investigation regarding the potential functional role of this, and other putative prophages, on the genotypic and phenotypic diversity of *Paraburkholderia* strains, and how these contributions might relate to symbiotic vs. free-living traits. *P. agricolaris* appears to be the most prevalent and phenotypically diverse *Paraburkholderia* symbiont species of *D. discoideum* (DuBose et al., 2022), possessing a genome approximately twice the size (8.7 Mbp) of those of *P. bonniea* and *P. hayleyella* (4.1 Mbp; Brock et al., 2018; Noh et al., 2022). Horizontal gene transfer, including prophage integration-based transduction, has been posited as an important contributing factor for genome expansion and diversification (Arnold et al., 2022), and the presence of prophage sequences correlates to some extent with genome size (Casjens, 2003). However, this relationship is tenuous, as some of the largest bacterial genomes lack significant prophage signatures and are more likely the result of genome duplication (Casjens, 2003; Han et al., 2013). Nonetheless, the features and environmental prevalence of *P. agricolaris* symbionts suggests that they are more readily environmentally acquired and horizontally transmitted (as well as reseeded into the environment) by host amoeba (Shu et al., 2020; Shu et al., 2018). By extension, *P. agricolaris* strains may be more vulnerable to environmental phage exposure and as such more heavily shaped by phage-predation and modification than the other two symbiont species.

The phage collection isolated in this study allowed us to co-culture and track different phage isolate by bacterial symbiont pairings within amoeba host populations, highlighting the influence of individual members and alternative partner pairings in driving multi-partner interaction outcomes. A powerful feature of the system is that the natural variation in infection characteristics across symbiont strains enables investigations into how specific characteristics associated with bacterial symbionts and/or phage isolates interrelate to produce novel outcomes. The phage-susceptible bacterial symbionts in this study differed in their infection prevalence rates, intracellular infection density characteristics, and fitness costs for host amoeba. While Ph171 and Pb433 symbiont strains both produce high infection rates, host spores infected with Ph171 harbor more symbiont cells than host spores infected with Pb433, while total host spore productivity is reduced by Ph171 infections but unaffected by Pb433 infections. In contrast, symbiont Pa159 produces an average spore infection rate of 60%, compared to only 10.9% for Pa1045, and while they both tend to reduce spore production for host amoeba, this reduction was only significant for Pa1045. Because of some overlap in host-specificity, we could detect differences in outcomes between different phage isolates when targeting the same symbiont and between the same phage isolate when targeting different symbionts. Furthermore, given the potential for phage and symbionts to persist in amoeba cultures over multiple developmental cycles, initially subtle variations may exacerbate over time to reveal striking differences, as trends from our small-scale serial transfer experiment potentially portends (i.e., Paranha and Balex appeared to lose efficacy over time, in contrast to their Bonzo and Scuba counterparts).

10.3389/fmicb.2025.1537073

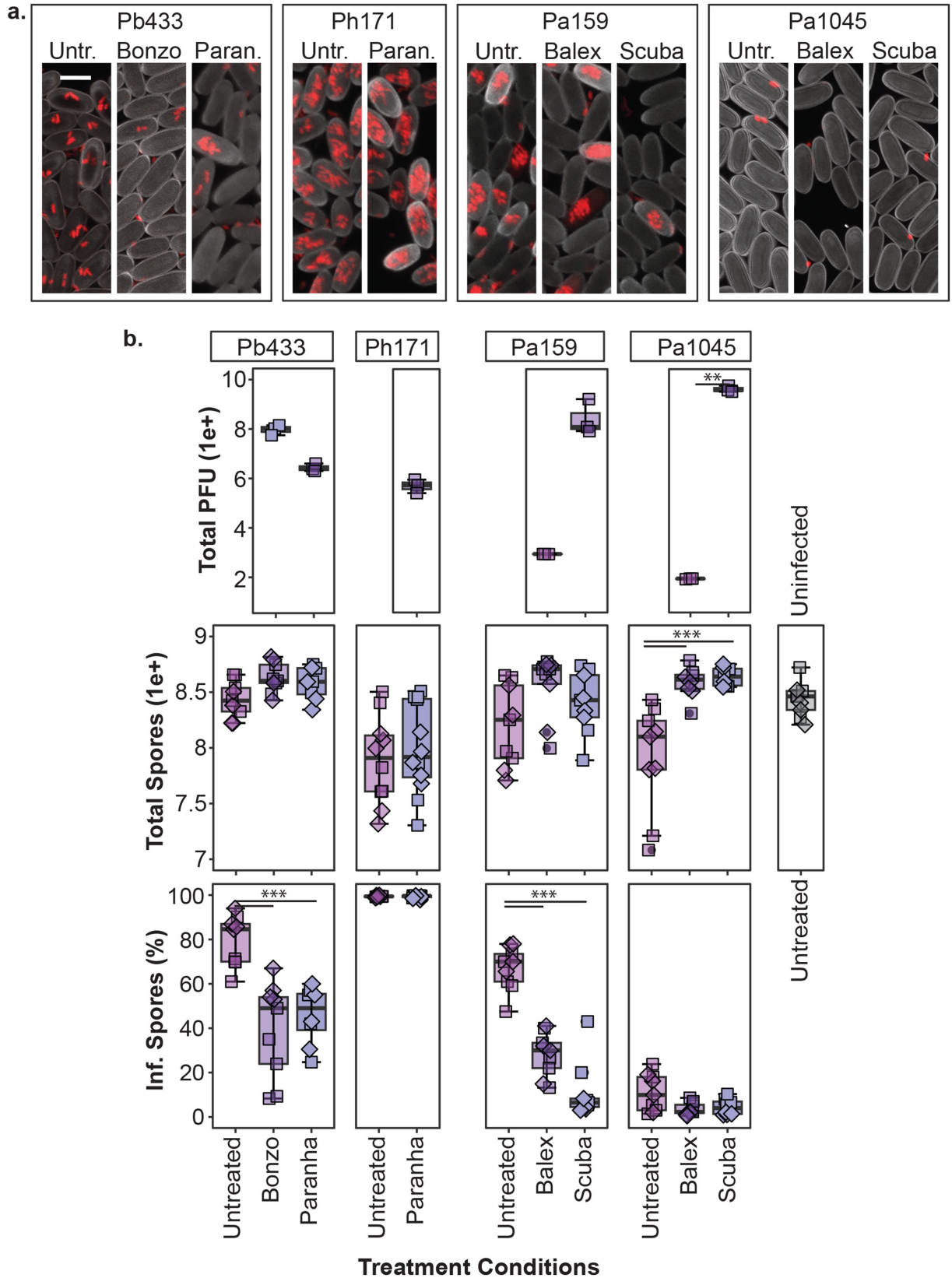

FIGURE 6
Phage treatment of *Paraburkholderia* infected amoeba. Representative confocal micrographs (z-projections) of sori contents **(a)** and box plots of total phage pfu's, amoeba spores, and intracellular infection prevalence in spore populations (top, middle, and bottom panels, respectively) **(b)** from developed amoeba cultures (1 week incubation) for the indicated phage treatment and *Paraburkholderia* (rfp) infection combinations. Scale bar represents 5um. Plot points represent individual biological replicates from V12 (boxes) and QS18 (diamonds) amoeba lines (n ≥ 4 per strain). Asterisks represent statistically significant differences between indicated groups (**p-value < *0.01*, ***p < 0.001).

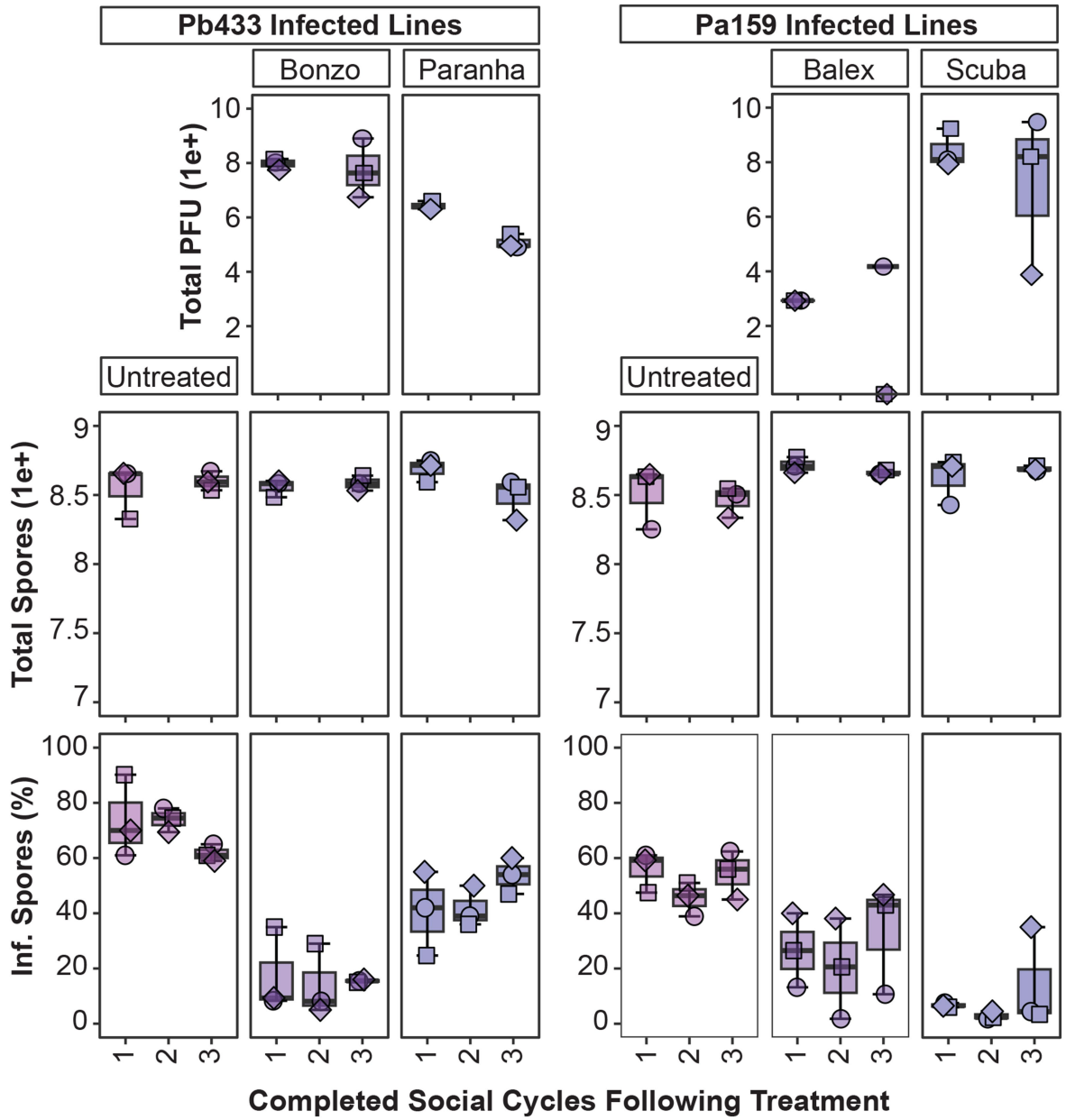

FIGURE 7
Tracking phage and symbiont infection parameters over multiple social cycles. Box plots of total phage PFU's, amoeba spores, and intracellular infection prevalence from spore populations (top, middle, and bottom panels, respectively) after plating phage treated amoeba spores for the indicated infected amoeba lines, sampling after one social cycle (1), and serially transferring spores from harvested fruiting bodies from the prior cycle to complete a second (2), and third (3), round of development. For the second (2) cycle, data was collected for intracellular infection prevalence (bottom panel) but not for total PFU and spore production (top panels). Plot points represent individual biological replicates from QS18 amoeba lines (n = 3).

In pairings where significant declines in infection prevalence were observed (Pb433, and Pa159), phage treatment did not completely eradicate intracellular infections in passaged hosts. For instance, Bonzo and Scuba phages were effective at reducing Pb433 and Pa159 infections, respectively, but low levels of infection persisted in the conditions tested. Additionally, for certain passaged amoeba host lines, phages appeared to have been lost entirely (e.g., Balex PFU's were not recovered from two of three Pa159 amoeba host lines), or were on the verge of extinction (e.g., Scuba PFU's declined in one of three amoeba lines). While immune mechanisms may improve phage therapy efficacy in mammals (Marchi et al., 2023), symbiont persistence in these phage treated amoeba lines does not rule out the possibility that primitive immune-like mechanisms in *D. discoideum* can act synergistically with phages. Indeed, as *Paraburkholderia* symbionts establish persistent (and in many cases, asymptomatic) infections these symbionts may be tolerated by, or act to dampen, *D. discoideum* pathogen clearance mechanisms (Brock et al., 2016). It may be that certain phage-symbiont pairings will result in more effective symbiont clearance. For example, in Pa1045 infected amoeba, despite detecting extracellular symbionts in treated amoeba cultures (Figure 6A), phage treatment reduced intracellular infections to almost

indetectable levels and improved amoeba host fitness. Although we did not carry these amoeba lines forward in the serial transfer experiment, this symbiont might represent a more pathogen-relevant context for assessing the interplay between phage and amoeba defense responses in pathogen targeting.

Phage-symbiont dynamics within amoeba populations may also reflect a balancing act driven by both co-evolutionary pressures and physiological constraints. A preliminary test on a small number of Bonzo treated Pb433 isolates hinted at emergence of variable phage resistant phenotypes, suggesting that evolution of resistance and counterselection may underly co-persistence (preliminary data not shown). However, host-specific features may also contribute to outcome dynamics (beyond immune system contribution mentioned above), as highlighted by other natural symbiont systems (Koskella et al., 2011; Xu et al., 2016). One compelling hypothesis is that intracellular symbionts are protected from phage predation and that this protection varies by cell-type (vegetative amoeba vs. spores), intracellular location, and/or symbiont-specific intracellular invasion and replication characteristics. For example, Paranha-induced reduction of Pb433, but not Ph171, could be related to different intracellular profiles between these two symbionts (Figure 6). Certainly, phage penetration into cells and tissues is an important factor for phage stability and targeting efficacy, and may be highly variable (Bichet et al., 2021; Fajardo-Lubian and Venturini, 2023; Nguyen et al., 2017). Ultimately, the observed dynamics in our system are likely to be shaped by a combination of phage, symbiont, host, and environmental characteristics (Castledine and Buckling, 2024).

In summary, this study demonstrates the feasibility of maintaining and analyzing tripartite interactions within the *Paraburkholderia*-amoeba symbiosis system while underscoring the inherent variability of these relationships. Our in-amoeba phage-symbiont pairings point to intricate links between phage, symbiont, and host traits, highlighting the need to unravel the underlying mechanisms shaping these dynamics. Moving forward, insights gleaned from our phage screening efforts will guide the optimization of future phage isolation strategies, enabling a deeper understanding of *Paraburkholderia* phages (and their relationship with *Paraburkholderia* host species) and expanding our toolkit of available phage isolates. Integrating a broader collection of characterized phage isolates with existing *Paraburkholderia*-amoeba resources will better enable identification of the genotypic and phenotypic determinants of interaction outcomes. Moreover, the ability to explore the influence of environmental conditions and long-term associations on outcomes in this system reinforces its utility as a model for understanding potential interaction trajectories relevant for more complex biological contexts. Together, these findings lay the groundwork for future studies aimed at dissecting the ecological and evolutionary dynamics of multipartite symbiosis.

Data availability statement

The original contributions presented in the study are publicly available. This data can be found at: https://figshare.com/articles/dataset/DiSalvo_et_al_Phages_specific_to_Paraburkholderia_symbionts_of_soil_amoeba_Frontiers_in_Micro_Submission_Nov_2024/27922041?file=50850939.

Author contributions

SD: Conceptualization, Formal analysis, Funding acquisition, Investigation, Methodology, Project administration, Visualization, Writing – original draft, Writing – review & editing. NM: Investigation, Writing – review & editing. AB: Investigation, Writing – review & editing. MT: Investigation, Methodology, Writing – review & editing. AH: Investigation, Writing – review & editing.

Funding

The author(s) declare that financial support was received for the research and/or publication of this article. This material is based upon work supported by the National Science Foundation CAREER Award under grant no. 2046869.

Acknowledgments

We thank all members of the DiSalvo lab at SIUE, particularly Paige Bangle, Lance Price, Niloufar Khojandi, Kalena Davis, Mainprice Essuman, Nicholas Wigge, and Ashleigh Stults for contributions toward phage isolation, preliminary data, and other insights generated from work on related projects. We thank Joan Strassmann, David Queller, and Tamara Haselkorn, for continued conceptual guidance and resource sharing. For helpful insights, editorial suggestions, and intellectual encouragement, we thank Nima Lotfi, Bonnie DiSalvo, and Richard DiSalvo.

Conflict of interest

The authors declare that the research was conducted in the absence of any commercial or financial relationships that could be construed as a potential conflict of interest.

Generative AI statement

The authors declare that Gen AI was used in the creation of this manuscript. To assist with editorial revisions on short sections of the manuscript.

Publisher's note

Supplementary material

The Supplementary material for this article can be found online at: https://www.frontiersin.org/articles/10.3389/fmicb.2025.1537073/full#supplementary-material

SUPPLEMENTARY FIGURE 1
Bonzo treatment of Pb433 infected amoeba reduces infection prevalence under a wide range of estimated phage to symbiont multiplicity of infection ratios. Pb433 infection prevalence (rfp-positive spores) from fruiting bodies developed after plating 10^5 Pb433rfp infected amoeba spores with 10^5, 10^6, 10^7, and 10^8 total Bonzo pfu's (reflecting 0.1 to 100 MOIs under the assumption that Pb433rfp cells outnumber spores in the sample by 10) or with phage buffer control (untreated).

SUPPLEMENTARY TABLE 1
Bacterial strains used for phage screening and host range analysis. For the main symbiont-relevant collection, information on isolation region and sample type is included. To generate the cladogram used to organize bacterial strains in the host range figure, the AtpD synthase GenBank accession number is indicated (associated with each isolate or, when necessary, a closely related representative). H. Arboretum and MLBS refer to the Houston Arboretum and Mountain Lake Biological Station, respectively.

References

Addy, H. S., Askora, A., Kawasaki, T., Fujie, M., and Yamada, T. (2012). The filamentous phage ϕRSS1 enhances virulence of Phytopathogenic *Ralstonia solanacearum* on tomato. *Phytopathology* 102, 244–251. doi: 10.1094/PHYTO-10-11-0277

Almeida, G. M. F., Laanto, E., Ashrafi, R., and Sundberg, L.-R. (2019). Bacteriophage adherence to mucus mediates preventive protection against pathogenic Bacteria. *MBio* 10, e01984–e01919. doi: 10.1128/mBio.01984-19

Annesley, S. J., and Fisher, P. R. (2009). Dictyostelium discoideum—a model for many reasons. *Mol. Cell. Biochem.* 329, 73–91. doi: 10.1007/s11010-009-0111-8

Arnold, B. J., Huang, I.-T., and Hanage, W. P. (2022). Horizontal gene transfer and adaptive evolution in bacteria. *Nat. Rev. Microbiol.* 20, 206–218. doi: 10.1038/s41579-021-00650-4

Avellaneda-Franco, L., Dahlman, S., and Barr, J. J. (2023). The gut virome and the relevance of temperate phages in human health. *Front. Cell. Infect. Microbiol.* 13:1241058. doi: 10.3389/fcimb.2023.1241058

Barisch, C., López-Jiménez, A. T., and Soldati, T. (2015). "Live imaging of *Mycobacterium marinum* infection in Dictyostelium discoideum" in Mycobacteria protocols, methods in molecular biology, vol. *1285*. eds. T. Parish, and D. M. Roberts (New York, NY: Humana Press), 369–385.

Barr, J. J. (2019). Missing a phage: unraveling tripartite symbioses within the human Gut. *mSystems* 4, e00105. doi: 10.1128/mSystems.00105-19

Barr, J. J., Auro, R., Furlan, M., Whiteson, K. L., Erb, M. L., Pogliano, J., et al. (2013). Bacteriophage adhering to mucus provide a non-host-derived immunity. *Proc. Natl. Acad. Sci.* 110:10771–10776. doi: 10.1073/pnas.1305923110

Beukes, C. W., Palmer, M., Manyaka, P., Chan, W. Y., Avontuur, J. R., Van Zyl, E., et al. (2017). Genome data provides high support for generic boundaries in Burkholderia Sensu Lato. *Front. Microbiol.* 8:1154. doi: 10.3389/fmicb.2017.01154

Bichet, M. C., Chin, W. H., Richards, W., Lin, Y.-W., Avellaneda-Franco, L., Hernandez, C. A., et al. (2021). Bacteriophage uptake by mammalian cell layers represents a potential sink that may impact phage therapy. *iScience* 24:102287. doi: 10.1016/j.isci.2021.102287

Bordenstein, S. R., and Bordenstein, S. R. (2016). Eukaryotic association module in phage WO genomes from Wolbachia. *Nat. Commun.* 7:13155. doi: 10.1038/ncomms13155

Bozzaro, S. (2013). "The model organism Dictyostelium discoideum" in Dictyostelium Discoideum protocols, methods in molecular biology. eds. L. Eichinger and F. Rivero (Totowa, NJ: Humana Press), 17–37.

Bozzaro, S., and Eichinger, L. (2011). The professional phagocyte Dictyostelium discoideum as a model host for bacterial pathogens. *Curr. Drug Targets* 12, 942–954. doi: 10.2174/138945011795677782

Brock, D. A., Callison, W. É., Strassmann, J. E., and Queller, D. C. (2016). Sentinel cells, symbiotic bacteria and toxin resistance in the social amoeba Dictyostelium discoideum. *Proc. Biol. Sci.* 283:2015.2727. doi: 10.1098/rspb.2015.2727

Brock, D. A., Douglas, T. E., Queller, D. C., and Strassmann, J. E. (2011). Primitive agriculture in a social amoeba. *Nature* 469, 393–396. doi: 10.1038/nature09668

Brock, D. A., Hubert, A. M., Noh, S., DiSalvo, S., Geist, K. S., Haselkorn, T. S., et al. (2018). Endosymbiotic adaptations in three new bacterial species associated with Dictyostelium discoideum: Burkholderia agricolaris sp. nov., Burkholderia hayleyella sp. nov., and Burkholderia bonniea sp. nov. *PeerJ*. doi: 10.1101/304352

Casjens, S. (2003). Prophages and bacterial genomics: what have we learned so far?: prophage genomics. *Mol. Microbiol.* 49, 277–300. doi: 10.1046/j.1365-2958.2003.03580.x

Castledine, M., and Buckling, A. (2024). Critically evaluating the relative importance of phage in shaping microbial community composition. *Trends Microbiol.* 32, 957–969. doi: 10.1016/j.tim.2024.02.014

Chan, B. K., Sistrom, M., Wertz, J. E., Kortright, K. E., Narayan, D., and Turner, P. E. (2016). Phage selection restores antibiotic sensitivity in MDR *Pseudomonas aeruginosa*. *Sci. Rep.* 6:26717. doi: 10.1038/srep26717

Chatterjee, A., and Duerkop, B. A. (2018). Beyond Bacteria: bacteriophage-eukaryotic host interactions reveal emerging paradigms of health and disease. *Front. Microbiol.* 9:1394. doi: 10.3389/fmicb.2018.01394

Chen, G., Zhuchenko, O., and Kuspa, A. (2007). Immune-like phagocyte activity in the social amoeba. *Science* 317, 678–681. doi: 10.1126/science.1143991

Clokie, M. R. J., Millard, A. D., Letarov, A. V., and Heaphy, S. (2011). Phages in nature. *Bacteriophage* 1, 31–45. doi: 10.4161/bact.1.1.14942

Compant, S., Nowak, J., Coenye, T., Clément, C., and Ait Barka, E. (2008). Diversity and occurrence of Burkholderia spp. in the natural environment. *FEMS Microbiol. Rev.* 32, 607–626. doi: 10.1111/j.1574-6976.2008.00113.x

Dąbrowska, K., Świtała-Jeleń, K., Opolski, A., and Górski, A. (2006). Possible association between phages, hoc protein, and the immune system. *Arch. Virol.* 151, 209–215. doi: 10.1007/s00705-005-0641-7

DiSalvo, S., Haselkorn, T. S., Bashir, U., Jimenez, D., Brock, D. A., Queller, D. C., et al. (2015). Burkholderia bacteria infectiously induce the proto-farming symbiosis of Dictyostelium amoebae and food bacteria. *Proc. Natl. Acad. Sci. USA* 112, E5029–E5037. doi: 10.1073/pnas.1511878112

Dobritsa, A. P., and Samadpour, M. (2016). Transfer of eleven species of the genus Burkholderia to the genus Paraburkholderia and proposal of Caballeronia gen. Nov. to accommodate twelve species of the genera Burkholderia and Paraburkholderia. *Int. J. Syst. Evol. Microbiol.* 66, 2836–2846. doi: 10.1099/ijsem.0.001065

Drulis-Kawa, Z., Majkowska-Skrobek, G., Maciejewska, B., Delattre, A.-S., and Lavigne, R. (2012). Learning from bacteriophages - advantages and limitations of phage and phage-encoded protein applications. *CPPS* 13, 699–722. doi: 10.2174/138920312804871193

DuBose, J. G., Robeson, M. S., Hoogshagen, M., Olsen, H., and Haselkorn, T. S. (2022). Complexities of inferring symbiont function: *Paraburkholderia* symbiont dynamics in social Amoeba populations and their impacts on the Amoeba microbiota. *Appl. Environ. Microbiol.* 88:e0128522. doi: 10.1128/aem.01285-22

Duerkop, B. A., Kleiner, M., Paez-Espino, D., Zhu, W., Bushnell, B., Hassell, B., et al. (2018). Murine colitis reveals a disease-associated bacteriophage community. *Nat. Microbiol.* 3, 1023–1031. doi: 10.1038/s41564-018-0210-y

Dunn, J. D., Bosmani, C., Barisch, C., Raykov, L., Lefrançois, L. H., Cardenal-Muñoz, E., et al. (2018). Eat prey, live: Dictyostelium discoideum as a model for cell-autonomous defenses. *Front. Immunol.* 8:1906. doi: 10.3389/fimmu.2017.01906

Estrada-de Los Santos, P., Palmer, M., Chávez-Ramírez, B., Beukes, C., Steenkamp, E. T., Briscoe, L., et al. (2018). Whole genome analyses suggests that Burkholderia sensu lato contains two additional novel genera (Mycetohabitans gen. Nov., and Trinickia gen. Nov.): Implications for the evolution of Diazotrophy and nodulation in the Burkholderiaceae. *Gene* 9:389. doi: 10.3390/genes9080389

Fajardo-Lubian, A., and Venturini, C. (2023). Use of bacteriophages to target intracellular pathogens. *Clin. Infect. Dis.* 77, S423–S432. doi: 10.1093/cid/ciad515

Gogokhia, L., Buhrke, K., Bell, R., Hoffman, B., Brown, D. G., Hanke-Gogokhia, C., et al. (2019). Expansion of bacteriophages is linked to aggravated intestinal inflammation and colitis. *Cell Host Microbe* 25, 285–299.e8. doi: 10.1016/j.chom.2019.01.008

Gómez, P., and Buckling, A. (2011). Bacteria-phage antagonistic coevolution in soil. *Science* 332, 106–109. doi: 10.1126/science.1198767

Han, K., Li, Z., Peng, R., Zhu, L., Zhou, T., Wang, L., et al. (2013). Extraordinary expansion of a *Sorangium cellulosum* genome from an alkaline milieu. *Sci. Rep.* 3:2101. doi: 10.1038/srep02101

Haselkorn, T. S., DiSalvo, S., Miller, J. W., Bashir, U., Brock, D. A., Queller, D. C., et al. (2018). The specificity of Burkholderia symbionts in the social amoeba farming symbiosis: prevalence, species, genetic and phenotypic diversity. *Mol. Ecol.* 28, 847–862. doi: 10.1111/mec.14982

Haselkorn, T. S., Jimenez, D., Bashir, U., Sallinger, E., Queller, D. C., Strassmann, J. E., et al. (2021). Novel Chlamydiae and *Amoebophilus* endosymbionts are prevalent in wild

isolates of the model social amoeba *Dictyostelium discoideum*. *Environ. Microbiol. Rep.* 13, 708–719. doi: 10.1111/1758-2229.12985

Hendrix, R. W. (2014). "Bacteriophage evolution and the role of phages in host evolution" in Phages. eds. M. K. Waldor, D. I. Friedman and S. L. Adhya (Washington, DC, USA: ASM Press), 55–65.

Horn, H., Slaby, B. M., Jahn, M. T., Bayer, K., Moitinho-Silva, L., Förster, F., et al. (2016). An enrichment of CRISPR and other defense-related features in marine sponge-associated microbial metagenomes. *Front. Microbiol.* 7. doi: 10.3389/fmicb.2016.01751

Hyman, P. (2019). Phages for phage therapy: isolation, characterization, and host range breadth. *Pharmaceuticals (Basel)* 12:35. doi: 10.3390/ph12010035

Jahn, M. T., Arkhipova, K., Markert, S. M., Stigloher, C., Lachnit, T., Pita, L., et al. (2019). A phage protein aids bacterial symbionts in eukaryote immune evasion. *Cell Host Microbe* 26, 542–550.e5. doi: 10.1016/j.chom.2019.08.019

Kaltenpoth, M., and Flórez, L. V. (2020). Versatile and dynamic symbioses between insects and *Burkholderia* Bacteria. *Annu. Rev. Entomol.* 65, 145–170. doi: 10.1146/annurev-ento-011019-025025

Kessin, R. H. (2001). Dictyostelium: Evolution, cell biology, and the development of multicellularity, developmental and cell biology series. Cambridge, UK; New York: Cambridge University Press.

Khojandi, N., Haselkorn, T. S., Eschbach, M. N., Naser, R. A., and DiSalvo, S. (2019). Intracellular Burkholderia symbionts induce extracellular secondary infections; driving diverse host outcomes that vary by genotype and environment. *ISME J.* 13, 2068–2081. doi: 10.1038/s41396-019-0419-7

Koskella, B., and Brockhurst, M. A. (2014). Bacteria–phage coevolution as a driver of ecological and evolutionary processes in microbial communities. *FEMS Microbiol. Rev.* 38, 916–931. doi: 10.1111/1574-6976.12072

Koskella, B., and Taylor, T. B. (2018). Multifaceted impacts of bacteriophages in the plant microbiome. *Annu. Rev. Phytopathol.* 56, 361–380. doi: 10.1146/annurev-phyto-080417-045858

Koskella, B., Thompson, J. N., Preston, G. M., and Buckling, A. (2011). Local biotic environment shapes the spatial scale of bacteriophage adaptation to Bacteria. *Am. Nat.* 177, 440–451. doi: 10.1086/658991

LePage, D. P., Metcalf, J. A., Bordenstein, S. R., On, J., Perlmutter, J. I., Shropshire, J. D., et al. (2017). Prophage WO genes recapitulate and enhance Wolbachia-induced cytoplasmic incompatibility. *Nature* 543, 243–247. doi: 10.1038/nature21391

López-Jiménez, A. T., Hagedorn, M., Delincé, M. J., McKinney, J., and Soldati, T. (2019). The developmental cycle of *Dictyostelium discoideum* ensures curing of a mycobacterial infection at both cell-autonomous level and by collaborative exclusion (preprint). *Microbiology*. doi: 10.1101/586263

Łusiak-Szelachowska, M., Weber-Dąbrowska, B., Żaczek, M., Borysowski, J., and Górski, A. (2020). The presence of bacteriophages in the human body: good, bad or neutral? *Microorganisms* 8:2012. doi: 10.3390/microorganisms8122012

Majkowska-Skrobek, G., Markwitz, P., Sosnowska, E., Lood, C., Lavigne, R., and Drulis-Kawa, Z. (2021). The evolutionary trade-offs in phage-resistant Klebsiella pneumoniae entail cross-phage sensitization and loss of multidrug resistance. *Environ. Microbiol.* 23, 7723–7740. doi: 10.1111/1462-2920.15476

Marbouty, M., Thierry, A., Millot, G. A., and Koszul, R. (2021). MetaHiC phage-bacteria infection network reveals active cycling phages of the healthy human gut. *eLife* 10:e60608. doi: 10.7554/eLife.60608

Marchi, J., Zborowsky, S., Debarbieux, L., and Weitz, J. S. (2023). The dynamic interplay of bacteriophage, bacteria and the mammalian host during phage therapy. *iScience* 26:106004. doi: 10.1016/j.isci.2023.106004

Martín-González, J., Montero-Bullón, J., and Lacal, J. (2021). *Dictyostelium discoideum* as a non-mammalian biomedical model. *Microb. Biotechnol.* 14, 111–125. doi: 10.1111/1751-7915.13692

Mattila, S., Ruotsalainen, P., and Jalasvuori, M. (2015). On-demand isolation of bacteriophages against drug-resistant Bacteria for personalized phage therapy. *Front. Microbiol.* 6. doi: 10.3389/fmicb.2015.01271

Miller, J. W., Bocke, C. R., Tresslar, A. R., Schniepp, E. M., and DiSalvo, S. (2020). Paraburkholderia symbionts display variable infection patterns that are not predictive of Amoeba host outcomes. *Gene* 11:674. doi: 10.3390/genes11060674

Mullins, A. J., and Mahenthiralingam, E. (2021). The hidden genomic diversity, specialized metabolite capacity, and revised taxonomy of Burkholderia Sensu Lato. *Front. Microbiol.* 12:726847. doi: 10.3389/fmicb.2021.726847

Nafarrate, I., Mateo, E., Amárita, F., De Marañón, I. M., and Lasagabaster, A. (2020). Efficient isolation of Campylobacter bacteriophages from chicken skin, analysis of several isolation protocols. *Food Microbiol.* 90:103486. doi: 10.1016/j.fm.2020.103486

Nguyen, S., Baker, K., Padman, B. S., Patwa, R., Dunstan, R. A., Weston, T. A., et al. (2017). Bacteriophage transcytosis provides a mechanism to cross epithelial cell layers. *MBio* 8, e01874–e01817. doi: 10.1128/mBio.01874-17

Noh, S., Capodanno, B. J., Xu, S., Hamilton, M. C., Strassmann, J. E., and Queller, D. C. (2022). Reduced and nonreduced genomes in *Paraburkholderia* symbionts of social amoebas. *Msystems* 7:e0056222. doi: 10.1128/msystems.00562-22

Oechslin, F. (2018). Resistance development to bacteriophages occurring during bacteriophage therapy. *Viruses* 10:351. doi: 10.3390/v10070351

Oliver, K. M., Degnan, P. H., Hunter, M. S., and Moran, N. A. (2009). Bacteriophages encode factors required for protection in a symbiotic mutualism. *Science* 325, 992–994. doi: 10.1126/science.1174463

Oromí-Bosch, A., Antani, J. D., and Turner, P. E. (2023). Developing phage therapy that overcomes the evolution of bacterial resistance. *Annual Rev. Virol.* 10, 503–524. doi: 10.1146/annurev-virology-012423-110530

Pichon, S., Bouchon, D., Liu, C., Chen, L., Garrett, R. A., and Grève, P. (2012). The expression of one ankyrin pk2 allele of the WO prophage is correlated with the Wolbachia feminizing effect in isopods. *BMC Microbiol.* 12:55. doi: 10.1186/1471-2180-12-55

Pratama, A. A., Chaib De Mares, M., and Van Elsas, J. D. (2018). Evolutionary history of bacteriophages in the genus Paraburkholderia. *Front. Microbiol.* 9:835. doi: 10.3389/fmicb.2018.00835

Pratama, A. A., and van Elsas, J. D. (2017). A novel inducible prophage from the mycosphere inhabitant Paraburkholderia terrae BS437. *Sci. Rep.* 7:9156. doi: 10.1038/s41598-017-09317-8

Sawana, A., Adeolu, M., and Gupta, R. S. (2014). Molecular signatures and phylogenomic analysis of the genus Burkholderia: proposal for division of this genus into the emended genus Burkholderia containing pathogenic organisms and a new genus Paraburkholderia gen. Nov. harboring environmental species. *Front. Genet.* 5. doi: 10.3389/fgene.2014.00429

Shropshire, J. D., On, J., Layton, E. M., Zhou, H., and Bordenstein, S. R. (2018). One prophage WO gene rescues cytoplasmic incompatibility in *Drosophila melanogaster*. *Proc. Natl. Acad. Sci. USA* 115, 4987–4991. doi: 10.1073/pnas.1800650115

Shu, L., Brock, D. A., Geist, K. S., Miller, J. W., Queller, D. C., Strassmann, J. E., et al. (2018). Symbiont location, host fitness, and possible coadaptation in a symbiosis between social amoebae and bacteria. *eLife* 7. doi: 10.7554/eLife.42660

Shu, L., Qian, X., Brock, D. A., Geist, K. S., Queller, D. C., and Strassmann, J. E. (2020). Loss and resiliency of social amoeba symbiosis under simulated warming. *Ecol. Evol.* 10, 13182–13189. doi: 10.1002/ece3.6909

Srinivasiah, S., Bhavsar, J., Thapar, K., Liles, M., Schoenfeld, T., and Wommack, K. E. (2008). Phages across the biosphere: contrasts of viruses in soil and aquatic environments. *Res. Microbiol.* 159, 349–357. doi: 10.1016/j.resmic.2008.04.010

Steinert, M., and Heuner, K. (2005). Dictyostelium as host model for pathogenesis. *Cell. Microbiol.* 7, 307–314. doi: 10.1111/j.1462-5822.2005.00493.x

Stiffler, A. K., Hesketh-Best, P. J., Varona, N. S., Zagame, A., Wallace, B. A., Lapointe, B. E., et al. (2024). Genomic and induction evidence for bacteriophage contributions to sargassum-bacteria symbioses. *Microbiome* 12:143. doi: 10.1186/s40168-024-01860-7

Suttle, C. A. (2005). Viruses in the sea. *Nature* 437, 356–361. doi: 10.1038/nature04160

Suttle, C. A. (2007). Marine viruses — major players in the global ecosystem. *Nat. Rev. Microbiol.* 5, 801–812. doi: 10.1038/nrmicro1750

Sweere, J. M., Van Belleghem, J. D., Ishak, H., Bach, M. S., Popescu, M., Sunkari, V., et al. (2019). Bacteriophage trigger antiviral immunity and prevent clearance of bacterial infection. *Science* 363:eaat9691. doi: 10.1126/science.aat9691

Thewes, S., Soldati, T., and Eichinger, L. (2019). Editorial: amoebae as host models to study the interaction with pathogens. *Front. Cell. Infect. Microbiol.* 9, 2235–2988. doi: 10.3389/fcimb.2019.00047

Weldon, S. R., Strand, M. R., and Oliver, K. M. (2013). Phage loss and the breakdown of a defensive symbiosis in aphids. *Proc. R. Soc. B* 280:20122103. doi: 10.1098/rspb.2012.2103

Wilde, J., Boyes, R., Robinson, A. V., Daisley, B. A., Botschner, A. J., Brettingham, D. J. L., et al. (2024). Assessing phage-host population dynamics by reintroducing virulent viruses to synthetic microbiomes. *Cell Host Microbe* 32, 768–778.e9. doi: 10.1016/j.chom.2024.04.001

Xu, Y., Buss, E., and Boucias, D. (2016). Impacts of antibiotic and bacteriophage treatments on the gut-symbiont-associated *Blissus insularis* (Hemiptera: Blissidae). *Insects* 7:61. doi: 10.3390/insects7040061

Zhang, X., Wang, S., Zhang, Q., Zhang, K., Liu, W., Zhang, R., et al. (2022). The expansion of a single bacteriophage leads to bacterial disturbance in gut and reduction of larval growth in *Musca domestica*. *Front. Immunol.* 13:885722. doi: 10.3389/fimmu.2022.885722

Zhang, X., Zhuchenko, O., Kuspa, A., and Soldati, T. (2016). Social amoebae trap and kill bacteria by casting DNA nets. *Nat. Commun.* 7:10938. doi: 10.1038/ncomms10938

Zuppi, M., Hendrickson, H. L., O'Sullivan, J. M., and Vatanen, T. (2022). Phages in the gut ecosystem. *Front. Cell. Infect. Microbiol.* 11:822562. doi: 10.3389/fcimb.2021.822562

Frontiers in Microbiology

Explores the habitable world and the potential of microbial life

The largest and most cited microbiology journal which advances our understanding of the role microbes play in addressing global challenges such as healthcare, food security, and climate change.

Discover the latest Research Topics

See more →

Frontiers

Avenue du Tribunal-Fédéral 34
1005 Lausanne, Switzerland
frontiersin.org

Contact us

+41 (0)21 510 17 00
frontiersin.org/about/contact